The deformation of rockfill : inter-particle behaviour, bulk properties and behaviour in dams.

Clements, Ronald Peter

THE DEFORMATION OF ROCKFILL; INTER-PARTICLE BEHAVIOUR, BULK PROPERTIES AND BEHAVIOUR IN DAMS

A thesis submitted to the
University of London (King's College)
for the degree of

Doctor of Philosophy in the Faculty of Engineering

by

Ronald Peter Clements

November, 1981.

King's College, London.

Abstract

The behaviour of rockfill has been investigated by a series of long-term oedometer tests, a study of the movements observed in dams and an experimental investigation of the crushing occurring at the points of contact of rock particles due to interparticle forces. Particular attention has been paid to the effect of saturation, inundation with water and the magnitude and variation of the load applied.

Using the results of the contact studies, a simple computer based numerical model has been developed to link local crushing with the bulk behaviour of an assembly of angular rock particles. This was successful for small overall displacements and has provided an interesting indication of the magnitude and distribution of contact forces and the extent of crushing occurring throughout the mass. Methods of improving the accuracy of the results at larger overall displacements have been suggested.

An extensive literature review has provided information about the movements of major rockfill dams. This has allowed the factors influencing the displacements to be pinpointed. The analysis of these results has shown existing methods of predicting post-construction movements to be inadequate and an alternative approach has been proposed.

Acknowledgement.

During my research I have been fortunate to enjoy the supervision of both Professor J.K.T.L. Nash and Professor J.W. Dougill. I would like to thank them for their very valuable help and guidance while carrying out the research and also in the writing of this thesis. Most of the equipment described was made in the Civil Engineering Department Workshop at King's College and I would like to thank Mr. R. Earll and his team of technicians for carrying out this work. Particular mention must also be made of Mr. C. St. C. Blakey who was extremely helpful in the day to day running of laboratory tests.

I am grateful to the Science and Engineering Research Council for supporting me financially throughout my research and the Yorkshire Water Authority (South Western Division) for providing rock and information from Scammonden Dam. All the computer programmes mentioned were run by the University of London Computer Centre.

My thanks go to my mother, Mrs. Cicely Clements, who had the arduous task of reading my writing and typing this thesis. Finally I would like to thank my wife, Anne, who has been an endless source of encouragement. After numerous discussions and lectures from me on the deformation of rockfill I am sure that she would be capable of submitting a thesis herself.

CONTENTS

List of Figures

List of Tables

page no.

Chapter 4 The Behaviour of Rock Contacts - the Load-Displacement Relationship

Chapter 5 The Behaviour of Rock Contacts - the Area of Contact

Chapter 6 The Behaviour of Rock Particles - Time Dependence

page no.

Chapter 1

Introduction

1.1 Rockfill Dams

The first rockfill dams are considered to have been built in the middle of the 19th century by Californian gold-miners. In the absence of the normal materials used to construct embankments, i.e. earthfill, the miners used the broken rock and timber which were readily available. These dikes consisted of a mound of dumped rockfill, with a timber upstream face which acted as an impervious membrane. After this the popularity of the rockfill dam grew but many of the early attempts to build dams with rolled earth cores suffered major piping failures, because of the lack of adequate filters. The complete failure, in 1928, of the 19 m high Schofield Dam in Utah (Sherard et al., 1963) discouraged the design of similar dams until the construction of the 76 m high Nantahala Dam in North Carolina in 1942. Extensive laboratory research into the design of filters was carried out before the construction of this dam and its successful performance encouraged the building of several dams to similar designs.

Fig. 1.1 is a histogram of all the dams with heights of over 10m built in Britain from about 1796 to 1980 and the number of earthfill, rockfill, concrete and combinations of these types constructed in each period are also given. Earth embankments have always been popular and the majority of British dams are of this type. Concrete dams were introduced in 1859 and have gained in popularity since then, becoming more popular than earthfill dams between 1950 and 1970. In the seventies there appears to have been a significant change in the attitude of dam designers with few concrete dams being constructed and earthfill dams regaining prominence. The exact definition of a rockfill dam has not always been clear and some of the dams listed as earthfill in the source of this data (World Register of Dams, 1964; 1973; 1976; 1979) would be considered to be rockfill. A widely accepted definition of a rockfill dam is 'an embankment in which rockfill is the major fill material'. The histogram figures show that although rockfill dams have been quite

scarce in Britain several, were constructed between 1970 and 1979.

Fig. 1.2 shows a histogram of the dam construction rates over the periods used in fig. 1.1. Between 1850 and 1950 the rate was fairly steady but there was a significant increase in the fifties. This was probably due to an increase in demand for water for new industry and the provision of better sanitation and water supply schemes. There would also have been construction of schemes delayed by the war during this period. Since then there has been a fall in the construction rate and the figures indicate a return to 3-4 dams/year, which is a similar rate to that in the 1850-1950 period.

Although increased economic pressures have led to the introduction of zoned dams, most rockfill dams can be placed in three general categories:-

(a) Central core section - fig. 1.3a

This consists of a centrally placed core of earth or impermeable wall, e.g. bituminous concrete supported by an upstream and downstream shoulder of rockfill. Llyn Brianne Dam (90 m high) constructed in Central Wales is an example of this type and is at present the highest rockfill dam in Britain.

(b) Sloping core section - fig. 1.3b

This section is also known as the 'Alcoa' or more commonly, the 'Growden' section (named after the consulting engineer, J.P. Growden, who was involved in the original design) and the core is placed on the upstream face of a mound of rockfill. Protection against wave action is given to the core by a layer of rockfill on its upstream face. Scammonden Dam (70 m high), completed in 1969 near Huddersfield, is an example of this type of section.

(c) Membrane - faced section - fig. 1.3c

This is similar to the dams constructed by the Californian gold-miners but more modern materials are used for the membrane now. The recently constructed 53 m high rockfill dam at Winscar, Yorkshire, is of this type and has a membrane of asphaltic concrete.

1.2 Deformation of Rockfill Dams

It has been recognised for many years that earth and rockfill

dams deform and settle both during and after construction. These movements may disturb a dam in such a way that failure or partial failure of the dam becomes possible. In assessing the relative importance of various areas of research needed for better design of dams, the ASCE Committee on Earth and Rockfill Dams (ASCE, 1967) lists 'Strength and Volume Change Characteristics of Gravel and Rockfill Materials under High Confining Pressures' as its highest priority. Extensive laboratory work on the overall behaviour of rockfill has been carried out in Mexico (Marsal, 1977) and California, U.S.A. (Becker et al., 1972) using large triaxial, oedometer and plane strain rigs. In his conclusion Marsal notes that the phenomena underlying the bulk behaviour was more complex than anticipated and suggests research to investigate the local behaviour.

Differential settlement can cause external cracking of the embankment which may lead to erosion of the core material or cracking of the membrane. The most dangerous cracks are those which open up seepage paths across the core. These are usually formed by differential settlements in the foundation material, e.g. a river bed foundation of alluvials and hard rock abutments, but such settlements may occur within the embankment, e.g. in a steep-sided valley where arching of the upper portion of the dam occurs, with equally devastating results.

Apart from dam-abutment interaction, recent research and discussion about differential settlement has concentrated on the interaction between the core and rockfill shells (Wilson and Marsal, 1979). If the core of a dam settles more than the shell (or the filter) material, then there is a transfer of load from the core to the shells and the core hangs on the shell by what is in effect an arching mechanism. This may lead to fracture i.e. horizontal cracking of the core and subsequent seepage through the core may cause failure. Sherard (1973) gives details of seven dams which are thought to have suffered differential settlement causing either external transverse cracking or internal cracking and subsequent hydraulic fracture.

There are a large number of factors which effect the amount and mode of the deformations but these can be grouped under a few general headings, as follows:-

(a) Site topography and geology

(b) Properties and gradings of materials used

(c) Dam design

(d) Construction methods

(e) External loading e.g. reservoir level changes and seismic activity

Most of these factors are influenced by the economic and regional situations and restrict the engineer's freedom to design and construct the dam how and where he wishes. One of his major considerations in design must be the amount of deformation likely to occur and how this will effect the stability of the dam. Several construction practices, such as sluicing and compaction of the rockfill, have been introduced and these help to limit the deformation. It is generally agreed that these are useful but there is still debate over the best way to apply them. Embankment instrumentation has become increasingly important during the last ten to fifteen years and information from this should help to resolve some of these problems.

1.3 Deformation Mechanisms

Although there are several factors which affect the deformation of rockfill, there are relatively few mechanisms which take place within the rockfill mass and contribute to the overall mass deformation. These mechanisms will either occur within each particle or at the points of contact between the particles.

1.3.i Interparticle Displacements

(a) Contact Crushing

Each piece of rock in a granular mass is subjected to forces at its contacts with other pieces. These forces create high stress regions at the contacts and crushing or spalling occurs to accommodate these stresses. The local displacements of particles contribute to the overall deformation of the mass.

(b) Rotation and Sliding of Particles

Contact crushing causes particles to move towards each other and can be considered to be a normal displacement on the contact plane. Tangential displacements may also take place and these are

seen as rotations or sliding of particles relative to each other. These processes will be opposed by friction between the particle surfaces but as the dynamic coefficient of friction is usually smaller than the static value, then once movement has started it will continue until the resulting redistribution of forces produces lower, stable values. These movements may also be accompanied by local breakage.

1.3.ii Intra-particle Deformations

(a) Bulk Deformation

When subjected to load rock undergoes an immediate deformation and if the load is maintained time-dependent deformations will be observed. Similarly each particle within the granular mass will respond to the variations in the forces applied to it and the strains produced will effect the overall deformation of the mass.

(b) Particle Breakage

If the forces applied to a particle produce stresses within the bulk of the particle which are greater than its strength along a particular plane, then the particle may break into two or more pieces. This will cause a redistribution of forces and change the structure of the mass. If the mass has a high porosity then large local movements may occur producing a significant change in the overall deformation.

1.3.iii The Concept of Inter and Intra-particle Deformations

The four mechanisms listed in 1.3.i and 1.3.ii help to explain the distinction between interparticle and intra-particle deformations. Broadly speaking interparticle displacements occur at the particle contacts whereas intra-particle deformations occur within the bulk of the particles. Interparticle displacements are 'surface phenomena' and the intra-particle deformations are 'volume changes'. These definitions are not very distinct since it must be assumed that there is a clear distinction between what constitutes the bulk of the particle and the contact zone. Similarly there are grey areas in distinguishing between the four mechanisms. This dilemma has not been resolved within this research. No attempt has been made to determine the exact limits of the bulk and contact zones and the broad definitions have been accepted as sufficient.

1.3.iv The Role of the Four Mechanisms in Rockfill Deformation

In measuring the deformations of a granular mass it is impossible to determine the exact contribution of each of the four mechanisms. It seems likely that the loads applied, the rock properties and particle shapes will all effect the relative importance of each mechanism in a particular situation. It is also possible that the main mechanism may change with time e.g. as a sample is compacted rolling and sliding may be restricted. At present, our knowledge of the possible role of each mechanism is limited and to understand and predict the deformations of granular masses and in particular rockfill dams, it is necessary to investigate each of the mechanisms involved.

1.4 Review of Research

Marsal (1977), in his work on granular materials, has laid great emphasis on the breakage of particles in oedometer and triaxial tests. This has led to the conclusion that breakage is the significant factor in the settlement of large dams during construction (Wilson and Marsal, 1979). In the development of his work little attention has been given to the role of contact crushing and rotation or sliding of particles. Other researchers (e.g. Charles, 1973; Kjaernsli and Sande, 1963), using similar equipment, have been more interested in the overall behaviour and deformation results rather than the processes involved.

Little attention has been given to the role of contact crushing, although some work has been carried out by researchers in tribology (e.g. Bowden and Tabor, 1949, 1964). Sowers et al. (1965) performed a series of tests on cylinders of greywacke. These were shaped to form a wedge or pyramid at one end and forced either against steel plates or flat, ground surfaces of the same material. Fig. 1.4 shows the results of these tests. Each sample showed an immediate displacement with a continuing settlement with time. Saturated contacts exhibited larger immediate displacements than dry contacts and wetting of the dry samples after about five days produced additional displacements. The use of an agent to reduce surface tension in the water increased the crushing and reduced the time lag between the

addition of water and the additional crushing. It was also noted that rock on rock tests produced sudden sporadic increased settlements but that the magnitude of these reduced with time. Rzadkowski and Zurek (1970) measured the total compression of sandstone particles when subjected to load between two metal platens. The particles were then inundated with water and the additional compression noted. Fig. 1.5 shows the graph of results they produced from these tests. Penman (1971) has shown that these results approximate to the relationship:-

$$d = c\,P^{\frac{2}{3}}$$

d - total displacement
P - load
c- constant

which is in agreement with the form of the theoretical relationship proposed by Hertz (1896). It should be noted that these tests were rock on platen tests and this conclusion is based on only a few graph points.

A large amount of theoretical work has been carried out into the behaviour of elastic contacts (e.g. Hertz, 1896: Mindin et al., 1951: Lubkin, 1951) and viscoelastic contacts (e.g. Lee and Radok, 1960: Yang 1966). Plastic contacts have been considered by Bowden and Tabor, 1949. Solutions for different load systems have been produced and usually expressions for the particle approach and dimensions of the contact area have been determined. In most of these analyses one of the main assumptions is that the contact shapes are ellipsoidal.

1.5 Outline of Research

The main emphasis of this research is an investigation into the phenomenon of contact crushing, the factors which influence its magnitude and its importance in the overall deformation of granular masses. The role of particle breakage and bulk deformations have also been considered, although not in as much detail. As a background to this work a study of the bulk behaviour of rockfill, as observed in dams, and a series of laboratory tests, has also been made.

The field data collected from a literature review of a large

number of rockfill dams has been presented in Chapter 2. This data has been used to test the accuracy of existing methods of predicting post-construction crest movements and an alternative approach to the problem has been proposed. The observed movements of dams and the major influences effecting these have also been discussed.

The material used in the laboratory tests was obtained from Scammonden Dam, near Huddersfield, Yorkshire and Chapter 3 contains a brief description of the dam and the results of classification and property tests carried out on this sandstone.

The experimental work on the behaviour of rock contacts is presented in Chapters 4 - 6 and is concentrated on three areas:-

(a) the load-displacement relationship

(b) the area of contact developed under load

(c) the time-dependent behaviour of the contact under constant load

A major influence on rock behaviour is saturation and particular attention has been paid to the effect of this throughout the research. The differences in behaviour of wet and dry contacts have been investigated as well as the effect of inundation. In analysing the results the influence of the material properties and the angularity of the particles have also been considered.

In Chapter 7 the results of a series of axial compressions tests on three gradings of the sandstone in a large oedometer creep rig have been discussed. These tests were carried out to investigate the magnitude of both immediate and time-dependent settlements when the samples were subject to different load levels, inundation and re-saturation. A study of the rebound on unloading and the subsequent time-dependent creep-recovery displacements has also been included.

A discussion of the importance of interparticle displacements (Chapter 8) suggests that a numerical computer model, based on the interparticle behaviour, can be developed to study the local behaviour of rockfill. Some success was obtained with a fairly simple model and the results of this investigation are given in Chapter 9.

The main results and conclusions of the research are presented in Chapter 10 (section 10.2) and summaries of the findings in the experimental contact tests are given in sections 4.5.ii and 6.4.iv.

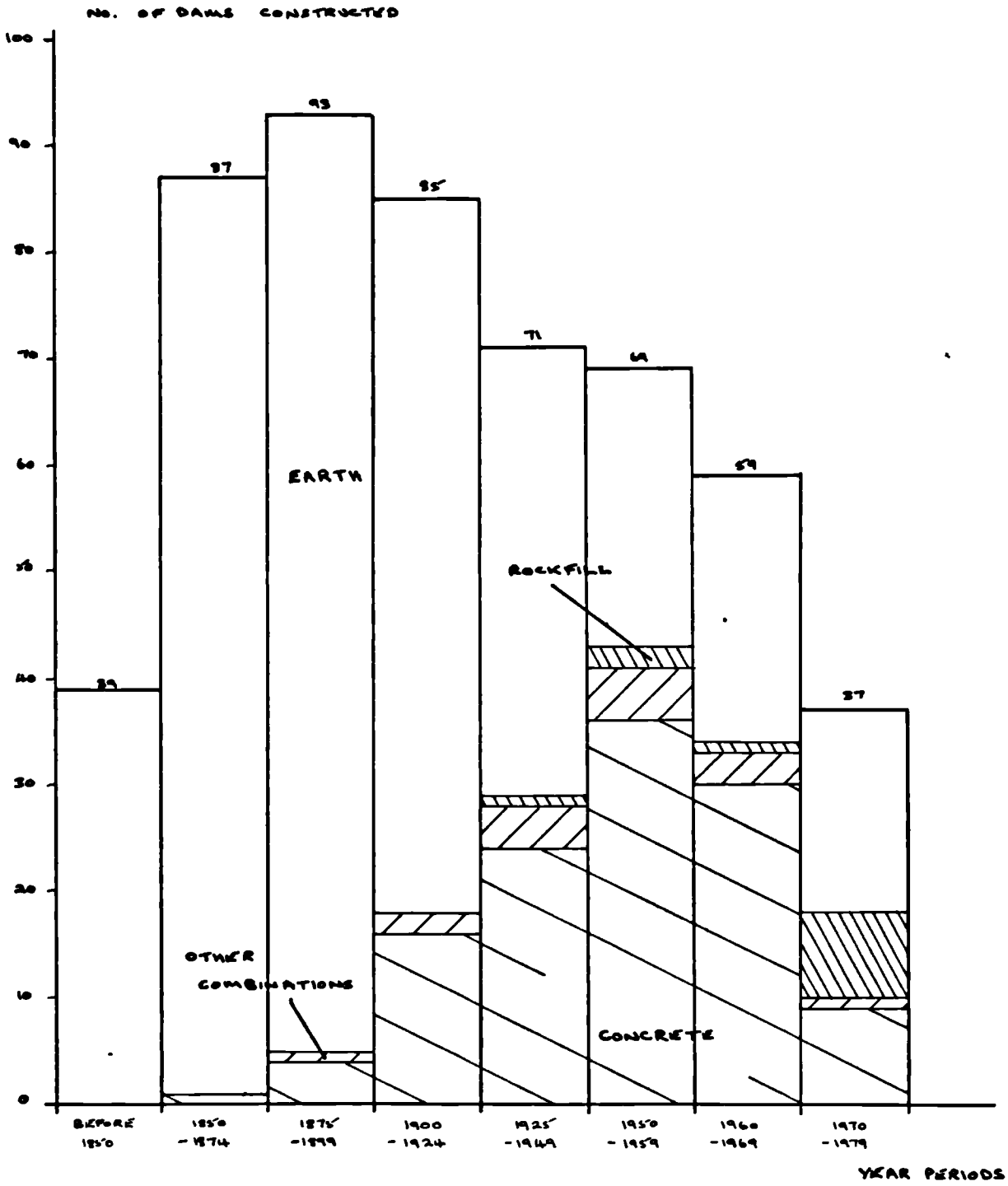

FIG. 1.1 :- HISTOGRAM OF DAMS (>10 m HIGH) CONSTRUCTED IN GREAT BRITAIN

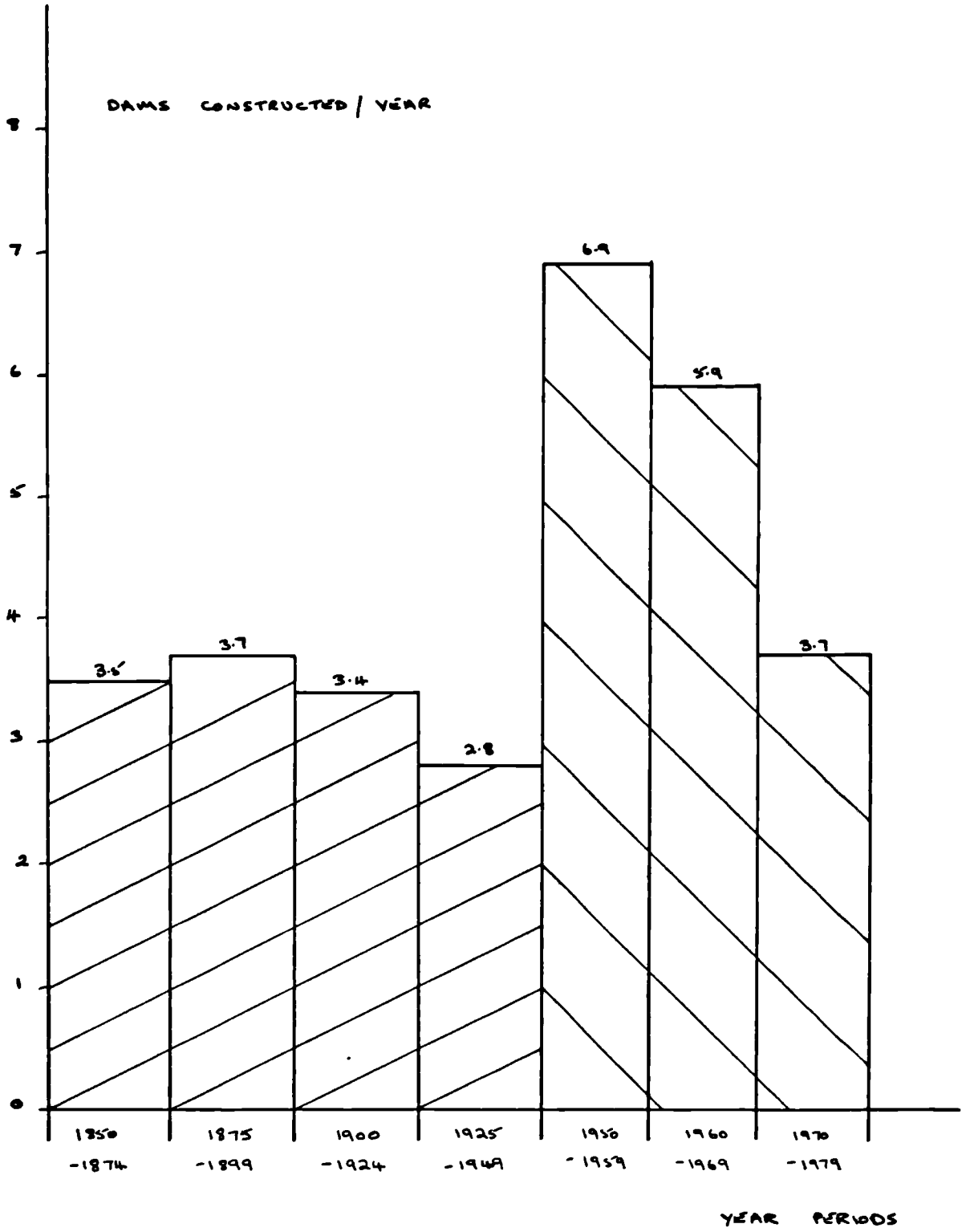

FIG. 1.2 :- HISTOGRAM OF RATES OF DAM CONSTRUCTION IN BRITAIN 1850 - 1980

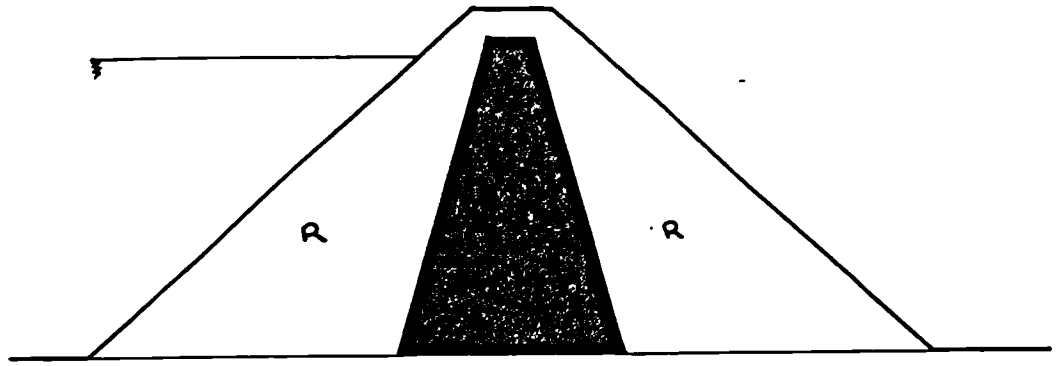

(a) CENTRAL CORE SECTION

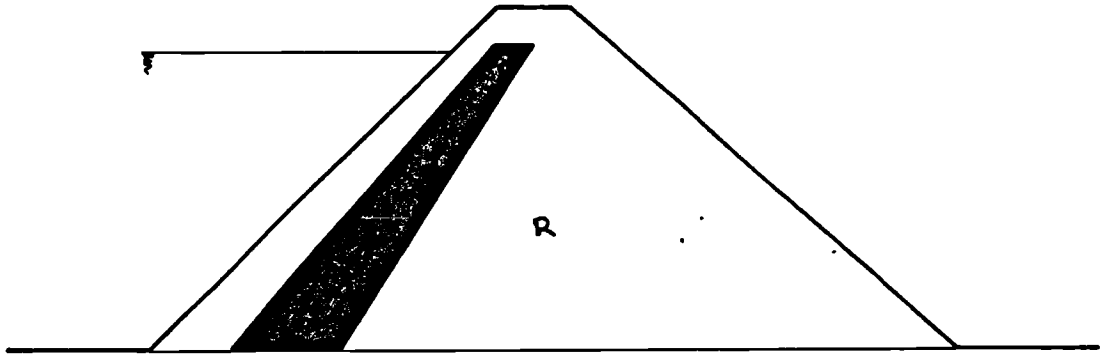

(b) SLOPING CORE SECTION

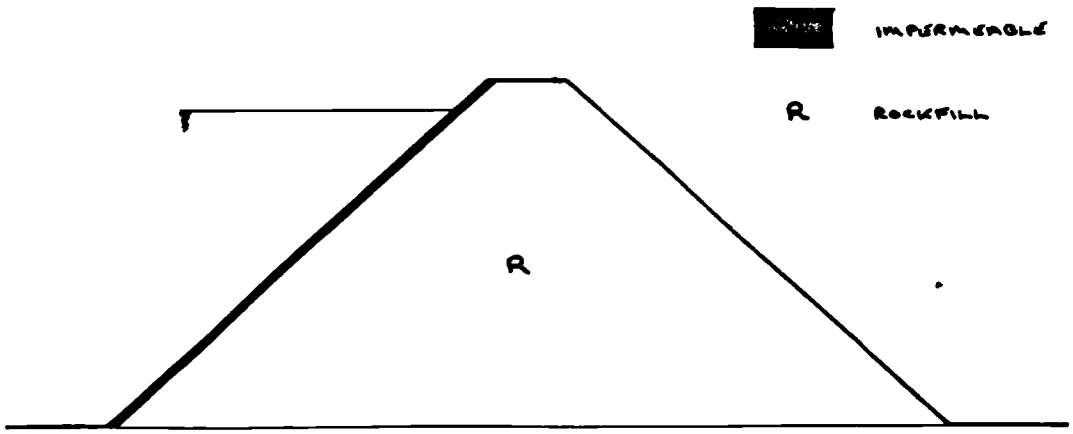

(c) MEMBRANE-FACED SECTION

FIG. 1.3 :- TYPICAL SECTIONS OF ROCKFILL DAMS

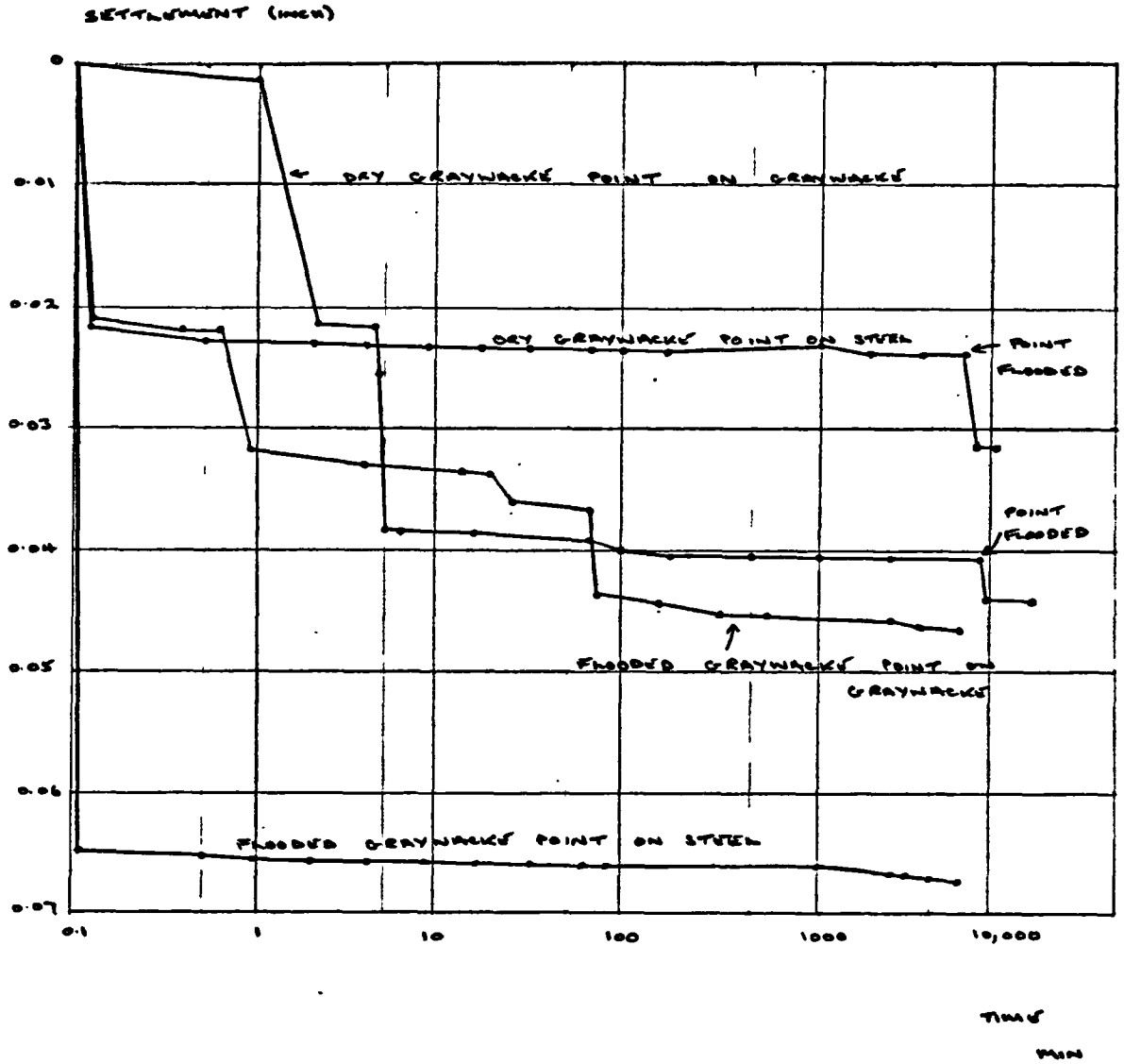

FIG. 1.4 :- TIME-DEPENDENT CRUSHING OF ROCK POINTS

(AFTER SOWERS ET AL., 1965)

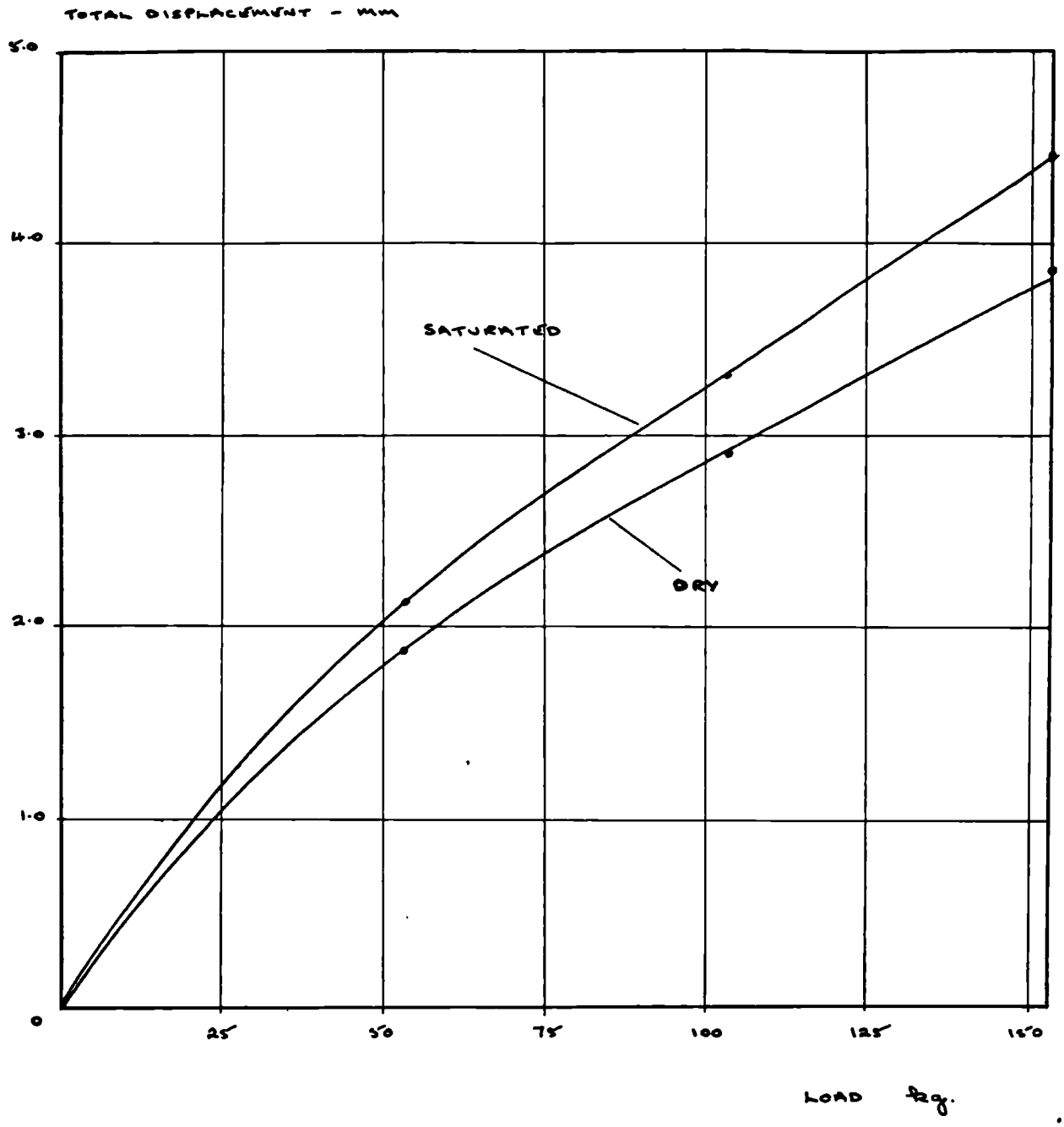

FIG. 1.5 :- RESULTS OF ROCK CONTACT CRUSHING TESTS

(AFTER RZADKOWSKI AND ZUREK, 1970)

Chapter 2

The Observed Post-construction Movements of Rockfill Dams. - their significance and prediction.

The movements of embankment dams may be divided into ~~two components - construction and post-construction displacements.~~ the displacements that occur during construction and those that occur afterwards. The first of these is concerned with the movements of the foundations and the section of the dam completed due to the addition of fill material. These include both large immediate displacements and smaller time-dependent movements. Post-construction movements are those of the completed structure and are mainly small time-dependent displacements, although external load changes may bring about larger movements.

While both sets of displacements are of importance, construction displacements may be compensated for by the addition of extra fill material. The post-construction movements are indicative of the structure's ability to perform the task it was designed for. Large movements may indicate problems within the dam which require attention and which would otherwise go unnoticed until the problem becomes more critical. Post-construction movements must also be considered at the design stage so that the designer can provide sufficient but not costly, excessive camber and freeboard. Lawton and Lester (1964) note a case where concern over large predicted settlements caused a dam to be changed from a sloping core to a central core type at the design stage.

2.1 The Prediction of Post-construction Movements.

2.1.i Methods of Prediction.

Although a wealth of material exists for predicting both construction and post-construction movements using the material properties, very little work has been carried out based on observations of dams already constructed. The finite element method has provided a useful tool in displacement prediction and may be adapted to most situations. However, its use should not go unquestioned and the present trend towards increased sophistication does not necessarily lead to greater accuracy. Materials such as rock and earthfill do not by their nature lend themselves

to precise numerical analysis techniques. It is interesting to note that a finite element analysis of Llyn Brianne Dam by Cathie and Dungar (1978), using both two and three dimensional meshes and elastic, non-linear elastic and elastic-plastic constitutive relationships, failed to improve on the elastic equivalent compressibility method used by Penman and Charles (1972). Cathie and Dungar conclude that their simple elastic 2-D analysis gave the best agreement with the observed movements. The use of inappropriate material behaviour models can produce meaningless results and it is felt that a greater understanding of material behaviour is needed to match the sophistication of analysis if the usefulness of the finite element method is to be increased.

Post-construction movement prediction based on observed displacements of existing dams has been approached in two ways.
(i) in terms of a displacement-time analysis and
(ii) in terms of a displacement-height relationship.

In considering dam movements there are a large number of factors to be taken into account viz. local topography, dam design, construction method, material properties and external loading. While it is difficult to assess the relative importance of each of these, studies of observed behaviour can provide valuable information for the dam designer. Time and height are readily available parameters and therefore provide a good basis for a prediction calculation.

(a) Displacement - time analysis

The first approach was used by Sowers et al. (1965). They collected vertical settlement data from fourteen dams noting the heights, design (sloping core, etc.), rock type and construction method. The settlement values were plotted as a percentage of the fill height against log time, fig. 2.1. Due to the fact that time-dependent displacements occur during construction and no 'creep threshold' can be defined, Sowers et al. assumed the mid-point of construction to be their zero time and plotted the values accordingly. Charles (1973), in considering Scammonden Dam, has used a point at three quarters of the construction time. From their study Sowers et al. concluded that the settlement per unit height was independent of the dam height, the design cross-section or the rock used and that the most important factor was the construction method. They also noted the narrow range of settlement

per unit height values (approximately 0.25 to 1.0% over 10 years) for the variety of dams considered. To aid prediction and as a comparison with oedometer test results presented in the paper, they suggested that a linear equation (2.1) could be applied to the curve of each dam.

$$E = \alpha (\log_{10} t_2 - \log_{10} t_1) \qquad (2.1)$$

Where E is the percentage settlement per unit height occuring between times t_1 and t_2. The value of α ranges from about 0.2 (Wolf Creek, East Fork, Chilhowee, Lower Bear River No. 1) to 1.05 (Dix River).

Parkin (1977) has reviewed the work of Sowers et al., and argues that analyses based on total settlements are subject to uncertainty and alternative interpretations. He proposes a creep rate analysis (Parkin 1971) which reduces the uncertainty, as it eliminates time-independent factors, and amplifies imperfections in the data which may be related to 'events'. He demonstrates his approach on the observed settlements of Cedar Cliff Dam and reproduces Sowers et al's equation. The application of this method is, however, not as useful as was envisaged. In this research the method was applied to data from several dams. It became apparent that the large number of 'events' which occur while a dam is in service make it difficult to distinguish the basic creep pattern from the imperfections.

(b) Displacement - height analysis

The second approach was used by Lawton and Lester (1964) who collected data from twenty-five dams of varying types. Of these, eleven were found to have attained creep rates of less than 0.02% of their heights per year. This arbitrary figure was selected as an indication that the dam had undergone its 'total effective settlement'. In using this approach no consideration was made of the length of time the dam had been in service. The values of 'total effective settlement' were plotted against the height of fill at the measuring point on a log-log graph, fig. 2.2. From this the following settlement (s) - height (h) relationship was obtained.

$$s = 0.001\ h^3/2 \qquad (2.2)$$

There is no discussion of the significance of the units of the

coefficient. A comparison of the 'rule of thumb' prediction, $s = 0.01\ h$, is made showing how this could lead to overestimation for small dams and serious underestimation for dams higher than 100 m.

A similar but more thorough study has been carried out by Soydemir and Kjaernsli (1975, 1979). They obtained information on forty-eight dams and distinguised between the various types, making a special distinction between dumped and compacted ~~membrane~~ rockfill dams. Unlike Lawton and Lester they have taken time into consideration and have also made use of data of horizontal deflections and displacements normal to the upstream face of membrane dams. Their analysis has produced a set of curves for each type of dam which allow the displacements in the three directions (vertical and horizontal crest movements, maximum displacements normal to the membrane) to be calculated from the height of fill. For some types of dams these curves have been produced for periods up to thirty years. Table 2.1.1 gives their values for the coefficient, α, and index, β, of the curves representing initial reservoir filling (0.5 - 3 years) and 10 years for equations of the form $s = \alpha H^{\beta}$. The ten year equation for the settlement of dumped (rockfill) membrane and sloping core dams is the same as that produced by Lawton and Lester. There is a similarity between the form of the normal displacement equations quoted here and that suggested by Steele and Cooke (1960) viz. $s \propto H^{2.1}$.

Dam Type	Dumped Membrane/sloping core				Compacted Membrane			
Time	Init. Res. Filling		10 years		Init. Res. Filling		10 years	
Displacement	α	β	α	β	α	β	α	β
Vertical	5×10^{-4}	1.5	1×10^{-3}	1.5	1×10^{-4}	1.5	3×10^{-4}	1.5
Horizontal	3.5×10^{-4}	1.5	6×10^{-4}	1.5	5×10^{-5}	1.5	1.5×10^{-4}	1.5
Normal	1×10^{-2}	2	-	-	2×10^{-3}	2	-	-

Table 2.1.1 Soydemir & Kjaernsli Prediction Formulae $s = \alpha H^{\beta}$

A comparison of the results of the two approaches reveals a discrepancy. Sowers et al. claim that settlement is proportional to height whereas a settlement-height approach indicates a variation with $H^{3/2}$. Sowers et al. also conclude that dam type is not

significant although no apparent attempt is made to separate the dams into their various types. The work of Soydemir and Kjaernsli indicates that the dam type may be of importance and especially the distinction between dumped and compacted rockfill dams.

2.1.ii Discussion of the Methods of Prediction

In view of the discrepancy between the two approaches it was decided to re-examine both approaches, reviewing the validity of the analyses, the conclusions and the error that may be expected in using the formulae produced. In order to do this an independent survey of the literature was carried out, gathering information on the construction methods, external loading, i.e. reservoir filling, rock and foundation materials as well as the observed vertical and horizontal displacements. Many of the dams considered have been used by Soydemir and Kjaernsli but a number of other dams have also been included. Tables 1 - 4 (Appendix I) give details of the sixty-eight dams studied and the references from which the information was obtained. The dams were classified according to their design and a distinction made between compacted and dumped rockfill membrane dams. A survey of this sort highlights how difficult it is to obtain good, concise information from the literature and several discrepancies were found even within papers by the same authors.

The displacements, expressed as a percentage of the height of fill, were plotted against a log time axis, fig. 2.3-2.9. The 'creep threshold' used was different from that suggested by Sowers et al. or Charles. Sowers' threshold is an arbitrary figure, whereas Charles bases his calculation on the method of load application for his large oedometer tests. In practice, however, the displacements were measured with respect to initial measurements at some ~~point in~~ time after the construction period. It seems more reasonable to consider the time of the initial measurements as the zero time rather than some convenient point in the construction period. From the dam designer's point of view, he may not know how long the construction period will be and calculations from a point within this period will not greatly help his determination of suitable freeboard for post-construction ~~movements.~~ settlements.

The use of a log (time) axis has disadvantages since log (zero time) has no real value. In order to overcome this and have a zero time-zero displacement origin a $\log_{10}(t + 1)$ (t in

months) axis has been used. It should be noted that as t increases then $\log (t + 1) \rightarrow \log t$.

A study of the settlement graphs reveals that the assumption of straight lines as suggested by Sowers et al. is not very good and that their coefficient, α, may be expected to increase with time. This can be seen at large time values, as well as being accentuated by the introduction of an origin. A comparison of the graphs for the different types of dam does show differences contrary to the conclusion of Sowers et al. but this will be discussed later in the chapter. The formula suggested by Sowers et al. also presents a problem to the designer in that he has a wide range of α values to choose from and there is no indication as to which factors influence its value.

The method of approach suggested by Lawton and Lester is more difficult to assess as no consideration is given to the length of service time of the dams. The choice of 0.02%/year as an indication of when the 'total effective settlement' is complete is an arbitrary figure and its significance depends on the height of the dam being considered. For a dam 30 m high this is a displacement of only 6 mm per year but for a 300 m high dam it amounts to 60 mm per year and this may represent a significant percentage of the freeboard. The number of dams considered in the analysis is small and no distinction is made between types of dam. Although twenty-six individual points are plotted, the majority of these are data from two dams, Kenny and Lower Bear River no. 1 (a sloping core and a dumped membrane dam). A log-log plot analysis is subject to individual interpretation of the results and a computer analysis of the points is useful. A best fit computer analysis gives the relationship $s = 0.001\ H^{3/2}$ if the settlements are assumed to be correct and the heights subject to error. However, if the heights are assumed to be correct and the settlements subject to error then a relationship $s = 0.0015\ H^{1.4}$ is obtained. The differences in settlements predicted from these two equations can become significant for higher dams and the choice of one rather than the other is a matter of opinion. Lawton and Lester have also plotted envelopes to show the margin of error of their functions, fig. 2.2. This gives values of approximately $\pm$ 30% of the settlement calculated by equation (2.2) for a given height. In real terms this is a range of 0.6 m for a 100 m high dam and greater than 3 m for a 300 m high dam. Clearly, this leaves the dam designer with a difficulty in designing an effective

freeboard and camber.

The method of analysis used by Soydemir & Kjaernsli requires examination and is essentially a contour curve fitting exercise Graphs of displacement against height have been plotted and each point designated its reported time value. By choosing suitable time values, e.g. 10, 20, 30 years it is possible to interpolate between the points plotted and obtain a series of points representing the selected time value. By joining these points together, like contours picking up points of equal magnitude, curves may be drawn for a number of discrete time values. These curves may then be used by the designer as estimates of the displacements for given heights and times. Soydemir and Kjaernsli have taken this type of analysis one step further and reproduced their contour curves together with known functions. Due to the similarity of their contour curves with these known functions, they have then used the known functions as the models of behaviour from which predictions can be made. The values of the coefficients and indices of some of these curves have already been given in Table 2.1.1.

This procedure smoothes out the data collected into a more 'manageable form'. Scatter of the data is to be expected and this 'manageable form' will necessarily contain a margin of error. However, if this smoothing out process is carried out on data with a large scatter then the margin of error will be significant and the predictions of the 'manageable form' of little value. It will be demonstrated that in analysing their data Soydemir and Kjaernsli have carried this process to unreasonable lengths and that the models they present are too simple with large margins of error.

Fig. 2.10 shows the data and curves plotted by Soydemir and Kjaernsli for vertical settlement of the crests of dumped membrane dams. The curves are not the actual discrete time contours but are the results of the smoothing out process. Fig. 2.11 shows the time contours for the same data using interpolation between the given points (extrapolation has not been used to extend the data). The contours show increasing settlement with time and height as expected. However, the choice of suitable curves to fit the contours is a matter of individual judgement and a linear relationship would be a reasonable fit for some of the contours e.g. 0.5, 5, 10 years. A comparison of the time contours and the curves of Soydemir and Kjaernsli (fig. 2.12) shows that they have

initially overestimated the settlements for higher dams. Only the two year curve shows good agreement with the time contour for all heights. Figs. 2.13, 2.14 and 2.15 show a similar comparison for the horizontal displacements of the dumped membrane dams. The time contours show large irregularities in the data and it is considered that there is insufficient data available after ten years to predict a reasonable settlement-height relationship. Fig. 2.15 illustrates clearly that the data available will in no way justify the smoothing out process used by Soydemir and Kjaernsli. Similar comparisons can be made from their data for normal displacements and other types of dams. It should be noted that these prediction curves have been further modified, as described above, by Soydemir and Kjaernsli to fit standard functions.

The above comparison is based on individual judgement and a more rigorous approach is needed. To do this a best fit computer analysis was carried out on the settlement data obtained from the independent survey. Since this data has been plotted on a displacement - time graph, displacements can be found at discrete time values by linear interpolation of the known values for each dam. Time values of one and ten years were chosen since these coincide with Soydemir and Kjaernsli's quoted function times. Table 2.1.2 gives the results of this analysis for a function of the form $s = \alpha H^{\beta}$, assuming the heights to be correct values. A comparison of the index values, β, with the 1.5 value of Soydemir and Kjaernsli indicates a value closer to 1.0 would be reasonable. There is little correlation of the coefficient values with those proposed by Soydemir and Kjaernsli. Of most importance are the correlation coefficients calculated, which range from 0.274 to 0.897 (1.0 indicating a perfect fit. i.e. a unique solution) implying that a unique solution cannot be reasonably used.

	Init. Res. Filling			10 years		
Dam type	α	β	Cor. coef	α	β	Cor. coef
Dumped membrane	1.8×10^{-3}	1.2	0.633	9×10^{-3}	0.9	0.683
Compacted "	2×10^{-2}	1.1	0.274	1.4×10^{-4}	2.6	0.437
Sloping core	7×10^{-3}	1.3	0.897	insufficient data		
Central "	2×10^{-4}	2.0	0.550	insufficient data		

Table 2.1.2 Results of Best Fit Computer Analysis

$s = \alpha H^{\beta}$ - vertical settlements.

As a final comparison the predicted and observed settlements for the individual dams were considered. The settlements predicted by Soydemir and Kjaernsli's equations were compared with the values found from the graphs at one and ten years. Table 2.1.3 shows the mean, maximum and minimum values of the function s_{calc}/s_{obs}. The mean values show an overestimation of settlements and in some cases this represents a significant error which could result in needless expenditure. Plots of s_{calc}/s_{obs} against the heights of the dams did not reveal any variation of error with height.

	Init. Res. Filling			10 years		
Dam type	Mean	Max	Min	Mean	Max	Min
Dumped Membrane	1.22	3.32	0.29	0.96	1.47	0.31
Compacted "	3.21	7.50	1.56	3.79	6.47	0.99
Sloping Core	2.68	7.59	0.89	1.71	2.52	0.90

Table 2.1.3 S_{calc}/s_{obs} - Predicted and Observed Settlements

These three analyses show clearly that the formulae and curves presented as prediction models by Soydemir and Kjaernsli are inadequate and produced by erroneous methods. The results of the computer analysis also throw doubt on the validity of using the prediction formulae of Sowers et al. and Lawton and Lester. It seems that the large number of factors which influence the displacements produce significant scatter and make the use of discrete prediction models inappropriate. While dam designers may desire such models, they must be made aware of the margins of error involved. An alternative approach to the problem is discussed in the following section.

2.1.iii Comparative Prediction Approach .

This approach recognises that a large number of factors influence the dam behaviour and that a simple prediction model is not available. It is based on the observed field performance of existing dams and takes into account the scatter of the data. It relies upon the experience and judgement of the designer and guidelines have been set out to aid his calculations.

Figs. 2.16 and 2.17 show the envelopes of the vertical and

horizontal displacements of the dam curves given in figs. 2.3 - 2.9. These envelopes contain the majority of the points plotted although a few of the more irregular points have been excluded. The envelopes provide the designer with quick method of ascertaining the range of displacements which a certain type of dam may be expected to undergo after a period of time. If, in the circumstances, these are unacceptable then a different design may be chosen.

The range of values given by the envelopes will not permit specific displacement values to be calculated. The selection of a mean, maximum or minimum value of the range is not a good approach to the problem. At this stage of design the location, local geology, proposed construction method and design will probably be known or the alternatives be under discussion. By consulting Tables 1-4 (Appendix I) dams with similar characteristics may be selected and their displacement time behaviour analysed from figs. 2.3 - 2.9. From this information and possibly extrapolation of the curves, a number of displacement values may be obtained. The designer may then decide how appropriate the various characteristics are to his own problem and calculate a reasonable displacement value. It is recommended that the references quoted are read in full as these will provide more background information and highlight problems encountered. Alternatively, the observed results from similar dams near the proposed site may be used.

2.2 Observed Displacements

This section contains guidelines for the designer in using figs. 2.3 - 2.9 to predict dam displacements and the behaviour of specific dams has been discussed. (The references for these dams are quoted in Tables 1-4 (Appendix I)). Other displacements not considered in the survey, viz. normal and lateral movements have been reviewed from the literature. Finally the factors which may influence the displacements e.g. construction methods are discussed.

2.2.i Vertical Settlement

The envelopes of settlements (fig. 2.16) show the differences

to be expected for the various types of dams. While the upper bounderies follow a sequence (increasing displacement for a given time) of compacted membrane (c.m.), sloping core (s.c.), central core (c.c.) and dumped membrane (d.m.) dams, this is not established for the lower boundaries until after nine years service. The most noticeable feature of these envelopes is the significant reduction in settlements of membrane dams when compacted. Although s.c. and c.c. dams of both compacted and dumped fills have been plotted there is not such a significant change in behaviour. A study of fig. 2.5 shows that the s.c. dams 9 and 11 which have compacted fill, lie along the lower boundary of the curves but Trängslet Dam (no. 10), which also has a compacted fill, lies in the middle of the envelope.

Three of the d.m. dams in fig. 2.3 show irregular behaviour viz. Swift, Shirokovsk and Wishon (nos. 3, 13, 14). Swift and Shirokovsk show small initial displacements followed by high settlements whereas Wishon has the opposite behaviour. Both Swift and Shirokovsk are built on alluvial deposits which may have caused the large settlements. Strawberry Dam (no. 4) is very similar to these but has a better construction method probably resulting in a better curve. It is probable that Swift and Shirokovsk were constructed from dry rockfill and the sharp increase in settlements may be a result of reservoir filling. The initial settlement of Wishon Dam is related to the first filling of the reservoir which took place in just thirteen days. After this the reservoir level was kept constant for six and a half months and then drawndown over the next nine months. This has resulted in the levelling off of the settlement curve. It is interesting to note that Dix River Dam (no. 5), which was singled out by Sowers et al. (1965) as having high settlements, shows similar behaviour to many other dams of its type.

Venemo (no. 4) and Nissastrom (no. 2) Dams (fig. 2.4) exhibit a rising effect initially before settling ~~as expected~~. Little information on Nissastrom is available but several factors may have influenced the behaviour of Venemo. This dam is situated in a relatively narrow valley which may have induced an arching action and together with freezing of the wet fill caused uplift. The upward movement is only noted prior to first filling when rapid settlement occured. The large settlements associated with the reservoir impounding are probably due to the construction

methods employed. The fill was initially dumped until field compaction tests were completed and then compacted fill used. While good sluicing was carried out during summer construction freezing conditions prevented this during winter and consequently winter fill was only sluiced the following spring.

The settlement-time graphs of s.c. dams (fig. 2.5) shows three dams which all exhibit the same behaviour. Two of these, Bersimis no. 1 and Deroches (nos. 5 and 6), are of similar construction and built next to each other for the same reservoir. Holjes (no. 2), however, is not particularly similar to the other two and there does not appear to be any reason for the small settlements recorded (as compared with the other dams) in all three cases.

In analysing the data from c.c. dams it must be remembered that the core plays a significant role in the behaviour. Cores may be relatively thin or very wide when compared with the dam cross-section. All the dams considered have earth cores, usually of clay, except Dhünn Valley Dam (no. 5) which has a vertical bituminous concrete core. The central position means that any crest settlements measured are those of the core rather than the rockfill shoulders. It is interesting to note that these earth core settlements are similar to those of rockfill for other types of dams. Central core dams suffer from core - filter - rockfill interactions due to the differences in stiffness of the zones and this complicates the behaviour as arching may occur. The reservoir filling introduces a further complication in that only one shoulder is saturated usually inducing additional settlements on that side. Despite these difficulties the settlement-time curves (fig. 2.6) show good correlation with each other and there are no particular irregularities of behaviour.

2.2.ii Horizontal Deflections

The graph of the envelopes of the various types of dams (fig. 2.17) shows again that compacted membrane dams have the smallest movements and dumped membrane dams the greatest. It is difficult to draw an envelope for c.c. dams and this is discussed more fully below. A comparison of the settlement and deflection envelopes shows that in general the horizontal movements are less than the vertical ones. The ratio of these two

values is different for different dams and times and a general relationship cannot be established.

The deflection - time curves of both compacted and dumped membrane dams have been plotted on one graph (fig. 2.7) due to the small amount of data available. All the displacements are in a downstream direction as would be expected because of the weight of the water on the upstream face. Both Wishon and Swift Dams show similar behaviour to their settlement-time curves. Malpaso Dam (no. 7) has horizontal displacements twice its settlements.

In fig. 2.8 the deflections of s.c. dams are plotted and, as expected, these are in a downstream direction. As before Holjes, Bersimis no. 1 and Deroches have the smallest movements. No conclusions can be drawn on the influence of compaction on the deflections of s.c. dams since data on only one dam, Furnas, was available. Both Kenny and Miboro Dams (nos. 1 and 4) have undergone quite large upstream movements after a period of time. The movement at Miboro can be related to the reservoir being lowered but this is not the case for Kenny. At Kenny the reservoir was impounded over a period of four years and has remained full since then. The increasing water level appears to have reduced the rate of downstream deflection but the full reservoir has induced a large downstream movement followed by an upstream and then downstream deflection. The reason for this is not clear but may be due to rotation of the foundation under the water load. The settlement curve does not show any particular irregular behaviour over the same period.

The c.c. dam deflections shown in fig. 2.9 are both upstream and downstream directions. As has already been discussed c.c. dams have a complicated behaviour and it is difficult to predict their movements. As the shoulders usually move in opposite directions placing of the measuring instrument or monument is very important. Cherry Valley Dam (no. 22) showed downstream movements on filling and upstream movements on drawdown. El Infiernillo (no. 12) showed upstream movements on impounding and then downstream deflection under a constant reservoir level condition. Although the movements at Tresna Dam (no. 24) are quite small, the downstream/upstream deflections are thought to be due to a culvert running under the centre of the dam. Other points along the crest at some distance from the maximum section show only downstream movements. Displacements at points upstream and

downstream on the crests were monitored at Gepatsch Dam in Austria (no. 2) and these are shown separately on the diagram. The initial upstream movement of both points was during drawdown of the half full reservoir. On refilling, the upstream shoulder moved upstream and the downstream shoulder in the opposite direction, which caused longitudinal cracking along the crest. Subsequent drawdowns and refillings have produced upstream and downstream deflections respectively with a continuing increase of the distance between the two crest movements.

2.2.iii Normal displacements to the upstream face

These displacements are of particular importance in the performance of membrane dams since differential displacements may cause cracking of the membrane and leakage. The local movements of the face are approximately normal to the face although in most cases the vertical settlement component is slightly greater than the horizontal component. During first filling the displacements are relatively large and usually have a maximum value at the maximum section and at a point 40% of the height from the base. This is due to the weight of water on the face and the dam effectively having a pin or rigid joint at the abutments. The dumped fill dams Salt Springs (fig. 2.18) Lower Bear River no. 1, Ishibuchi and Nozori and the compacted fill Venemo Dam all have maximum movements at approximately 40% of the height. Wishon and Paradela Dams have their maximum values at 56% and 85% of the height respectively. At Wishon no points below this were monitored, while at Paradela filling the reservoir during construction created difficulties in interpretation of the results. The lower regions of rockfill had already been loaded before measurement started and. therefore the measurements in these regions could be expected to be small.

Once impounding has been completed refilling and natural ageing movements appear to be a maximum at the crest e.g. Salt Springs (fig. 2.18) and Nozori Dams. This is to be expected since repeated loadings i.e. water weight produce only small displacements and if these are less than those of the natural movements of the dam mass under its own weight then the net effect will be maximum movements at the crest. Cethana Dam (fig. 2.19) is an exception to this as its maximum displacement point moves

from 55% to 40% of its height after first filling. There is a pronounced kink in the deflection curve and although Fitzpatrick et al. (1973) can find no reason for this, this may be the cause of downward movement of the point of maximum displacement.

2.2.iv Cross-valley Movements

Observations of the cross-valley or lateral movements have been made only at a few dams. Movements are, as expected, away from the abutments and towards the centre but in some dams the bulk of the dam tends to move towards one abutment. At Salt Springs (fig. 2.20), Lower Bear River no. 1 and Kenny Dams this has been attributed to the dumping from one abutment only in the direction of the movement. A similar conclusion may be reached at Paradela Dam but the shape of the abutments and the weathered rock at the abutment being approached may have contributed to the movement.

These cross-valley movements are usually small and remedial action is not required. However, since the abutment zones of the dam are in tansion, transverse cracking may occur resulting in leakage if adequate freeboard is not provided. Pipes, etc. running along the crest may also suffer damage (fig. 2.21) if precautions are not taken.

2.3 Factors Influencing the Displacements

2.3.i Local Topography and Geology

The topography of a site may effect the displacement if the valley is narrow with steep abutments. This can produce an arching effect in the dam which reduces the settlements, particularly a valley with abutments of different slopes may cause cross-valley movements towards the flatter abutment.

The foundation movements are not always monitored separately and therefore influence the observed dam displacements. If alluvials and weathered rock are removed before construction then it may be assumed that post-construction displacements of the foundation are minimal. If these are not removed then zones of the dam above these may undergo larger settlements and therefore calculations must be made to determine the value of these.

Strength values for foundation rock and rockfills are rarely

quoted in the literature making it difficult to assess the influence of this parameter. While it may be expected that sound rockfill is less compressible than weathered rockfill this does not necessarily effect the post-construction movement directly. The strength of the rockfill will determine its displacement during construction (either by dumping or compaction) due to crushing at the contacts or breakage. This then will effect the relative density of the fill and it is this parameter which will influence the post-construction displacements. The relative density is also determined by the amount of energy input and, therefore, a comparison between displacements of dams due to the influence of their rockfill strengths cannot reasonably be made unless the construction methods are similar.

2.3.ii Construction Methods

(a) Dumping or compaction?

As has already been noted compaction has a significant effect in reducing displacement of membrane dams but not as great (if at all) for sloping core dams. It is, therefore, better to compact the fill in membrane dams unless circumstances dictate otherwise. On the basis of the survey of dams carried out in this research there appears to be room for discussion as to whether sloping core dams should be compacted or not.

If dumping is to be used then the direction of dumping and the heights of the lifts can effect the movements. By dumping from both abutments and producing a more uniform fill, it is likely that cross-valley movements can be reduced. Dumping from the abutment with the flatter slope may also counteract cross-valley movements due to the topography of the site.

A study of the settlement-time curves for the dumped fill dams in the survey does not produce a general conclusion as to whether high (>10m) or low lifts (<10m) are better. For membrane dams the high lifts tend to produce lower settlements whereas central core dams show lower settlements with low lifts. For sloping core dams there is no pattern and both types of construction produce high and low settlements. It is interesting to note that in the survey the majority of membrane dams had high lift construction, approximately equal numbers of the sloping core dams had high and low lifts and most of the central core dams had low lifts.

Terzaghi (1960) argues that single-stage construction i.e. one lift produces a gradually, changing fill due to segregation, with coarse material at the base and fine at the crest. In a multi-stage construction coarse particles will rest on finer ones and larger displacements can occur. Nottely, Watauga and South Holston are three dams built in the U.S.A. in one, two and three sessions respectively using dumping. Fig. 2.6 shows that, under similar reservoir level conditions, Nottely has the smallest displacements and South Holston the largest in ~~accordance with~~ support of the above argument ~~Terzaghi's theory~~. Reinus (1964) observed from field tests that dumping on top of the existing fill and then pushing with a bulldozer produced lower porosities than dumping directly onto a slope. Fills of 2 - 4 m lifts produced lower porosities than 1 m lifts with or without sluicing.

If a fill is to be compacted then test fills may be used to determine the best method with the plant available.

(b) Sluicing

Past experiences with dams have shown how useful sluicing can be in construction. At Cogswell Dam in California (Baumann, 1960) the fill was dumped without sluicing due to the scarcity of water. A storm yielding fifteen inches of rain at the site when the dam was 80% complete, produced settlements of about 4% of the height causing severe damage to the upstream placed rock face. Subsequent sluicing increased the settlement to 6% within a few months. Sluicing reduces the compressive strength of the rock particles and allows greater crushing which decreases the porosity and compressibility (Terzaghi, 1960).

The volume of water required is a matter of debate and ratios from 0.15:1 (water to rock) to 4:1 were used on the dams in the survey. Terzaghi, (1960) recommends a ratio of 0.2:1 on the basis of calculations from Cogswell Dam. Kawase, (1960) comments that a ratio of 2:1 was not sufficient in the construction of Ishibuchi Dam. Some construction procedures have relied upon heavy rainfall at the site.

Comparison of the curves of the individual dams does not produce any conclusions as to which ratio is best. If the best ratio is substantially less than the 1:1 - 1:4 ratios normally used then it will not be possible to distinguish any noticeable effect between these values. Cethana Dam with the lowest ratio of 0.15:1 has higher settlements and deflections than most dams of

a similar type but the compaction method used may influence this behaviour as well.

This difference of opinion is not very important where abundant water supplies are available but in more arid areas sluicing may be costly and for any particular dam, field tests are needed to resolve this matter.

Restrictions on sluicing during winter placing can be detrimental to dam performance and liberal sluicing during the spring should be carried out. Settlements of up to 20% of the height of placed fill can occur during this sluicing (Soydemir and Kjaernsli, 1975).

2.3.iii External Loading

(a) Reservoir Impounding

As has already been noted the reservoir level can effect the performance of the dam and the initial filling is the most critical. Large movements are produced on first filling in a downstream direction for membrane and sloping core dams but in either direction for central core dams. Subsequent fillings are not as important and movements are much smaller. Membrane and sloping core dams appear to deform under their own weight rather than due to the reservoir load after first filling. Central core dams exhibit a more elastic behaviour and respond to the fluctuations in the reservoir level, e.g. Gepatsch Dam. Flooding at El Infiernillo dam which raised the reservoir level by 5 m three years after it had been impounded, produced large additional movements in both vertical and horizontal directions.

(b) Earthquakes

This subject is very prominent in discussions at the moment and method of analysis and defensive measures are being put forward to avoid failure or damage to dams under earthquake conditions. Little observed behaviour data has been collected or published and it is difficult to approach the problem in this way. It should be noted that on the whole dams do resist earthquake shocks very well and only a few total failures have occurred.

2.4 Conclusion

The study of existing dams and their behaviour can provide a source of useful information for the dam designer. Problems encountered during construction are usually discussed in the literature and may be avoided or dealt with. A study of this sort should be used in conjunction with field and laboratory tests since some of the problems cannot be solved from the information available and may be peculiar to the dam being designed. The influence of various factors on behaviour can be evaluated and used to ensure better performance. Of these factors, sluicing, compaction of the fill and the initial reservoir filling are the most important. The dam cross-section appears to have a small effect on the magnitude of the displacements and certain topographical and geological conditions are also important. Using these and other observations, the dam designer can predict vertical and horizontal displacements by considering existing dams with similar characteristics to that he is concerned with.

As this study of observed displacements shows, the behaviour of rockfill can be complex and existing prediction methods, based on this information, are too simple. A better understanding of the basic mechanisms occurring within the rockfill is needed, in order to understand why rockfill behaves in the manner observed and to improve the methods of behaviour prediction.

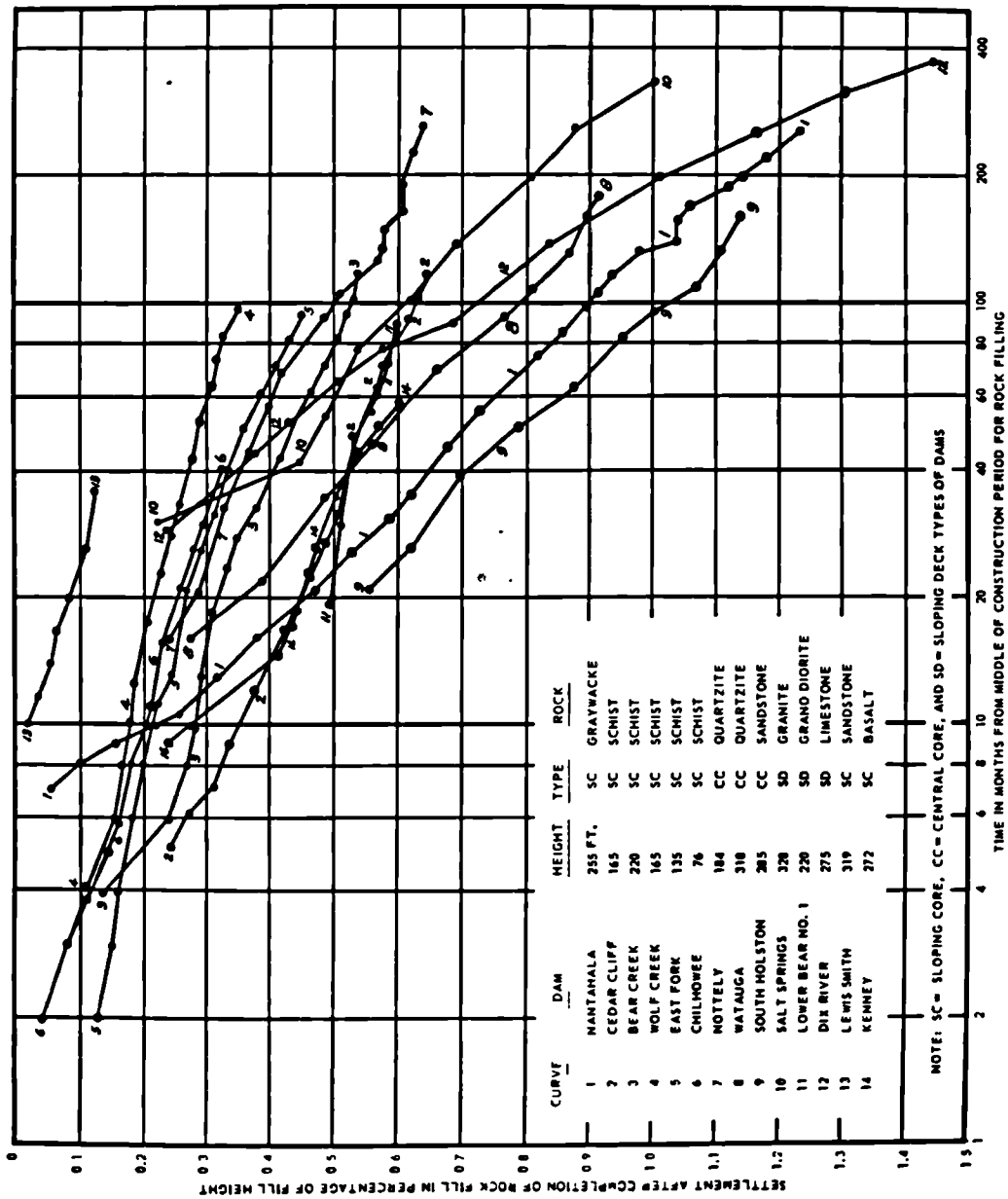

Fig.2.1 :- Observed Post-construction Settlements of Rockfill Dams
(after Sowers et al., 1965)

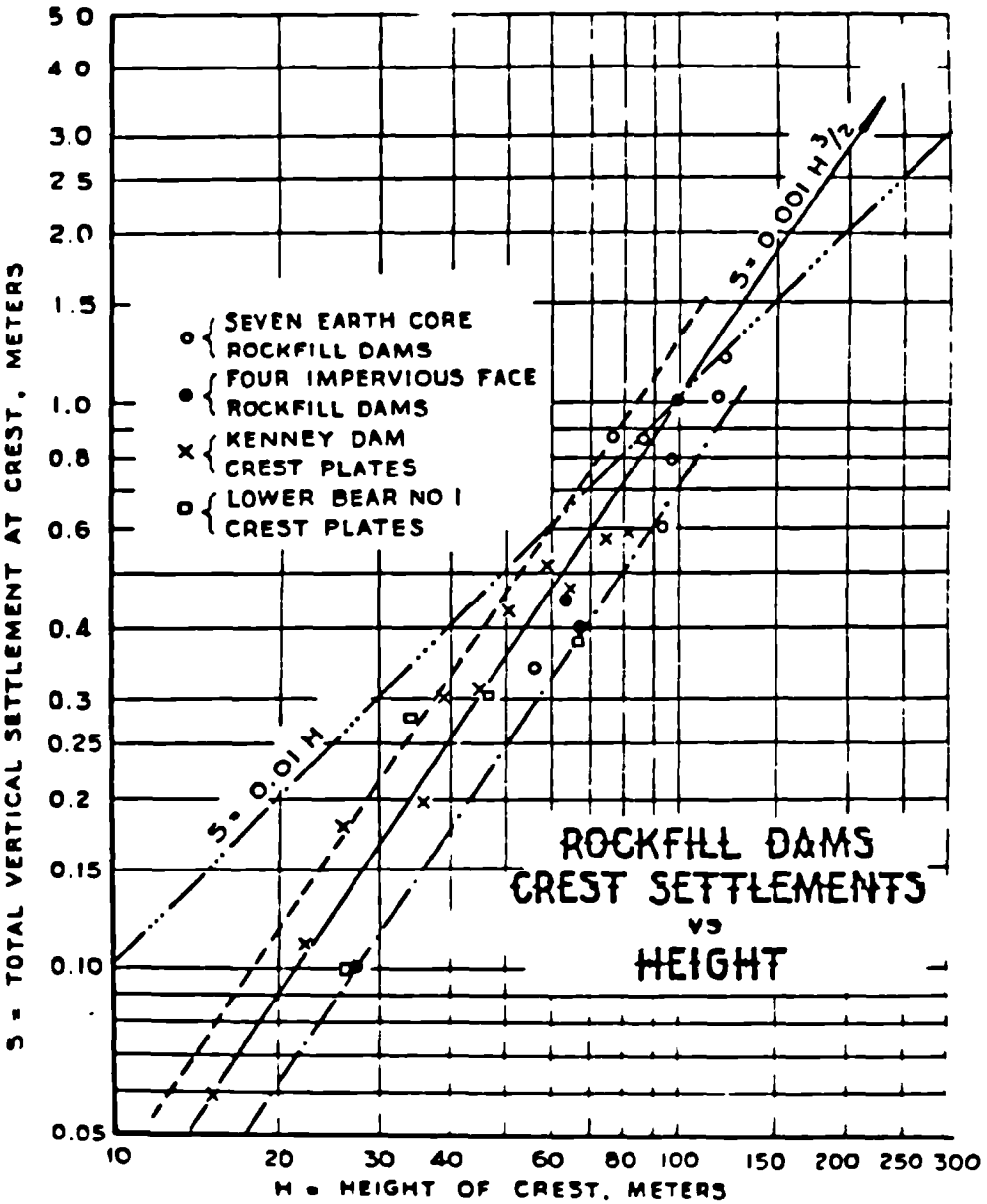

Fig. 2.2 :- Relation between Settlement and Height of 11 Rockfill Dams

(after Lawton and Lester, 1964)

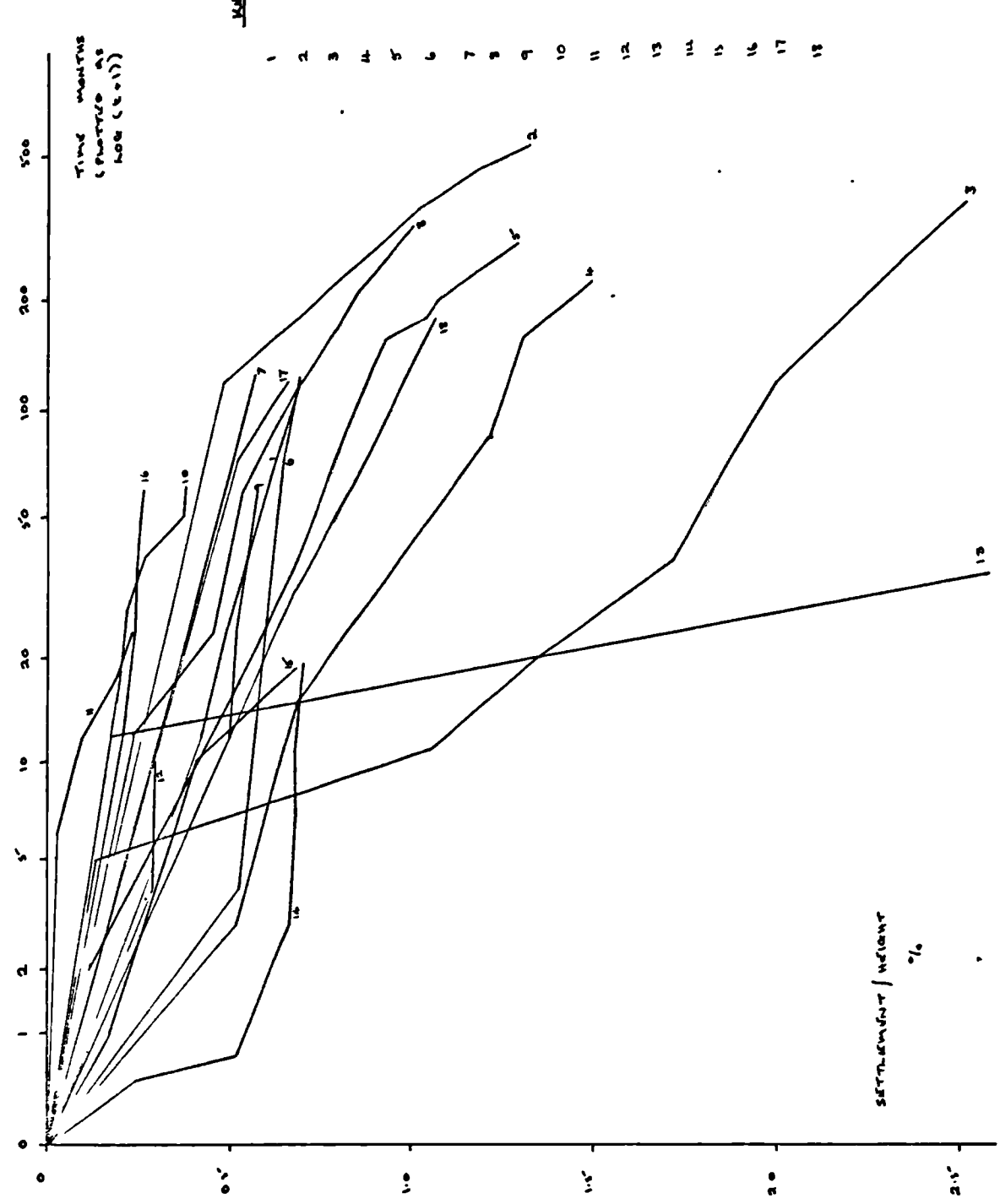

FIG. 2.3 :- OBSERVED POST-CONSTRUCTION SETTLEMENTS OF MARMOREAND DAMS (DUMPED)

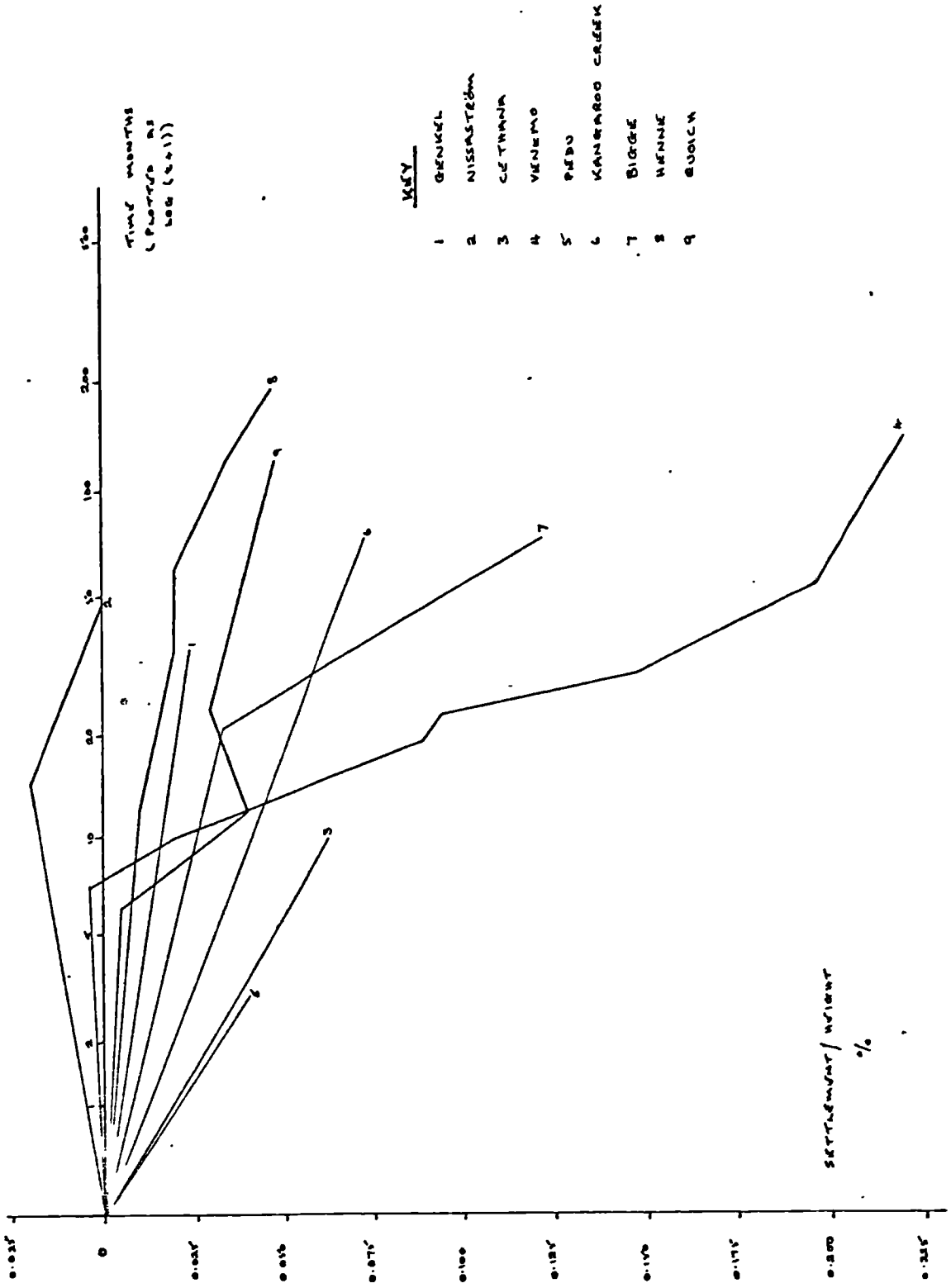

FIG. 2.42:- OBSERVED POST-CONSTRUCTION SETTLEMENTS OF MUNGERNIE DAMS (COMPACTED)

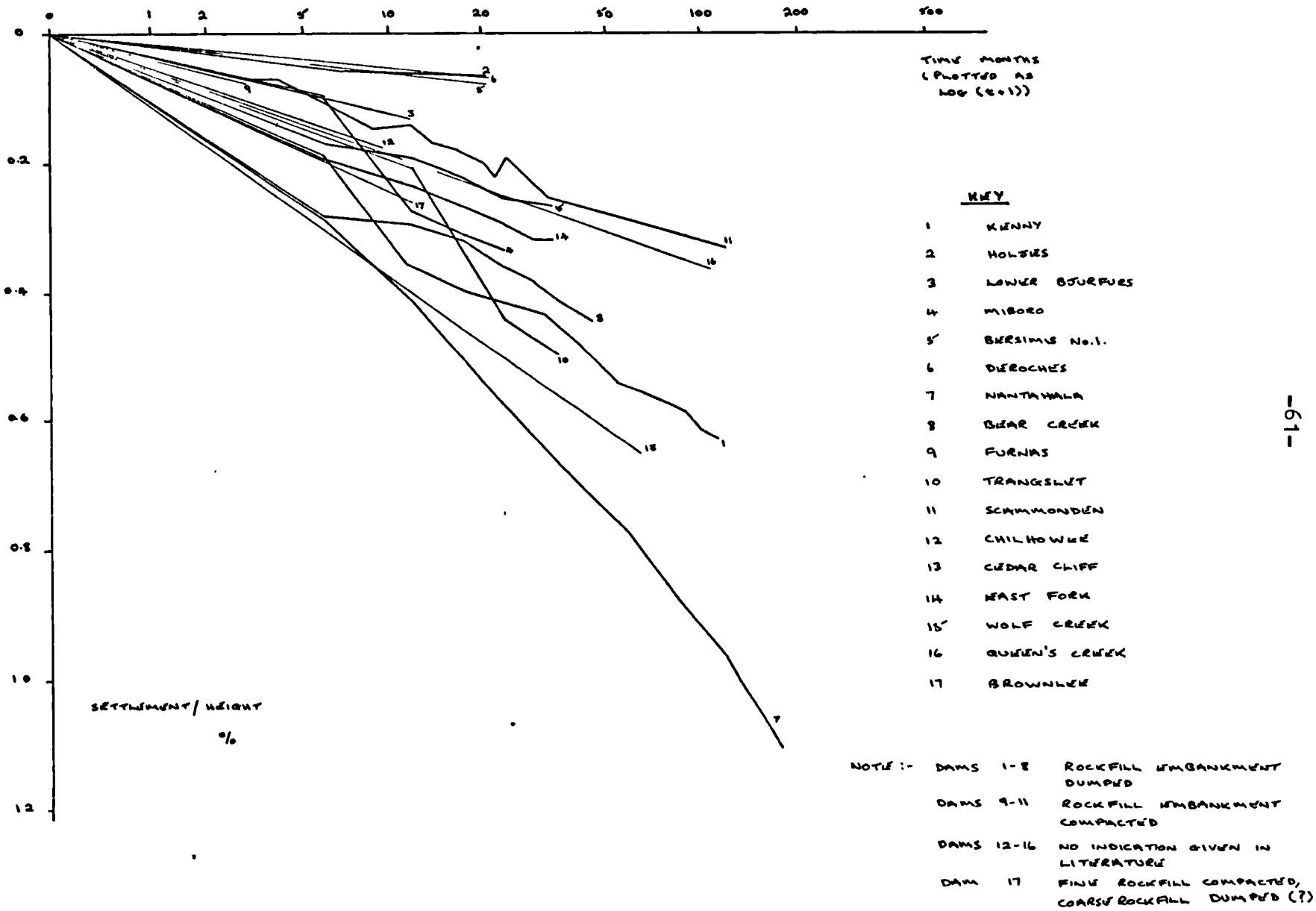

NOTE :-

DAMS	1-8	ROCKFILL EMBANKMENT DUMPED
DAMS	9-11	ROCKFILL EMBANKMENT COMPACTED
DAMS	12-16	NO INDICATION GIVEN IN LITERATURE
DAM	17	FINE ROCKFILL COMPACTED, COARSE ROCKFILL DUMPED (?)

FIG. 2.5:- OBSERVED POST-CONSTRUCTION SETTLEMENTS OF SLOPING CORE DAMS

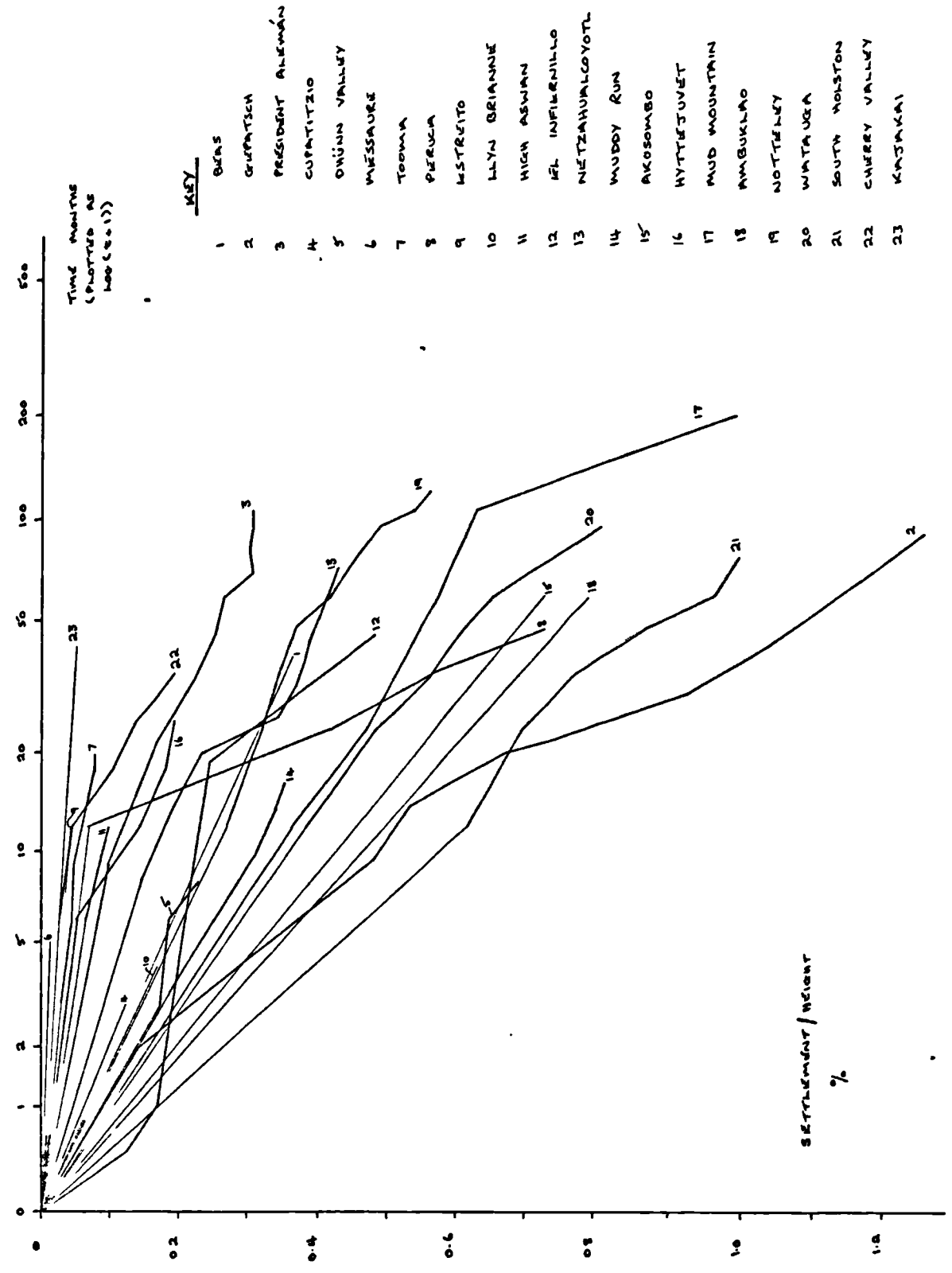

FIG. 2.6 :- OBSERVED POST-CONSTRUCTION SETTLEMENTS OF CENTRAL CORE DAMS

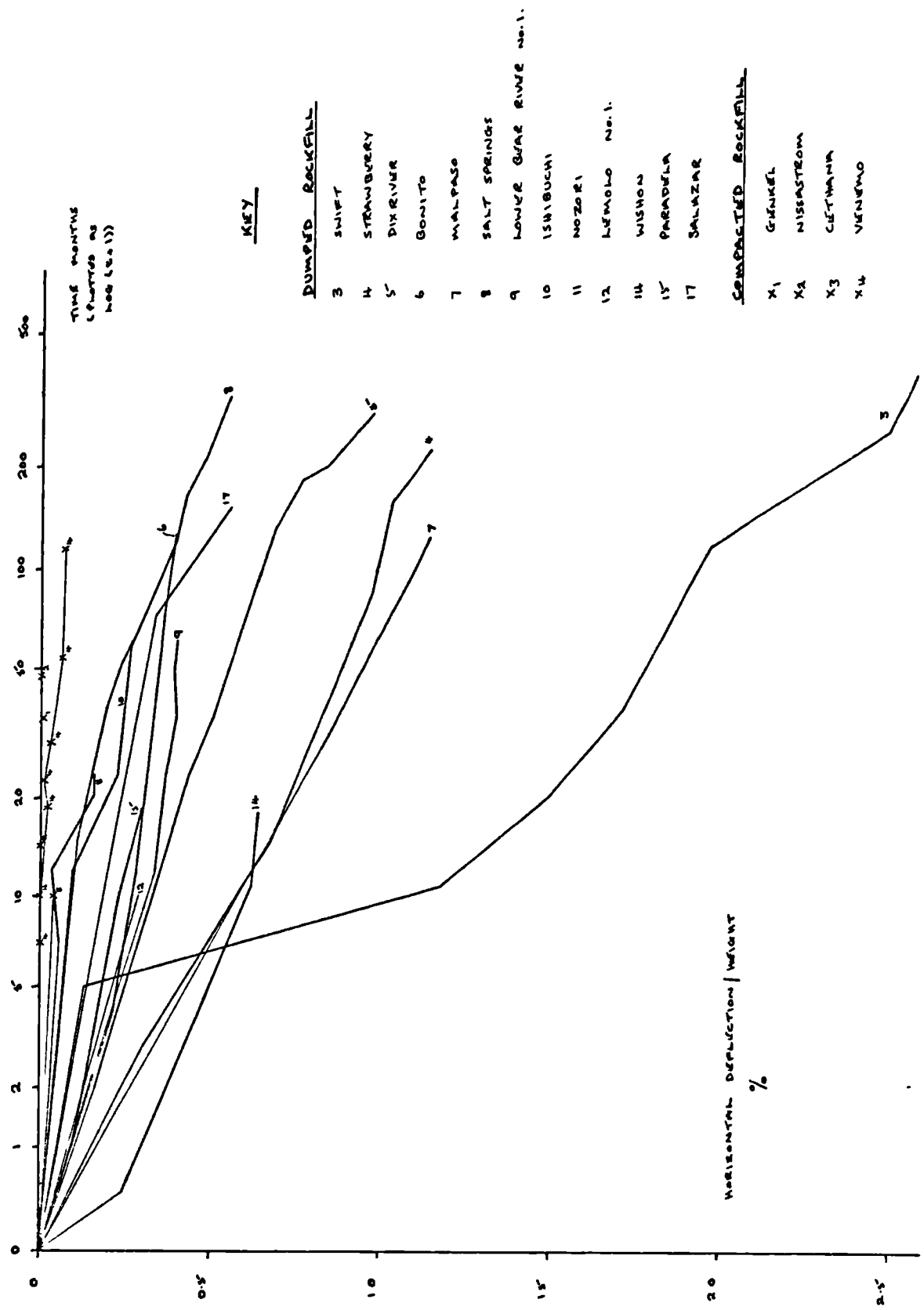

FIG. 2.7 :- OBSERVED POST-CONSTRUCTION HORIZONTAL DEFLECTIONS OF MEMBRANE DAMS

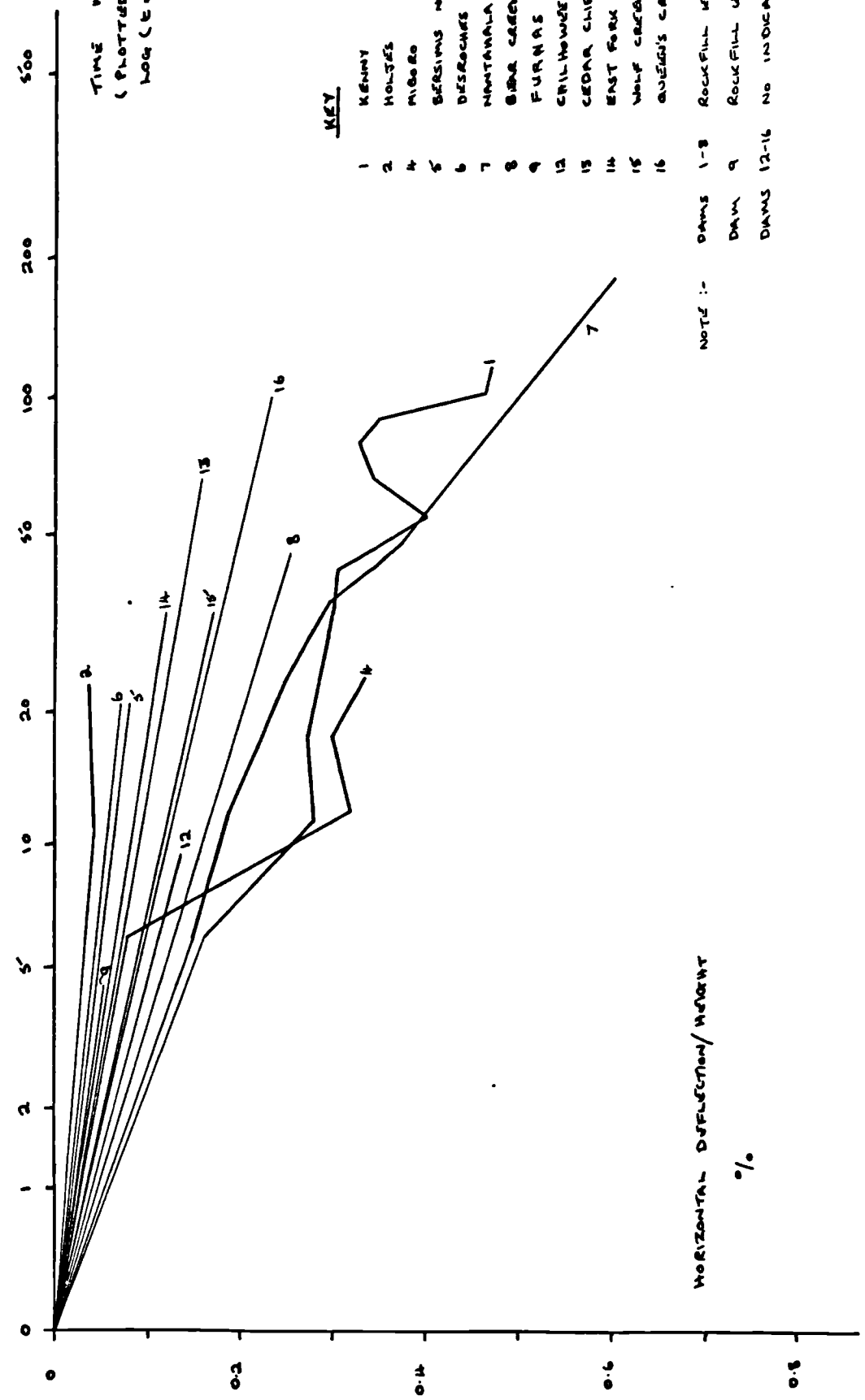

FIG. 2.3 :- OBSERVED POST-CONSTRUCTION HORIZONTAL DEFLECTIONS OF SLOPING CORE DAMS

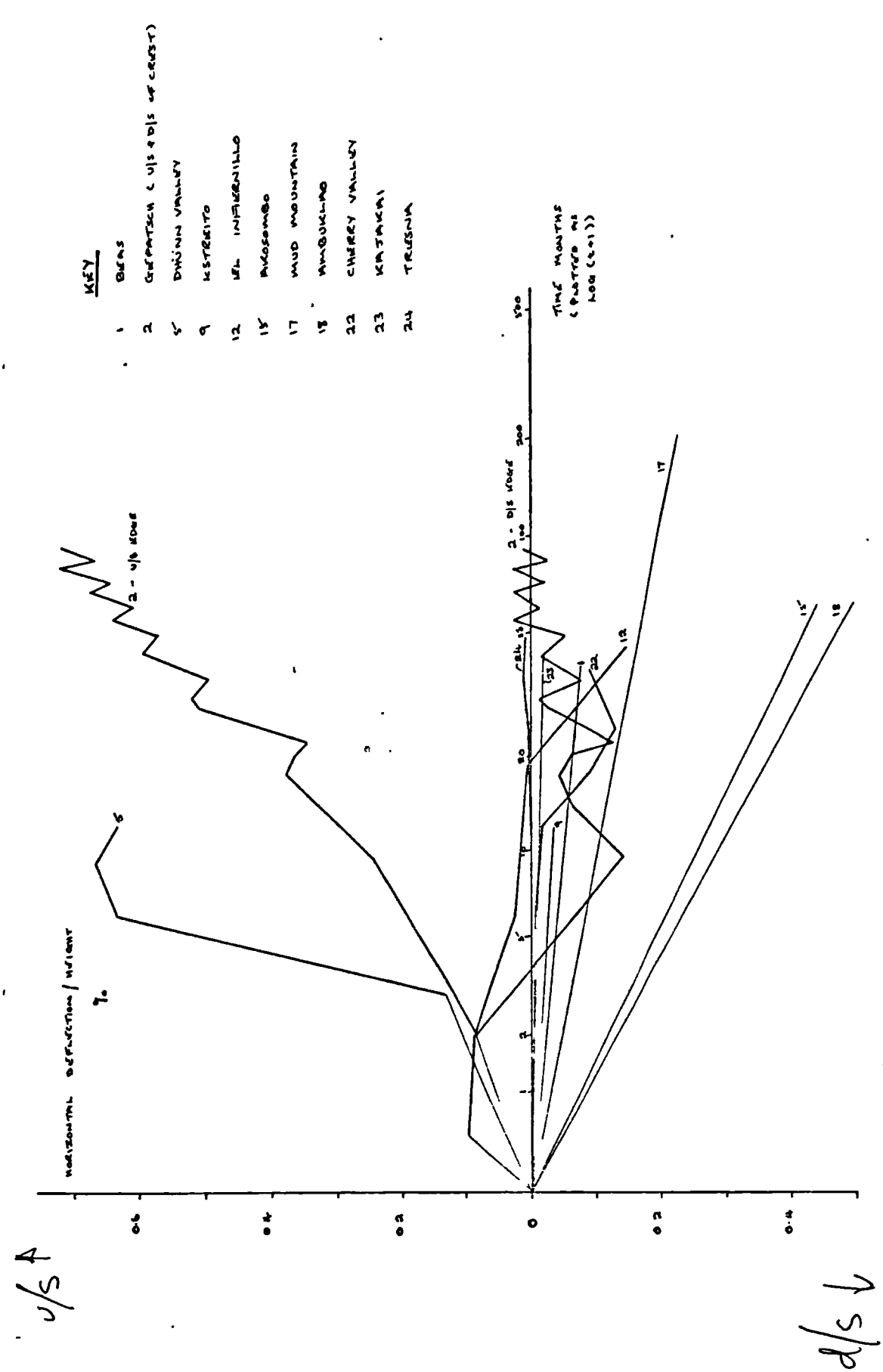

FIG. 2.9 :- OBSERVED POST-CONSTRUCTION HORIZONTAL DEFLECTIONS OF CENTRAL CORE DAMS

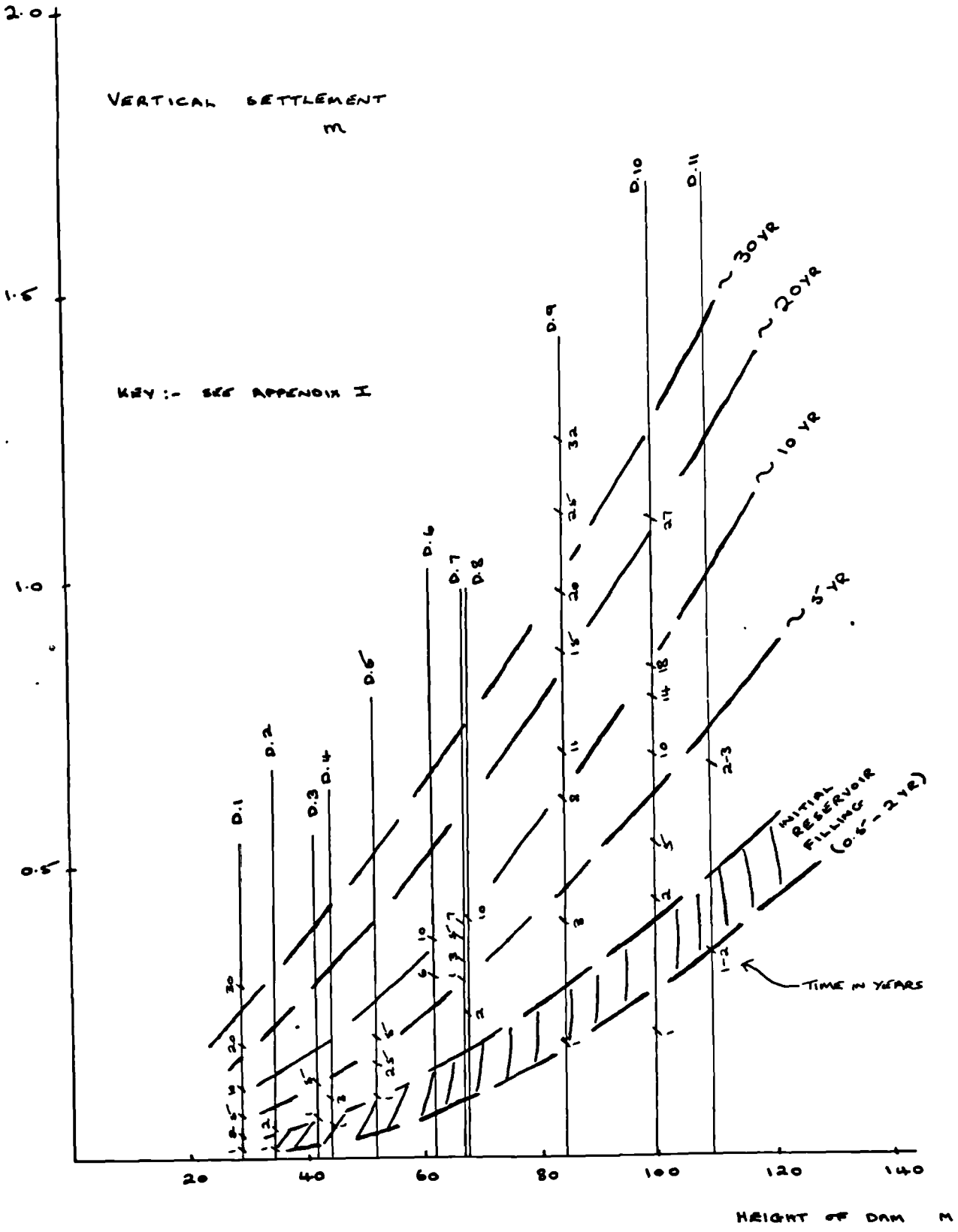

FIG. 2.10 :- SETTLEMENT - HEIGHT GRAPH - DUMPED MEMBRANE DAMS

AFTER SOYDEMIR & KJAERNSLI (1975)

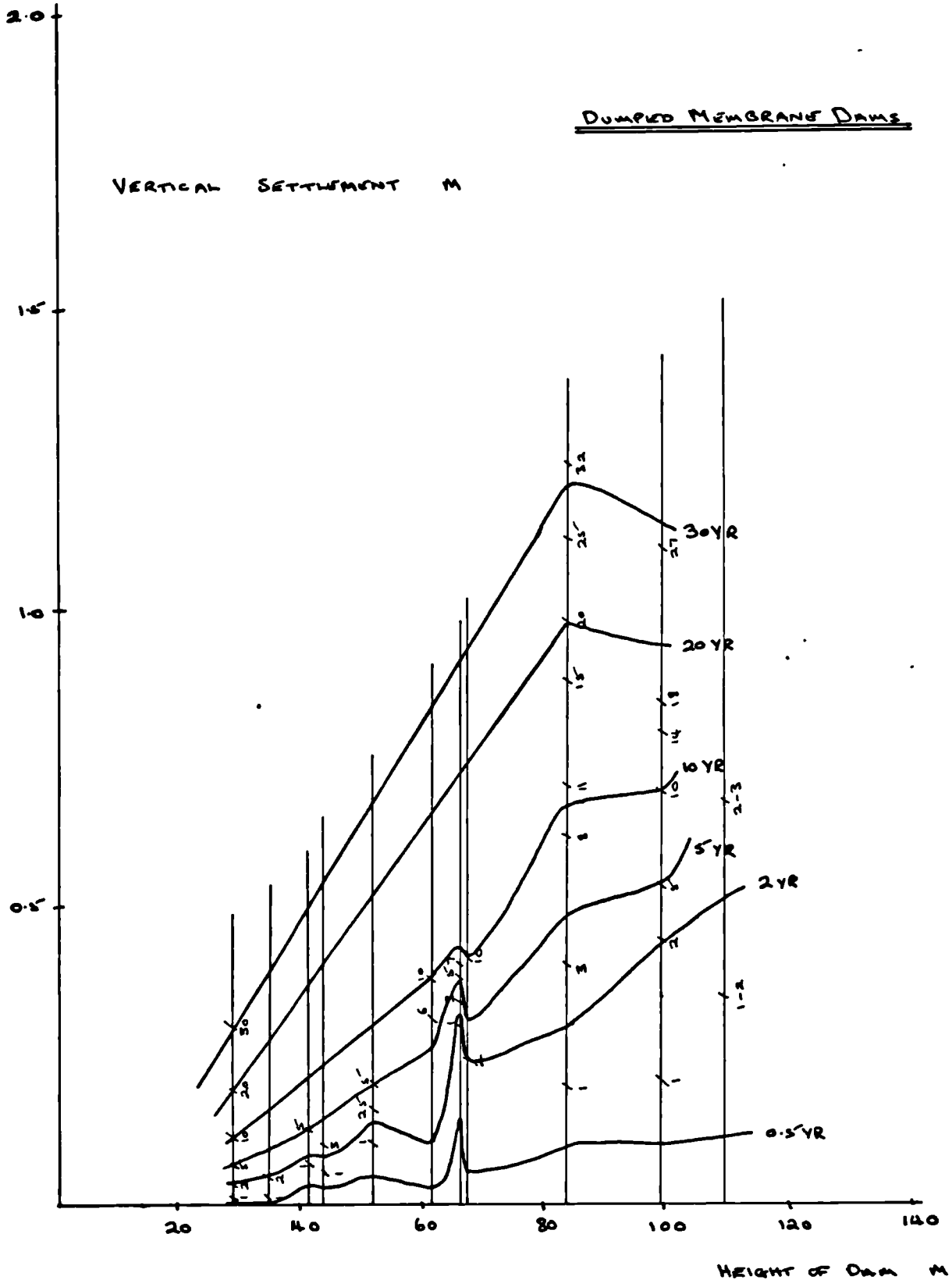

FIG. 2.11:- SETTLEMENT - HEIGHT GRAPH - CONTOURS OF TIME REDRAWN USING DATA FROM SOYDEMIR AND KJAERNSLI

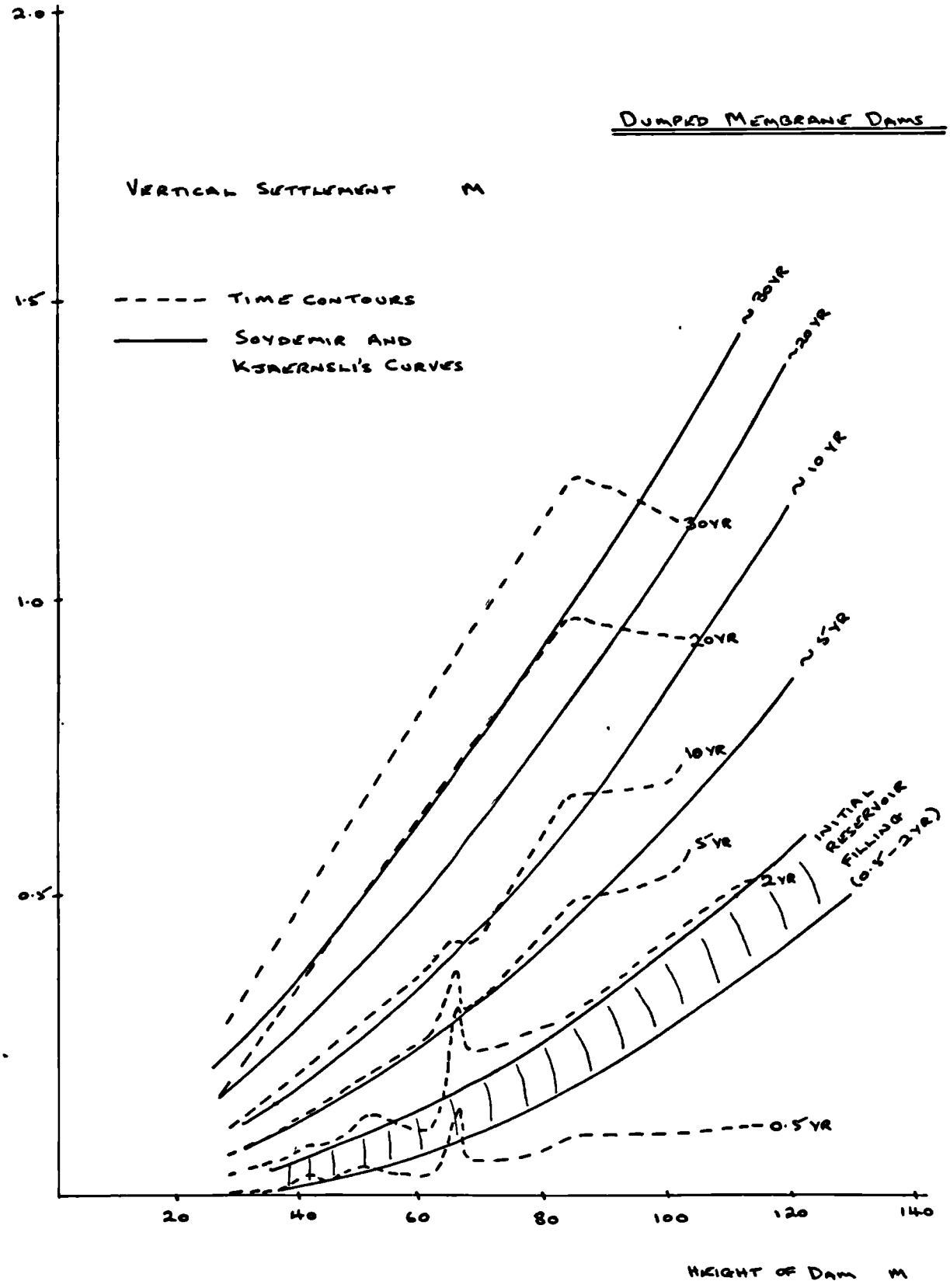

FIG. 2.12 :- COMPARISON OF TIME CONTOURS AND SOYDEMIR AND KJAERNSLI'S CURVES

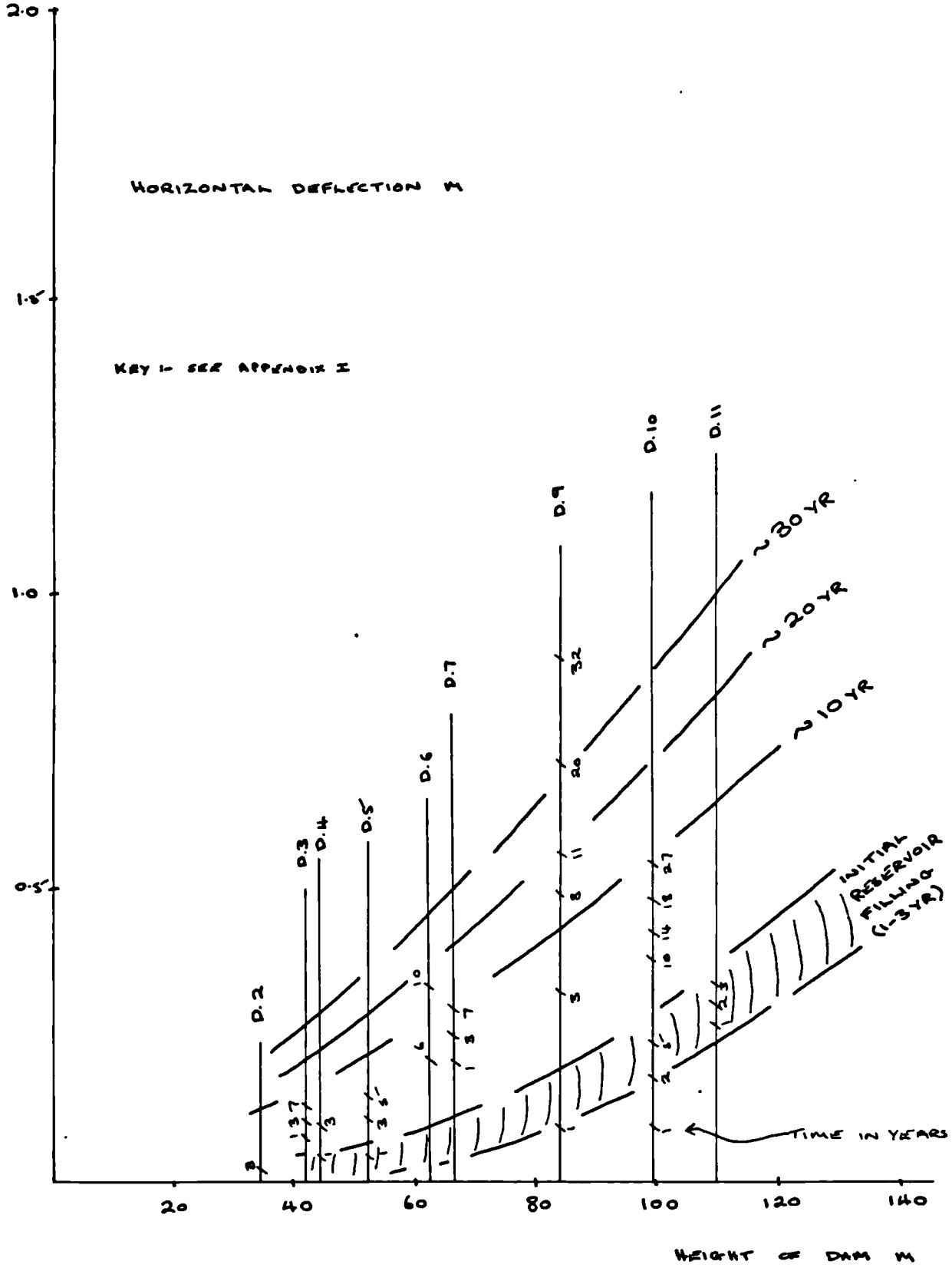

FIG. 2.13 :- DEFLECTION v HEIGHT GRAPH - DUMPED MEMBRANE DAMS

AFTER SOYDEMIR & KJAERNSLI (1979)

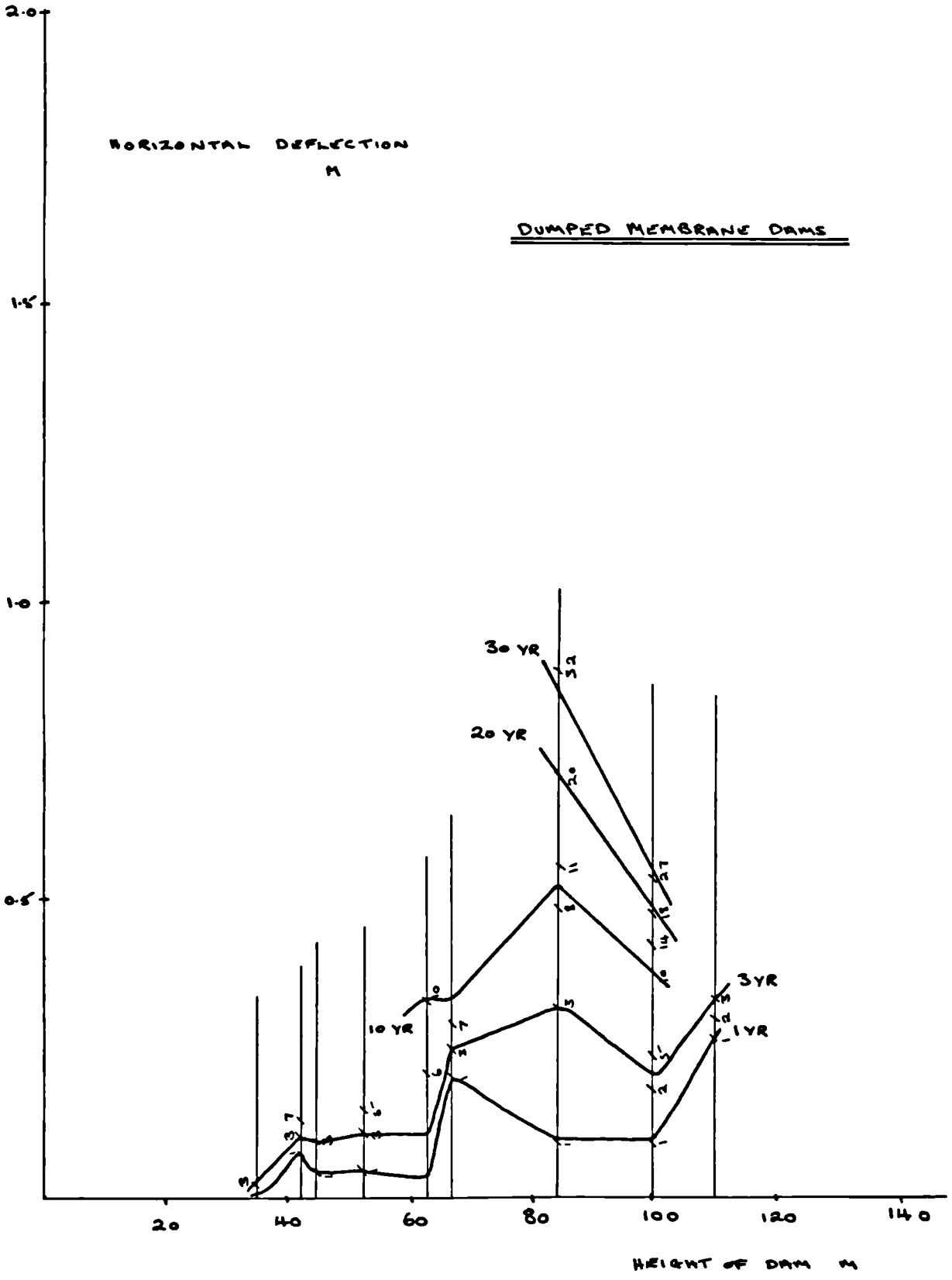

FIG. 2.14 :- DEFLECTION v HEIGHT GRAPH - CONTOURS OF TIME REDRAWN USING DATA FROM SOYDEMIR & KJAERNSLI

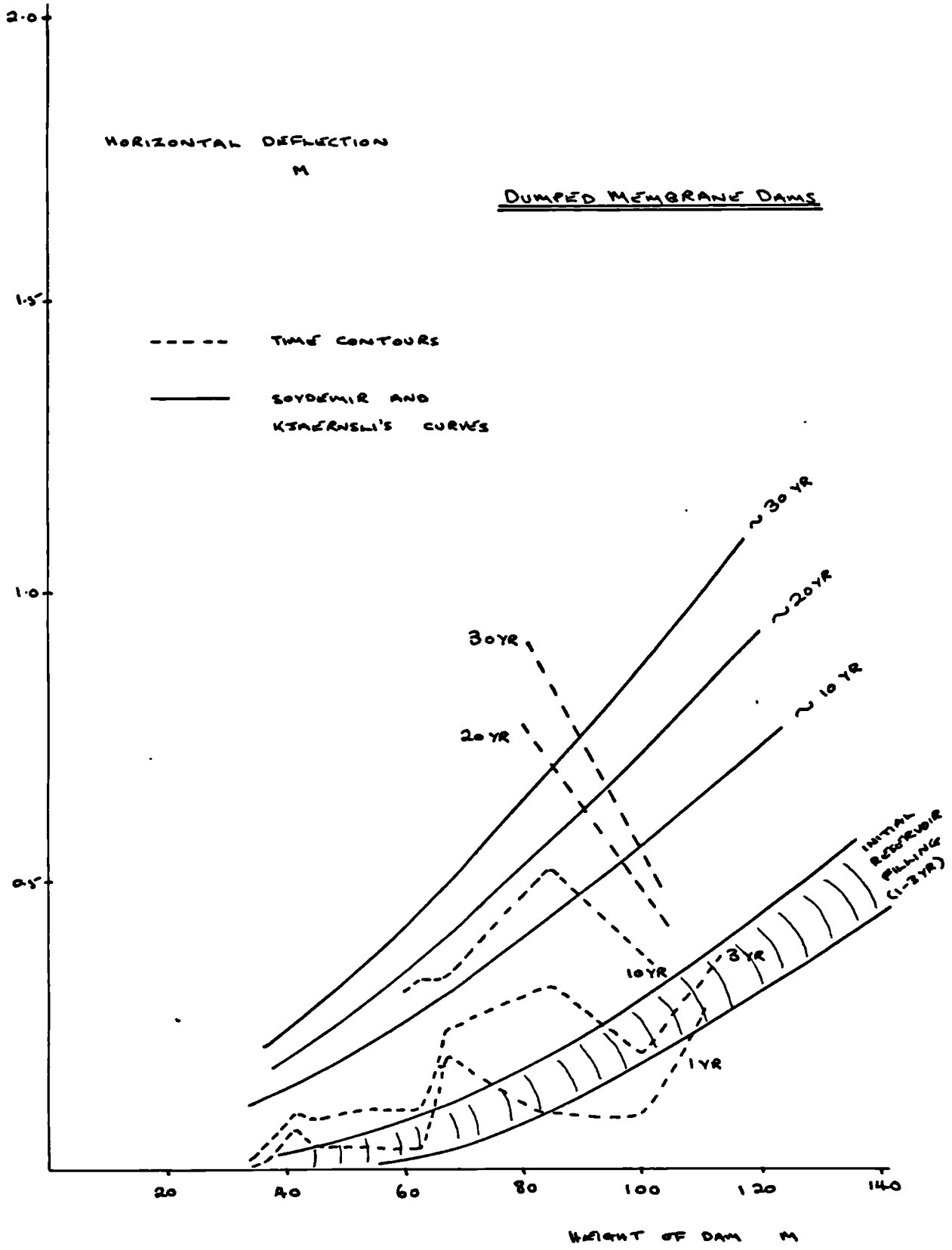

FIG. 2.15 :- COMPARISON OF TIME CONTOURS AND SOYDEMIR AND KJAERNSLI'S CURVES

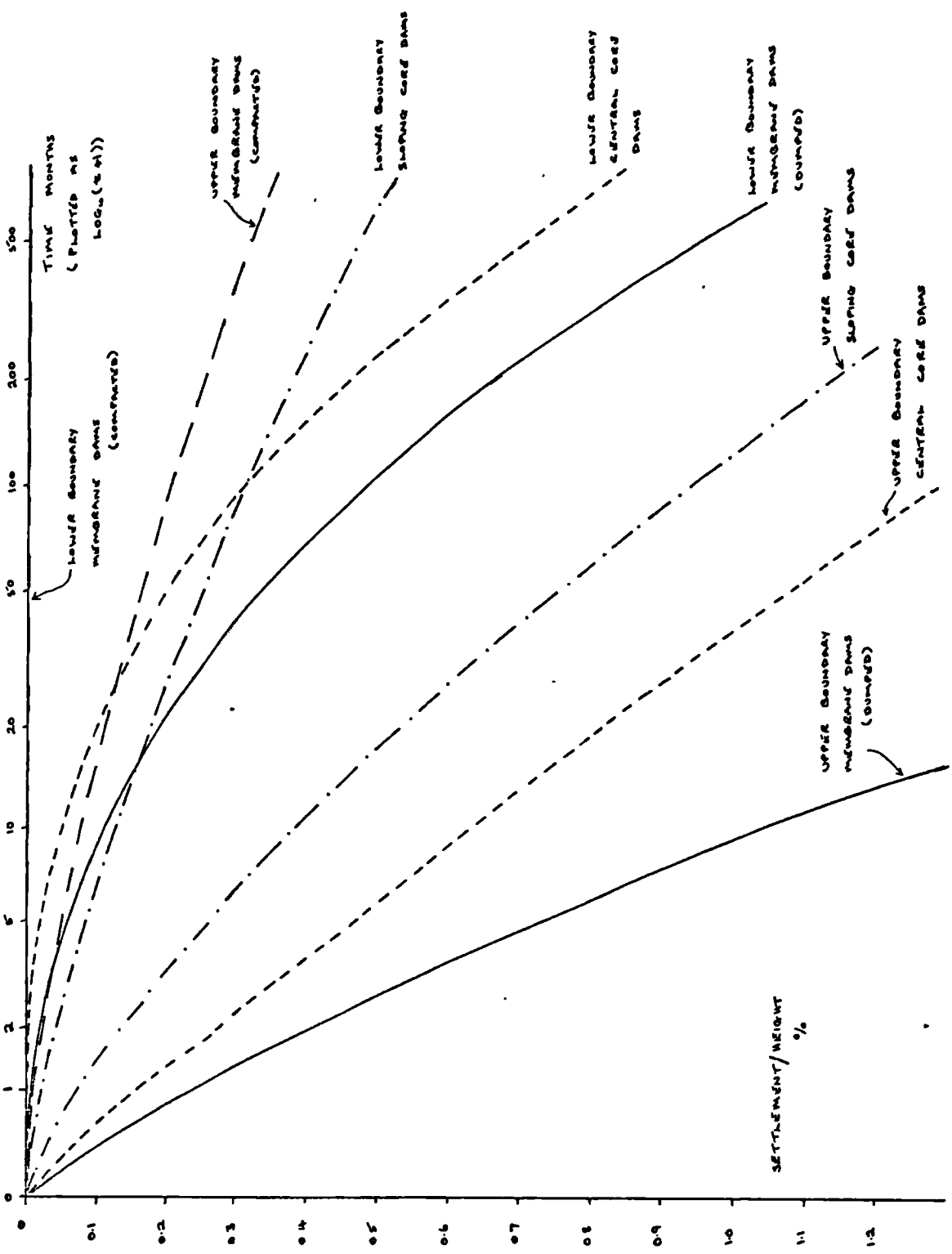

FIG. 2.16 :- ENVELOPES OF POST-CONSTRUCTION SETTLEMENT CURVES OF ROCKFILL DAMS

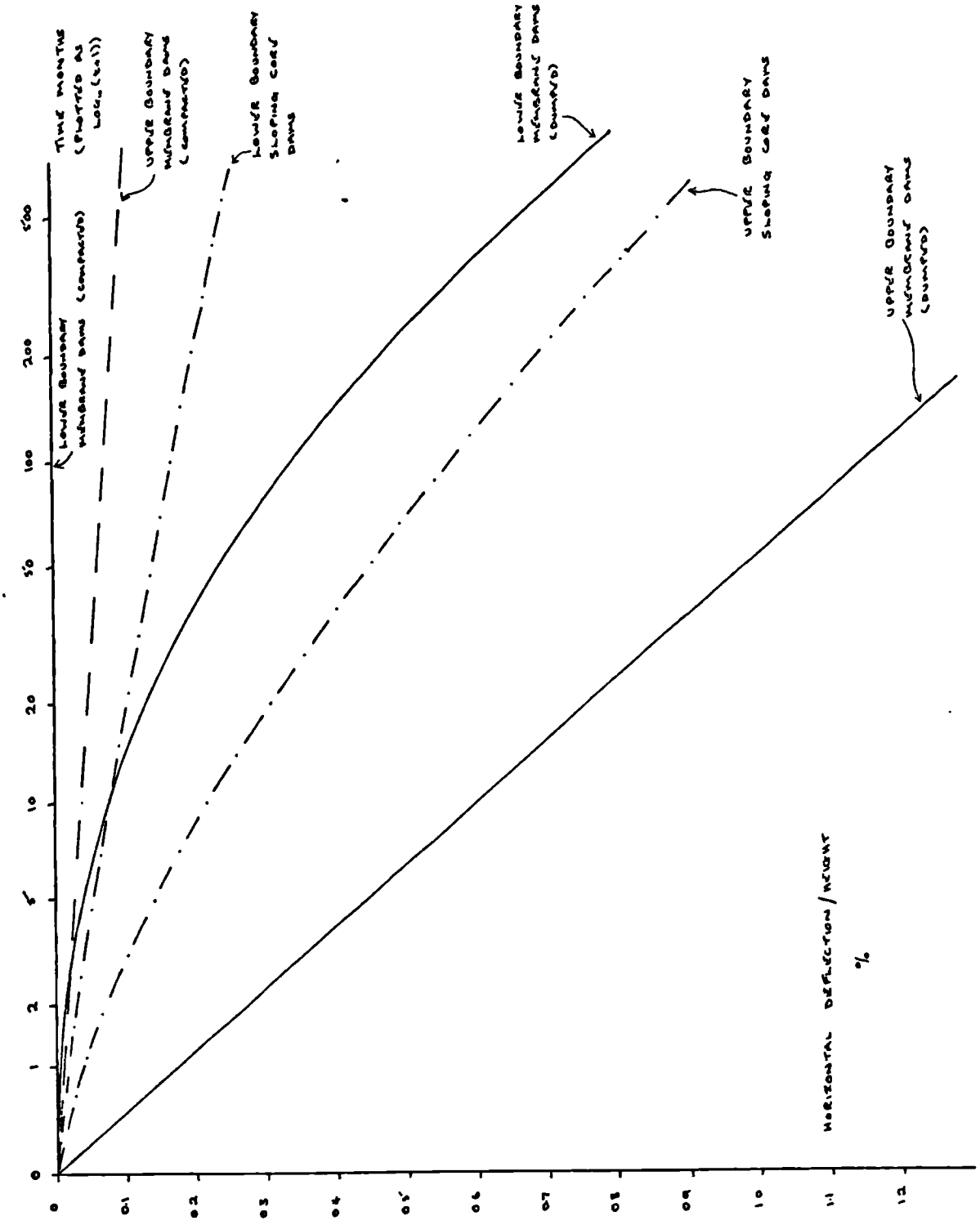

FIG. 2.17 :- ENVELOPES OF POST-CONSTRUCTION HORIZONTAL DEFLECTION CURVES OF ROCKFILL DAMS

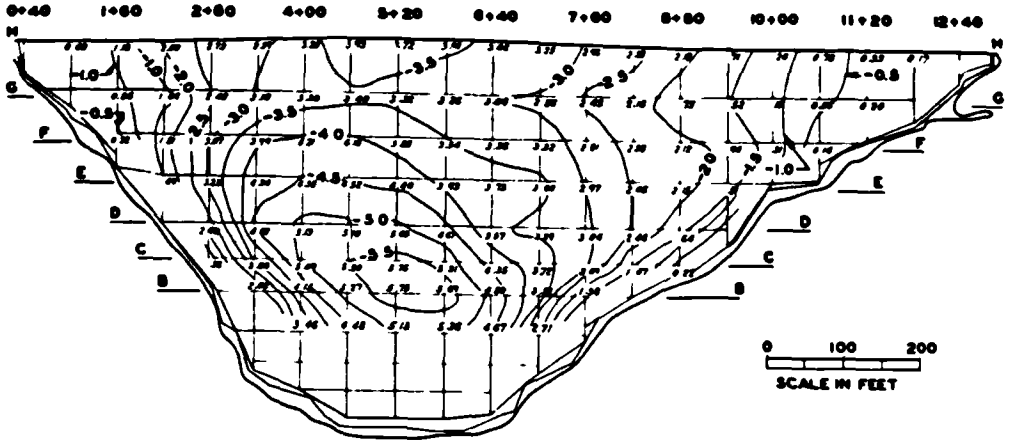

5C. TOTAL SETTLEMENT SINCE COMPLETION OF DAM - SUM OF 5A AND 5B CONTOURS - MARCH 1931 TO MARCH 1958 - 27 YEARS.

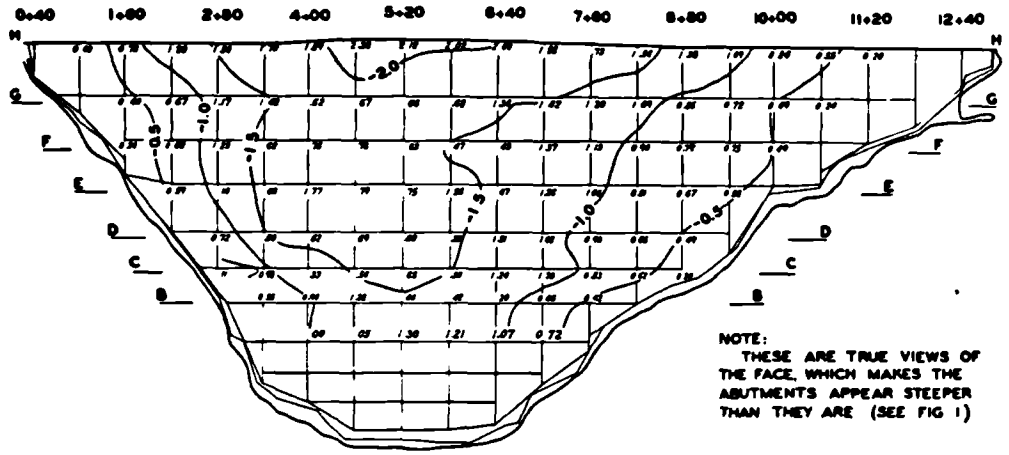

5B. DUE TO AGING AND REAPPLICATIONS OF WATER LOAD AFTER FIRST COMPLETE FILLING - MARCH 1933 TO MARCH 1958 - 25 YEARS

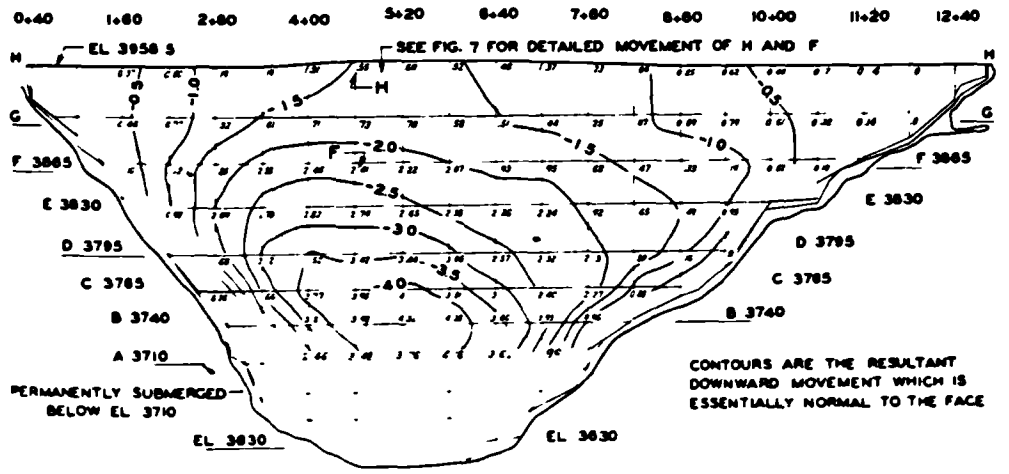

5A DUE TO FIRST COMPLETE FILLING - MARCH 1931 TO MARCH 1933 - 2 YEARS

Fig. 2.18 :- Settlement Contours - Salt Springs Dam
(after Steele and Cooke, 1960)

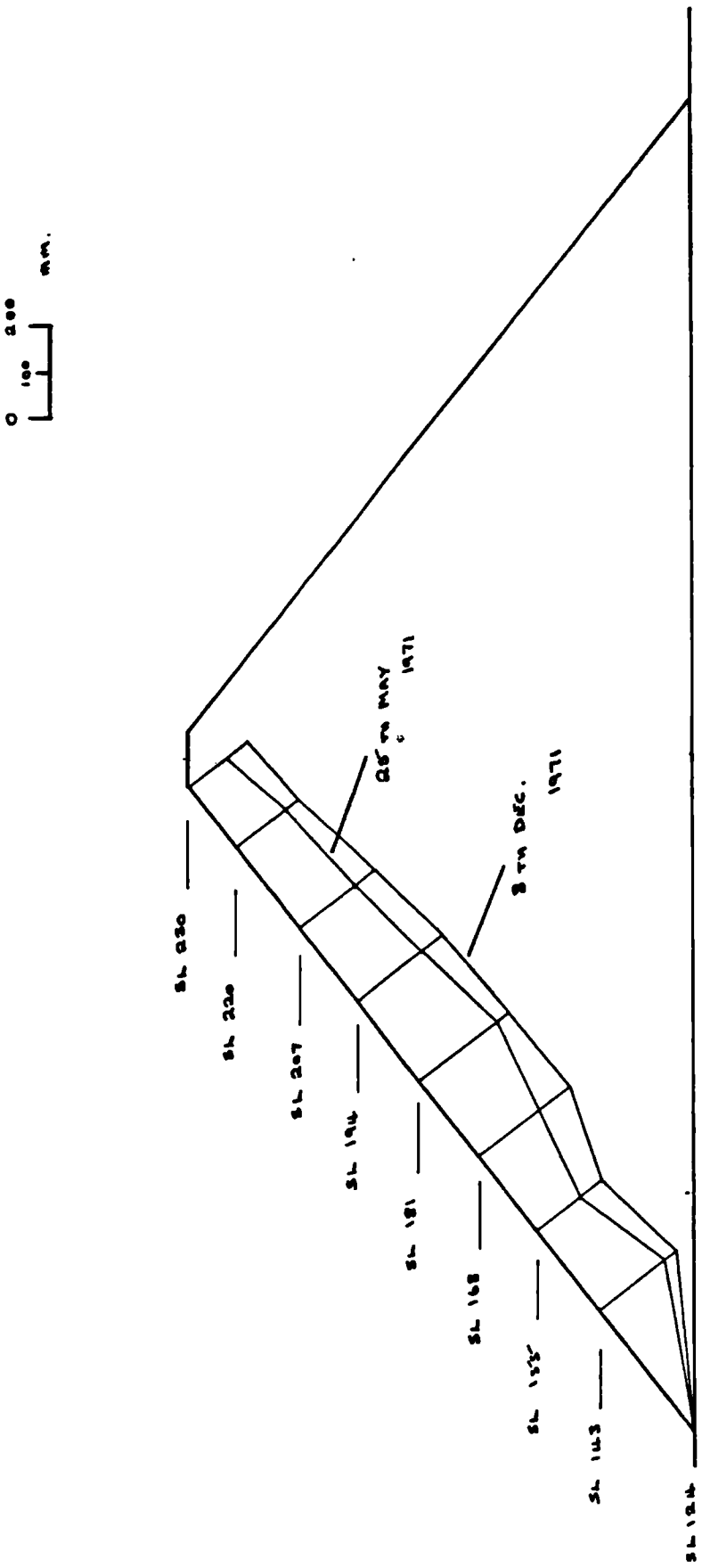

FIG. 2.19 :- MEMBRANE NORMAL DEFLECTION AT CETHANA DAM
(METZE FITZPATRICK ET AL., 1973)

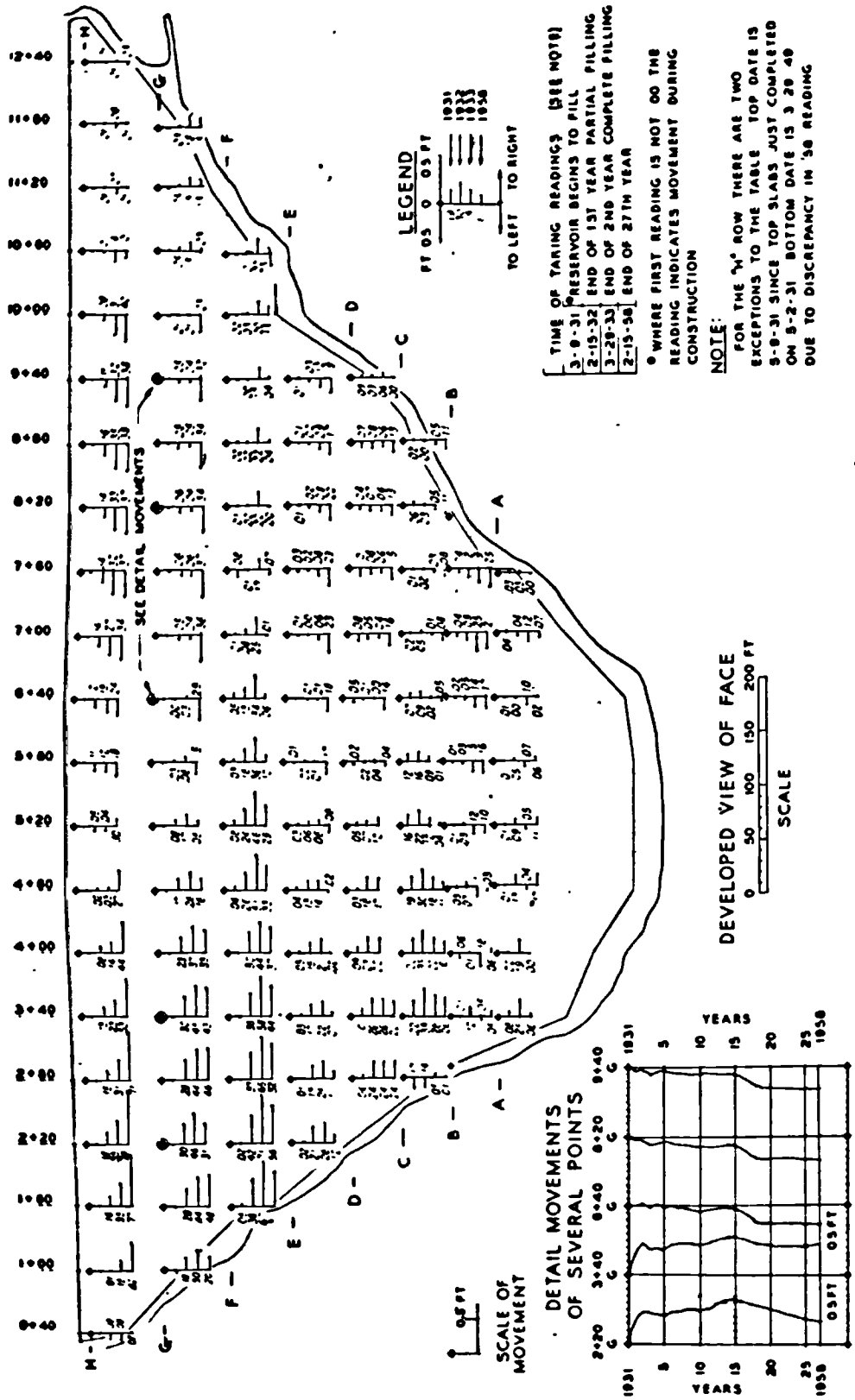

Fig. 2.20 :- Cross-valley Movements - Salt Springs Dam
(after Steele and Cooke, 1960)

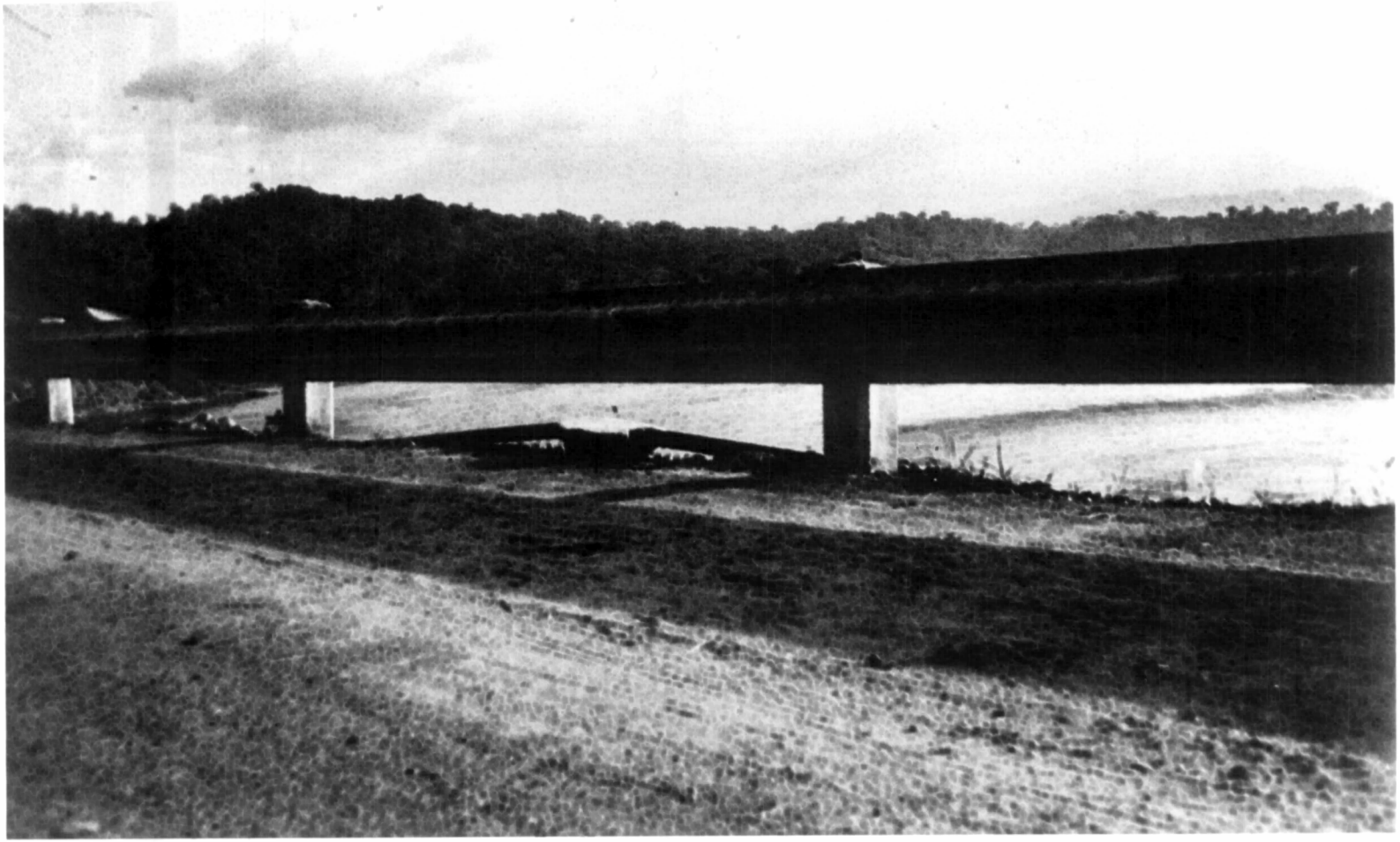

Fig. 2.21 :- Compression Buckling of Electrical Conduit at Netzhualcoyotl Dam
(after Wilson, 1973)

Chapter 3

Material Classification Tests.

The material used for the tests carried out over the period of research was obtained from the site of Scammonden Dam near Huddersfield, Yorkshire (figs. 3.1 and 3.2). As has already been mentioned this is a rockfill dam with a sloping core of three zones of clay. The majority of the rockfill is a carboniferous sandstone with small zones of mudstone and shale (fig. 3.3). The dam, which is 70 m high, serves a dual role and has the M62 Pennine Motorway running along its crest as well as being used for water storage. During construction the dam was well instrumented with piezometers, pressure cells, strain gauges and deformation instruments to monitor the behaviour of the core and rockfill shoulders, both during and after construction. More detailed reports of the dam and its construction have been given by Penman and Mitchell (1970) and Charles (1973). Charles has also published results of the early post-construction behaviour.

The material was obtained from an open rock face close to the crest on the upstream left abutment (figs. 3.4 and 3.5). The lumps varied in colouring from dark brown to a sandy-white and although most of the pieces were the typical plates of laminated material, a significant percentage were lumps without laminations. Two of the larger sandy-coloured blocks, which did not appear to be laminated, were used to obtain cores for the classification tests and also for the point contact tests.

A number of classification tests were carried out on the rock after it had been broken down into fractions using a large hammer. These provide basic information on the properties of the rock as well as giving a description of the material. A similar set of tests (although other tests have been included in this research) were carried out by Charles (1973) on material obtained during the construction of the dam from the blasting quarries. A comparison of the results shows general agreement in the values obtained and similar behaviour of the material.

3.1 Grain Shape

Sedimentary particles have two properties - shape and roundness

- which are distinct and should not be confused. The shape of a particle depends on its surface area and volume whereas the roundness is a measure of the roughness of the surface. Due to difficulty in calculating the surface area of a particle the shape is usually defined in terms of the ratio of the volume of the particle and the circumscribing sphere. The cube root of this ratio, Ψ, is called the sphericity. Krumbein (1941) has developed a method of determining three mutually perpendicular dimensions of a particle and expressing the volume in terms of an ellipsoid. Hence,

$$\Psi = \frac{\text{Volume of ellipsoid}}{\text{Volume of sphere}}$$

$$= \frac{(\pi . abc/6)}{(\pi . a^3/6)} \qquad a > b > c$$

where a, b and c are the dimensions of the particle. This leads to the expression

$$\Psi = \left(\frac{b}{a}\right)^2 \cdot \left(\frac{c}{b}\right) \qquad (3.1)$$

and Krumbein has used this to produce a chart from which Ψ can be calculated if b/a and c/b are known. Since the expression is a simple one, it is much easier to use this and avoid interpolating values which lie between the curves determined by Krumbein.

Krumbein's method may be used for large particles but it is difficult to measure the dimensions of smaller grains. To deal with this problem, Rittenhouse (1943) has produced a series of charts showing the outlines of particles with known sphericity values. A visual comparison of the shape of smaller grains, magnified in some manner, may be made giving a rapid determination of the associated sphericity. These charts are, however, based on a different definition of sphericity, where the volume of the particle is expressed in terms of a sphere of the same volume.

Zingg (Zeller and Wullimann, 1957) classified particles into four basic shapes, determined by the ratios b/a and c/b, as given in Table 3.1.1. Marsal (1963) has also defined two shape parameters based on the ratios of measured surface area and volume to those of a nominal sphere. The methods of measurement involved are tedious and time-consuming and this means that use of these parameters is very limited for field calculations.

Shape	Condition
spherical	$b/a > 2/3$; $c/b > 2/3$
disc-shaped	$b/a > 2/3$; $c/b < 2/3$
rod-like	$b/a < 2/3$; $c/b > 2/3$
bladed	$b/a < 2/3$; $c/b < 2/3$

Table 3.1.1 Zingg's classification

Krumbein (1941) has also produced a rapid method of determining the roundness of a particle. The particle is compared with outlines of particles of known roundness values ranging from 0.1 to 0.9. The lower value being associated with very angular surfaces and the higher with smooth, rounded particles. An average roundness value for a set of particles is determined by summing the products of the roundness values with the number of particles of each value and then dividing by the total number of particles observed. Another classification test which may be used has been produced by von Moos (Zeller and Wullimann 1957). He defined six classes of surface roughness which may be determined by observation. Table 3.1.2 gives the definitions of classes I, II, and III. Classes IV to VI, associated with very rounded surfaces, did not apply to the particles considered.

Class	Definition
I	sharply angular, spiky contours
II	projections slightly rounded, recesses sharply indented
III	projections and recesses slightly rounded, small radii curvature

Table 3.1.2 von Moos classification

Recently Bros and Orzeszyna (1979) have performed a number of tests on nine different sands to investigate the effect of angularity and surface roughness on the properties of these sands. They conclude that the limiting void ratios of a sample and crushing of particles decrease with increasing smoothness and roundness. Drained triaxial tests indicate that the interlocking

of the angular and rough grains contribute to higher angles of internal friction.

The sphericities of nine fractions of the sandstone were determined. Krumbein's equation (3.1) was used for the five largest fractions with a random selection of 25 particles from each fraction but measurement of grains below 2 mm was found to be impossible. The percentages of particles falling into the four classes of shape defined by Zingg were also calculated for these fractions. For the smaller fractions the grains were photographed (in some cases under a microscope) and the prints enlarged to allow comparisons of shape to be made with Rittenhouse's charts, (fig. 3.6).

Fraction	Sphericity
-76+37.5	0.74
-37.5+19	0.75
-19+9.5	0.71
-9.5+4.75	0.67
-4.75+2.36	0.73
-2.36+1.18	0.76*
-1.18+0.6	0.77**
-0.6+0.3	0.77*
-0.3+0.15	0.79**

*50 particles
**30 particles

Table 3.1.3 Sphericity results

Fraction	Spherical %	Disc-shaped %	Rod-like %	Bladed %
-76+37.5	44	48	0	8
-37.5+19	44	32	12	12
-19+9.5	36	32	20	12
-9.5+4.75	28	36	12	24
-4.75+2.36	44	12	32	12

Table 3.1.4 Results Zingg Classification

The mean sphericity values, given above, show that using Krumbein's definition the sphericity generally decreases with particle size. The increase noted for the -4.75+2.36 mm fraction

may indicate a boundary where the shape is determined by the sand grains rather than the manner in which the rock was originally laid down, i.e. in layers. Rittenhouse's definition produces the opposite behaviour and the results show a slight increase in sphericity with decreasing size. However, since the methods are based on different definitions the relative values obtained by the two tests cannot be compared. Zingg's classification of the larger fractions shows the predominance of spherical and disc-shaped pieces in all five fractions.

Both Krumbein's and von Moos' methods of determining the roundness of the particles were used for each of the nine fractions. The results are based on observation of 50 particles (except in two cases) which were selected at random from each fraction. The photographs used to calculate the sphericities of the smaller fractions were again used in these tests.

Fraction	Roundness	Class I%	Class II%	Class III%
-76+37.5	0.29	16	26	58
-37.5+19	0.29	16	34	50
-19+9.5	0.27	18	36	46
-9.5+4.75	0.25	36	32	32
-4.75+2.36	0.24	32	42	26
-2.36+1.18	0.23	36	36	28
-1.18+0.6*	0.19	27	50	23
-0.6+0.3	0.17	30	52	18
-0.3+0.15*	0.17	33	50	17

* 30 particles

Table 3.1.5 Roundness results Krumbein's and von Moos methods

Krumbein's method shows a definite decrease in roundness with decreasing particles size from 0.29 to 0.17. This trend is confirmed by the percentages of the three von Moos classes obtained for each fraction. These show the predominance of class III type particles in the coarse and medium gravels with a more even distribution of all three classes in the fine gravel size. In the remaining fractions there is a low percentage of rounded grains and a large number of class II type particles.

3.2 Specific Gravity

Table 3.2.1 shows the results of specific gravity tests carried out on ten fractions of the rockfill. The fractions -2.36+1.18 to -0.15 mm were tested using density bottles according to the procedure set out in B.S. 1377 (1975). The remaining sizes were tested using a pycnometer, to B.S. 1377 (1961) although this recommends a maximum particle size of $1\frac{1}{2}$" (38mm) for reasonable accuracy of results.

The results show an increase in the S.G. value with decreasing particles size down to the -1.18+0.6 fraction. This is because air is trapped in pieces of the rock and the amount of air increases as the surface area from which it can escape decreases i.e. as the fraction sizes increase. The pycnometer cannot be relied upon to give accurate results unless it can be ensured that all the rock pieces are 100% saturated, otherwise a lower S.G. than the true value will be attained. The values obtained for the four smallest fractions are the same and this value, 2.67, has been used in all subsequent calculations.

Fraction	S.G.	Fraction	S.G.
-76+37.5	2.45	-2.36+1.18	2.65
-37.5+19	2.55	-1.18+0.6	2.67
-19+9.5	2.55	-0.6+0.3	2.67
-9.5+4.75	2.60	-0.3+0.15	2.67
-4.75+2.36	2.60	-0.15	2.67

Table 3.2.1 S.G. Values

3.3 Porosity and Void Ratio

The porosity, n, of a material is defined as the ratio of the volume of voids to the total volume. A mean porosity value for individual lumps of the sandstone was obtained from nine cylinders of the rock. These were prepared from 1" (25 mm) diameter cores, their dimensions measured using a pair of vernier calipers and then they were weighed after being oven-dried for 24 hours. The mean porosity was calculated to be 15.6% with a standard deviation in the results of 1.3%

The void ratio, e, is defined as the ratio of the volume of voids

to the volume of solid material and may be calculated from the porosity.

$$e = \frac{Vv}{Vs} = \frac{Vv}{Vt - Vv}$$

$$= (1/n - 1)^{-1} = \frac{n}{1 - n}$$

Hence, for $n = 15.6\%$, $e = 0.185$

3.4 Relative Density and Porosity

The influence of grain shape on the porosity of a granular medium means that a given value of porosity is not enough to determine whether the medium is in a loose or dense state. If this value is compared with values for the loosest and densest conditions then the degree of compaction may be determined. In soil mechanics the relative density, Dr, is used to measure this where

$$Dr = \frac{e_{max} - e}{e_{max} - e_{min}}$$

and e_{max}, e_{min}, and e represent the void ratios of the loosest, the densest and the actual state of the soil. An alternative parameter, called the relative porosity, has been used by researchers into the behaviour of rockfill (Pigeon, 1969) and this is defined as

$$R.P. = \frac{n_{max} - n}{n_{max} - n_{min}}$$

This may also be expressed in terms of the dry density i.e.

$$R.P. = \frac{\gamma_d - \gamma_{dl}}{\gamma_{dd} - \gamma_{dl}}$$

where γ_d, γ_{dl}, γ_{dd} are the dry densities of the rockfill in its actual, loosest and densest states.

In order to calculate the relative porosity of a particular sample of rockfill, then the maximum and minimum dry densities must be known. The dry density of the loosest state may be found quite easily and the results are fairly consistent for different methods

of determination. The value for the densest state is difficult to obtain and different methods may produce very different results.

The minimum dry density for a rockfill with a grading curve similar to that used at Scammonden (maximum particle size 76 mm) was obtained by carefully placing a 30 kg sample into the oedometer cylinder using a scoop. The test was repeated four times and a mean value of 1665 kg/m^3 obtained, which is equivalent to a maximum porosity of 37.6%. An alternative method has been suggested by Kolbuszewski (1948) which involves allowing the sample to be deposited through water.

The maximum dry density was not calculated since there was no guarantee that any of the methods available would produce the maximum value. The maximum value obtained during the oedometer tests was 2000 kg/m^3 i.e. a minimum porosity of 25.1%. The maximum value obtained during field trials at the site of the dam prior to construction was 2180 kg/m^3 (Williams and Stothard, 1967).

3.5 Angles of Friction

In addition to the angle of internal friction (or angle of shearing resistance) usually calculated for cohesionless soils, another angle of friction can be found. This is the angle of repose and this is the slope which a heap of the soil naturally forms. This has been defined as the friction angle under zero pressure (Taylor, 1948) and differs from the friction angle under pressure in several ways. In a pile of soil the angle of repose is determined by the grains on the slopes of the heap which are effectively at the loosest state possible. The angle of internal friction is a measure of the average conditions of all the grains and hence this is larger than the angle of repose. On the surface there is very little strength generated by interlocking of the grains whereas this is a major factor in the angle of internal friction. A small amount of cohesion between particles, if the sample is not dry and clean, can produce a significant increase in the angle of repose but its effect is small on the angle of internal friction for samples under larger pressures. Terzaghi (1943) noted that the angle of repose for dry or wet sands is independent of the height of the slope and that the angle of internal friction increases with density.

3.5.i Angle of Repose

Four fractions of the sandstone were oven-dried at 105°C for twenty-four hours prior to testing. The four samples, each weighing 200g were cooled in a desicator and then passed through a funnel, falling from a height of 70 mm onto a level surface. The heap of material was photographed and the test repeated twice on the same sample. The angle of repose was determined from the photographs to the nearest 0.25° and a mean value found for each fraction.

Fraction	Angle of Repose
-1.18+0.6	42.5°
-0.6+0.3	34.5°
-0.3+0.15	35.5°
-0.15	39.5°

Table 3.5.1 Results-angle of repose

The results of these tests, given in Table 3.5.1 are quoted to 0.5° and do not show any distinct trend with particle size. The results showed a maximum deviation of 2.5° from the mean values which is large, but reasonable, bearing in mind the crudeness of the test. Charles (1973) determined the angle of repose by carefully pouring the material over a 120 mm vertical wall. While a similar scatter of results was observed, the angle decreased with particle size.

3.5.ii Angle of Internal Friction

For most practical applications the angle of repose has limited value and the angle of internal friction needs to be calculated. The simplest method of determining this value is the direct shear test using a Casagrande shear box. For a uniformly graded sample Lewis (1956) showed that the maximum particle size which could be tested should be one-fortieth of the width of the box. The maximum grain size allowable for a well graded sample was greater than this but the increase was not significant. The shear box used in these tests was 60 mm wide and the maximum size used was 1.18 mm in accordance with

Lewis' specification.

The four samples used in calculating the angle of repose were used to determine the angle of internal friction. The samples were dried and cooled as before so that a direct comparison of results could be made. Each sample was split into two and two shear tests carried out under different normal stresses. The rate of shearing was maintained at 1.35 mm/minute and measurements of the shear stress and dilatancy taken at regular intervals. Table 3.5.2 gives the results of these tests.

	Normal Stress 39.12 kN/m^2		Normal Stress 88.76 kN/m^2	
Fraction	Shear strength kN/m^2	ϕ	Shear strength kN/m^2	ϕ
-1.18+0.6	40.43	45.94°	74.35	39.95°
-0.6+0.3	35.19	41.97°	71.98	39.04°
-0.3+0.15	34.44	41.36°	72.86	39.38°
-0.15	36.98	43.39°	76.42	40.73°

Table 3.5.2 Shear box test results

The results show that as the normal stress increases then the shear strength at failure also increases. Fig. 3.7 shows a typical set of load-deformation curves under different normal stresses. Once the peak stress has been reached the shearing stress remains practically constant for the reminder of the deformation. The angle of internal friction decreases with increased normal stress, indicating a curved strength envelope.

A comparison of the dilatancy results shows that the three largest fractions act in a similar manner to a dense sand but the -0.15 mm fraction acts more like a loose sand, although in preparing the samples each was subjected to approximately the same degree of compaction. Fig. 3.8 shows the dilatancy curves for the -0.6+0.3 mm fraction under the two sets of normal stress. These show the initial negative dilatancy as the particles settle under load and the subsequent positive dilatancy as the particles are lifted over each other by the shearing load. An increase in the normal load gives an increase in the amount of negative dilatancy as expected. Figs. 3.9 and 3.10 show the load-deformation and dilatancy curves

for the -0.15 mm friction. In this case very little positive dilatancy is seen and the peak stress is just reached before the 10% maximum travel is exhausted. As before the increase in normal stress produces an increase in the negative dilatancy.

The angles of internal friction are greater than the angles of repose for each fraction, as predicted by the theory. The variation of the angles of internal friction with particle size is similar to that of the angles of repose and this indicates that although the angle of repose method of calculation may be rather crude, the results may be used with some degree of confidence.

In addition to the tests on the sandstone obtained directly from the parent rock, a few tests were carried out on the same fractions of material taken from the resieving of the sample used in test A.1 of the large oedometer tests. The conditions this sample was subjected to are described in chapter 7. In general the same trends were noted in these tests as in the first set. The tested material, however, showed a larger drop in shearing strength after the peak strength than seen in the first tests. This appeared to be a general trend although the peak strengths were not necessarily less than before.

3.6 Unconfined Compression Strength

The standard method of determining the unconfined compression strength of rock is to prepare cylinders of the material and obtain their failure stress in a testing machine. While the testing procedure and analysis of results are quite straightforward, the preparation of samples can be very time consuming and weaker samples may break during machining. Hobbs (1964) has developed a method of testing which avoids sample preparation. This involves testing lumps of rock in a testing machine with the smallest dimension parallel to the direction of loading. The area of contact between the sample and the platens is determined by placing pieces of graph paper and carbon paper on the platens. The samples are loaded to failure and the blackened squares on the graph paper counted to obtain the area of contact (fig. 3.11). This method allows more samples to be tested because of the short preparation time but since the results show substantial scattering, this is necessary to obtain a reasonable mean value. Measurement of the area of contact is open to errors as it is difficult to sum

the fractions of squares, and the imprints are obscured by smudging and tearing. The fracture mechanism is similar to that seen in the irregular blocks of rock under loading in an oedometer or a dam.

Hobbs determined a relationship (3.2) between the compressive strength, q, of a cylinder 25 mm in length and 25 mm diameter and a strength index, I_a, of a lump of rock weighing 32 g. I_a is defined as the fracture load divided by the mean area of contact.

$$q = 0.91\ I_a - 21900 \qquad (kN/m^2) \qquad (3.2)$$

This is an approximate relationship and has the disadvantage that if the strength index is less than 24000 kN/m^2 then a negative value of q results. A different relationship is needed if softer rocks are to be tested by this method and meaningful results obtained.

Both the standard and Hobbs tests were used to determine the strength of the sandstone. The specimens were tested in an Instron 1195 testing machine with a 100 kN load cell and a constant rate of crosshead (screw driven) movement of 1mm/min. This rate was selected since the length of time to fracture was approximately the same as that Hobbs obtained using a constant rate of loading.

Twelve cylinders, 25 mm long, were prepared from cores taken from a block of the sandstone using a 25 mm diameter diamond tipped coring tool. More accurate measurements of their dimensions were made using a pair of vernier calipers. Half of the cylinders were saturated in water at 20°C for twenty-four hours and tested immediately on removal from the water. The remaining samples were oven dried at 40°C for twenty-four hours and air-cooled before testing (fig. 3.12). The results in Table 3.6.1 show that saturation causes a 40% reduction in strength.

Conditions of test	No.of samples	Mean compression strength kN/m^2	Standard deviation kN/m^2
oven dried air cooled	6	51520	5000
saturated surface dry	6	31300	7400

Table 3.6.1 Compression strength results on 25 mm cylinders

The specimens for the Hobbs test were obtained by breaking up parent material with a small hammer and selecting 50 lumps with weights of 31-33 g. The lumps were saturated and dried in the same way as described above, (fig. 3.13).

Conditions of test	No. of samples	Mean I_a kN/m^2	Standard deviation I_a kN/m^2	q kN/m^2
oven dried air cooled	25	62320	26970	34800
saturated surface dry	25	41020	23010	15430

Table 3.6. 2 Compression strength results Hobbs test

As before the results from the Hobbs test, shown in table 3.6.2 indicate a reduction in strength due to wetting. The compression strengths are much smaller than those found above; four reasons may account for this discrepancy. The material used for the cylinders was obtained from a block of homogeneous rock whereas the material for the lumps of rock varied considerably. This is reflected in the large scatter of results. It is probable that the Hobbs specimens were more weathered than the block, therefore having a lower strength. As already mentioned the determination of the area of contact is subject to errors but this would only effect the results slightly. Finally the relationship suggested by Hobbs may not be valid for this material. If a correlation of the results obtained by these two methods is assumed then the following relationship would be obtained.

$$q = 0.95\ I_a - 7640 \qquad (kN/m^2)$$

This has a similar gradient to Hobbs' formula but the absolute intercept value is reduced considerably.

Hobbs noted that the direction of the laminations did not appear to matter, and comparable strengths were obtained whether the laminations were parallel or perpendicular to the direction of loading. A similar study was carried out during the strength tests and the same conclusion was reached.

Source	Type of test	Conditions	Depth m	q kN/m^2	E kN/m^2
Penman and Mitchell (1970)	cores	-	21.6	56500	9,440,000
		-	53.0	80600	19,220,000
Charles (1973)	Hobbs	dry	-	69000	-
		wet	-	51800	-

Table 3.6.3 Compression strengths of Scammonden sandstone

Table 3.6.3 gives the results of compression tests carried out by other reseachers. The results obtained with the cylinders show reasonable agreement with these values. The Hobbs test results do not compare very well and the possible reasons for this have already been stated.

3.7 Young's Modulus and Poisson's Ratio

To determine the Young's modulus and Poisson's ratio of the sandstone, three 2.5 mm diameter cores, with length-diameter ratios of approximately 2:1 were prepared. The strains were measured using electrical resistance strain gauges attached to the surface of the rock cylinders. The four gauges, equi-spaced on the mid-length circumference, were placed alternatively horizontal and vertical so that both transverse and longitudinal strains could be recorded. During the testing of sample 1 each gauge was monitored seperately using a half bridge circuit but in subsequent tests the mean transverse and longitudinal strains were measured using a full bridge circuit.

The true values of these material parameters can only be obtained in this way if the sample is subject to uniform loading. In order to ensure this, three steps were taken. The ends of each cylinder were made as parallel as possible using a special attachment arm on an Isomet low speed saw (model 11-1180). A rig was designed and constructed which would ensure that each sample was placed centrally on the testing machine load cell. In order to match the ends of the cylinders to the machine platens a thin layer of a hard dental cement (trade name Kemroc) was applied to each end and allowed to set while the sample was under a small load in the machine. Kemroc was used because, when dry, it has a strength comparable with

that of the rock and has a quick setting time of twenty minutes.

The tests were carried out in the Instron 1195 testing machine with a constant rate of crosshead movement of 1 mm/min. For sample 1, the load was applied in cycles, with the maximum load increasing from 5 kN to 25 kN by 2.5 kN on each cycle. Samples 2 and 3 were tested in a similar manner with the maximum load increasing by 5 kN on each cycle from 5 kN to failure.

Sample	Load range kN	E kN/m^2
1	0-3.5	9,410,000
	7.5-15	19,260,000
2	0-5.0	10,090,000
	10-26	21,520,000
3	0-3.0	5,780,000
	10-28	18,140,000

Table 3.7.1 Young's modulus of sandstone

Table 3.7.1 shows the values obtained for the Young's modulus of the three cylinders over the given load ranges. These show clearly the work-hardening effect under increasing load which is to be expected in a porous material. The stress-longitudinal strain graph for sample 3 is shown in fig. 3.14. During each cycle energy is dissipated and the length of the specimen is reduced. On reloading the curve passes close to the tip of the loop of the previous cycle but as the maximum load increases the discrepancy also increases. These features were noted in all the tests carried out.

$Load_{kN}$	Poisson's ratio - ν		
	Sample 1	Sample 2	Sample 3
5	0.032	0.022	0.013
10	0.075	0.060	0.038
15	0.117	0.104	0.075
20	0.173	0.152	0.124
25	0.271	0.223	0.199

Table 3.7.2 Poisson's ratio (in terms of total strains)

The Poisson's ratio values were obtained at different loads using the total strains at those loads and these are given inTable 3.7.2. These show that ν increases with load and that the rate of increase also increases with load. Sample 3 has a smaller set of values than 1 and 2 but as it has a smaller initial E value i.e. larger longitudinal strains for the same stress, then a Poisson's ratio determined from the total strains will reflect this. Fig. 3.15 shows the stress-transverse strain graph obtained for sample 3. In this and the other tests a small negative (compression) residual strain after the first cycle was noted. This means that the sample undergoes a volume decrease during the first cycle. After subsequent cycles larger, positive residual strains were produced but the net volume change was still negative.

Although steps, described above, were taken to ensure uniform loading, the graphs obtained by monitoring each gauge of sample 1 show that large differences may still occur in the transverse strains on either side of the cylinder. An additional test of the sensitivity of the transverse strains to position was carried out by rotating the specimen through 90, 180, and 270 degrees and recording the mean strains under loads of 1, 2, 3 and 4 kN. As expected the results varied widely depending on the position. The longitudinal strain graphs obtained from each gauge for sample 1 were very similar and the differences seen were negligible over the whole load range. Tests carried out when the centering rig and cement end pads were not used produce similar Young's modulus values but much larger Poisson's ratios.

Table 3.6.3 gives the results reported by Penman and Mitchell (1970) for the sandstone used in Scammonden Dam. These are similar to the values obtained in this research but no details are given of the experimental procedure. In the tests described above all the samples tested were air dried after coring and cutting. From other literature it appears that wetting does alter the Young's modulus value but no agreement on this has been reached. Jaegar (1972) reports a 50-70% reduction in the modulus for a phyllite immersed in water for three days. Obert and Duval (1967), however, noted increases of 38 and 40% for granite and marble as the water content increased from a dry to a saturated condition.

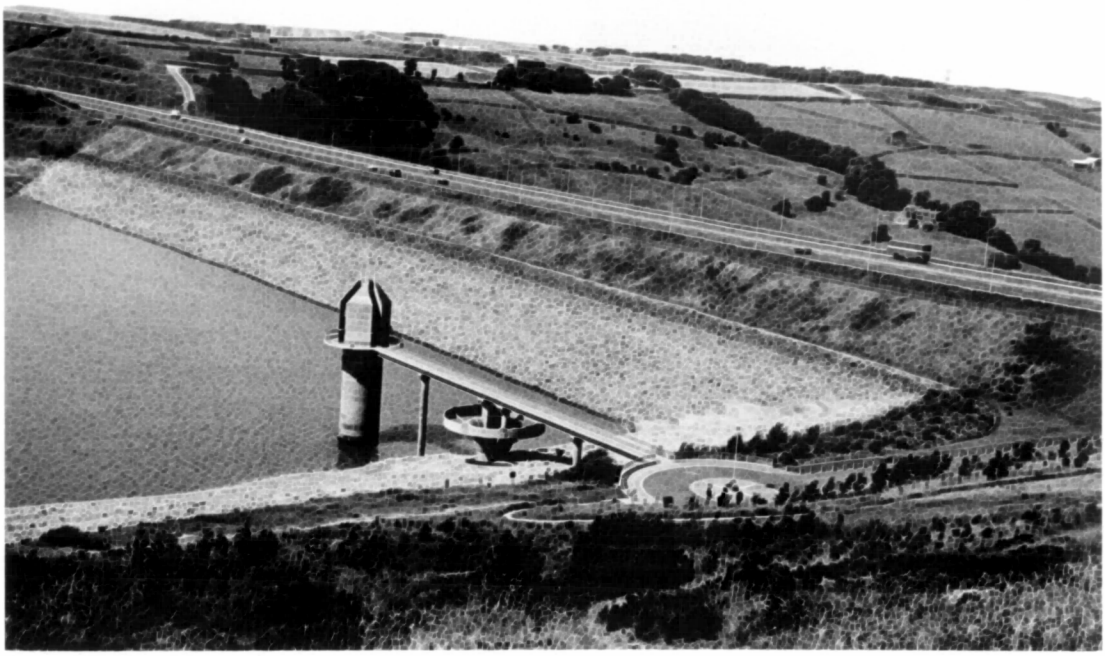

Fig. 3.1 :- Scammonden Dam

Fig. 3.2 :- Downstream Face of Scammonden Dam

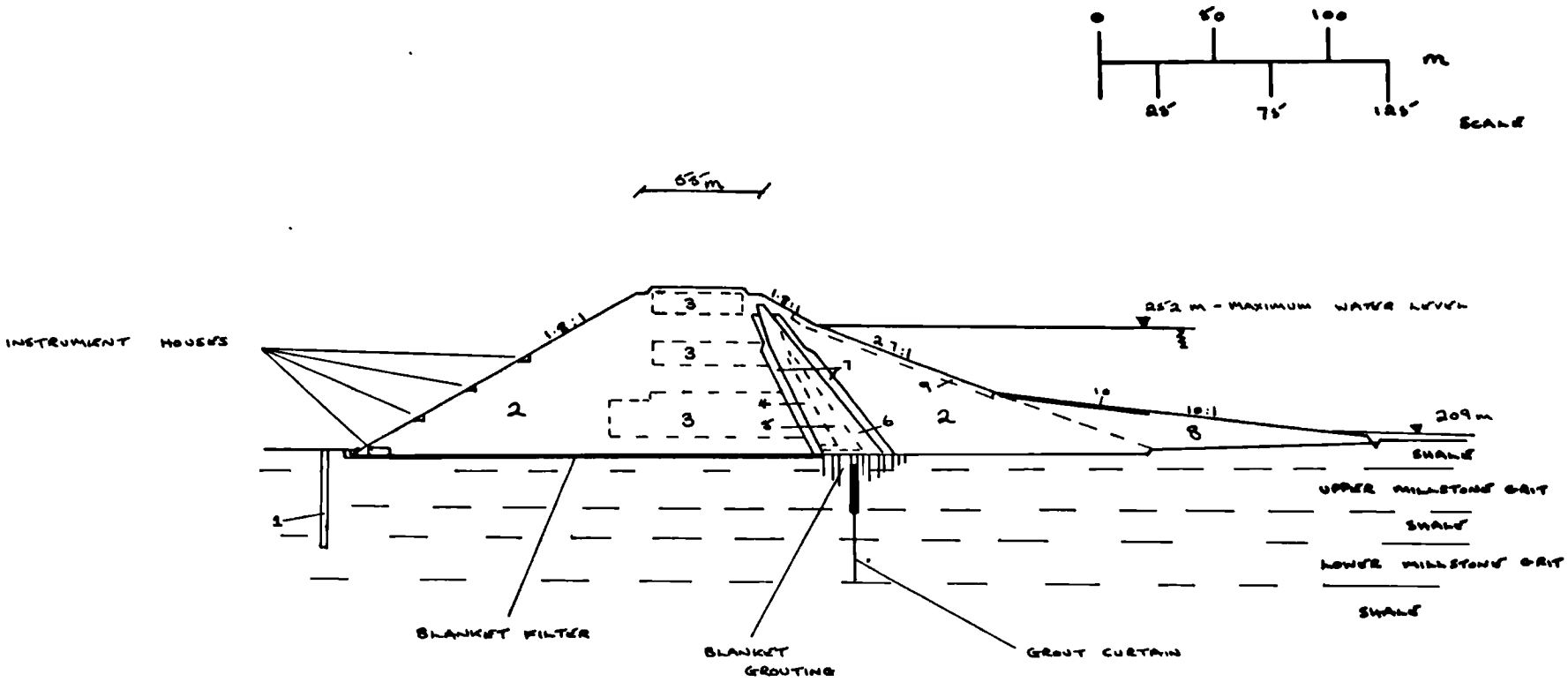

FIG. 3.3 :- SECTION OF SCAMMONDEN DAM

1. PRESSURE RELIEF WELL
2. SANDSTONE ROCKFILL
3. MUDSTONE ZONES
4. THIRD CLASS CLAY ZONE
5. SECOND CLASS CLAY ZONE
6. FIRST CLASS CLAY ZONE
7. FILTERS
8. TOE WEIGHTING
9. FILTER AND RIP-RAP
10. BEACHING

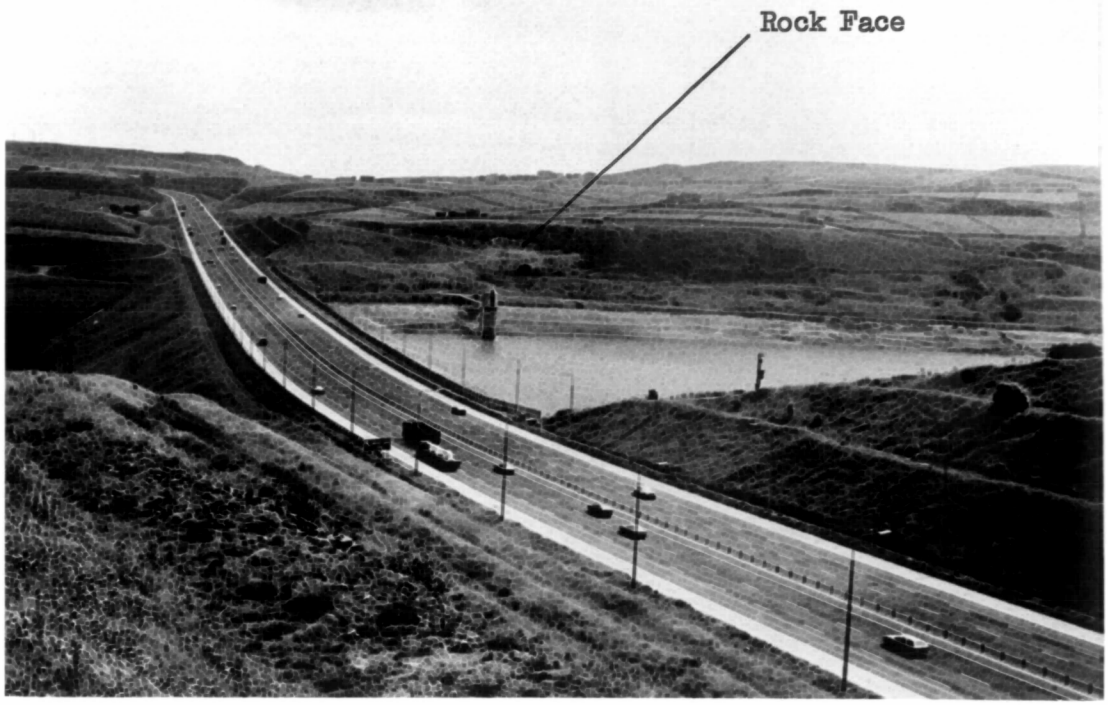

Fig. 3.4 :- Source of Rock used for Laboratory Tests

Fig. 3.5 :- Open Rock Face on Dam Abutment

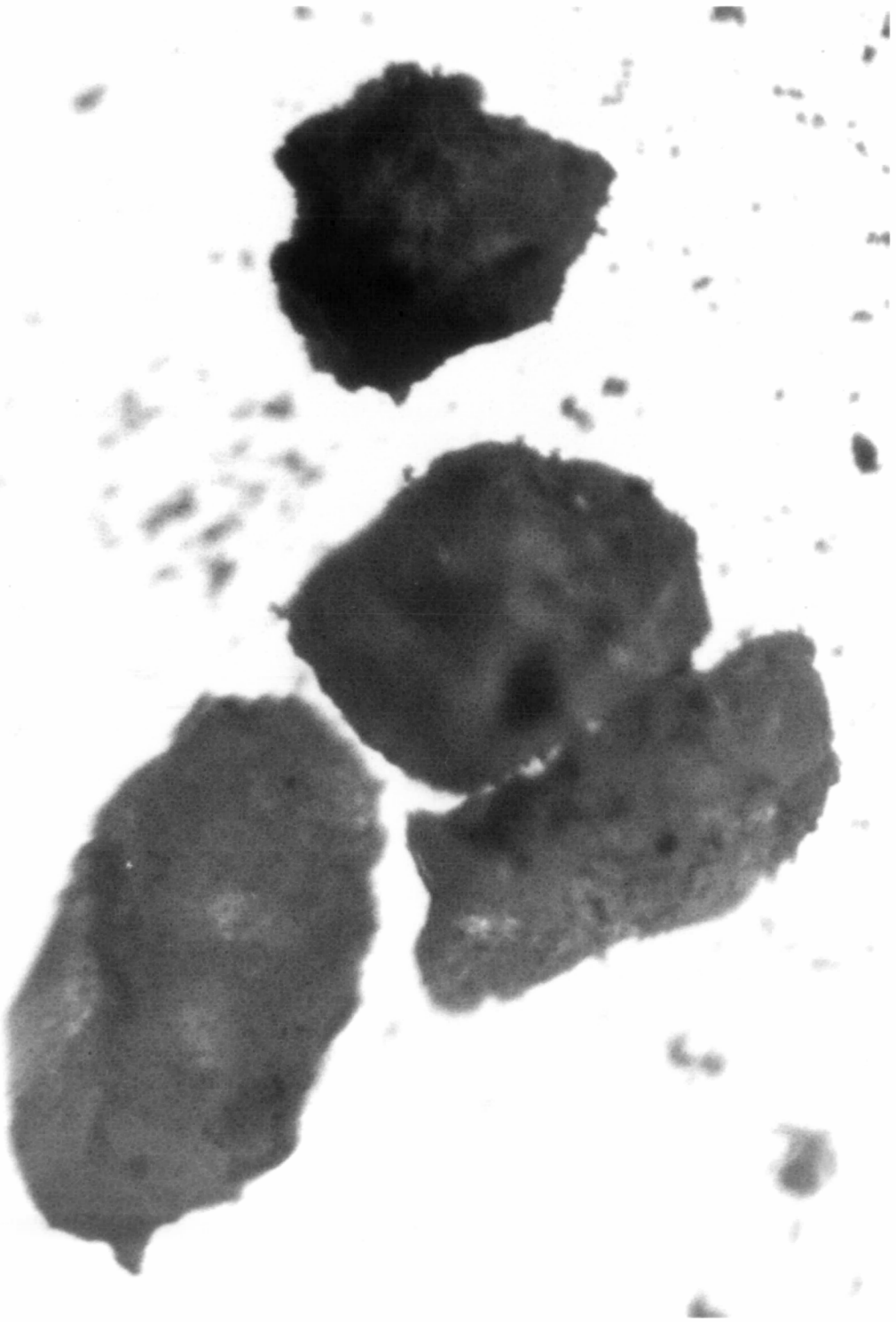

Fig. 3.6 :- Rock Particles - -0.6+0.3mm Fraction

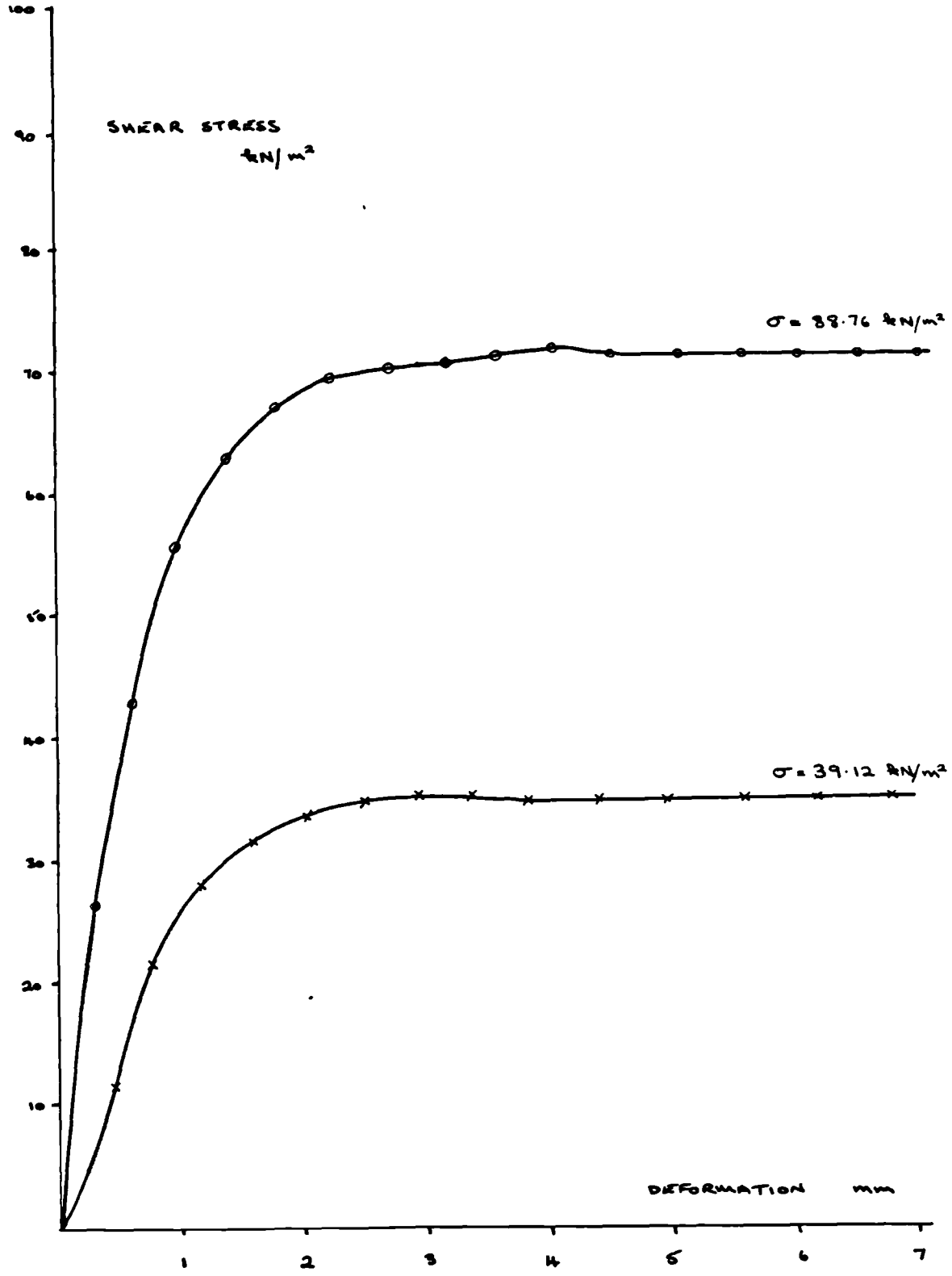

FIG. 3.7 :- SHEAR STRESS v DEFORMATION CURVES

SHEAR BOX TESTS ; -0.6 + 0.3 mm FRACTION

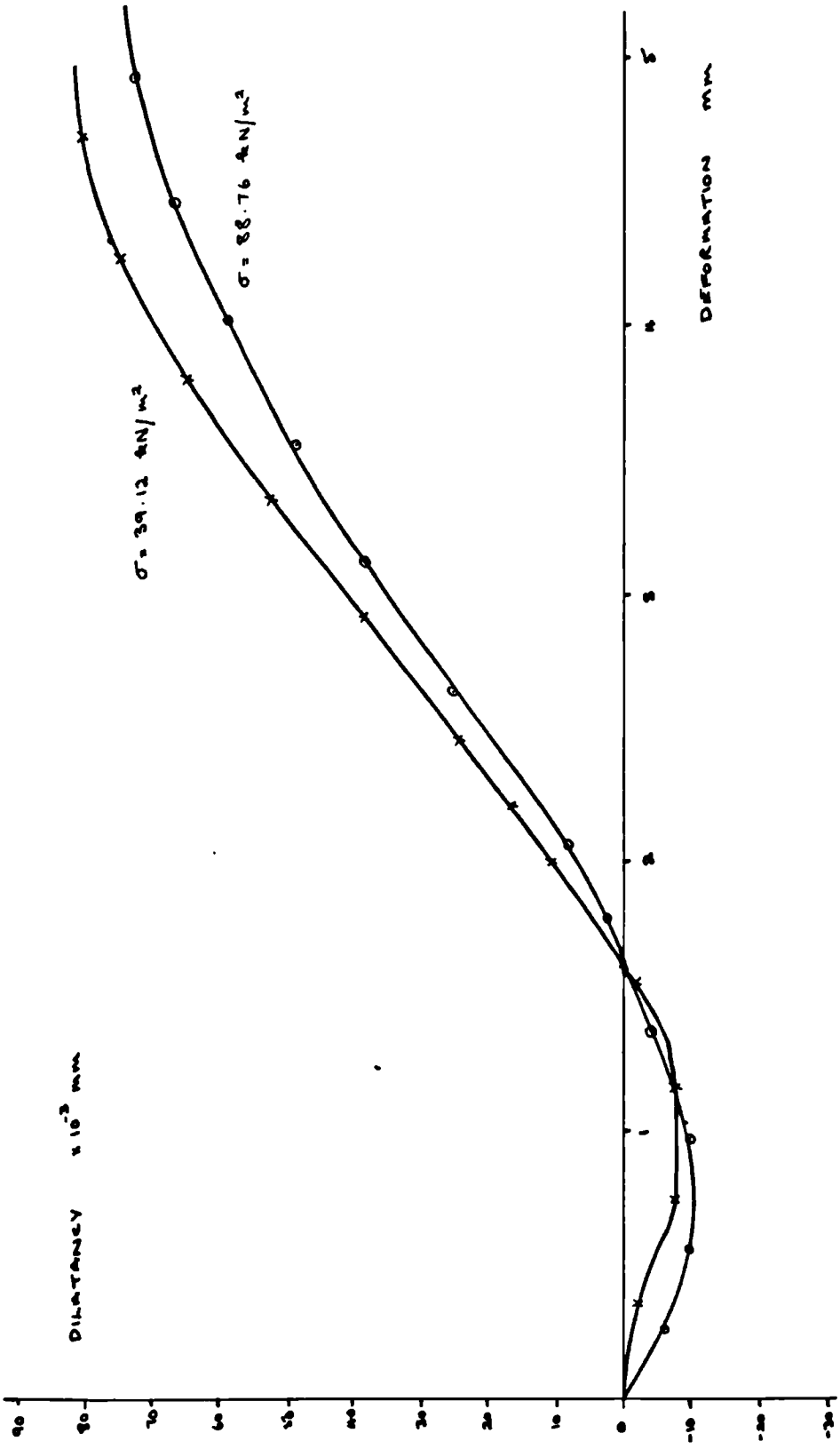

FIG. 3.8 :- DILATANCY BEHAVIOUR
SHEAR BOX TESTS ; -0.6 + 0.3 mm FRACTION

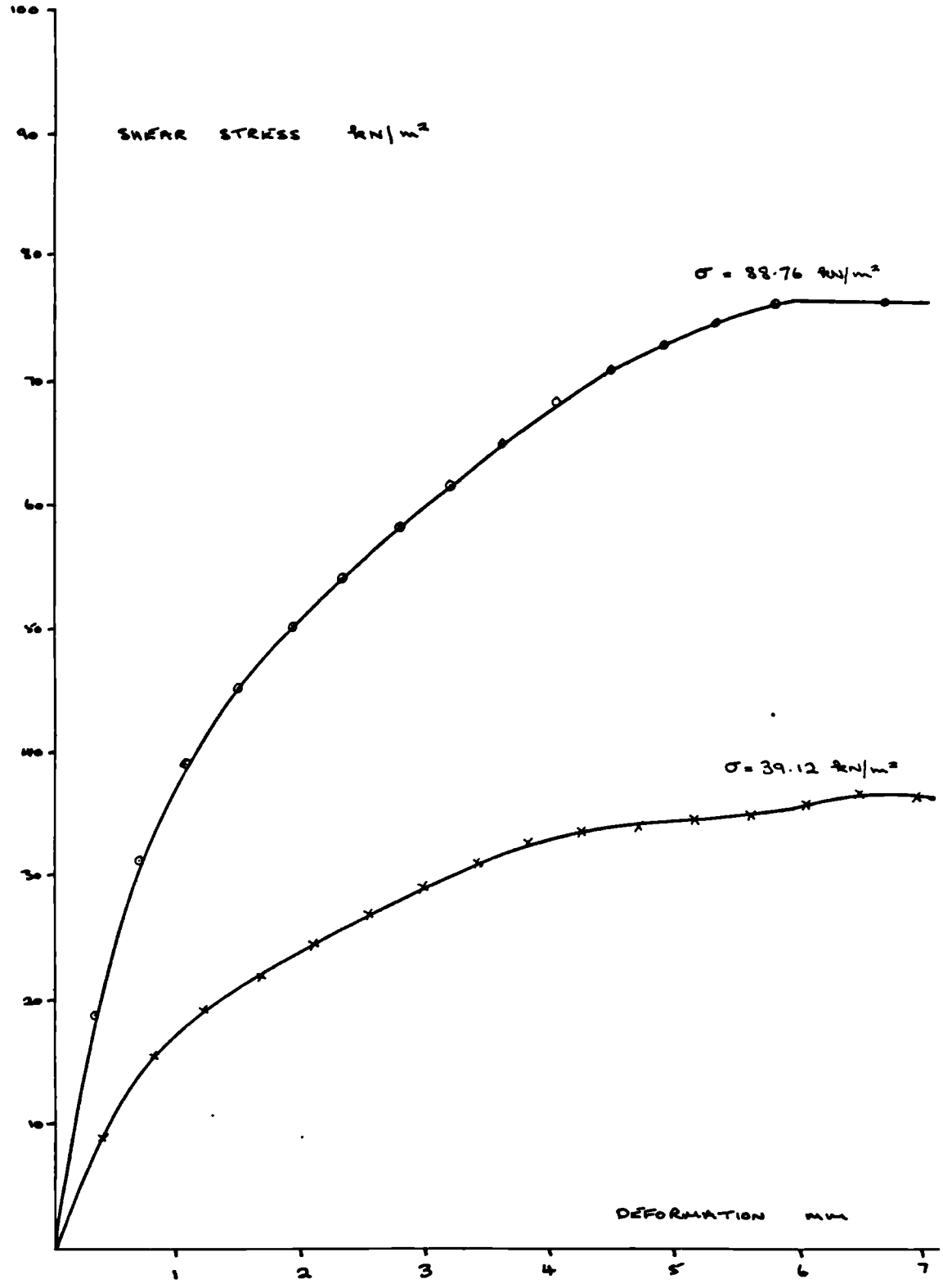

FIG. 3.9 :- SHEAR STRESS v DEFORMATION CURVES

SHEAR BOX TESTS ; -0·15 mm FRACTION

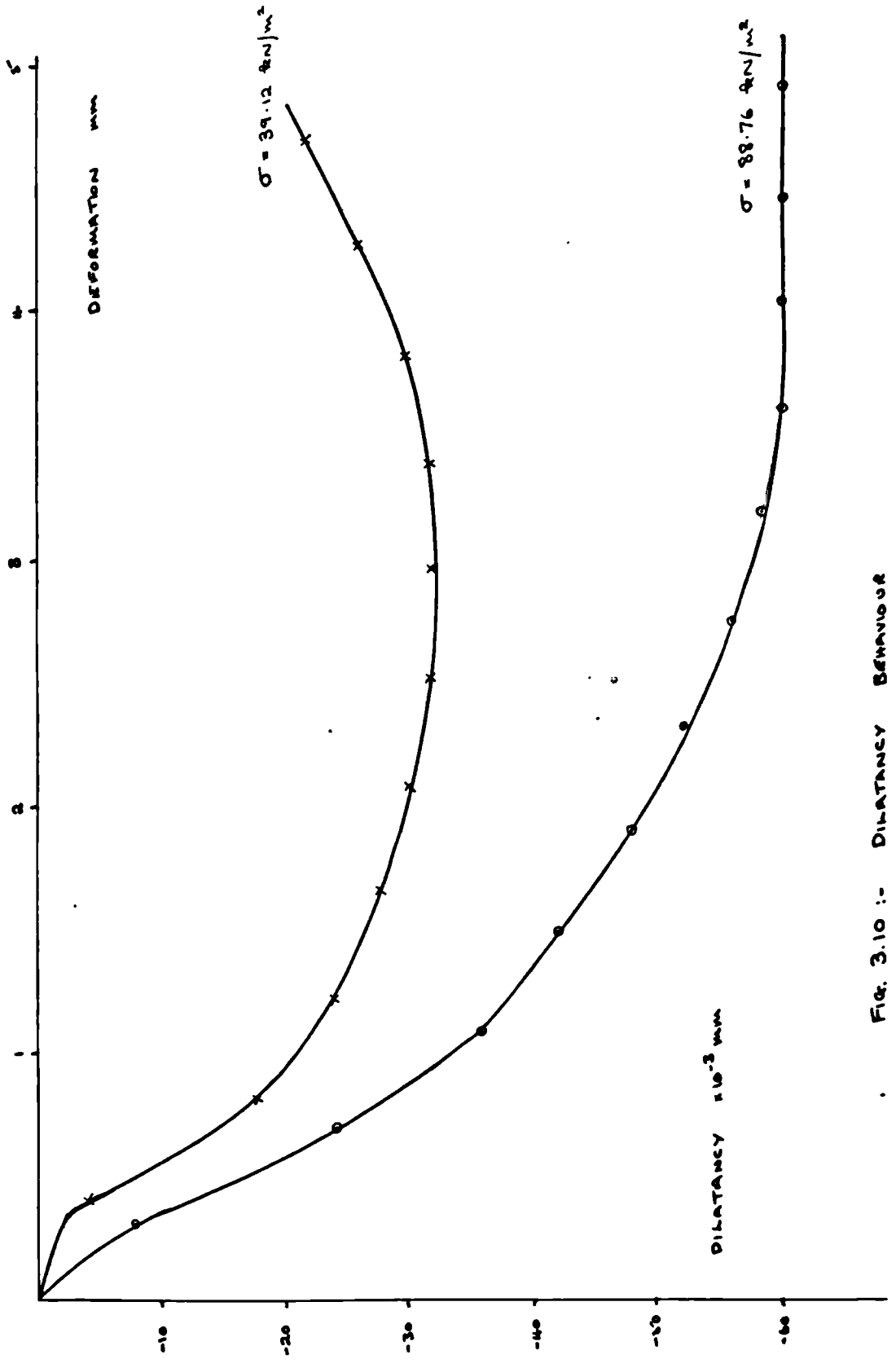

Fig. 3.10 :- Dilatancy Behaviour
Shear Box Tests ; -0.15 mm Fraction

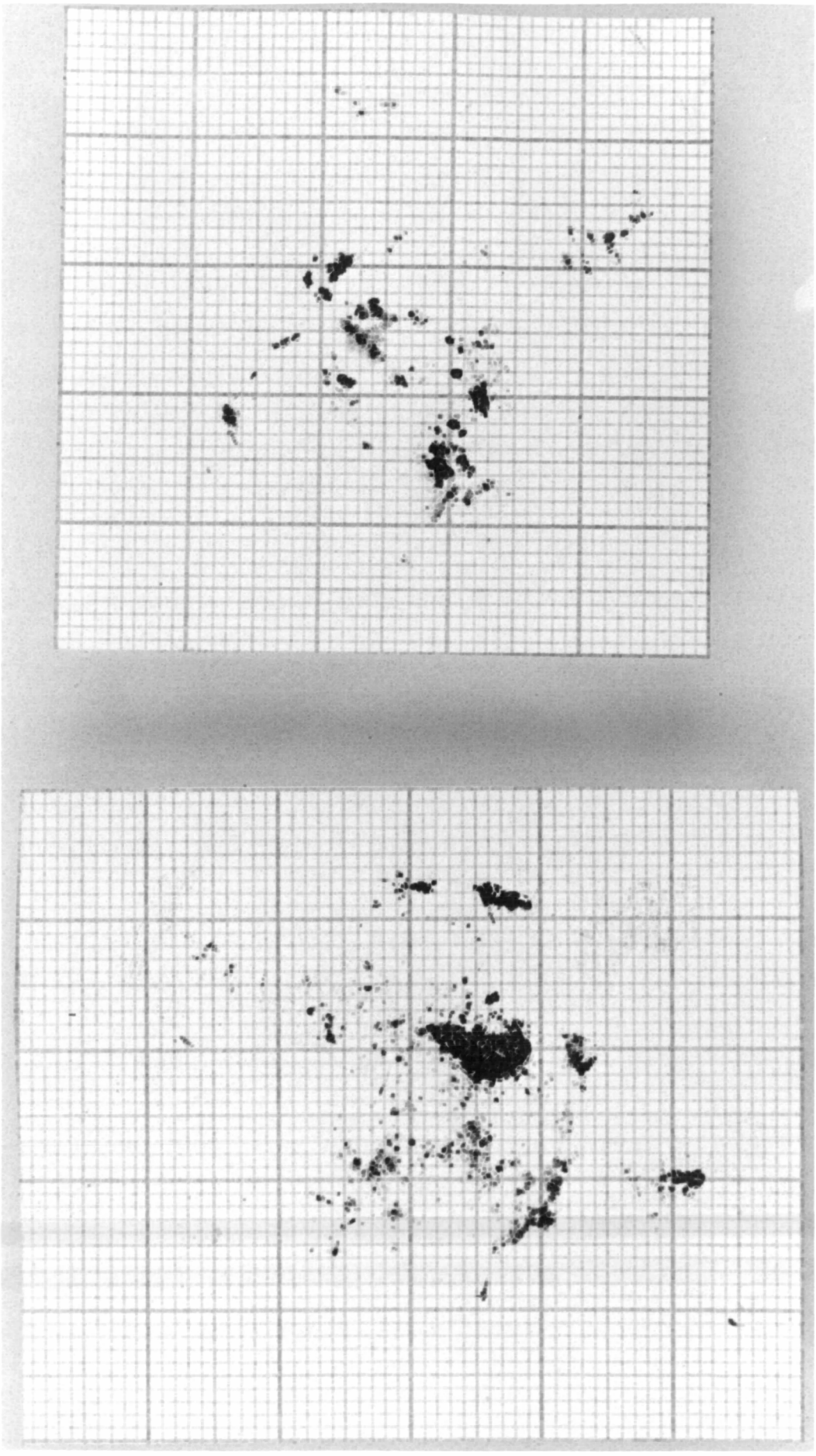

Fig. 3.11 :- Area of Contact Imprints - Hobbs Test

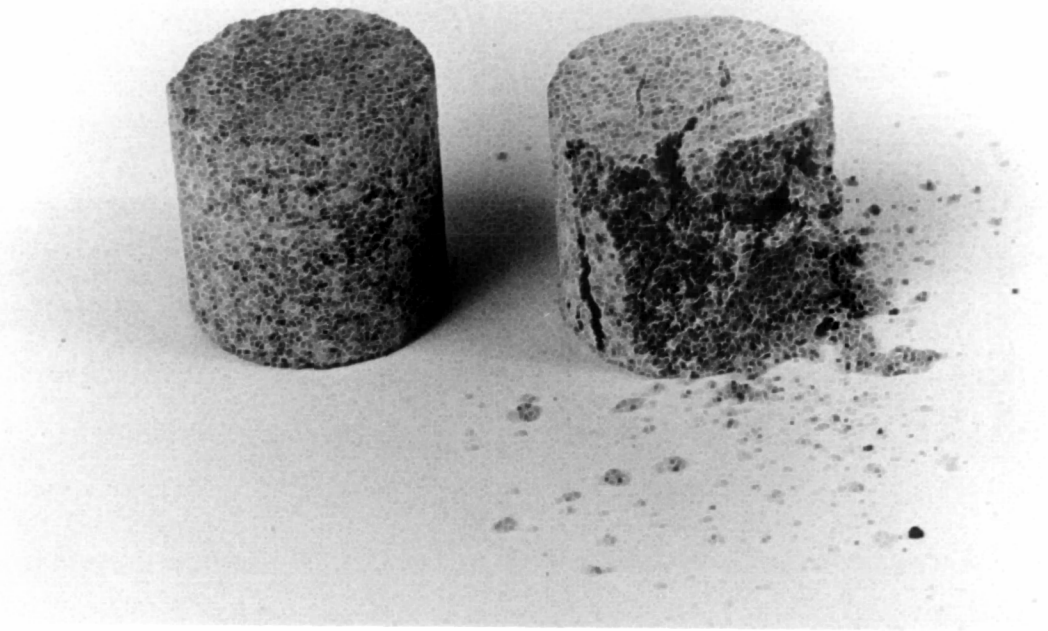

Fig. 3.12 :- Rock Cylinders used in Compression Strength Tests

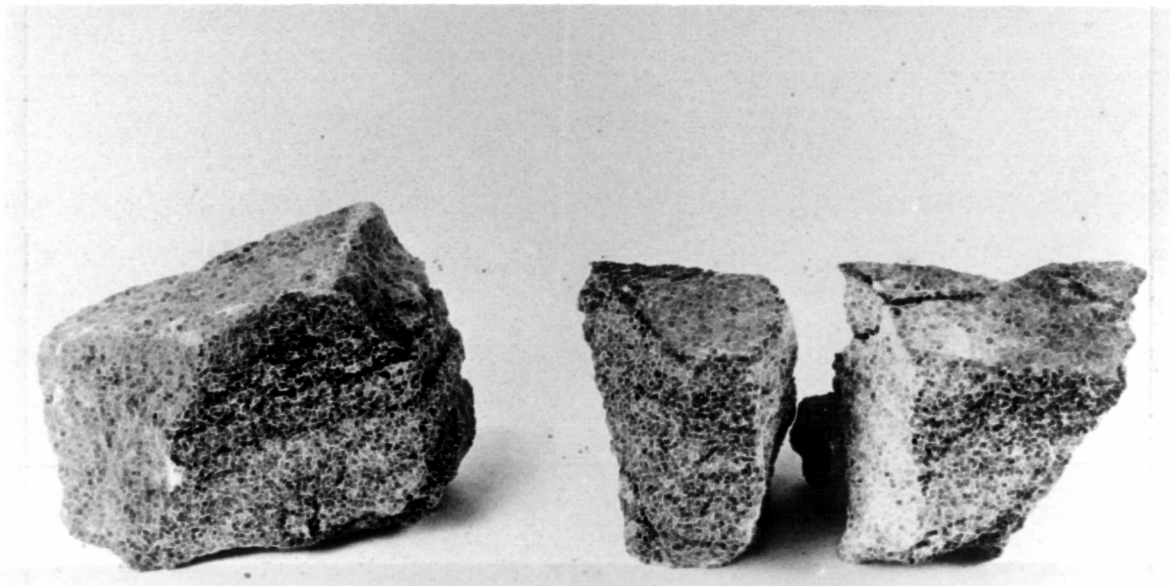

Fig. 3.13 :- Irregular Samples used in Hobbs Test

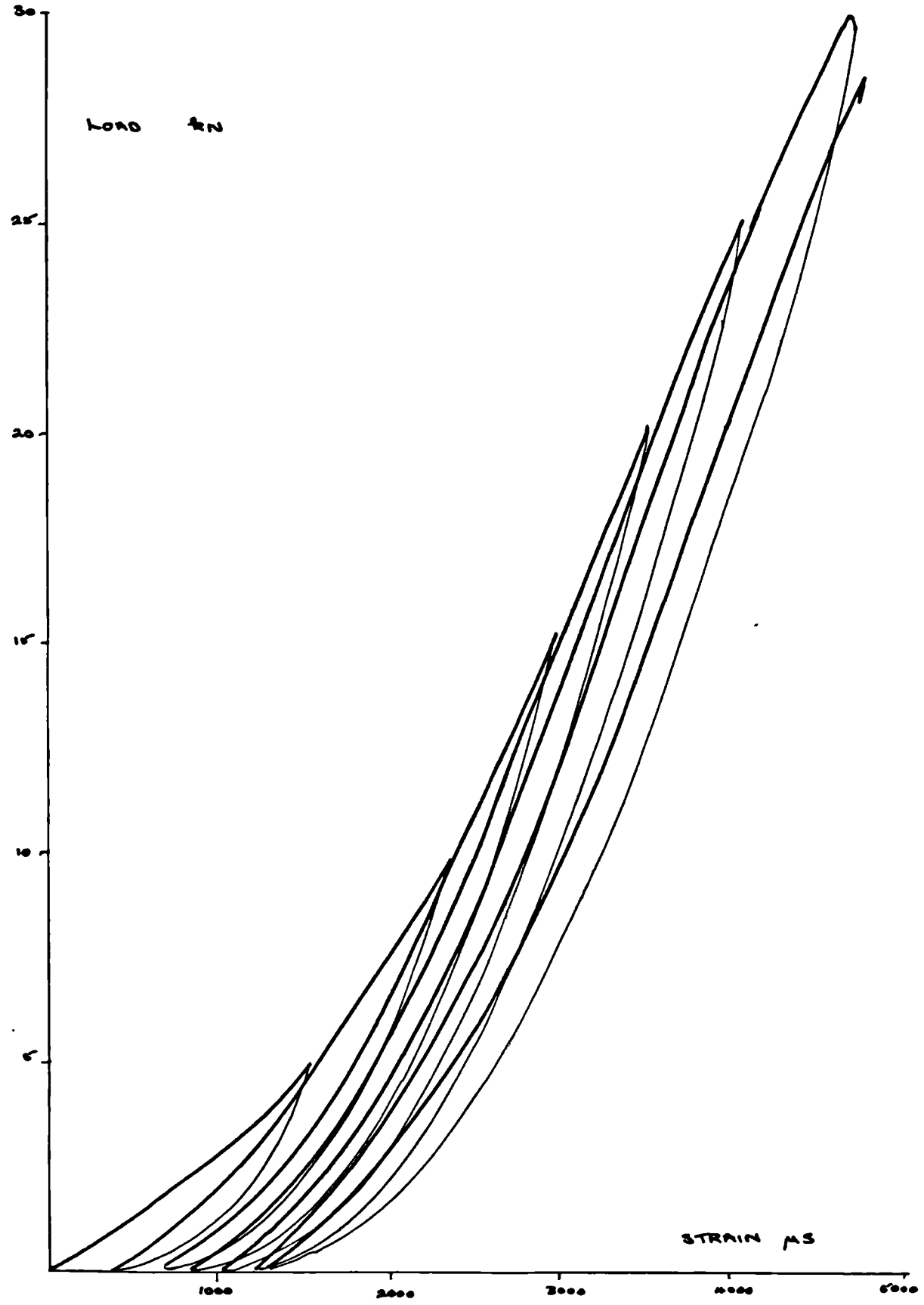

FIG. 3.14 :- LOAD v LONGITUDINAL STRAIN; SAMPLE 3

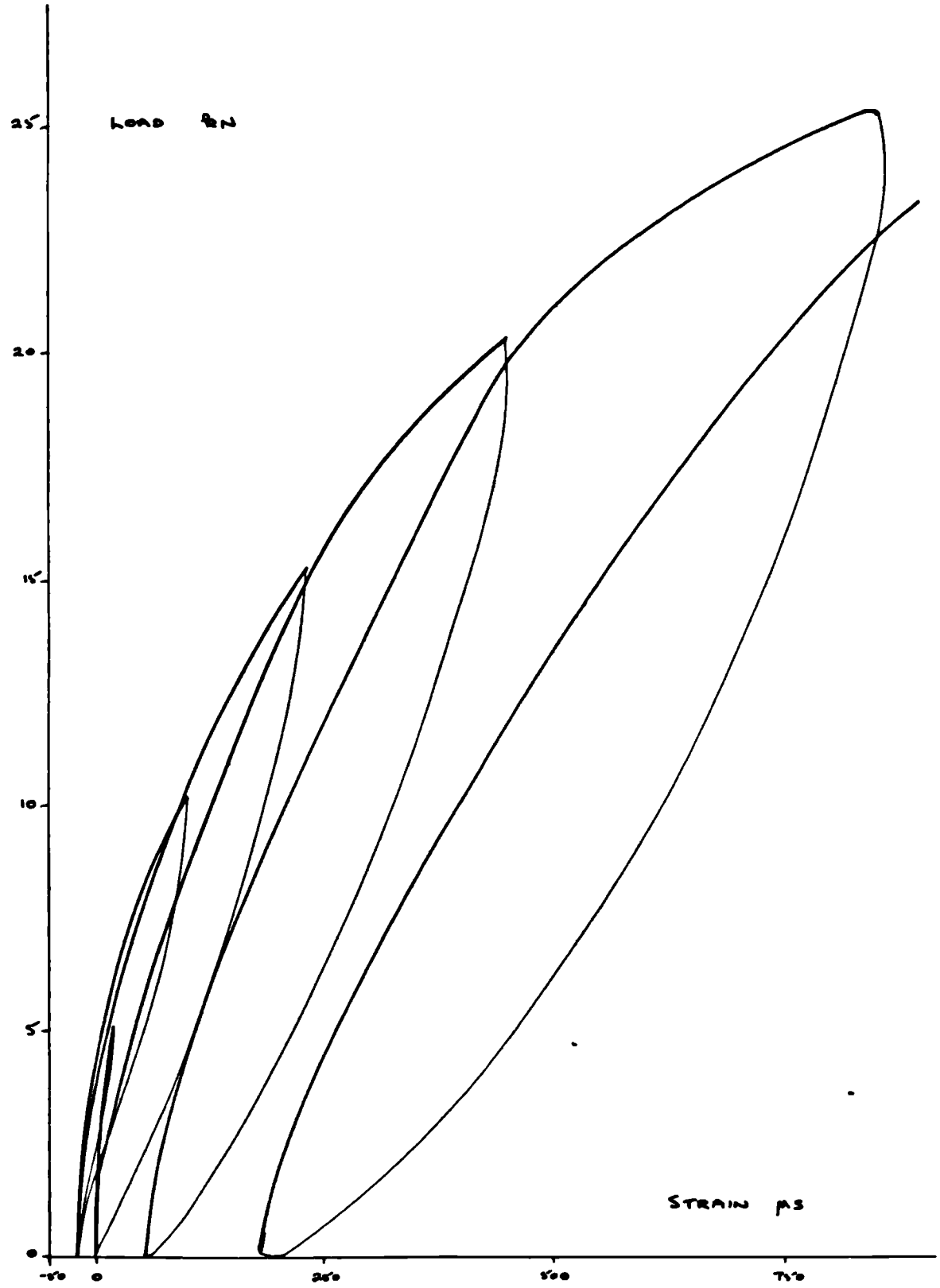

FIG. 3.15 :- LOAD v TRANSVERSE STRAIN; SAMPLE 3

Chapter 4

The Behaviour of Rock Contacts - the Load-Displacement Relationship

In considering granular media two approaches have usually been used. The first is concerned with the overall behaviour and considers the medium to be a continuum, whereas the second recognises the medium as having a structure determined by the particle arrangement. This second approach is usually used in computer models where the particles are considered to be spheres and properties (usually obtained from theoretical work) are ascribed to each contact, in order to predict overall behaviour under certain loading conditions.

The work presented in this chapter and in chapters 5 and 6 is an investigation of the behaviour of single point contacts between rock particles. The various parameters which might be expected to influence the behaviour have been considered and particular attention has been paid to the effect of saturation and drying. This experimental work provides a basis from which a model of contact behaviour can be developed and an insight into the significance of contact deformations in the overall behaviour of granular media. The work has concentrated on three topics.

(a) the load-displacement relationship
(b) the area of contact
(c) time-dependence

In each case only normal loading has been considered.

4.1 Theoretical Analyses of the Contact Problem

4.1.i Elastic Theory

The problem of determining the pressure distribution on the surface of contact of two elastic bodies, brought into contact by the application of known forces, was first solved by Hertz in 1881 (Hertz, 1886). He considered the application of a force normal to the plane of contact (fig. 4.1) and made the following assumptions:-

(a) Each body has isotropic elastic properties.

(b) The surface of each body may be represented by a quadratic function

(c) The area of contact is small compared with the other dimensions of the bodies - i.e. the problem is reduced to a plane problem.

(d) The surfaces of contact are perfectly smooth

(e) Body forces, temperature and inertia effects may be neglected

By comparing this problem with that of the distribution of electricity of a given potential on a plane Hertz showed that the area of contact was an ellipse with semi-axes a and b. He produced the following formulae to calculate the approach of the two bodies, d, and two parameters A and B.

$$d = \frac{P.D}{\pi} \int_0^\infty \frac{de}{\sqrt{(a^2 + e)(b^2 + e)\, e}}$$

$$A = \frac{P.D}{\pi} \int_0^\infty \frac{de}{(a^2 + e)\sqrt{(a^2 + e)(b^2 + e)\, e}}$$

$$B = \frac{P.D}{\pi} \int_0^\infty \frac{de}{(b^2 + e)\sqrt{(a^2 + e)(b^2 + e)\, e}}$$

Where P is the applied load and D a parameter calculated from the Young's modulus, E, and the Poisson's ratio,

$$D = \frac{3}{4}\left[\left(\frac{1 - \nu_1^2}{E_1}\right) + \left(\frac{1 - \nu_2^2}{E_2}\right)\right]$$

(subscripts 1 and 2 denote the body referred to)

A and B can be expressed in terms of the principal radii of curvature, R and R', of the bodies and the angle, ρ, between the planes containing these radii.

$$A + B = \frac{1}{2}\left(\frac{1}{R_1} + \frac{1}{R_1'}\right) + \frac{1}{2}\left(\frac{1}{R_2} + \frac{1}{R_2'}\right)$$

$$B - A = \frac{1}{2}\left[\left(\frac{1}{R_1} - \frac{1}{R_1'}\right)^2 + \left(\frac{1}{R_2} - \frac{1}{R_2'}\right)^2 + 2\left(\frac{1}{R_1} - \frac{1}{R_1'}\right)\left(\frac{1}{R_2} - \frac{1}{R_2'}\right)\cos 2\rho\right]^{\frac{1}{2}}$$

By manipulating these equations the values of d, a and b can be expressed more simply in terms of the complete elliptic integral of the first and second kind, K (k) and E (k), where k is the modulus and k' the complementary modulus.

$$d = 1.P^{\frac{2}{3}}\ D^{\frac{2}{3}}\ (A + B)^{\frac{1}{3}}$$

$$a = m.P^{\frac{1}{3}}\ D^{\frac{1}{3}}/\ (A + B)^{\frac{1}{3}} \qquad (4.1)$$

$$b = n.P^{\frac{1}{3}}\ D^{\frac{1}{3}}/\ (A + B)^{\frac{1}{3}}$$

where $m^3 = \frac{2}{\pi} \cdot \frac{E(k)}{k'^2}$

$$n^3 = \frac{2}{\pi} . k'\ E(k)$$

$$ln = \frac{2}{\pi} . k'\ K(k)$$

For the simple case of spherical bodies these equations reduce to very simple expressions and the values can be easily determined. If the bodies are not spheres then it is necessary to use iterative methods of solution.

The Hertzian approach to the contact problem is idealised by the assumptions made and its validity in real problems is questionable. Cattaneo (1947) extended the assumption of surfaces represented by quadratic functions to include fourth degree terms for two solids of revolution.

$$\text{Hertz}\quad zi = ai.r^2$$
$$\text{Cattaneo}\quad zi = ai.r^2 + bi.r^4 \qquad i = 1,$$

Storey (1968) has used a different approach to the same problem and compared the results of first and second order approximations for two spheres with different radii and two cylinders, one inside the other. It is concluded that for these cases the differences in results are negligible and can be ignored. Work by Goodman and Keer (1965) and Torvik (1967) has shown that extension of Hertz's theory to higher order approximations of the surface is inconsistant with the assumption of a plane problem. Torvik shows that the assumption of infinitesimal strains produces greater errors than that of quadratic surface functions for values of $a/R \leq 0.22$.

Goodman and Keer also show that for an extension of the Hertz theory to be made to large areas of contact then the radii of curvature must be of similar magnitude and of opposite sign.

The assumption of smooth surfaces avoids the problem of interfacial slip on the area of contact by ignoring the possibility of resistance to slip. If the bodies have similar elastic properties then the assumption is valid, since displacements of one body will be matched by equal displacements, in the same direction, of the other. Goodman (1962) has considered the variation of normal and shear stresses over the contact area of two rough spheres of different materials under normal loading. It is assumed that no slip occurs between two points of contact once they enter the area and that the normal displacements due to surface shears are negligible compared with those due to the normal loading. Experimental evidence is presented to support this latter assumption and theoretical work by Feng (1963) provides additional confirmation of its validity. From his analysis Goodman investigates the variation of the ratio of the shear and normal stresses at a point with the distance from the area's axis of symmetry. The ratio is approximately linear for distances of up to 80% of the area radius but increases rapidly at the area boundary as the stresses approach zero. Slip, therefore, takes place on an annulus at the boundary where the ratio exceeds the coefficient of friction. The width of this annulus is dependent upon the coefficient of friction and the difference in the elastic properties of the bodies.

4.1.ii Programme 'Contact'

In order to be able to compare the theoretical results from the Hertzian analysis with the experimental results a computer programme, 'Contact', was written. This consists of two sections, a simple circular area analysis (contact of spheres) and a general elliptical area analysis. This allows comparison of the analyses and gives an indication of the improvement in accuracy of prediction in using a general analysis.

While the circular area analysis integrals are easily reduced to the standard forms given below,

$$d = P^{\frac{2}{3}} D^{\frac{2}{3}} \left(\frac{1}{R_1} + \frac{1}{R_2} \right)^{\frac{1}{3}}$$

$$a = P^{\frac{1}{3}} D^{\frac{1}{3}} / \left(\frac{1}{R_1} + \frac{1}{R_2} \right)^{\frac{1}{3}} \qquad (4.2)$$

the general analysis equations contain complete elliptic integrals (4.1) and are solved by iterative methods. The elliptic integrals were generated by series approximation and Newton's iterative method used. A similar computer analysis has been carried out by Cooper (1969).

4.1.iii Linear Viscoelastic Theory

The theory developed by Hertz and other researchers deals with materials exhibiting only an initial instantaneous response to load. The ability of materials, such as rock, to exhibit time-dependent behaviour subsequent to this initial response has led to the development of theories which take this into account. Most of these problems can be solved by applying a Laplace transformation to the associated elastic problem to remove the time variable. The solution is then obtained in the transform parameter and the viscoelastic solution found by inversion. This method is only applicable if the boundary conditions do not vary with time and therefore cannot be used to solve contact problems.

Lee and Radok (1960) first produced a solution for a rigid sphere indenting a viscoelastic halfspace using 'functional equations', which involve replacing the elastic constants by partial differential operators. Their solution for the case of continuous indentation shows that the initial distribution of pressure over the contact area is similar to the elastic case. As time increases the distribution departs from the elastic solution but at the edges of the area a good agreement with the elastic case is maintained. This analysis is restricted to situations where the contact area is monotonically increasing.

Yang (1966) has used Lee and Radok's finding, that a viscoelastic solution can be directly obtained from the elastic solution subject to the increasing area restriction, to develop a solution for the general Hertz problem. The analysis is similar to that originally used by Hertz but includes time-dependent behaviour. The examples given reproduce the elastic solution at zero time before the time-dependent behaviour distorts the results.

4.1.iv Plastic Theory

In tribology research it has been discovered that surfaces are not smooth, even when polished, but have many irregularities

or asperities. The contact between two surfaces occurs only at the tips of these asperities (fig. 4.2) and this has led to the concept of real and apparent areas of contact. If these asperities are assumed to be spherical then it can be shown for metals (Bowden and Tabor, 1949) that plastic deformations occur under small normal loads in the contact regions. For tool steel it is calculated that full plasticity is reached at loads of 1.4×10^{-5} N for radii of 10^{-4} cm and 1.4 kN for radii of 1 cm. If the material is not work-hardening then the area of contact is proportional to the load,

$$\text{Area} \propto P$$

If work-hardening does occur then Bowden and Tabor suggest a relationship

$$\text{Area} \propto P^{n} \qquad \text{where } 0.8 < n < 1.0$$

Bowden and Tabor have also considered the indentation of a hard pyramid or cone into a softer half-space and vice versa. They conclude that in both cases for annealed or work-hardening metals that area is proportional to load.

Taking the case of a rigid perfectly plastic sphere indenting a rigid plate the relationship between the load applied and the approach, d, can be found (fig. 4.3) assuming d is small.

$$P \propto \text{Area}$$
$$P = Cr^2 \qquad \text{where C is a constant}$$

since $r^2 = R^2 - h^2$

$$P = C(R^2 - h^2)$$

and $h = R-d$

$$P = Cd\ (2R - d)$$

For an ellipsoid the area is an ellipse and the relationship is

$$P = Cd\ \left[(2R - d)(2R' - d)\right]^{\frac{1}{2}}$$

For the case of a cone or a four sided pyramid indenter, the relationship is

$$P = Cd^2$$

4.2 Sample Preparation

Two different sets of samples were tested, fig. 4.4

4.2.i Shaped Samples

These were prepared from 25 mm diameter, 25 mm length cylindrical cores, one end of each being shaped into a four sided pyramid using a lap wheel. Four apex angles were chosen as a rough guide to the amount of shaping needed - 160°, 140°, 110°, 80°. Each sample was photographed prior to testing to enable an accurate measurement of the apex angle to be made. The heights and diameters of each sample were also recorded.

4.2.ii Irregular Samples

To prepare these, lumps of rock were broken down into small pieces measuring about 50-75 mm. The pieces were given flat bases on which to stand using a circular saw and then photographed so that the contact angles and base areas could be measured. The heights were also recorded prior to testing.

In all the rock on rock tests the upper piece was a 25 mm diameter, 25 mm long cylinder. Samples were tested dry, saturated and saturated/surface dry, saturation being carried out for twenty-four hours before testing.

In practice contacts are very varied in their shapes, size and properties. The testing of irregular samples takes all these factors into account and allows general behaviour trends to be recognised. The testing of shaped samples, taken from the same block of material with constant contact angles and approximately equal heights and base areas, reduces the number of factors which need to be considered, allowing the influence of the remaining factors to be monitored. If the conclusions drawn from simple contacts are the same as those drawn from more complex ones, then a behaviour model can be developed on the basis of the simple

contact behaviour. This model may then be used for describing the behaviour of real contacts.

4.3 Angle of Contact

Theoretical solutions to contact problems for ellipsoids indicate that the principal radii in the contact region effect the behaviour. The results of the roundness studies of various fractions of the rockfill, described in chapter 3, indicate that this is an angular material. If the material had high roundness values (>0.4) e.g. river gravel then it would be possible to calculate principal radii values but this is not appropriate for angular particles. It is, therefore, necessary to define a 'contact angle' for particles with low roundness values, which is a measure of the shape of the contact region.

4.3.i Irregular Samples

The manner in which the contact angle is defined is shown in fig. 4.5. The contact angle, α, is the inclusive angle of lines drawn from the rock point to points on the rock surface equidistant from a line perpendicular to the rock piece base through the rock point.

The angle of contact is dependent on which section is taken through the sample point and it is necessary to select sections which may be considered typical. Two angles, α and α', were obtained from two photographs of each sample, the first looking along the major axis and the second perpendicular to this. Since the angle is also dependent on the distance x, three values of x were choosen, i.e. 1mm, 2 mm and 5 mm giving angles denoted $\alpha_1, \alpha_2 \alpha_5$ respectively. The mean value of α and α' is denoted as α_m.

4.3.ii Shaped Samples

In this case the angle is not dependent upon and there is no major axis. The angle of contact, β, is therefore defined as the maximum solid angle of the pyramid, fig. 4.6. This is, in fact, a special case of the irregular sample definition.

4.4 Details of Tests

In order to investigate the behaviour of single point rock

contacts under normal loading and to determine a load-deformation relationship, 20 shaped and 50 irregular samples were prepared. Details of these samples and the test conditions are given in Tables 4.4.1 and 4.4.2. The tests were carried out in the Instron 1195 testing machine and the rock pieces - an angular piece and a small cylinder - were placed between the steel platens so that the point of the angular piece was pressed against the centre of the end of the cylinder, fig. 4.7. The pieces were then subjected to load cycles, with the maximum load increasing on each cycle upto 5.0 kN, under a constant cross-head displacement rate of 0.2 mm/min. The displacements were monitored by a Boulton Paul (Sangamo) transducer and recorded on a Bryans X-Y plotter against the Instron load output. In testing the irregular samples the displacements were limited to 1 mm but this was increased to 3-4 mm for the shaped samples. A perspex tube was placed around the saturated samples and filled with water to ensure saturation during testing.

Approx Angle	No.	Conditions	Approx Angle	No.	Conditions
80^{o}	1	Dry, RoR	140^{o}	1	Sat. RoR
	2	Sat. RoR		2	Dry RoP
	3	Dry RoP		3	Dry RoR
	4	Dry RoR		4	Dry RoR
	5	Dry RoP		5	Dry RoR
110^{o}	1	Dry RoP	160^{o}	1.	Dry RoP
	2	Dry RoR		2	Dry RoR
	3	Sat. RoR		3	Sat. RoR
	4	Dry RoR		4	Sat. RoR
				5	Dry RoR
				6	Dry RoR

Table 4.4.1 Details of tests - Shaped Samples

Key:- RoR Rock on Rock
RoP Rock on Platen (steel)

Conditions	Block	Nos.
Dry, Rock on Rock	H	1-10
	F	11-15
Dry init. Rock on Rock Saturated later	D	16-20*
Saturated, Rock on Rock	B	21-25
	F	26-30
	G	31-40
Saturated/Surface dry, Rock on Rock	A	41, 42
	C	43-45
	E	46-50

Table 4.4.2 Details of tests - Irregular Samples

* Due to operator difficulties, sample 20 not saturated

4.5 Test Results

4.5.i Irregular Samples

(a) General behaviour

Figs. 4.8-13 show the load displacement curves of 6 typical irregular sample tests under the three test conditions. Fig. 4.14 gives an idealised curve shape based on all the test curves. The curves become quite complex in the latter stages of the tests, and hence several possible 'paths' have been drawn.

The load-deformation curve can be divided into two sections. The initial behaviour is that of a work-hardening material showing an increasing gradient. At some point the 'smooth' curve ceases and is replaced by more complex behaviour which is introduced either by a fall in load or a decrease in gradient. In this research this point is referred to as the 'Damage Load'. This point should not be confused with any minor unsettled behaviour at the start of the test.

The observed mechanism of failure at the contact is a brittle material showing crushing and tensile fracturing, in the form of splitting and spalling, determined by the weaknesses and imperfections in the rock at the contact. This is seen more frequently once the Damage Load has been reached. A study of the unloading/ reloading curves shows that deformation is not reversible although

an element of elastic behaviour is present. This elastic behaviour probably stems from strains being relieved within the mass of the particles rather than at the contact. This behaviour contrasts with the elastic models usually used to describe contact behaviour.

A number of the samples were subjected to cycling to the same load once the limit of 1 mm was reached, e.g. fig. 4.13. With the exception of one sample, 38, these 15 samples exhibited work-hardening. The additional displacements at the maximum load (1.0 kN) on the first cycle vary from 0.023 to 0.063 mm and reduce to 0.013 mm after about four cycles. The magnitude of these displacements do not appear to depend on the maximum cycle load or the test conditions. It seems likely that the magnitude depends on the stability of the contact region and the history of loading. Sample 38 work-hardens initially but then shows increasing additional displacements indicating the rock point was approaching failure.

(b) Inundation during testing

The graphs of the four samples, 16-19, saturated during testing are shown in figs. 4.15-18 and these show that the saturation causes additional displacements on reloading (see samples 16, 18 and 19 particularly). During the slow, steady saturation the rock points were observed and in the case of sample 16 rock particles were displaced from the area of contact. This would cause additional displacements on reloading as the area of contact would need to be built up to its previous value. However, no displacement of particles was noted for the other samples and the additional displacements are probably due to strength loss through saturation.

(c) Unloading/Reloading behaviour

As has already been noted, the unloading curves exhibit the presence of small elastic strains. The reloading curves are similar to the unloading curves and produce hysteresis loops, passing close to the point of unloading before apparently returning to the original curve. The unloading/reloading curves are similar inspite of the point of unloading and whether or not the Damage Load has been reached, indicating that the contact is

not the source of the elastic rebound. Saturation appears to reduce the gradients of these curves slightly.

4.5.ii Shaped Samples

(a) General behaviour

Figs. 4.19-22 show the load-displacement curves produced from the shaped sample tests. In reproducing these the unloading/reloading curves and any minor deviations have been omitted. The curves have been grouped according to the angle of contact, β, of the samples i.e. $\beta \simeq 80^{\circ}$, 110°, 140°, 160°.

In fig. 4.19 all the curves reach the Damage Load at a low displacement ($\simeq$ 0.1 mm) and exhibit complex behaviour after this. Sample 3, a rock on platen test, is different from the others and reaches relatively high loads but sample 5, another rock on platen test, has very similar behaviour to the dry rock on rock tests. Initially there appears to be little difference between the saturated sample, 2, and the dry samples but under higher displacements lower loads are achieved. In the second group of curves ($\beta \simeq 110^{\circ}$, fig. 4.20) the rock on platen test curve agrees very well with the rock on rock curves but the saturated sample, 3, shows distinct behaviour being noticeably lower than the rest. Although these curves are a little smoother than the first set, the Damage Load is reached at a similar displacement.

The curves in fig. 4.21 are much smoother than those for smaller angles of contact and the Damage Load is reached at a displacement of approximately 0.4 mm. As before there is no difference in the rock on platen and rock on rock curves but the saturated sample, 1, shows no distinct behaviour either. In the final group of curves ($\beta \simeq 160^{\circ}$, fig. 4.22) the effect of saturation is very noticeable reducing the loads to approximately half those of the dry tests.

The above points can be summarised as follows:-

(i) the displacement at which the Damage Load is reached increases with contact angle.

(ii) rock on platen tests can be considered to be similar to rock on rock tests.

(iii) as the angle of contact increases local failures are less frequent and become progressive rather than sudden in nature.

(iv) saturation may reduce the loads a rock point is able to carry.

The load-displacement curves display the behaviour seen in the irregular sample tests, with an initial smooth curve followed by complex behaviour after the Damage Load has been reached. Crushing and tensile fracture at the point of contact were also noted during loading of the samples. Similar conclusions can be drawn from the unloading/reloading curves as noted for the irregular samples.

(b) Influence of contact angle

In figs. 4.23-26 the curves for the dry, rock on rock tests have been reproduced again to illustrate the similarity in behaviour of samples with similar contact angles. It is clear that tests of this type will produce consistent results and it is only necessary to carry out a few tests in order to provide a basis from which models of contact behaviour can be produced. From these curves simplified mean curves have been constructed and compared in fig. 4.27. This shows the manner in which the load-displacement relationship of a single, dry rock point being pressed into a flat rock surface may be expected to vary with its angle of contact. The load-displacement curve equivalent to a Young's modulus of 10 kN/mm for a cylinder, 50 mm long and 25 mm in diameter, has also been included. This is effectively a rock on platen test for a contact angle of 180^{o} and can be seen to be quite consistent with the test results.

Fig. 4.27 also shows the point of failure of the lower rock piece for the three larger contact angles. None of the samples with angles of contact of 80^{o} failed under the displacements imposed. Fig. 4.28 illustrates the two modes of tensile splitting - three or four way - noted after the tests.

4.6 The Significance of the Damage Load

4.6.i Variation with Contact Angle

The values of the Damage Loads were measured from all the load-displacement graphs and plotted against the mean contact angle of each piece. Additional data (presented in chapter 5) from rock on platen tests of irregular samples was also plotted. A ranking analysis of the α_m values with the loads indicated no significant relationship and these graphs were not plotted. All

the graphs (figs. 4.29-36) show the general trend of increasing Damage Load with increasing mean contact angle.

(a) Rock on platen tests

A comparison of the dry and saturated rock on rock (figs. 4.31-34) with the rock on platen results (figs. 4.29-30) for both the $\alpha_2 m$ and $\alpha_3 m$ angles indicates that the rock on platen Damage Loads are slightly greater for the same angles. This conclusion is not bourne out by the dry, shaped sample values which are similar for both conditions. The main difference in the graphs is at angles below 110° where the rock on rock values are lower.

(b) Effect of saturation

For contact angles greater than 100° saturation reduces the Damage Load but below this figure there is no significant difference in the results. This suggests that breakage of the small angle contact is mainly dependent upon the angle, whereas breakage of the large angle contact is influenced by the reduction in strength caused by saturation. The same conclusion can be drawn from the results for saturated/surface dry samples (figs. 4.35 and 4.36).

(c) Comparison of $\alpha_2 m$ and $\alpha_3 m$

Since irregular samples have been assigned three angles of contact, it is necessary to assess which of these is most representative of the rock point. As already noted the $\alpha_1 m$ values were not found to be representative and were not plotted.

A study of the rock on platen results show that the shaped sample points form an upper bound to the irregular sample points in the $\alpha_2 m$ graph with one 'wild' result. In the $\alpha_3 m$ graph the shaped and irregular sample results are more mixed and the 'wild' result is absorbed into the spread of points. In the dry rock on rock graphs the $\alpha_2 m$ points are more dispersed than the $\alpha_3 m$ points and again form an upper bound of the shaped sample results. These comparisons indicate that α_3 and α_3' are more representative of the dry samples. The opposite conclusion is reached in a study

of the saturated test results as the $\alpha_1 m$ values have a greater spread at large angles. A similar trend is seen in the saturated/surface dry graphs.

These comparisons do not lead to any real conclusion as to which of these angles is the more representative. It is possible that saturation does influence this choice although it may indicate that an angle between $\alpha_2 m$ and $\alpha_1 m$ should have been measured.

4.6.ii Variation with Height and Base Area

These parameters were measured prior to each test as they could be factors influencing the results which are not encountered in real situations but result from the preparation and testing procedure. The shaped samples have equal base areas and heights thus avoiding this problem.

Ranking the irregular sample results with the measurements does not appear to produce a good correlation of either height or base area with the Damage Load. In some sets of results correlations may be seen but these are not general trends. Since the shaped sample results fit in very well with those of the irregular samples, this suggests that the contact angle is more important and that the influence of these parameters is minimal.

4.6.iii Variation from Block to Block

This has been investigated on the grounds that particles from the same block should have similar strengths and hence form a consistent 'Damage Load - contact angle' relationship. However, good trends noted in $\alpha_2 m$ graphs are not necessarily seen in $\alpha_1 m$ graphs, and vice versa, which makes it difficult to reach any firm conclusion. A more definite result could be reached by comparing strength values and 'Damage Load - contact angle' curves for different types of rock.

4.7 The Initial Curve

The curve upto the Damage Load is a work-hardening curve with a smooth change in gradient. The curves were analysed using a best straight line technique to describe a curve of the form

$$d = \eta P^{\lambda}$$

This analysis was carried out on both shaped and irregular samples, although it was not possible to analyse all the curves because of low Damage Loads. The shaped sample curves with contact angles of approximately 80° and 110° were not analysed for this reason.

Condition	No.	$\alpha_{im}^{\cdot}$	$\alpha_{im}^{\cdot}$	$\alpha_{im}^{\cdot}$	η	λ
Dry,	1	145.9	142.1	128.7	0.398	0.785
Rock	2	146.4	141.6	120.8	0.854	0.699
on Rock	6	167.3	151.0	110.2	0.929	0.723
	7	142.7	148.8	119.8	0.319	0.540
	8	172.5	151.0	120.7	0.341	0.546
	9	169.3	142.7	120.8	0.361	0.620
	10	135.0	130.0	134.0	0.683	0.772
	13	154.8	137.8	125.6	0.418	0.687
	15	169.3	156.6	138.0	0.286	0.866
	16	127.9	118.0	104.5	0.355	0.774
	18	168.5	157.0	117.7	0.234	0.626
Sat.	21	137.1	139.5	119.6	0.573	0.805
Rock	22	167.6	153.3	119.3	0.840	0.641
on Rock	25	133.6	126.0	132.5	0.431	0.637
	27	156.5	137.4	125.9	0.444	0.687
	28	143.0	134.5	127.8	0.436	0.792
	32	128.8	130.3	146.3	0.824	0.719
	33	167.0	158.5	146.0	0.303	0.601
	35	141.8	129.8	113.2	0.402	0.734
Sat/surface	42	132.2	141.3	134.8	0.694	0.672
dry,	46	130.3	130.8	113.1	0.870	0.845
Rock on	48	129.8	126.7	113.0	0.765	0.651
Rock	49	135.8	119.7	101.0	0.576	0.596
	50	170.8	155.0	150.5	0.505	0.591

Table 4.7.1 Irregular Samples - calculated η and λ values

Condition	Approx. Angle	No.	β°	η	λ
Dry, Rock on Rock	140°	3	142.3	0.261	0.617
		5	133.5	0.389	0.704
	160°	2	162.3	0.191	0.633
		5	162.9	0.156	0.624
		6	167.7	0.175	0.646
Dry, Rock on Platen	140°	2	137.6	0.277	0.697
	160°	1	162.4	0.152	0.602
Sat. Rock on Rock	140°	1	137.2	0.316	0.629
	160°	3	156.5	0.369	0.564
		4	164.7	0.339	0.636

Table 4.7.2 Shaped Samples - calculated η and λ values.

The results of this analysis are presented in Tables 4.7.1 and 4.7.2 and the λ values summarised in Table 4.7.3. The results show that the mean λ values lie between 0.6 and 0.7 irrespective of the conditions of testing. Saturation does not effect the results and does not increase or decrease the scatter. The shaped and irregular samples show the same range of values indicating that this index is independent of the contact angles, base areas and heights. For all the curves analysed the correlation coefficients of the points were greater than 0.98 and the majority greater than 0.997.

	Condition	No. of Samples	Mean λ	Standard Deviation
Shaped	Dry, RoP	2	0.650	0.067
	Dry, RoR	5	0.645	0.035
	Sat. RoR	3	0.610	0.040
Irregular	Dry, RoR	11	0.694	0.103
	Sat. RoR	8	0.702	0.074
	Sat./sur dry RoR	5	0.671	0.103

Table 4.7.3 Summary of λ values

Having determined experimentally a mean value for λ, it is interesting to compare this with theoretical solutions of the

contact problem. The index value of 2/3 predicted by Hertz is within the range of λ values calculated and there is good agreement in the form of the equations. This conclusion is supported by Penman's work (1971) on experiments carried out by Rzadkowski and Zurek (1970).

The Hertz equation (4.2) for a sphere on a plane indicates that the cube of the approach is inversely proportional to the sphere radius for a given load. If the contact between angular rock particles exhibits Hertzian behaviour then an inverse relationship between the approach and the contact angle would be expected. Fig. 4.27 shows that as the contact angle of the shaped samples is decreased the displacements, generated by loads less than the Damage Load, increase. The variation of η with the contact angle, β, for both the dry and saturated shaped sample tests is shown in fig. 4.37. The dry samples show very clearly the expected behaviour but the saturated results do not suggest a similar relationship. Although the 160° samples show that saturation increases the value significantly, this is not as marked for the 140° samples.

The irregular sample results do not produce any firm conclusions and there is no indication that saturation increases η. Inverse relationship trends between η and α_m noted for one angle are not necessarily seen for the other angles or test conditions and the dependence may alter from one angle to another for ranges of η. This confused picture stems from the varying contact shapes of each sample, making it difficult to select a particular angle to represent the shape under all the different test conditions. It is worth noting that a distinct inverse relationship of η with the α_{1m} values for the saturated/surface dry samples and the α_{sm} values for the saturated samples can be seen. For η values below 0.45 the relationship with the α_{2m} values of the dry samples correlates well with the shaped sample results.

4.8 Conclusion

Although the descriptions of the irregular and shaped sample results have been dealt with seperately in this chapter, it is clear that they are similar. Both exhibit the two distinct types of behaviour before and after the Damage Load and similar failures and crushing modes can be observed. The analyses of the Damage Load and initial curves show that the shaped sample results

are representative of the irregular sample results. This implies that models of contact behaviour can be obtained from testing a few shaped samples and that each contact shape may be described by a single contact angle.

The initial curve is a work-hardening curve but the behaviour is more complex after the Damage Load has been reached as crushing and local failure occur more readily. Analysis has shown that this initial curve could be modelled by use of an expression of the form

$$d = \frac{C}{\beta^n} \cdot P^{\frac{2}{3}} \qquad (4.3)$$

where C and n are constants. Alternatively use could be made of Hertz's theoretical solution for an elastic sphere on an elastic halfspace, which has a similar form to (4.3), by replacing the angle with an equivalent radius. This would have the advantage of describing the load-displacement behaviour of particles over the whole range of roundness values. It is not clear why behaviour which is not elastic may be described by an elastic solution. Gillam (1969) notes that the Hertz analysis predicts that brittle materials will fail at the boundary of the contact area under tensile stresses which is the behaviour observed during the tests.

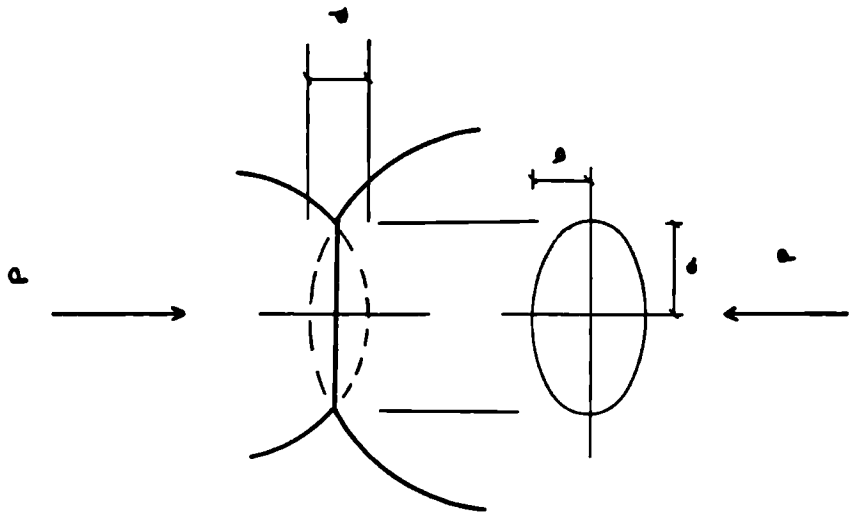

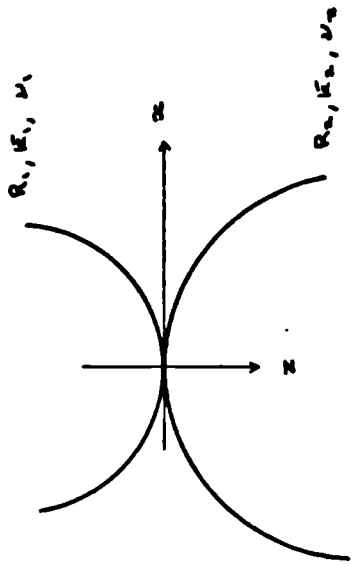

FIG. H.1 :- CONTACT OF ELLIPSOIDS UNDER NORMAL LOAD

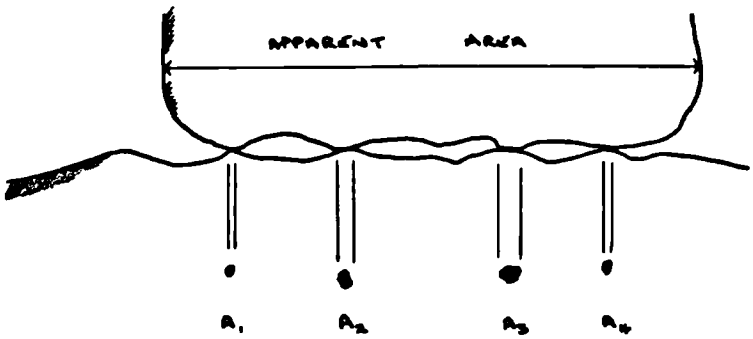

REAL AREA = $\sum_{1}^{4} A_i$

FIG. 4.2 :- CONTACT OF 'FLAT' SURFACES

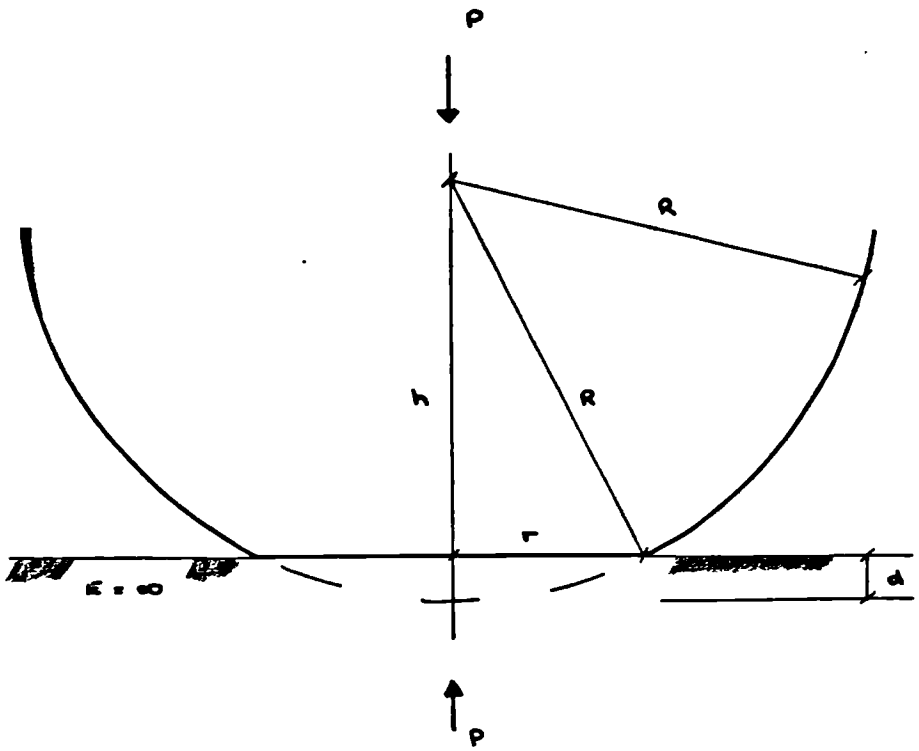

FIG. 4.3 :- CONTACT OF A RIGID PERFECTLY PLASTIC SPHERE WITH A RIGID PLATE

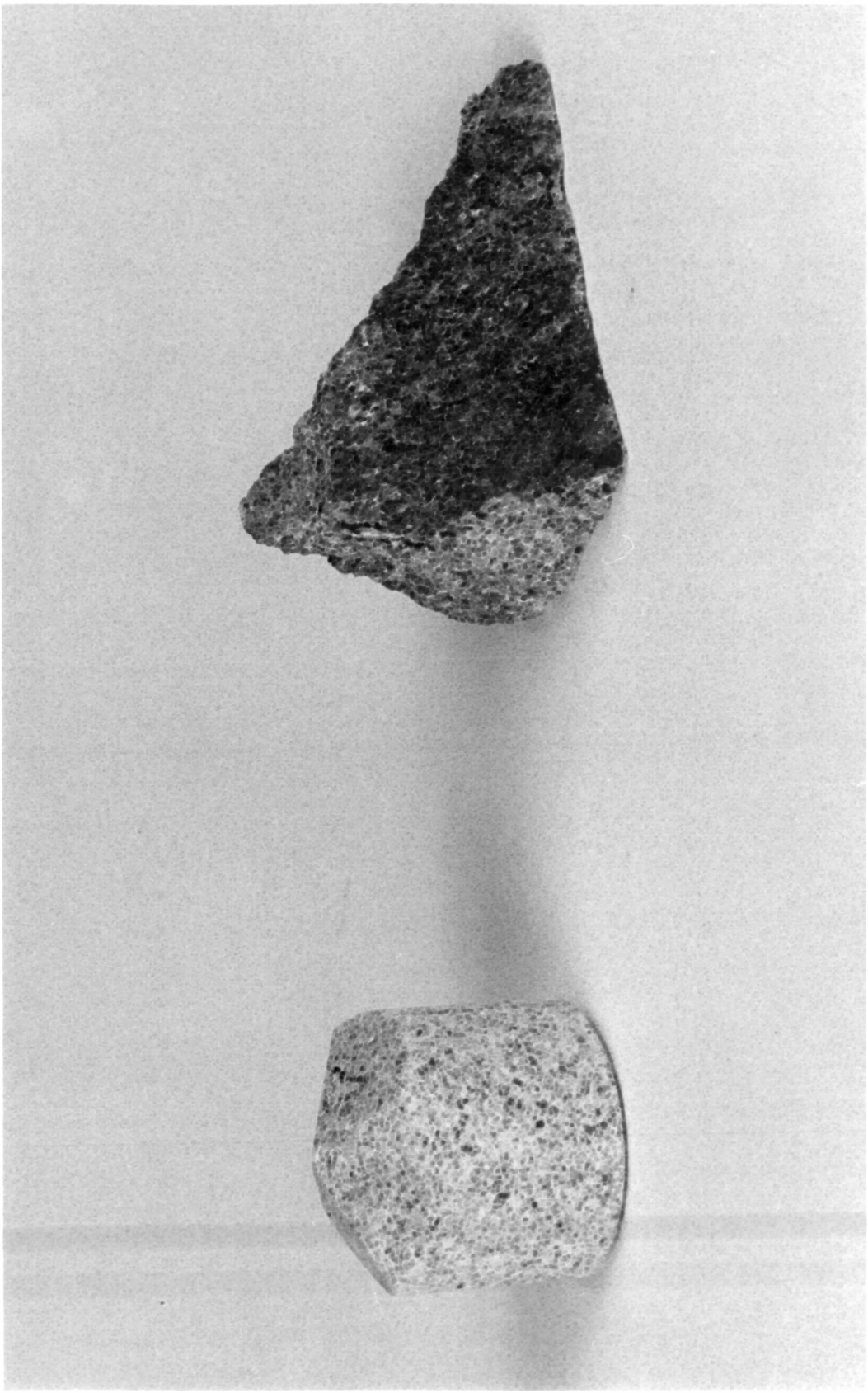

Fig. 4.4 :- Shaped and Irregular Test Samples

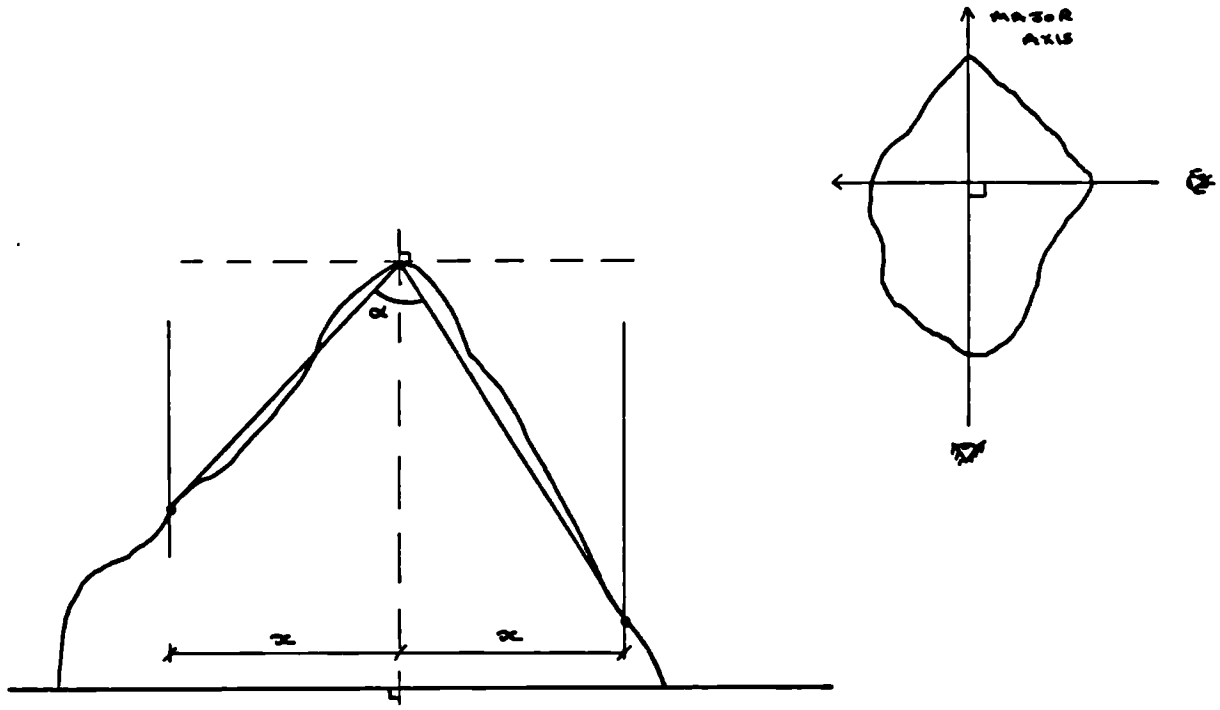

FIG. 4.5 :- ANGLE OF CONTACT, α - IRREGULAR SAMPLE

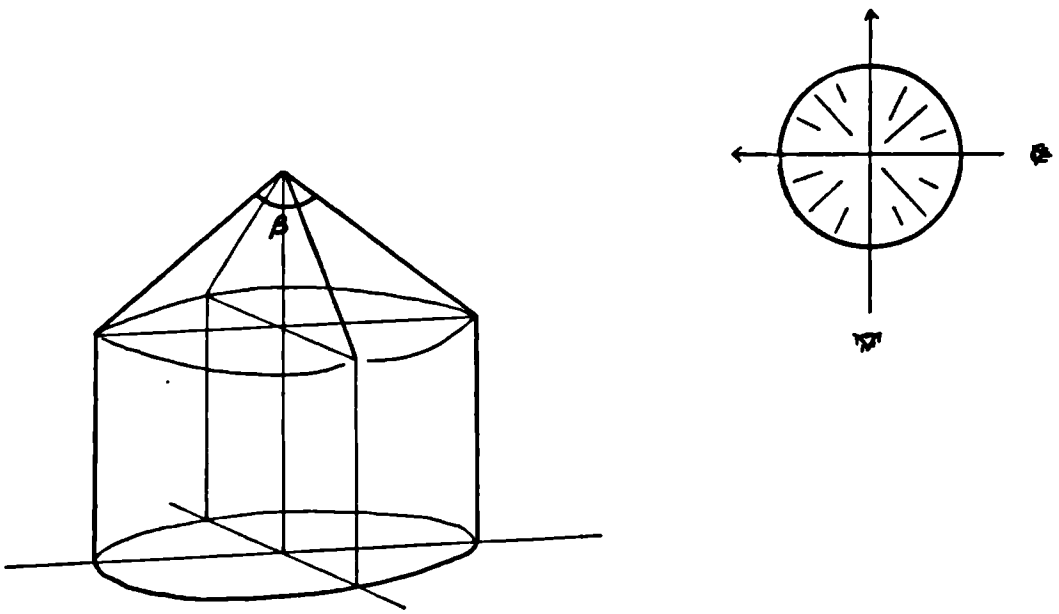

FIG. 4.6 :- ANGLE OF CONTACT, β - SHAPED SAMPLE

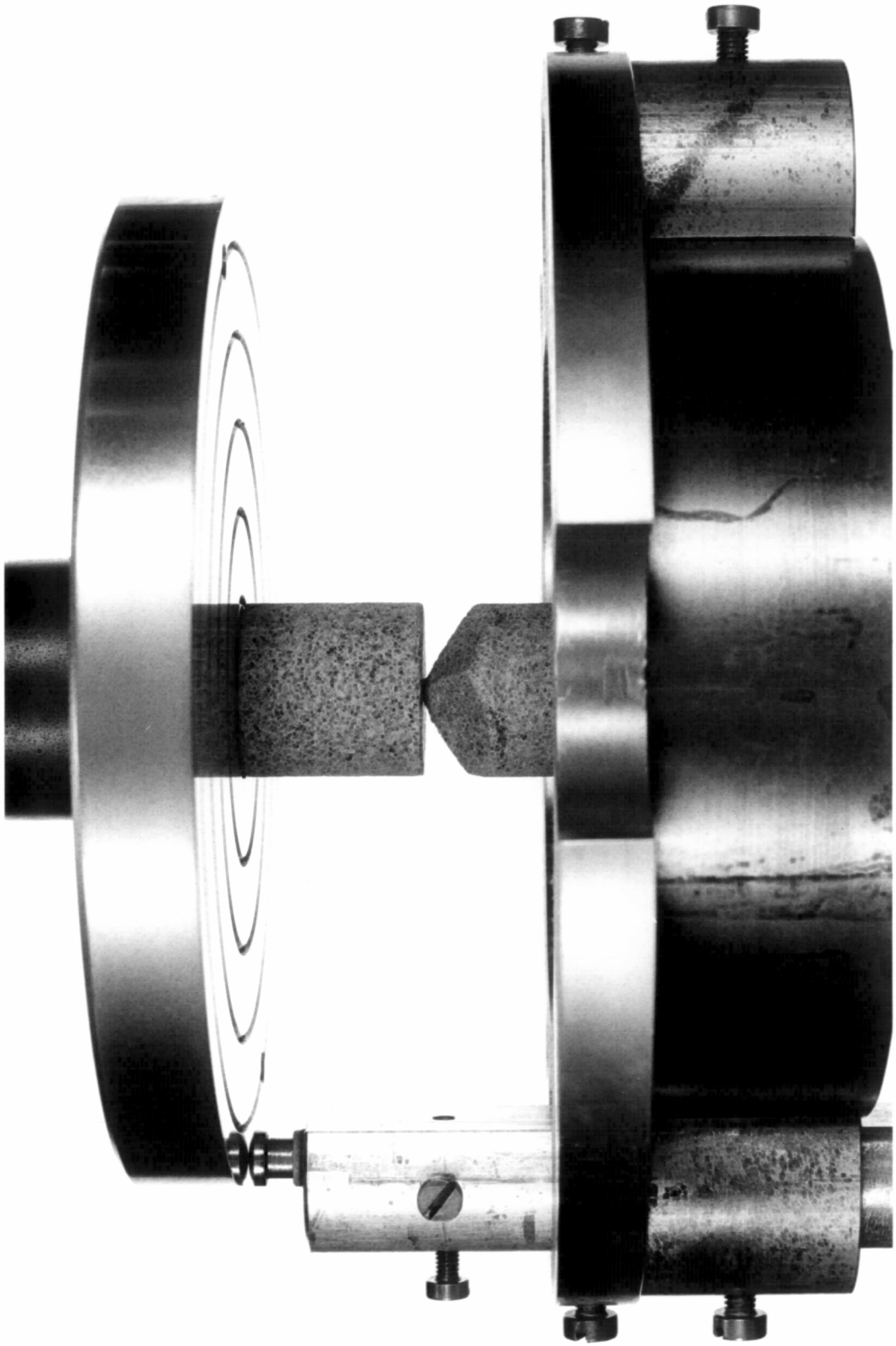

Fig. 4.7 :- Experimental Set-up for investigating Behaviour of Rock Contacts

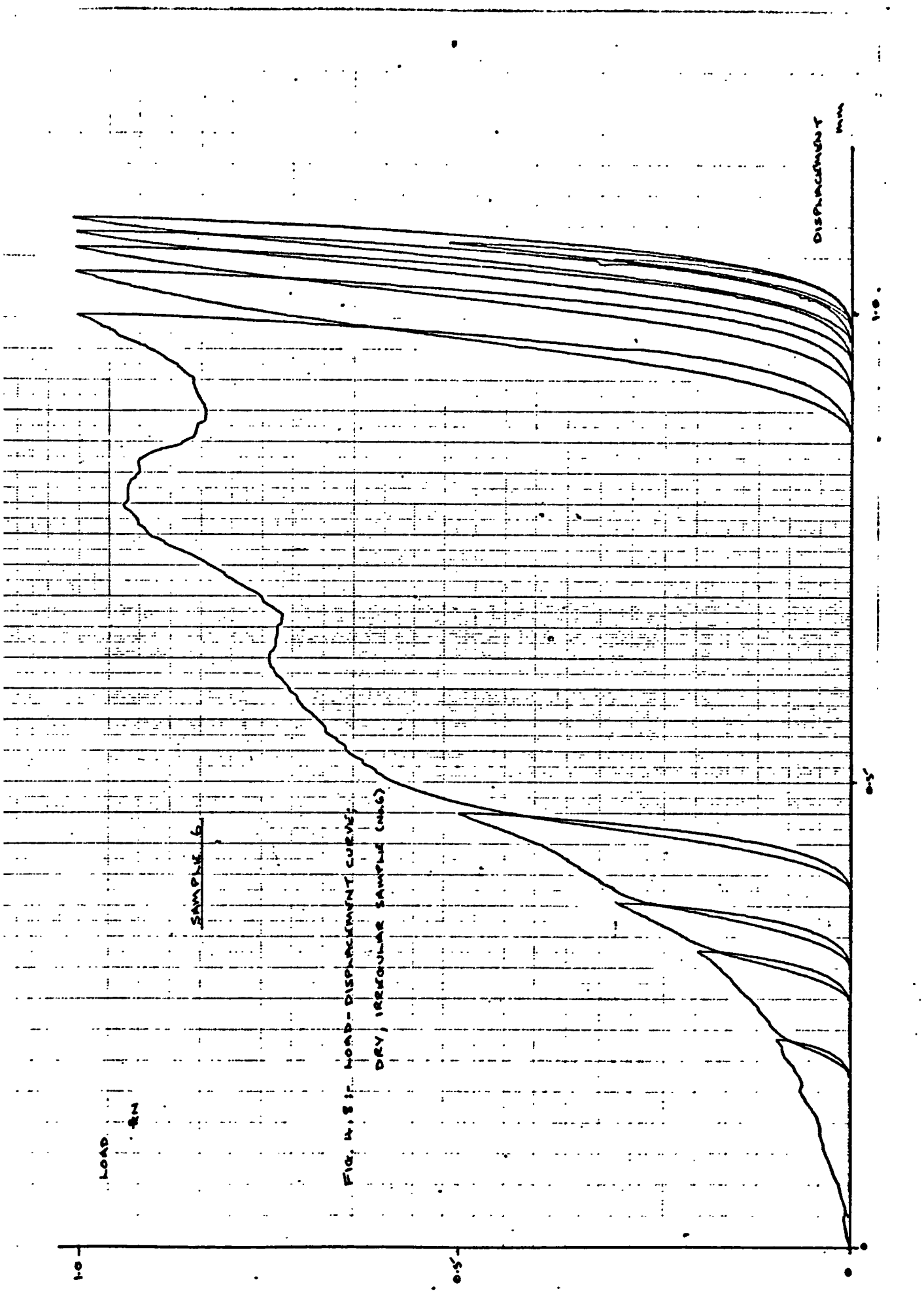

FIG. 4.3 : LOAD-DISPLACEMENT CURVE; DRY, IRREGULAR SAMPLE (NO.6)

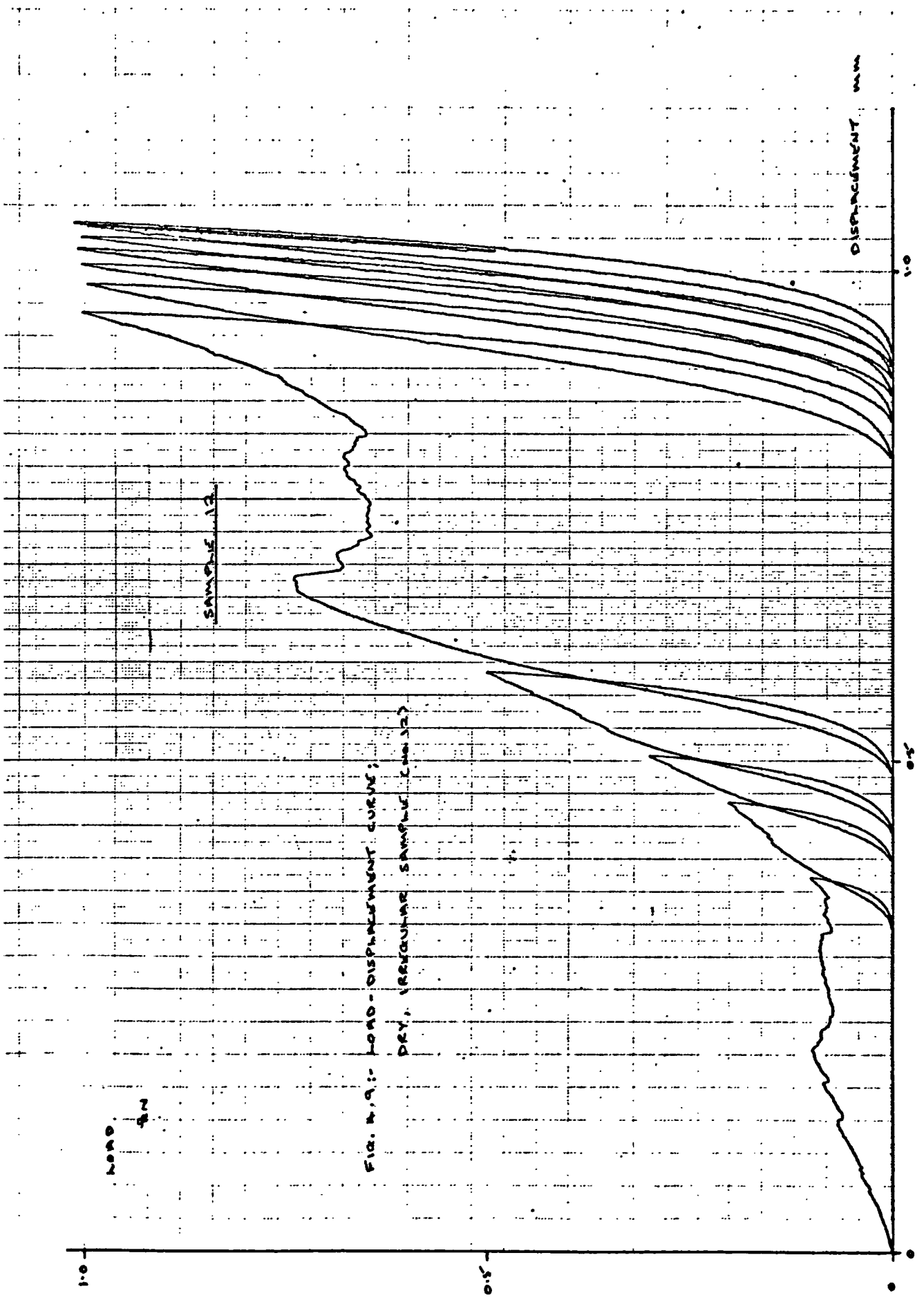

FIG. 4.9:- LOAD-DISPLACEMENT CURVE: DRY, IRREGULAR SAMPLE (No. 12)

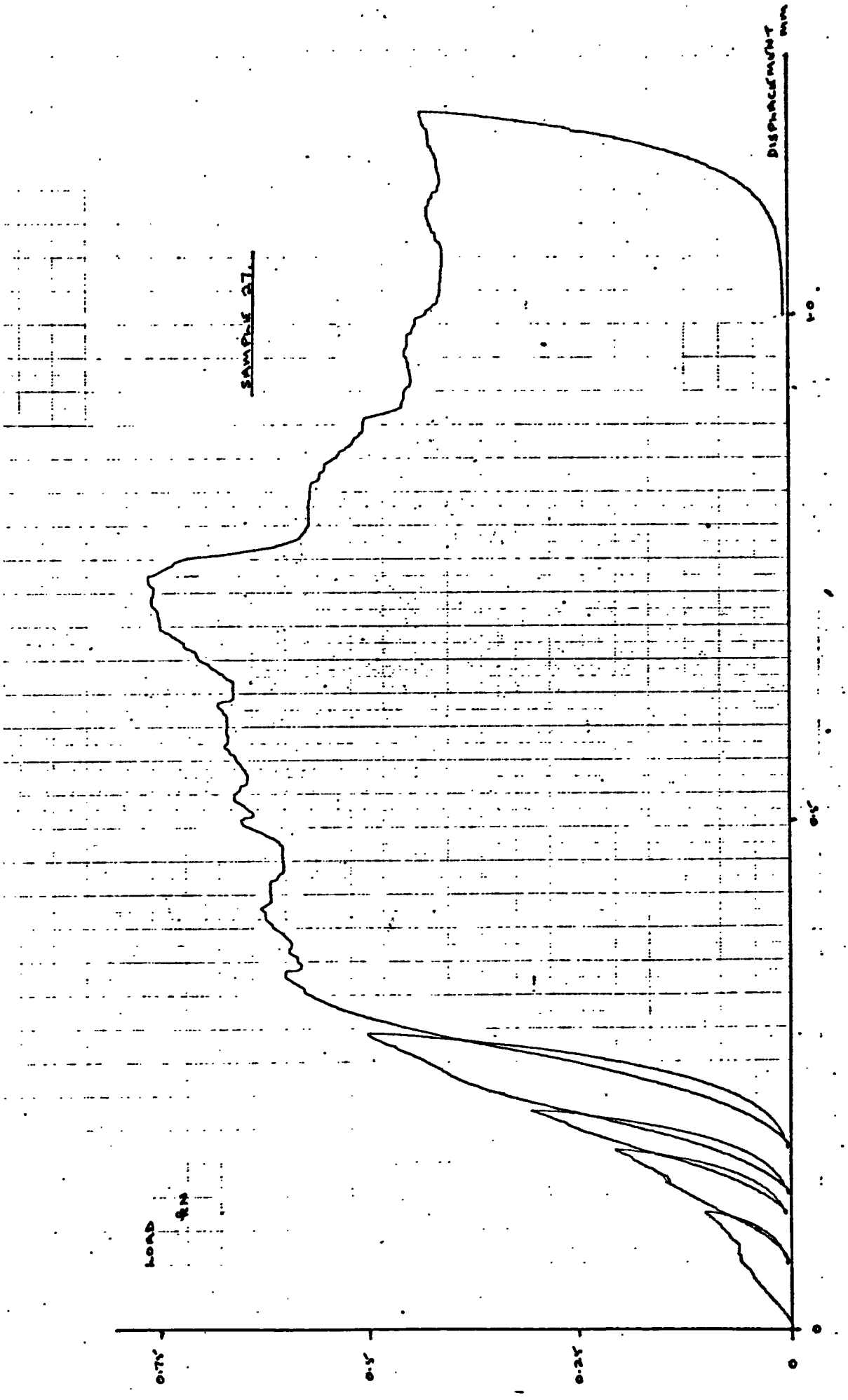

FIG. 4.10 :- LOAD - DISPLACEMENT CURVE ; SATURATED, IRREGULAR SAMPLE (No. 27)

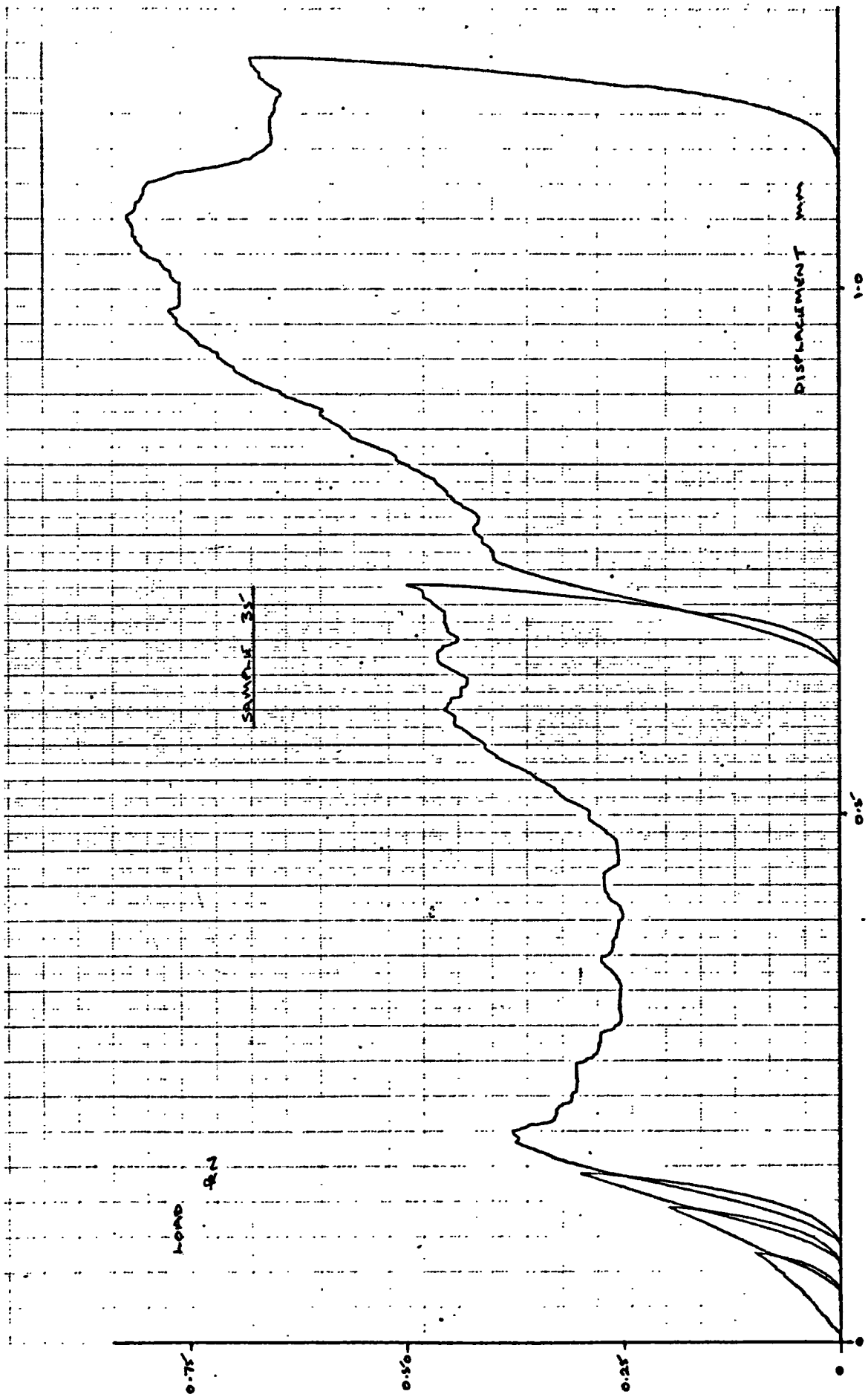

FIG. 4.11 :- LOAD - DISPLACEMENT CURVE ; SATURATED, IRREGULAR SAMPLE (NO. 35)

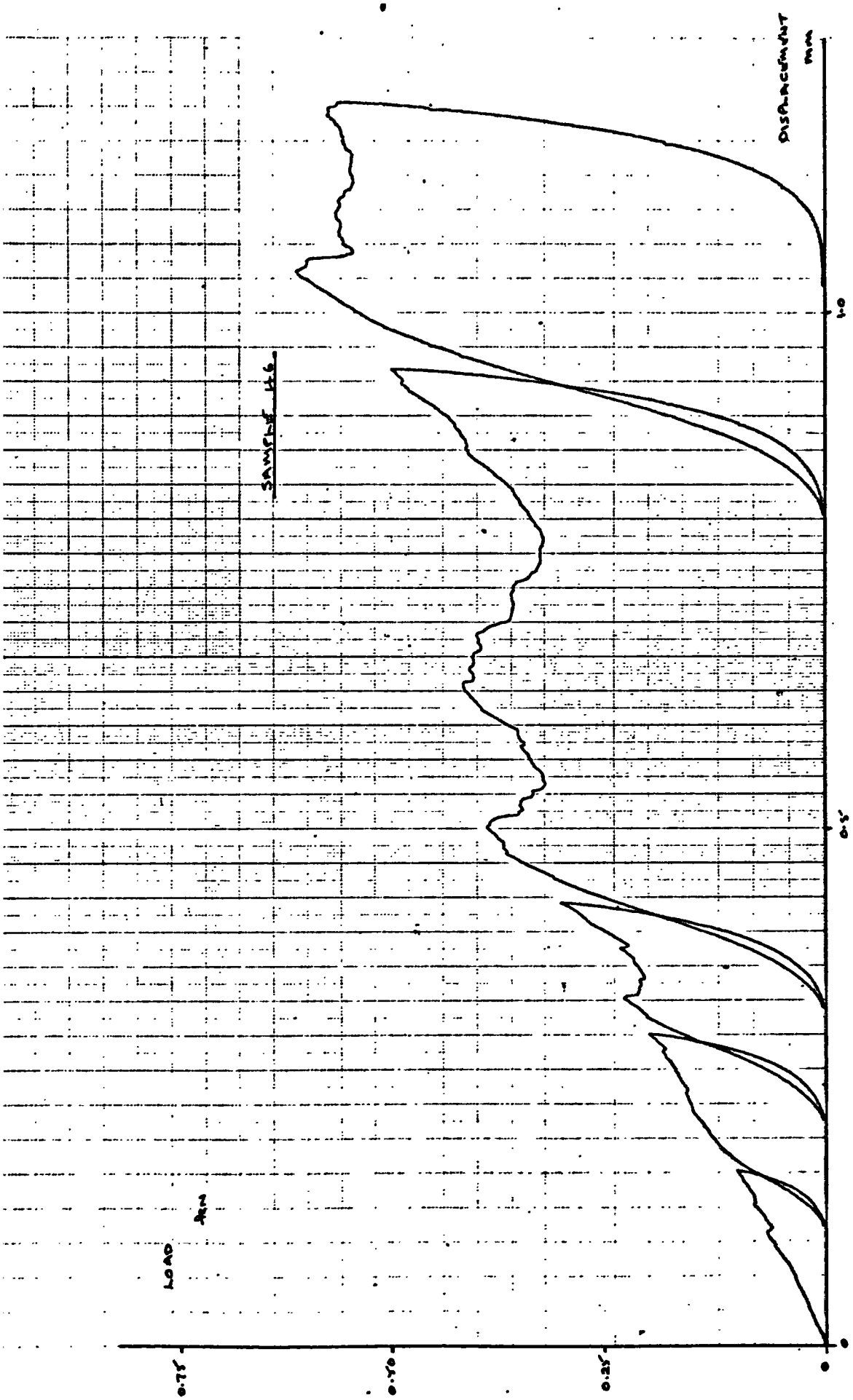

FIG. 4.12 :- LOAD - DISPLACEMENT CURVE ; SATURATED/SURFACE DRY, IRREGULAR SAMPLE (NO. 46)

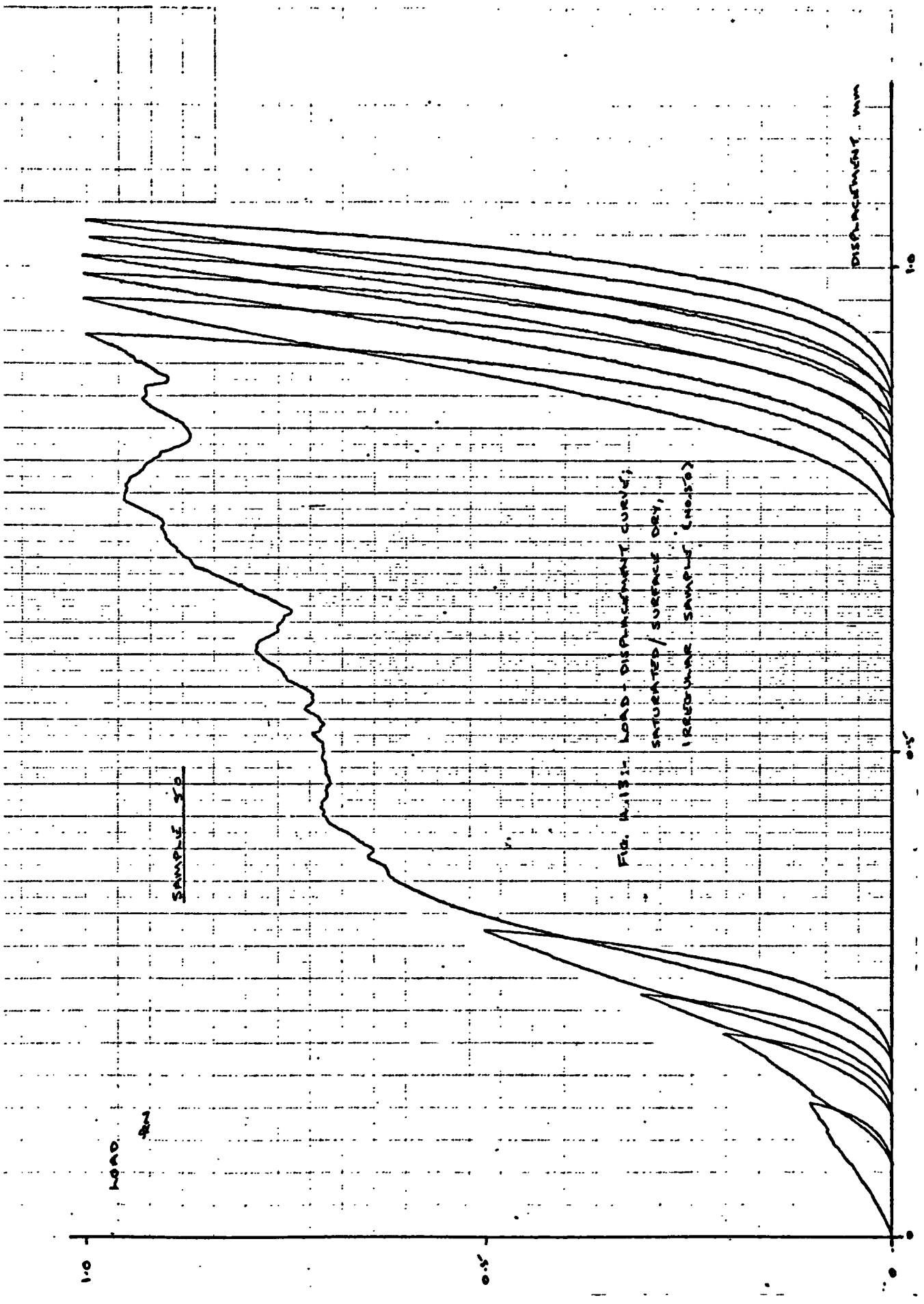

FIG. A.13:- LOAD - DISPLACEMENT CURVE; SATURATED / SURFACE DRY, IRREGULAR SAMPLE (NO. 50)

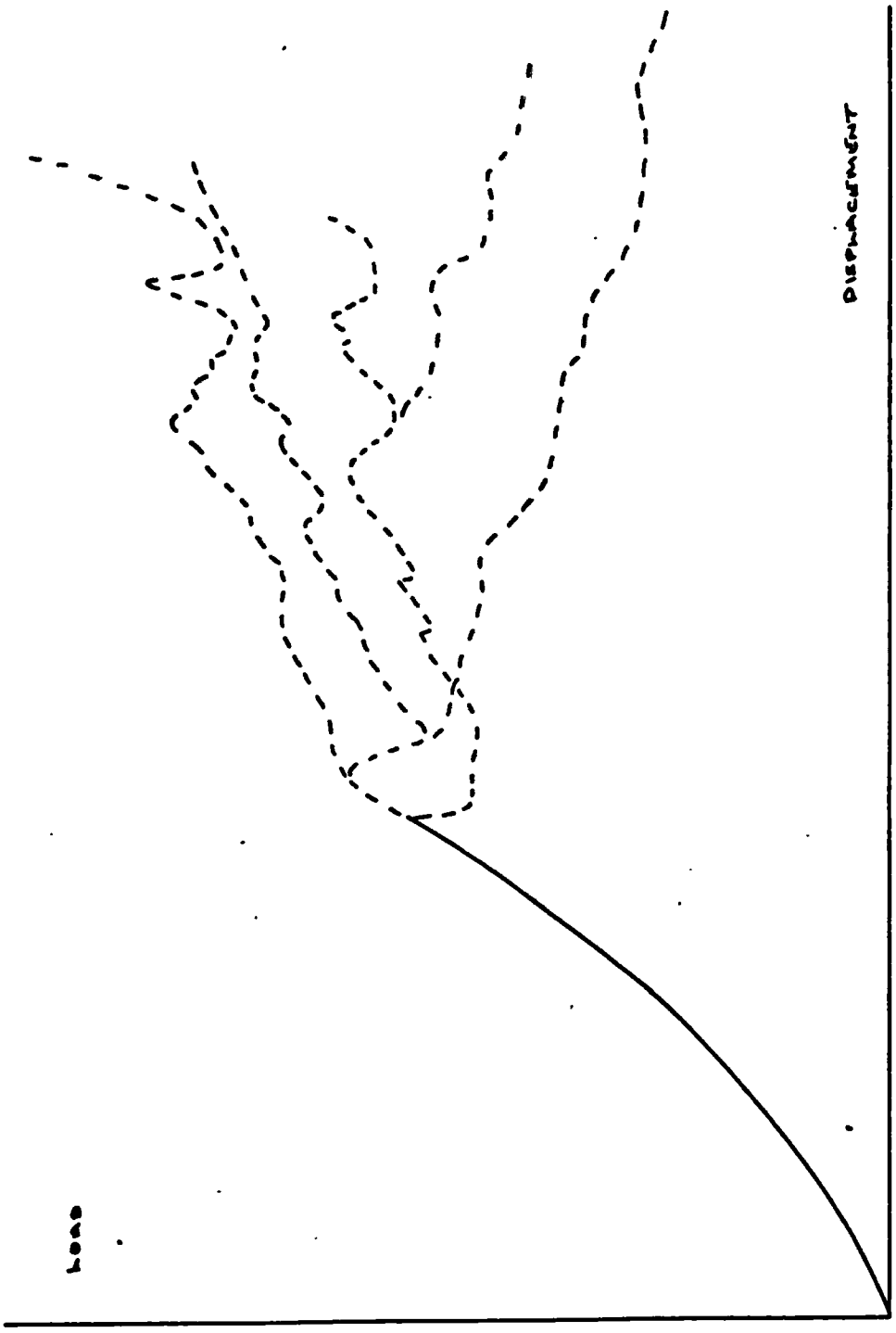

FIG. 4.14 :- TYPICAL CONTACT NORMAL LOAD-DISPLACEMENT CURVES

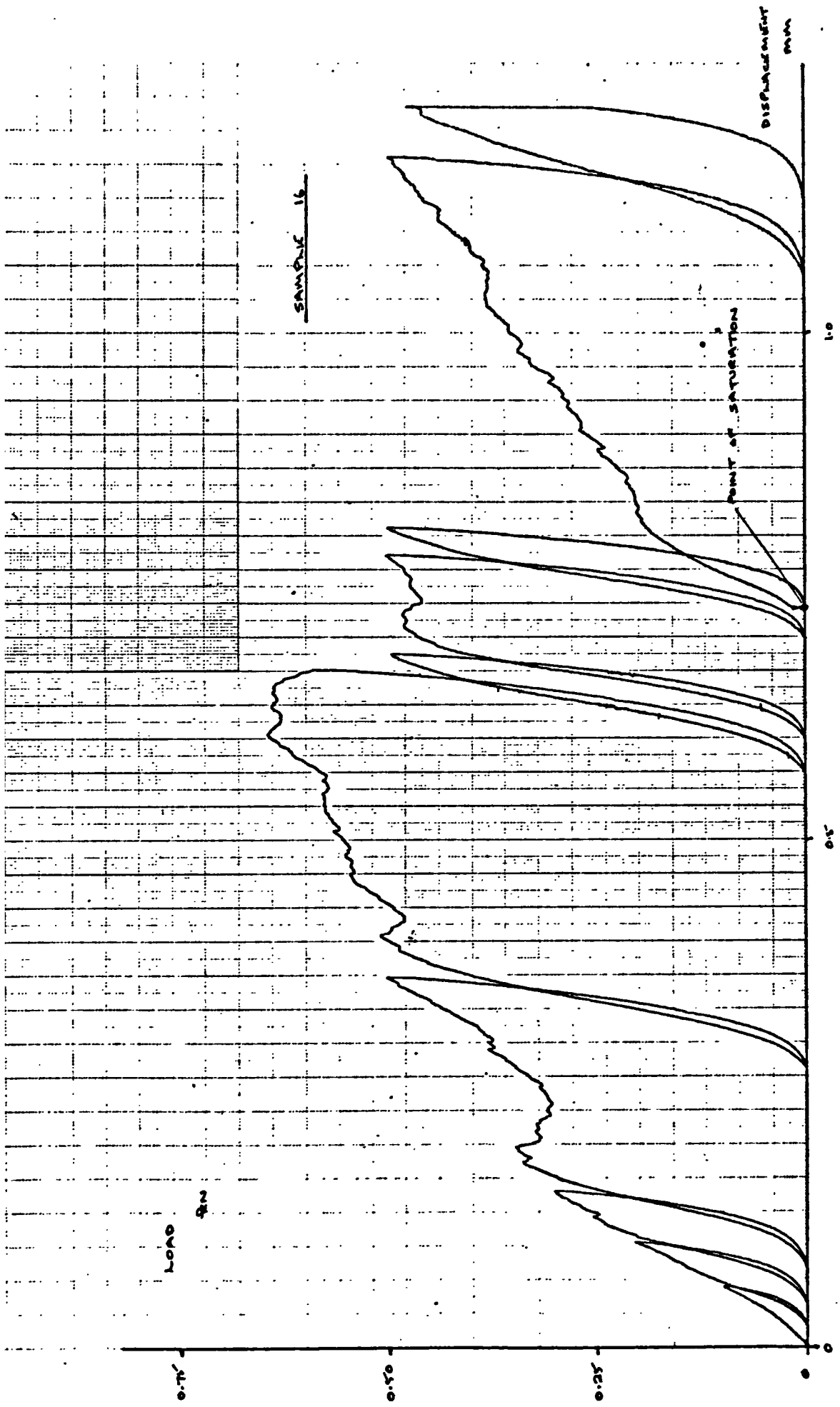

FIG. 4.15 :- EFFECT OF SATURATION ON LOAD-DISPLACEMENT RELATIONSHIP; IRREGULAR SAMPLE (No. 16)

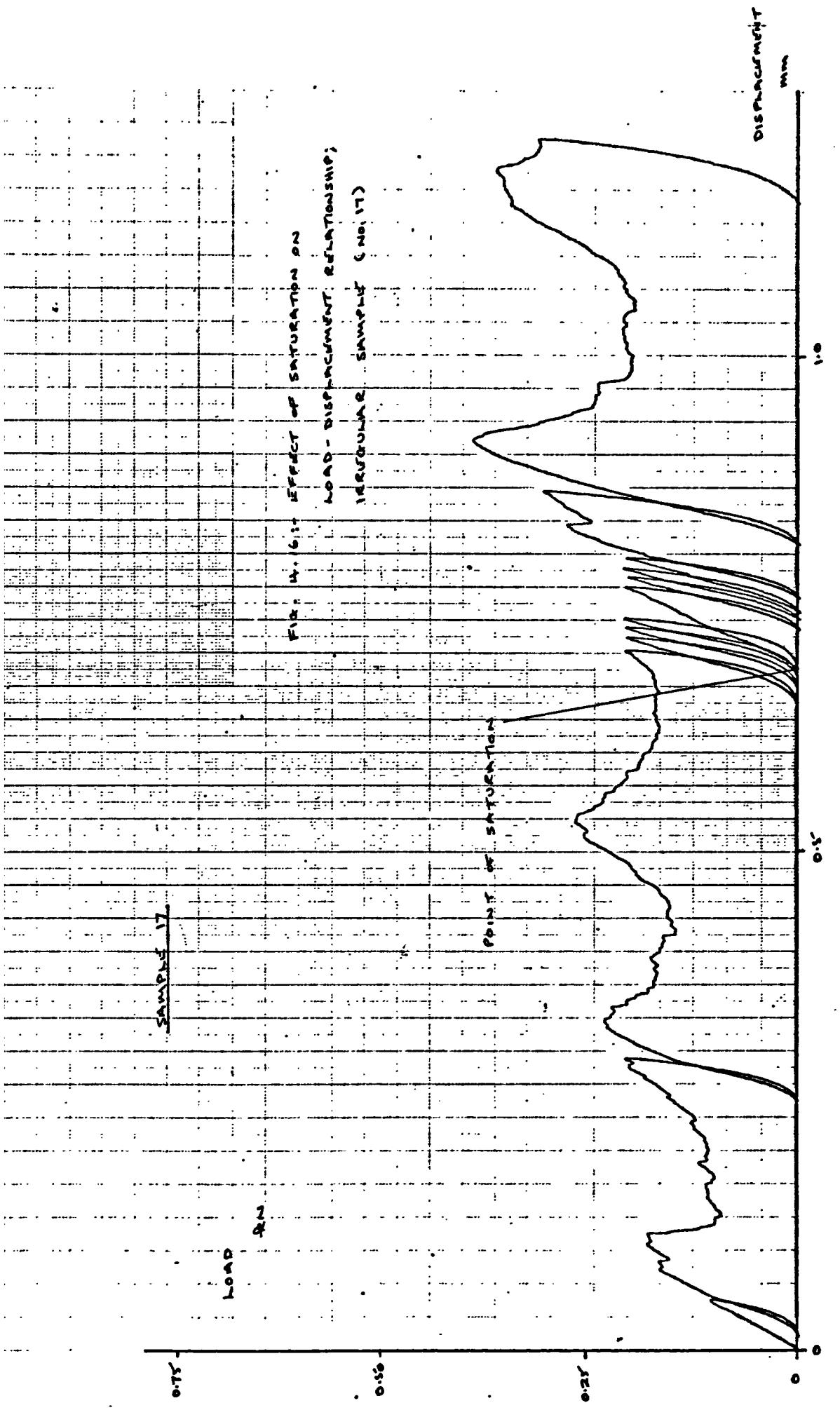

FIG: 4.16:1 EFFECT OF SATURATION ON LOAD - DISPLACEMENT RELATIONSHIP; IRREGULAR SAMPLE (NO: 17)

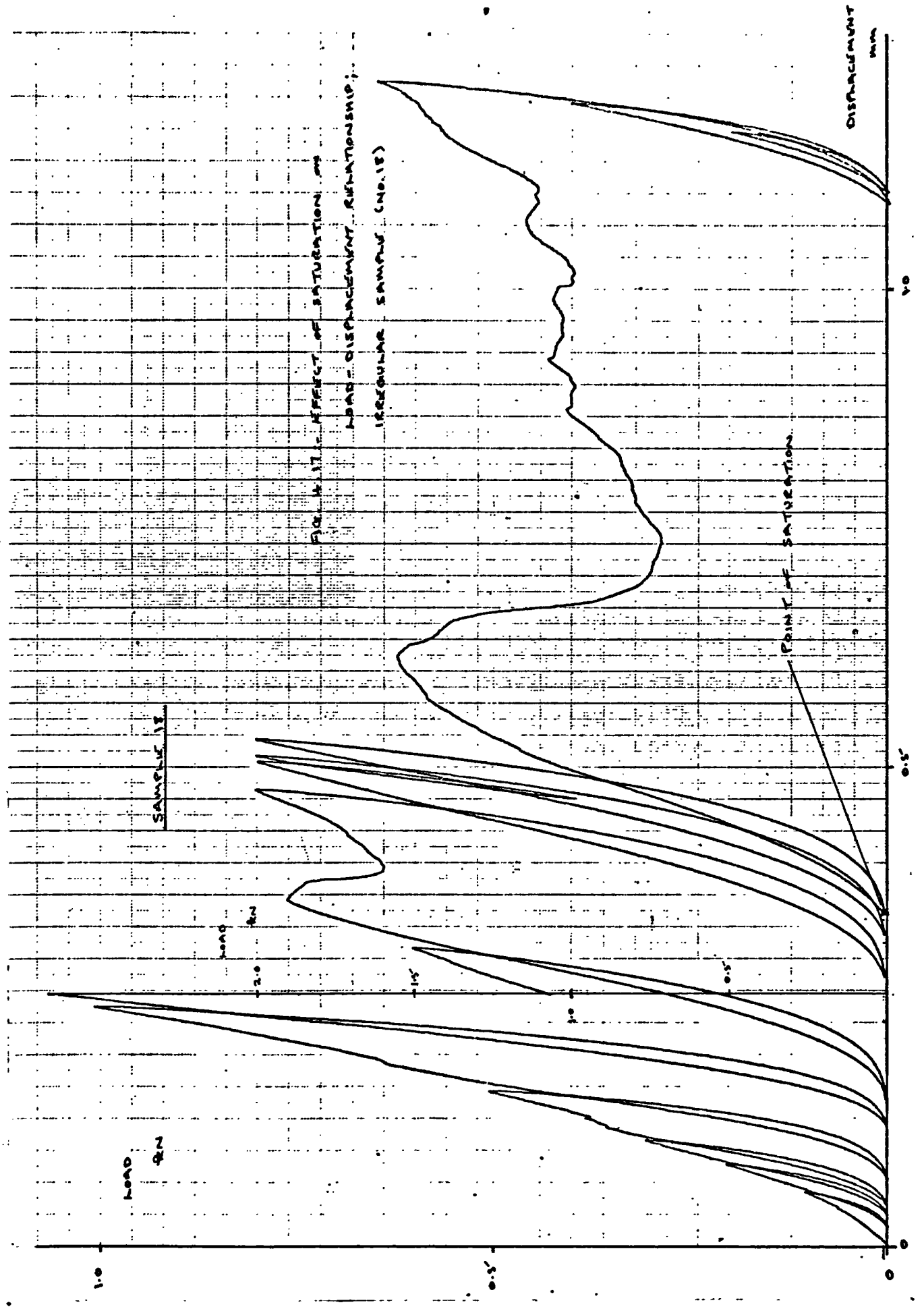
FIG. 11. EFFECT OF SATURATION ON LOAD-DISPLACEMENT RELATIONSHIP.
IRREGULAR SAMPLE (NO. 12)
SAMPLE 12
LOAD kN
DISPLACEMENT mm
POINT OF SATURATION
2·0
1·5
1·0
0·5
0
0·5
1·0

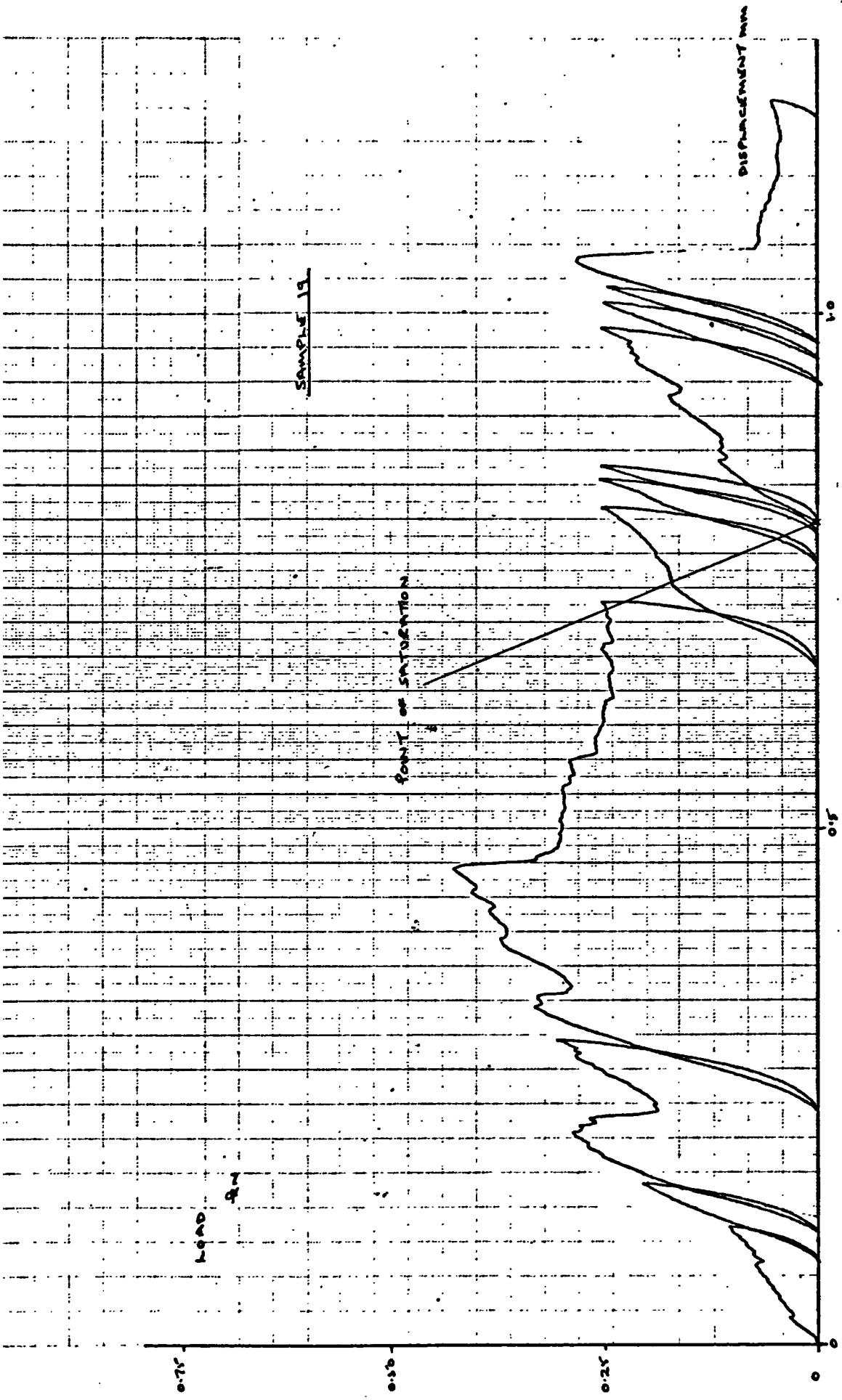

Fig. 4.18 :- Effect of saturation on load-displacement relationship ; Regular sample (No. 19)

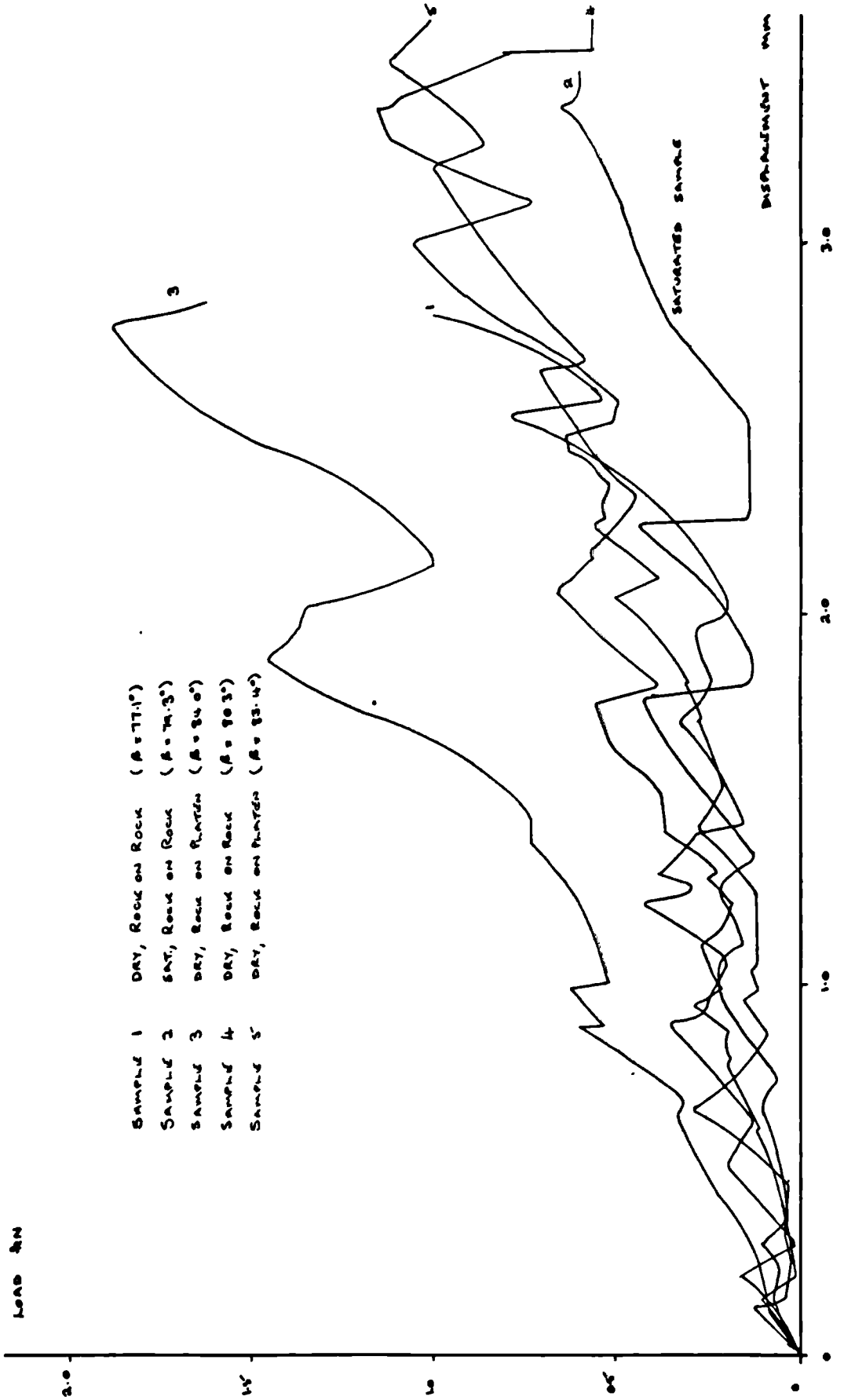

FIG. 4.19 :- LOAD - DISPLACEMENT CURVES ; SHAPED SAMPLES, β ≈ 90°

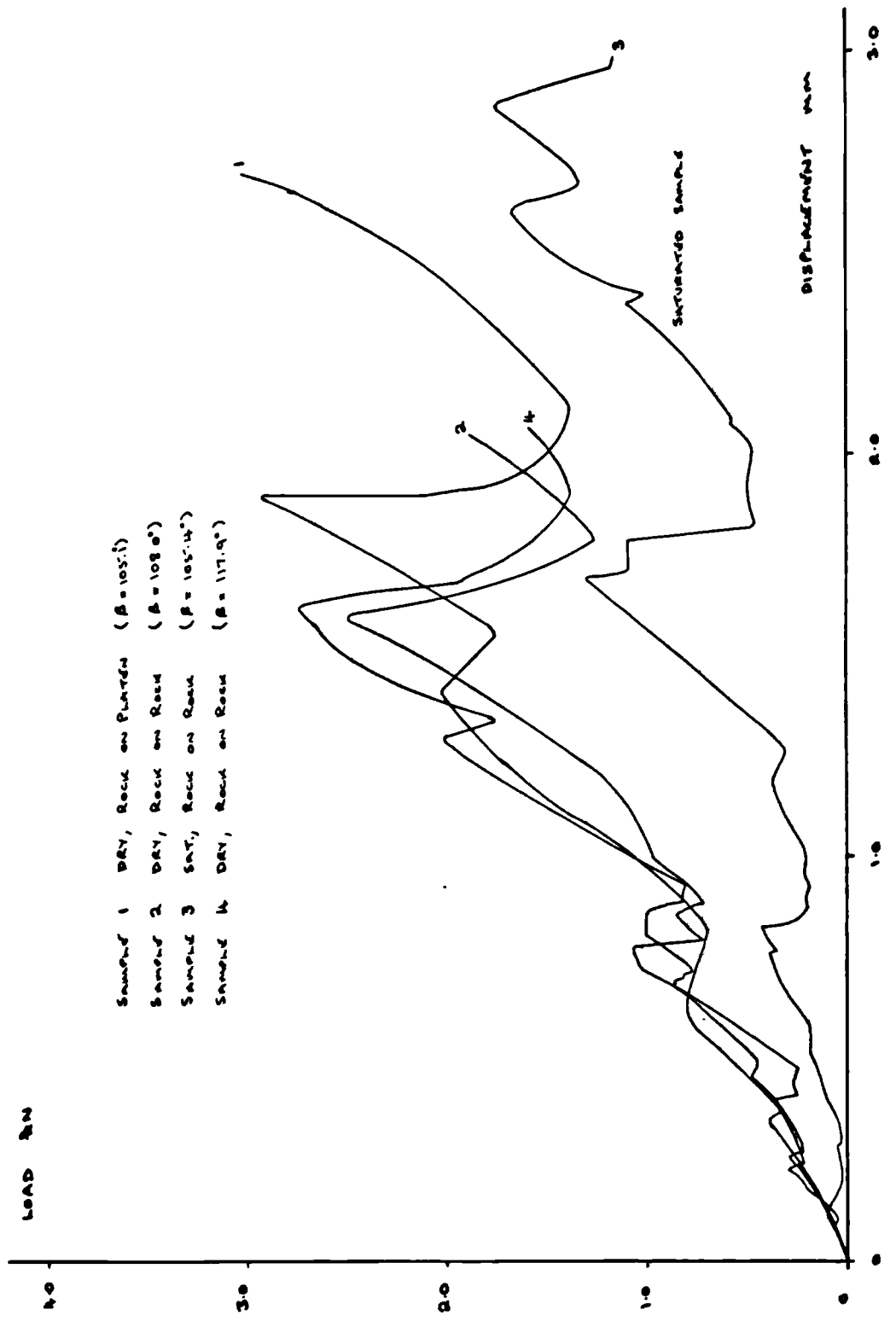

FIG. A.20 :- LOAD - DISPLACEMENT CURVES; SHAPED SAMPLES, β ≈ 110°

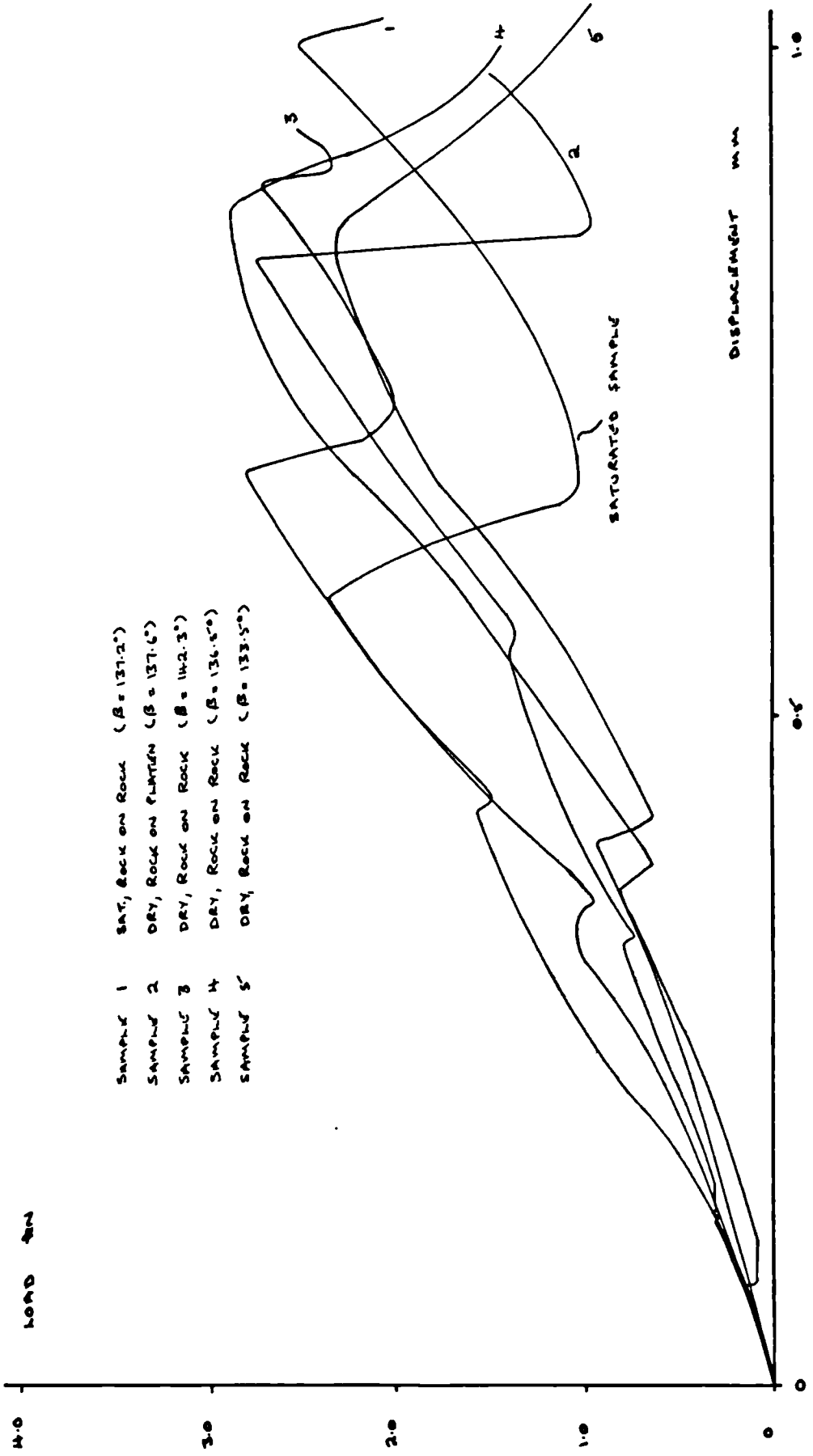

FIG. 4.21 :- LOAD - DISPLACEMENT CURVES ; SHAPED SAMPLES, β = 140°

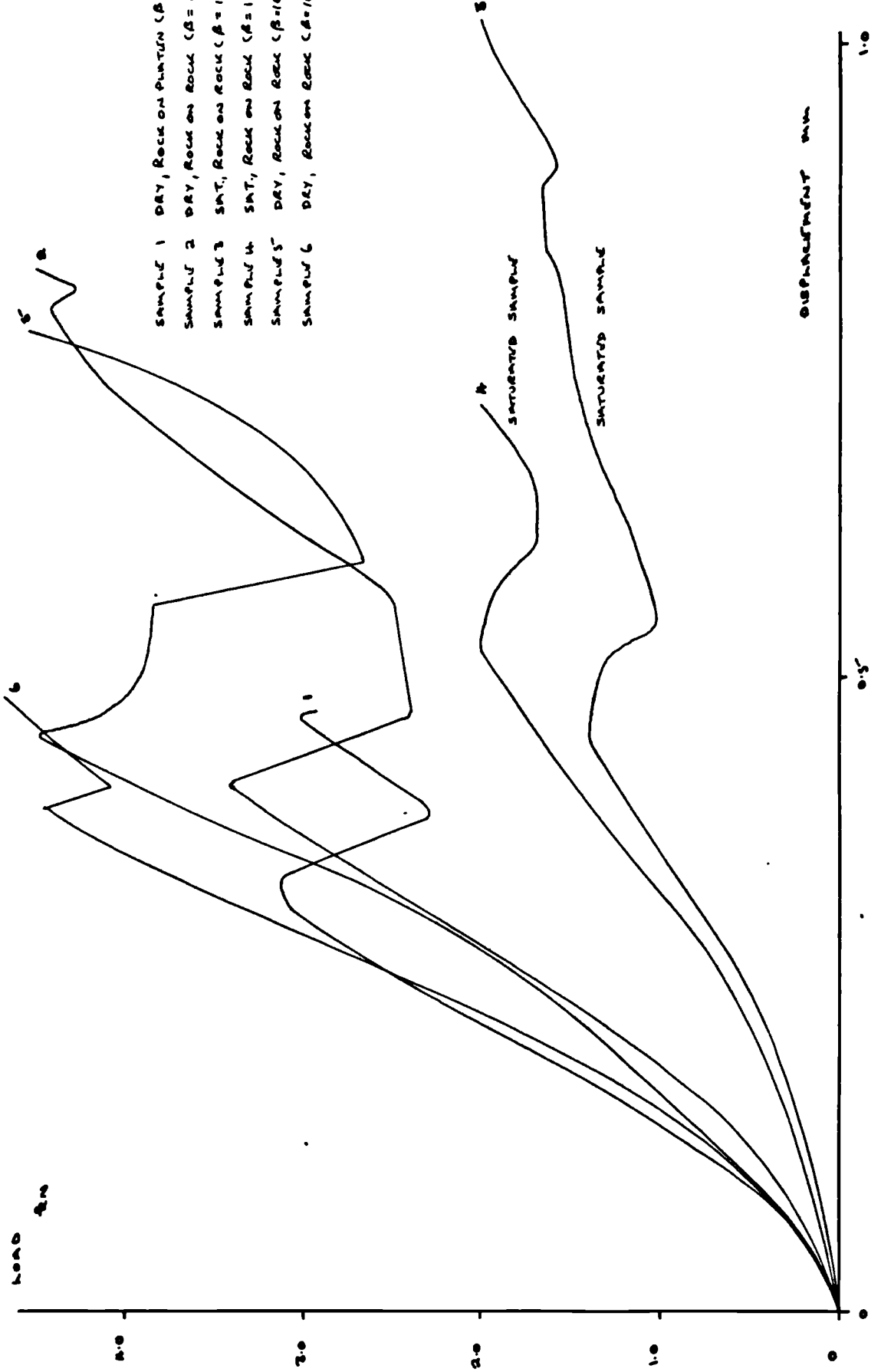

Fig. 4.22 :- LOAD - DISPLACEMENT CURVES ; SHARED SAMPLES, β ≥ 160°

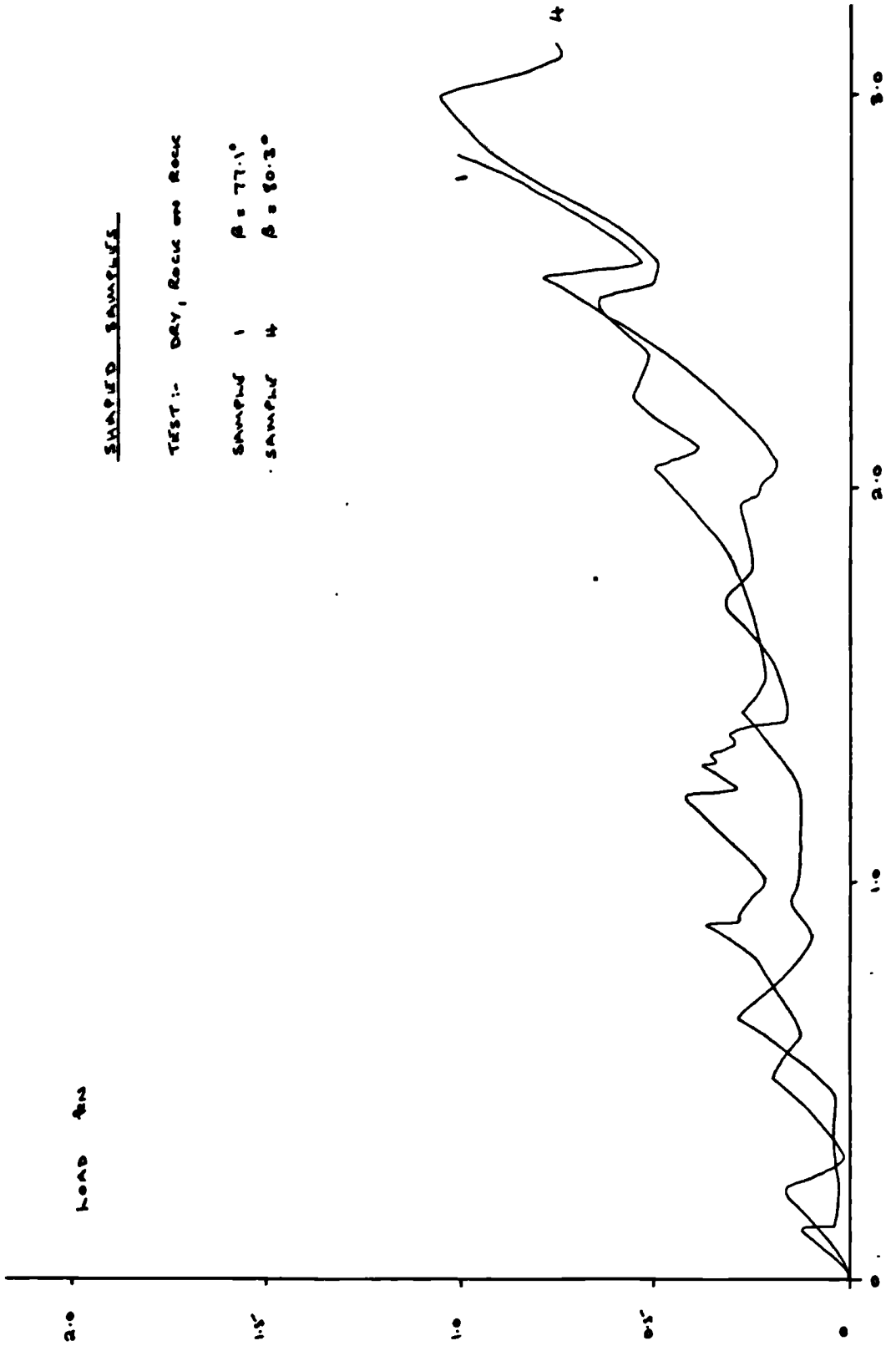

Fig. 4.23 :- LOAD-DISPLACEMENT CURVES ; DAY, SHAPED SAMPLES, β = 80°

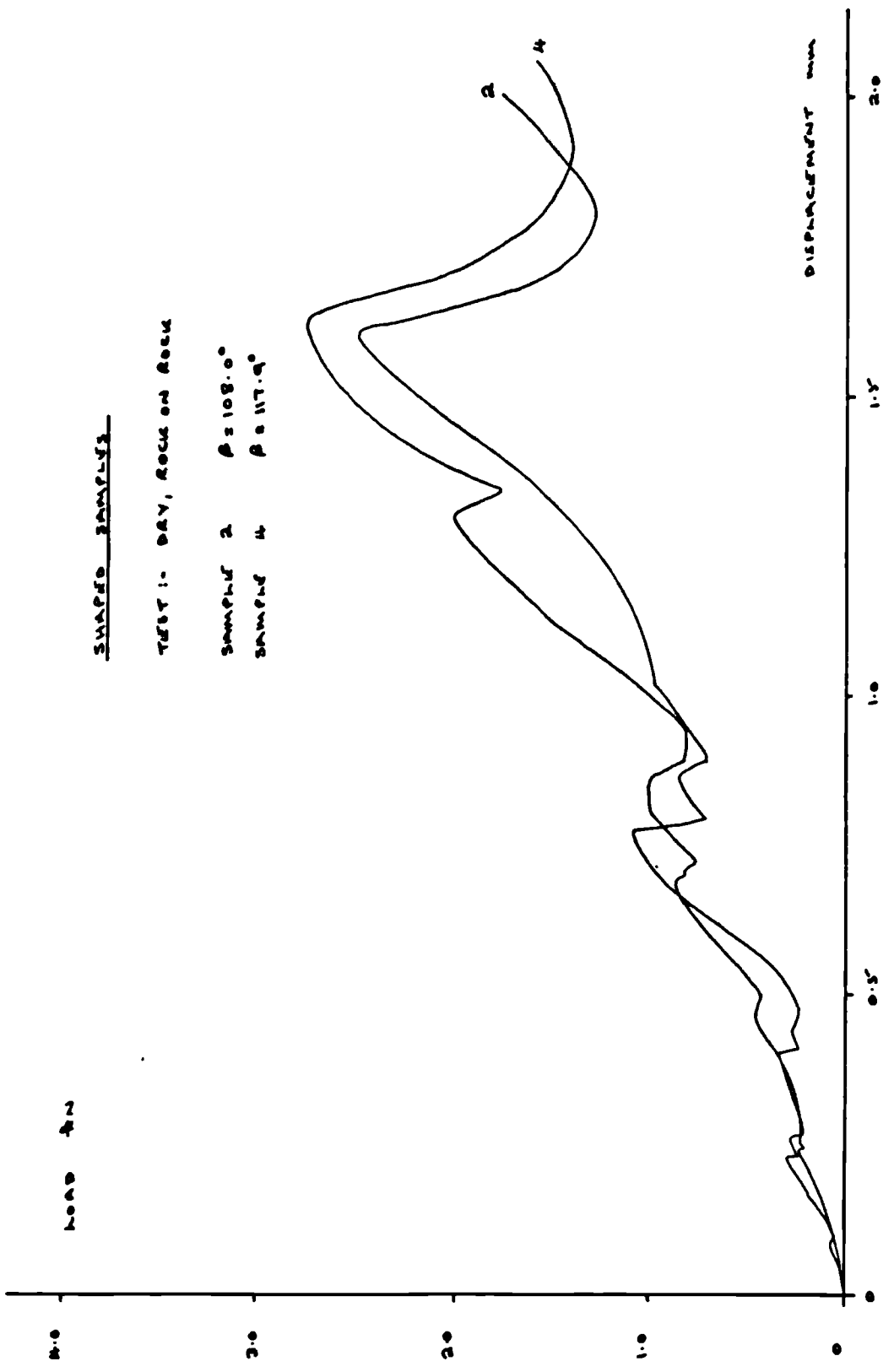

Fig. 4.24 :- LOAD - DISPLACEMENT CURVES ; DRY SHAPED SAMPLES, β ≈ 110°

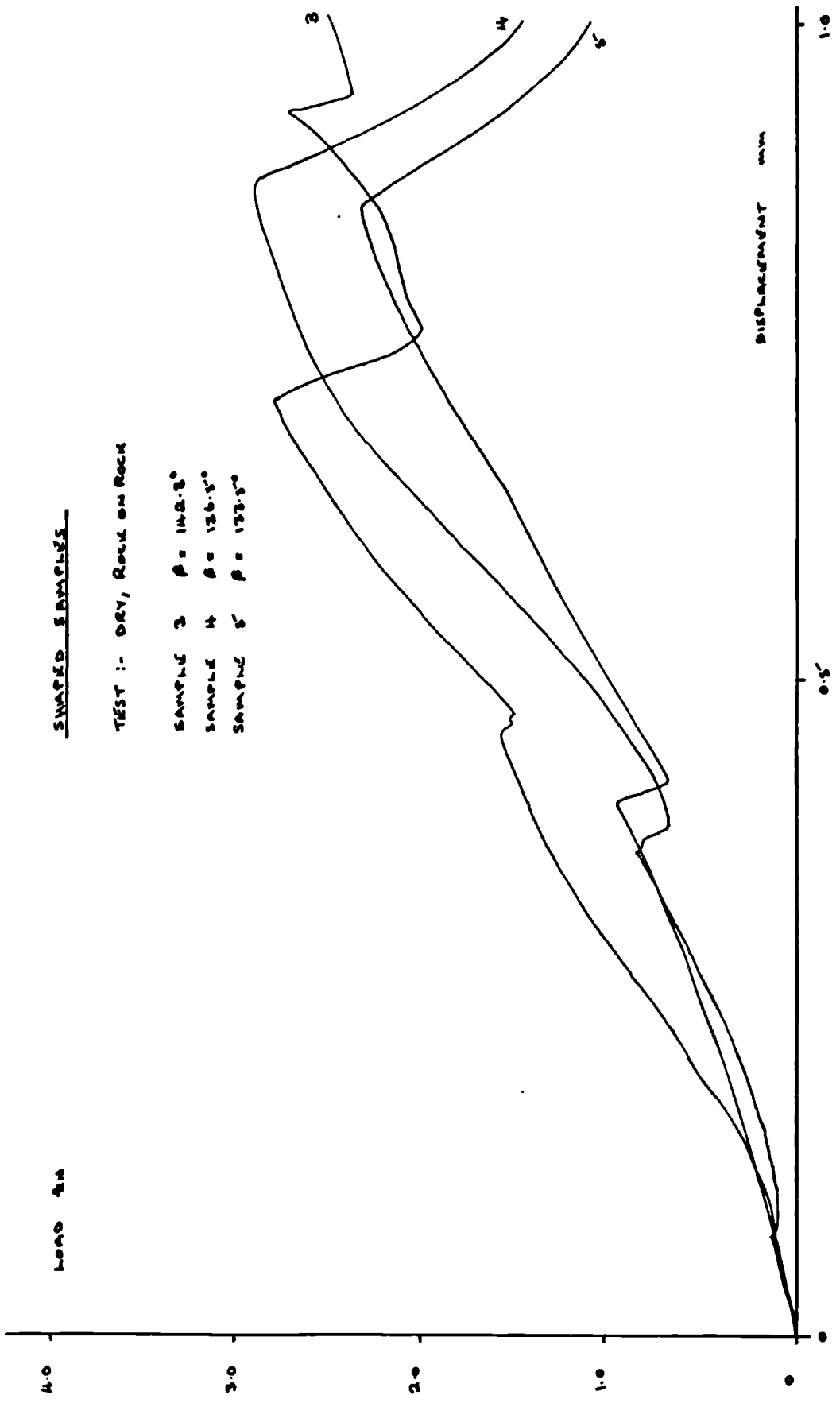

FIG. 4.25 :- LOAD-DISPLACEMENT CURVES ; DRY, SHAPED SAMPLES, $\beta \approx 140°$

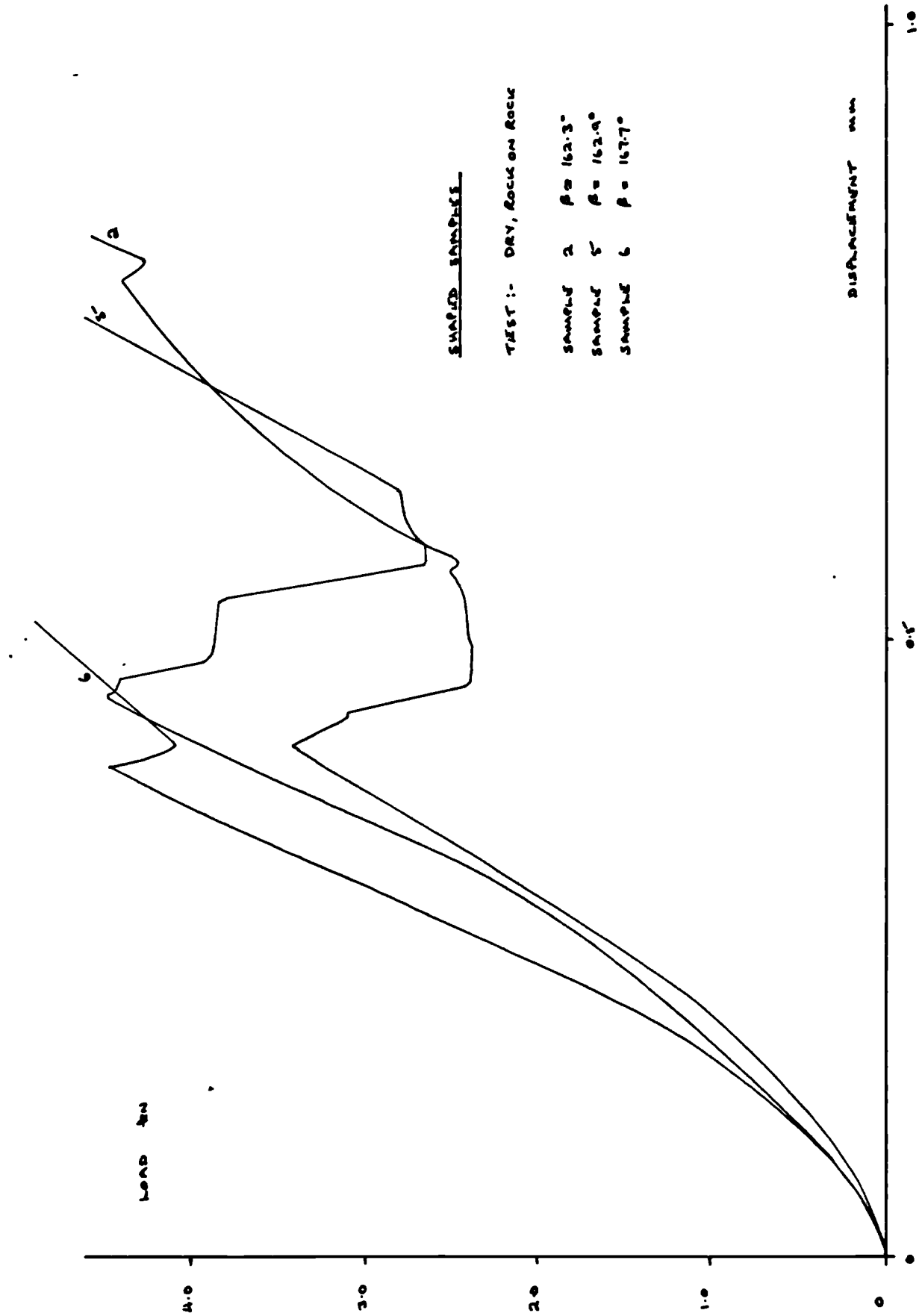

FIG. 4.26 :- LOAD - DISPLACEMENT CURVES ; DRY, SHAPED SAMPLES, β ≈ 160°

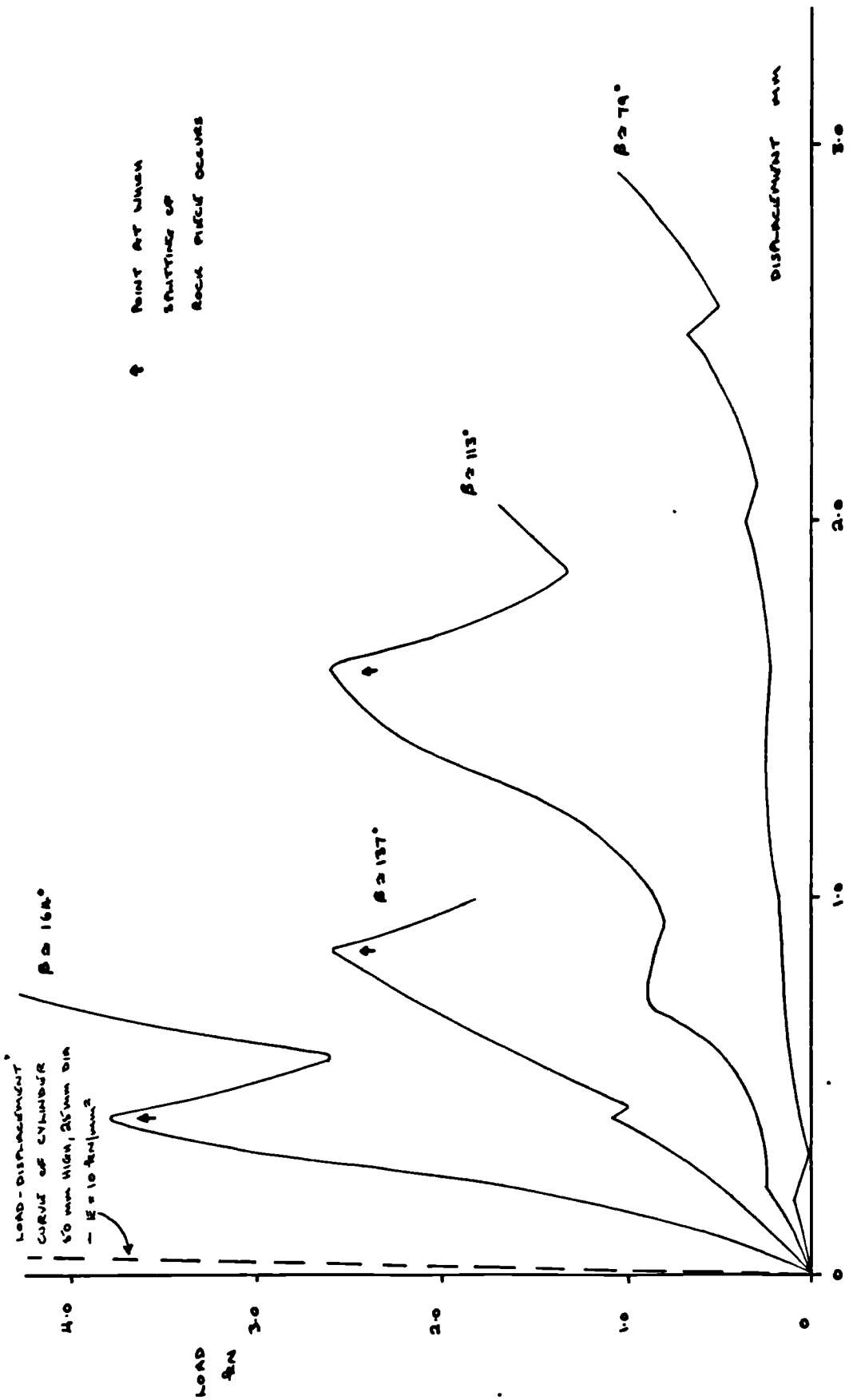

FIG. 4.27 :- COMPARISON OF MEAN LOAD-DISPLACEMENT CURVES OF DRY, SHAPED SANDSTONE CONTACTS FOR DIFFERENT CONTACT ANGLES

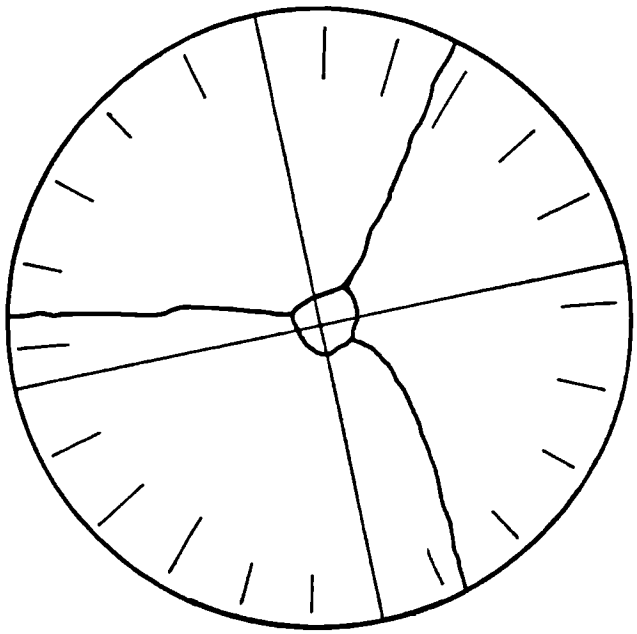

THREE WAY MODE

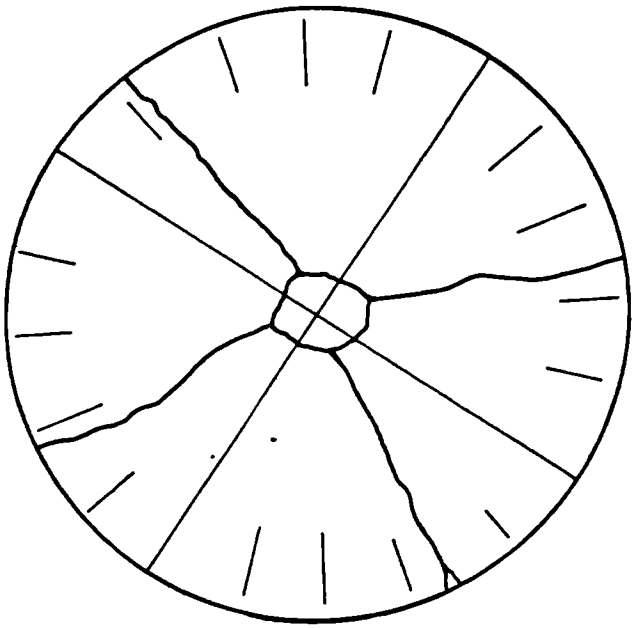

FOUR WAY MODE

FIG. 4.28:- SPLITTING MODES OF SHAPED SAMPLES

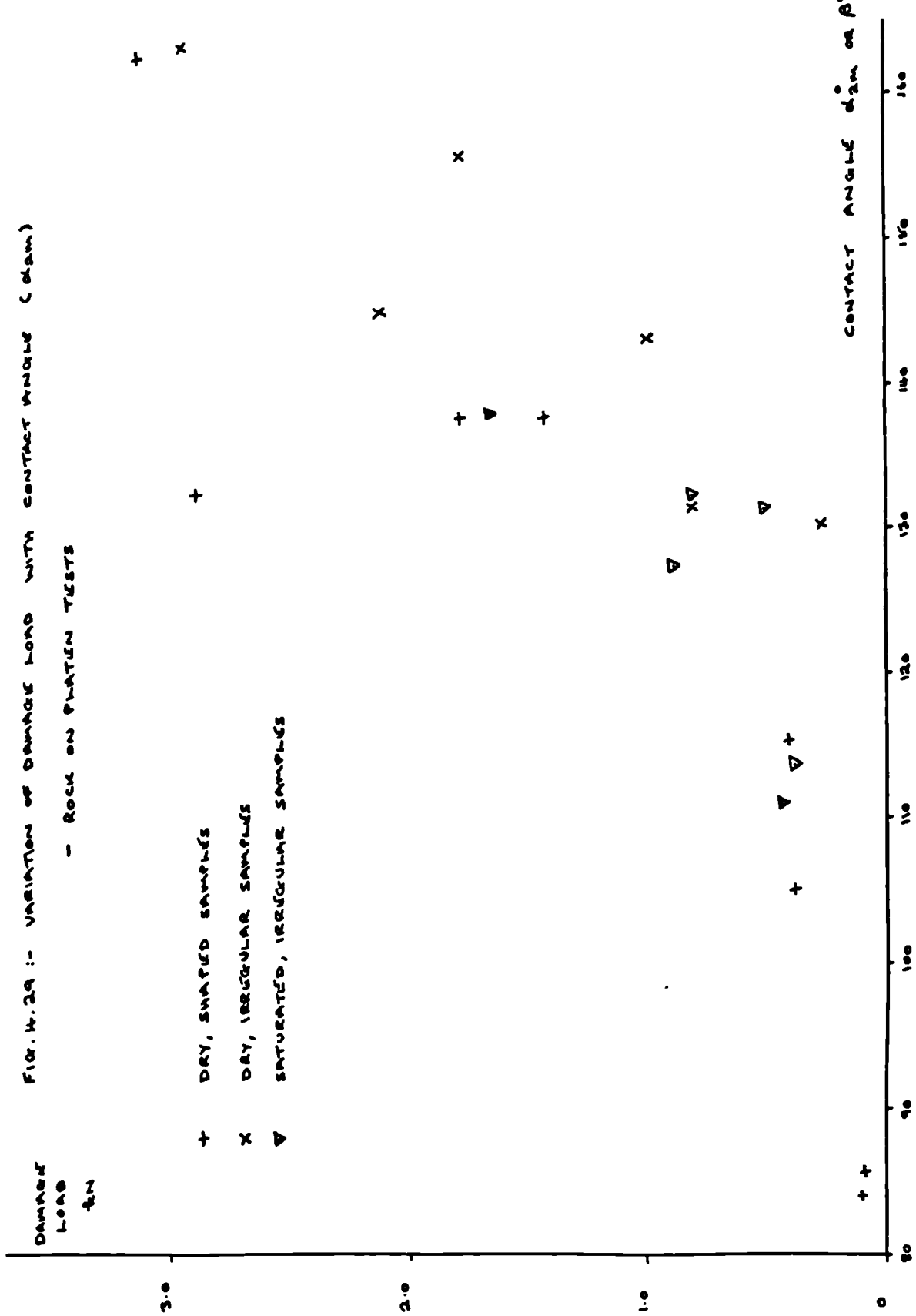

Fig. 4.29 :- VARIATION OF DAMAGE LOAD WITH CONTACT ANGLE (diam)
- ROCK ON PLATEN TESTS

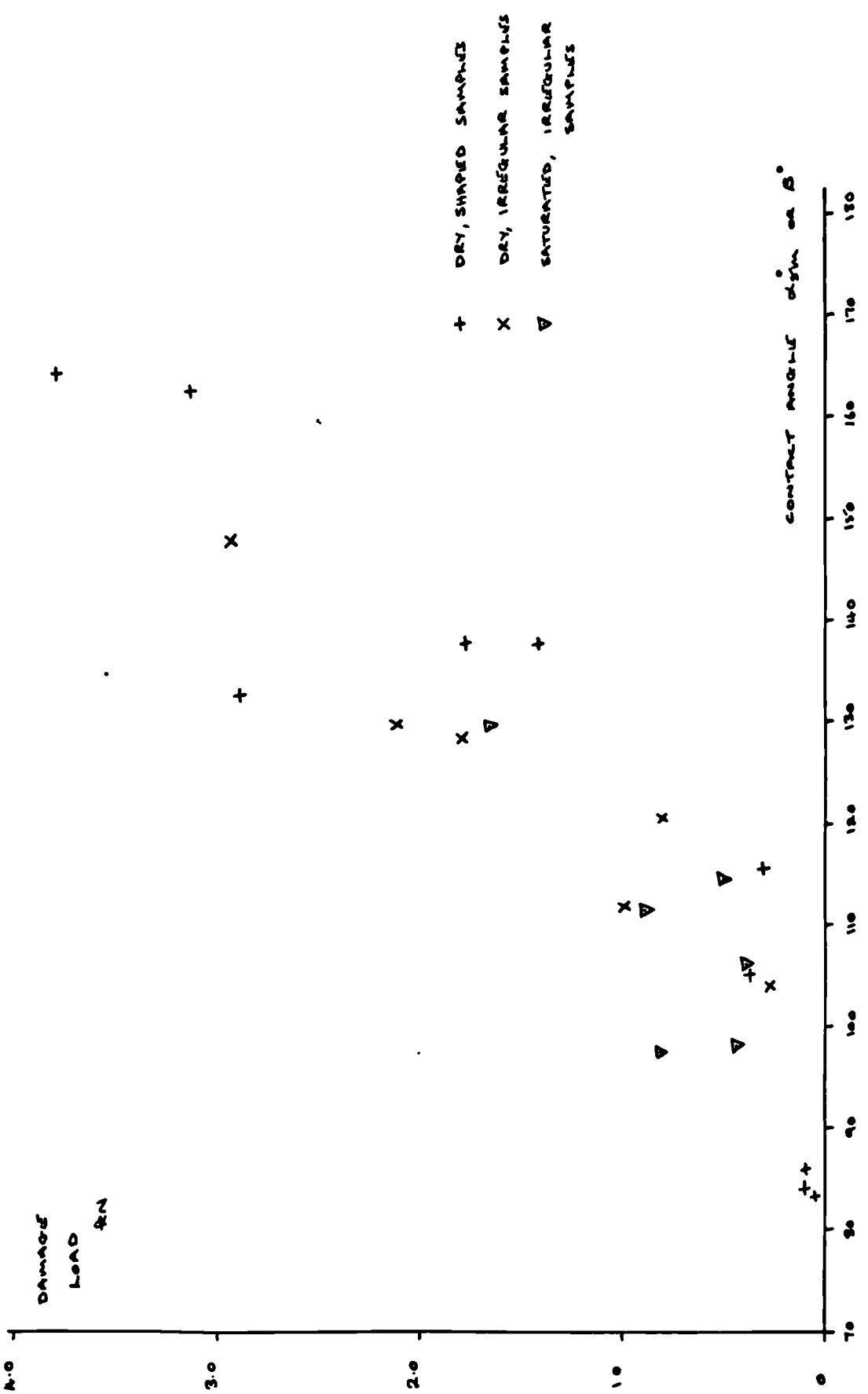

FIG. 4.30 :- VARIATION OF DAMAGE LOAD WITH CONTACT ANGLE (degrees)
- ROCK ON PLATEN TESTS

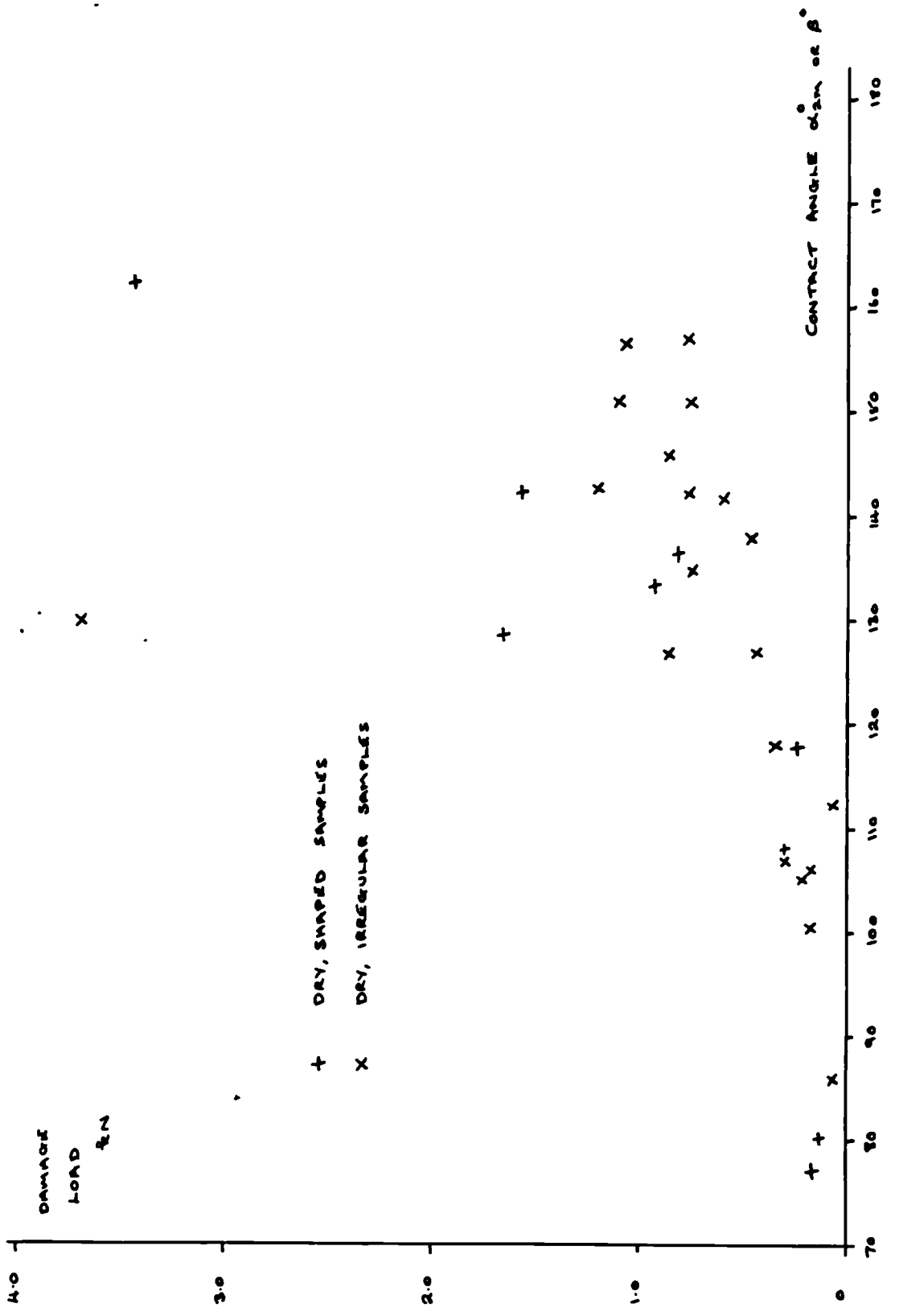

FIG. 4.31 :- VARIATION OF DAMAGE LOAD WITH CONTACT ANGLE (deg.)
- DRY, ROCK ON ROCK TESTS

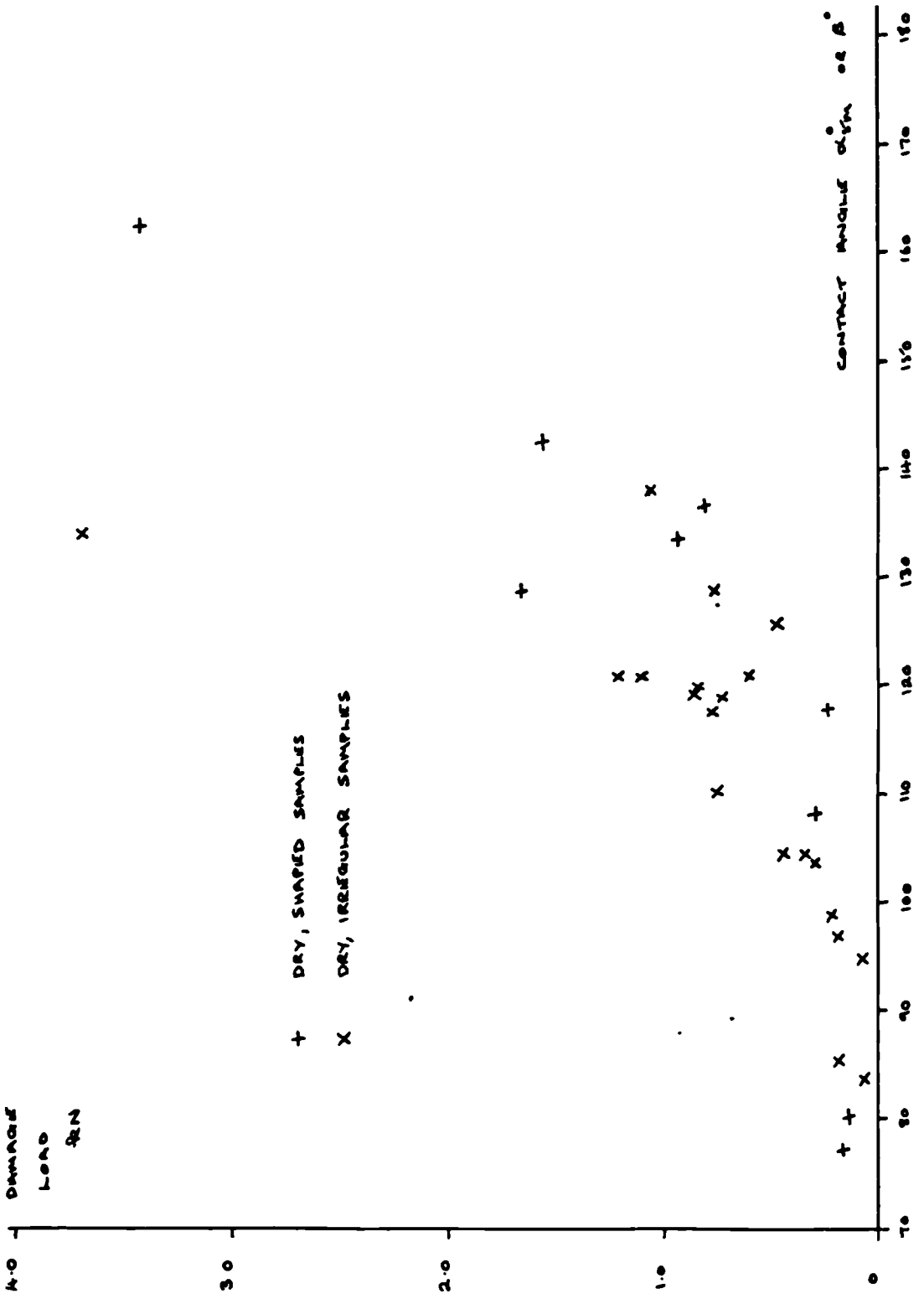

FIG. 4.32 :- VARIATION OF DAMAGE LOAD WITH CONTACT ANGLE (dgrs)
- DRY, ROCK ON ROCK TESTS

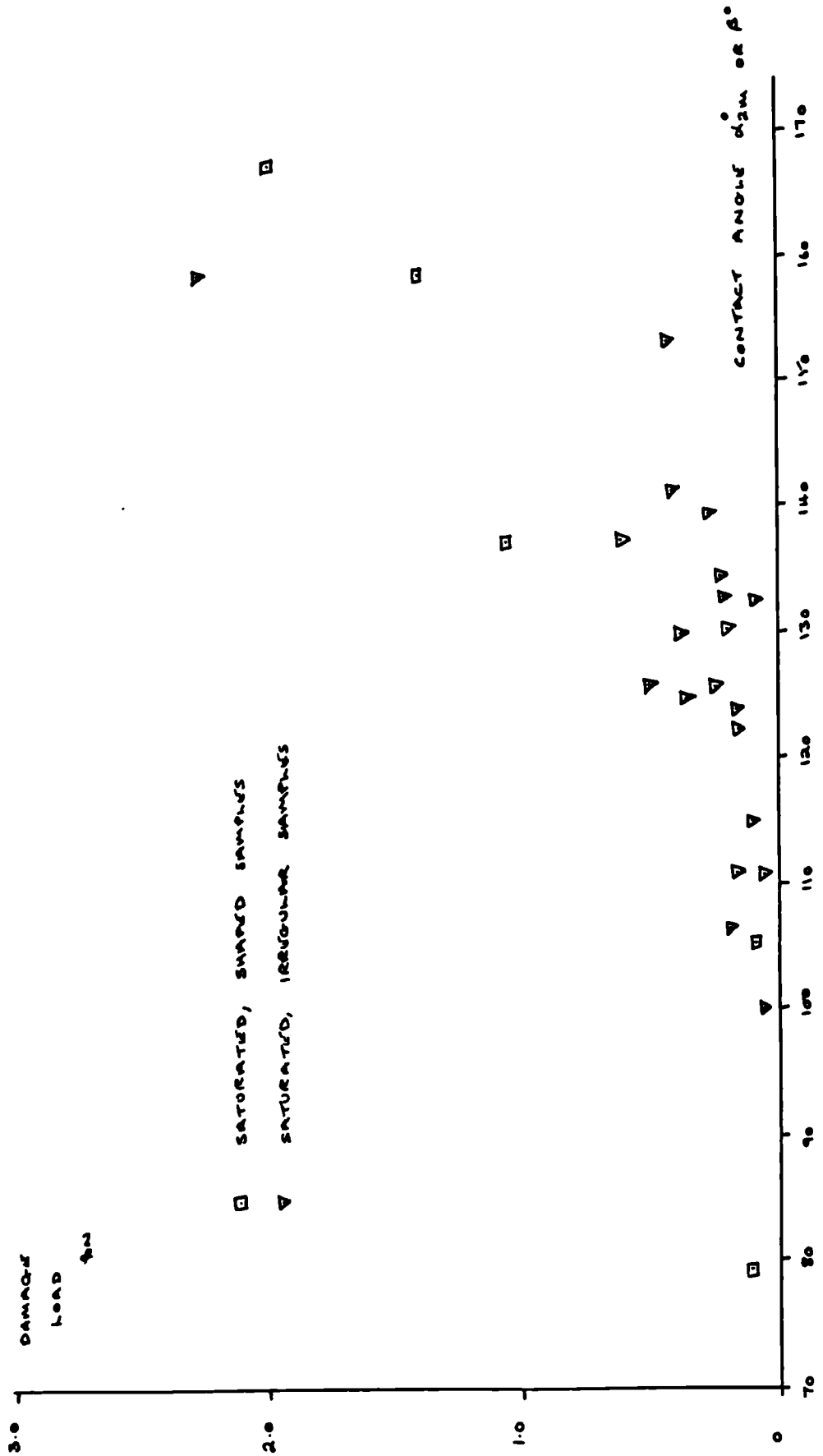

Fig. 4.33 :- VARIATION OF DAMAGE LOAD WITH CONTACT ANGLE (α'_{2m})
- SATURATED, ROCK ON ROCK TESTS

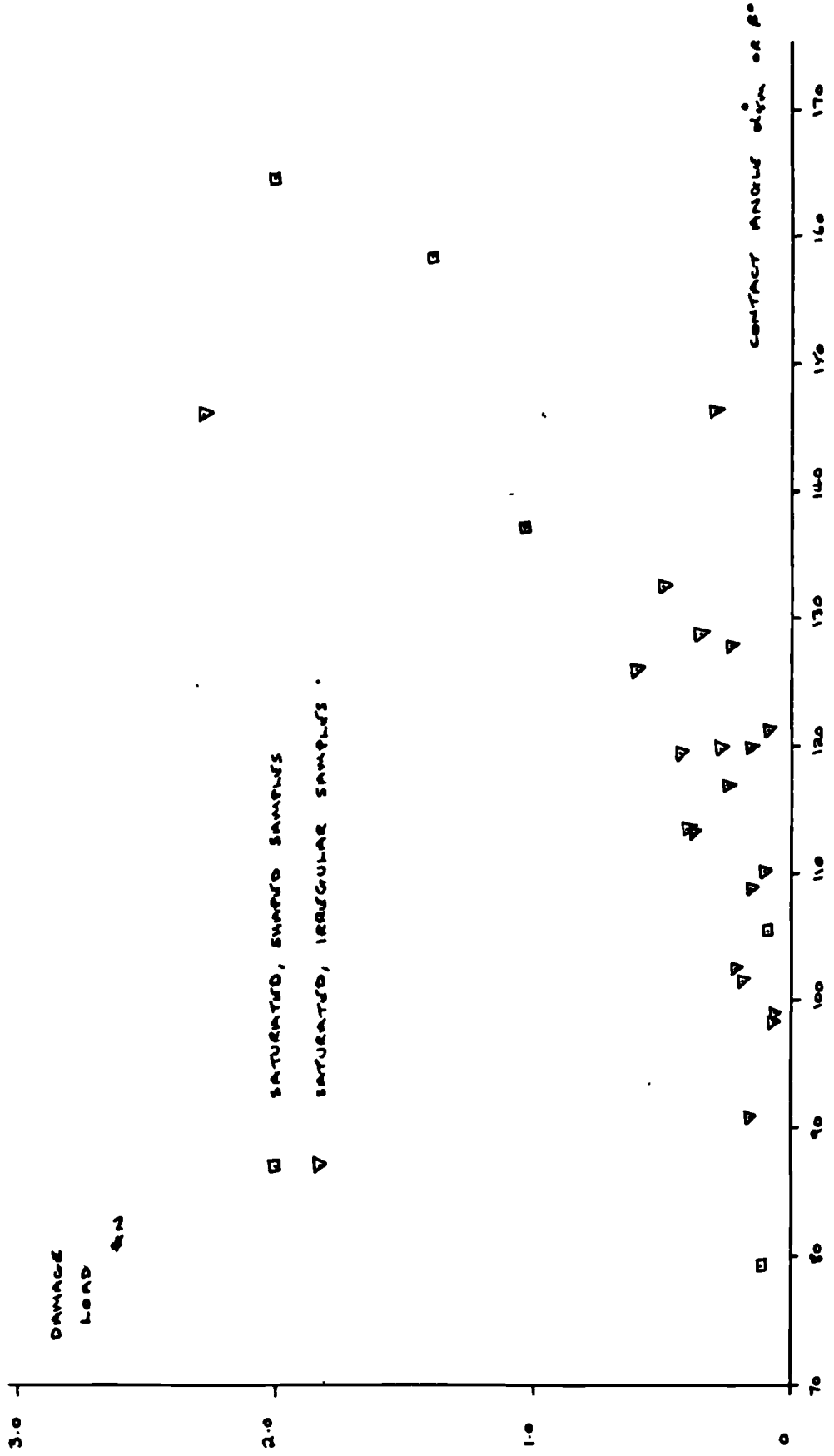

FIG. 4.34 :- VARIATION OF DAMAGE LOAD WITH CONTACT ANGLE (deg.)
- SATURATED, ROCK ON ROCK TESTS

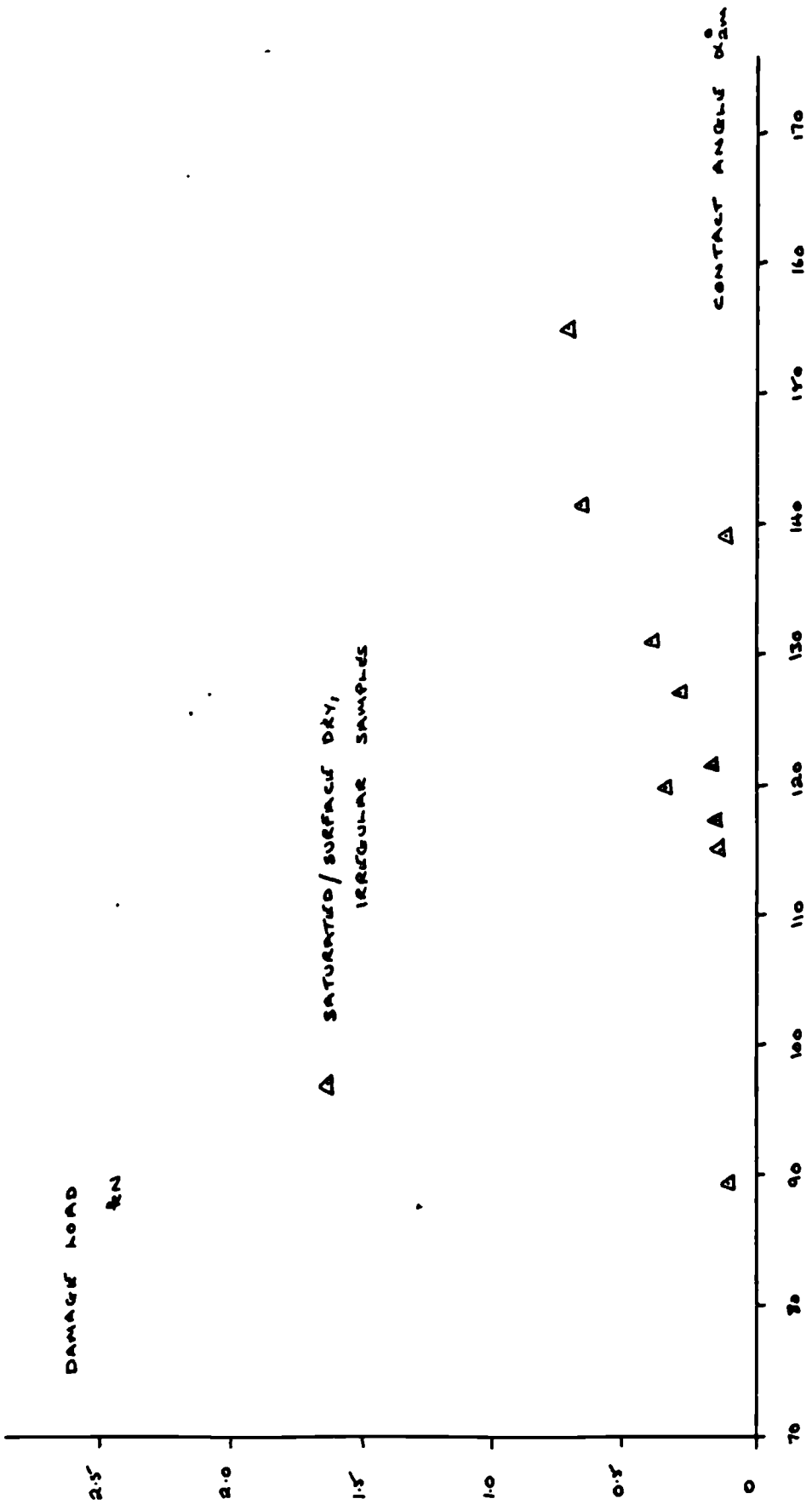

Fig. 4.35 :- VARIATION OF DAMAGE LOAD WITH CONTACT ANGLE (θ_{cm})
- SATURATED/SURFACE DRY, ROCK ON ROCK TESTS

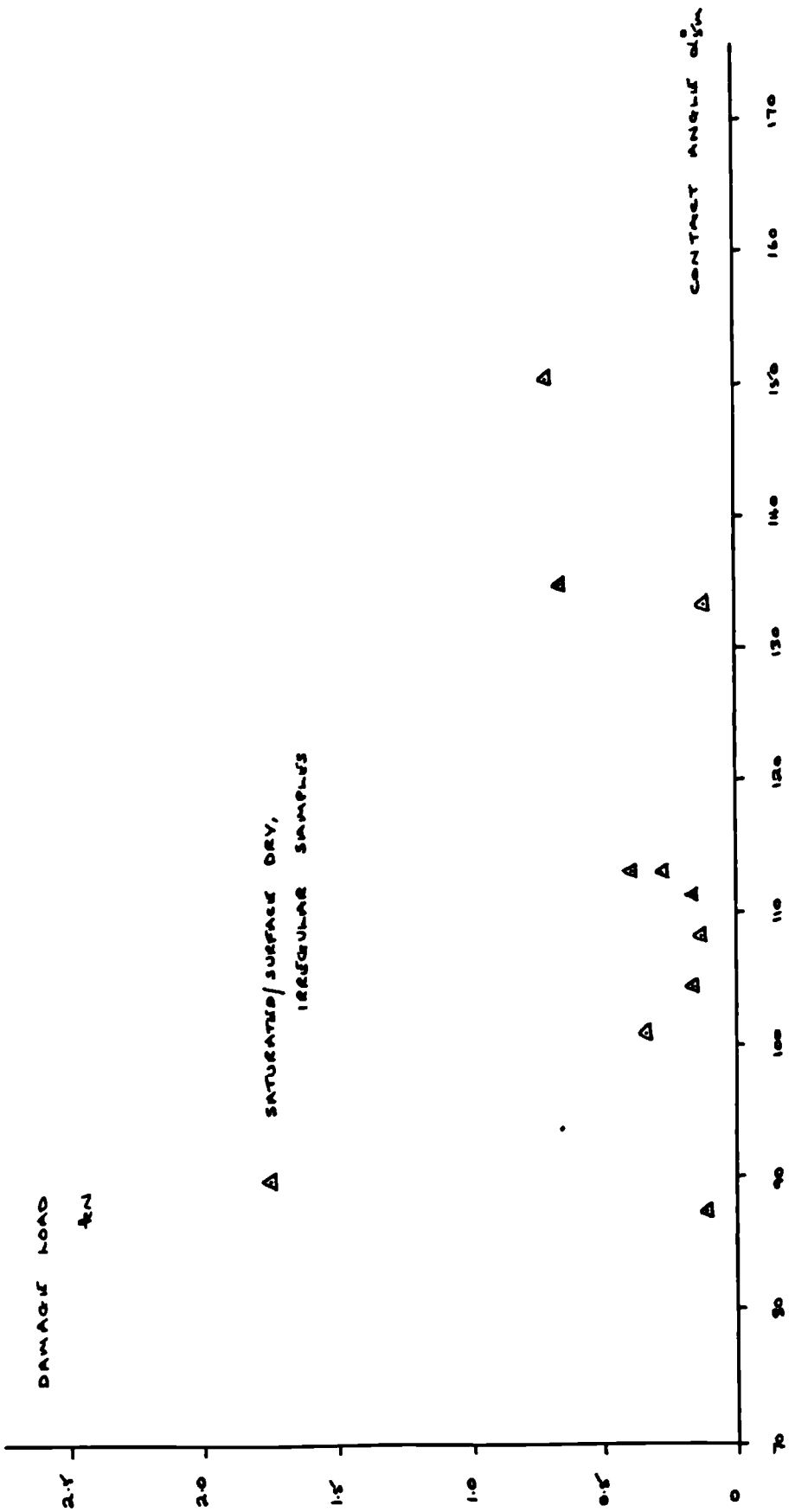

FIG. 4.36 :- VARIATION OF DAMAGE LOAD WITH CONTACT ANGLE (deg.)
- SATURATED/SURFACE DRY, ROCK ON ROCK TESTS

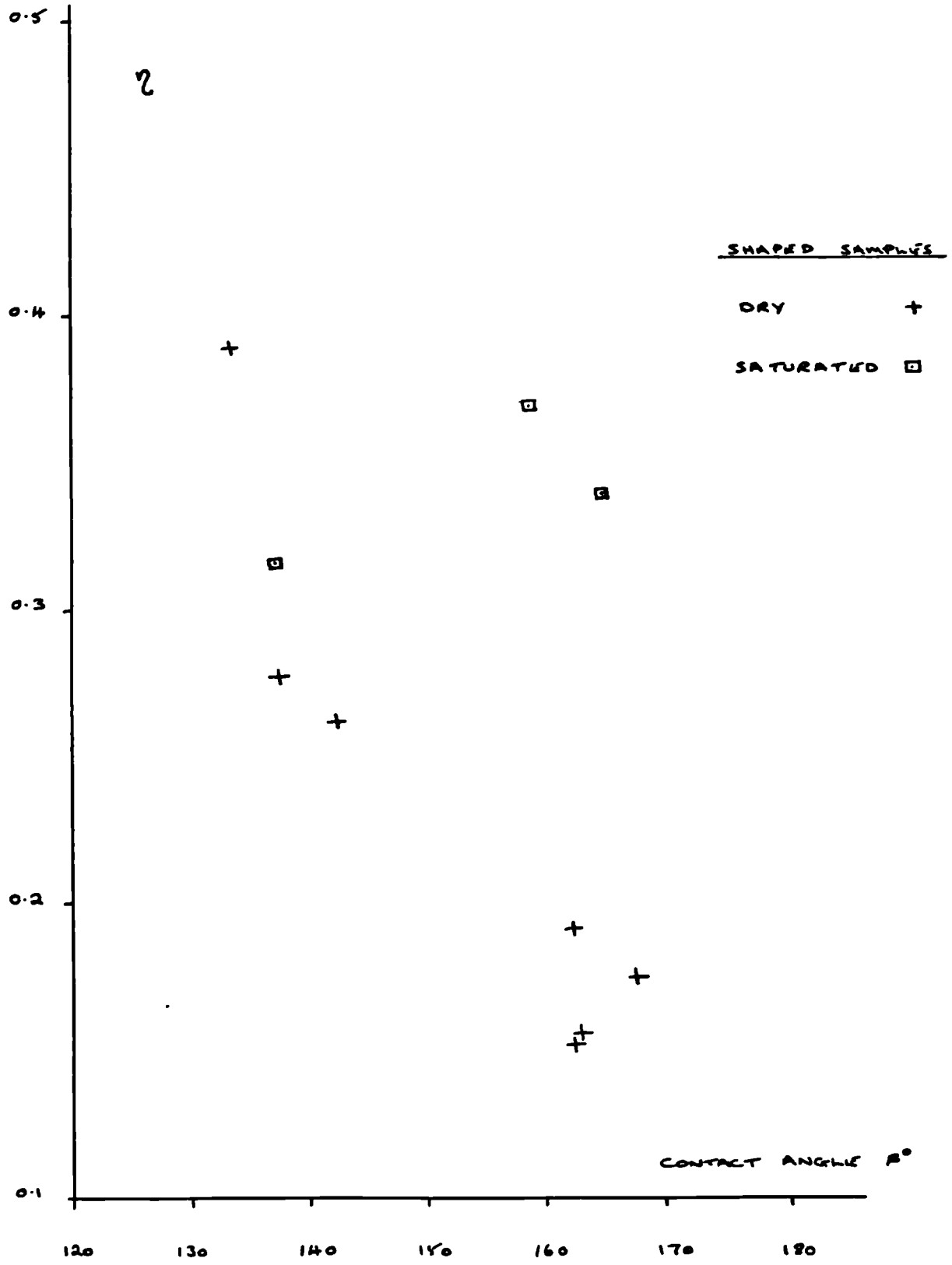

FIG. 4.37 :- VARIATION OF EXPERIMENTAL COEFFICIENT, η, WITH SHAPED SAMPLE CONTACT ANGLE, θ

Chapter 5

The Behaviour of Rock Contacts - the Area of Contact

5.1 Contact Area Measurement

While studies in tribology have not been particularly concerned with the load-displacement relationship of contacts, a great deal of attention has been paid to the area of contact and this has led to the distinction between real and apparent area, fig. 5.1. The real area is defined as the sum of the areas of the regions between the surfaces where there is 'atom-to-atom' contact. The total interfacial area, which consists of both contact regions or 'junctions' and areas of apparent contact, is defined as the apparent area. In tribology the real area is considered to determine the behaviour and interactions of the two surfaces and therefore several methods of determining the area have been proposed.

The area of contact for metallic asperities has been shown to be proportional to the load, although Bowden and Tabor (1949) indicate that the load index may reduce to 0.8 in certain work-hardening cases.

$$A_p = P/_{hp} \qquad (5.1)$$

where hp is the penetration hardness, i.e. the largest compressive stress a region of material can carry without plastic yielding. The penetration hardness is determined from simple indentation experiments.

The elastic theory proposed by Hertz produces a different equation, from (4.1)

$$Ae = \pi a b$$

$$A_e = \pi . m . n \left[\frac{P.D.}{(A+B)} \right]^{\frac{2}{3}} \qquad (5.2)$$

where m = n = 1 for a circular area of contact.

Rabinowicz (1965) has discussed five other methods of area

determination using experimental techniques such as the electrical resistance and sectioning methods. These methods are inappropriate for determining the area of rock contacts and different methods are needed. In this chapter two alternative methods of approach have been proposed and their advantages and limitations discussed. As in chapter 4 the factors influencing the magnitude of the contact area have been investigated and conclusions drawn as to their relative importance.

5.2 Method I - Carbon Paper Technique

5.2.i Sample Preparation

Three sets of samples were prepared for these tests, set 1 and 2 consisting of six irregular sandstone samples about 16 - 28 mm high and the third set of four shaped samples. The samples were prepared in the same way as those described in section 4.2. Sets 1 and 3 were tested dry but the samples in set 2 were saturated prior to and during the tests. Tables 5.2.1 - 5.2.3 give the measured contact angles, base areas and heights of the samples.

5.2.ii Method of Testing

Each sample was placed in the Instron 1195 and pieces of carbon copying paper and plain paper placed between the tip of the sample and the platen. The samples were then subjected to cycles of loading, using a rate of crosshead displacement of 0.2 mm/min. and the maximum load increased in each cycle. After each cycle the pieces of paper were removed and replaced by fresh pieces. In the saturated tests the pieces of paper were placed in polythene pockets to avoid getting them wet. By measuring the area of the imprints left on the plain paper using a graticule, it was possible to obtain data relating the area of contact and the maximum load during any cycle.

5.2.iii Test Results

The values of the area calculated for each sample are presented in Tables 5.2.1 - 5.2.3. The areas are given in mm^2 and were calculated to the nearest 0.25 mm^2.

Sample	1	2	3	4	5	6
$\dot{\alpha}_{1m}$	156.5	165.1	174.9	175.7	150.2	155.9
$\dot{\alpha}_{2m}$	130.3	144.9	150.6	163.2	131.4	143.1
$\dot{\alpha}_{5m}$	104.0	129.6	128.4	147.7	120.5	111.8
Height mm	21.30	17.97	17.89	15.94	16.02	17.04
Base area mm^2	1044	1133	1376	1230	992	1089
Load kN	Area of contact results mm^2					
0.1	1.00	1.50	2.25	1.00	1.00	1.00
0.25	2.00	3.00	3.25	1.50	1.50	1.25
0.5	6.25	3.25	5.25	2.50	2.25	1.75
0.75	7.00	3.75	12.25	3.00	3.00	2.50
1.0	11.50	4.75	13.25	4.25	9.25	4.50
1.5	13.75	5.50		5.75	10.50	8.50
2.0		7.25		9.75		12.00
Failure	16.00	12.25	22.25	14.25	19.00	17.50

Table 5.2.1 Details and Results - Dry, Irregular Samples - Set 1

Note:- For sample 3 all loads should be multiplied by 2.5

Sample	1	2	3	4	5	6
$\alpha_{1m}^{\bullet}$	148.3	132.5	132.5	152.1	133.7	147.3
$\alpha_{2m}^{\bullet}$	137.9	113.8	111.2	131.4	127.5	132.3
$\alpha_{5m}^{\bullet}$	129.5	106.1	98.0	114.5	111.4	97.5
Height mm	23.50	25.26	23.36	28.20	23.98	28.00
Base area mm^2	1001	751	1025	1449	1272	613
Load kN	Area of contact results mm^2					
0.1	2.50	3.00	2.25	2.25	1.75	2.00
0.2	3.50		2.75		3.00	2.75
0.25		4.50		3.75		
0.3	4.00		3.25		3.75	3.75
0.5	6.25	11.25		4.50	5.00	5.75
0.75	7.50			7.50	7.25	8.00
1.0	7.50			9.50		
1.5	8.75					
Failure	10.25	19.5	7.25	11.75	11.25	11.25

Table 5.2.2 Details and Results - Saturated, Irregular Samples - Set 2

Sample	1	2	3	4
β°	85.6	115.5	140.1	164.3
Height mm	25.12	24.98	26.30	26.08
Base Area mm^2	4950	4950	4950	4950
Load kN	Area of contact results mm^2			
0.1	1.00	1.00	0.75	1.00
0.2	2.00	1.00	1.25	1.25
0.3	2.00	1.25	1.25	1.50
0.5	4.00	2.25	1.50	2.75
0.75	4.75	4.00	2.75	3.75
1.0	5.75	4.50	3.50	4.25
1.5	12,75	11.50	4.75	5.25
2.0		13.25	8.50	6.75
3.0			11.50	9.00
Failure			21.50	45.00

Table 5.2.3 Details and Results - Dry Shaped Samples - Set 3

The results, plotted in figs. 5.2 - 5.4, show very clearly that the contact area increases with the maximum load but there is significant divergence of the points at higher loads. There does, however, appear to be a lower bound line to each graph. The graphs also show the points at which the Damage Load occurred for each sample, and it can be seen that the divergence of the points from the lower bound line occur once the Damage Load has been reached. The spread of results make it difficult to establish any relationship between the two parameters, but if attention is concentrated on the behaviour before the Damage Load is reached a clearer picture emerges.

5.2.iv Behaviour prior to the Damage Load

Figs. 5.5 - 5.7 show the results obtained from cycles of loading with maximum loads less than the Damage Load. These points correspond to points on the initial smooth section of the load-displacement curves described in Chapter 4. Since these modified graphs show much less scatter, it is possible to use curve fitting techniques to obtain relationships between the two parameters. The results of this analysis are given below (5.3) and it should be noted that the influence of contact angles, base areas etc. was not taken into account.

Set 1:- dry, irregular samples

$$A = 4.25\ P^{0.62} \qquad \text{(correl. coeff. = 0.94)}$$

Set 2:- saturated, irregular samples

$$A = 7.95\ P^{0.56} \qquad \text{(correl. coeff. = 0.96)}$$

Set 3:- dry, shaped samples

$$A = 3.72\ P^{0.68} \qquad \text{(correl. coeff. = 0.97)}$$

A = area in mm^2

P = load in kN (5.3)

5.2.v Effect of Saturation

The mean curves given above have been reproduced in fig. 5.8. There is a good agreement in the curves for the dry samples indicating again that results from shaped samples are representative of results produced from real but more complex irregular contacts. There is a distinct difference in the behaviour of the dry and saturated samples showing that the areas needed to sustain the same loads are much greater for a saturated sample than for a dry one over the range of loads at which samples can be realistically tested. This implies that loss of strength caused by saturation allows more crushing of the contact to take place under load. It is interesting to note from Table 3.6.2 that saturation reduces the rock strength to approximately half its dry value and that the areas determined for saturated samples are approximately double those for dry samples.

5.2.vi Variation of Strength

If the strength of the material is a factor which influences the area generated under load, then it would be expected that pieces with equal strengths would produce similar curves. In set 1 samples 2 and 3 were taken from the same block of material and in set 2 samples 3, 4, 5 and 6 were obtained from the same block. A study of the positions of the curves for these samples indicates similarities, although care must be taken in drawing any firm conclusions.

5.2.vii Variation with Contact Angle

A study of the relative positions of the curves and the contact angles of each sample does not suggest that a relationship exists. This is surprising in view of conclusions reached in Chapter 4 and this discrepancy has been investigated in section 5.4.

5.2.viii Variation with Height and Base Area

Since the shaped sample have approximately equal heights

and base areas and produce results consistant with those from irregular samples, it seems unlikely that these two parameters influence the areas generated. The positions of the curves for the irregular samples do not show any correlation with either parameter.

5.2.ix Behaviour after the Damage Load

Figs. 5.2 - 5.4 also reveal some interesting behaviour once the Damage Load has been reached. On the cycle in which the Damage Load is reached and in subsequent cycles the increases in area generated are alternatively large and small, producing a 'stepping' effect in the curve (see figs. 5.2 and 5.4 particularly). This is due to the way in which damage occurs at the contact. If the tip is subjected to a load it cannot sustain, then breakage occurs along the weaknesses in the contact zone material. This may result in the tip breaking down to form an area which is more than sufficient to sustain the applied load and possibly even the maximum load in the cycle. This will be seen as a large increase in area for that cycle. On the subsequent cycle the area will only increase once the load it can carry has been exceeded. Providing the maximum load of the subsequent cycle is not much greater than this load then only a small increase in area will be needed and it is possible that no further damage will occur during this cycle.

5.2.x Advantages and Limitations of Method I

The main advantage of this method is that tests can be performed simply and quickly, once the samples have been prepared, without using highly sophisticated instrumentation. This means that large amounts of data can be obtained allowing statistical methods to be used with a higher degree of confidence. The method also allows measurements of area to be made at points throughout the test, rather than obtaining just one result per sample. A picture of the behaviour of each sample can be built up and any anomalies spotted, as well as combining all the results to obtain models describing the 'average' behaviour. Another advantage is that the imprint produced is the real area of contact, although spurious marks may be produced if excessive damage occurs. This contrasts with many methods where it is necessary to make assumptions about the shape, size or number of

the junctions.

Although the tests are easily performed, difficulties may arise in obtaining the data from the imprints. It was found that at the higher loads the paper was quite often torn and the imprint distorted due to the breakage at the contact. Wetting of the paper during saturated tests also caused smudging. Although it is an obvious advantage to obtain an imprint of the real area, this imprint is small (especially in the initial stages of the test) and care must be taken in measuring the area. Unless the imprint can be magnified quite considerably to allow instruments, such as planimeters, to be used, the measurement is based on observation and is therefore open to human error. In the tests carried out in this research the imprints were observed through a camera lens and measured against a 1 mm graticule. The areas were measured at least six times and the mean value used.

This method is based on the assumption that a sample requires a specific area to carry a specific load i.e. there is a unique load-area relationship. The area generated under a certain load is independent of the load-path and of any damage the contact may have undergone. In this method the area of contact is disturbed each time the carbon paper is removed and a fresh piece inserted. It was found in some cases that particles of rock were transferred from the contact to the paper and removed with the paper. Unloading may also allow particles to fall away from the contact region. Despite this the area values calculated are assumed to be exactly the same as those which would have been obtained if the contact had not been disturbed. Whereas the cases encountered in practice mainly involve rock on rock contacts, only rock on platen tests can be performed with this method.

In order to overcome these problems a method was required, which allowed rock on rock tests to be carried out and in which the contact was not disturbed or unloaded. This would give a truer picture of the contact area variation with load under conditions seen in practice. To do this a second method was devised and investigated.

5.3 Method II - Camera Technique

This method is based on a graphical analysis which produces

an upper bound solution for the area. Fig. 5.9 shows a view of the two particles from a point on the edge of the cylinder in a rock on rock test (fig. 4.7). From such a view, it is possible to measure the distances a' and a" from the cylinder axis to the edges of the contact area. Having obtained several values of a'i, a"i and θ_i, where θ_i is the angle of rotation from the initial view (fig. 5.10) and i the point number, these may be replotted on cartesian axes. Lines are drawn parallel to and at distances a'i and a"i from the line radiating from the origin at θ_i to the x-axis, fig. 5.11. Repeating this for all the data points produces a graph similar to that shown in fig. 5.12. Since these parallel lines represent the boundaries of the area of contact then the shaded area included within these lines must represent the area of contact. Fig. 5.13 shows the same example with the actual boundaries of an area drawn in. This shows that the calculated area is always greater than or equal to the real area. If the real area is a convex shape e.g. an ellipse then the error in the calculated area will be small.

5.3.i Area of Contact Rig

In order to use this method a special rig was designed and made. It was decided to use a camera as the means of storing the information, rather than making direct measurements during the tests, so that the tests could be performed quite quickly and the data preserved for analysis afterwards. In order not to have to disturb the samples at any time during tests a 'roundabout' was made and the camera hung from this, fig. 5.14. This was able to rotate freely about the central column so that photographs could be taken from any angle.

Fig. 5.15 shows the finished rig in the Instron 1195 testing machine. A cine camera, with a single shot facility and macro lens, was used, since this provides a relatively cheap method of storing a lot of information. As fig. 5.15 shows, it is also necessary to provide sufficient lighting and it was found that two lamps were needed to avoid casting shadows on the rock surface. Fig. 5.16 shows the central pivot of the 'roundabout' which was marked every 5° so that the angle of rotation could be easily calculated.

5.3.ii Sources of Error

(a) Theoretical work

The accuracy of the analysis depends upon the number of views taken and therefore the variation in error with the viewing angle interval i.e. ($\theta_i - \theta_{i-1}$) was investigated. To do this a number of standard shapes were analysed using the graphical method. A computer programme 'Area' was written to calculate the points of intersection of the lines and the inclusive area as well as producing a picture of the area. This general programme was adapted to analyse each of the standard shapes, fig. 5.17 shows the original point of viewing of the shapes and the general expressions obtained for a'i and a"i. For the ellipse three ratios of b/a viz. 0.25, 0.5, 0.75 were considered.

Fig. 5.18 shows the variation of the error with the viewing angle interval. There is less than a 5% error for most of the shapes if the angle interval is less than 20° i.e. taking 9 views at regular intervals. The expressions (ii) (fig. 5.17) for a square produce no error whatever the angle interval but quite large errors can be introduced if one of the views is not parallel to the sides of the square. This implies that for any area there is a set of data points which will generate an optimum area value. The ellipse results indicate that as the ratio b/a decreases, then for a particular viewing angle interval, the error increases.

Since contact areas generally approximate to ellipses this final point was investigated further. Taking an angle interval of 5° the percentage errors calculated were plotted against ratios of b/a, fig. 5.19. While the errors become relatively quite significant for values of $b/a < 0.2$, for $b/a > 0.4$ the errors are approximately constant. If a larger angle interval is used then relatively significant errors would occur at higher values of b/a.

This analysis of standard shapes highlights two factors which should be taken in account when considering irregular area shapes.

(i) Accuracy increases with decreasing angle interval

(ii) The original viewing point may effect the accuracy if the angle interval is too large.

Although a 20° angle appears to be sufficient to obtain good area

approximations for standard shapes, the accuracy will be substantially reduced for irregular shapes. In these tests a 5^{o} angle interval was found to be quite reasonable and, although the amount of data to be analysed for a test is quite large and time-consuming, the results can be quoted with greater confidence.

(b) Other sources

In usingthis method it is assumed that the contact region is viewed from a point at infinity which is reproduced in the computer by drawing lines parallel to the directionof viewing. The use of a camera at a finite distance from the contact area means that these lines are not parallel and meet the edges of the area at an angle to the direction of viewing.

(i) Circular Area

If the area is a circle then for a tangent to the circle at α^{o} to the direction of viewing, the radius is measured as x" instead of x' and the error, E, is

$$E = (1 - \cos^{2} \alpha) \times 100\ \%$$

If α is less than ~~17.5~~ 13^{o} the error is less than 5% but at large angles the error becomes quite substantial, fig. 5.20.

(ii) Irregular Area

The situation arising for an irregular area shape presents more difficulties as a point which would have been picked up by the parallel line tangent is in the shadow of the angle α tangent, fig. 5.21. The error, E, is dependent upon the distance l and as long as $x' > x''$ and $x' < (l + h) \tan\alpha$ then an incorrect measurement will be made. Since the distance l is dependent on the unknown area shape then the error cannot be quantified.

The problem can be dealt with by using an iterative method of solution. The determined area shape will reveal anomalies at various points on the area boundaries in the form of small triangles, fig. 5.22. By adjusting the data appropriately and repeating the calculation a satisfactory solution can be obtained. This method is not very easy to use if a small viewing angle interval

is used as the pictures can become quite complicated.

In order to determine the likely error in assuming parallel lines for the camera position in this research, the variation of α with the distance across the contact area at the centre of the cylinder was calculated, fig. 5.23. Comparing this with fig. 5.20 the error in the measured diameter of the rock cylinder is found to be about 1.5%. Since the distances measured across the contact area were never greater than 4 mm the expected error for a circular area is less than 0.2% and it was decided that error introduced by the assumption of parallel lines could be assumed to be negligible.

5.3.iii Testing Procedure

Three irregular samples were prepared as before from two different blocks of material, samples 1 and 2 being taken from the same block. The samples were placed in the Instron 1195 as before and the camera set up, looking along the interface of the two particles and with the central column axis in the centre of the viewfinder, fig. 5.15. The samples were then loaded under a constant crosshead displacement rate of 0.2 mm/min upto 0.1 kN and the loading stopped. Rotating the camera through 5° intervals from a designated point, thirty six photographs were taken and then the loading continued. This process was repeated at loads 0.2, 0.3, 0.5, 0.75, 1.0, 1.5 kN or until the Damage Load was reached and then the sample unloaded.

5.3.iv Analysis of Results

Having completed the tests and developed the films, the values of a'i and a"i were collected from each frame. As the information was stored on 8 mm cine film it was necessary to use a 35x magnifying lens in a microfilm reader, the information being taken directly from the reader screen to avoid distortions in printing. Three measurements were taken from each frame, a'i and a"i and the diameter of the rock cylinder. This third measurement provides a calibration of the distances measured in each frame since the real diameter value of the cylinder is known.

Fig. 5.24 shows typical pictures of the area produced by the computer programme 'Area' from the sets of data. Although on applying the appropriate calibration factors the measurements were

accurate to about 0.06 mm, inaccuracies in the data still occur due to difficulties in determining the extent of the contact region. It was found that even with the magnification used it was often very difficult to pin-point the edge of the area of contact accurately. An inaccuracy in the placing of the edge of the area of 1 mm on the screen, leads to the intersection point of two lines in the computer picture, meeting at an angle of 5°, being about 3 mm from its true position. These inaccuracies produce a graph of a central area with spurious lines around it instead of the neat convex shape anticipated. This then is the result of an averaging process of the results rather than the plotting of exact values as in the case of the standard shapes.

Due to the difficulties in defining a unique area three methods of analysis were used.

(a) Equivalent Circle Method

This method determines the mean value of all the measured distances across the contact area for a particular load and assumes this to be the diameter of a circle.

$$D = \sum^{n}(a'i + a''i)/n$$

$$A = \pi D^2/4$$

(b) 72 Point Method

All the data from the thirty-six photographs for each load is used in 'Area' to produce pictures of the type shown in fig. 5.24. By blowing up these pictures to reasonable proportions, fig. 5.25, and estimating the shape of the contact area (shaded), its magnitude may be determined using a planimeter.

(c) 12 Point Method

The 72 Point Method is a subjective observation of the results which may introduce further error, whereas the 12 Point Method is an objective measurement. The data is split into six sets, each set consisting of the data from frames seperated by a 30° viewing angle interval e.g. 1, 7, 13, 19, 25, 31. These are seperately

analysed by 'Area' producing six pictures as shown in fig. 5.26. The shaded inclusive areas are calculated using a planimeter. From these six areas the contact area may be determined in one of two ways.

(i) the mean value

(ii) discard the largest and smallest values and take the mean of the remaining four

Both these approaches were used but it was found that the second method results were always within 0.1 mm^2 of the first and therefore only the first approach results have been presented.

5.3.v Results

The results of the three analyses and details of the samples are given in Table 5.3.1 and have been plotted in figs. 5.27 - 5.29, together with the equation (5.3) produced for dry irregular samples by the carbon-paper technique.

The graphs show increasing area with increasing load as before and the values are of the same order of magnitude as those determined by the carbon-paper technique. Both the equivalent circle and 12 point method results show good trends of increasing area but the 72 point results do not seem as consistent and have a greater scatter. The equivalent circle area values for sample 1 increase rapidly at higher loads, a trend not seen in the other two approaches.

Figs. 5.30 - 5.32 show the results replotted to allow comparisons to be made of the values calculated for each sample. The graphs for samples 1 and 3 show a good correlation between the values calculated by the 72 point and the 12 point methods but this is not seen for sample 2. In all these cases, apart from the higher load values of sample 1, the equivalent circle method results are approximately twice those obtained by the 12 point method.

5.3.vi Influence of Height, Base Area and Contact Angle

A study of the heights and positions of the curves in figs.

	1			2			3		
α_{1m}	155.4			141.9			132.4		
α_{2m}	150.4			123.9			97.0		
α_{5m}	132.4			123.5			99.6		
Height mm	27.48			28.62			33.12		
Base Area mm^2	2076			981			1284		
Load kN	Area (a)	Area (b)	Area (c)	Area (a)	Area (b)	Area (c)	Area (a)	Area (b)	Area (c)
0.1	1.8	0.6	0.6	0.6	0.3	0.6	1.2	0.4	0.8
0.2	2.0	0.8	0.8	1.0	0.5	1.1	1.4	0.7	0.8
0.3	2.4	0.9	0.9	1.4	0.4	2.2	1.8	0.9	0.9
0.5	3.5	1.6	1.8	2.1	1.1	2.6	2.7	1.1	0.9
0.75	5.8	2.3	2.4				3.7	1.9	1.4
1.0	7.8	2.8	3.0				4.5	2.3	2.0

Table 5.3.1 Details and Results - Dry, Irregular Samples

Note:- Area (a) - Equivalent Circle Method: Area (b) - 12 Point Method: Area (c) - 72 Point Method.

5.27 - 5.29 does not suggest any relationship of the height with the area of contact. The base areas increase with increasing contact area in the equivalent circle results and it may be argued that a similar trend is seen in the 12 point method values but this is less distinct. There does not appear to be any reason why a larger base area should produce greater contact areas.

Neither the equivalent circle or 72 point methods show any correlation of the curve positions and the angles, $\alpha_1 m$, $\alpha_2 m$ and $\alpha_3 m$. The 12 point method results show a similar trend to the variation of the $\alpha_2 m$ and $\alpha_3 m$ angles but again this is not very distinct.

5.3.vii Comparison of Methods I and II

Comparison of the results and conclusions of the carbon paper and camera techniques should give some indication of which of the three approaches viz. equivalent circle, 12 or 72 point gives the best results. The 72 point results do not show any particular correlation with the equation (5.3) line and although the 12 point results follow this line quite well, the area magnitudes are much smaller. The equivalent circle analysis results, however, show a good distribution of points on either side of the equation line.

5.3.viii Limitations of Method II

Although the errors likely to occur in the analysis have been investigated and taken into account, the method is very sensitive to errors in the data. Small inaccuracies in fixing the contact boundaries are accentuated by the analysis and obscure the area of contact. An alternative test was devised using a parallel light source and a convex lens as shown in fig. 5.33. If the lens is placed so that the contact region is at the focal length then an image of the samples may be thrown up onto a screen. Measurements taken from this image are more accurate because of the large magnifications which can be achieved and because the area boundary is much more distinct. However, the method has practical difficulties, since the samples cannot be rotated very easily without disturbing the contact and the Instron 1195 has wide side pillars which obscure the image over a large portion of

the 'roundabout' rotation. Photographing samples with a light source behind them produced distorted pictures of the contact region.

5.4 Comparison of Results with Theoretical Work

The work presented in section 5.1 gives the theoretical load-area relationships for plastic and elastic materials, (5.1) and (5.2).

Plastics:- $A_p = P/hp$

Elastic:- $A_e = \pi . m . n . \left[\frac{P.D}{(A + B)} \right]^{\frac{2}{3}}$

For a circular area of contact of a shpere on a plane, which has a similar load-displacement relationship to rock contacts, the elastic expression reduces to

$$A_e = \pi . R^{\frac{2}{3}} D^{\frac{2}{3}} P^{\frac{2}{3}} \qquad (5.4)$$

For a sandstone rock on rock contact three expressions have been determined by the carbon-paper technique for the initial behaviour, section 5.2.iv

Dry, irregular samples

$$A = 4.25\ P^{0.62}$$

Saturated, irregular samples

$$A = 7.95\ P^{0.56} \qquad (5.5)$$

Dry, shaped samples

$$A = 3.72\ P^{0.68}$$

A = area in mm^2
P = load in kN

The index of the load obtained from experimental work shows very good agreement with the elastic equation index, particularly for the dry samples. This agrees with the conclusion reached in the study of the initial load-displacement curves.

There is, however, a major difference between the experimental results and this theoretical expression. The theoretical equation shows a variation of the area with the sphere radius, R, whereas in the experimental work of both the camera and carbon-paper techniques no correlation of the results with the angle of contact was found. The study of contact load-displacement behaviour in Chapter 4 showed that

$$d = \frac{C}{\beta^{\wedge}} P^{\frac{2}{3}}$$

β is contact angle

which compares with the Hertzian equation

$$d = \frac{C'}{R^{\frac{1}{3}}} P^{\frac{2}{3}}$$

and indicates that the contact angle has a similar role to the sphere radius. If the load is considered to be a function of the contact area and the strength, S i.e. $P=g(A)$. $f(S)$ then

$$d = \frac{C}{\beta^{\wedge}} g(A)^{\frac{2}{3}}. f(S)^{\frac{2}{3}}$$

Unfortunately, the displacement-area relationship could not be investigated to see whether or not this relationship was dependent on the contact angle, because in using the carbon-paper method the sample was distrubed when removing and replacing the carbon paper.

The theoretical load-area relationship (5.4) does not contain a term representing the strength of the material but the experimental results do suggest that the strength is important. This is seen in the higher area values obtained from the saturated results (fig. 5.8) and the similarity of the results of samples from the same blocks of material (section 5.2.vi). Fig. 5.34 shows a plot of the inverse strength values (Tables 3.6.1 and 3.6.2) against the experimental coefficients (5.5). A best fit analysis of these results produces the following strength (S) - coefficient (C) relationship with a correlation coefficient of approximately 0.99

$$\frac{1}{S} = 2.874\, C^{1.516}$$

Assuming a load index of $\frac{2}{3}$, the area of contact may be calculated as follows

$$A = \frac{0.495}{S^{0.66}} \quad P^{\frac{2}{3}}$$

$$\frac{1}{2}\left[\frac{P}{S}\right]^{\frac{2}{3}}$$

Taking a dimension analysis of this equation the 0.5 coefficient has units of $(\text{distance})^{\frac{2}{3}}$ and since it does not vary with test condition, angle of contact, base area or height of sample, it appears to be a constant for the rock material. The information available here does not allow a conclusion to be reached but the distance dimension does suggest a volume/area or elasticity modulus/density ratio. Experiments on other types of rock may provide a better understanding of the role of this parameter.

5.5 Conclusion

Fig. 5.35 shows a comparison of typical load-area and load-displacement curve shapes. In the initial stages of the test, before the Damage Load is reached, both graphs show a smooth change of gradient. At this stage experimental evidence suggests that the load-displacement behaviour is dependent upon the angle of contact, whereas the load-area behaviour is dependent on the strength of the material. It has been suggested in Chapter 4 that loss of strength due to saturation also effects the load-displacement relationship.

Once the Damage Load has been reached the load-displacement behaviour becomes quite complex due to crushing and spalling at the contact. This is reflected in the load-area graph by a stepped curve as the tip breaks down to give alternatively large and small area increases as described in section 5.2.ix.

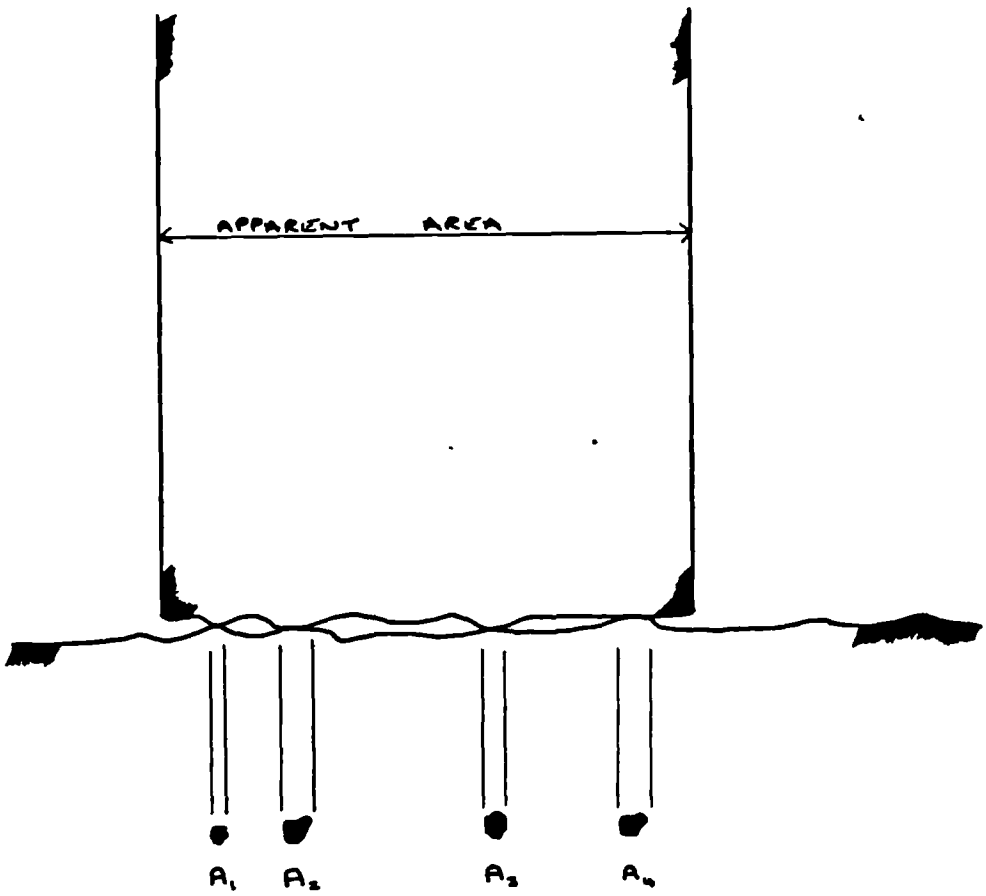

$$\text{REAL AREA} = \sum_{i}^{n} A_i$$

FIG. 5.1 :- REAL AND APPARENT AREA OF CONTACT

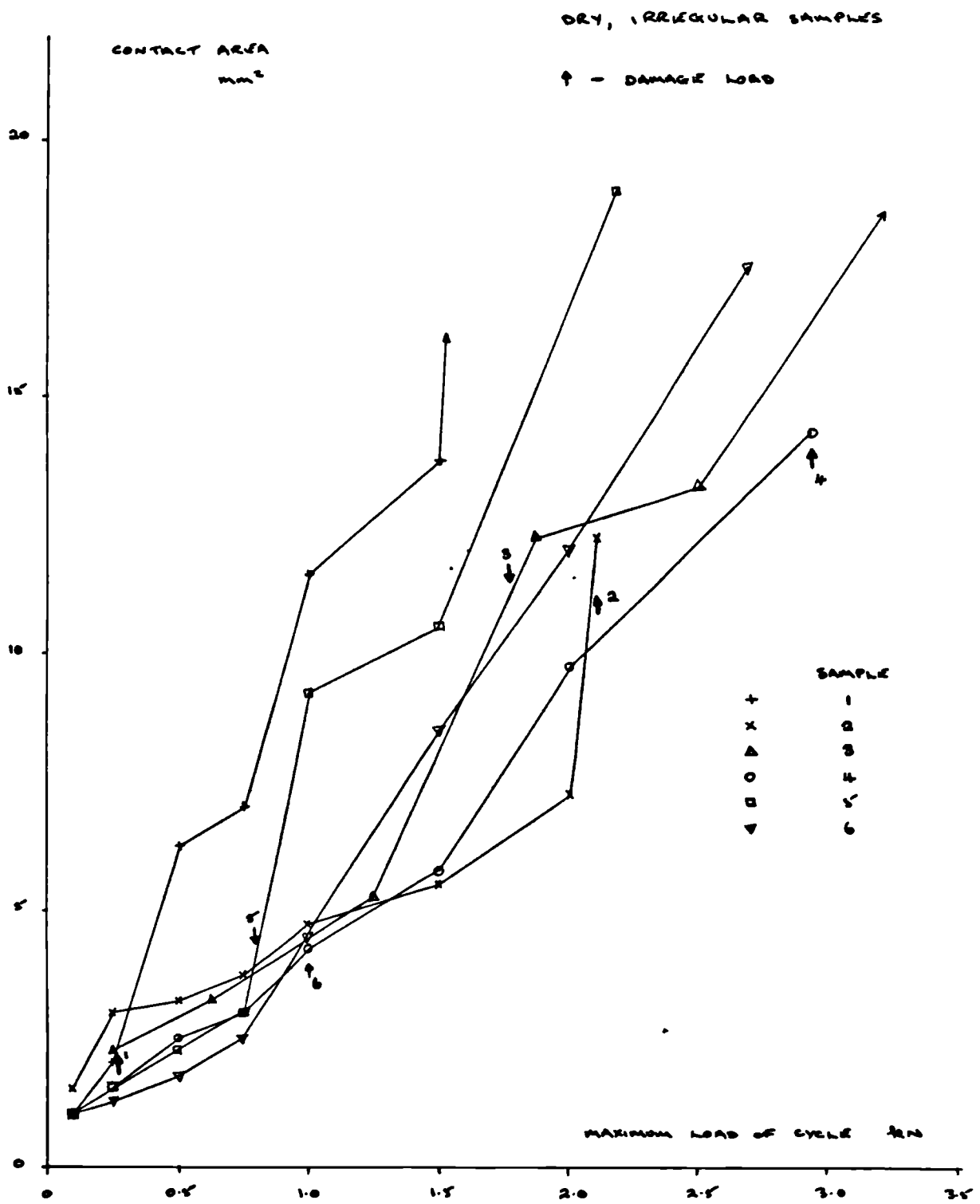

FIG. 5.2 :- METHOD I AREA RESULTS - SET 1 SAMPLES

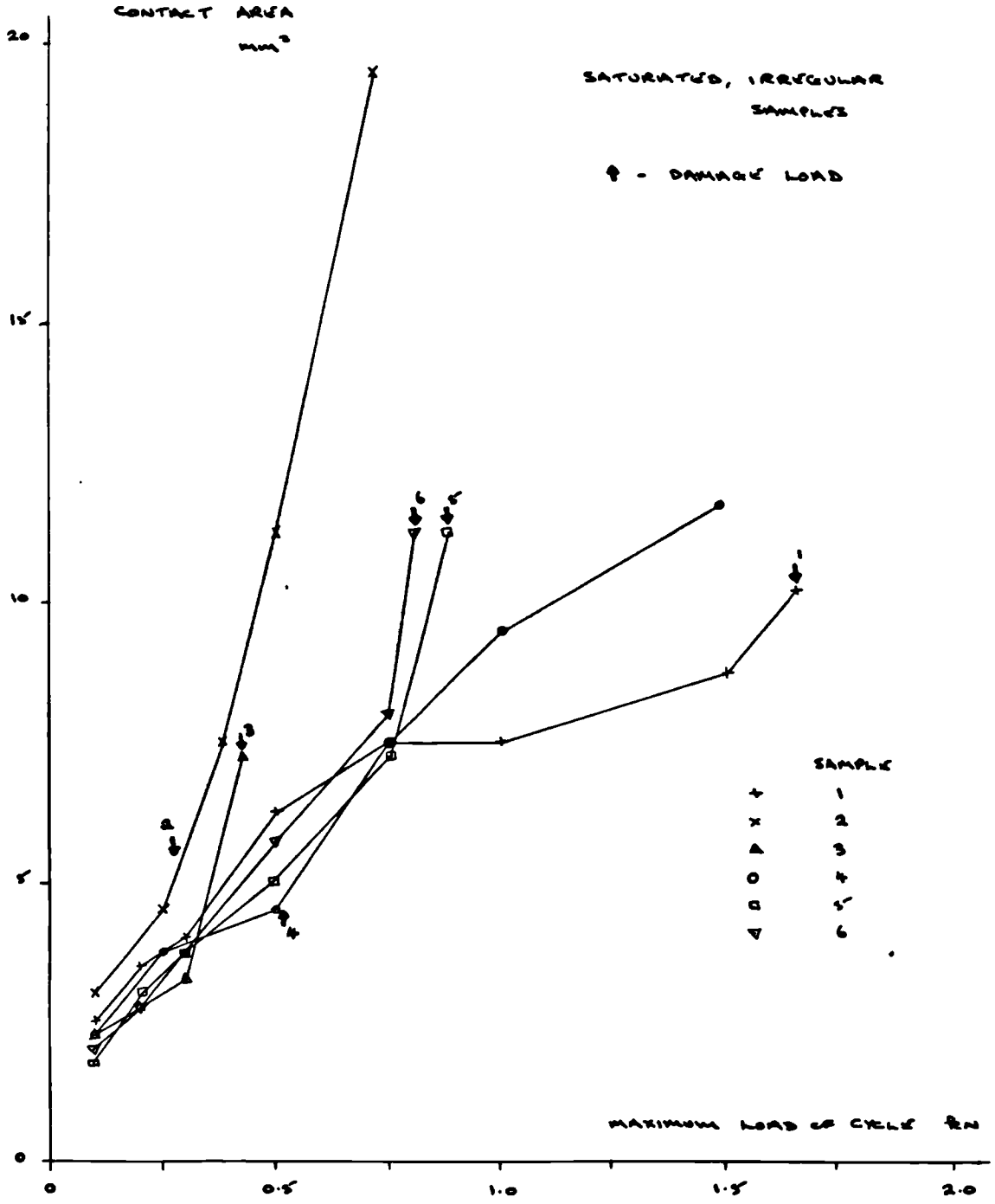

FIG. 8.3 :- METHOD I AREA RESULTS - SET 2 SAMPLES

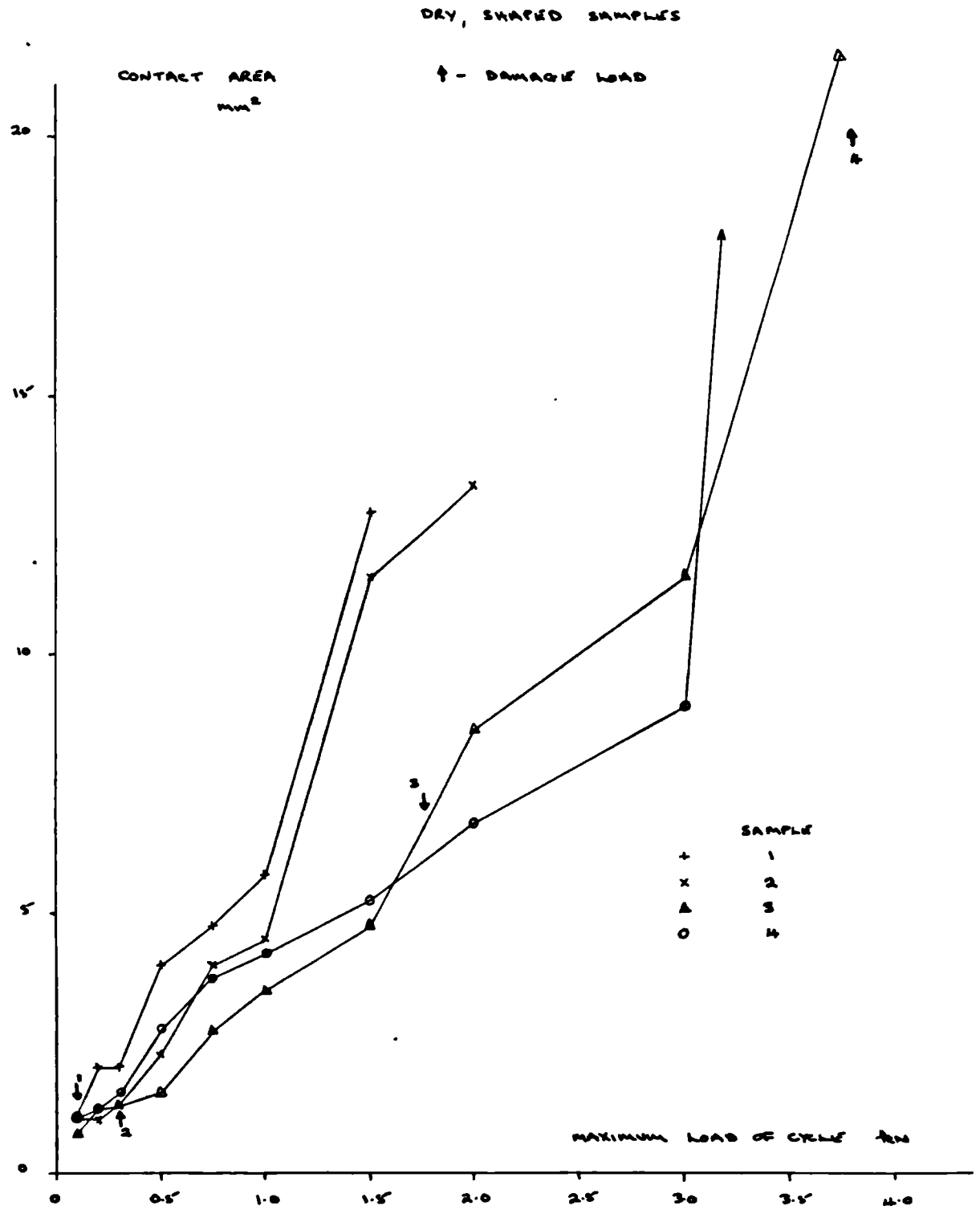

FIG. 8.14 :- METHOD I AREA RESULTS - SET 3 SAMPLES

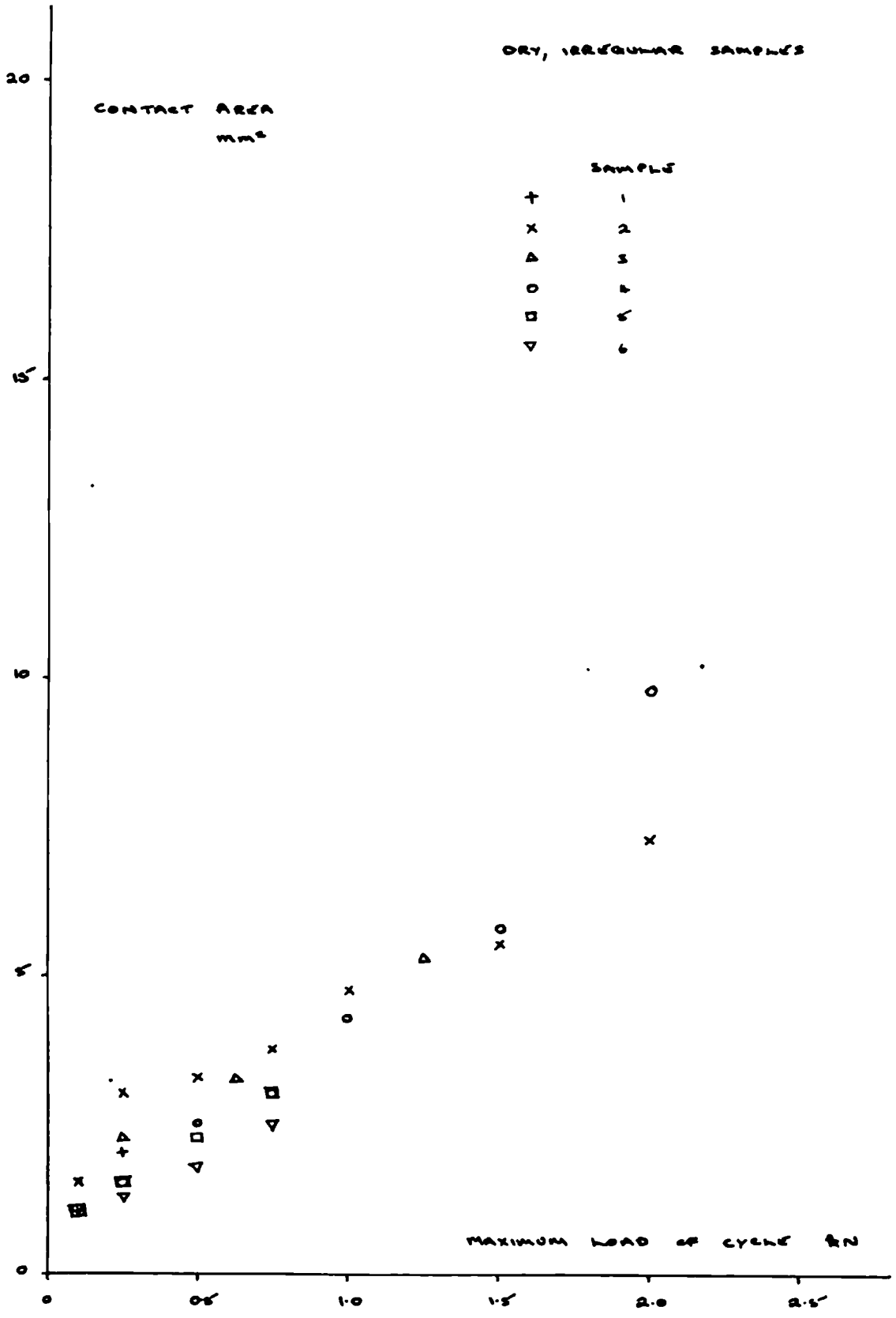

FIG. 5.5 :- MODIFIED GRAPH OF SET 1 SAMPLE RESULTS

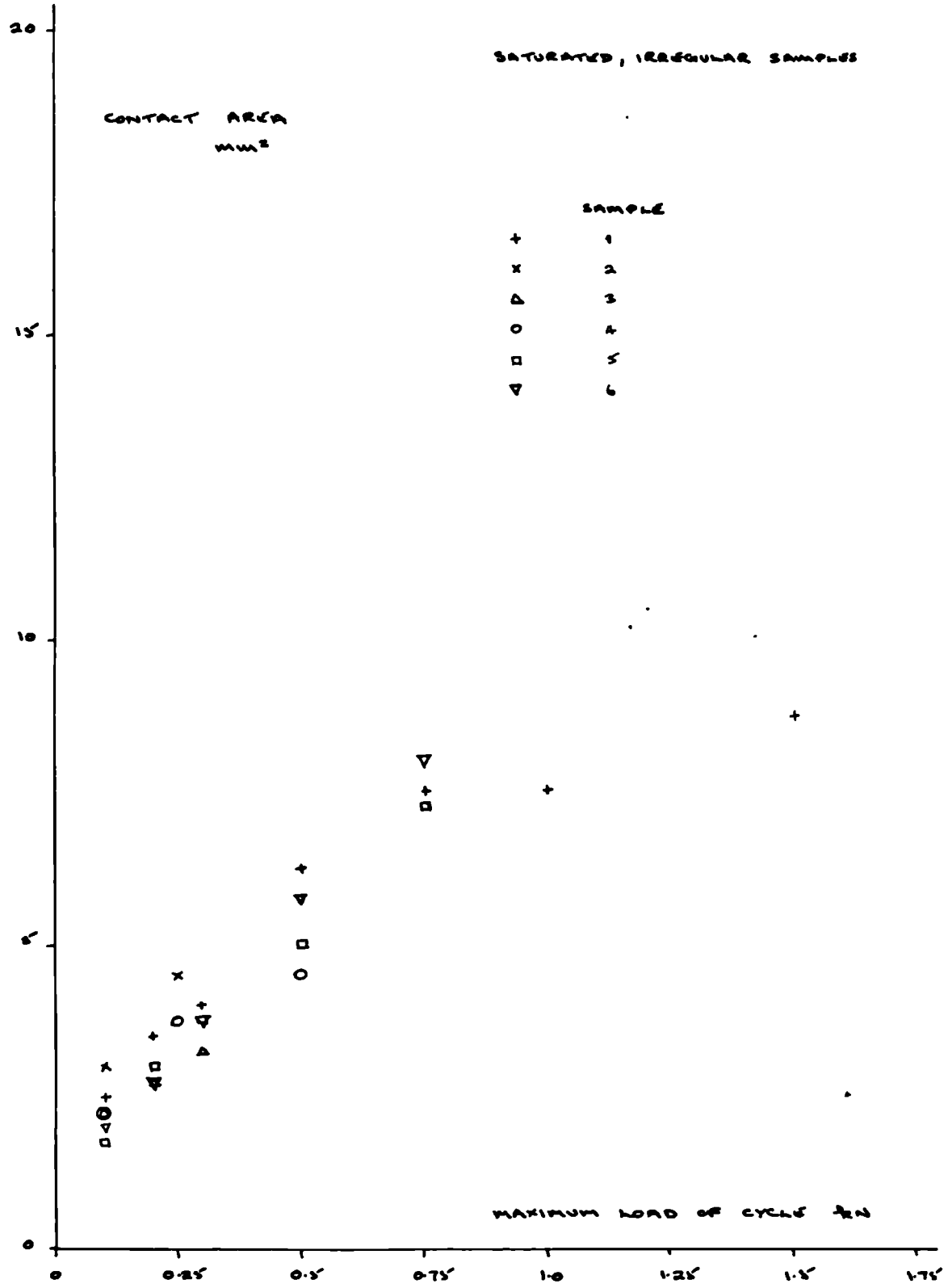

FIG. 5.6:- MODIFIED GRAPH OF SET 2 SAMPLE RESULTS

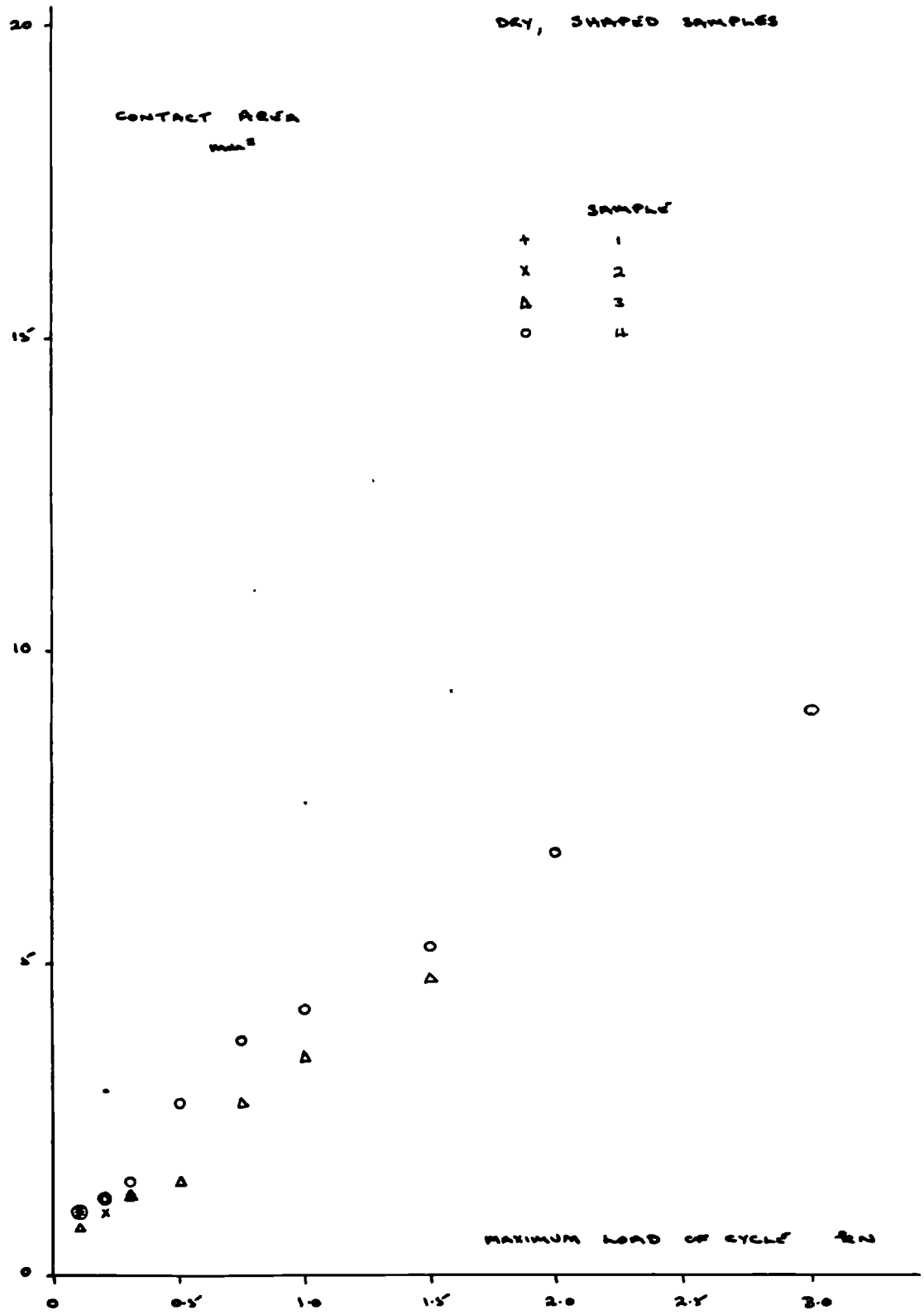

FIG. 5.7 :- MODIFIED GRAPH OF SET 3 SAMPLE RESULTS

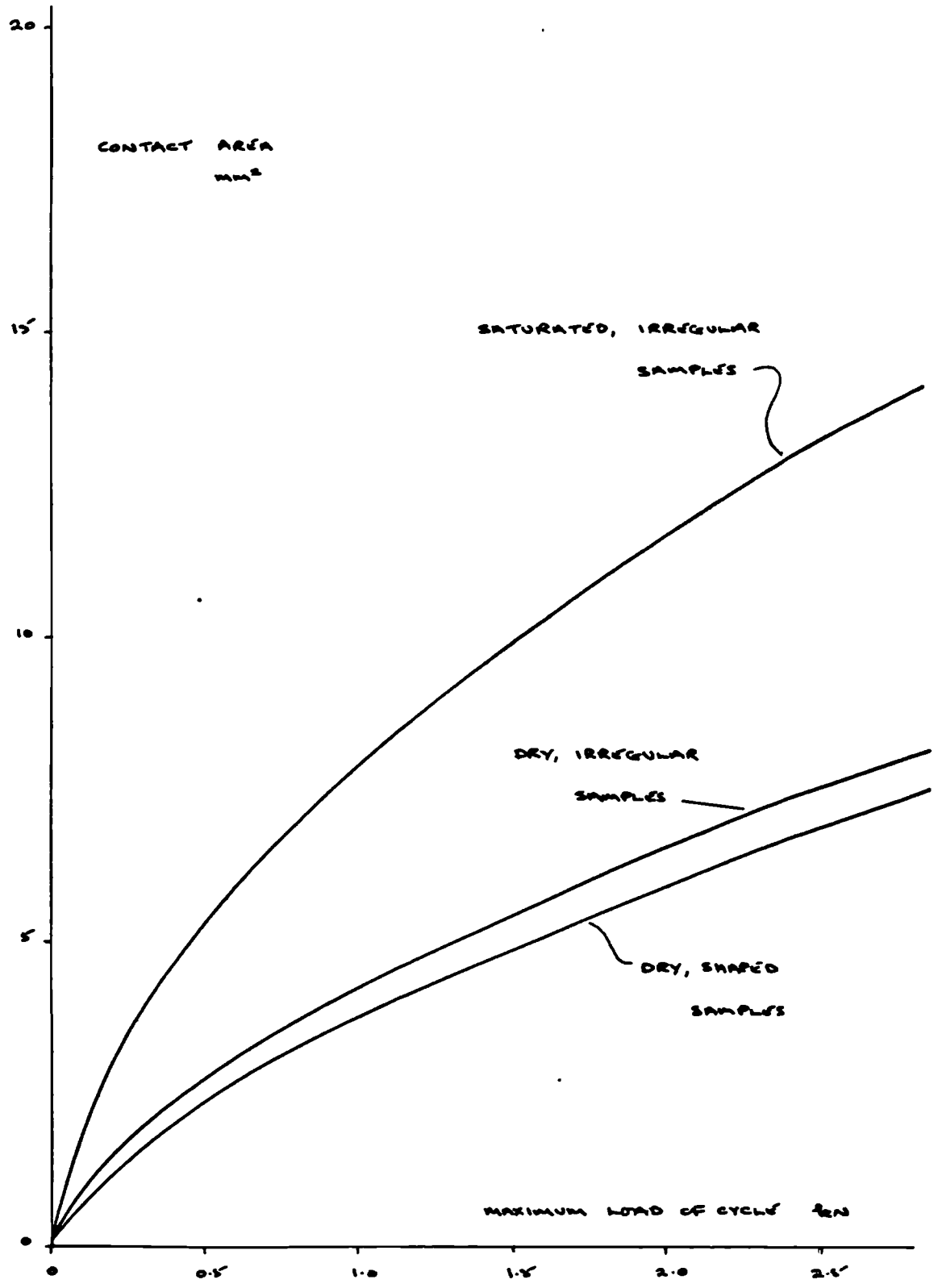

FIG. 5.8 :- COMPARISON OF MEAN CURVES FOR DRY AND SATURATED SAMPLES

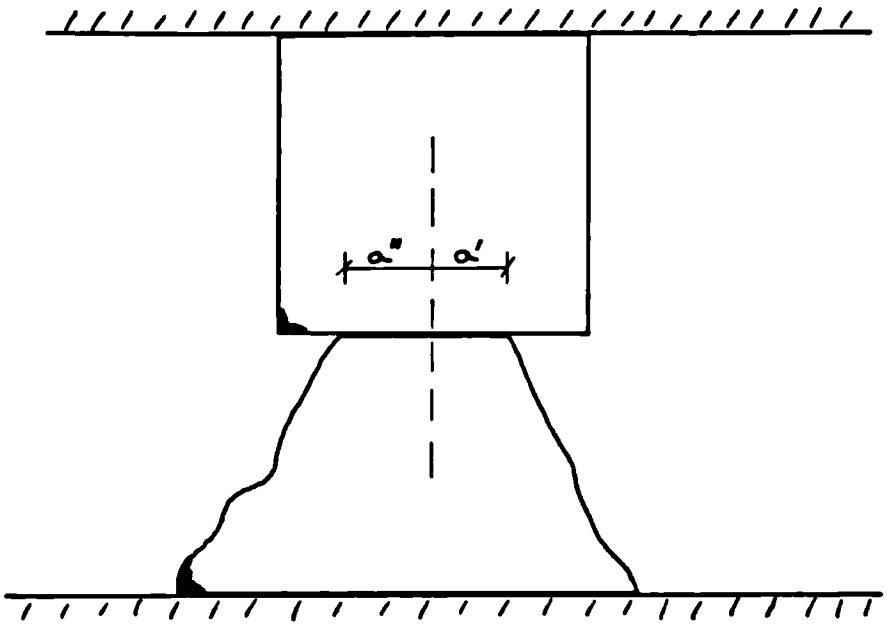

FIG. 5.9 :- ELEVATION OF ROCK ON ROCK TEST

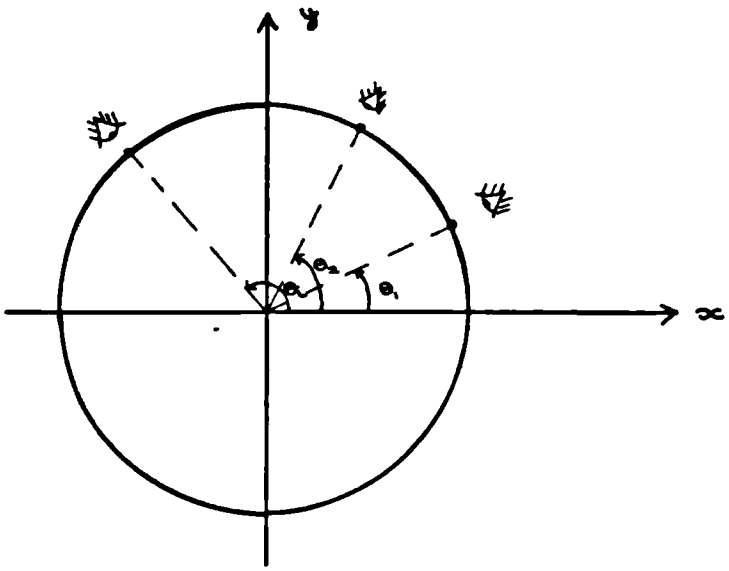

FIG. 5.10 :- MEASUREMENT OF θi

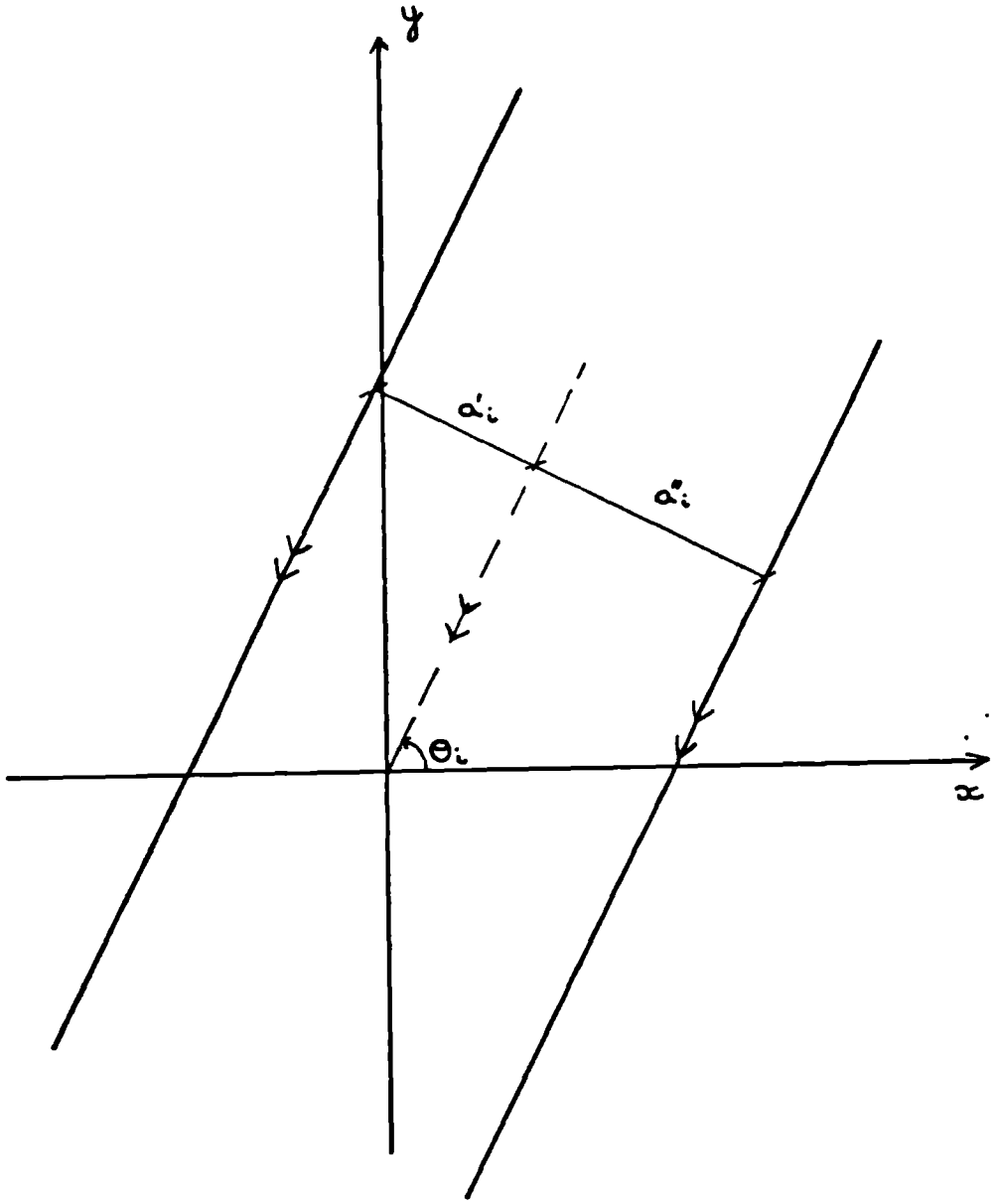

FIG. 5.11 :- GRAPHICAL METHOD - INITIAL STAGE

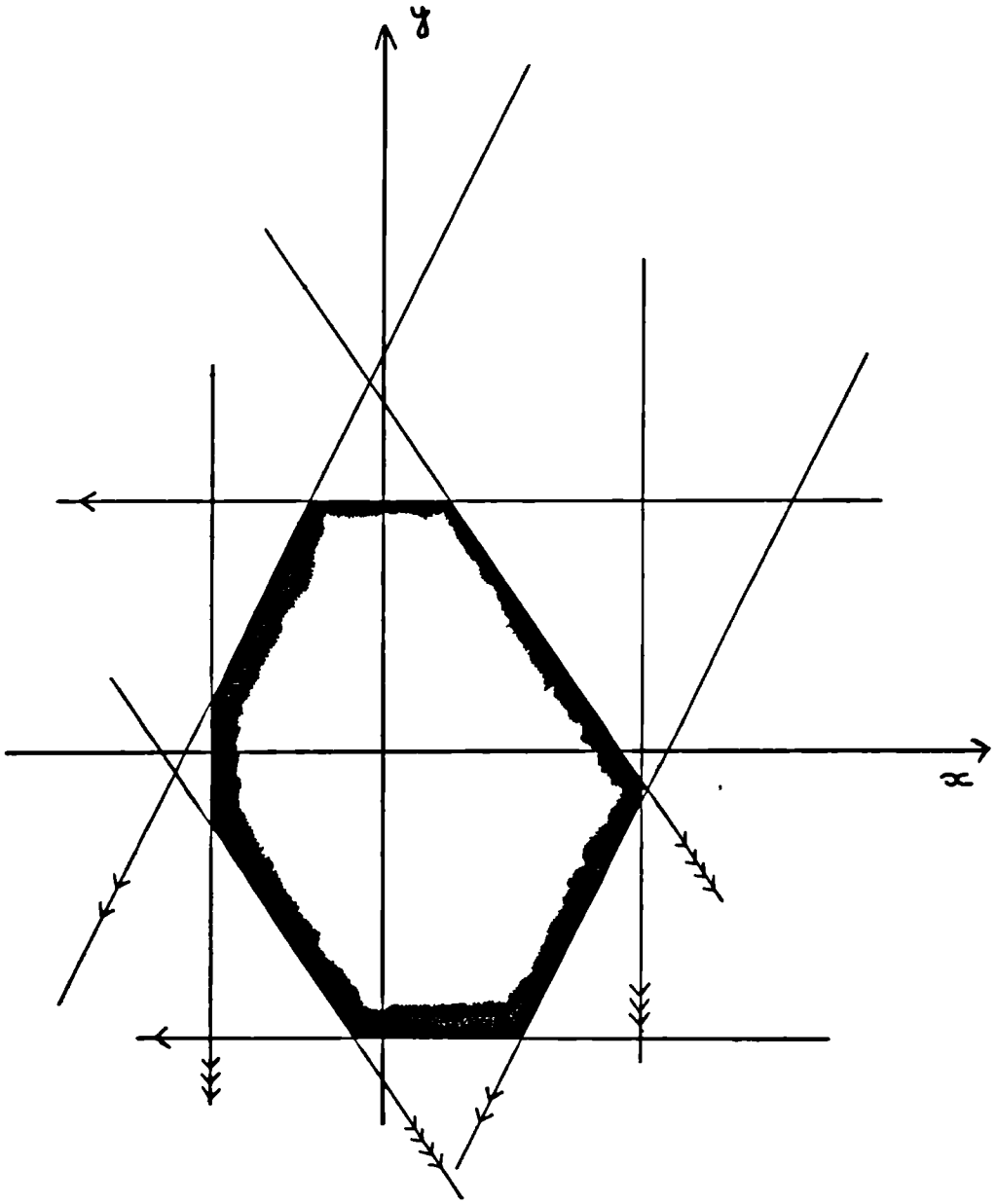

FIG. 5.12 :- GRAPHICAL METHOD - FINAL STAGE

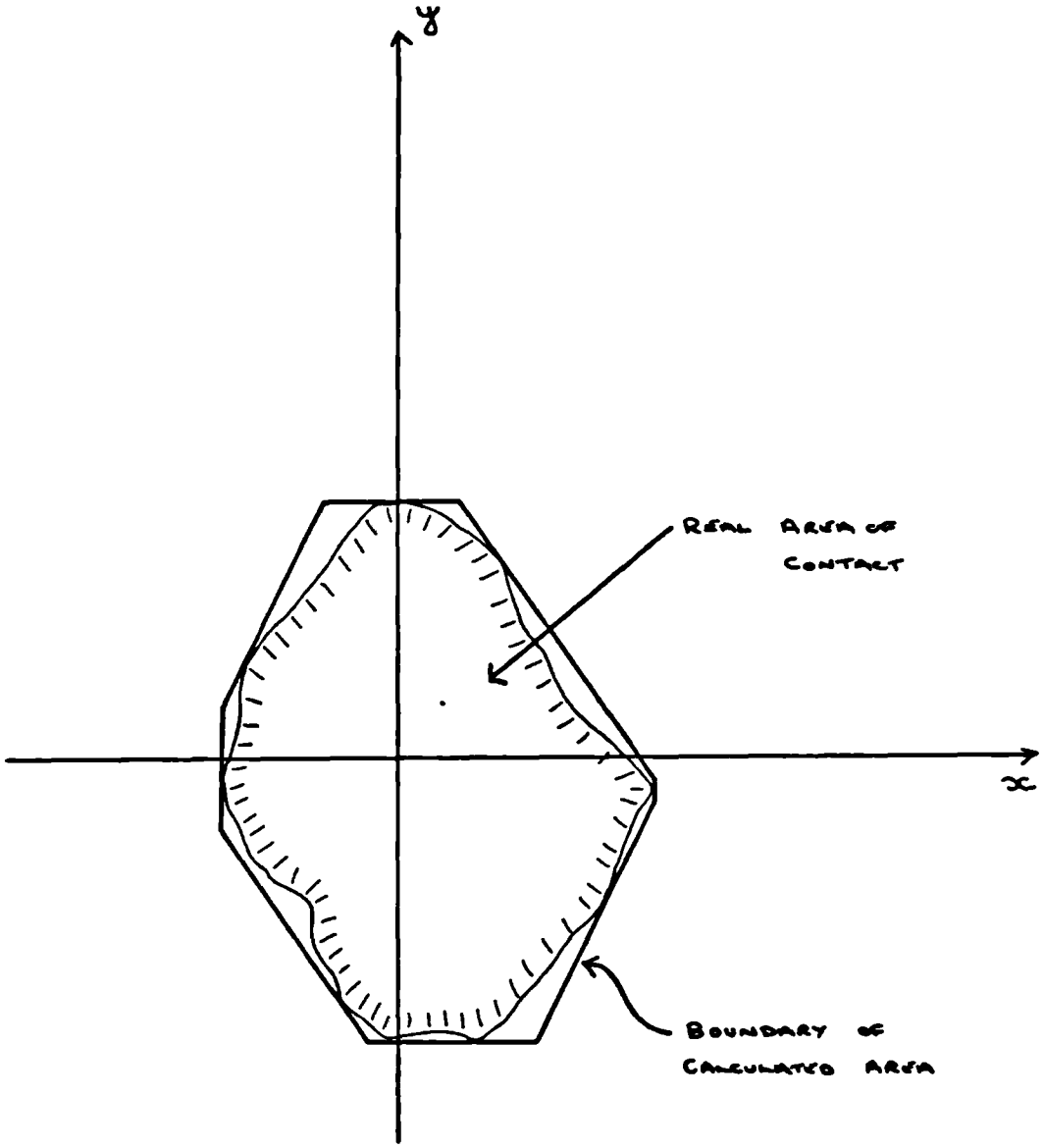

FIG. 5.13 :- COMPARISON OF REAL AND CALCULATED AREA

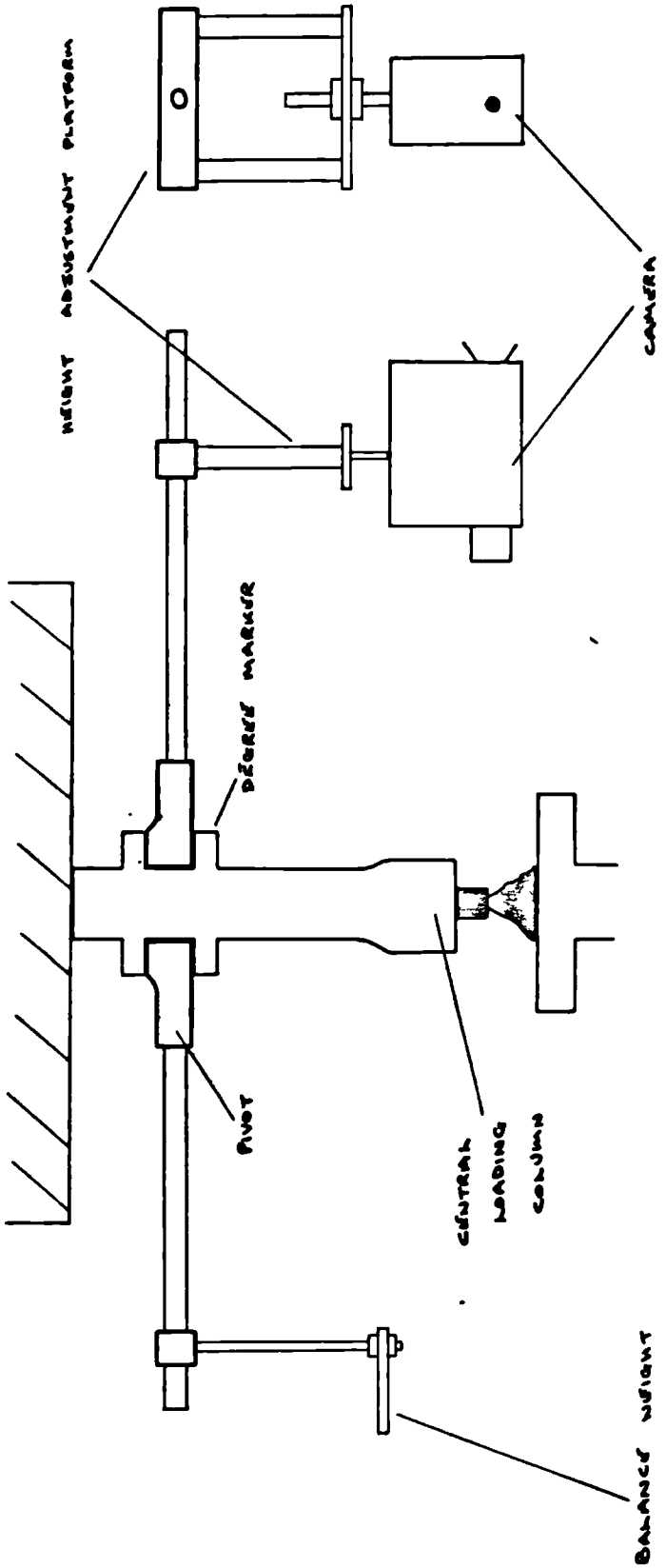

Fig. 5.14 :- CONTACT AREA RIG

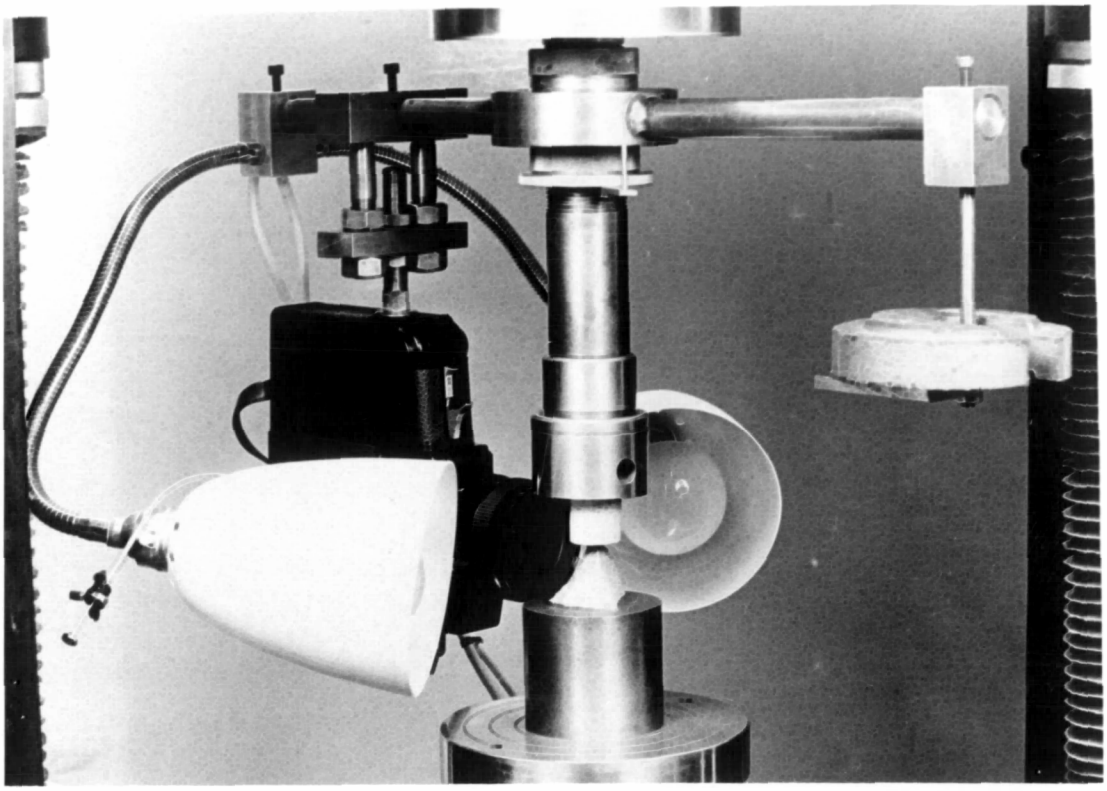

Fig. 5.15 :- Contact Area Rig

Fig. 5.16 :- Contact Area Rig: Detail of Pivot and Angle Measurement Scale

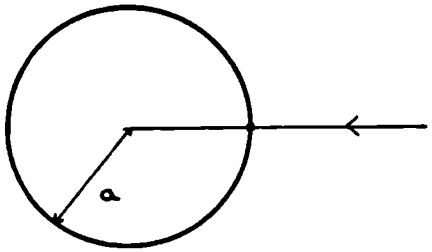

(i) CIRCLE

$a'_i = a \qquad a''_i = -a'_i$

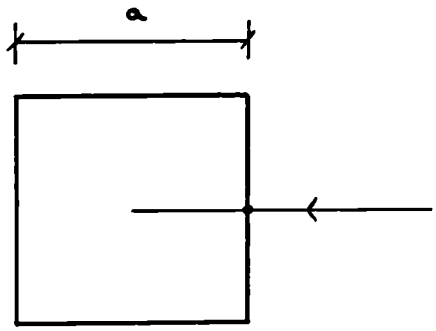

(ii) SQUARE

$a'_i = \sqrt{2} \cdot \frac{a}{2} \cos(45° - \theta_i) \qquad 0 \leq \theta_i \leq 90°$

$a'_i = \sqrt{2} \cdot \frac{a}{2} \cos(135° - \theta_i) \qquad 90° \leq \theta_i \leq 180°$

$a''_i = -a'_i$

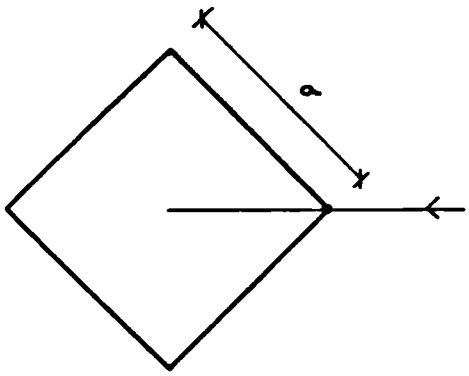

(iii) SQUARE

$a'_i = \sqrt{2} \cdot \frac{a}{2} \cos\theta_i \qquad 0 \leq \theta_i \leq 45°$

$a'_i = \sqrt{2} \cdot \frac{a}{2} \sin\theta_i \qquad 45° \leq \theta_i \leq 135°$

$a'_i = -\sqrt{2} \cdot \frac{a}{2} \cos\theta_i \qquad 135° \leq \theta_i \leq 180°$

$a''_i = -a'_i$

(iv) ELLIPSE

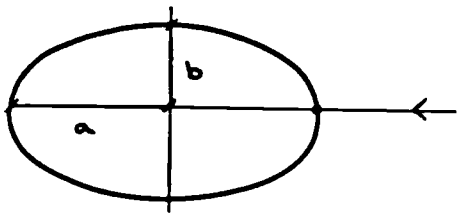

$a'_i = B \cos\theta_i \qquad 0 \leq \theta_i < 90°$

$a'_i = a \qquad \theta_i = 90°$

$a'_i = -B \cos\theta_i \qquad 90° < \theta_i \leq 180°$

$a''_i = -a'_i \qquad B = (a^2 \tan^2\theta_i + b^2)^{1/2}$

FIG. 5.17 :- GENERAL EXPRESSIONS AND ORIGINAL VIEWING POINTS OF STANDARD SHAPES

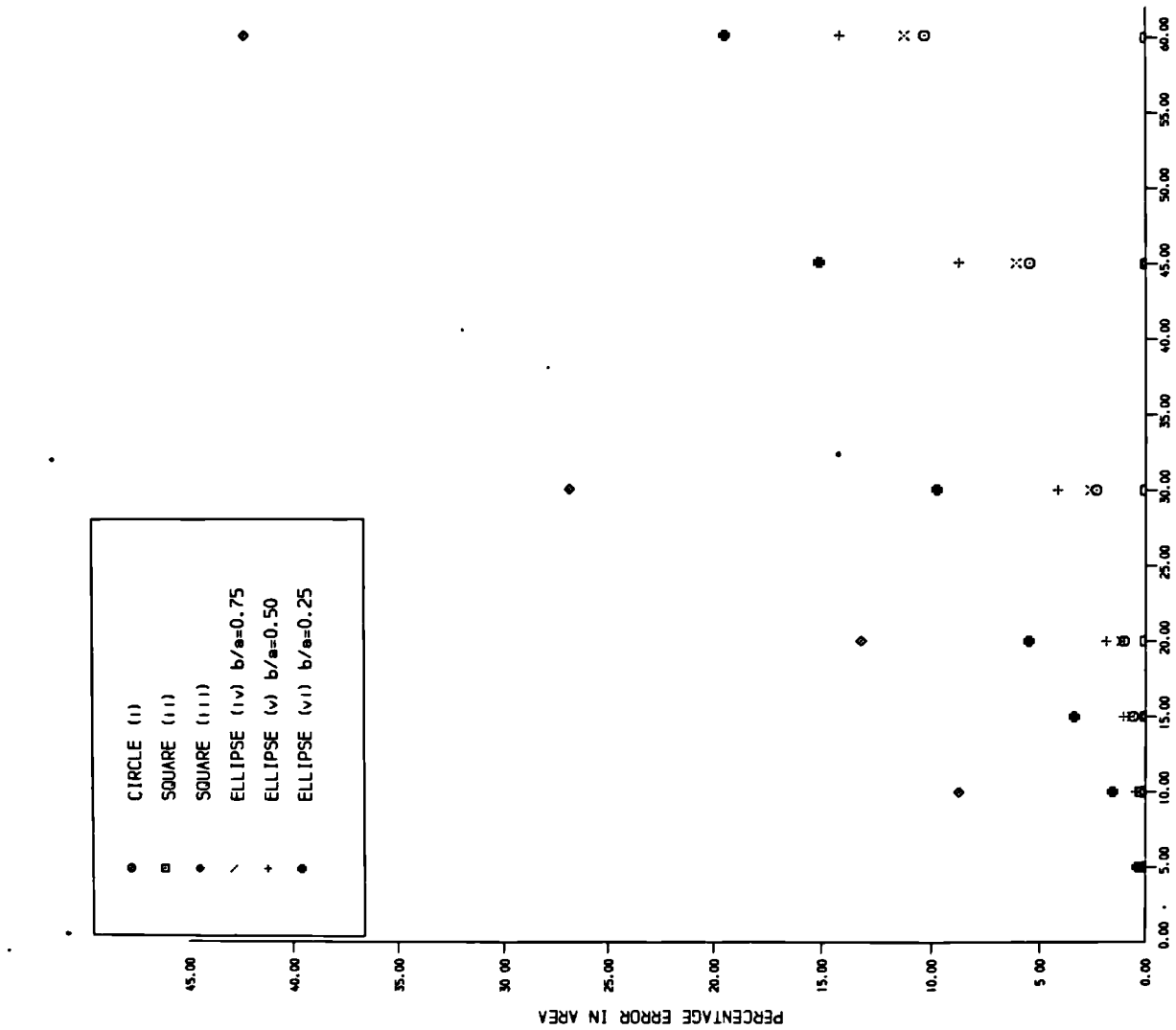

FIG.5.18. VARIATION OF ERROR WITH VIEWING ANGLE INTERVAL

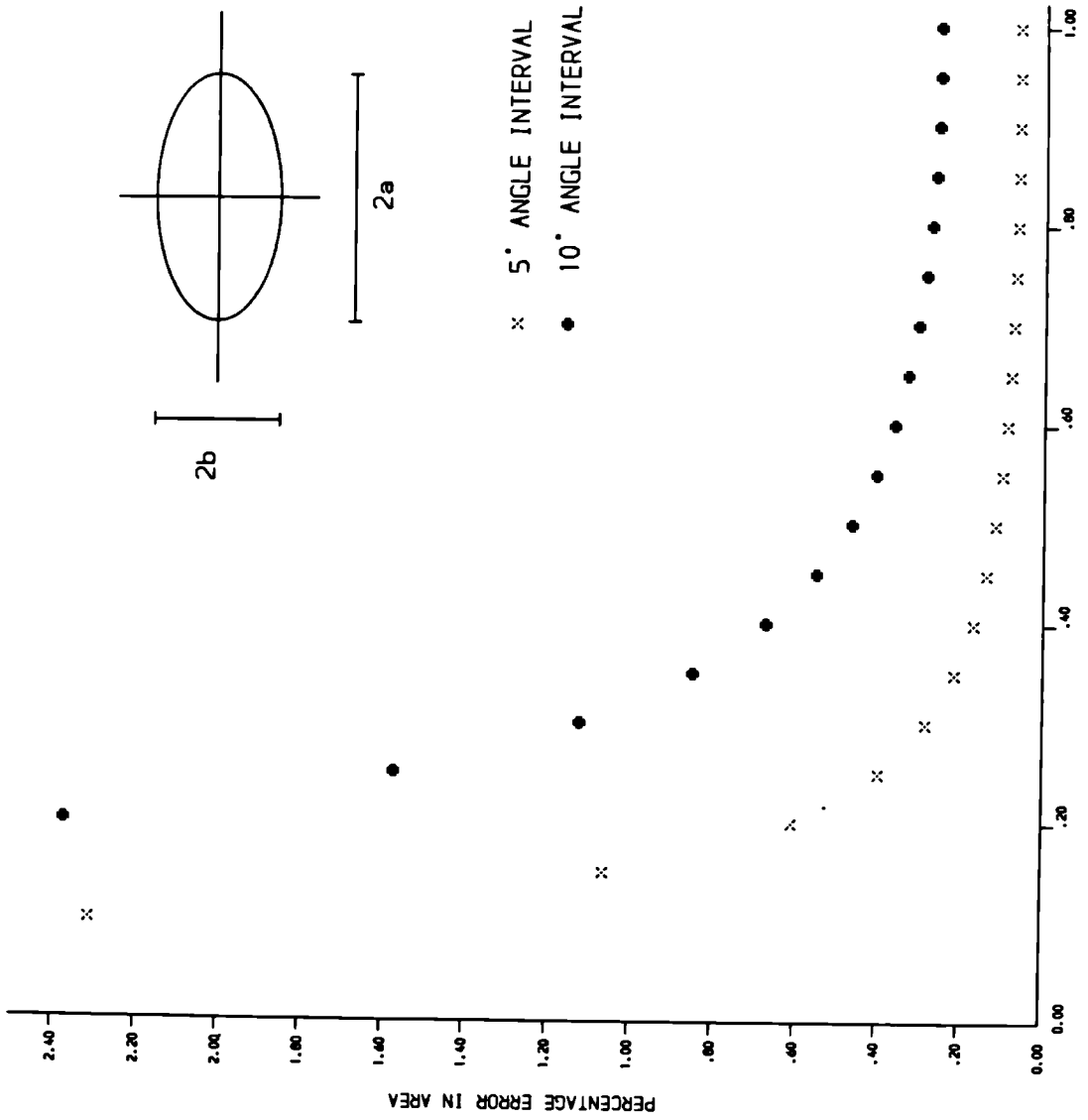

FIG.5.19.- ERROR IN AREA CALCULATED - ELLIPSE

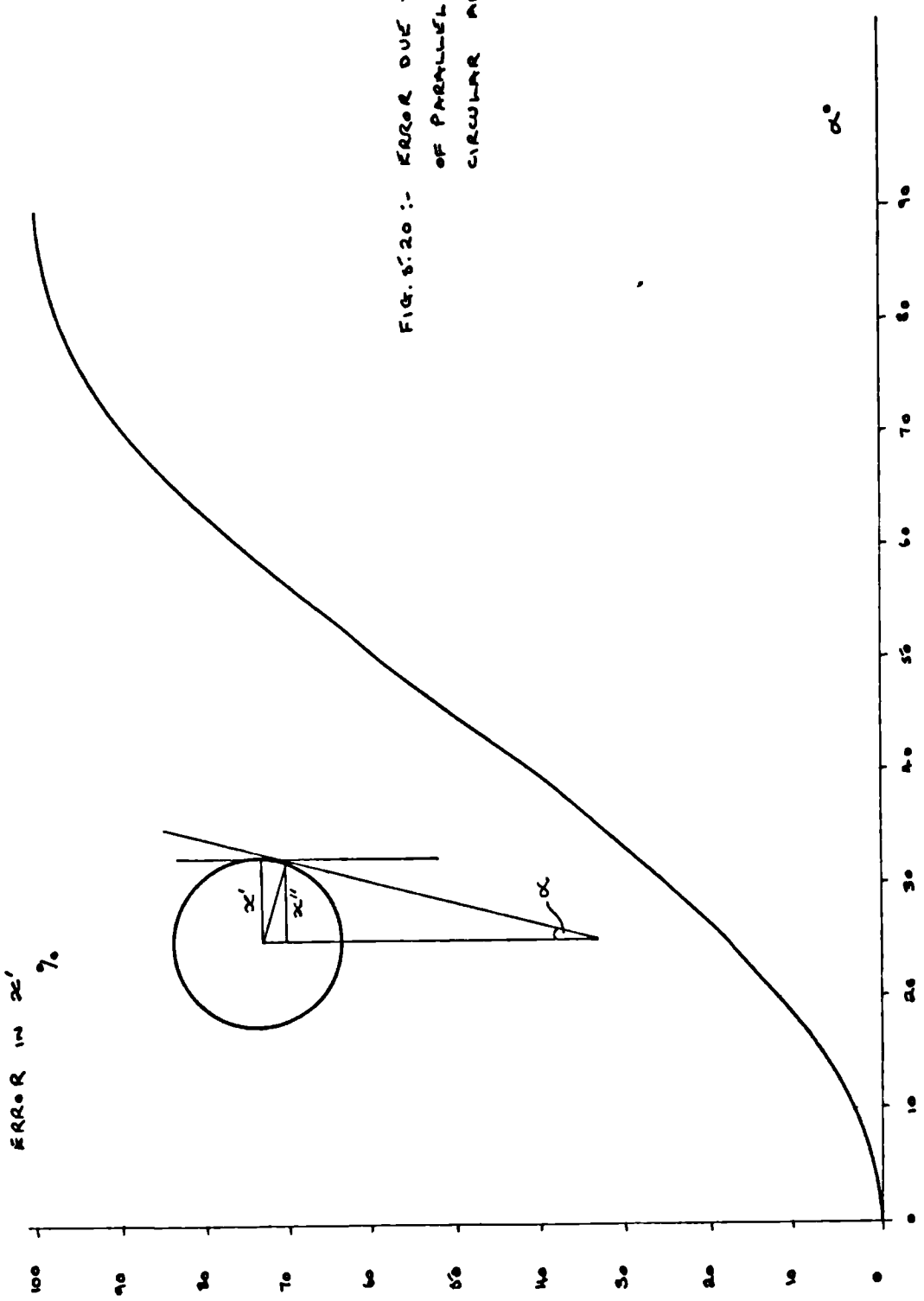

FIG. 5.20 :- ERROR DUE TO ASSUMPTION OF PARALLEL LINES FOR CIRCULAR AREA OF CONTACT

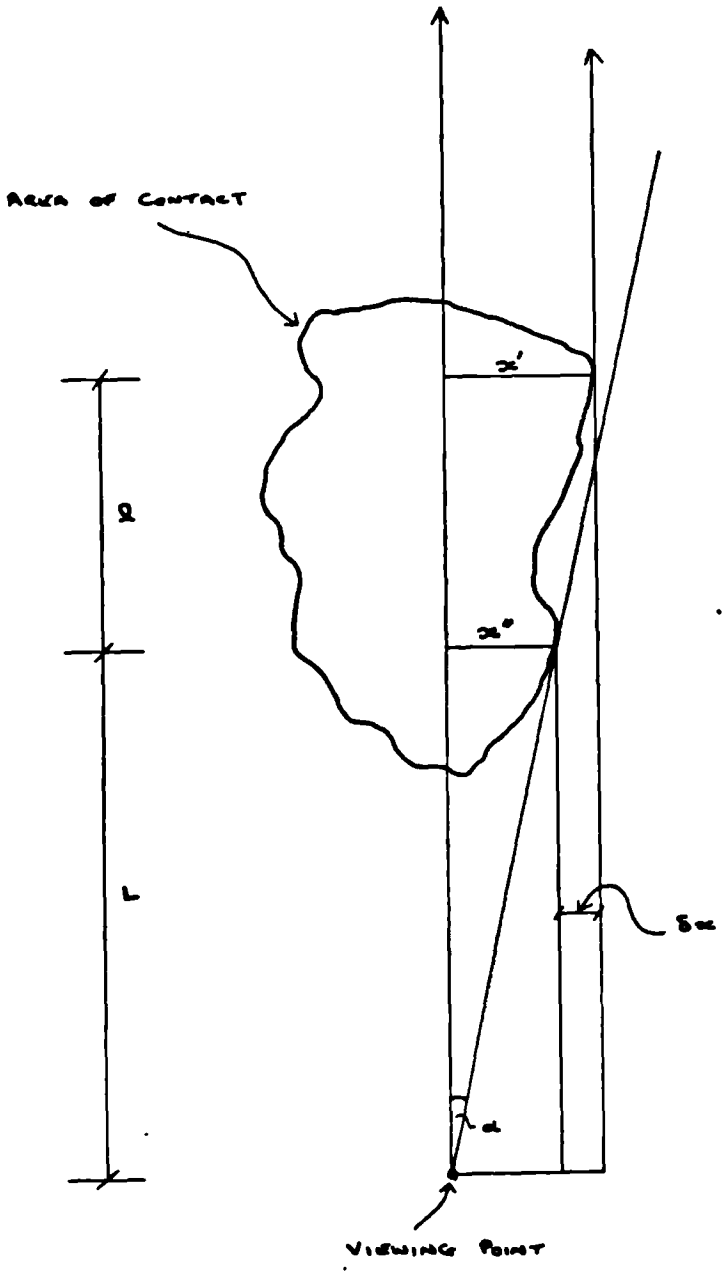

$$E = \frac{\delta x}{x'} \times 100\ \%$$

FIG. 5.21 :- POSSIBLE SOURCE OF ERROR IN METHOD II - IRREGULAR AREA

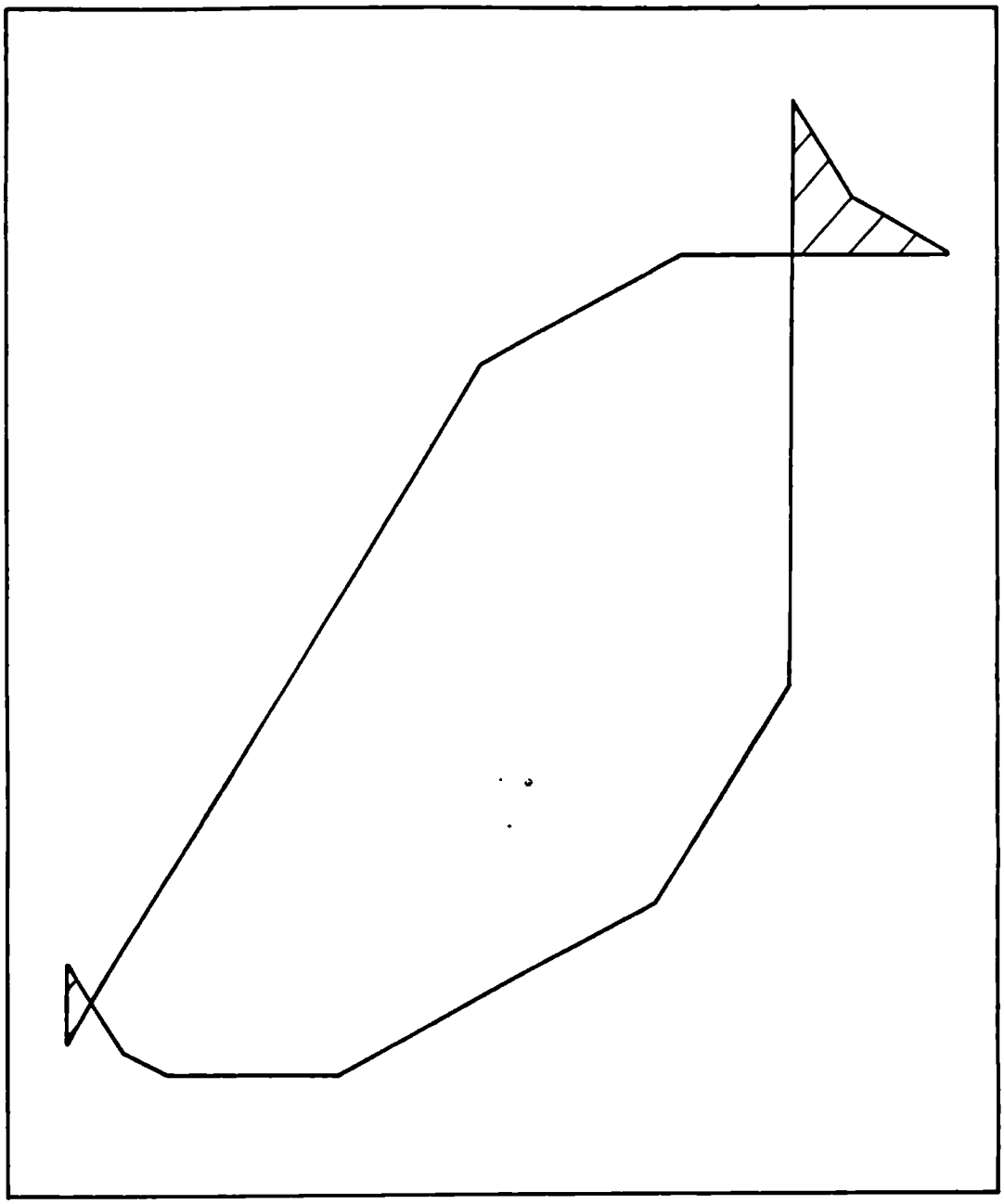

FIG. 5.22 :- AREA OF CONTACT USING INCORRECT DATA

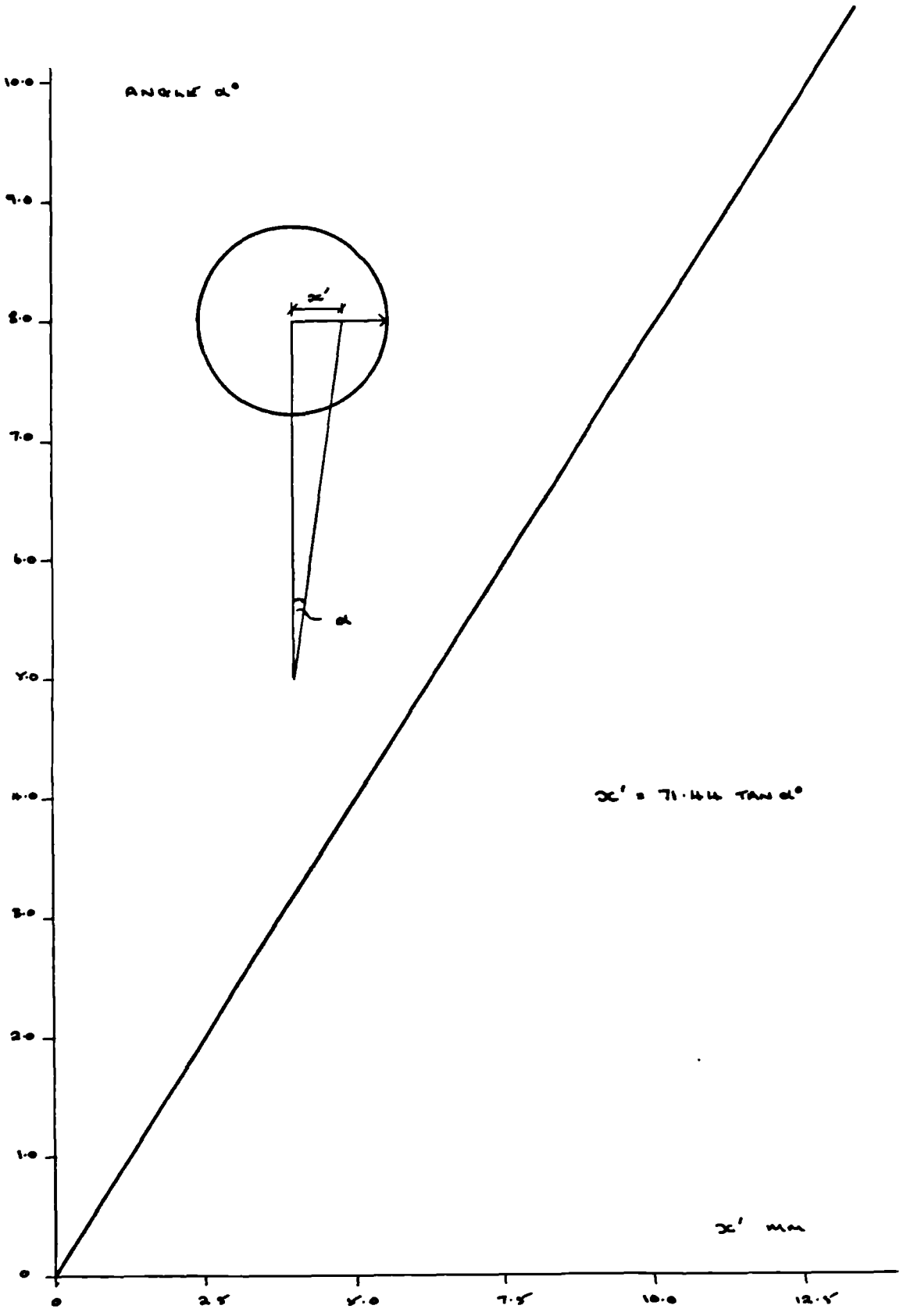

FIG. 5.23 :- RELATIONSHIP BETWEEN ANGLE TO PARALLEL TANGENT AND DISTANCE ACROSS AREA OF CONTACT

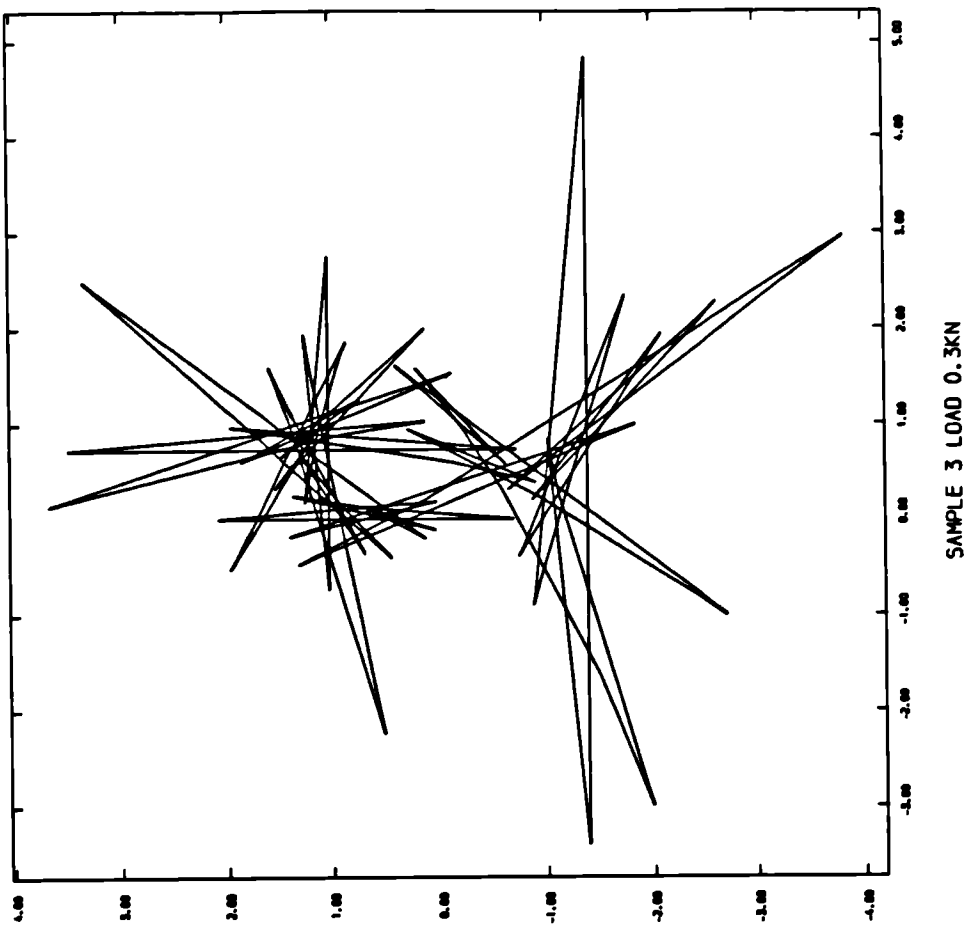

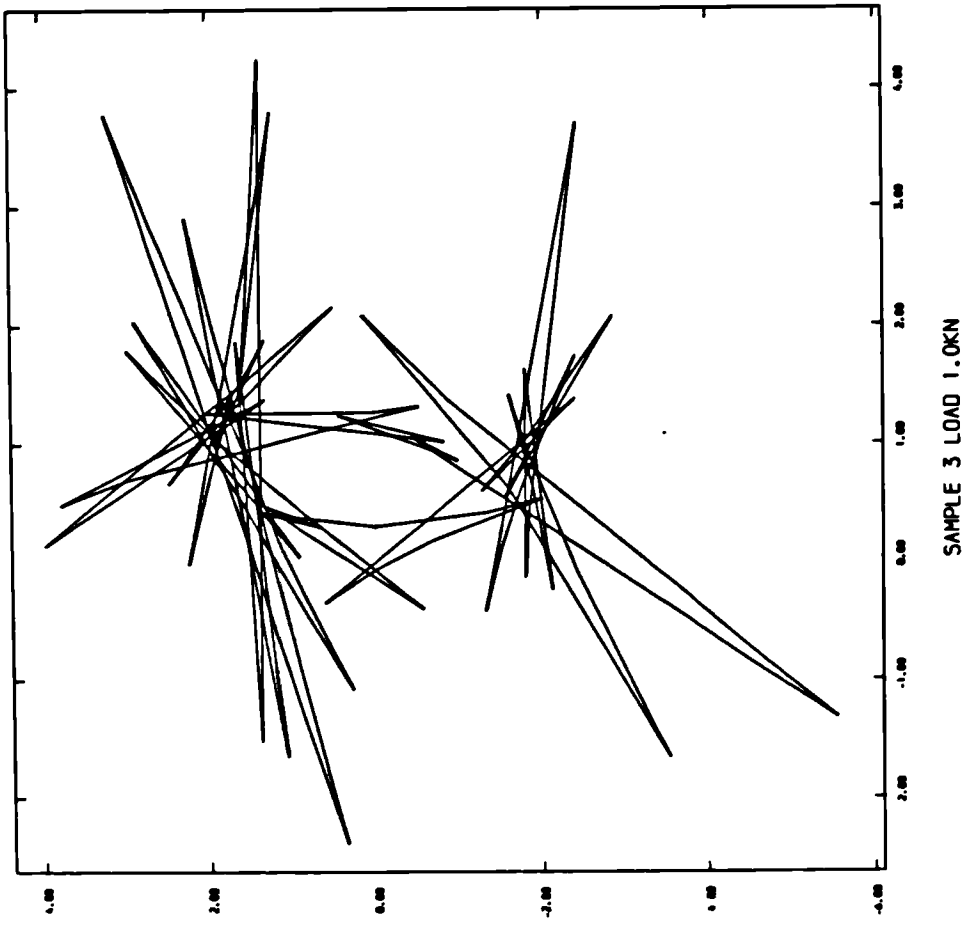

FIG.5.24,- COMPUTER PLOTS OF CONTACT AREA DATA

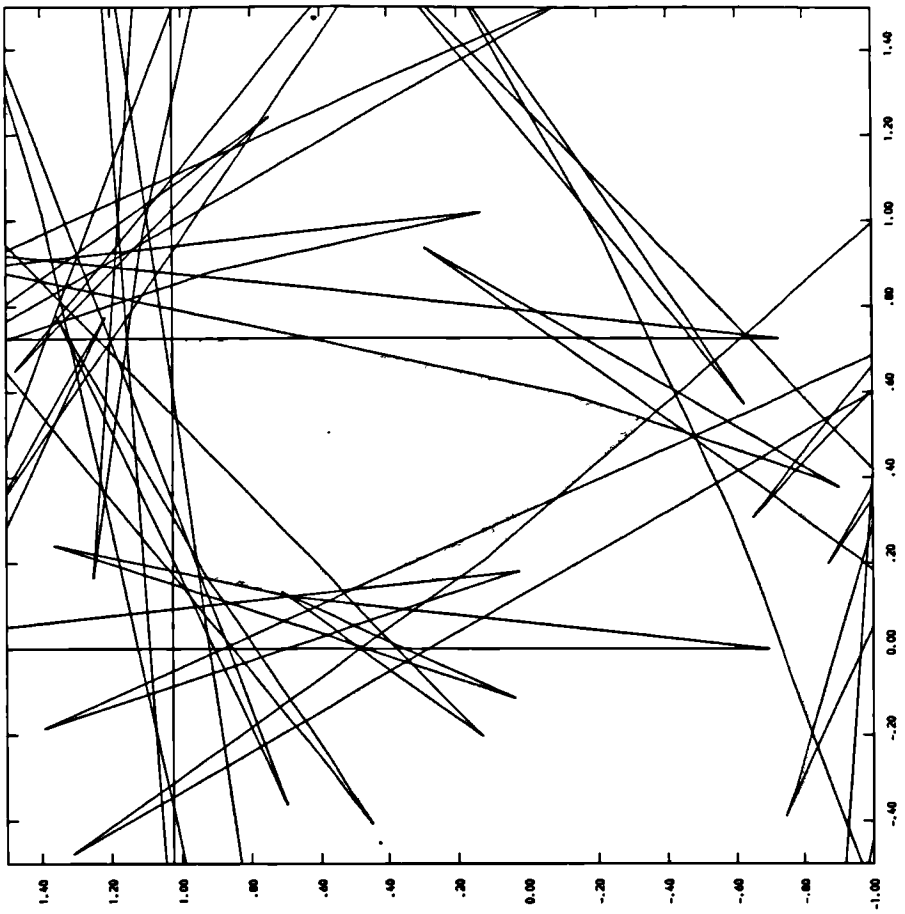

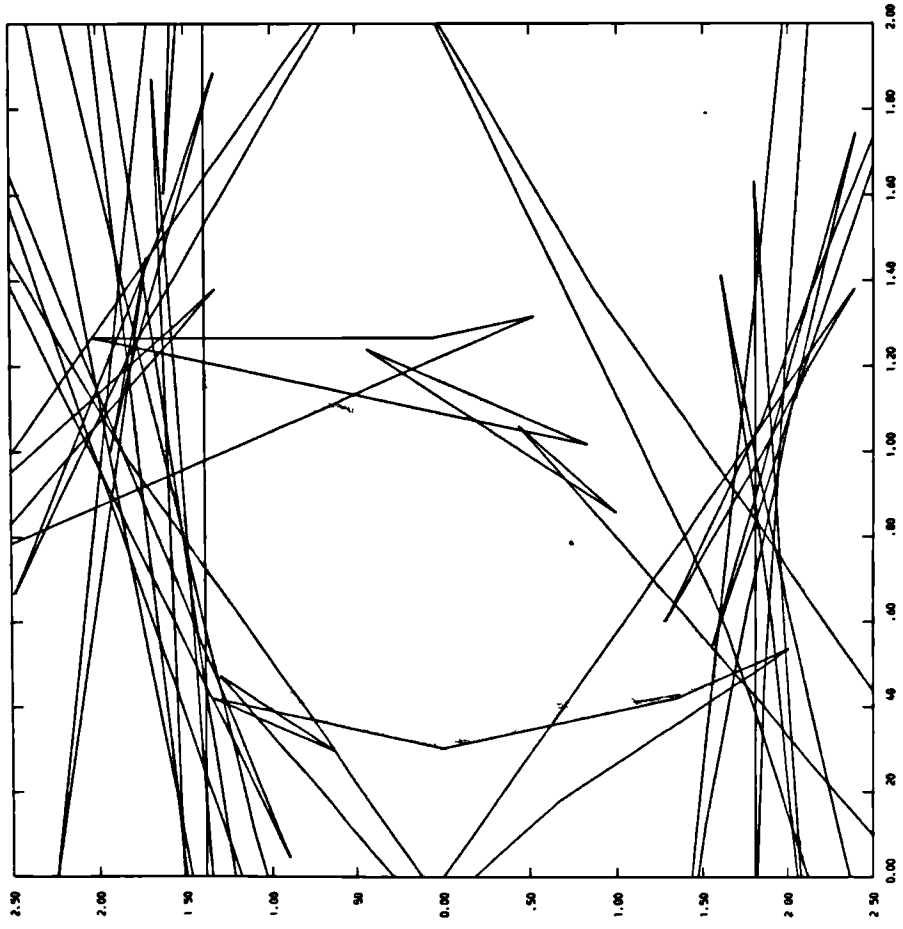

FIG.5.25;- CONTACT AREA PLOTS ENLARGED

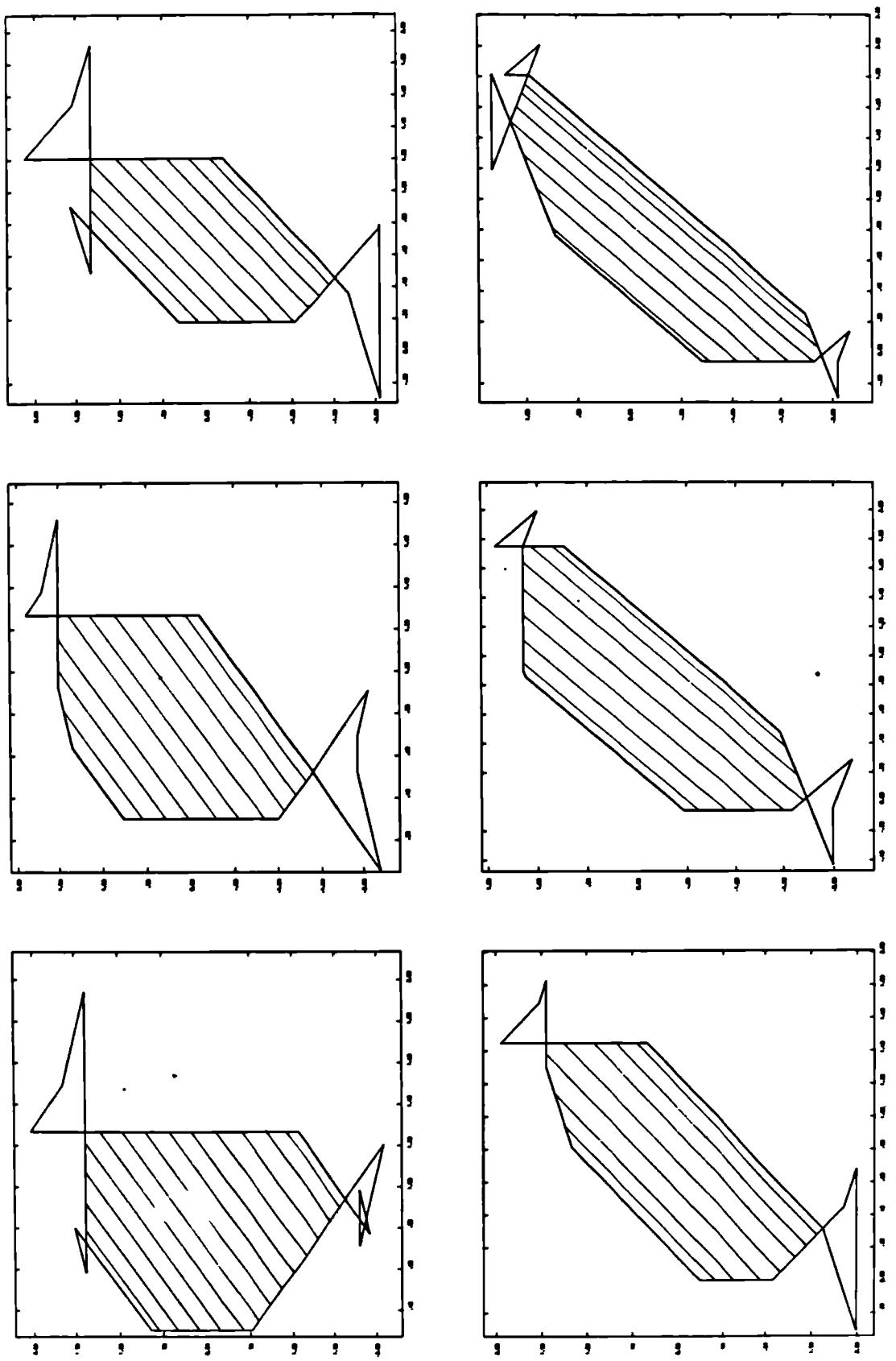

FIG.5.26:- AREA OF CONTACT RESULTS - 12 POINT METHOD

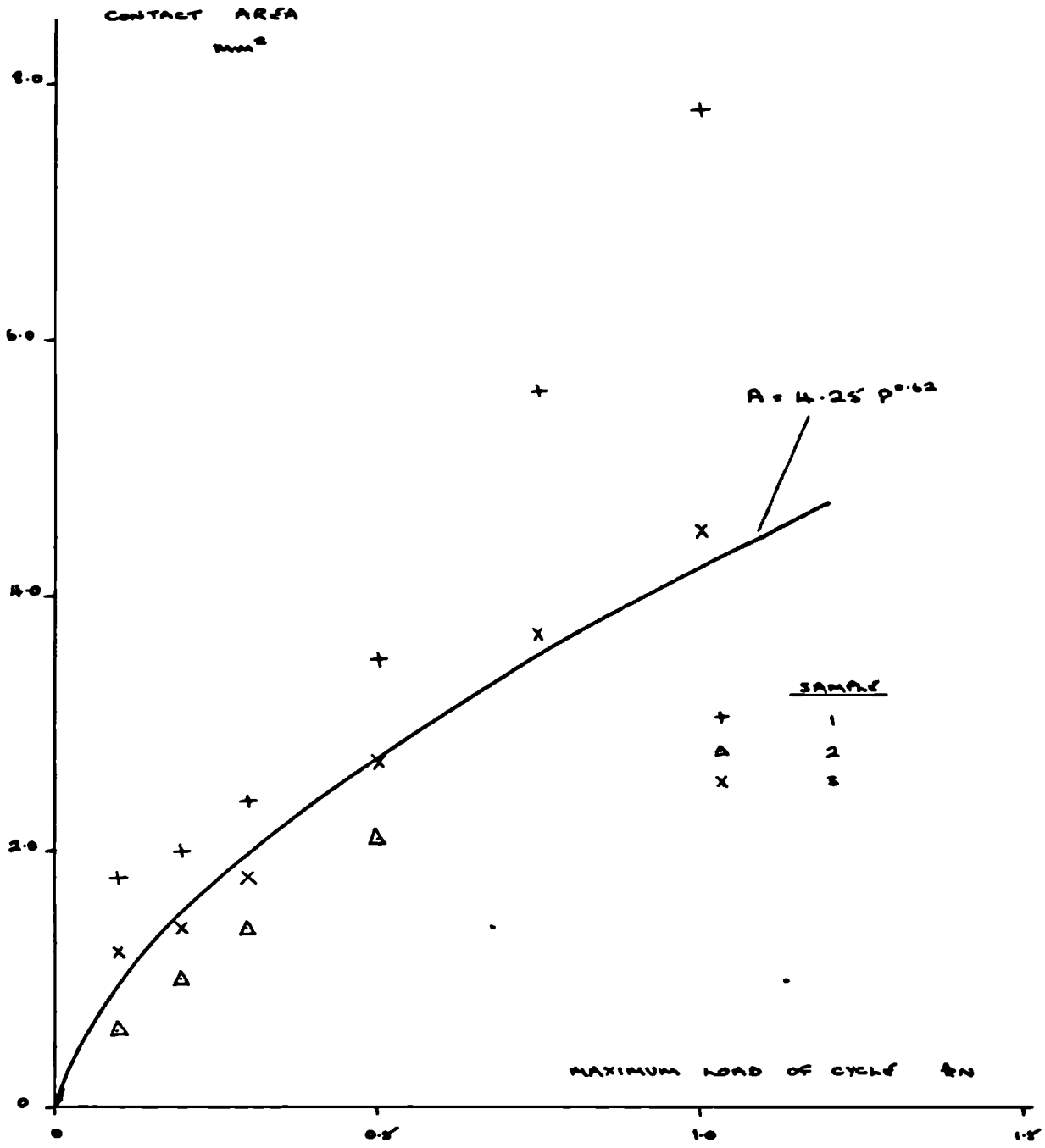

FIG. 5.27 :- METHOD II AREA RESULTS - EQUIVALENT CIRCLE METHOD

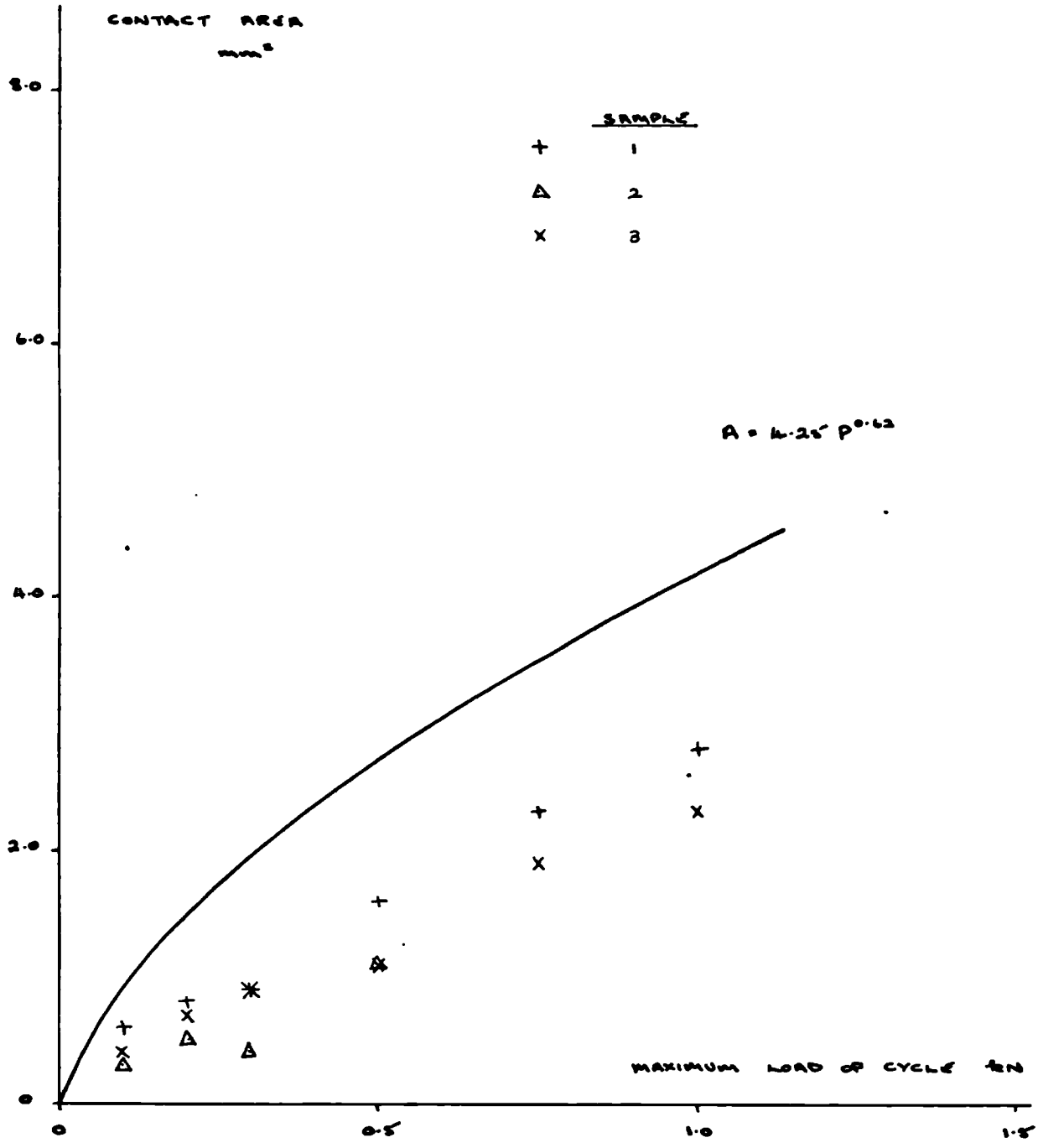

FIG. 5.28 :- METHOD II AREA RESULTS - 12 POINT METHOD

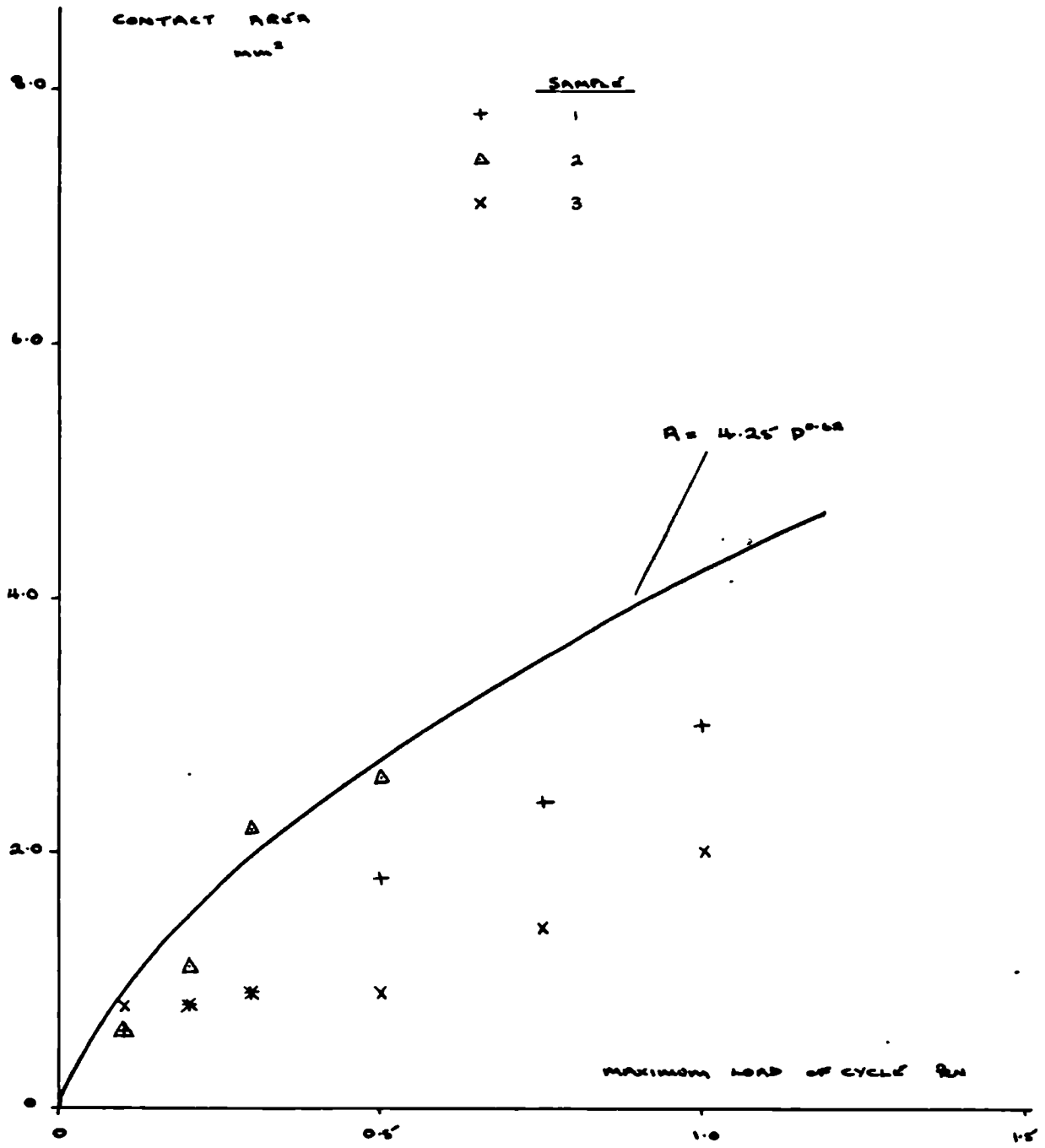

FIG. 5.29 :- METHOD II AREA RESULTS - 72 POINT METHOD

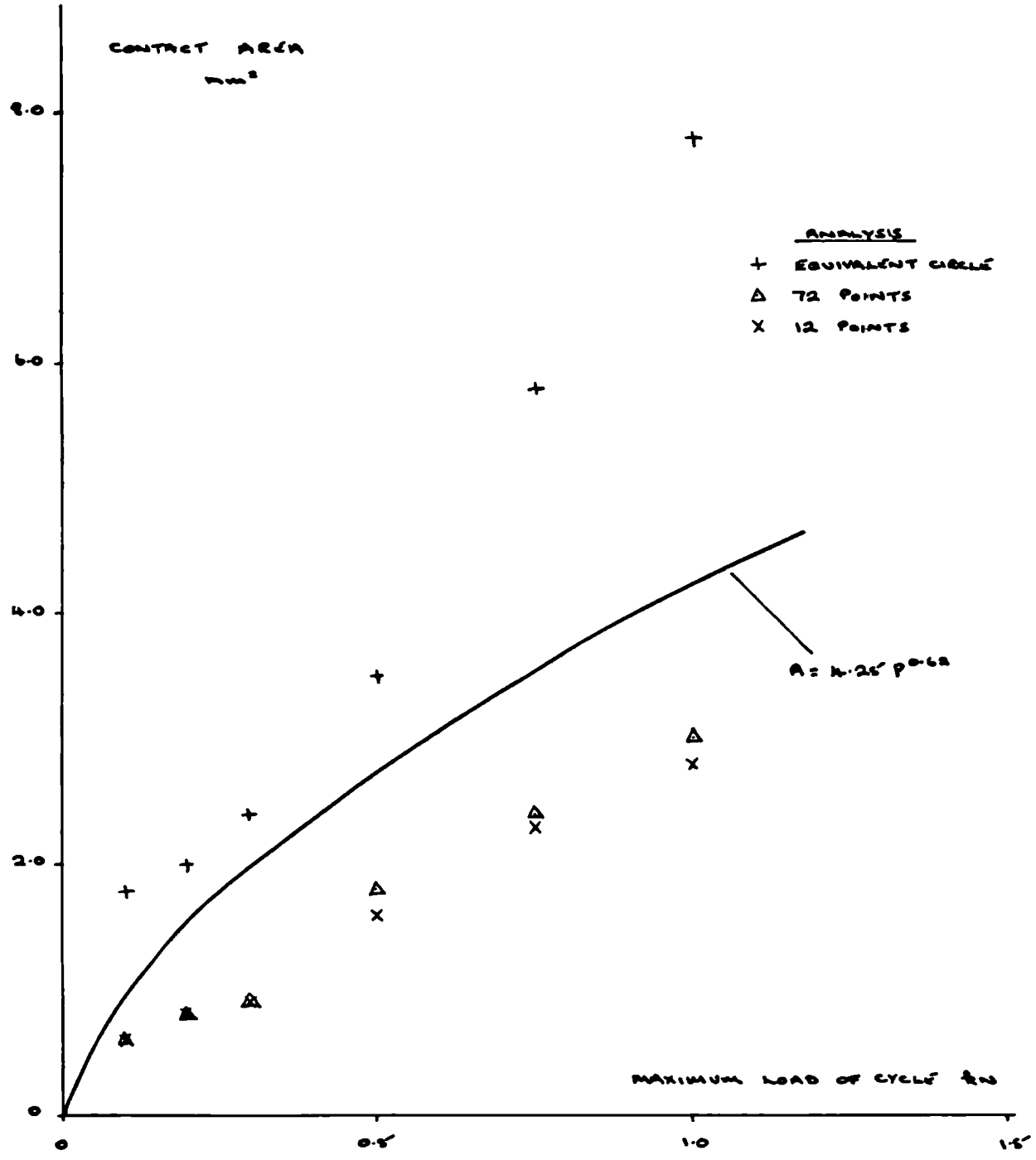

FIG. 5.30 :- METHOD II AREA RESULTS - SAMPLE 1

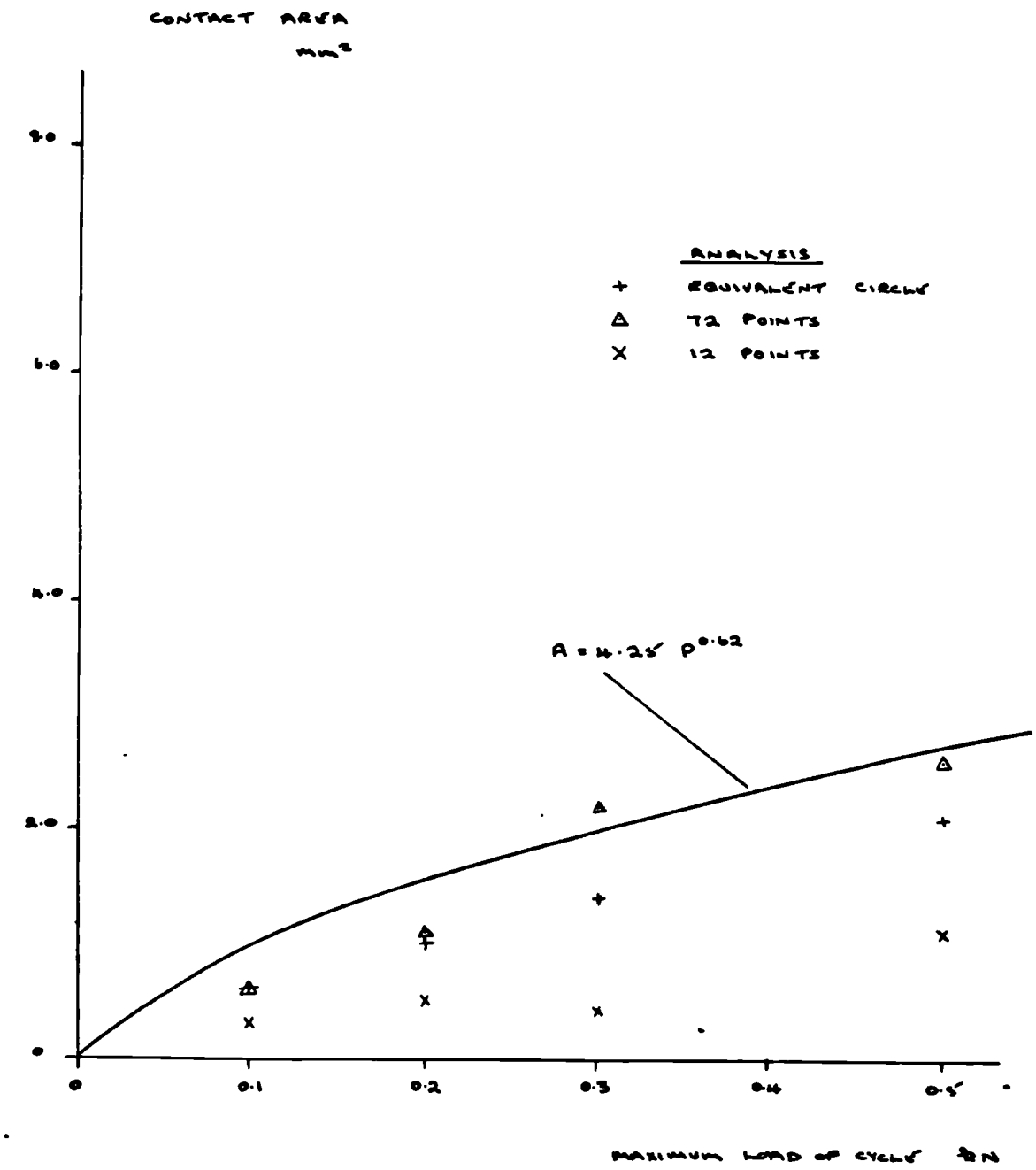

FIG. 5.31 :- METHOD II AREA RESULTS - SAMPLE 2

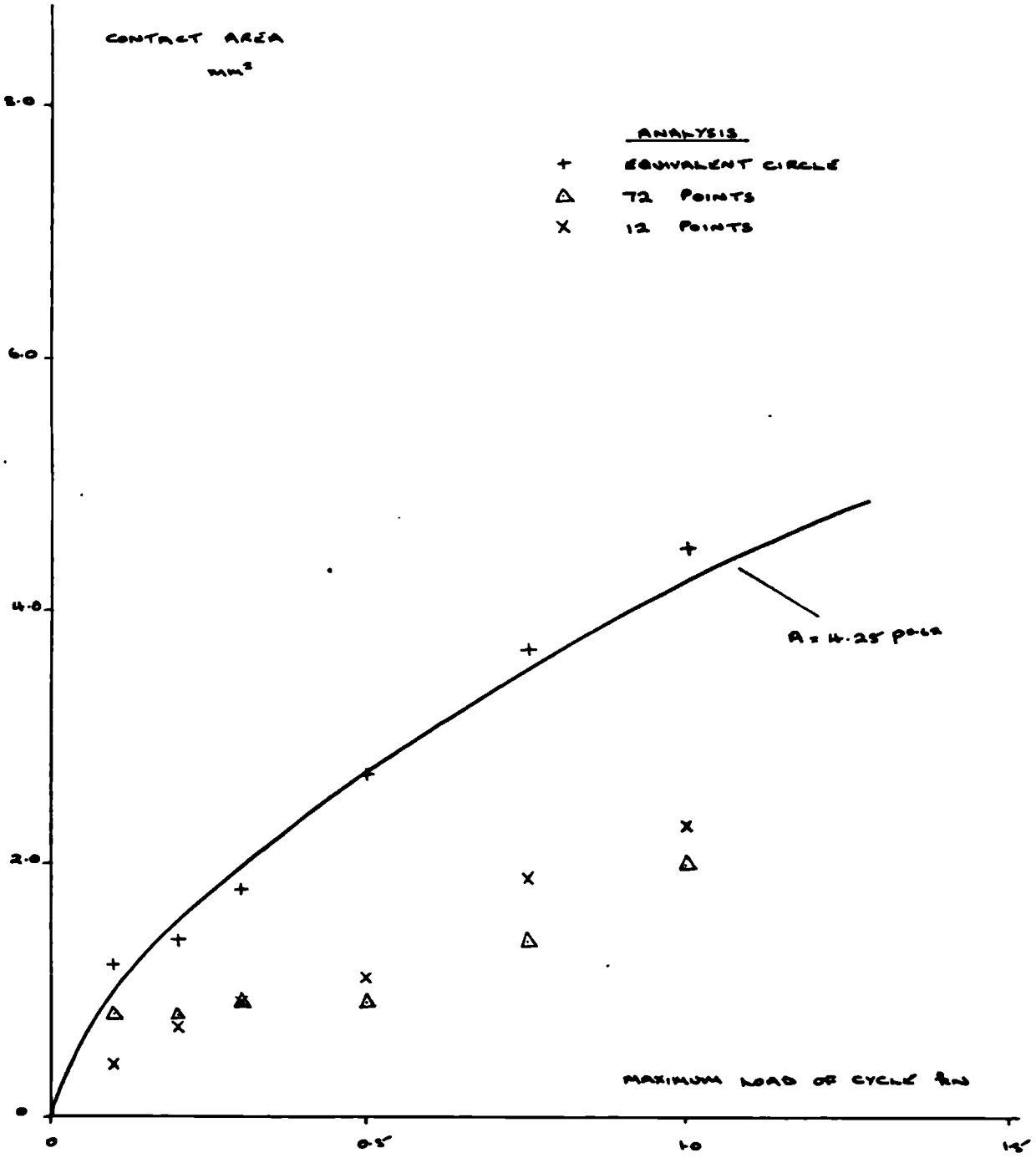

FIG. 5.32 :- METHOD II AREA RESULTS - SAMPLE 3

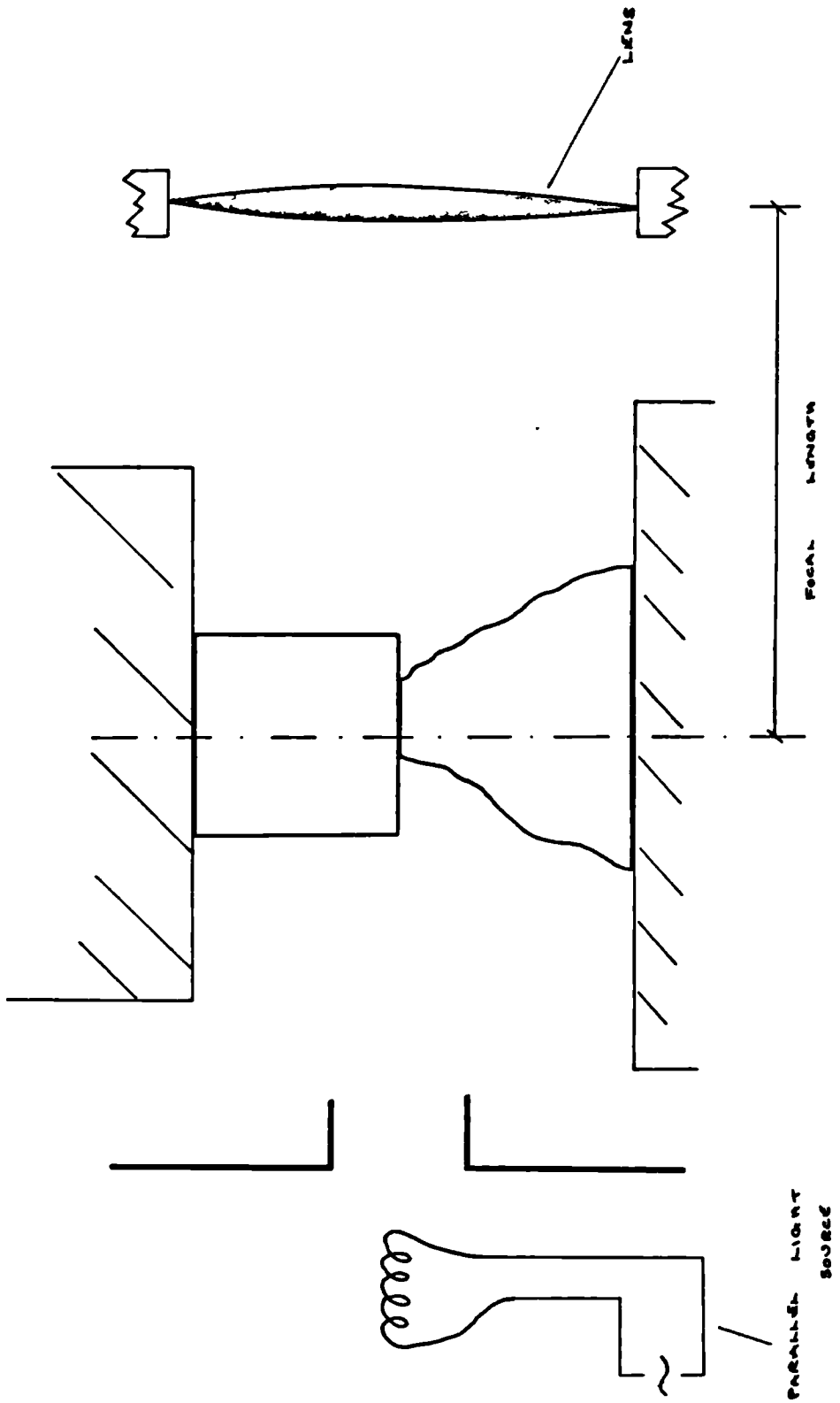

FIG. 5.38 :- ALTERNATIVE TEST TO DETERMINE THE AREA OF CONTACT

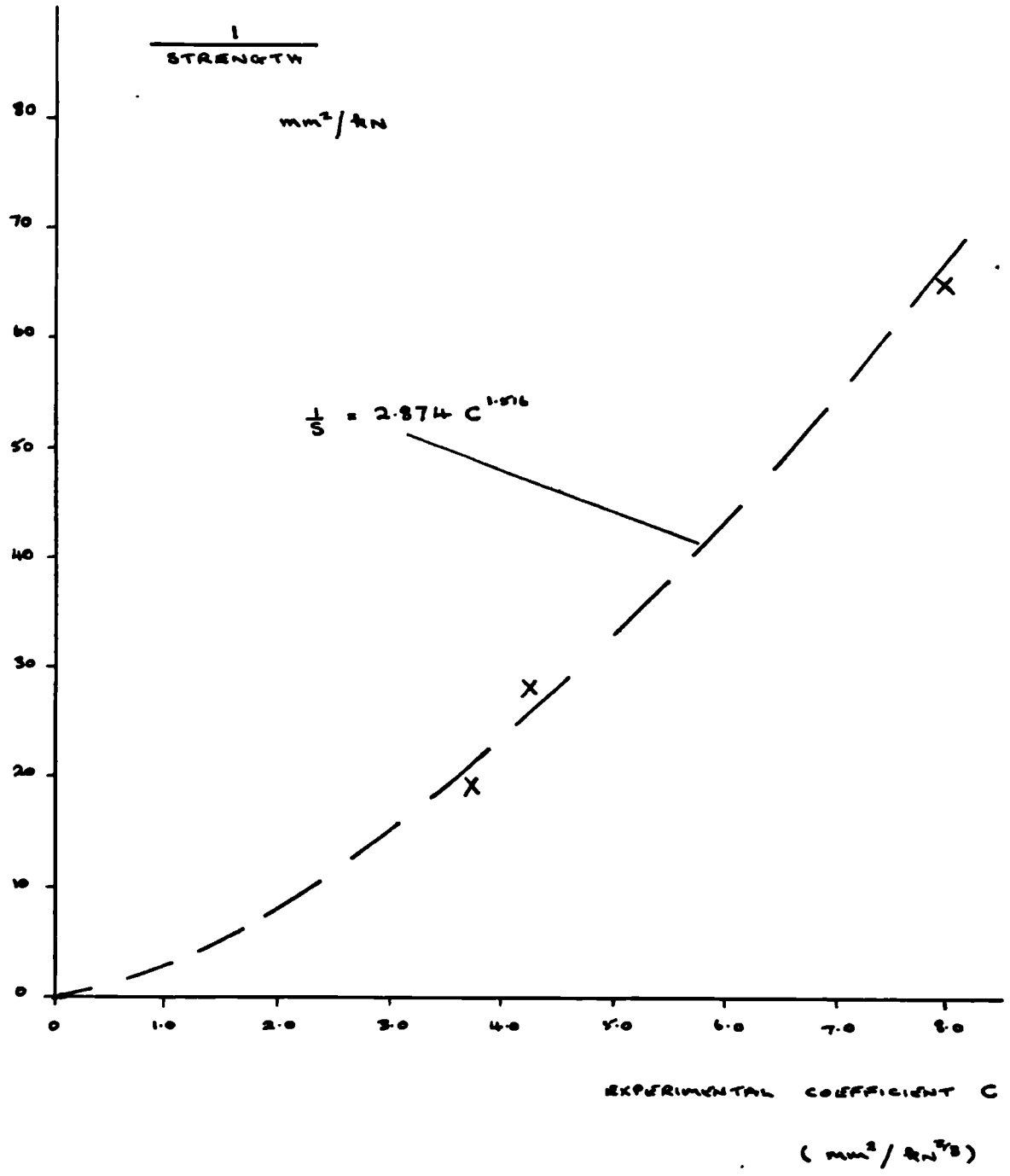

FIG. 5.34 :- CORRELATION OF EXPERIMENTAL COEFFICIENTS FROM AREA OF CONTACT EXPRESSIONS WITH ROCK STRENGTH VALUES

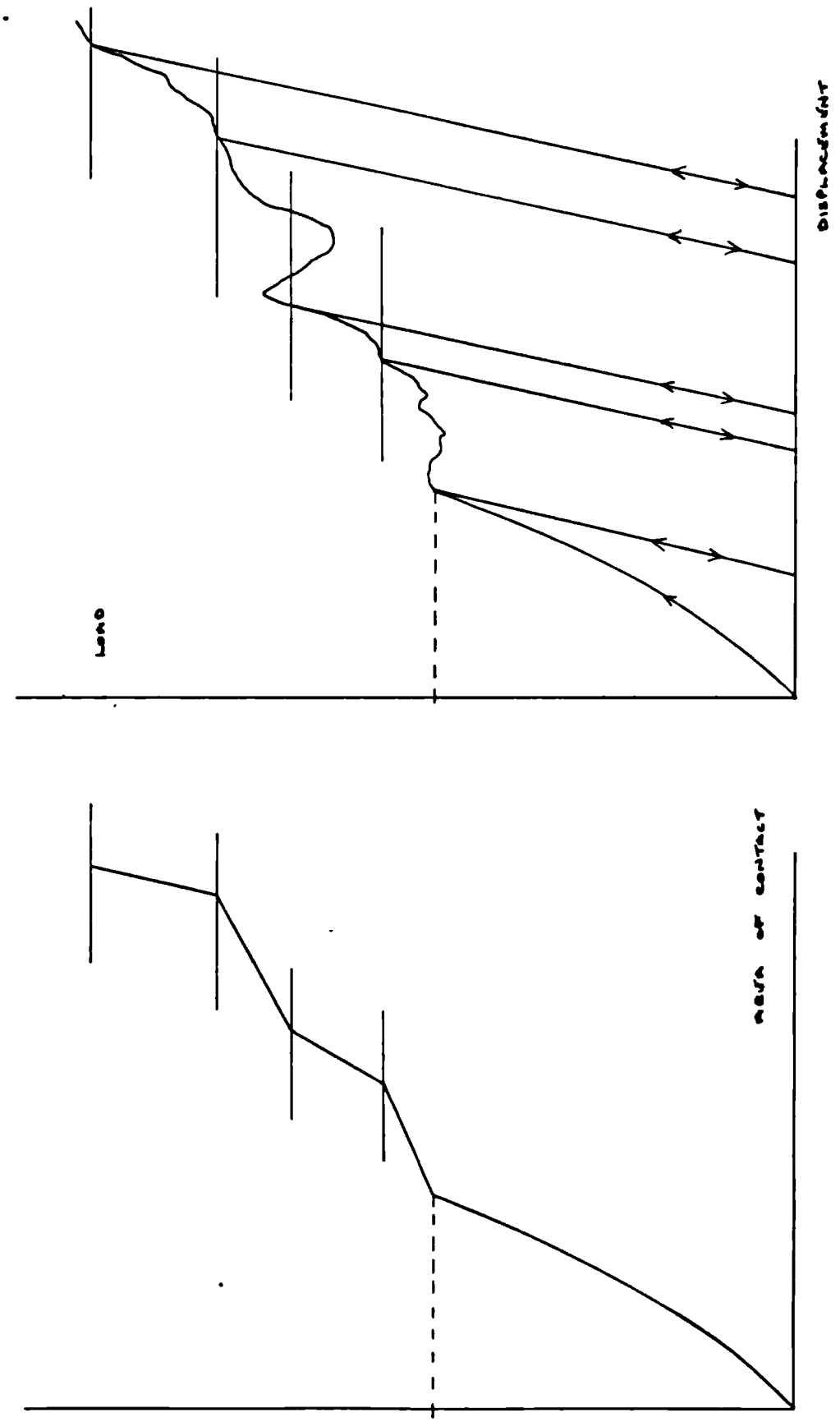

Fig. 5.35:- Comparison of load-area and load-displacement curves

Chapter 6

The Behaviour of Rock Contacts - Time Dependence

6.1 Time-dependence of Rock

When placed under load rock displays time-dependent behaviour and this is an important aspect of design for construction in or with rock. A large number of laboratory and in-situ experiments have been carried out to produce behaviour theories and 'laws', relating the various parameters involved in rock creep. Uniaxial compression tests have been carried out by Griggs (1939) and Price (1964) and triaxial loading has been considered by Le Compte (1965) and Cogan (1976). Michelson (1917) and Lomnitz (1956) performed a series of torsion tests on several materials, including igneous and sedimentary rocks, and Price (1964) used bending tests to provide information on the creep of sandstone.

The information gathered from these tests allows general rules of behaviour to be formulated, fig. 6.1. As the temperature at which the test is carried out is increased, then the creep rate increases. A similar result is noted if the magnitude of the load is increased, although triaxial tests appear to produce contradictory conclusions. There is some evidence that an increased grain size produces a decrease in creep rate but this has not yet been shown to be conclusive. The creep rate also shows an immediate response, increasing significantly, when a dry sample is inundated with water.

The standard behaviour curve, fig. 6.1, can be divided into four components or states of creep. The initial, instantaneous deformation, O-A, is an elastic, reversible response to the load. The section A-B represents the primary or transient creep and this is also recoverable. The secondary or steady-state creep, B-C, is not recoverable and removing the load produces a permanent set. The final stage is called tertiary or accelerating creep and leads to failure of the sample. Not all these stages may be seen during testing since this depends on the material and the test conditions.

However, in considering the time-dependent behaviour of rockfill, the work presented in Chapters 4 and 5 suggests that

the contact deformations would dominate the behaviour and have a greater influence on the overall displacements than the bulk deformations. Experimental work on the time-dependent behaviour of rock contacts has been limited, although Sowers et al. (1965) have performed a number of tests on shaped greywacke cylinders, as described in Chapter 1. The main conclusions of this work are listed below.

(a) Samples show an immediate deformation and continuing settlement with time.

(b) Saturated points exhibit larger deformations than dry points.

(c) Wetting of dry points while under load induces further large settlements.

(d) Addition of agents to reduce surface tension increases crushing and reduces the time lag between wetting and additional crushing.

(e) Rock on rock tests show sudden sporadic increased deformations but the magnitude of these reduces with time.

In this chapter the influence of contact angle, saturation, load, temperature and local damage on the time dependent behaviour of rock on rock contacts has been investigated. Tests were performed on irregular and shaped contacts and both creep and relaxation behaviour were considered. In order to demonstrate the dominance of the contact behaviour a number of creep and relaxation control tests were carried out on the bulk material. These provide a measure of the expected creep (or relaxation) in the material away from the contact and can be compared with the results of the contact tests.

6.2 Contact Creep Rig

For the contact creep tests a creep rig was designed to meet the specifications of the proposed tests and sample sizes. The rig, fig. 6.2, has a base plate on which sits a small load cell and the sample platform. This platform was made from hardened steel whereas the other parts of the rig were made from mild steel.

Above the platform a floating plate acts as an upper platen for the samples and this moves vertically along three guide rods connecting the base and top plates.

In tests of this kind it is necessary to ensure that the maximum amount of load is transferred to the sample and that little is lost in friction between the guide rods and floating plate. Jamming and excessive friction at these points may cause a stick-slip situation so that the samples are not loaded smoothly or the operator does not have complete control of the loading procedure. To overcome this problem three long brass sleeves are provided to act as the contact between the rods and plate. Although the length of these sleeves increases the metal on metal contact, this reduces the possibility of tilting and jamming which is considered to be the greater problem.

A linear clockwise spring is placed between the floating and top plates to maintain the applied load at a constant value. The spring used in the rig had an outer diameter of $1\frac{7}{8}$" (47.6 mm) and a wire diameter of 7/16" (11.1 mm) and the spring rate was found to be 430 N/mm. Once loading is completed the load may be transferred to the rig by tightening the three nuts on the guide rods above the top plate.

Fig. 6.2 shows the basic outline of the rig and its dimensions are given in Imperial units as it was designed to these specifications. Where necessary contact faces were ground to provide good bearing surfaces. An optional facility shown is the use of a perspex tube on the platform which allows saturated tests to be carried out. The tube was filled and emptied using plastic tubing passing over the lip of the tube. This was not very efficient and it is felt that a hole bored through the platform would have been more useful. Another problem encountered was the coarseness of the threads at the top of the guide rods. This was not fine enough to adjust the loads as accurately as would have been liked and the loading machine was used to ease this problem. Fig. 6.3 shows the completed rig set up for an experiment.

6.2.i Instrumentation

(a) Load Cell

The load cell is placed beneath the sample platform and measures the actual load carried by the samples. The cell, fig. 6.4 was designed to carry a working load of 10 kN and has two

bearing plates, outer diameter 88.9 mm ($3\frac{1}{2}$"), seperated by four legs (2 mm thick and 25 mm (1") long) equi-spaced on a 25 mm radius. The cell, which is 34.9 mm ($1\frac{3}{8}$") high, was made from a single block of HE 15 duraluminium. In order to obtain a load measurement a four arm bridge of electrical resistance foil strain gauges was used; a calibration factor of 395 μs/kN was obtained.

(b) Displacement Measurement

The transducers, used to measure the displacements, should be well clamped during testing but must also be moved fairly simply and quickly due to the variations in sample size and the possibility of large displacements occurring. Fig. 6.5 shows the duraluminium transducer collar designed to cope with these problems and fig. 6.6 illustrates how the collar works. The transducer is held firm in a sleeve which runs freely in a second sleeve. The second sleeve is attached to a collar which sits on the rim of the sample platform. The first sleeve is clamped in position using two screws in the second sleeve and this also clamps the collar to the platform so that it cannot rotate. By sitting the collar on the sample platform and allowing the transducers to bear on the floating plate, the only deformations measured are those of the samples and not the load cell.

6.3 Laboratory Conditions

As has been noted in fig. 6.1, apart from the level of loading, one of the major influences on the rate of creep is the temperature. All the time-dependent tests and the oedometer tests, described in Chapter 7, were carried out in the same laboratory and a study of the temperature variations in the laboratory was carried out at different times over a period of a year.

The graphs produced from this study, figs. 6.7 and 6.8, show that the variation is from approximately 19° C to 24° C and $\pm$ 1.5° C in any given week. These variations are small, especially if compared with temperatures used by other researchers e.g. 1000° C (Jaegar and Cook, 1969), and it would be expected that these would not influence the test results. Temperature readings were recorded during the tests and no correlation of the variations with the behaviour was observed.

6.4 Contact Creep Tests

Using the set up described for previous contact tests i.e. a rock cylinder above the shaped or irregular sample, fig. 6.9 the creep rig was placed in the Instron 1195 and the load applied under a constant crosshead displacement rate of 1 mm/min. The load and displacements were monitored and recorded on a Bryans X-Y plotter. The weight of the plates and spring ($\sim$ 0.2 kN) above the sample were also taken into account.

To monitor the displacements two different measuring systems were employed. For the irregular samples two 5 mm stroke Taylor Hobson transducers were used, fig. 6.10, connected to a meter giving a single digital display of the mean displacement, accurate to 0.0002 mm. A different system was used for the shaped samples, fig. 6.11, as one of the transducers developed a fault. The Taylor Hobson transducers were replaced by two 5 mm stroke Boulton Paul (Sangamo) and since no averaging unit was available the outputs were monitored seperately by Sangamo meters. The meter outputs were added together before recording them on a continuous plot and a scale of 1 mm chart = 2.3×10^{-3} mm was used. In using this method the calibrations of the transducers should be the same to obtain a true mean value. With both systems of measurement, recording the loading curve means that a zero-time point is not recorded, and therefore only results subsequent to 1 minute were considered.

6.4.i Shaped Samples

Six different tests were carried out on the shaped samples and two samples with different contact angles subjected to each test, Table 6.4.1. Small contact angles were not considered as the irregular sample tests showed that these usually suffered excessive damage under load which introduced complications in observing the general behaviour trends.

(a) Results

In order to analyse the results, values of the creep were taken from the continuous time plot at specific time values e.g. 1 minute, 2 minutes and replotted. These points have been joined by straight lines to give an impression of the change of creep rate with time.

Sample	β^{o}	Height mm	Temp. Variation ^{o}C	Load kN	Condition	Duration hrs.	Remarks
1	164.8	25.04	19.5	1.0	Dry	3	
2	136.4	25.18	20.125 ± 0.125				
3	169.1	25.00	20.25 ± 0.25	1.0	Dry	3	Saturated after 2 hours
4	135.9	25.40	21.75 ± 0.25				
5	165.3	25.54	20.375 ± 0.375	1.0	Saturated	3	
6	137.4	25.96	21.625 ± 0.375				
7	165.7	28.84	22.375 ± 0.125	1.0	Saturated	3	Water removed after 2 hours
8	138.1	25.70	21.375 ± 0.625				
9	167.8	25.00	22.625 ± 0.125	-	Dry	4	Loads- 0.5, 1.0, 1.5, 1.0 for 1 hour
10	140.9	24.70	21.125 ± 0.125				
11	166.4	26.08	20.875 ± 0.375	-	Saturated	4	Loads- 0.5, 1.0, 1.5, 1.0 for 1 hour
12	143.4	24.82	22.625 ± 0.125				

Tables 6.4.1 Details of Shaped Sample Contact Creep Tests

Fig. 6.12 shows the results of the four samples, 1 - 4, tested under a 1 kN load in a dry condition. Samples 1 and 3 have contact angles greater than 160° whereas samples 2 and 4 have contact angles of about 136°. This appears to be reflected in the positions of the curves: the greater the contact angle, the lower the creep displacements. Sample 4 exhibits quite marked behaviour after six minutes with a sudden increase in deformation before settling down to a similar curve to the other samples. This behaviour is probably due to an unstable situation at the contact which becomes stable once local damage has occurred. A study of the loading curves shows that sample 4 reached its Damage Load before reaching 1 kN, whereas the other samples did not.

A similar comparison can be made of the saturated samples, 5 - 8, and these results are shown in fig. 6.13. Samples 5 and 7 and samples 6 and 8 have similar contact angles and initially the higher angles have lower creep displacements. After about one hour, however, sample 7 has similar displacements to sample 6 and has a greater creep rate. Samples 6, 7 and 8 reached their Damage Loads during loading but sample 5 did not.

Fig. 6.14 compares the results for dry and saturated samples and apart from sample 4, the dry samples have lower displacements than the saturated ones over the first 20-30 minutes. Taking into account the contact angles this period is extended to about two and a half hours when the displacements may become similar.

(b) Effect of Saturation

The dry samples, 3 and 4, were inundated with water and the effect of this is clearly shown in fig. 6.15. The curves show an immediate increase in displacement and a subsequent curve with a decreasing creep rate. These tests show the displacements to be quite substantial and much greater than the values noted for tests on saturated samples. This is unexpected since it would be thought that saturation would merely transfer the behaviour from the 'dry curve' to the 'saturated curve' in a manner similar to the 'preload' effect described by Kjaernsli (1965) for oedometer tests. It is possible that saturation displaces particles from the contact area inducing greater deformation but attempts to simulate this by using a compressed air jet on dry samples did not produce similar behaviour. It is also possible that additional displacements due to the difference between the dry and

saturated loading curves are being produced on saturation. The graph also indicates greater crushing on saturation with decreasing contact angle but this may be due to the unstable nature of sample 4.

(c) Effect of Water Removal

The saturated samples, 7 and 8, were tested saturated for two hours and then the water removed from the perspex tube, fig. 6.16. While a slight disturbance occurs at the point of removal, the subsequent curve is essentially the same as the original curve. Leaving the samples for one hour should dry out the surfaces although surface tension may keep the contact wet for some time. Rewetting after an hour does not cause any further changes in the displacements.

(d) Effect of Load Variation

The tests on samples 9 - 12 involved varying the load applied and allowing the sample to creep under each load for one hour, figs. 6.17 and 6.18. The curves indicate increasing displacement with increasing load and there is almost a linear variation for samples 9 and 11. The samples with lower contact angles do not show linear variation but both these samples underwent damage at stages during loading. Sample 12 was not tested at 1.5 kN due to failure occurring as this load was approached. In general the graphs seem to indicate increasing displacement with saturation and decreasing angle.

After loading to 1.5 kN the samples were unloaded to 1.0 kN and the behaviour observed. An additional creep displacement of 0.3×10^{-3} mm was noted for sample 9 and negative displacements of 1.6×10^{-3} and 0.9×10^{-3} mm for 10 and 11 respectively. It is thought that this negligible displacement is due to slight variations in the applied load and constant values are achieved within about fifteen minutes.

(e) Effect of Damage Load

In general these tests seem to indicate that if the Damage Load is reached before the maintained load then complications may arise once creep commences. These complications may take the form of sudden failures (sample 4), a greater creep rate (sample 7) or several sudden minor displacements. Sowers et al.'s (1965) observation of sudden sporadic increased deformations decreasing in magnitude with time was not particularly noted in these tests.

6.4.ii Irregular Samples

A number of tests were performed on irregular samples at a stage in this research when the significance of the contact angle had not been realised and therefore was not measured. The results have been presented as they provide information about real rock contacts and confirm some of the conclusions drawn from the shaped sample results. Table 6.4.2 gives details of the tests carried out.

(a) Results

Fig. 6.19 shows the creep displacements of the dry samples and these are slightly greater than those seen in fig. 6.12. Although none of the samples reached their Damage Loads, sample 3 underwent a sudden deformation after about twenty-five minutes, followed by a high creep rate which did not stabilise for a further hour. Samples 4 - 6 and 9, 10 (fig. 6.20) were saturated and of these samples 5, 9, 10 suffered a large amount of damage. This is reflected in the time-dependent behaviour of 5 and 9, as sample 5 failed due to crack propagation after fifty-five minutes and 9 continued to creep at a high rate throughout the test. Sample 6 also underwent failure after about one hour of constant loading. A comparison of the dry and saturated results suggests again that saturation produces larger creep displacements in the first sixty minutes but the values are not substantially different after this.

Fig. 6.21 shows the curves of the two saturated/surface dry samples and these appear to behave in a similar manner to the saturated samples. The drying out does not effect the curves but since the dry and saturated curves have similar creep rates after about one hour, this is to be expected.

(b) Effect of Water Removal

The results for samples 9 and 10 are shown in fig. 6.22. Neither removing the water nor re-saturating the samples has any significant effect on the creep curves, although the values for sample 10 are erratic initially after re-saturating.

(c) Effect of Load Variation

The creep curves for samples 11 and 12 (fig. 6.23) again indicate that creep displacements increase with increased load

Sample	Temperature Variation °C	Load kN	Condition	Duration hrs.	Remarks
1	23.25 ± 0.25	1.0	Dry	3	
2	22.375 ± 0.125				
3	22.75 ± 0.25				
4	22.5	1.0	Saturated	3	
5	22.625 ± 0.375				
6	22.625 ± 0.125				
7	23.25 ± 0.25	1.0	Saturated-surface dry	3	
8	24.0				
9	23.25	1.0	Saturated	3	Water removed after 1 hr. Water replaced after 2 hrs.
10	23.0 ± 0.5				
11	22.125 ± 0.375	-	Dry	4	Loads 0.5, 1.0, 2.0, 1.0 kN for 1 hr.
12	22.625 ± 0.125	-	Saturated	4	Loads 0.5, 1.0, 2.0, 1.0 kN for 1 hr.

Table 6.4.2 Details of Irregular Sample Creep Tests

and for 11 the values observed at 1.0 kN are approximately double those at 0.5 kN. Damage occurred in loading sample 11 from 1.0 to 2.0 kN and this is reflected in the large displacements seen under 2.0 kN. On unloading this sample to 1.0 kN subsequent displacements of less than 0.4×10^{-3} mm were recorded. Sample 12 could not be loaded to 2.0 kN due to continual failure under load.

6.4.iii Effect of Creep on the Load-Displacement Behaviour

If the loading of a contact is continued after a period of constant load, then the load-displacement relationship will be affected by the period of creep. Figs. 6.24 and 6.25 illustrate this effect as observed for shaped sample 9 and irregular sample 11. The samples were subject to initial loads due to the weight of the plates and spring and then constant loads of 0.5 and 1.0 kN. Initially the graphs show a distinct increase in gradient (compared with the general loading curve) on reloading before returning to approximately the same curve as before. This behaviour is similar to Kjaernsli's 'preload' effect, (1965).

This effect is similar to the stepping seen in the load-contact area graphs, since the time-dependent displacements produce a small increase in area, reducing the stress at the contact. On reloading this stress must be built up to its previous level before the sample can follow the general load-displacement relationship. This 'building-up' period is seen as a large load increase for small displacement, producing an increased gradient. Similar results can also be seen for the other samples tested in this way but these are complicated by damage occurring during loading.

6.4.iv Conclusion

The main conclusions of the contact creep tests on the shaped and irregular samples can be summarised as follows:-

(a) Creep displacements increase with decreased contact angle

(b) Saturated samples initially have higher creep rates than dry samples but after a short period of time there is little difference.

(c) Saturated/surface dry samples act like saturated samples.

(d) Saturation of a dry sample produces much greater displacements than those seen for saturated samples.

(e) Removal of water and rewetting have a negligible effect on the time-dependent behaviour.

(f) Increased loads produce increased creep displacements.

(g) No creep or recovery occurs if a sample is unloaded to a lower load.

(h) Damage occurring during loading may lead to unpredictable behaviour under constant load.

(i) The period of constant load effects the load-displacement relationship.

These conclusions are general trends noted from the tests but there are exceptions to some of these due to the complications introduced by damage.

6.5 Contact Relaxation Tests

6.5.i Test Procedure

The prepared samples were placed in the 1195 Instron, using the creep rig sample platform as the base platen, and saturated if necessary. The samples were then loaded under a constant cross-head displacement rate of 0.2 mm/min upto 1 kN and allowed to relax under a fixed displacement. The tests were carried out over seventy-two hours and the load variation with time plotted using the machine load signal. Details of the four shaped samples and the test conditions are given in Table 6.5.1.

6.5.ii Results

Fig. 6.26 shows the results obtained from the time plots for the first four hours and fig. 6.27 the results for the final sixty eight hours. In fig. 6.26 the relaxation rates appear to decrease

quite smoothly and the curves have distinct positions. The percentage loss of load at any time increases with decreased contact angle and with saturation for a given angle of contact. After the first four hours the behaviour is not as well established and the curves do not maintain their positions but this may have been caused by other factors e.g. instrumentation stability.

Sample	1	2	3	4
β°	166.3	137.3	167.6	138.6
Height mm	25.14	24.98	24.86	25.06
Load kN	1.0	1.0	1.0	1.0
Condition	Dry	Dry	Saturated	Saturated
Temp.Variation $^\circ C$	21.75 $\pm$ 0.5	22.50 $\pm$ 0.5	20.25 $\pm$0.25	21.75 $\pm$0.75

Table 6.5.1 Details of Shaped Samples and Contact Relaxation Tests

6.6 Bulk Creep Tests

These tests were carried out as control tests to provide information about the creep properties of the bulk material so that a measure of the relative importance of contact time-dependent behaviour could be made.

6.6.i Test Procedure

Creep and recovery tests were carried out on three 25 mm diameter sandstone cylinders, with lengths of approximately 76 mm, prepared in the normal manner. The longitudinal strains were measured using a four arm bridge arrangement of electrical resistance gauges giving double sensitivity. The two active gauges of the bridge were attaced on opposite sides of the core and connected in series with two passive gauges. These samples were tested in an Avery constant load machine, fig. 6.28, and dental cement endpads (as described in section 3.7) used to ensure an even load distribution across the ends of the samples.

The bridge circuit was connected to a Peekel 581 DNH strain meter and the output from this monitored on a X - Y plotter. The samples were tested at loads of 5, 10 and 15 kN and allowed to creep for seventy-two hours before unloading. The recovery strains

were then recorded for a further seventy-two hours.

6.6.ii Results

Table 6.6.1 gives details of the three samples and the temperature variations recorded during the tests. Fig. 6.29 shows the results of the first four hours of the test and fig. 6.30 the remaining sixty-eight hours; the recovery curves are shown in figs. 6.31 and 6.32.

Sample	Length mm	Load kN	Temp. Variation ^{o}C	Loading Strains $\mu\varepsilon$
1	76.02	5.0	20.75 ± 1.25	948
2	75.79	10.0	21.625 ± 1.625	2121
3	75.67	15.0	20.00 ± 1.00	1991

Table 6.6.1 Details of Bulk Creep Tests

The creep strain graphs show that the samples continue to deform with time under constant load. The 10 kN sample shows higher creep strains than the 5 kN sample although these are not double the 5 kN strains. Sample 3, however, shows rather unexpected behaviour and is initially similar to the 5 kN sample behaviour. After four hours the curve shows an increased creep rate and at twelve hours there is a sudden large deformation. This ceases abruptly and the creep rate is approximately constant for the rest of the test. This may have been caused by the propagation and blunting of a crack but the strange behaviour of this sample on recovery, discussed below, suggests that the results are not typical. The loading strains, given in Table 6.6.1, indicate that the strains for sample 3 are low when compared with the values for samples 1 and 2.

The graphs demonstrate the states of creep noted in fig. 6.1 after the initial instantaneous response to the load. All three samples show transient creep initially and the 10 kN sample appears to reach a state of secondary creep after about thirty-six hours. Sample 3 shows typical tertiary creep behaviour between four and twelve hours but then returns to a state of secondary creep.

The recovery results, figs. 6.31 and 6.32, again show the expected increasing recovery with time. As before the 10 kN

sample values are greater than the 5 kN results but the 15 kN sample values are similar to the 5 kN results. The 15 kN results after twenty-four Hours are not presented as rather strange behaviour occurred at this point. The continuous plot indicates large increases and decreases in length (of the order of 300 μs) with a net increase in recovery strains of approximately 36 μs over the twenty-four hour value at seventy-two hours. Checks on the instrumentation and gauges were made but these seemed to be working correctly.

The recovery strains noted after seventy-two hours for sample 1 are approximately the same as the creep strains over the same period, which is in accordance with the behaviour shown in fig. 6.1 for transient creep, although there is a permanent set of 252 μs because the initial response is not completely reversible. For sample 2 there is a permanent set of 607 μs and although the recovery strains are greater than the creep strains, the recovery values are constant after thirty-six hours which corresponds to the point of steady-state creep.

6.6.iii Conclusion

These results give an indication of the creep characteristics of the material and are generally in accordance with behaviour noted from other research. Variations in the continuous plots may be correlated with temperature fluctuations but a more major influence on the results was the amount of activity in the laboratory. Variations from the mean curve were less than 10 μs and usually less than 5 μs. Another source of inaccuracy was the use of resin backed strain gauges which may cause 'creep drag'. This can be reduced by using foil gauges.

6.7 Bulk Relaxation Tests

6.7.i Test Procedure

Three samples were prepared in the same way as the creep samples but subjected to constant deformation rather than constant load. These tests were carried out in the Instron 1195 and a direct output of load variation taken from the machine load cell. The samples were loaded to 5, 10 and 15 kN under a crosshead displacement rate of 1 mm/min. Since the stiffness of the machine

varies with the applied load, the variation in strain with time was also recorded. The tests were carried out over seventy-two hours as before.

6.7.ii Results

Table 6.7.1 gives details of the samples tested and the loading strains and variations during testing. These values show variations of less than 2.0% for sample 1 and 1.0% for samples 2 and 3. Since the variaions appear to be random and not dependent upon the load, they have not been taken into account in analysing the results. The amount of load loss, fig. 6.33 and 6.34, varies with the applied load i.e. increased loss with larger load and the curves are approximately parallel after about four hours. Replotting the values as a percentage of the applied load, figs. 6.35 and 6.36, shows similar curves for the 10 and 15 kN samples and it is reasonable to assume that the material properties are also similar, whereas sample 1 exhibits slightly different properties. A study of the Young's moduli indicates that sample 1 has a modulus 2 to 3 times that of the other samples over the 0.5 kN load range.

Sample	Length mm	Load kN	Strain Variation $\mu\varepsilon$
1	76.40	5.0	605 ± 10
2	75.54	10.0	1903 ± 7.5
3	76.45	15.0	3278 ± 7.5

Table 6.7.1 Details of Bulk Relaxation Tests

6.8 Comparison of Bulk and Contact Time-dependent Behaviour

If the results of the creep test on the core under a load of 5 kN (fig. 6.29) can be considered typical of the material behaviour, then it is possible to calculate the approximate deformation of a 50 mm long sample of similar diameter. Under a 5 kN load this sample would shorten by 3×10^{-3} mm in about three hours. Assuming a linear variation of creep displacement with applied load, the shortening is approximately 6×10^{-4} mm for a 1 kN load. A similar calculation for the 10 kN sample given a value of 4×10^{-4} mm.

Fig. 6.12 shows that for samples with contact angles ranging from 135° to 170°, deformations are approximately $5\text{-}10 \times 10^{-3}$ mm which are 10 to 20 times those for the compression of a cylinder.

A comparison of the results of the relaxation tests on the contacts and cylinders can also be made, although it should be noted that the cylinders were 76 mm long as opposed to the combined length of 50 mm for the contact samples. Comparing figs. 6.35 and 6.36 with figs. 6.26 and 6.27, the percentage loss of load for the typical cylinders (10 and 15 kN) is about 5.75% after four hours and 8.0% after seventy-two hours, whereas the values for the dry contact samples are about 13-19% and 20% after the same periods.

These comparisons show that in situations where time-dependent processes are allowed to occur, the contact behaviour is very dominant and the material time-dependence plays only a minor role.

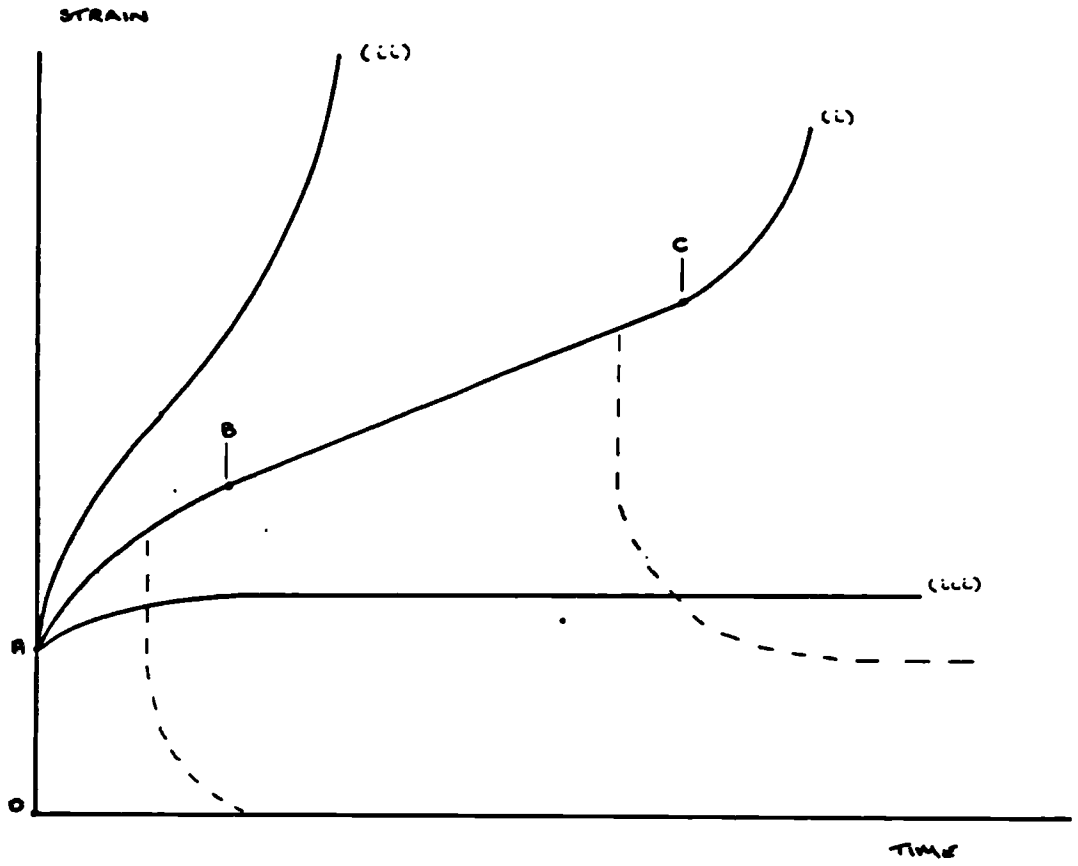

——— LOADING

– – – UNLOADING

(i) STANDARD CURVE

(ii) CURVE FOR HIGH STRESSES AND HIGH TEMPERATURES

(iii) CURVE FOR LOW STRESSES AND LOW TEMPERATURES

FIG. 6.1 :- TIME-DEPENDENT BEHAVIOUR OF ROCK UNDER CONSTANT LOAD

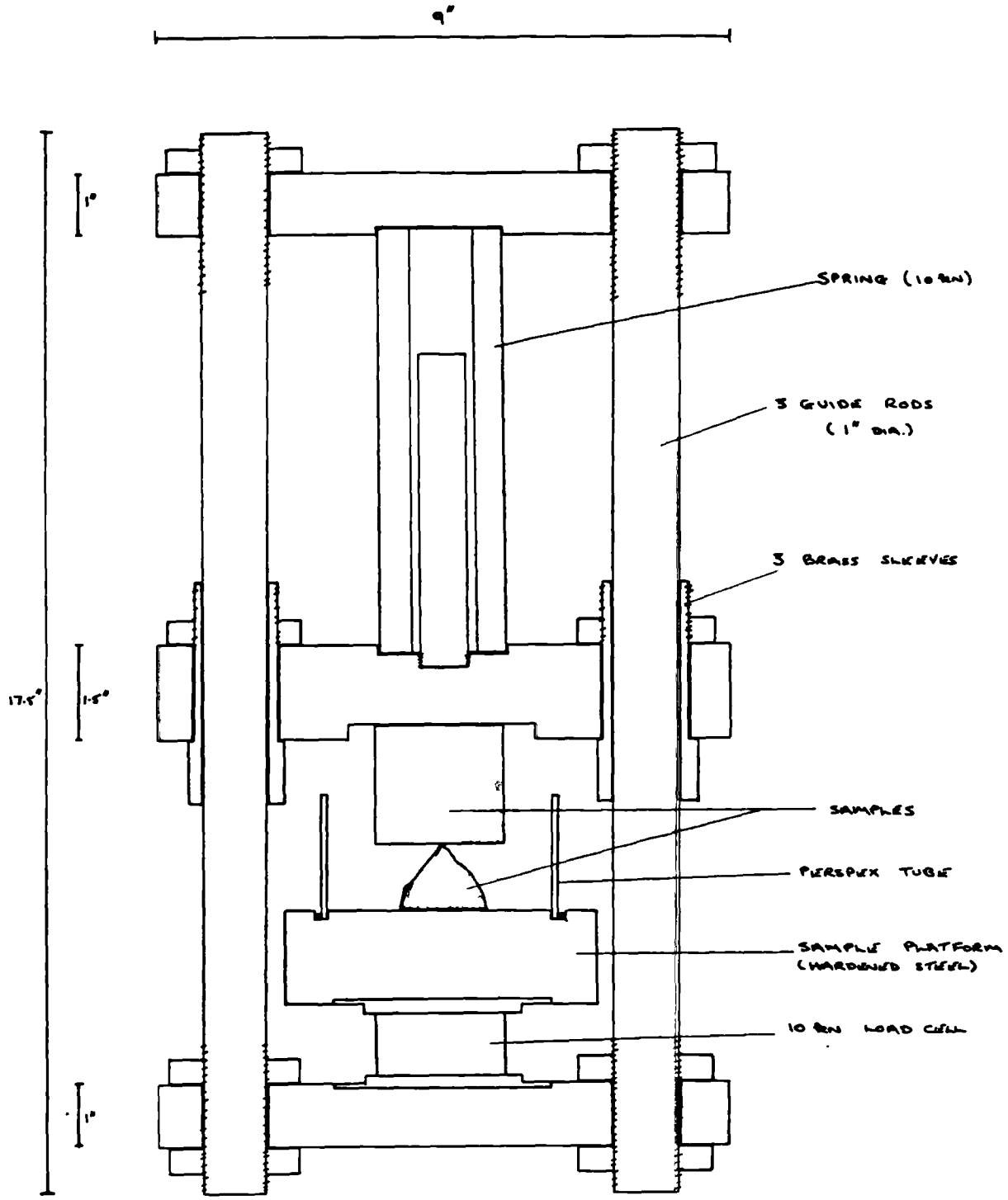

FIG. 6.2:- CONTACT CREEP RIG

Fig. 6.3 :- Contact Creep Rig

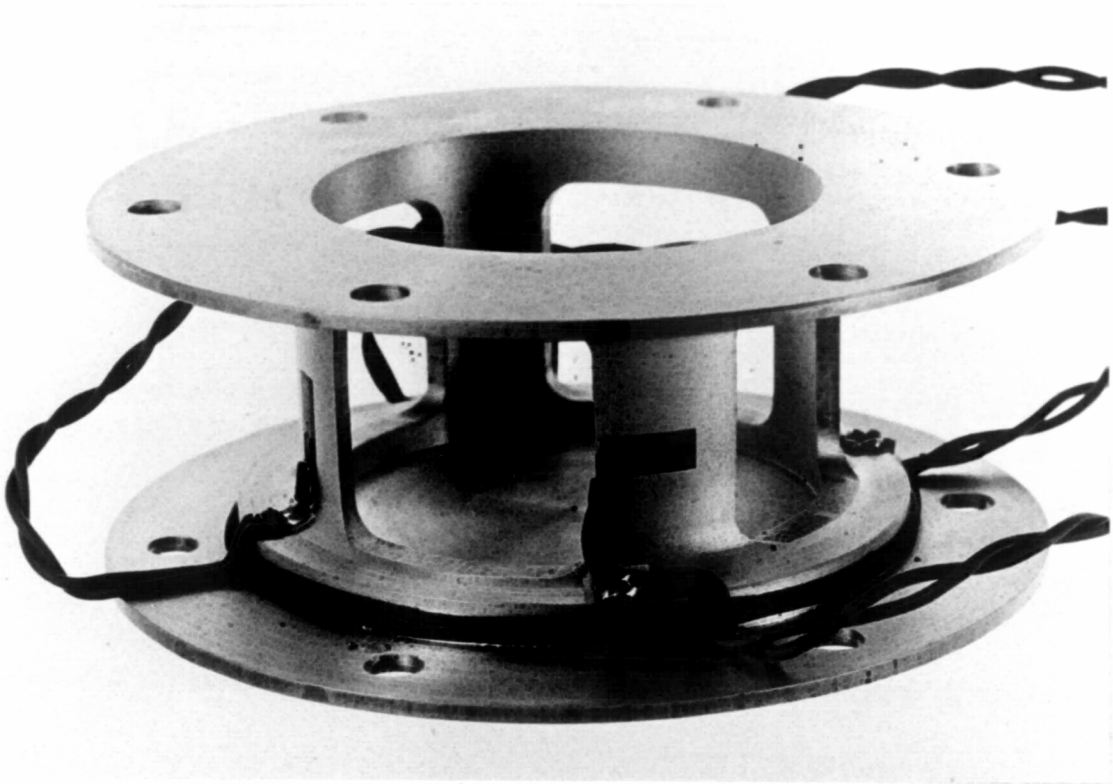

Fig. 6.4 :- 10 kN Load Cell

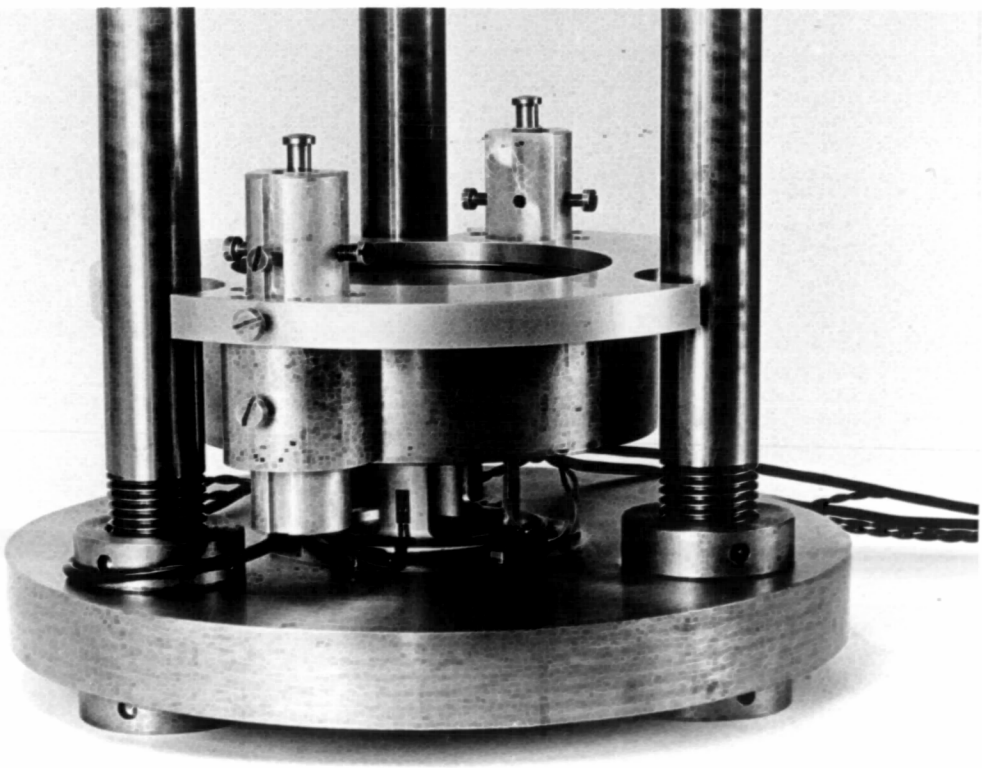

Fig. 6.5 :- Transducer Collar

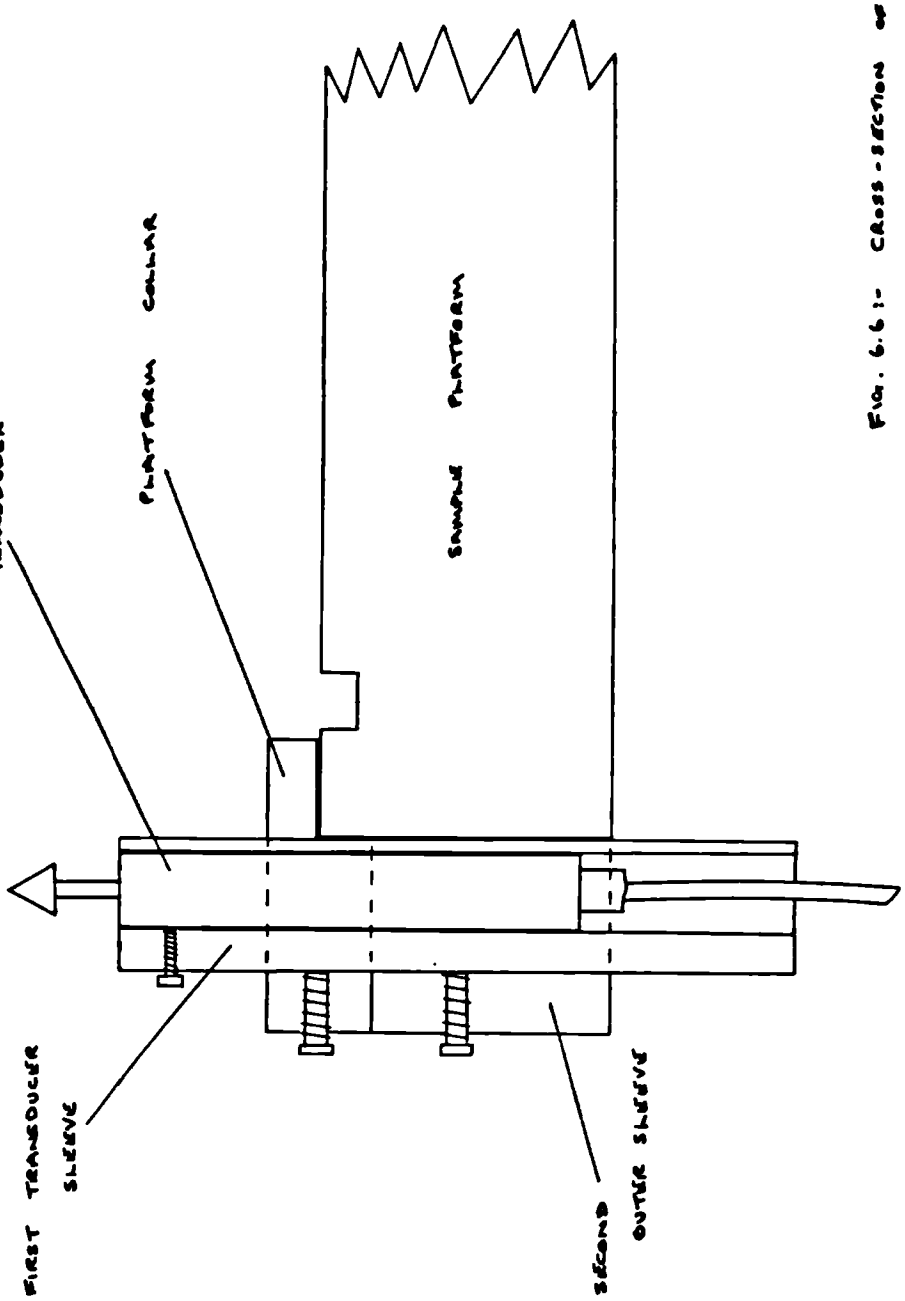

FIG. 6.6 :- CROSS-SECTION OF TRANSDUCER COLLAR

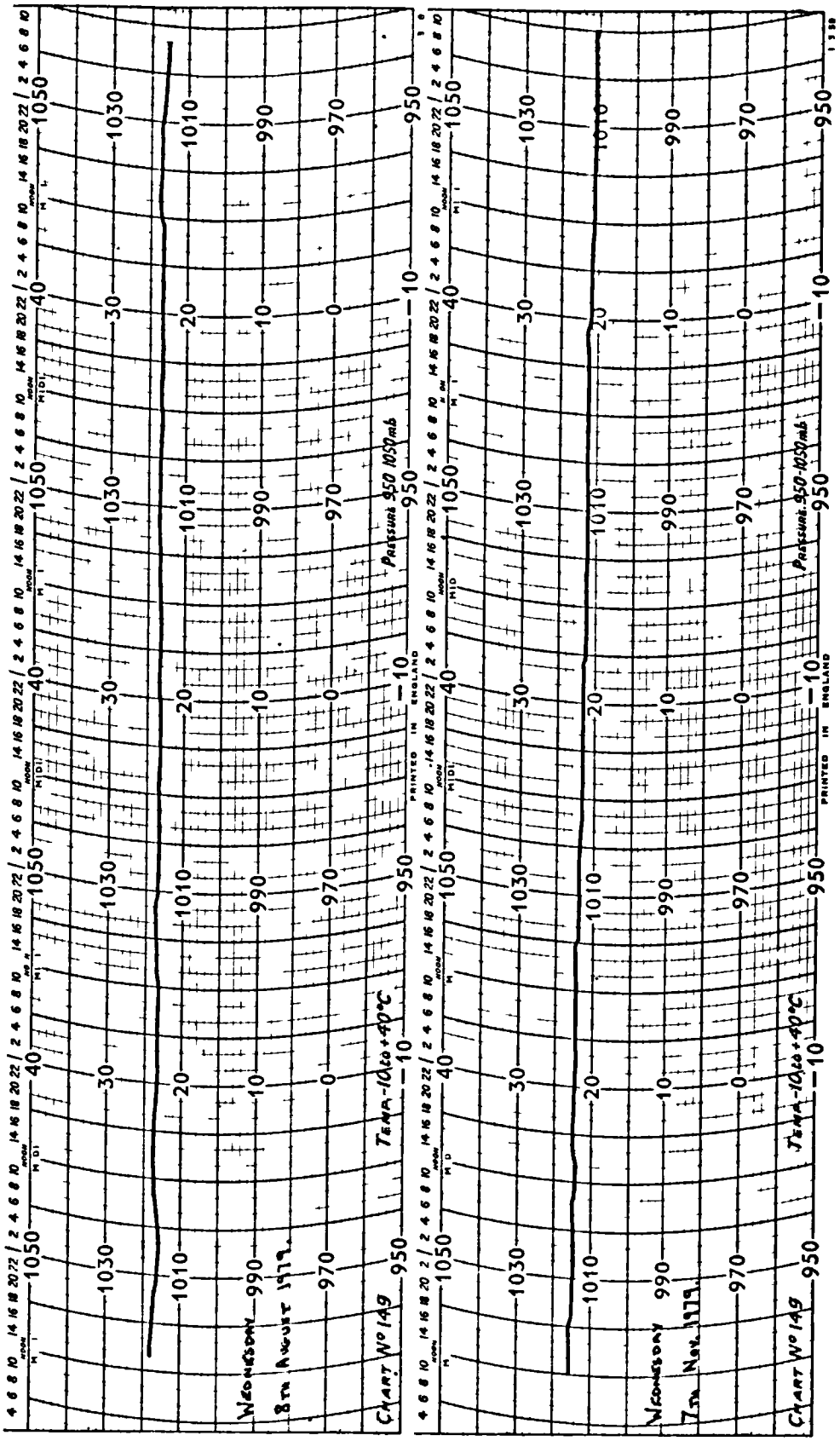

Fig. 6.7 :- Temperature Variation in Laboratory (i)

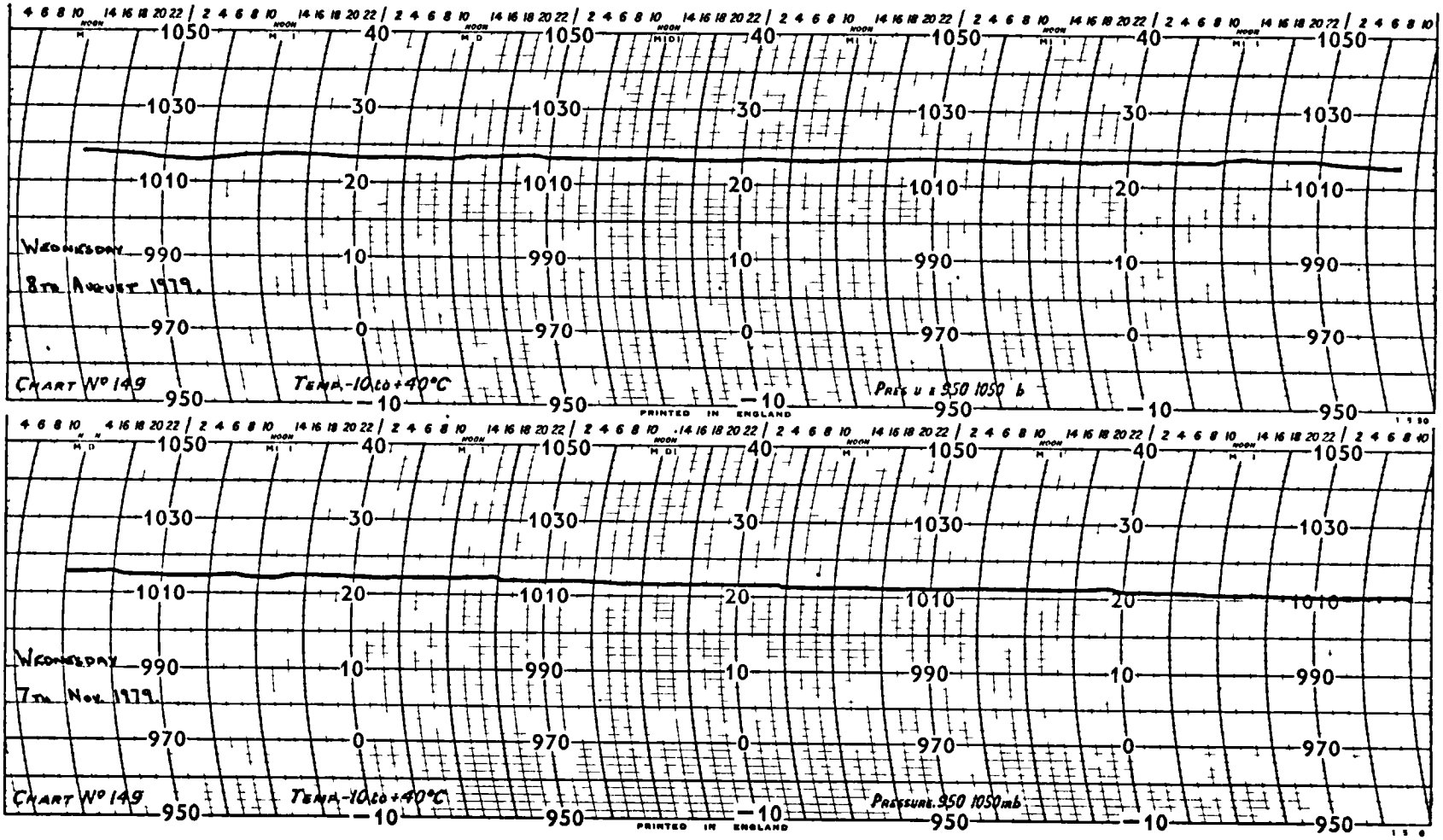

Fig. 6.7 :- Temperature Variation in Laboratory (i)

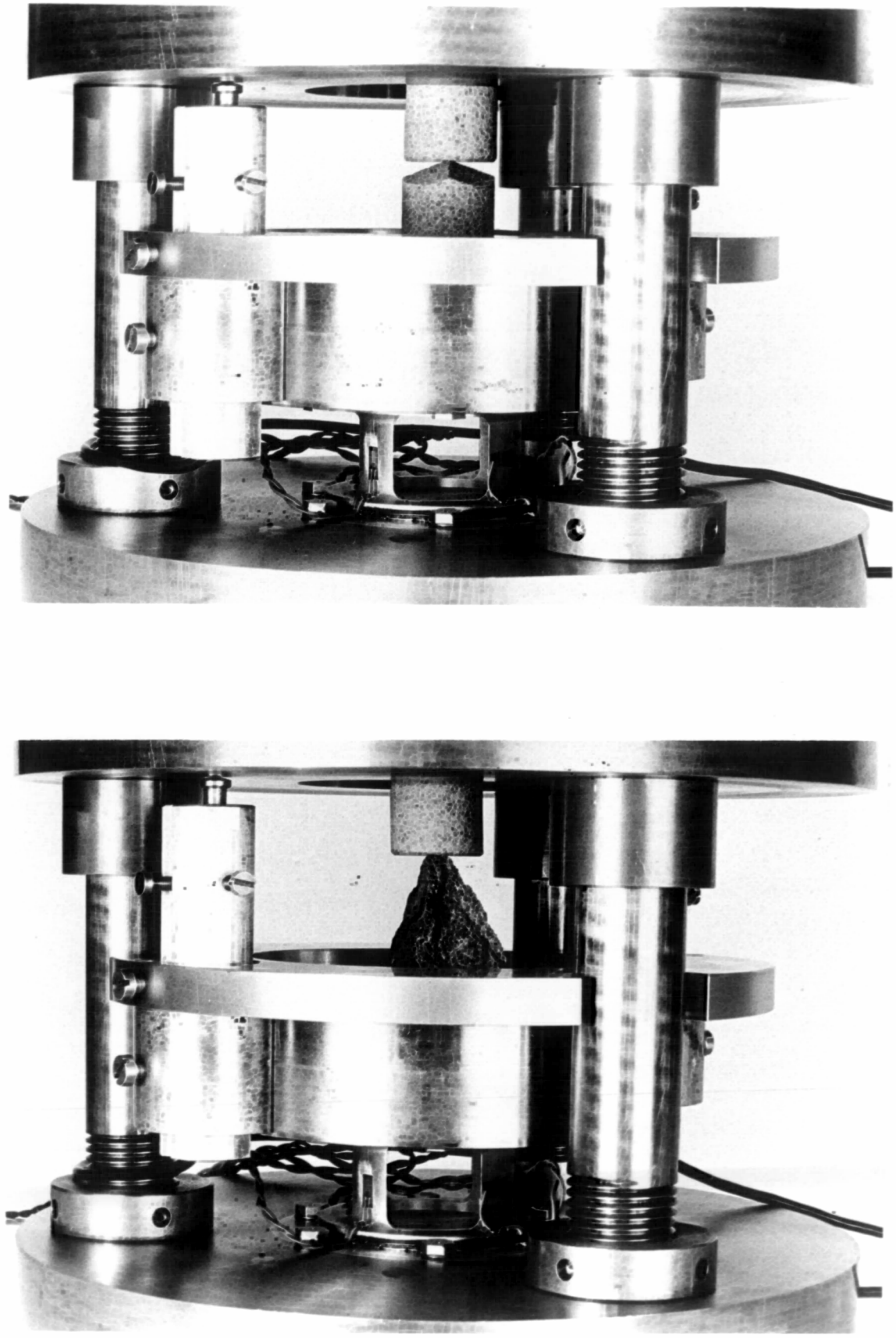

Fig. 6.9 :- Testing of Shaped and Irregular Samples in Contact Creep Rig

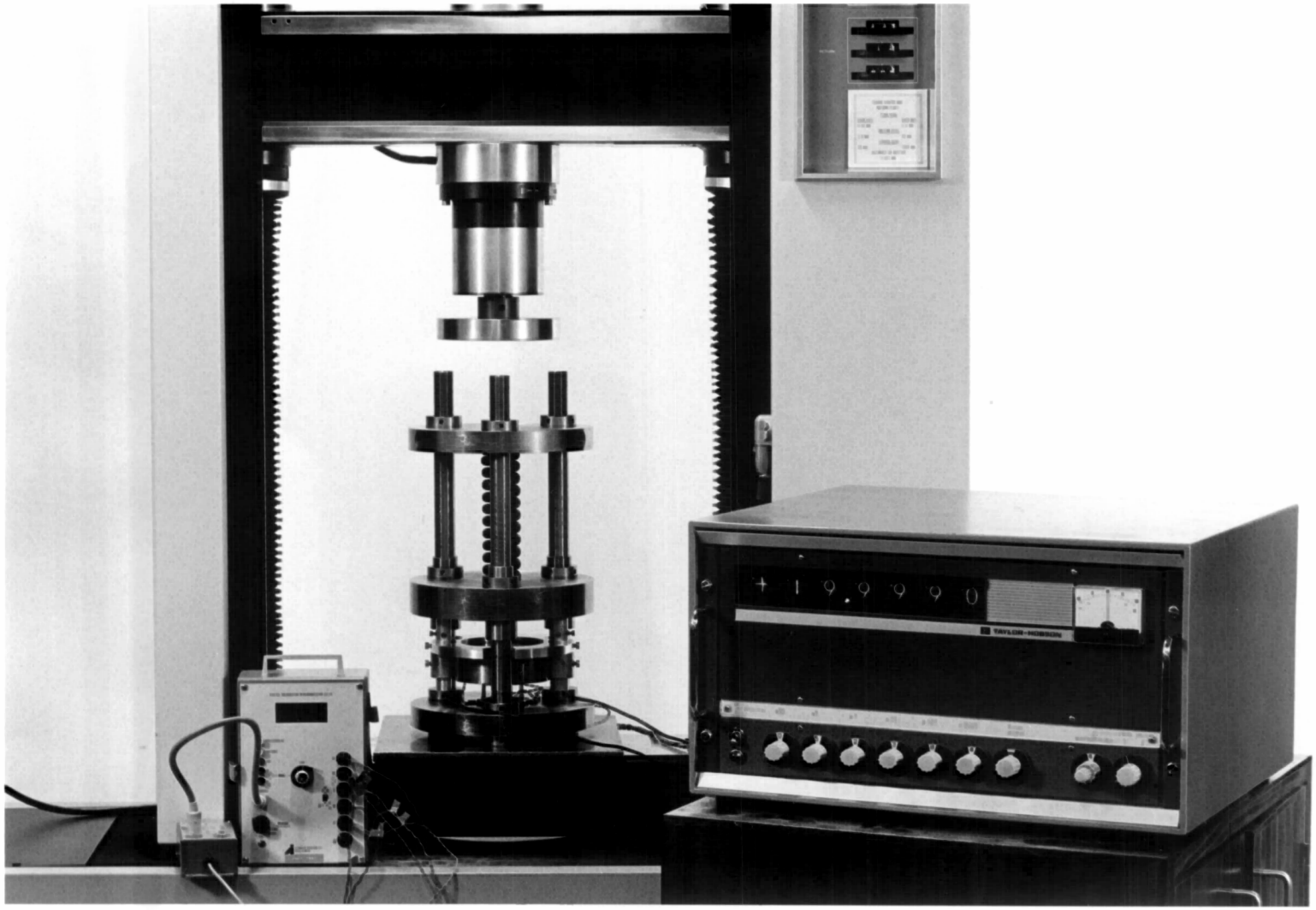

Fig. 6.10 :- Experimental Set-up using Taylor Hobson Instrumentation

Fig. 6.11 :- Experimental Set-up using Sangamo Instrumentation

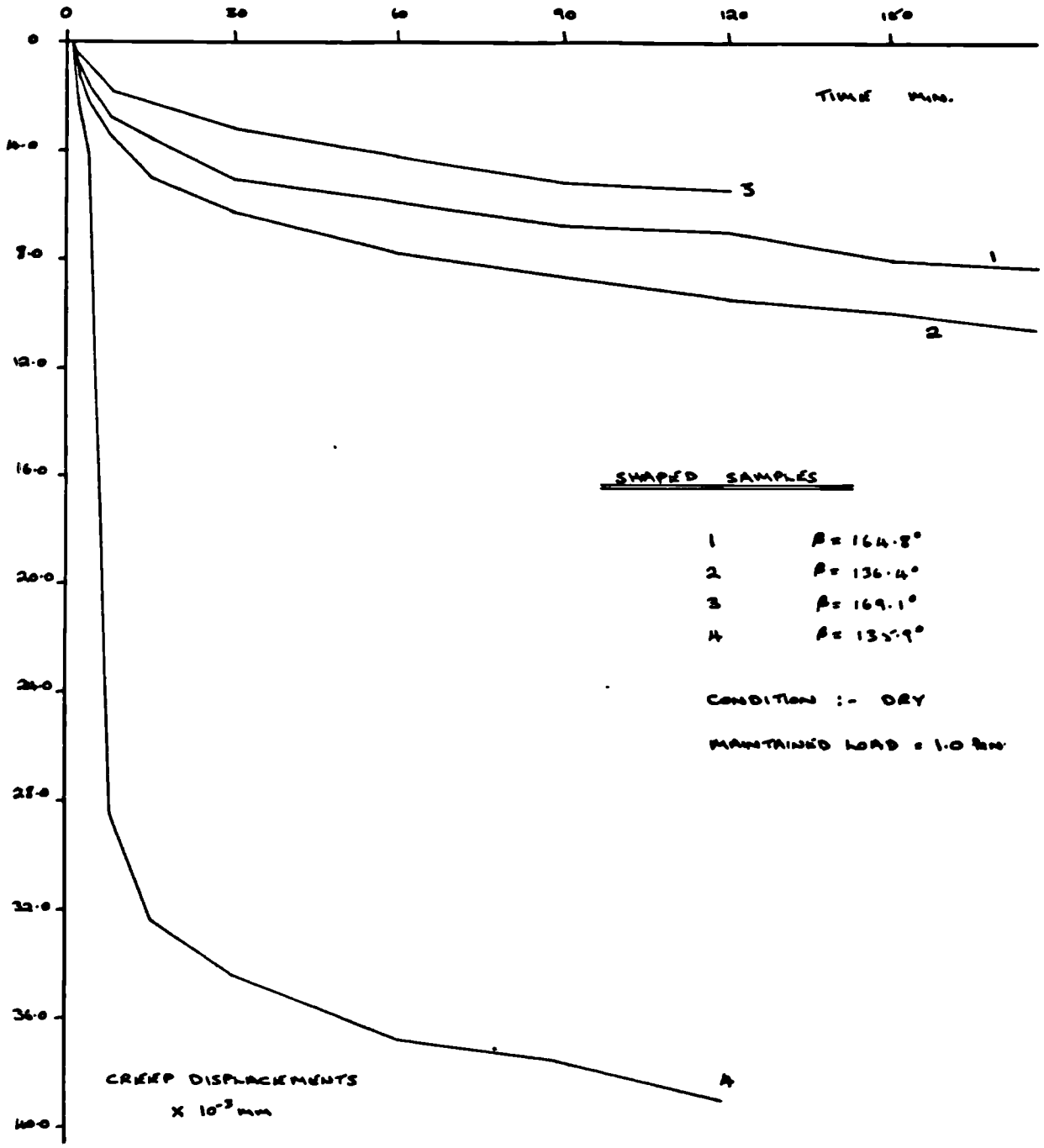

FIG. 6.12 :- CONTACT CREEP DISPLACEMENT RESULTS;
DRY, SHAPED SAMPLES

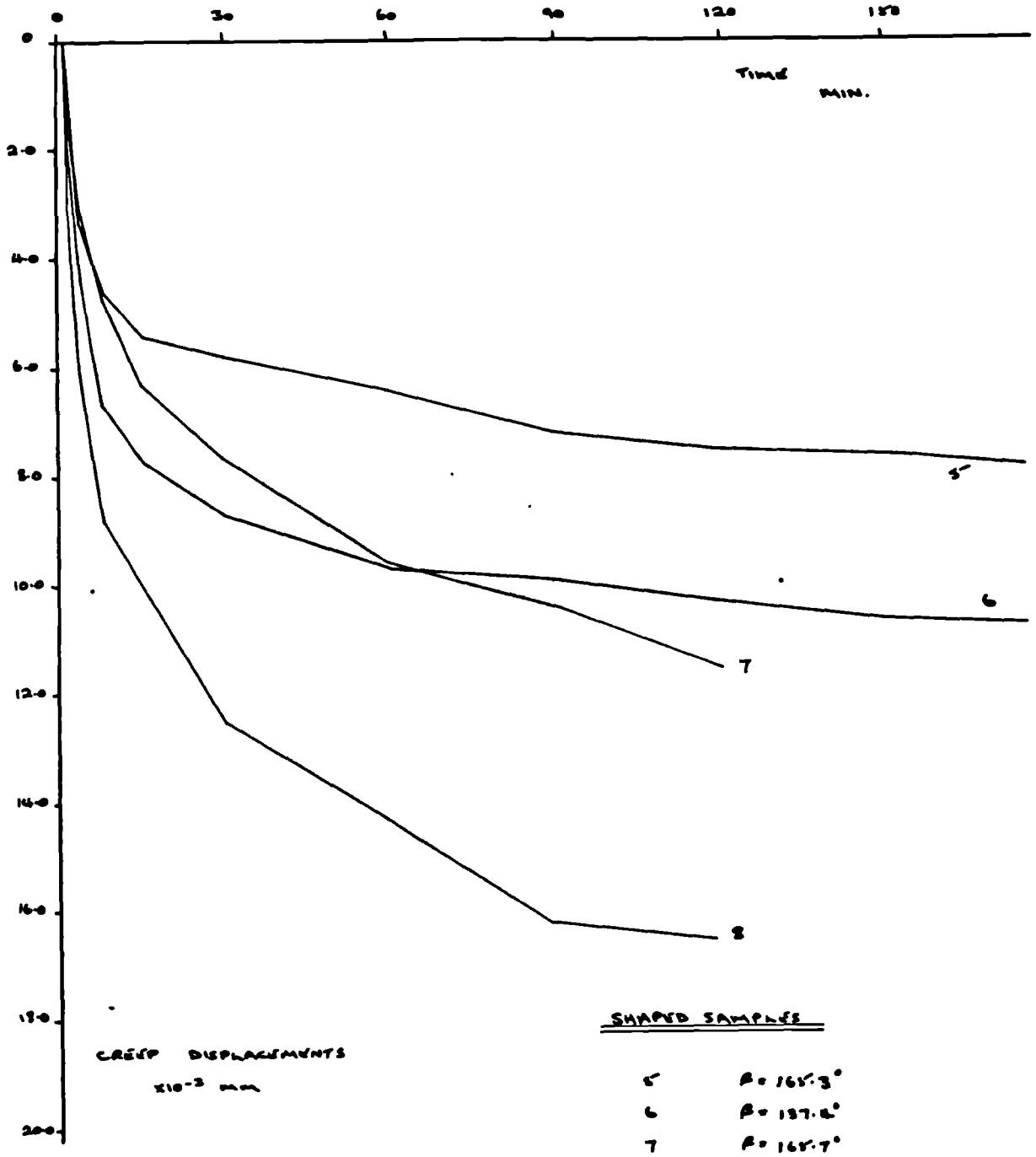

SHAPED SAMPLES

5	$\beta = 161.3°$
6	$\beta = 137.6°$
7	$\beta = 161.7°$
8	$\beta = 138.1°$

CONDITION :- SATURATED

MAINTAINED LOAD = 1.0 kN

FIG. 6.13 :- CONTACT CREEP DISPLACEMENT RESULTS ;

SATURATED, SHAPED SAMPLES

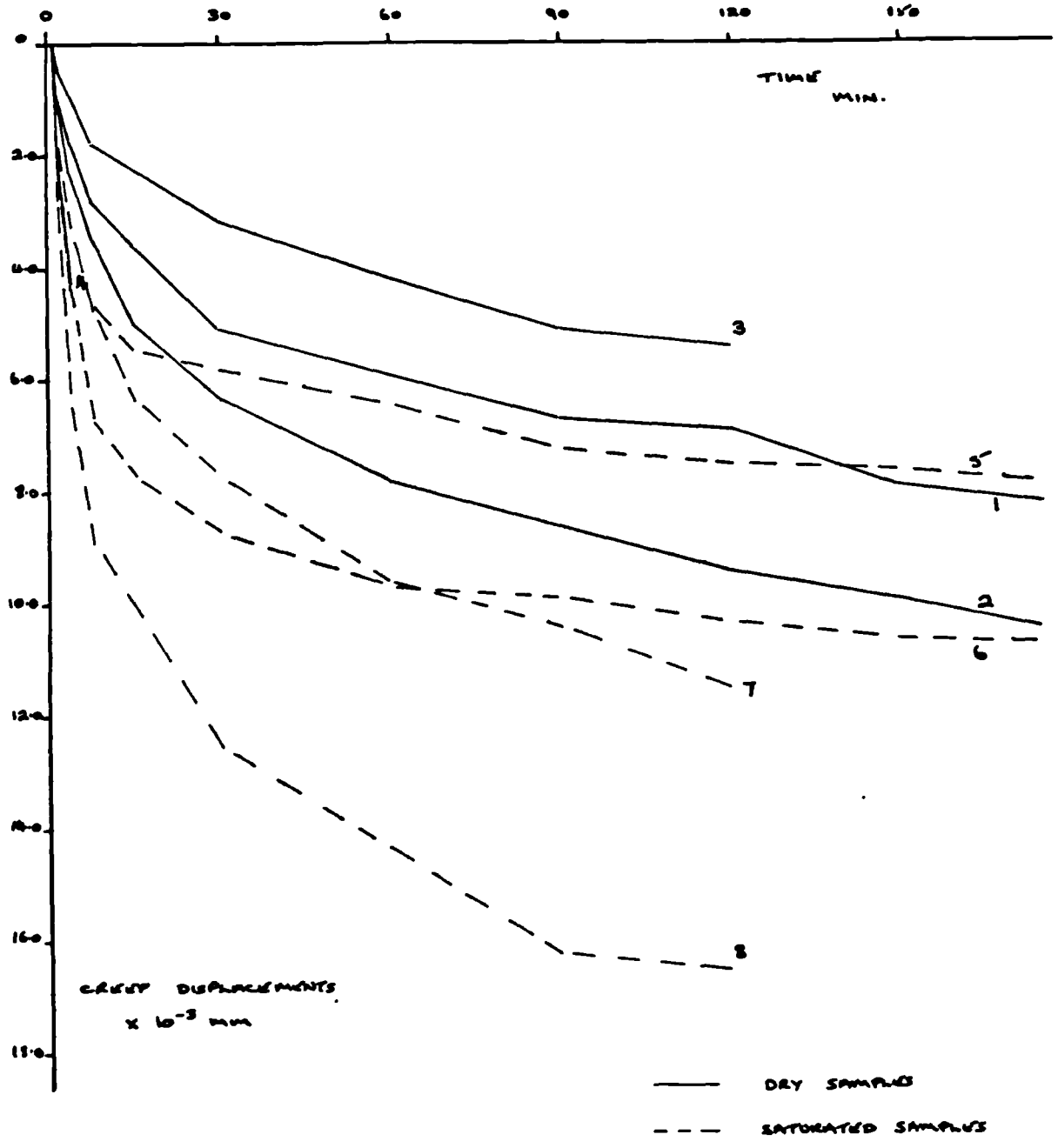

FIG. 6.14:- COMPARISON OF DRY AND SATURATED SHAPED SAMPLE CONTACT CREEP DISPLACEMENT RESULTS

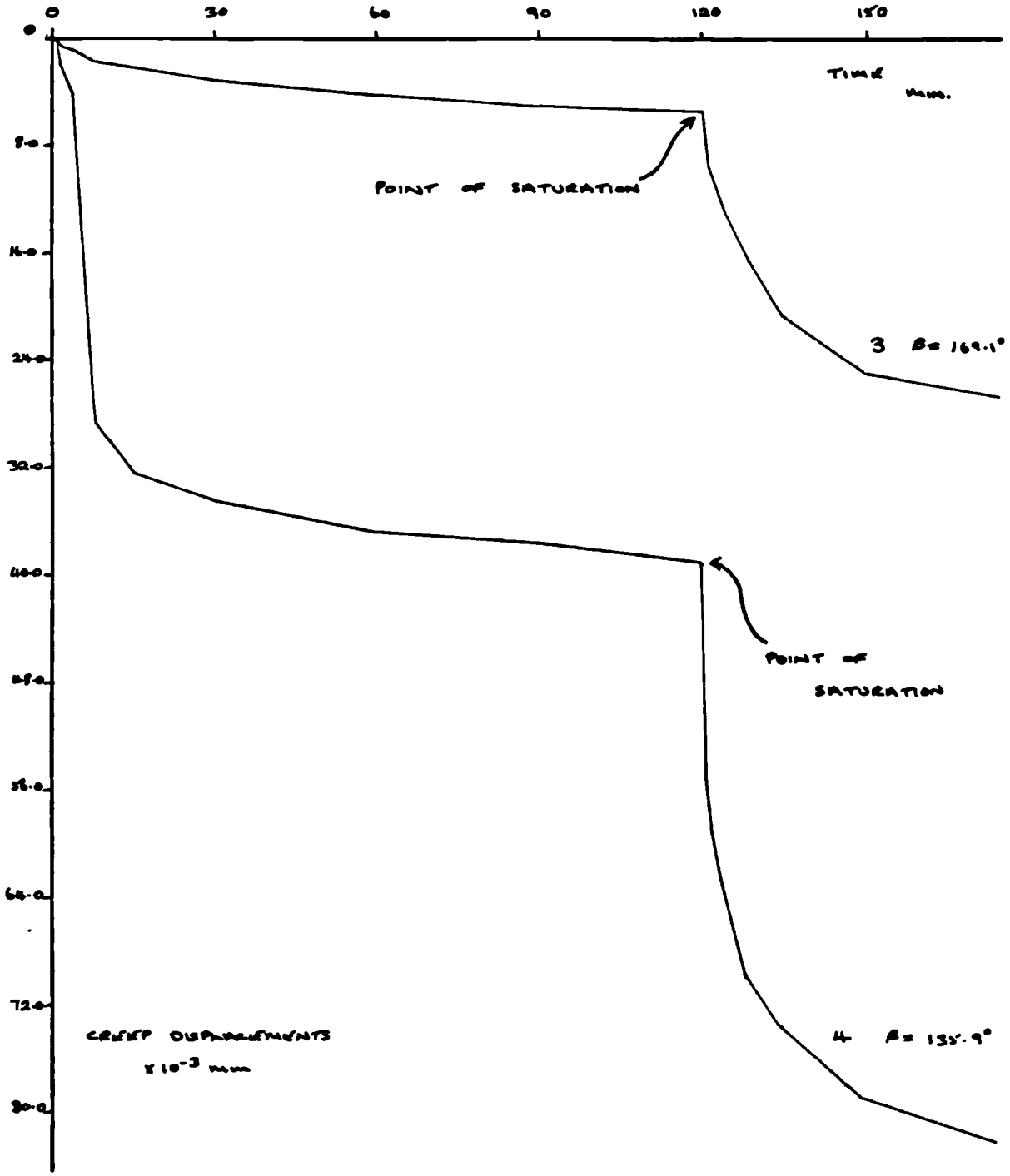

FIG. 6.15 :- EFFECT OF SATURATION ON CONTACT TIME-DEPENDENT BEHAVIOUR; SHAPED SAMPLES

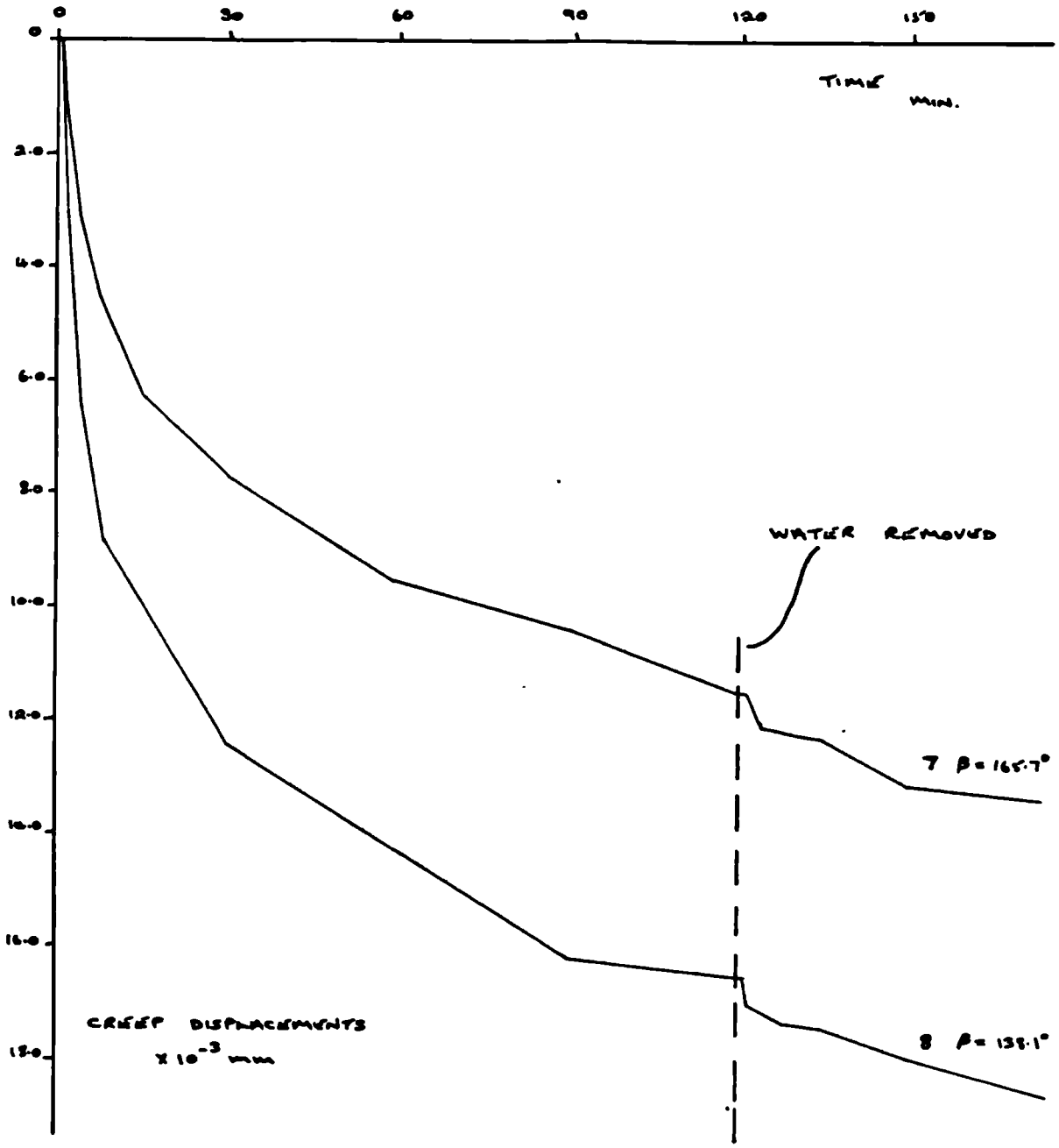

FIG. 6.16 :- EFFECT OF REMOVING WATER ON CONTACT TIME-DEPENDENT BEHAVIOUR ; SHAPED SAMPLES

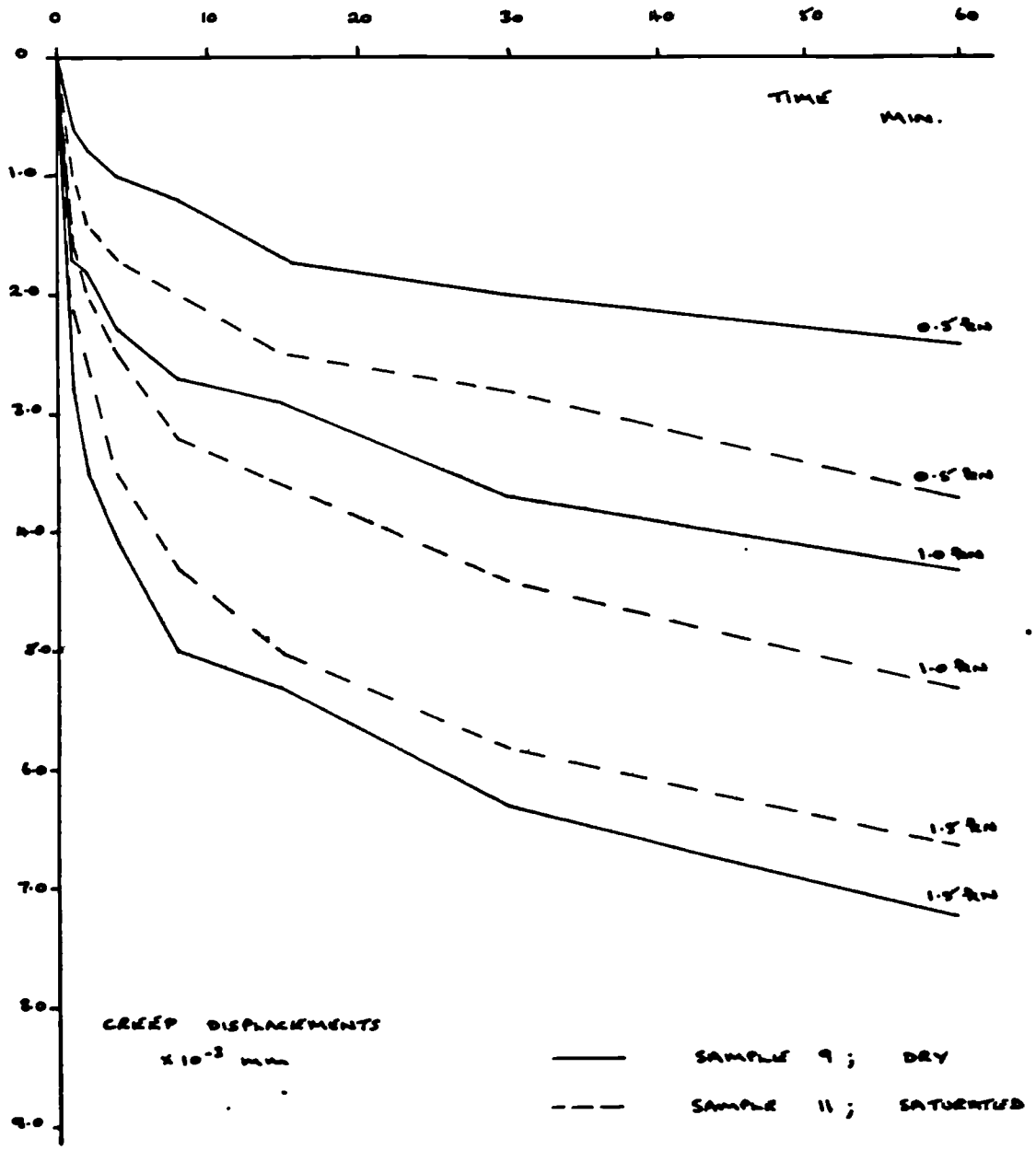

FIG. 6.17 :- EFFECT OF INCREASED LOAD ON CONTACT TIME-DEPENDENT BEHAVIOUR ; SHAPED SAMPLES (B=160°)

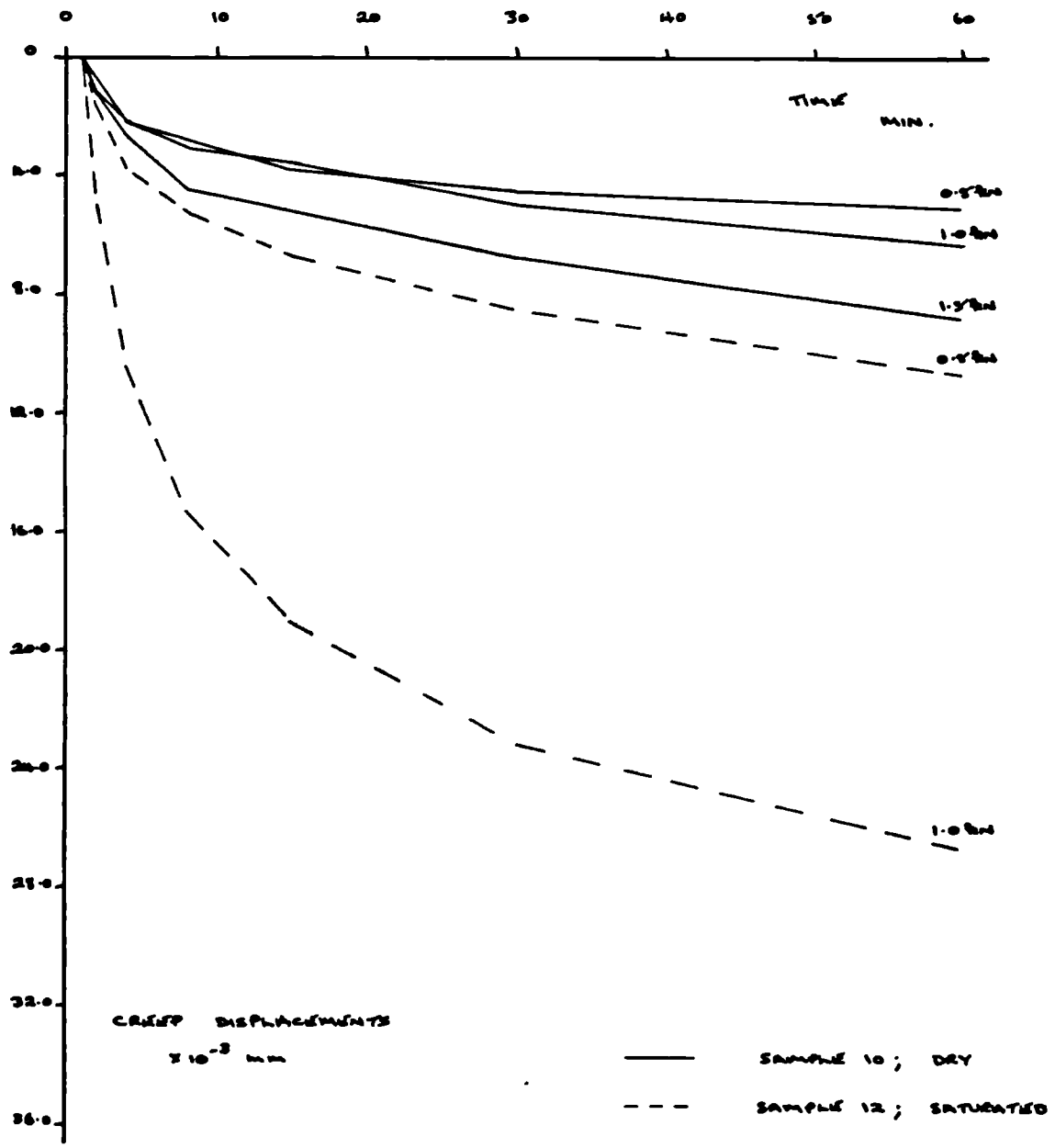

FIG. 6.19 :- EFFECT OF INCREASED LOAD ON CONTACT TIME-DEPENDENT BEHAVIOUR ; SHAPED SAMPLES ($\beta \simeq 120°$)

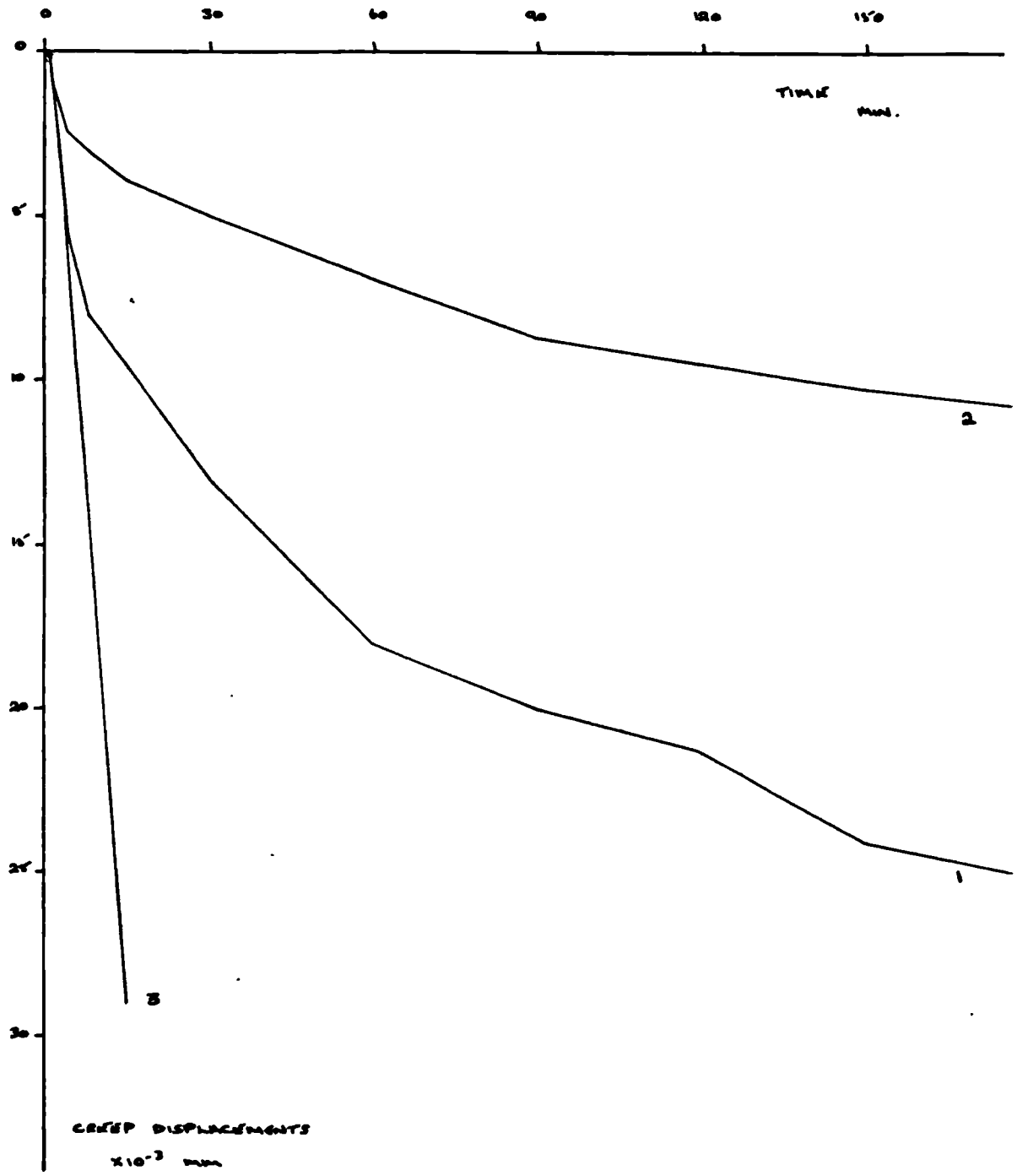

FIG. 6. 19 :- CONTACT CREEP DISPLACEMENT RESULTS;

DRY, IRREGULAR SAMPLES

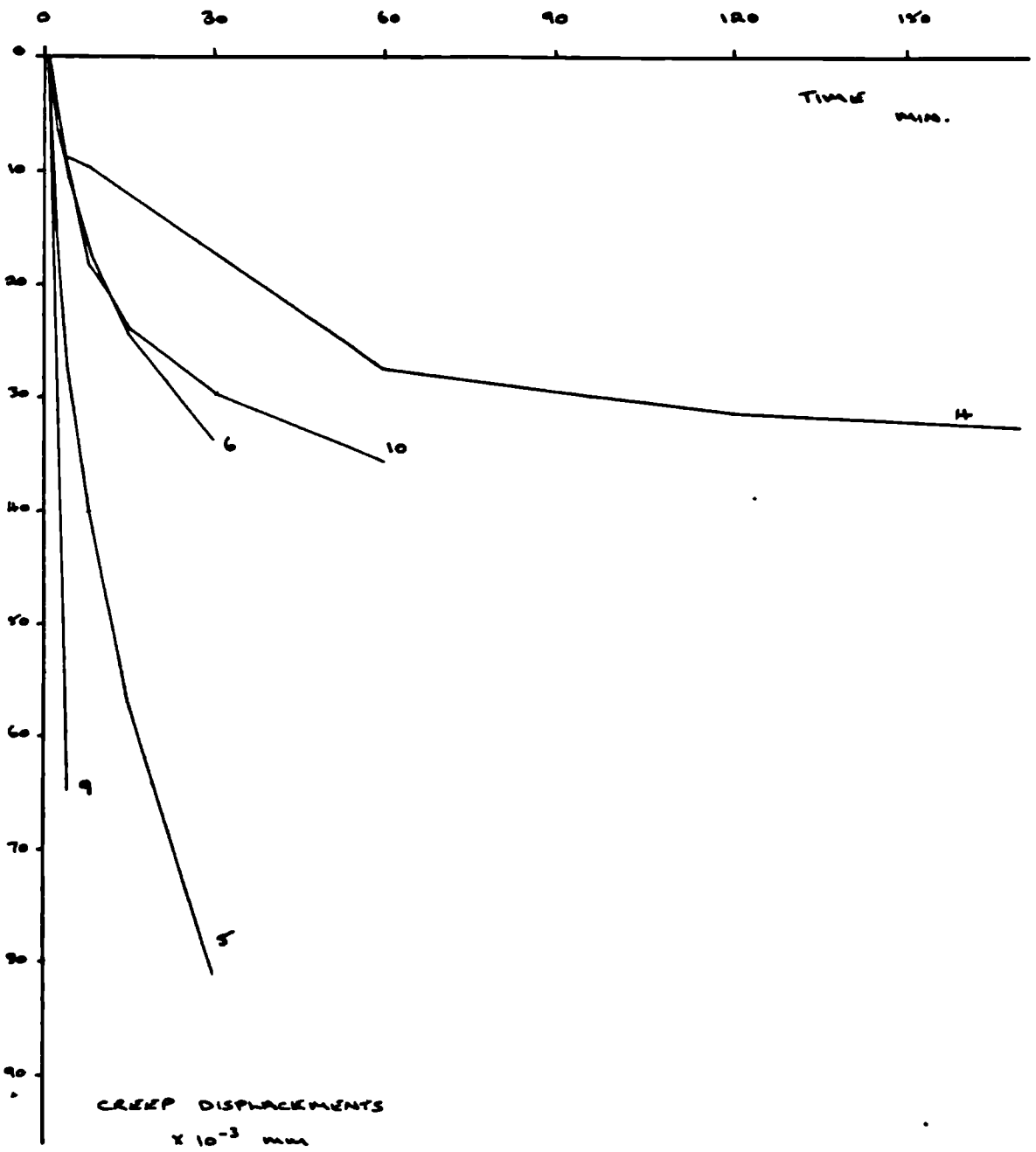

FIG. 6.20 :- CONTACT CREEP DISPLACEMENT RESULTS;
SATURATED, IRREGULAR SAMPLES

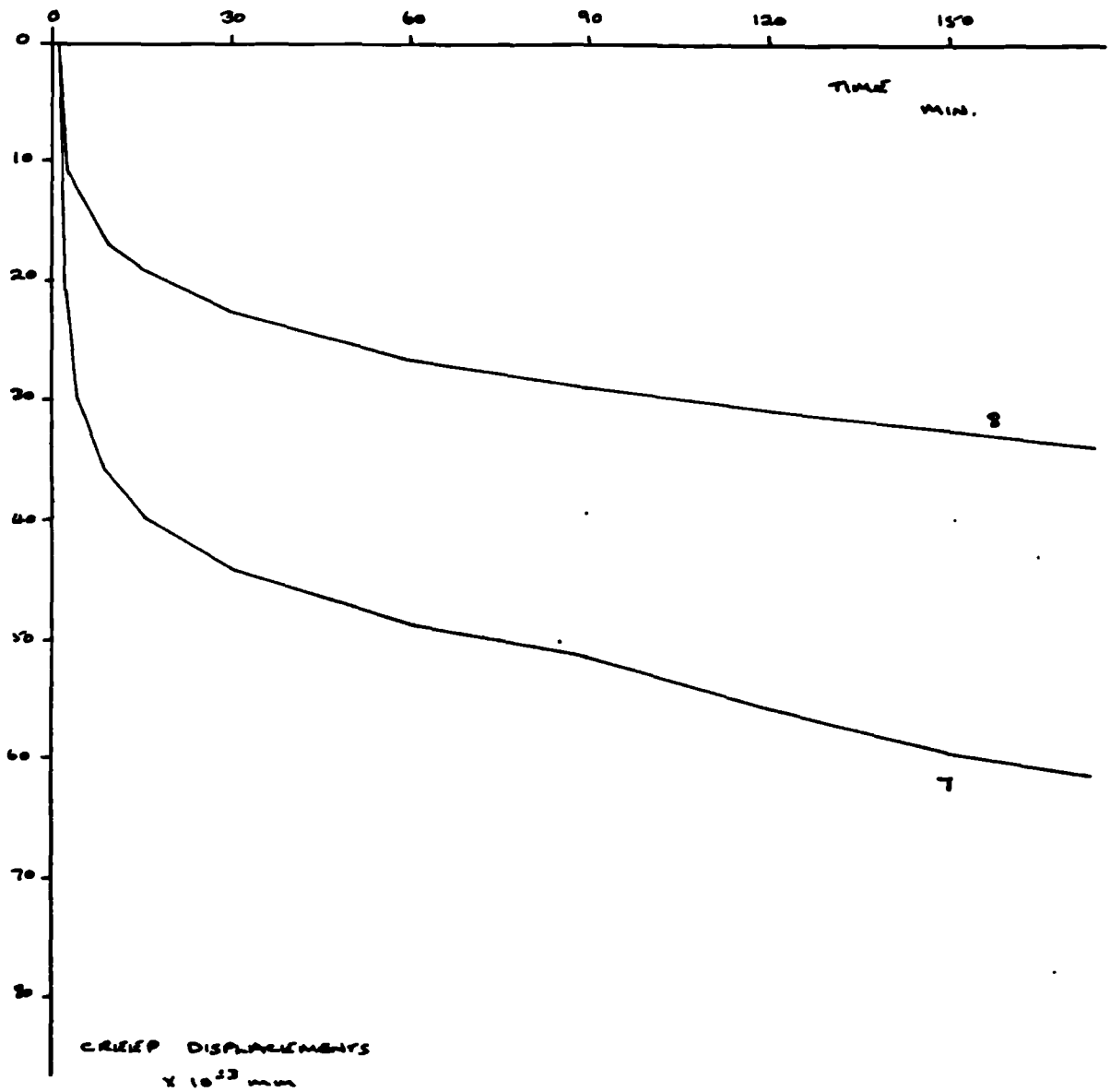

FIG. 6.21 :- CONTACT CREEP DISPLACEMENT RESULTS;
SATURATED / SURFACE DRY, IRREGULAR SAMPLES

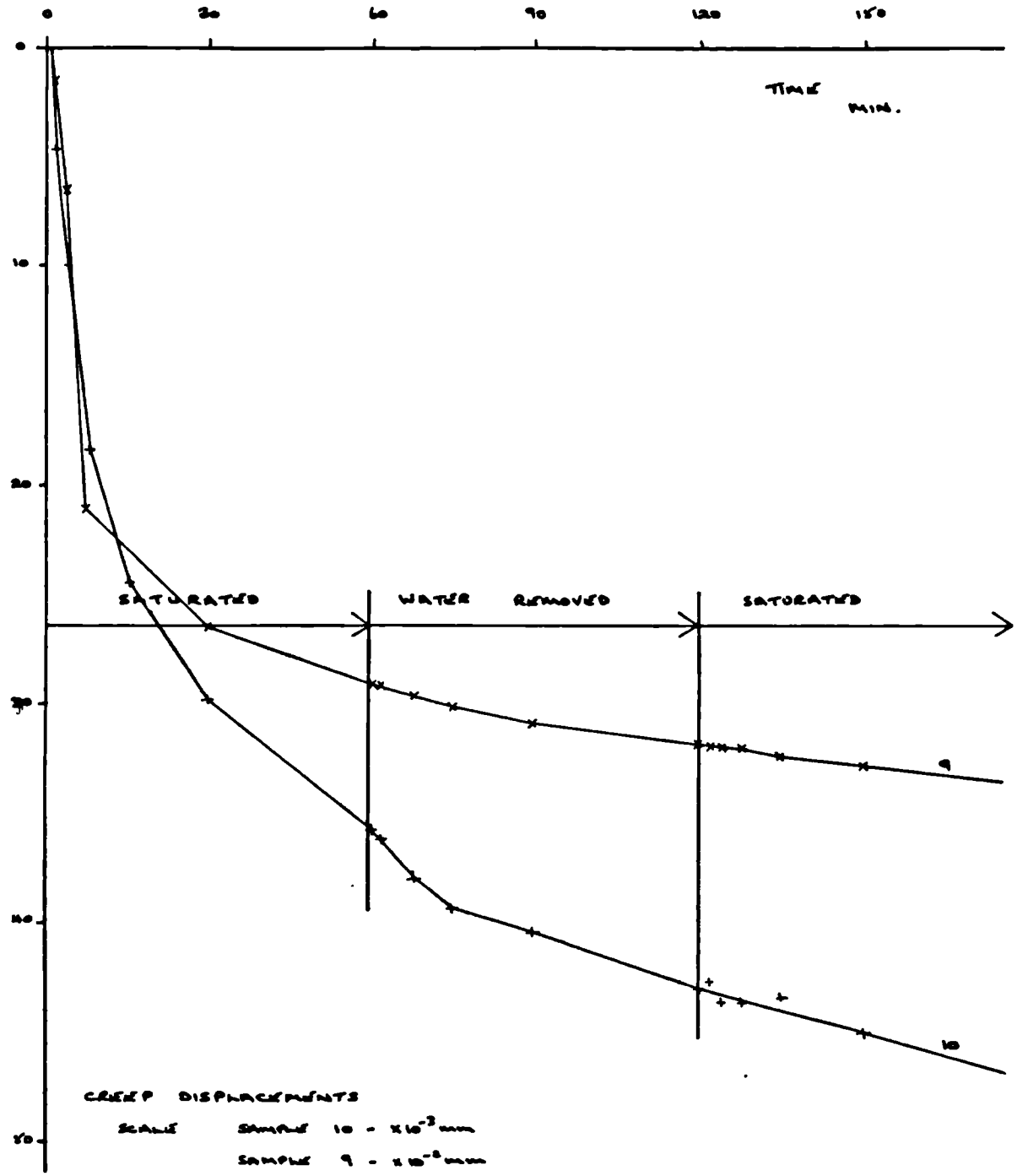

FIG. 6.22 :- EFFECT OF REMOVING WATER AND RESATURATION ON CONTACT TIME-DEPENDENT BEHAVIOUR ; IRREGULAR SAMPLES

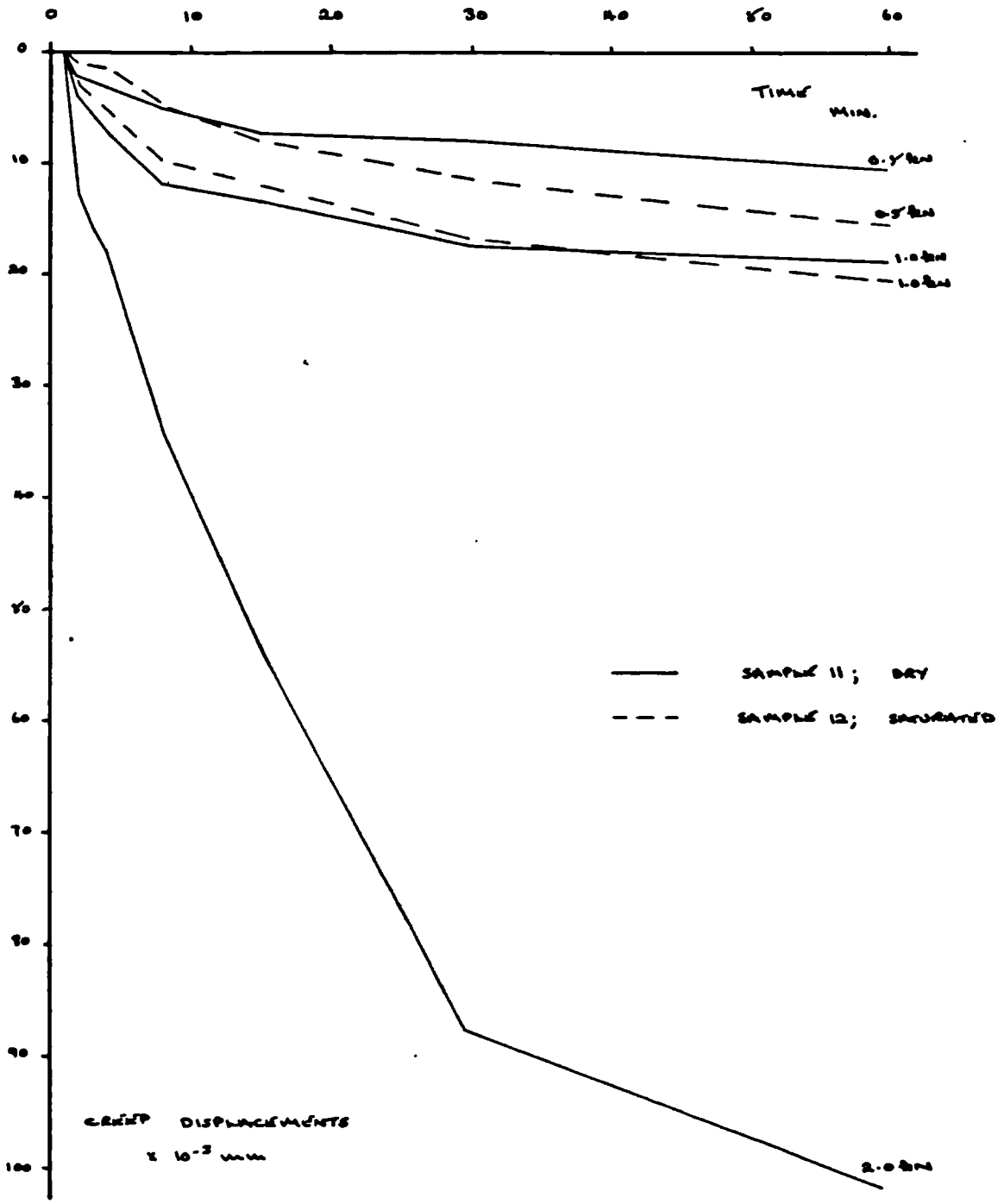

FIG. 6.23 :- EFFECT OF INCREASED LOAD ON CONTACT TIME-DEPENDENT BEHAVIOUR ; IRREGULAR SAMPLES

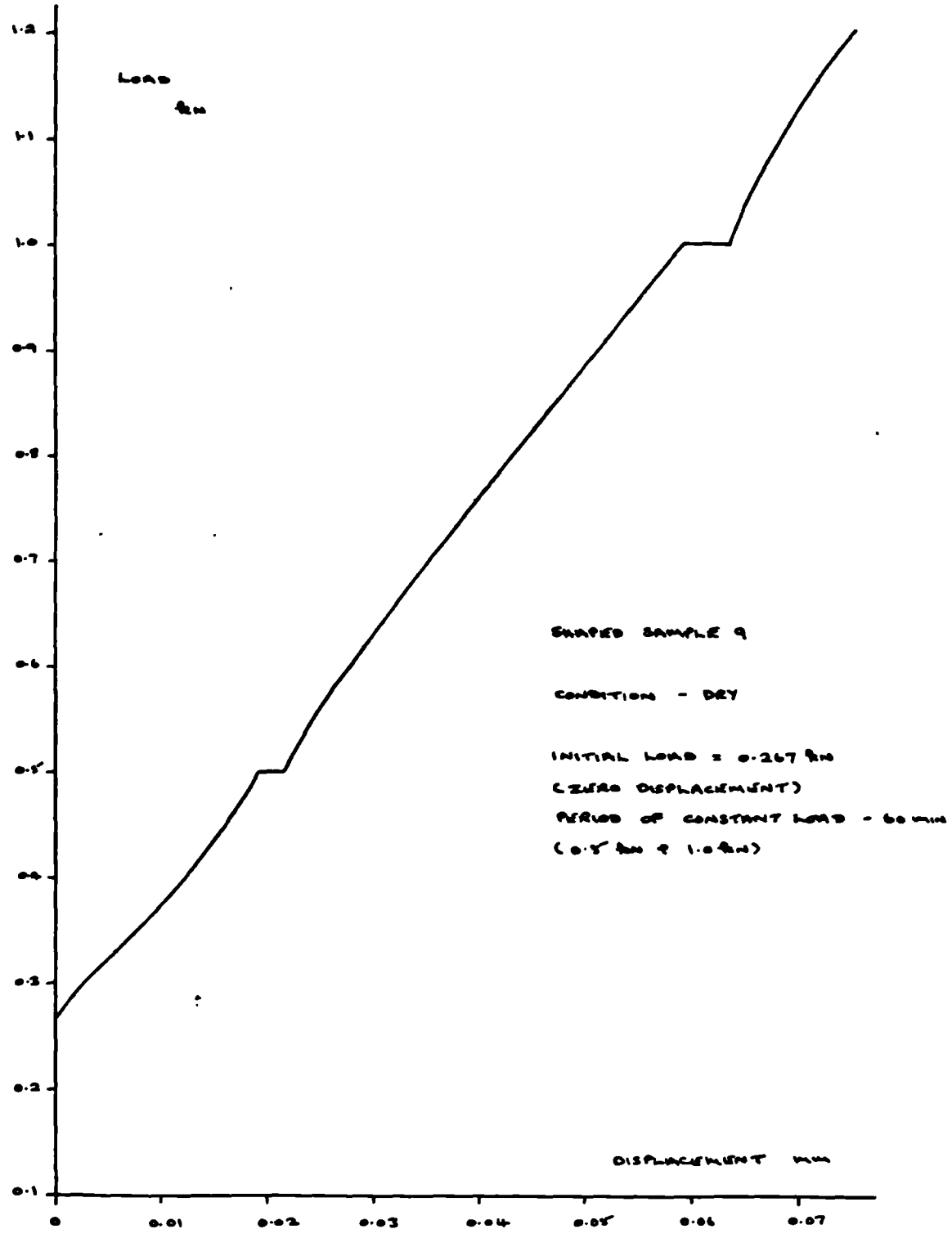

FIG. 6.24 :- EFFECT OF PERIOD OF CONSTANT LOAD ON LOAD - DISPLACEMENT CURVE ; DRY, SHAPED SAMPLE (No. 9)

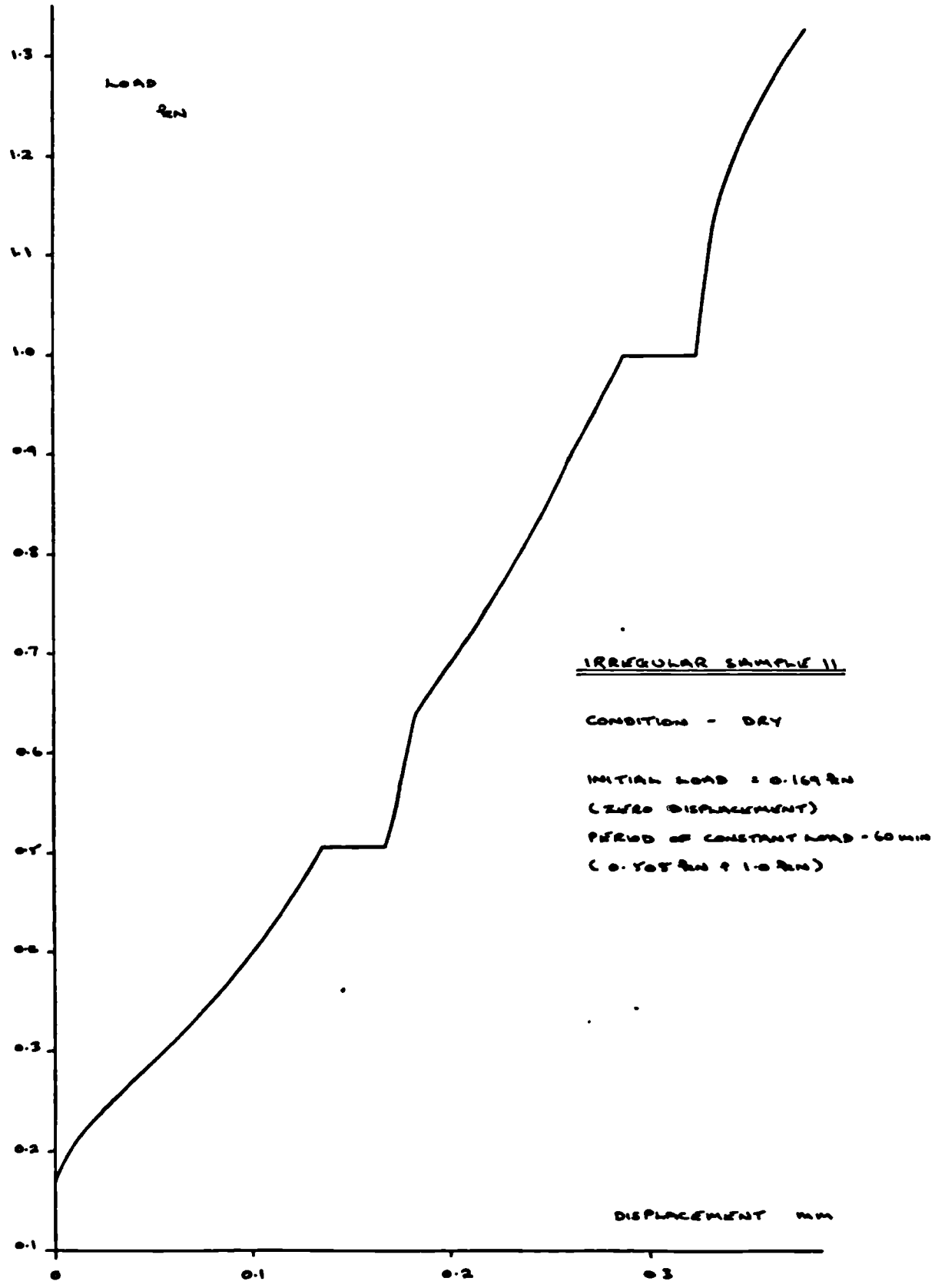

FIG. 6.25 :- EFFECT OF PERIOD OF CONSTANT LOAD ON LOAD - DISPLACEMENT CURVE; DRY, IRREGULAR SAMPLE (No.11)

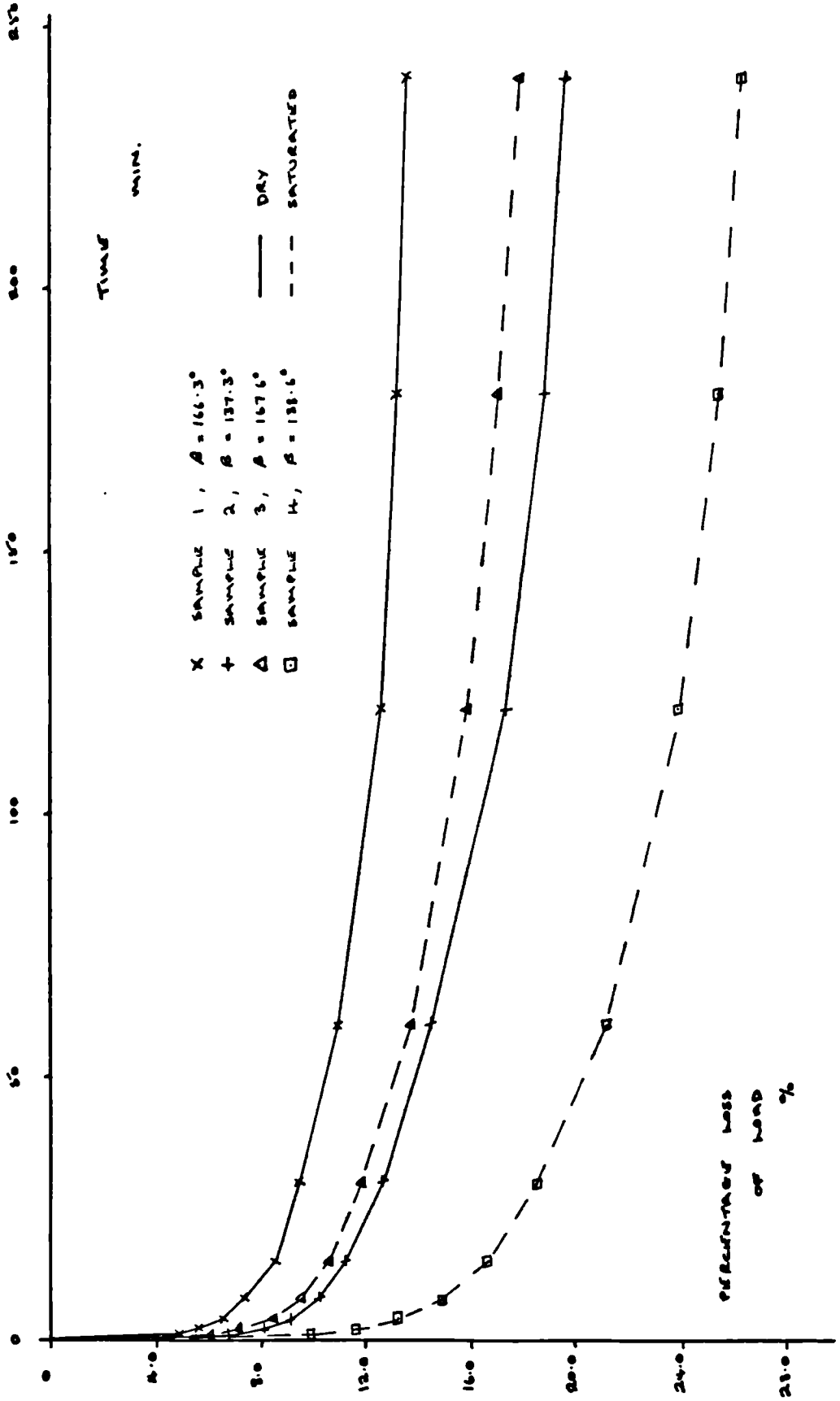

FIG. 6.26 :- RESULTS OF SHAPED SAMPLE CONTACT RELAXATION TESTS (0 - 4 HRS)

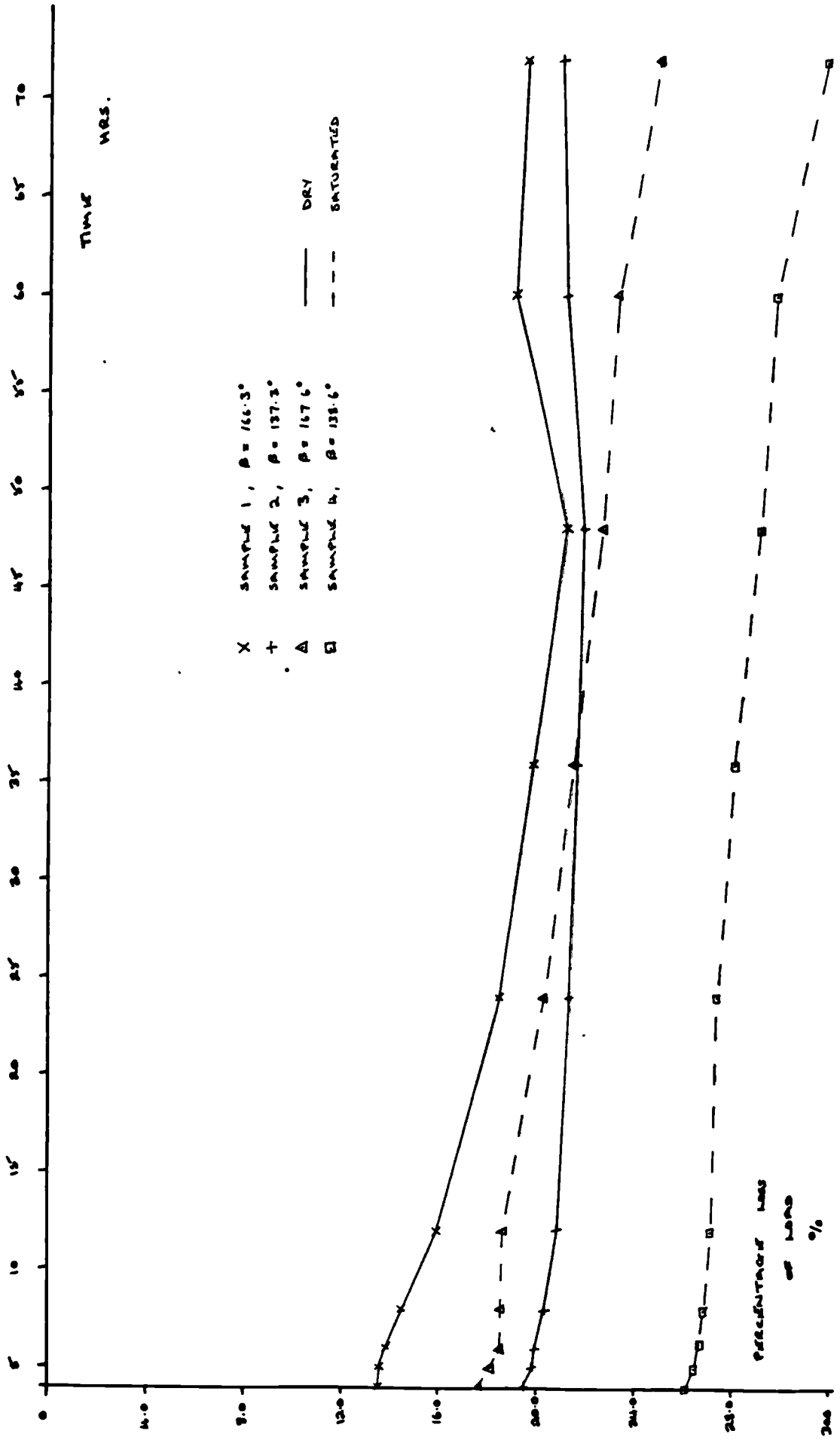

FIG. 6.27 :- RESULTS OF SHAPE SAMPLE CONTACT ABRASION TESTS (4-72 HRS)

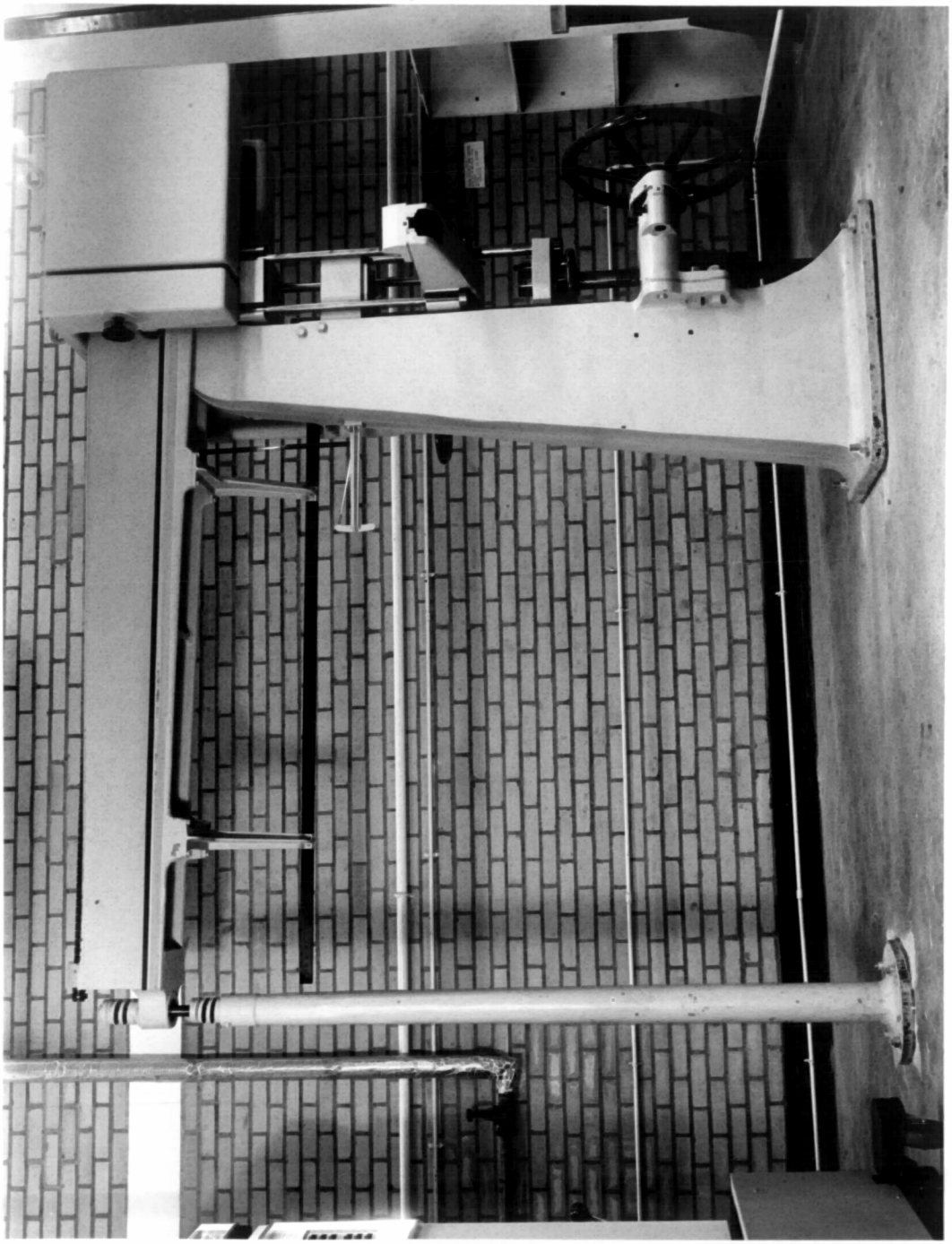

Fig. 6.28 :- Avery Constant Load Machine

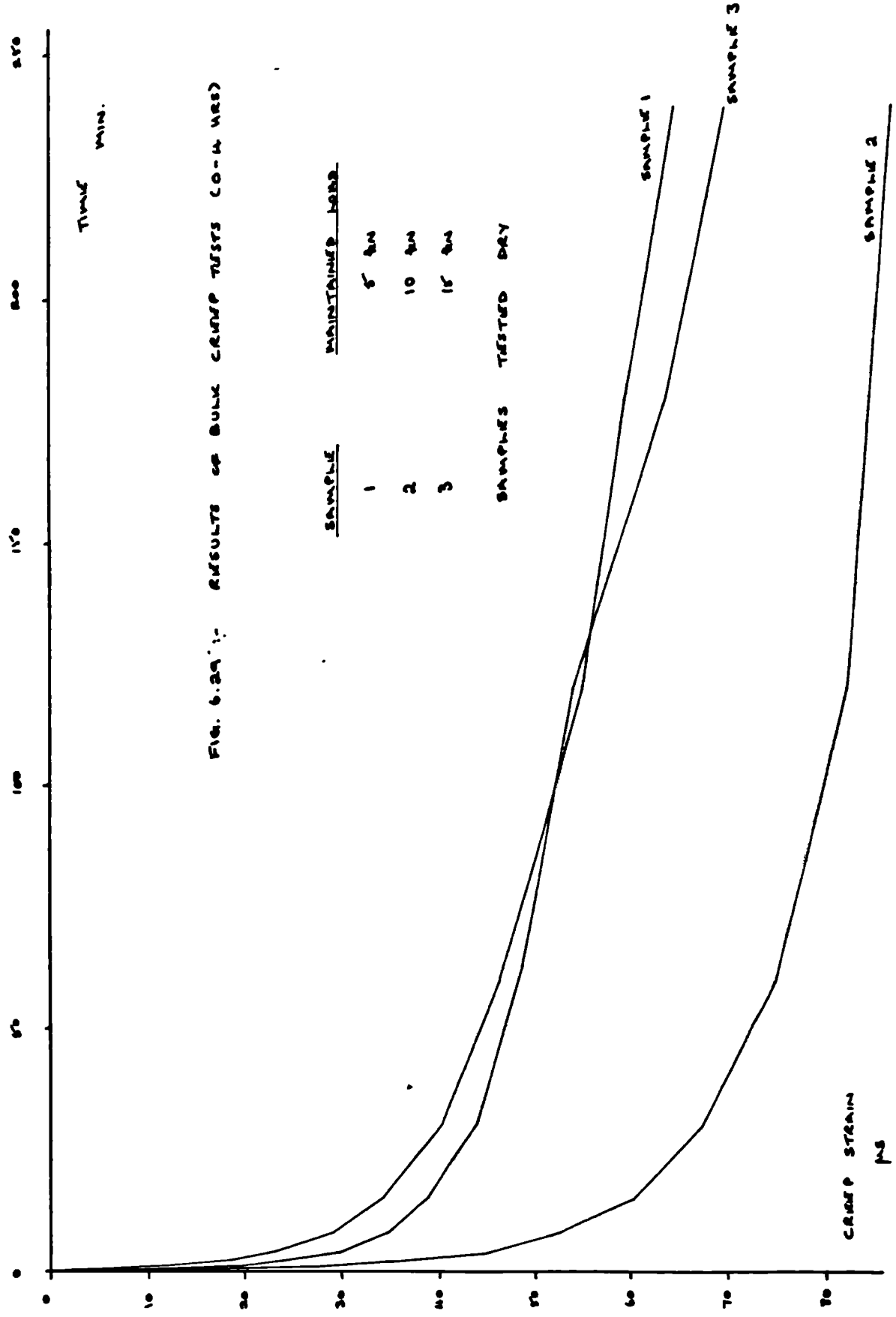

FIG. 6.29 :- RESULTS OF BULK CREEP TESTS (CO-4 WKS)

SAMPLE	MAINTAINED LOAD
1	5 kN
2	10 kN
3	15 kN

SAMPLES TESTED DRY

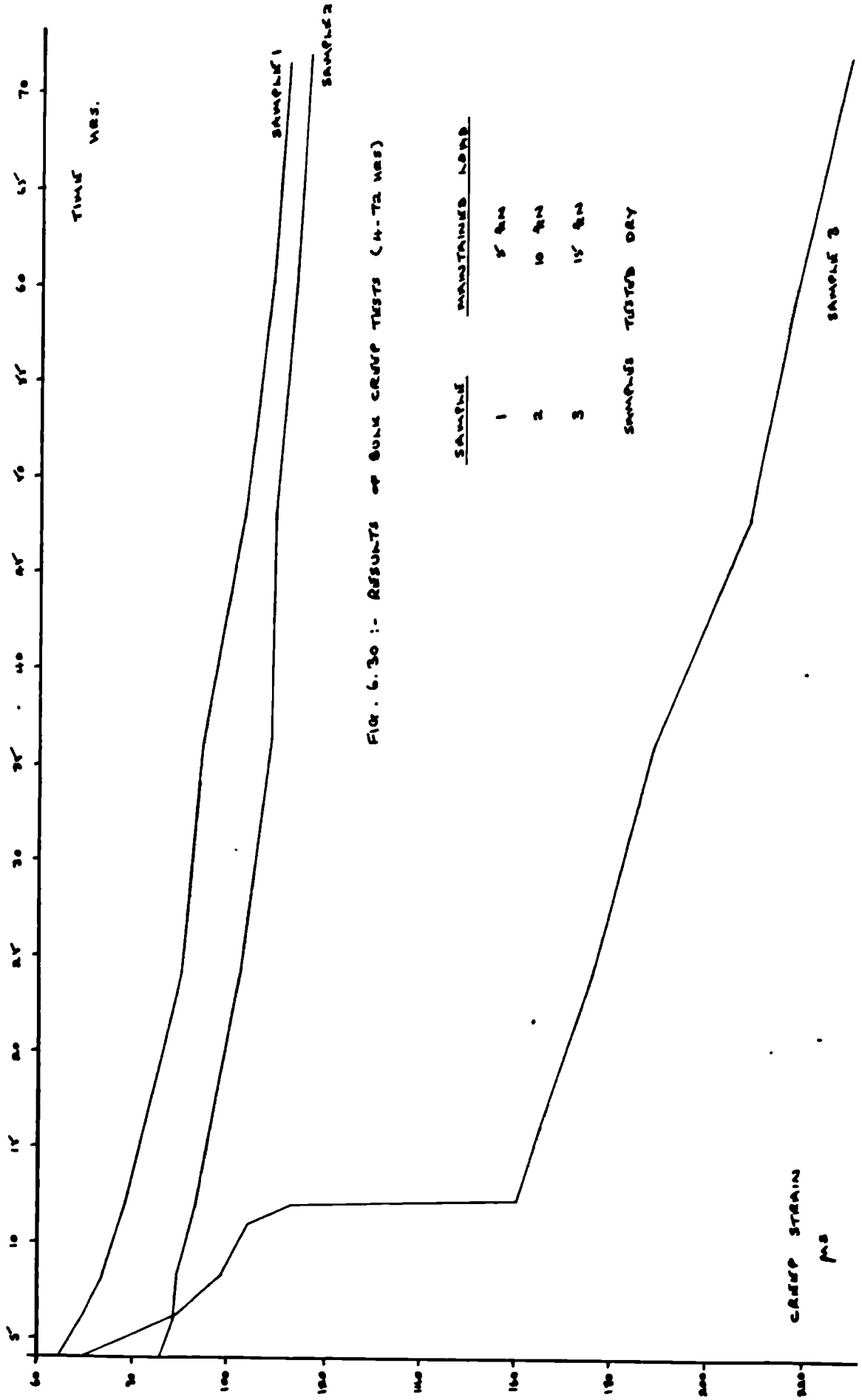

Fig. 6.30 :- Results of Bulk Creep Tests (4-72 hrs)

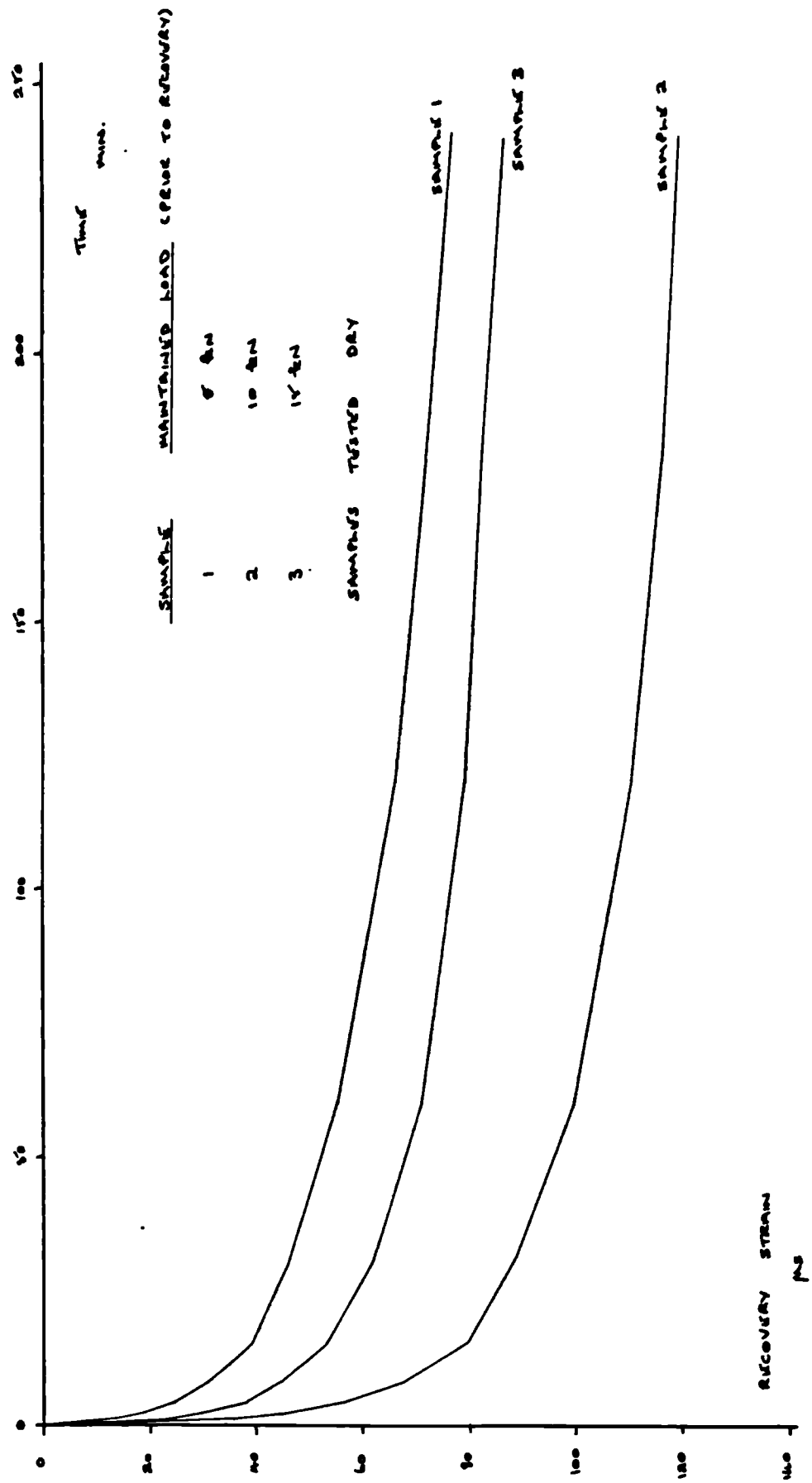

Fig. 6.31 :- Results of Bulk Recovery Tests (0-4 hrs)

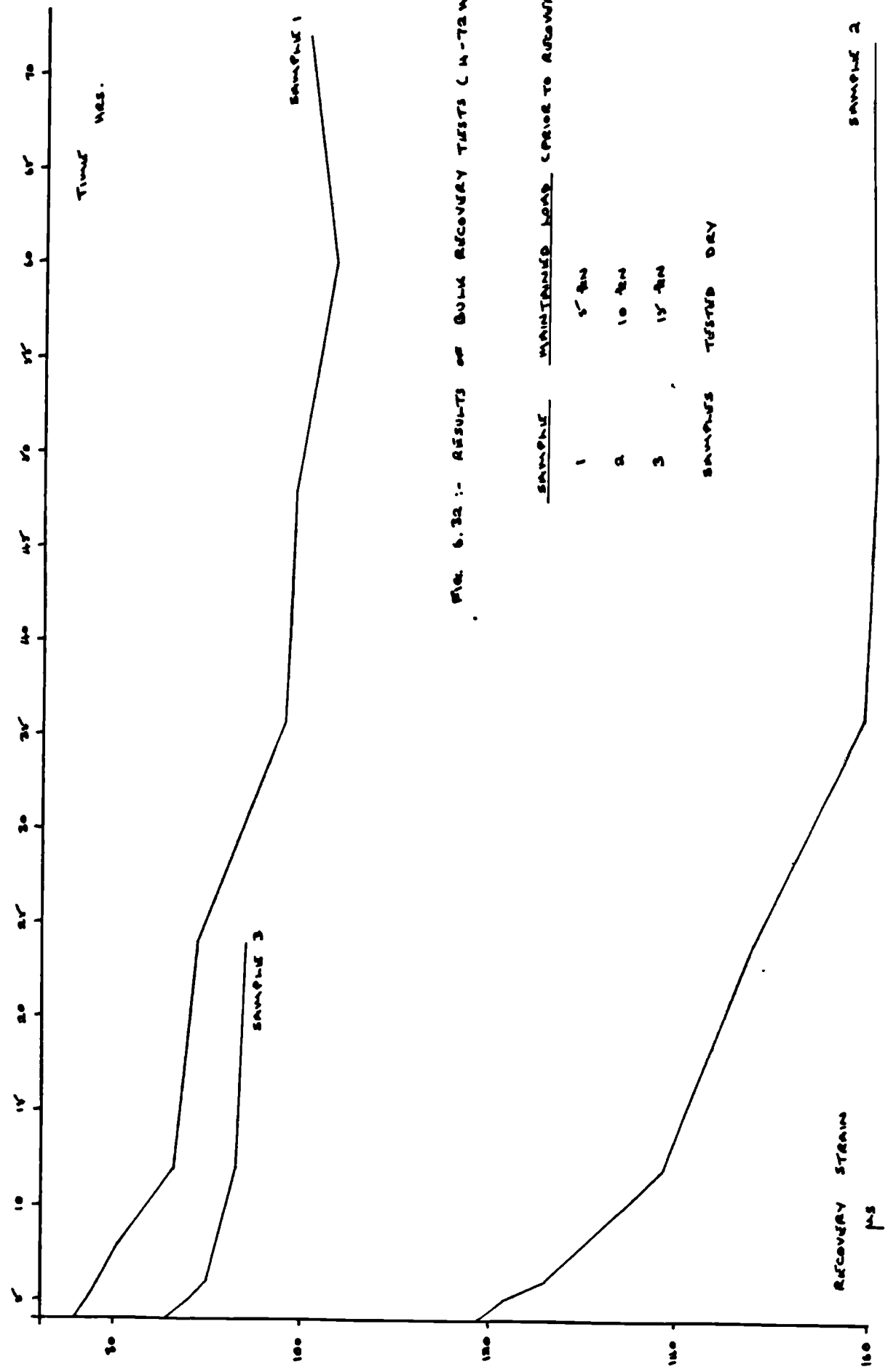

Fig. 6.32 :- Results of Bulk Recovery Tests (4-72 Hrs)

Samples	Maintained Load (Prior to Recovery)
1	5 Kn
2	10 Kn
3	15 Kn

Samples Tested Dry

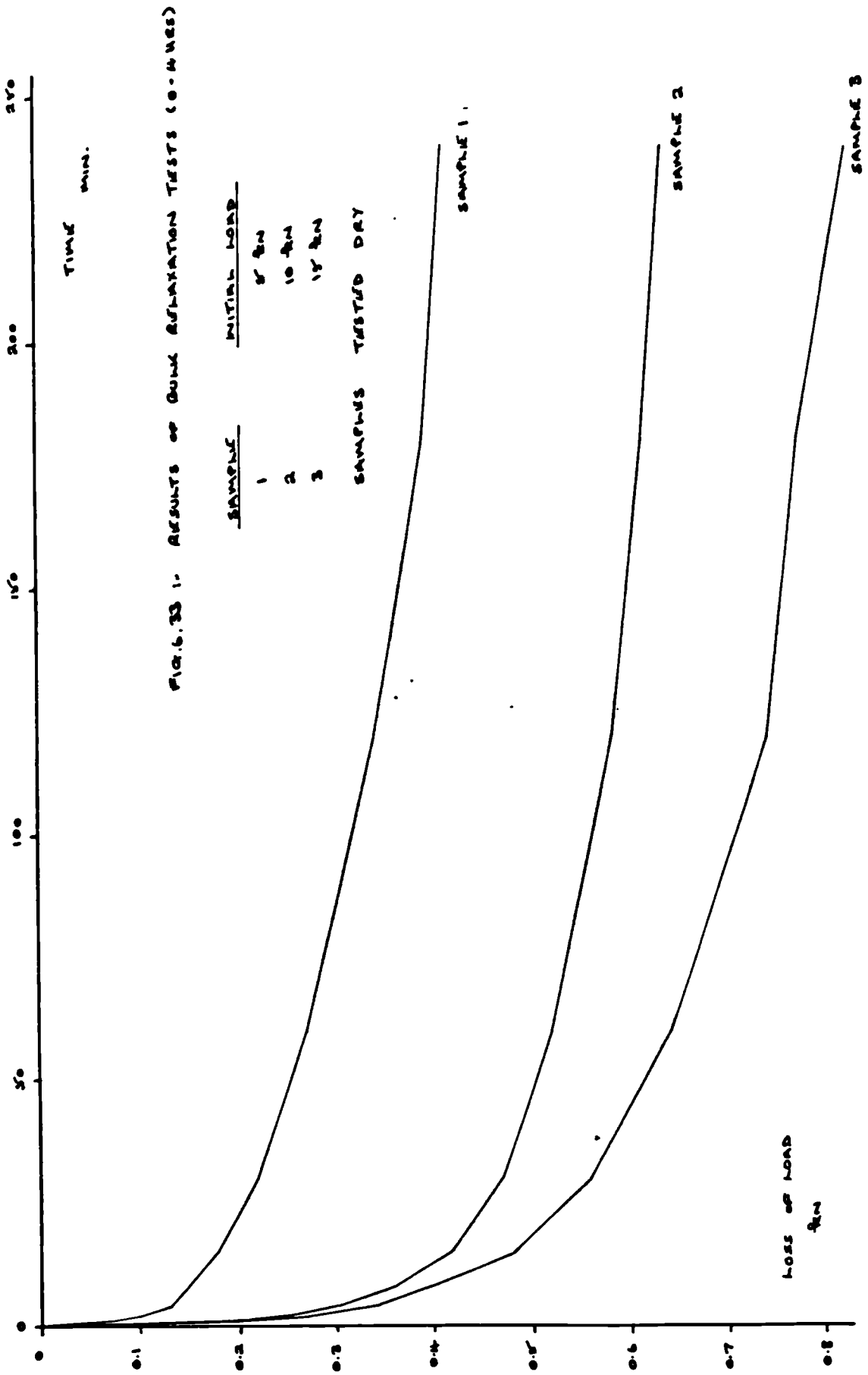

FIG. 6.33 :- RESULTS OF CHUNK RELAXATION TESTS (10 - 14 WEEKS)

SAMPLE	INITIAL LOAD
1	5 kN
2	10 kN
3	15 kN

SAMPLES TESTED DRY

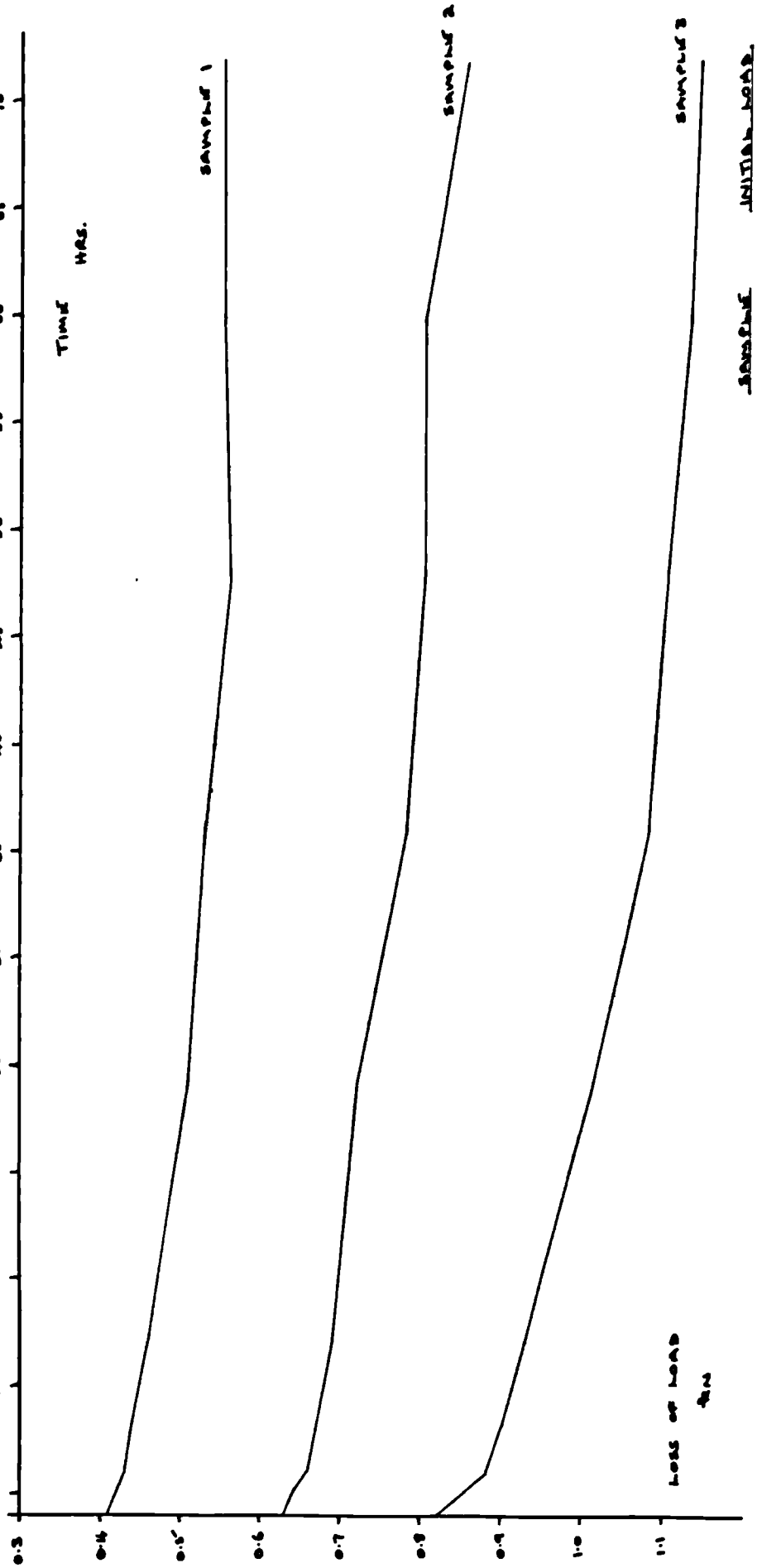

Fig. 6.34 :- Results of Bulk Relaxation tests (4-72 hrs)

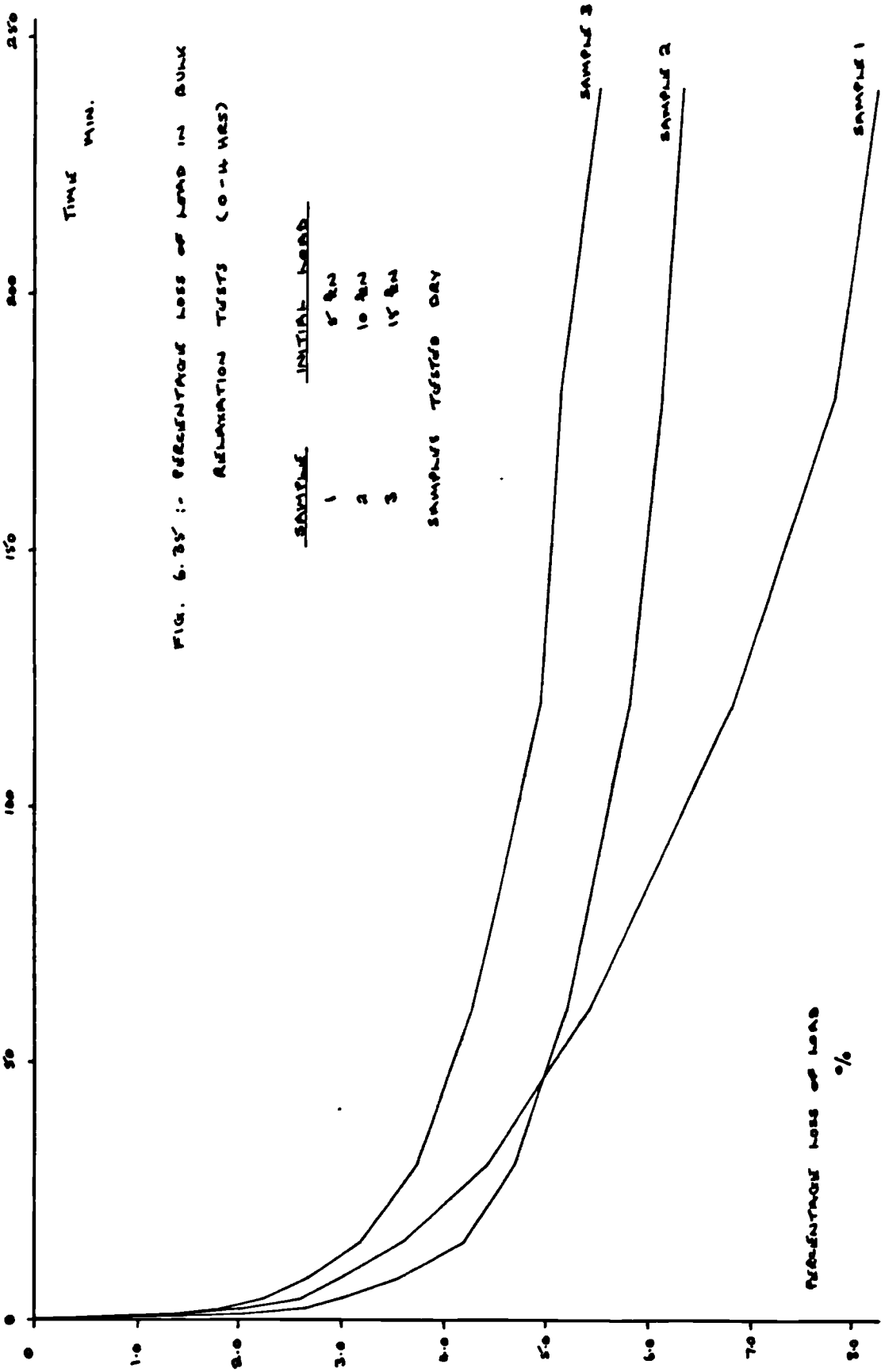

FIG. 6.35 :- PERCENTAGE LOSS OF LOAD IN BULK RELAXATION TESTS (0-14 HRS)

SAMPLE	INITIAL LOAD
1	5 Kn
2	10 Kn
3	15 Kn

SAMPLES TESTED DAY

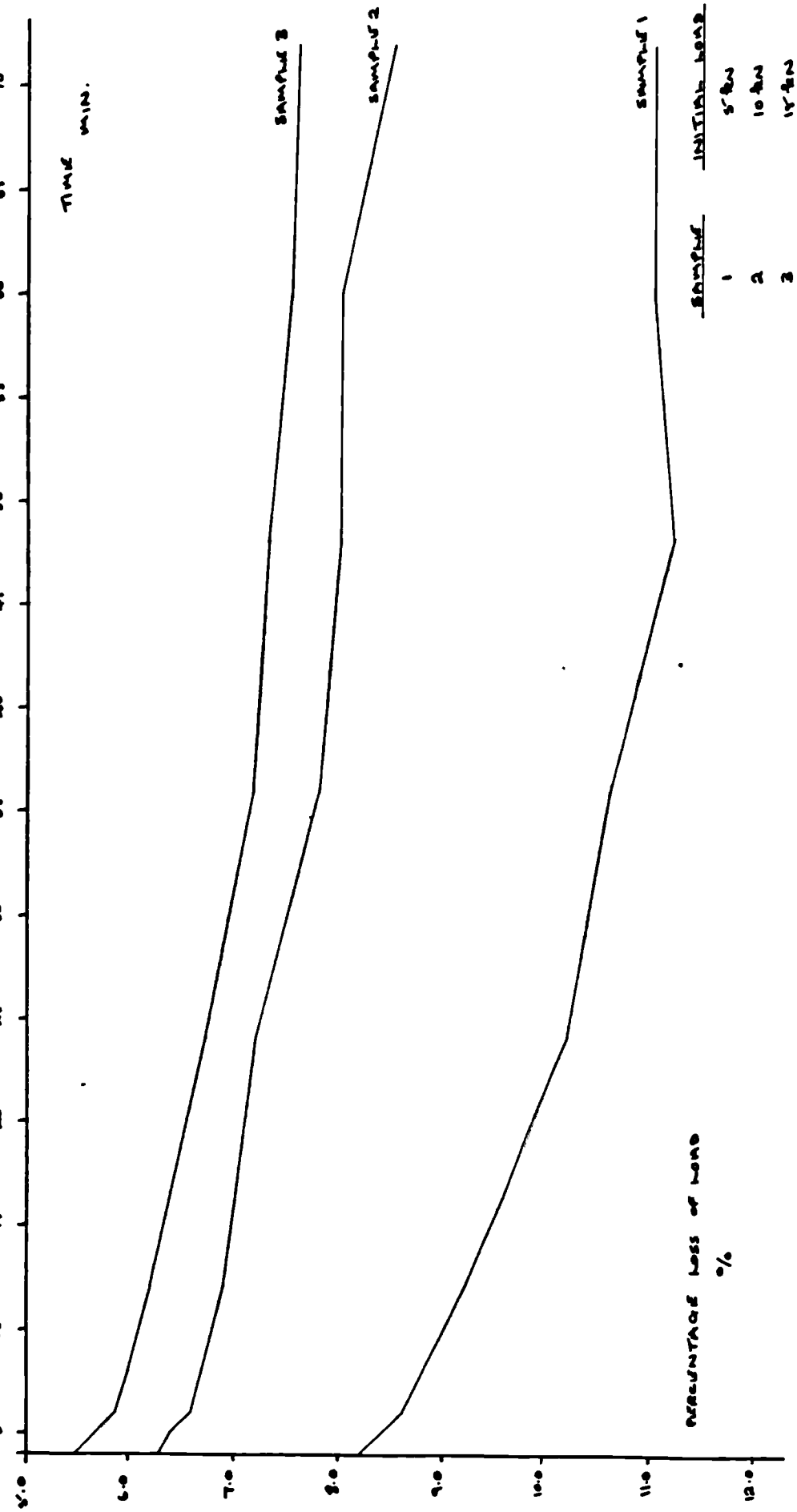

FIG. 6.36 :- PERCENTAGE LOSS OF LOAD IN BULK RELAXATION TESTS (14-72 HRS)

Chapter 7

Study of the Behaviour of Rockfill in Oedometer Tests

Charles (1973) has considered the creep behaviour of Scammonden rockfill in a series of oedometer tests using a range of applied stresses (108 - 2700 t/m^2) and dry densities (1.5 - 2.0 t/m^3). In addition to reporting some general overall behaviour patterns, he has made a direct comparison of test creep rates with values obtained from instrumentation within the dam and shown the test rates to be 4-14 times smaller than the observed values. A similar test has been carried out and this discrepancy commented on in section 7.5.i.

The other tests presented here have been used to investigate various aspects of rockfill deformation and particular emphasis has been placed on the influence of saturation and the significance of particle breakage. Three gradings of the rockfill have been tested and comparisons between the results made where possible. On unloading samples after tests short-term (rebound) and long-term (recovery) expansions were noted and a study of these movements has been made.

7.1 The Oedometer Rig

The tests were carried out in an oedometer previously used by Pigeon (1969) and Charles (1973) and they give more detailed descriptions of the apparatus. An outline of the rig is shown in fig. 7.1 and fig. 7.2 shows it in use. The jack applies a load to the sample in the cylinder via the set of springs and the total applied load is measured by the load cell situated between the platen and top plate. If the load is to be maintained, the lower plate can be held in place by the nuts below it and the springs used to sustain the load. The sample cylinder (diameter 0.45 m) rests on three small load cells and this enables the frictional load, transferred from the sample to the cylinder walls, to be measured. The problem of friction is discussed more fully in section 7.3. Samples may be saturated or drained using the channels shown in the platen and floating plate.

The rig was slightly different from its original state, as described by Pigeon. Only twelve of the thirteen springs were available and these were arranged symmetrically beneath the floating plate. The floating plate originally used for a 0.6 m (24") diameter sample (also described by Pigeon) was used as the top plate. While these adaptions reduce the maximum load which can be applied, it is calculated that for a 0.45 m (18") diameter sample stresses of 3000 kN/m^2 can be safely achieved. The protective cage around the springs was made of aluminium mesh and fastened to the floating plate, fig. 7.2.

7.2 Instrumentation

7.2.i Displacement

The displacement of the sample was measured by dial gauges standing on the floating plate and bearing on anvils connected to the platen, fig.7.1. Measurements were made at three points equi-spaced around the sample and the mean value calculated.

7.2.ii Load

The friction loads were measured by three 15 tonne load cells placed beneath the cylinder. These were connected via an 8-way swithh box to a Sangamo C 61 strain-meter which has a set of decade balancing switches. Calibration curves were obtained for each cell and appropriate adjustments made to compensate for long-term variations.

Charles and Pigeon used a single load cell to measure the total applied load and this system was used in the first two tests (samples A.1. and A.2. - Table 7.4.1). The squat cylinder with a turned down central portion, fig. 7.3, was capable of carrying 750 kN and the full bridge circuit was monitored on a Peekel 581 DNH meter.

For the other tests three 350 kN cells, standing equi-spaced on the edge of the platen, were designed. This system was used to reduce the possibility of tilting and jamming of the platen in the cylinder which may increase the friction substantially. Each cell, fig. 7.4, is a 152 mm (6") high duraluminium

cylinder with a 25 mm (1") wall thickness. The central portion has been turned down to a wall thickness of 12.5 mm (0.5") and eight electrical resistance strain gauges attached to form a full bridge circuit. Plastic tubing was used to protect the gauges.

The total applied loads were measured by the Peekel 581 DNH meter during loading but by the Sangamo C 61 meter once constant loading was in progress. Interposed between the meters and the cells were the 8-way switch box and a 3-way switch box. This second box enabled each cell to be monitored seperately during constant load but had an averaging switch which was used during loading. Calibration and long-term stability tests were carried out and appropriate strain-load relationships determined.

7.3 Wall Friction

The friction developed in the oedometer between the sample and the cylinder wall produces a decrease in the vertical stress applied along the length of the sample. If this friction is significant it may seriously distort the expected deformation pattern causing greater crushing at the top of the sample than at the bottom. Kjaernsli and Sande (1963) measured high friction values of 12-40% and Charles (1973) 12-34% on cylinder height-diameter ratios of 1:2, while Fumagalli (1969) measured 20% for a 2:1 ratio.

Several measures have been used in the past to reduce friction including

(a) low height - diameter ratios e.g. 1:2

(b) lubricants and teflon linings

(c) floating ring cylinder

but none of these have been particularly satisfactory. Measure (c) involves not placing load cells under the cylinder, allowing it to float, so that the maximum friction load occurs at the centre of the sample rather than the base. There are, however, difficulties in obtaining a friction value with this approach. Fumagalli (1969) built a cylinder of alternate steel and deformable hoops and

reported this to be successful although he did not discuss the performance or any difficulties encountered.

As has been noted previously the frictional load was measured during each test and the mean values are shown in Table 7.4.2. Pigeon (1969) determined the following equation to calculate the load applied to a sample, P', and this has been used in these tests.

$$P' = P - (P_f/2)$$

where P is the total applied load and P_f the total friction load measured. In addition to this, the cylinder walls were coated with Castrol LM Grease.

The measured friction loads ranged from 6% to 28% of the total applied load and these values are lower than those reported by other researchers. In analysing the results comparisons were made between samples A.1. and A.2., samples C.2. and C.3. and samples C.4. and D.1. A study of the friction loads, Table 7.4.2, shows similar values for the samples in each pair and this suggests that such comparisons are not unreasonable. The values obtained for samples C.4. and D.1. are significant and caution must be used in interpreting these results.

7.4 Sample Gradings and Preparation

Three different gradings A, C and D were used in preparing the samples, fig. 7.5. Grading A has a curve parallel to that used for the construction of Scammonden, with a maximum particle size of 76 mm (3"). Gradings C and D are uniform gradings with maximum sizes 76 mm and 38 mm ($1\frac{1}{2}$") and minimum sizes 38 mm and 19 mm ($\frac{3}{4}$") respectively. A maximum particle size of 76 mm was used in accordance with the sizes suggested by Pigeon.

The rock particles were prepared from large irregular blocks broken down using a hammer and sieved, washed and air dried. Each fraction of the sample was weighed before mixing and placed in the cylinder by hand or using a scoop. Samples with grading A were compacted using a kango hammer to achieve the desired dry density. The other samples were not compacted but the surface was made level by hammering with a rubber hammer on a piece of wood lying on the surface. After each test the sample was air dried if necessary and re-sieved and weighed to determine the

particle breakage. This process took one-two weeks and since most of the tests lasted four weeks the number of tests, which could be carried out over the period of research, was limited to seven.

The details of each test are given in Table 7.4.1 and the sample details and some of the results are given in Table 7.4.2. The samples are denoted by two figures e.g. A.1.; the first indicating the sample grading and the second its sequence number. In each case loading and unloading were carried out in a single step to the desired load.

7.5 Test Results

7.5.i Samples A.1. and A.2.

(a) Immediate and Creep Displacements

The friction generated in testing these two samples was quite small (6-7%) and therefore the results can be assumed to be reliable. A study of the immediate strains, given in Table 7.4.2 for these two samples shows that despite being subjected to a slightly lower stress the saturated sample has almost twice the deformation of A.1. This correlates well with the ratio of strength values determined in Chapter 3.

Fig. 7.6 shows the creep strains plotted against $\log_{10}$ (time) and this again indicates that saturation produces larger displacements. Both sets of results may be approximated by a series of straight lines: the central portions having lower gradients than the initial and final behaviour. For A.2. this behaviour may be related to the temperature variation during the test; the temperature being lower between 70 and 300 hrs. Due to paucity of results in this region for A.1. this conclusion, that lower temperatures reduce the creep rate, cannot be confirmed here.

Charles (1973) carried out a similar test on a saturated sample with the same initial dry density and grading under a maintained stress of 696 kN/m^2 for three years and approximated the creep behaviour to the linear relationship

$$\Delta\varepsilon = \alpha(\log t_2 - \log t_1)$$

$\Delta\varepsilon$ - % creep strain

t - time

Sample	Duration Weeks	Test Details		
A.1.	4	Maintained Stress = 1852 kN/m^2	Condition - dry	Saturated on final day for 8 hrs.; drained for further 16 hrs.
A.2.	4	Maintained Stress = 1715 kN/m^2	Condition - saturated	
C.1.	-	"Quick" loading - max. applied stress = 1372 kN/m^2		Condition - dry
C.2.	4	Loaded to 1218 kN/m^2 Unloaded to 663 kN/m^2	Maintained Stress Wk.1 - 663 kN/m^2 Wk.3 - 1010 kN/m^2 Wk.2 - 834 kN/m^2 Wk.4 - 1218 kN/m^2	Condition - dry
C.3.	4	Loaded to 1199 kN/m^2 Unloaded to 642 kN/m^2	Maintained Stress Wk.1 - 642 kN/m^2 Wk.3 - 1039 kN/m^2 wk.2 - 833 kN/m^2 Wk.4 - 1199 kN/m^2	Condition - saturated
C.4.	4	Maintained Stress = 417 kN/m^2	Wk.1 - dry Wk.2,-3, 4 - Saturated (24 hrs)/Drained	
D.1.	4	Maintained Stress = 377 kN/m^2	Wk.1 - dry Wk.2 - sat. (24 hrs.)/Drained	Wk.3 - Saturated Wk.4 - Drained

Table 7.4.1:- Details of Oedometer Tests.

Sample	Initial Heights mm	γ_d t/m³	No. of Particles	Immediate Strains	Friction/ Total Load %	Particle Breakage %	Rebound/ Total Disp. %	Rebound parameter %	Temperate Variation °C
A.1.	228.6	2.00	-	0.019	6.3	2.2	27	-	24.75 ± 1.75
A.2.	228.6	2.00	-	0.035	7.1	2.5	18	-	22.00 ± 2.00
C.1.	188,9	1.24	218	0.132	-	20.9	8	-	-
C.2.	214.3	1.29	214	0.112	17.1	13.7	4	92.1	21.125 ± 1.625
C.3	211.1	1.22	220	0.114	13.1	23.2	5	89.7	22.375 ± 1.625
C.4	219.9	1.37	190	0.029	19.5	4.5	7	90.2	22.375 ± 1.875
D.1.	219.1	1.33	1563	0.043	27.8	10.3	6	89.9	22.875 ± 1.375

Table 7.4.2:- Details of Oedometer Samples and Results.

Ignoring the central portion of the curves, values of the gradient α can be calculated for A.1. and A.2.

A.1. $\alpha = 0.04$

A.2. $\alpha = 0.05$

Charles produced a value of 0.051 from his test which is in good agreement with the A.2. sample result. This agreement is contrary to the conclusion of Charles, Pigeon (1969) and Sowers et al. (1965) that α increases with increased vertical stress. However, it should be noted that they loaded their samples incrementally, taking creep measurements after each increment, whereas these samples were loaded in a single step.

From a study of the post-construction movements within Scammonden Dam, Charles has calculated α values ranging from 0.2 to 0.7 for the fill. The discrepancy between these values and the oedometer test results may be due to size effects. The oedometer sample had a maximum particle size of 76 mm whereas a 1 m maximum size was specified for the dam (a ratio of 1:13). The oedometer test is a confined uniaxial loading test whereas material within the dam is not confined and bulging of the fill does occur at the base of the dam. It is difficult to assess what effect this will have in the middle of the fill but larger α values would be expected at points near the dam faces.

(b) Effect of Saturation

After subjecting the dry sample A.1. to a constant stress of 1852 kN/m^2 for about four weeks, water was allowed to flow through the sample for eight hours and then drained for a further sixteen hours. The stress of 1852 kN/m^2 was not maintained over this period but was allowed to fall to a lower level. As the sample was compressed, due to the reduction in material strength by saturation, the oedometer springs expanded and the load applied to the sample was reduced. Twenty-four hours after the saturation was started the applied stress had fallen to 1447 kN/m^2.

The sample did not respond immediately to saturation but after one or two minutes the creep rate increased substantially. Fig. 7.7 shows the increase in contraction of the sample with time and this indicates that it was three-four hours before the creep rate became constant again. It is interesting to note

that the α value for the final portion of this curve is approximately 0.05, which is the same as that determined for the saturated sample A.2.

The total displacements noted for A.1 and A.2. were 5.723 mm and 8.488 mm respectively, although the value for A.1. would have been greater if the load had been maintained during saturation. Despite this, the values suggest that greater compaction can be achieved if the rockfill is saturated for some time before compaction, rather than compacting first and then saturating.

(c) Recovery of Samples

The recovery curves for A.1. and A.2. are shown in fig. 7.8 together with the rebound displacements noted on unloading. Similar rebound displacements are obtained for both samples, although the value for A.2. is slightly smaller. The curves indicate that rockfill will continue to expand for some time after compaction has ceased. Unlike the constant load creep curves, plotting recovery displacements against log time does not produce a linear relationship, fig. 7.9.

The total rebound (short and long term) displacements are 27% and 18% of the total displacements measured under load for A.1. and A.2. respectively and these values are quite significant. The similarity of the A.1 and A.2. results suggests that the rebound is dependent upon the elasticity of the bulk material and to a lesser extent on the amount of compaction applied.

7.5.ii Sample C.1.

The test on this sample was carried out to determine a load-displacement relationship for the uniform grading C. The test was carried out quite quickly (approximately ten minutes) so that the effect of time-dependent displacements would be small. The displacements of the sample were recorded at regular intervals of 12.5 kN (upto 250 kN) during loading and every 25 kN on unloading.

A value for the friction load was not measured during this test and so a mean value of 15% obtained from the other tests has been used. Fig. 7.10 shows the load-displacement curve obtained for this sample and although this is not smooth, the variations from the mean curve do not suggest that friction was significant since there is no evidence of stick-slip situations

occurring. These variations from the mean curve are probably due to contacts reaching their Damage Loads or particles breaking and the chain reaction this produces as the interparticle forces are redistributed. The mean curve shows the expected increasing gradient as compaction occurs.

The unloading curve is very steep initially and most of the rebound appears to occur as the last 25% of the load is removed. Although a final zero load reading was not taken it seems that the total expansion would be about 8% of the loading displacement, much lower than noted for samples A.1. and A.2. The uniform sample has a much lower initial dry density and therefore a greater void ratio, which should produce larger permanent displacements since compaction and particle rotation can occur more readily.

The results of this test have been used and discussed further in Chapter 9 in connection with the development of a numerical computer model of rockfill.

7.5.iii Samples C.2. and C.3.

The sequence of loading in these tests was chosen to mirror a sequence of loading which a layer of rockfill may undergo during dam construction. Having been compacted under high loads the layer will then be reloaded more slowly as the construction proceeds. The samples were loaded to about 1200 kN/m^2 and then the stress immediately decreased to approximately half this value. Having allowed the samples to creep for one week, the load was increased by equal increments each week for a further three weeks back to the maximum applied stress of 1200 kN/m^2. This maximum applied stress is equivalent to applying 200 kN to the samples. A study of the compaction loads used in constructing the dams mentioned in Chapter 2 indicates loads of 50-100 kN were generally used. Loads of 500 kN have been reported for the construction of Brownlee and Ambuklao dams.

Fig. 7.11 shows the creep curves after one hour of maintained load for each load stage for the dry sample C.2. together with the total displacements after one hour. The increase in total displacements is quite small between weeks one and two,

and two and three but increases substantially in the final week. The creep displacements under 633 kN/m^2 are ngegligible and practically zero over the first twelve hours. A similar curve is seen under 834 kN/m^2 although the magnitudes are approximately double those under 633 kN/m^2. In the final two weeks the creep displacements are much larger and comparable with the magnitude of strains seen when the sample is loaded normally. The increase in magnitude of the creep displacements with applied stress is not linear.

These results and those obtained for C.3 show that significant creep of granular masses can still occur after compaction if the mass is reloaded to more than about 70% of the maximum compaction stress. This behaviour is reflected in dam post-constructinn movements which continue long after construction has finished.

(a) Effect of Saturation

Fig. 7.13 shows the results obtained for the saturated sample C.3. The total displacements are only slightly greater than those for the dry sample which is surprising in the light of the results for samples A.1. and A.2. The total displacements show the very low increases in the second and third weeks and the large increase on the final increment as seen before.

There are also similarities between the creep curves of C.2. and C.3., both in curve shape and magnitude of displacements. Under 642 kN/m^2 sample C.3. expands slightly over the one hundred and sixty-eight hours. This was not due to tilting of the platen as all three dial gauges show the increase. This suggests that half the maximum compaction stress is a threshold below which recovery occurs and above which creep occurs.

These results indicate that saturation has little effect on either the immediate or creep displacements. This is contrary to the expected behaviour of rockfill but may be due to the fact that C.3. was saturated only ten-fifteen minutes before loading instead of the twenty-four hours normally used. While this might affect the loading behaviour, because the particles were not fully saturated, some effect on the subsequent behaviour would be expected.

(b) Recovery of Samples

Fig. 7.13 shows the recovery of the samples and this is

slightly different from that seen for the well-graded samples, A.1. and A.2. Although the curves indicate increasing expansion and increasing gradient with time, the displacements noted in the first minute and the positions of the curves reveal greater expansion of the saturated sample.

7.5.iv Samples C.4. and D.1.

These tests were carried out to investigate another aspect of dam behaviour - repeated saturation of the rockfill. This may occur in sluicing or in raising and lowering the reservoir level. Having loaded the dry samples to a stress of about 400 kN/m^2 and allowed them to creep for one week, the samples were subjected to cycles of saturation and drainage while the applied stress was maintained using the rig jack.

(a) Sample C.4.

The initial loading of this sample produced a displacement of 6.5 mm which was almost double that observed on saturation after one week, fig. 7.14. The creep curves for these two weeks show greater displacements for the sample saturated than for the sample dry.

The displacements on the second and third saturations are substantially smaller than before and it became clear on the third saturation that the small displacement recorded was due to returning the load to its 'maintained' value rather than by saturation. The curves show decreasing creep rates with time and it is felt that these curves are merely an extension of the first saturated curve and are not particularly affected by the saturation/drainage cycles being applied. The 'sudden' increases during weeks two and three are difficult to explain as these occurred overnight while the test was not being supervised. High friction values were measured for this test and this may be the result of a stick-slip situation.

(b) Sample D.1.

The grading for D.1., although uniform, had a smaller particle size range, i.e. - 38 + 19 mm, than sample C.4. The initial dry density and applied stress were similar but a slightly different saturation/drainage sequence was used, Table 7.4.1. The initial loading strain, Table 7.4.2. is much greater than that obtained for C.4. although this is partly due to the lower dry

density. This is unexpected as a smaller particle size range increases the number of particles and hence the magnitude of the interparticle forces decrease. A study of the particle breakage values, Table 7.4.2 shows that a higher percentage (by weight) of the D.1 particles broke. This suggests that breakage may occur more readily within certain size ranges and emphasises the difficulties in extrapolating results from one range of sizes to another. The initial displacements each week on saturating and maintaining the load are similar to the C.4. values, fig. 7.15,

The creep displacements for the two samples are similar in magnitude and it is again felt that saturation and drainage have little effect in the third and fourth weeks. The saturated sample creep displacements in week two are again greater than the dry values.

These tests show clearly that repeated saturation has little effect on the behaviour of rockfill. In practice there seems to be little benefit in repeatedly sluicing fill in order to achieve lower densities by compaction.

(c) Recovery of Samples

The recovery curves, fig. 7.16, for these samples are similar in shape to those seen previously. The magnitudes are similar to those recorded for C.2. although this sample was tested dry and subjected to stresses three times those for the saturated samples C.4. and D.1. The displacements recorded for the smaller size range sample, D.1. are greater than those for C.4.

7.6 Particle Breakage

The deformation of a rockfill mass will be affected by the number and frequency of particles breaking down into smaller particles. This is difficult to quantify but Marsal (1973) has proposed the following definition:- fig. 7.17

"The particle breakage (P.B.) is equal to the sum of the positive ΔW_k, expressed in percent, where ΔW_k is the difference between the percentage of the total sample contained in each grain size fraction before and after the test."

This definition is quite reasonable when considering a uniform grading but some breakage in a well-graded sample will be disregarded because of the different fractions involved.

The results of the particle breakage determined using Marsal's definition are given in Table 7.4.2 and have been plotted against the maximum applied stress, fig. 7.18. The samples with grading C show the expected increased breakage with increased stress and a comparison of C.3 with C.2. indicates increased breakage with saturation. The well-graded samples only show a small amount of breakage compared with the uniform sample values.

It is difficult to assess when the particle breakage becomes an important influence on the deformation behaviour of rockfill. Clearly the 2-3% values measured for the grading A samples under high stresses can be considered as negligible. Uniform gradings show greater breakage but the amount is a function of the applied stress. It seems reasonable to assume that the influence is small at stresses below about 750 kN/m^2 (approximately half the stress exerted on the fill under the crest at the base of Scammonden Dam) for dry densities between 1.25 and 1.4 t/m^2.

7.7 Rebound and Recovery

The rebound reflects the elasticity of the rockfill and is the sum of the bulk material recovery in each particle as the load is removed. The recovery curves also show that this is a time-dependent process. The curves indicate that the recovery rate decreases with time but the relationship between the recovery and log (time) is not linear. The expansion of a sample appears to increase with vertical stress but the effect of saturation varies with the grading.

The ratios of total expansion and total settlement, given in Table 7.4.2, range from 4 to 27%. The values for the well-graded samples are quite significant but those for the uniform gradings are approximately the same and may be considered to be small. The rebound parameter shown in Table 7.4.2 is the ratio of total expansion at one and twenty-four hours. The parameter is approximately 90% for the uniform gradings and is apparently not dependent upon the test conditions. This shows the rapid decrease in recovery rate which occurs and that the majority of the expansion may be expected to occur either on unloading or soon after this.

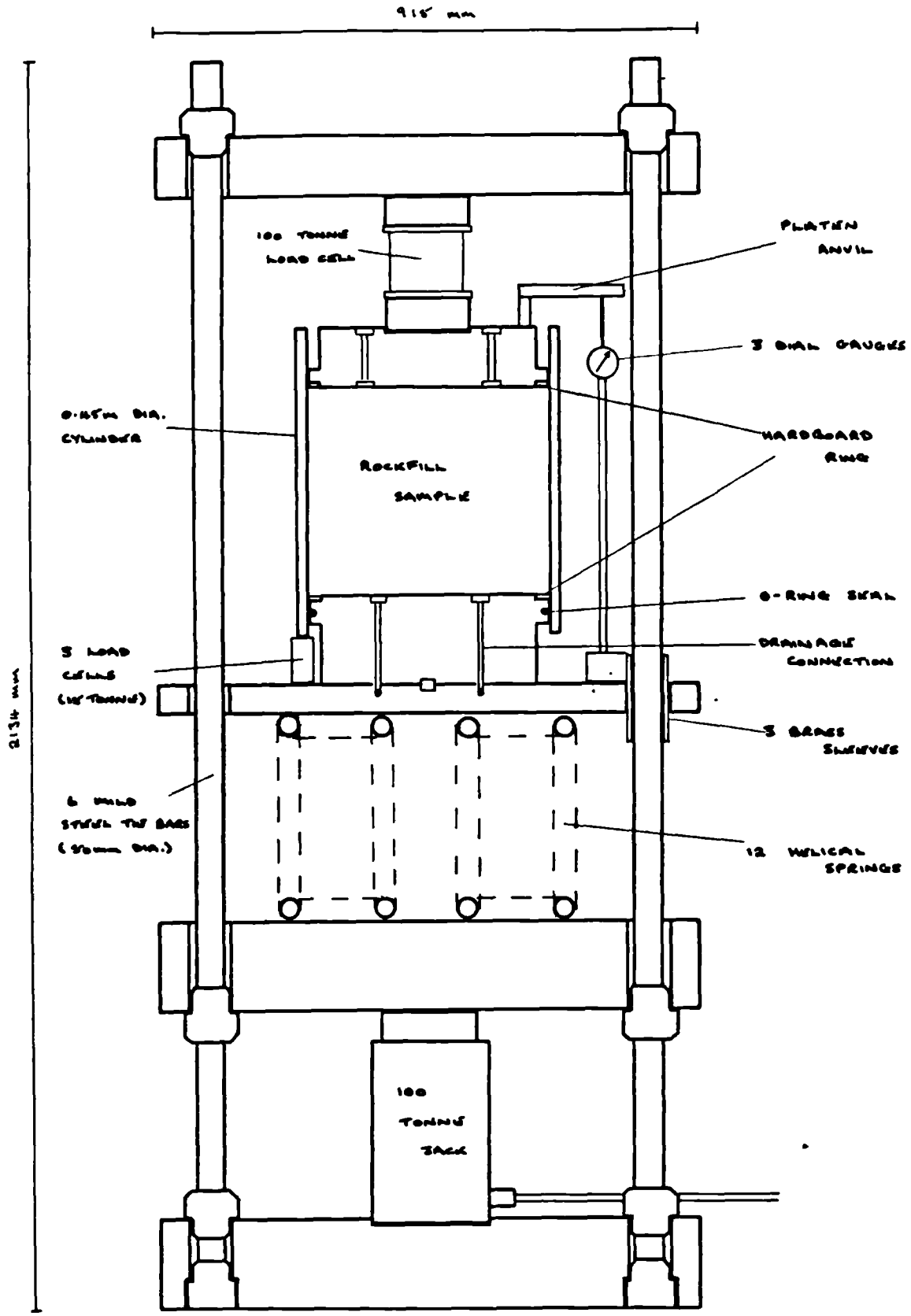

FIG. 7.1 :- 0·45m OEDOMETER RIG

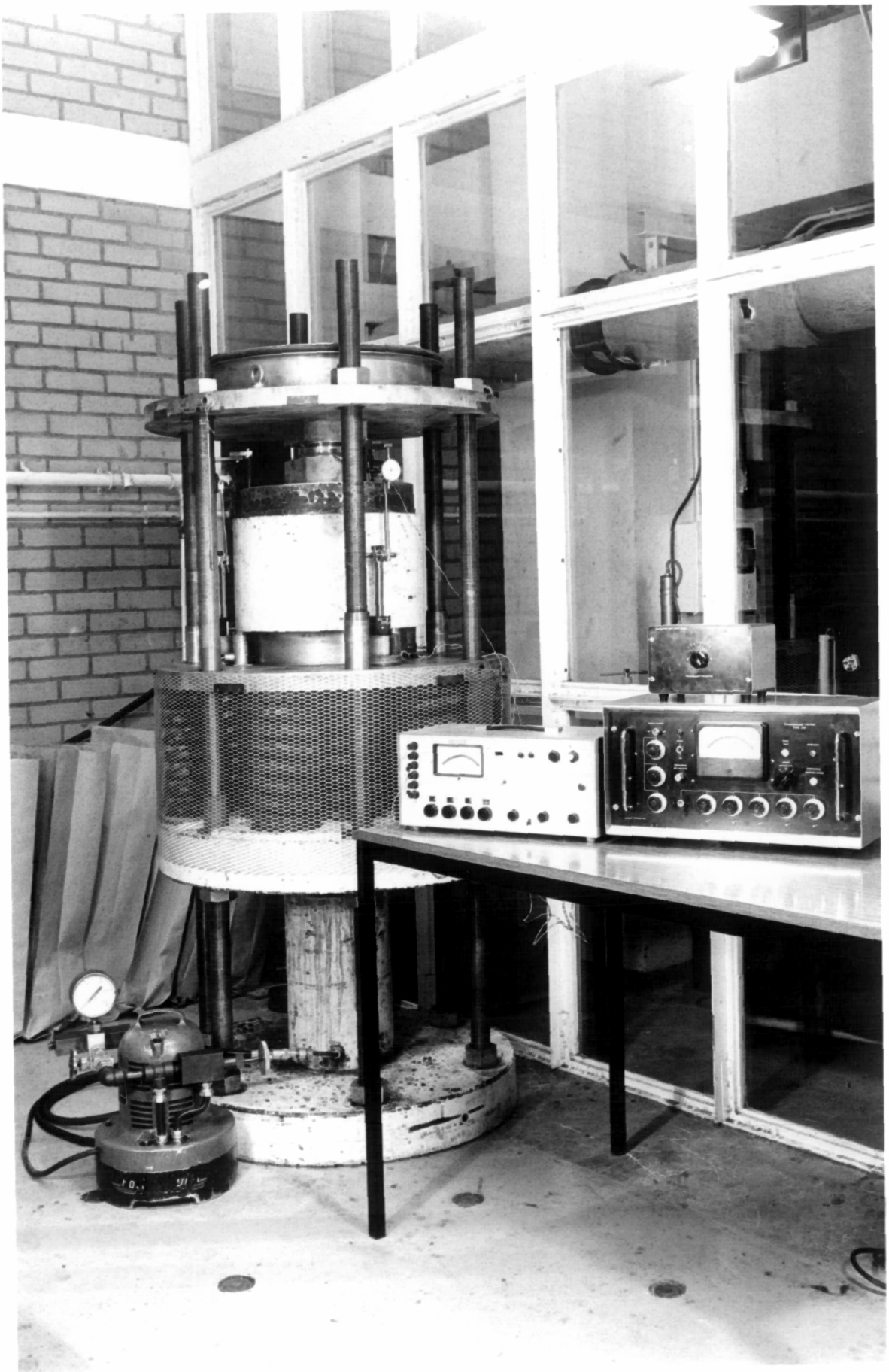

Fig. 7.2 :- Oedometer Rig and Instrumentation

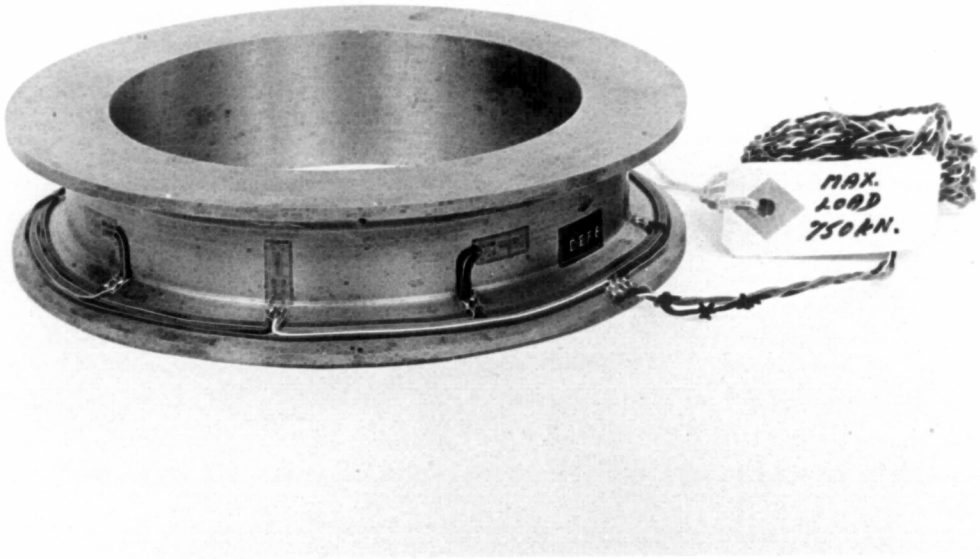

Fig. 7.3 :- 750 kN Load Cell

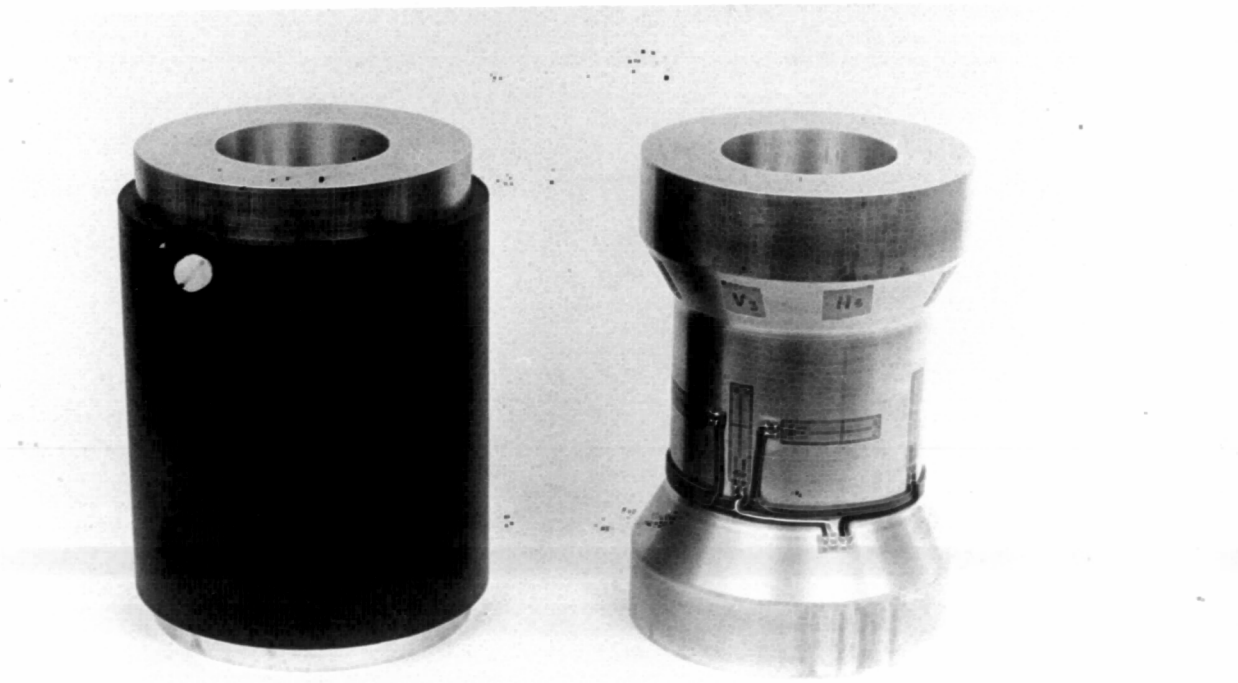

Fig. 7.4 :- 350 kN Load Cells

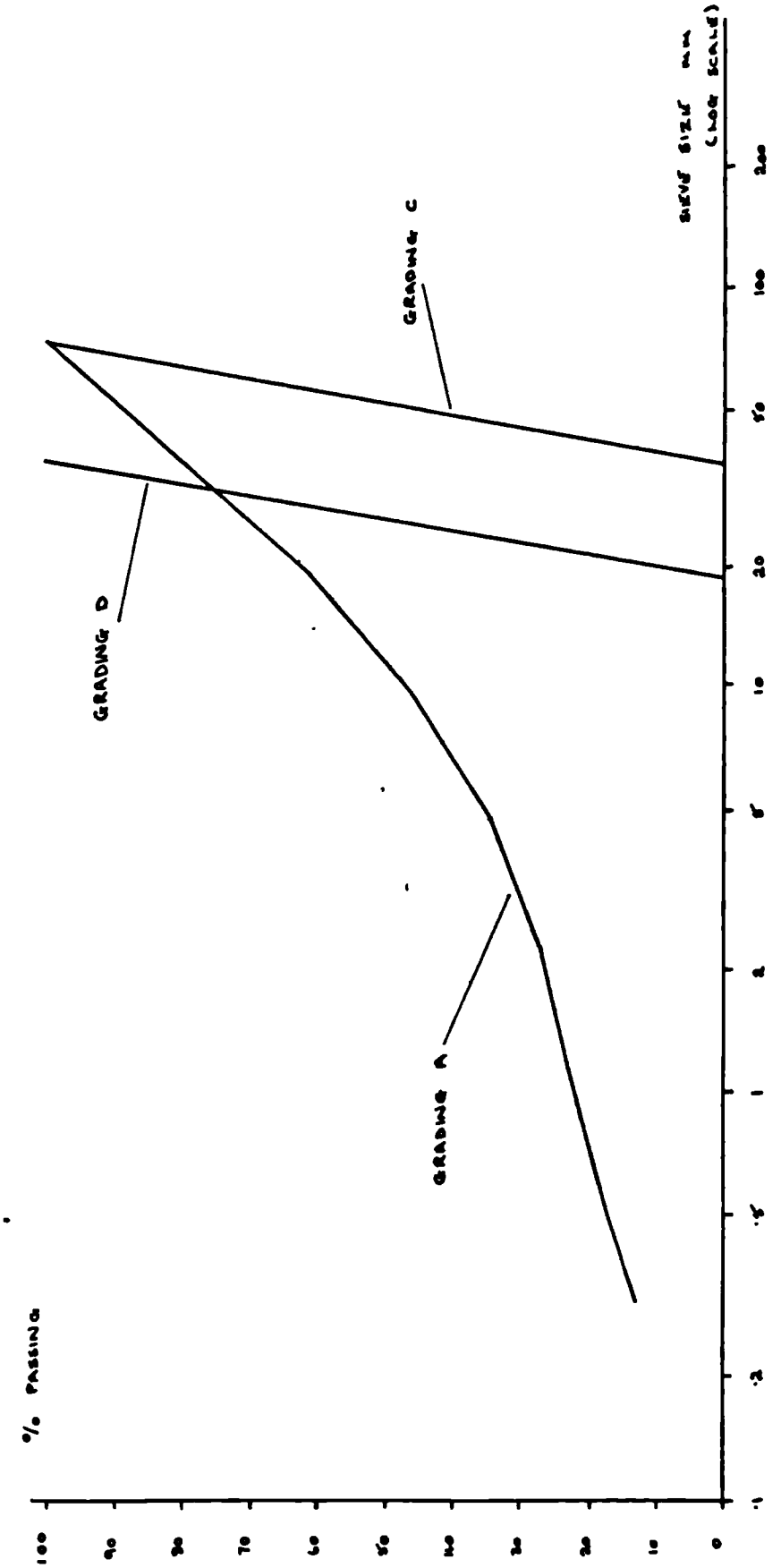

FIG. 7.5:- GRADING CURVES OF OEDOMETER SAMPLES

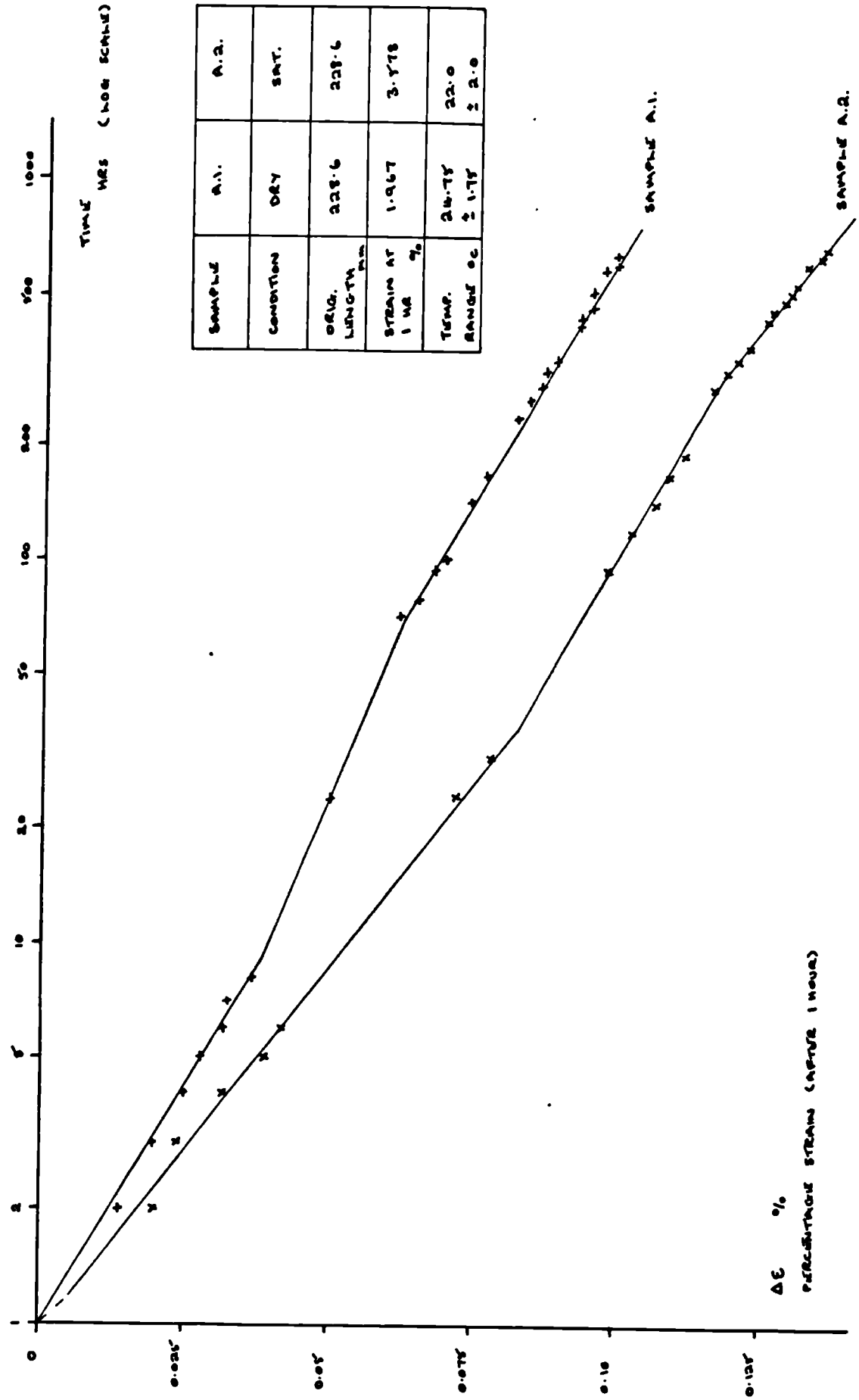

FIG. 7.6 :- TIME-DEPENDENT STRAIN RESULTS FOR SAMPLES A.1. AND A.2.

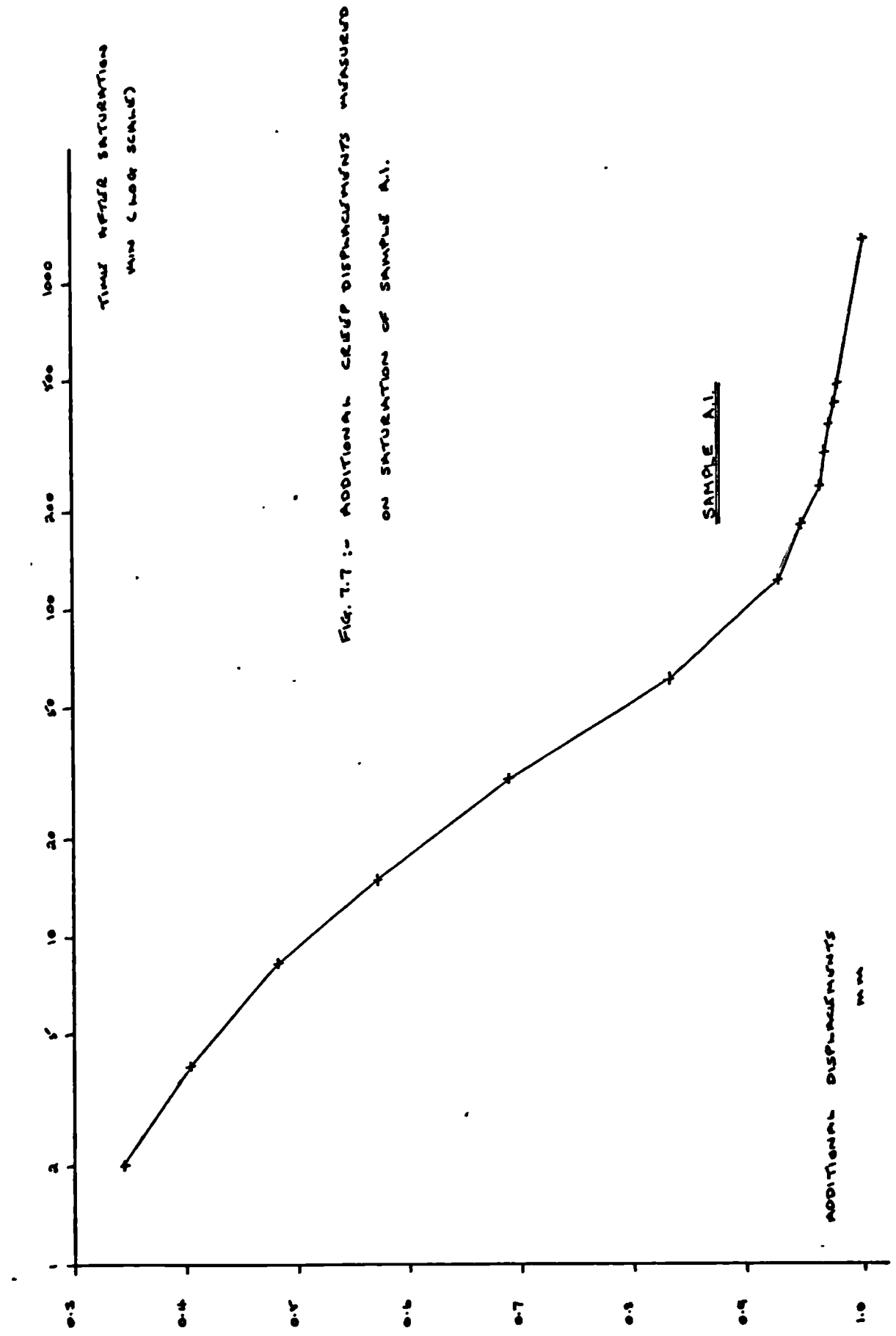

Fig. 7.7 :- ADDITIONAL CREEP DISPLACEMENTS MEASURED ON SATURATION OF SAMPLE A.1.

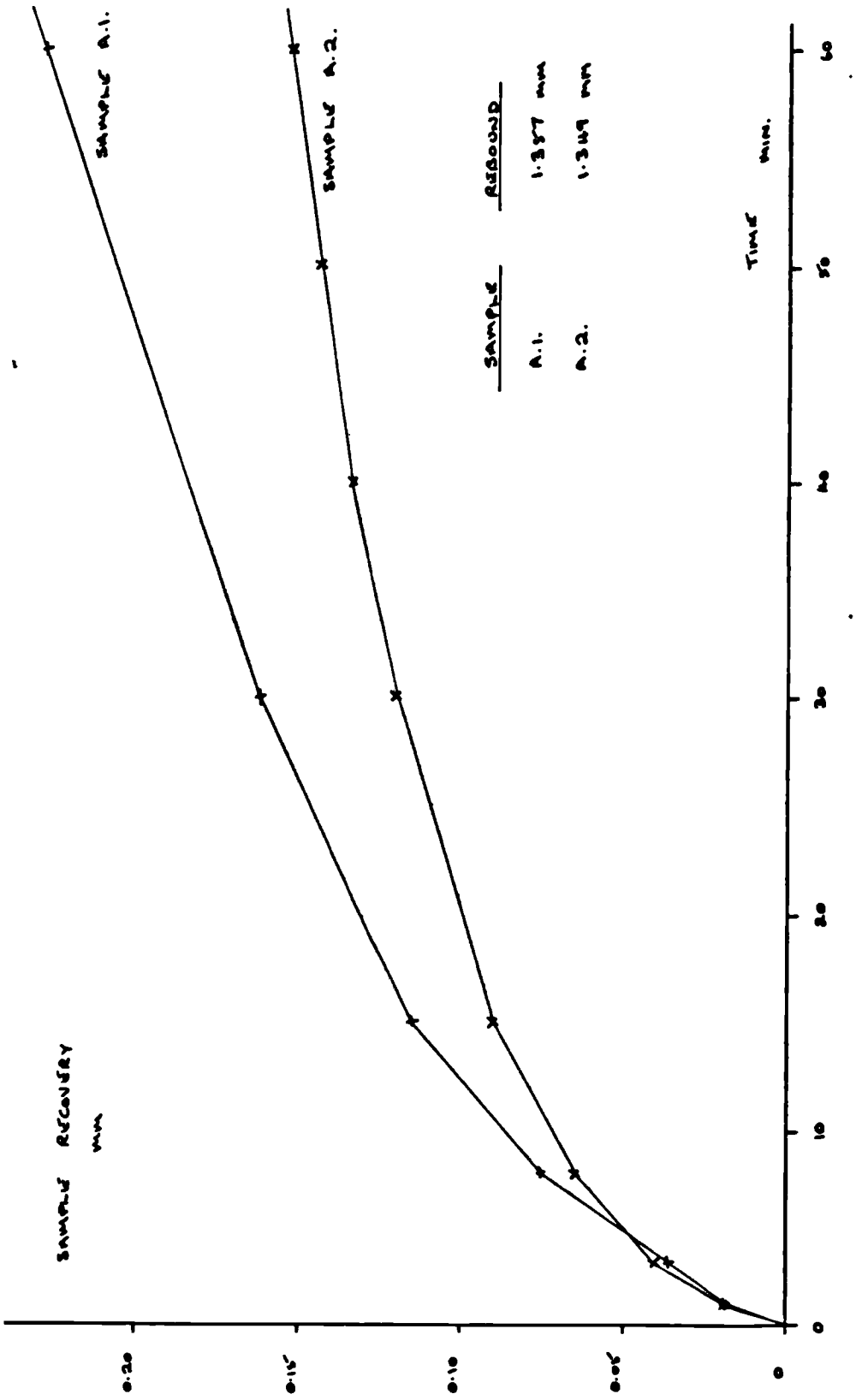

FIG. 7.9 :- RECOVERY OF SAMPLES A.1. AND A.2.

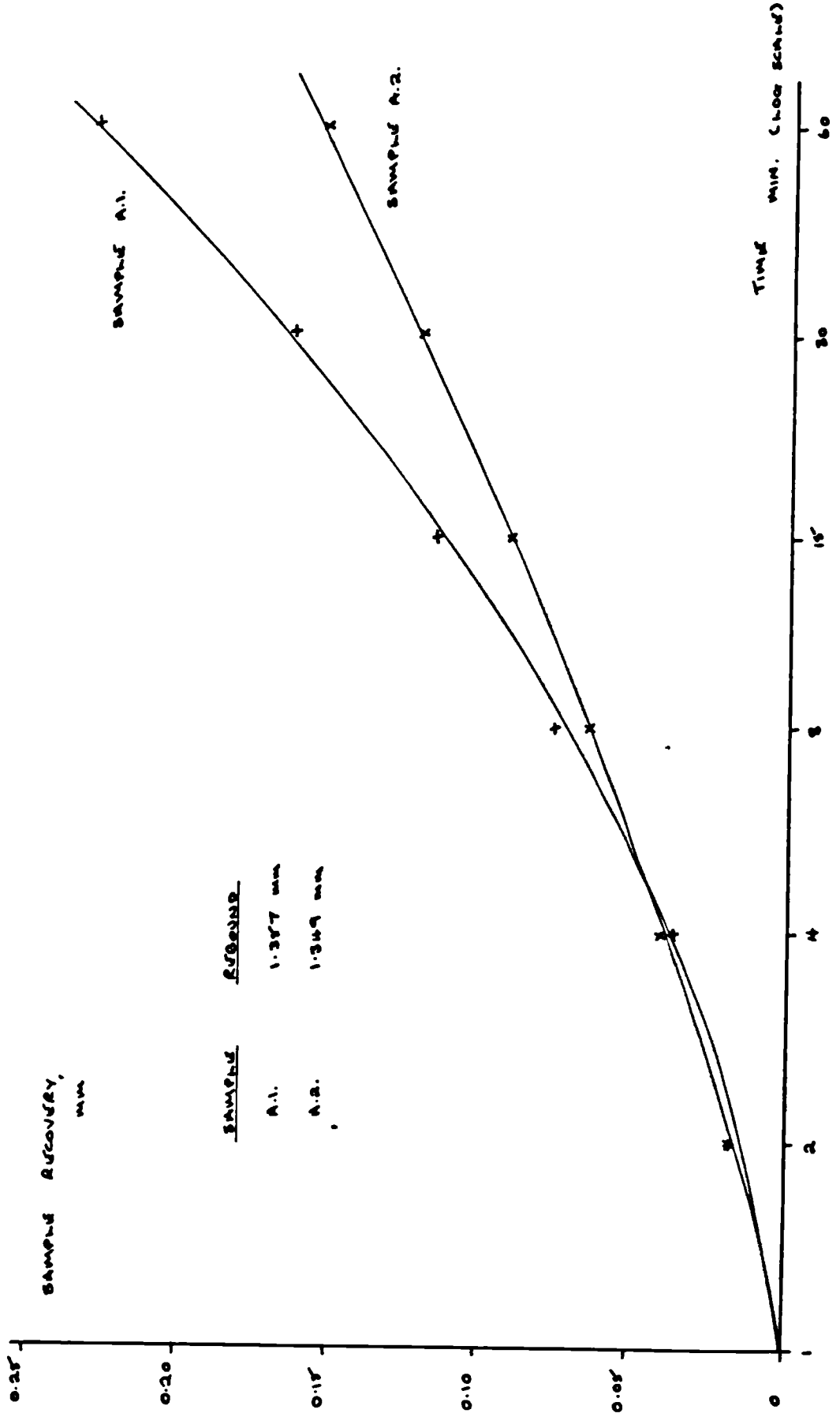

FIG. T.9 :- RECOVERY OF SAMPLES A.1. AND A.2. (LOG TIME)

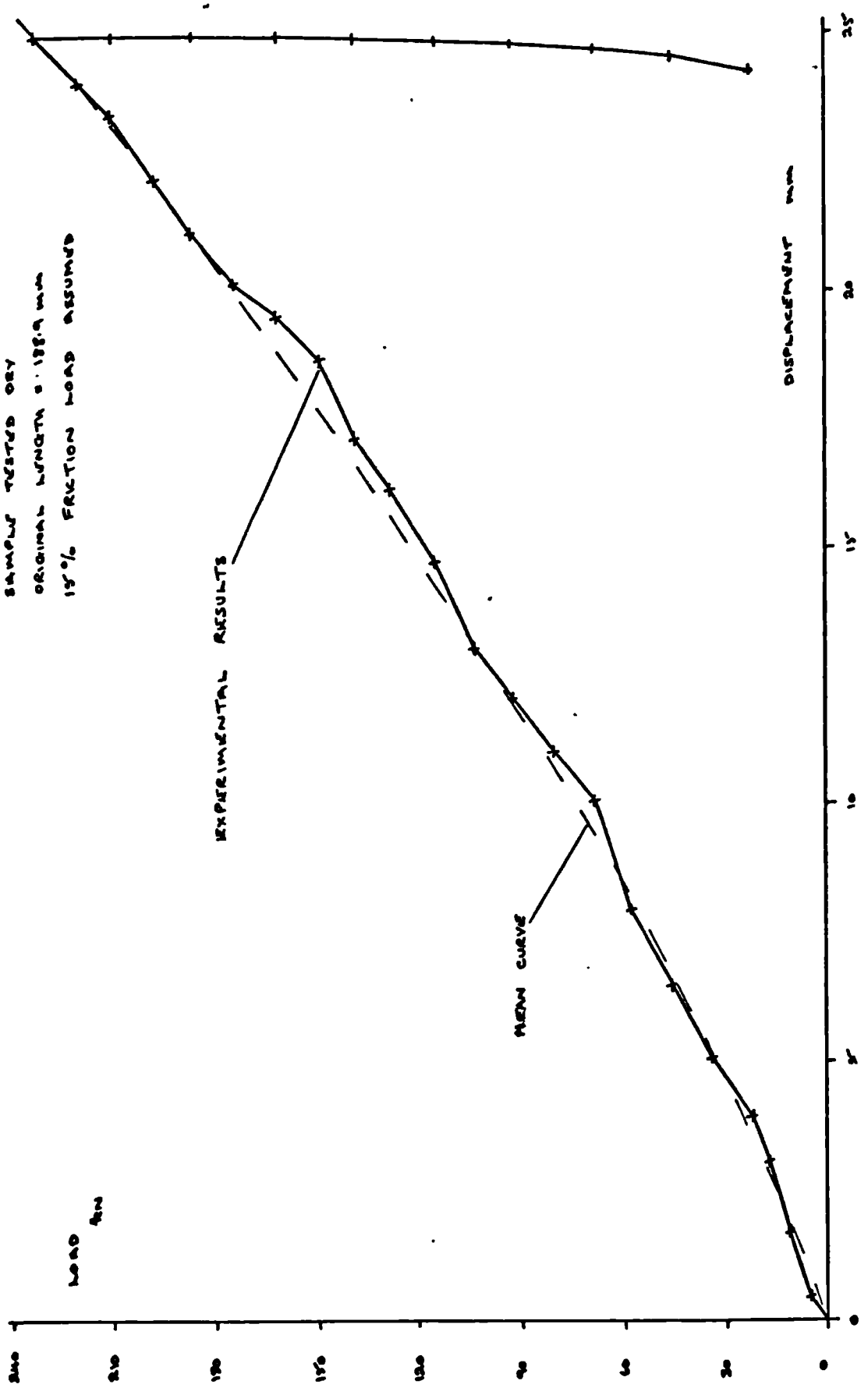

FIG. 7.10 :- LOAD-DISPLACEMENT CURVE FOR SAMPLE C.1.

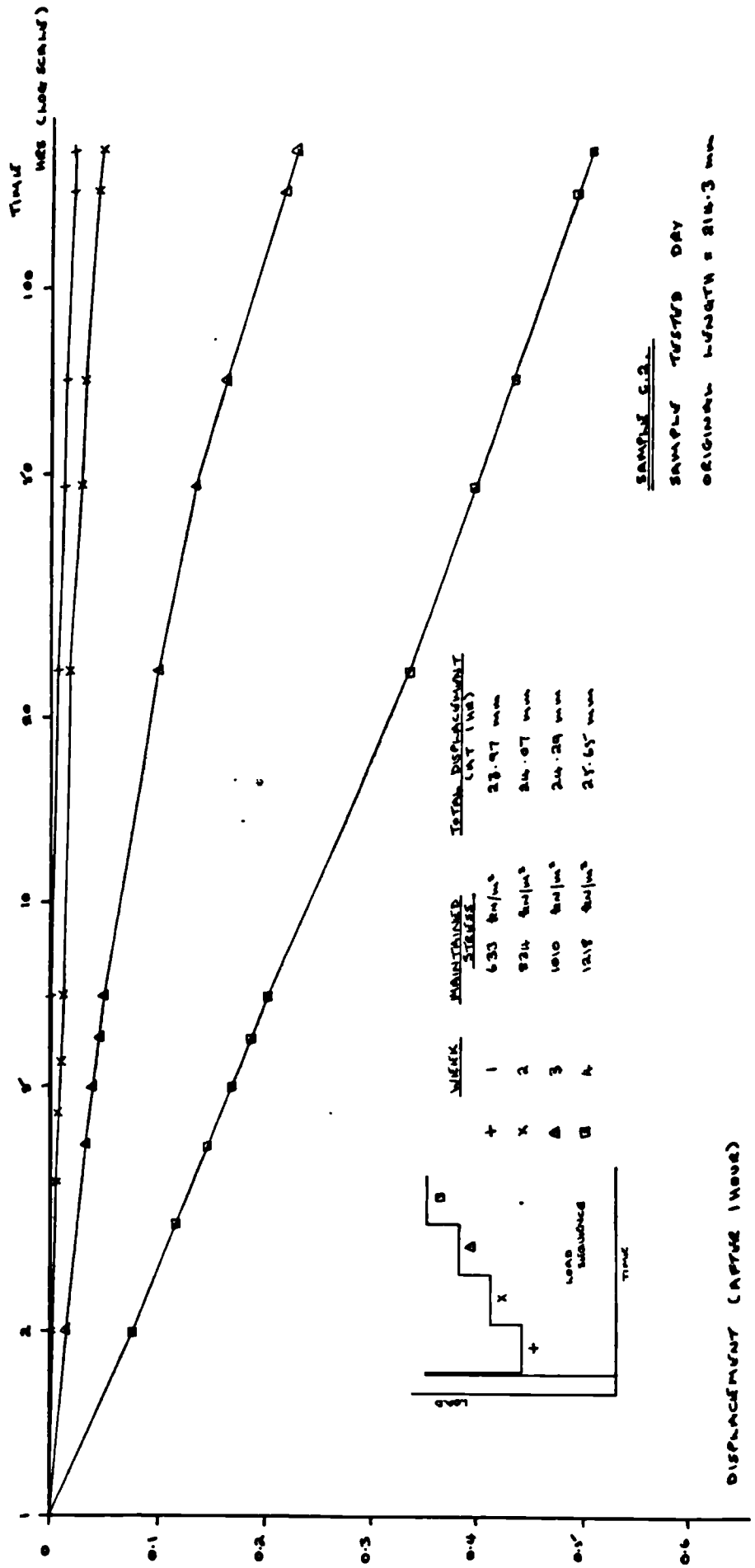

FIG. 7.11 :- CREEP DISPLACEMENT RESULTS RECORDED FOR SAMPLE C.B.

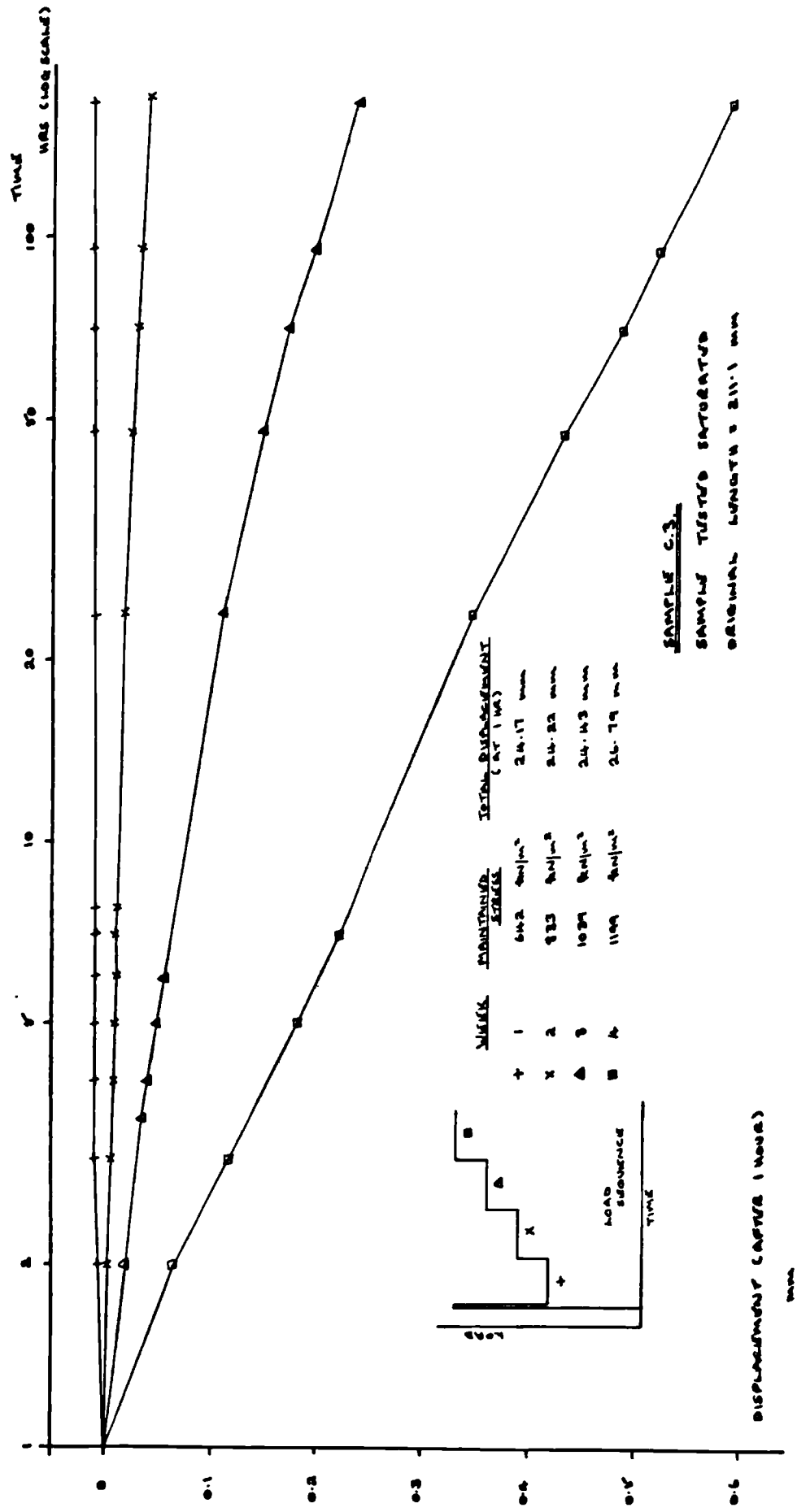

FIG. 7.12 :- CREEP DISPLACEMENT RESULTS RECORDED FOR SAMPLE C.3.

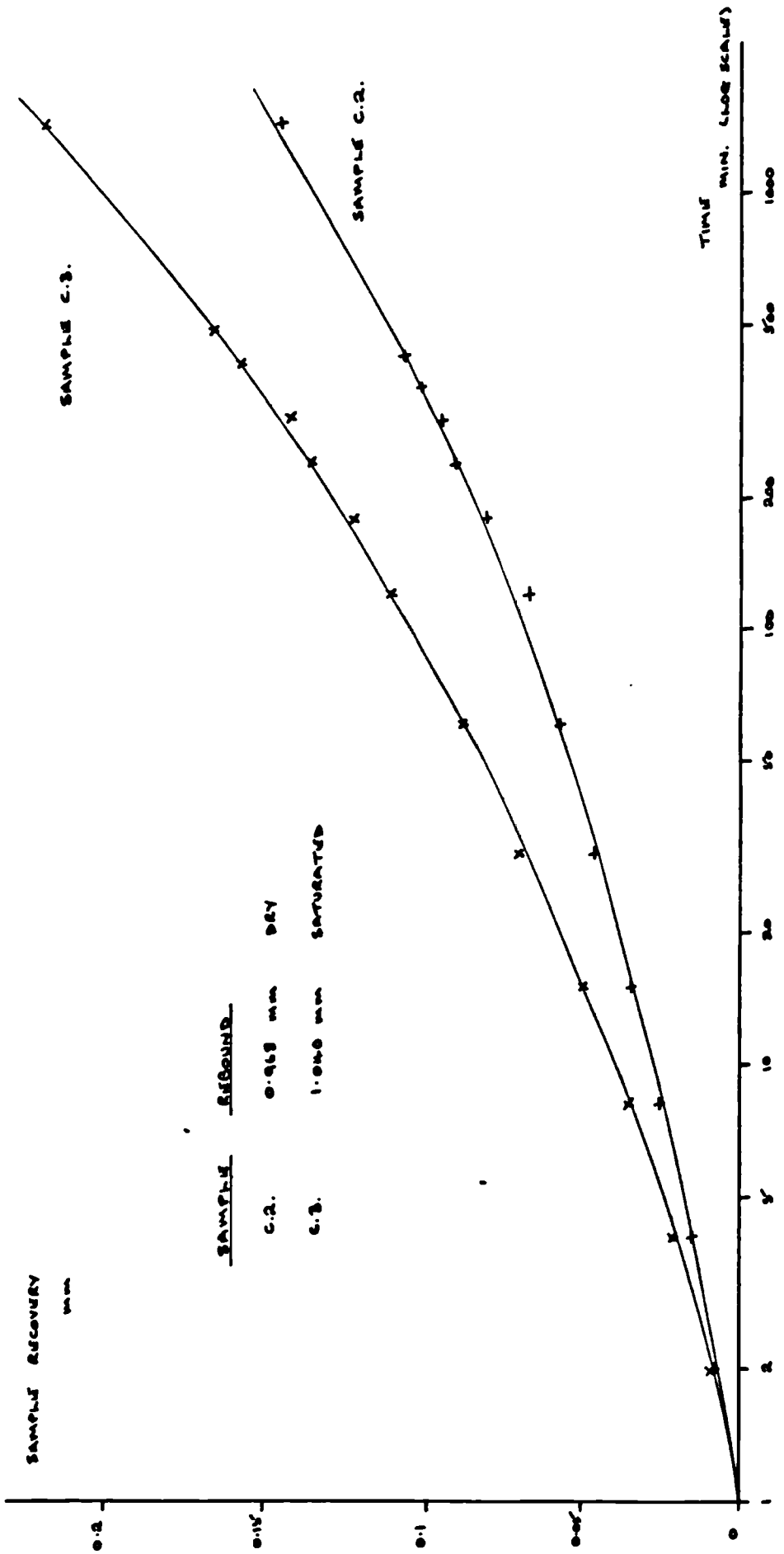

Fig. 7.13:- Recovery of samples C.2. and C.3. (Log Time)

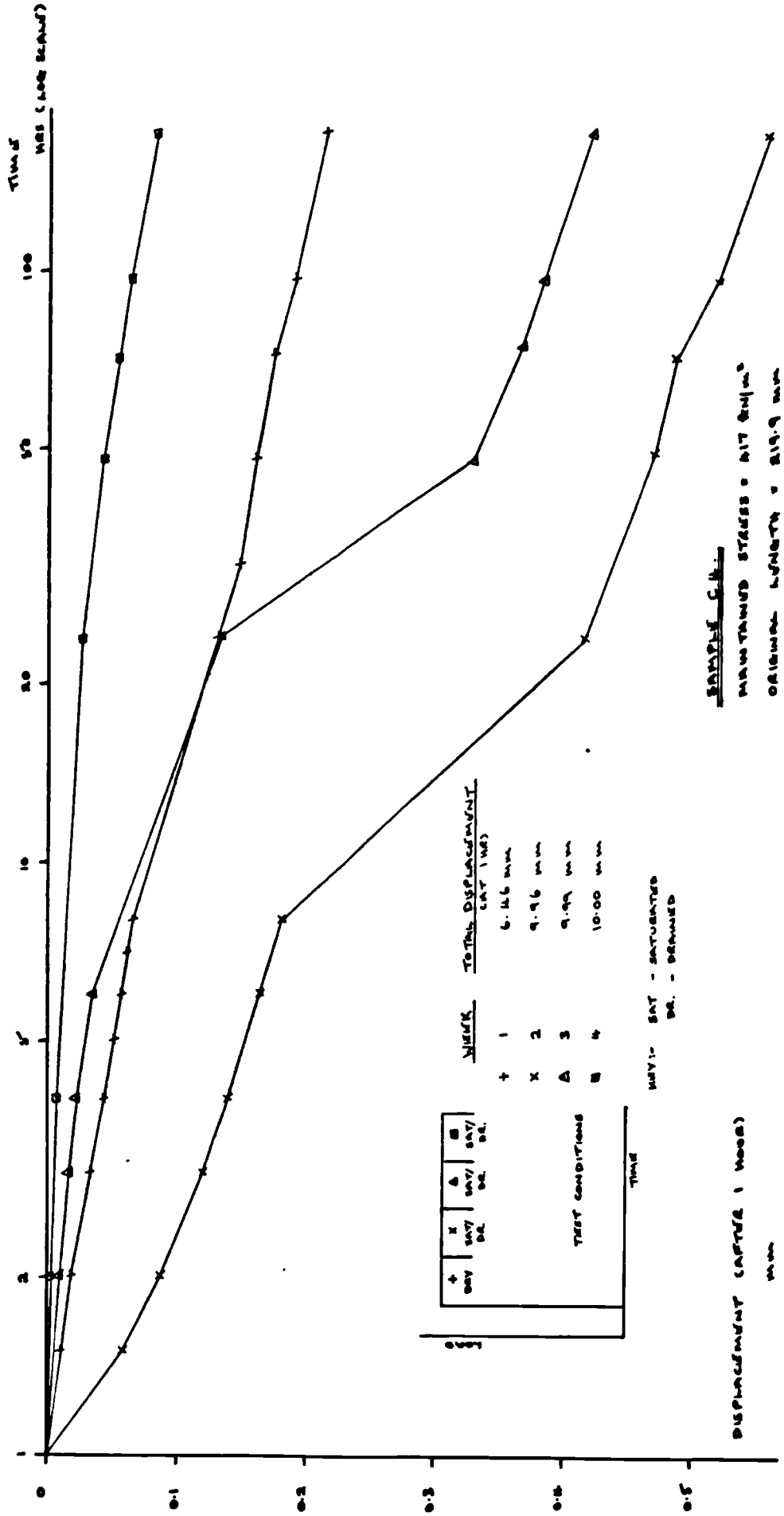

Fig. 7.14 :- Creep displacement results recorded for sample C.14.

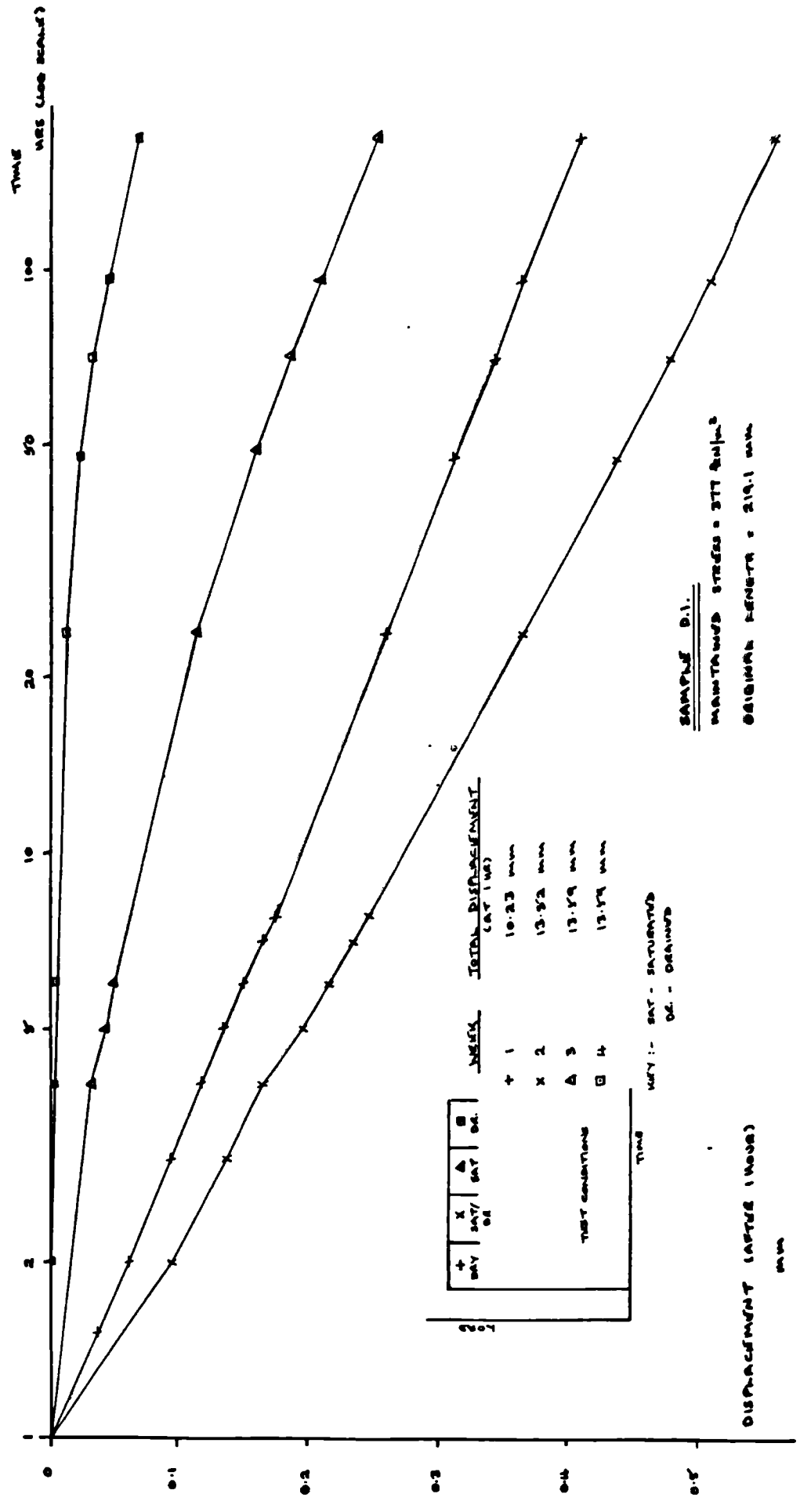

FIG. 7.15 :- CREEP DISPLACEMENT RESULTS RECORDED FOR SAMPLE D.1.

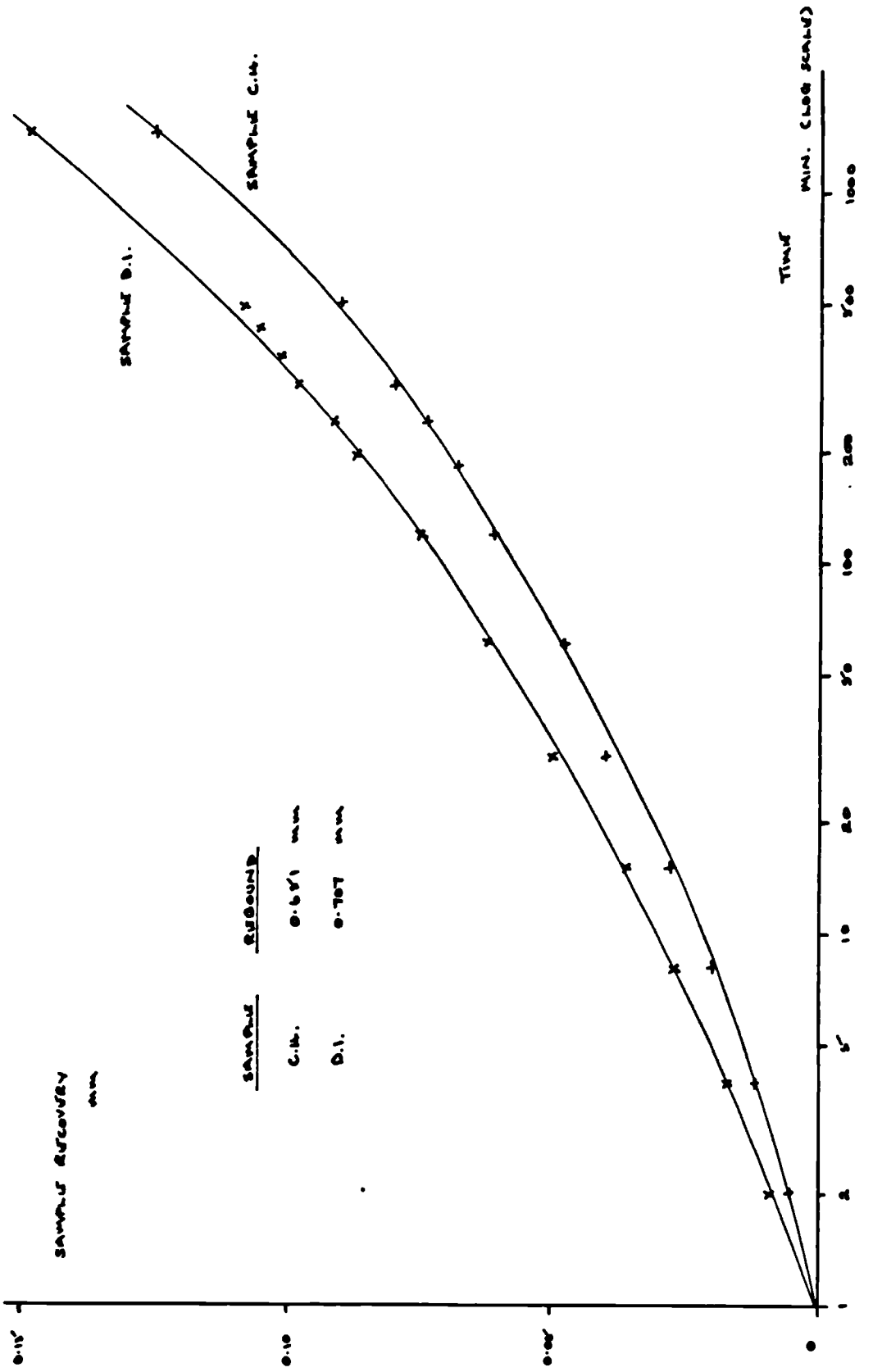

FIG. 7.16 :- RECOVERY OF SAMPLES C.H. AND D.I. (LOG TIME)

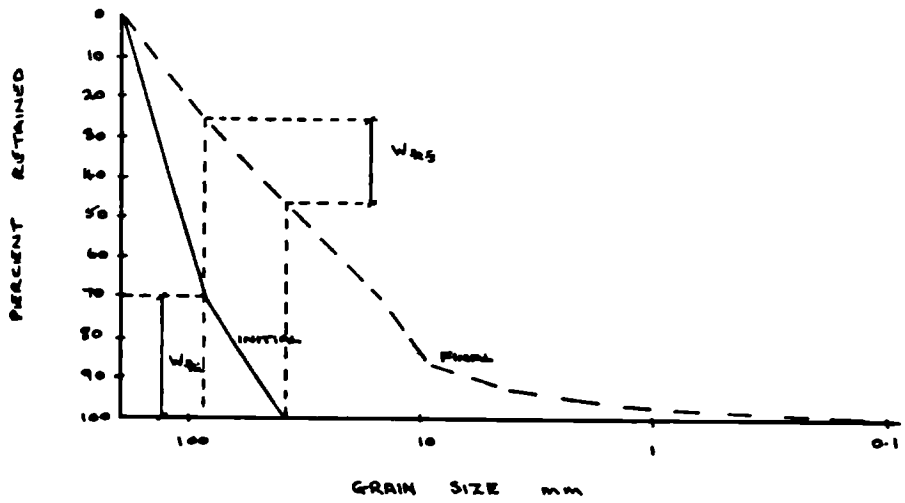

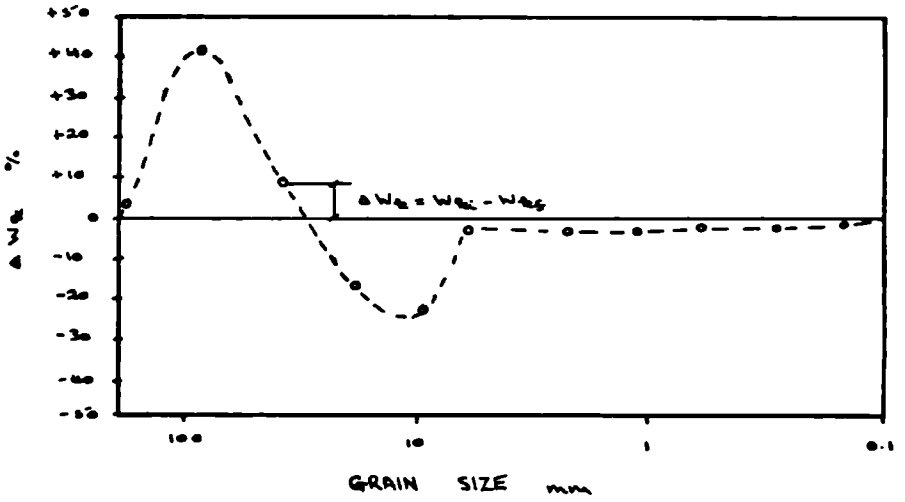

W_{Ri} = WEIGHT OF Rth FRACTION BEFORE TESTING EXPRESSED AS PERCENTAGE OF TOTAL WEIGHT

W_{Rf} = WEIGHT OF Rth FRACTION AFTER TESTING EXPRESSED AS PERCENTAGE OF TOTAL WEIGHT

FIG. 7.17 :- VARIATION OF GRADING CURVE PRODUCED BY PARTICLE BREAKAGE

(AFTER MARSAL, 1973)

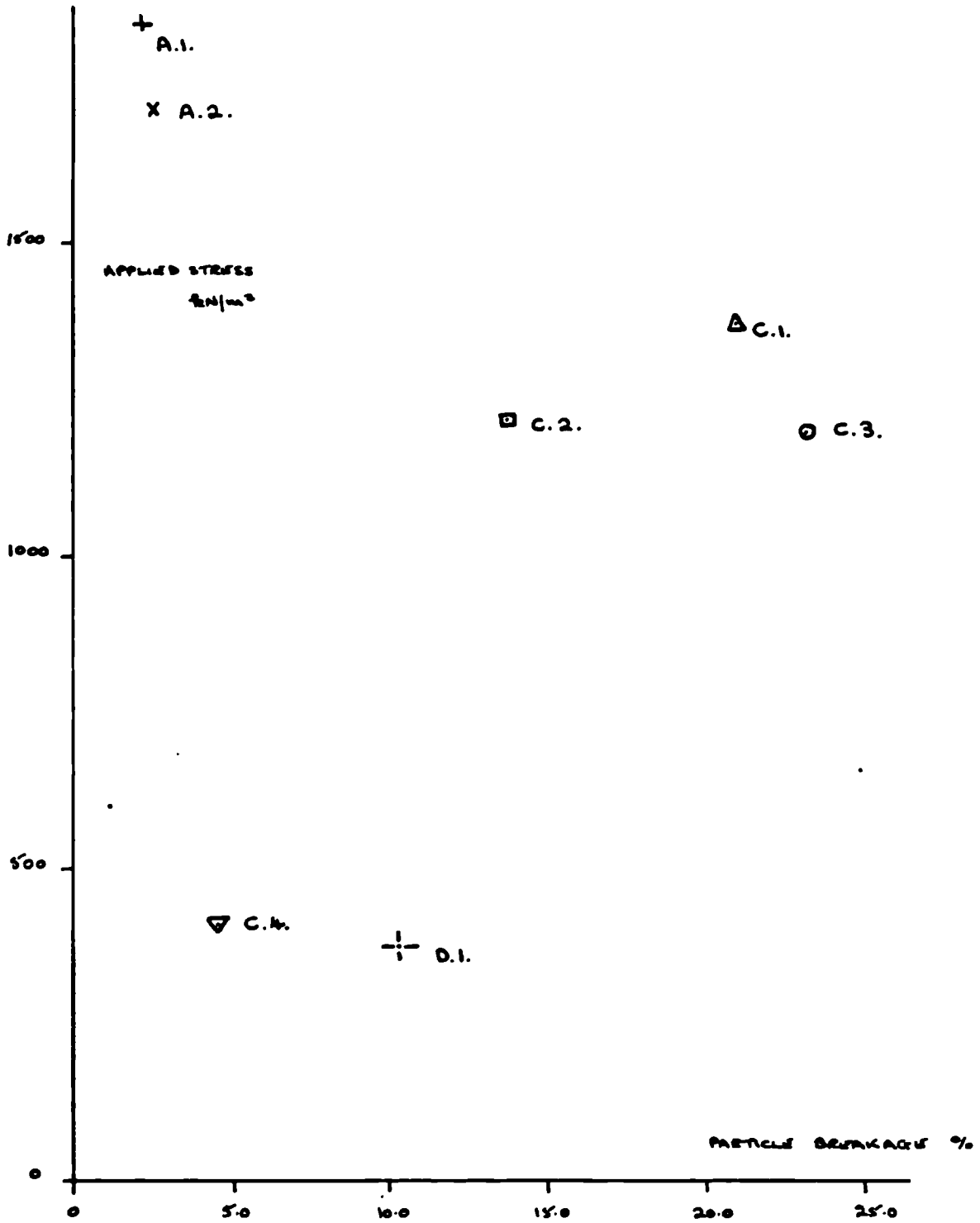

	γ_d t/m³	CONDITION
A.1.	2·00	DRY / SATURATED
A.2.	2·00	SATURATED
C.1.	1·24	DRY
C.2.	1·29	DRY
C.3.	1·22	SATURATED
C.4.	1·37	DRY / SATURATED
D.1.	1·33	DRY / SATURATED

FIG. 7.18 :- VARIATION OF PARTICLE BREAKAGE WITH APPLIED STRESS

Chapter 8

The Role and Importance of Contact Crushing

As has been discussed in Chapter 1 there are two phenomena which contribute to the overall deformation of a granular mass - interparticle and intra-particle behaviour. Interparticle displacement is observed as the crushing occurring at each contact due to the inter-particle force and as particles rotating and sliding relative to each other. Intra-particle deformations are seen as the strains induced in the bulk material of the particles and as particle breakage. When a granular mass is loaded or unloaded, some, if not all, of these mechanisms will occur and the relative importance of these will depend upon the load level, the sample condition and its history. In Chapters 4 to 6 the mechanism of contact crushing has been investigated. If these results are to be useful in predicting the behaviour of rockfill, as well as helping to understand observed behaviour, it is necessary to consider the relative importance of this and the other mechanisms.

8.1 The Relative Importance of the Deformation Mechanisms

8.1.i Contact Crushing

The loads applied to a granular mass are always transmitted from particle to particle at the particle contacts unless the interstitial medium carries some of the load. The deformation of each particle will be dependent upon the magnitude and direction of the contact forces. The shapes and orientations of the particles will determine the direction of the contact forces and their magnitude will depend on the total number of contacts within the mass. Marsal (1973), using a statistical method, has determined values of the mean contact forces acting on a plane due to a resultant stress of 100 kN/m^2 (which represents an overburden of 6-7 m) for uniform gradings.

sand (dia. ≃ 0.05 cm)	1×10^{-5} kN
gravel (dia. ≃ 2 cm)	1×10^{-2} kN
rockfill (dia. ≃ 70 cm)	10.0 kN

Under these loads crushing occurs at the contacts to accommodate the stresses induced so that they are no greater than the rock strength and this local displacement contributes to the overall deformation of the rockfill. Since the interparticle forces are always applied at the contacts, the amount of contact crushing must always contribute towards the overall deformation. Contact crushing is a permanent action since the displacement cannot be reversed on unloading.

8.1.ii Rotation and Sliding of Particles

Rotation and sliding movements are also permanent since removal of the load will not cause the particles to return to their initial position. Applying opposite moments and shear forces will not necessarily produce the original configuration since the local movements are path dependent and any breakage (either of particles or at the contacts) is irreversible.

The role of rotation and sliding in a granular mass has not been considered in this research and it is difficult to assess the importance of these. It would be expected that a well-graded sample would exhibit less rotation and sliding than a uniform grading since, due to the greater number of contacts, the shear forces would be smaller. A dense sample would have less void space than a loose one, restricting the amount of movement. A sample of smooth rounded particles would be expected to exhibit more rotation and sliding than a set of angular particles because of the lower coefficient of friction and less interlocking.

8.1.iii Bulk Deformation

Fig. 4.27 shows the mean load-displacement curves determined for contacts with various angles together with a curve representing the bulk displacements of a cylinder with the same height and diameter as the contact samples. This cylinder curve gives an indication of the proportion of the bulk dis-

placement occurring in the contact samples. For a contact angle of 160° under 2.0 kN the bulk deformation is approximately a tenth of the total and about a sixtieth for an angle of 110°.

A comparison of the contact and bulk time-dependent displacements (section 6.8) reveals that the contact displacements can be ten to twenty times the bulk displacements for contact angles ranging from 135° to 170°. These calculations do not take into account the possibility of the Damage Load having been reached which may increase the contact creep displacements substantially.

These results indicate that in comparison with the contact displacements the bulk displacements are not very significant. However, the rebound and recovery of a granular mass cannot be dependent upon the contact displacements or the particle breakage since these are permanent and not reversible. A proportion of the bulk deformation is reversible and therefore this is important in cases where unloading of the granular mass or some of the particles occurs.

8.1.iv Particle Breakage

If the stresses set up along a plane or set of planes within a particle by the interparticle forces are greater than the material strength, then cracking of the particle will occur. The magnitude of the deformations resulting from breakage is dependent on the amount and shape of the voids in the vicinity of the broken particles. Breakage is an irreversible process and therefore contributes to the permanent deformation of the granular mass.

The significance of breakage as measured in the oedometer tests has been commented on in section 7.6. The values obtained for the well graded samples (2.2.and 2.5%) under stresses of 1800 kN/m^2 are considered to be of little significance, whereas quite large values (upto 23%) were noted for the uniform samples. This again illustrates the importance of the number of contacts; the very large numbers in well-graded samples reduce the contact forces significantly compared with those expected in a uniform grading.

Fig. 8.1 shows a section of the load-displacement curve obtained from the oedometer test on sample C.1. described in

Chapter 7. The curve is made up of a series of steps but the mean gradient shows an increasing trend. If the deformation of a granular mass is considered to result from particle breakage only, then it would be expected that the gradient would decrease with increasing load (since as has been shown breakage increases with load and therefore the overall displacement increases) until all the interstices had been filled. In practice, breakage increases the number of particles and therefore the number of contacts, which reduces the mean contact force. This is seen as a stiffening of the sample until further breakage occurs. This suggests that even though significant breakage may occur the full effect is reduced by the introduction of new contacts.

8.1.v Conclusion

In the above remarks an assessment of the importance of each of the four mechanisms has been made. The contact crushing is important, since interparticle forces are always transmitted from particle to particle at the contacts and therefore the behaviour at the contact will always effect the overall behaviour. Bulk deformations have been shown to be always small compared with the contact displacements, although these are of importance in unloading behaviour because the other mechanisms produce permanent displacements. Particle breakage may be significant if the initial dry density is low and sufficient stress applied but the phenomena serves to increase the number of contacts and while stepping of the load-displacement curve reflects this, the overall trend is an increasing gradient. Rotation and sliding have not been assessed but the amount of movement is dependent upon the sample grading, the initial dry density and the coefficient of friction of the particles.

The importance of the interparticle behaviour compared with the intra-particle behaviour stems from the fact that the interparticle force is determined by the number of contacts within the mass. Both bulk deformations and particle breakage are dependent upon the magnitude of these forces. The magnitude of the forces also determines the points at which irreversible displacements occur within the mass. This has the effect

of introducing a non-linear aspect into the behaviour of granular masses so that the overall behaviour depends on the particle sizes and configuration.

If the interparticle behaviour is important in the overall behaviour of a granular mass, then it would be expected that similarities between the local and overall behaviour would be observed. By comparing the behaviour of contacts with that seen in the oedometer tests and more generally with that in dams, a further confirmation of the relative importance of the interparticle behaviour can be obtained.

8.2 Comparison of Contact Behaviour with Rockfill Behaviour

8.2.i Effect of Load Level

(a) Maintained Load

Maintained loads produce time-dependent displacements both at a contact point and in oedometer samples. The post-construction movements of dams, observed even when other external loading is not applied, reflect these internal local displacements.

(b) Increased Load

Increasing the load on a rock point causes an immediate displacement and the creep rate of the time-dependent displacements is also increased. Similar behaviour may be seen when the load on the upstream face of membrane dams is increased by the initial filling of the reservoir. This behaviour was not reproduced in any of the oedometer tests but the work carried out by Pigeon (1969) indicates that the gradient of the strain v log (time) graph increases with increased vertical stress. Inspection of the oedometer samples after tests revealed evidence of substantial contact crushing.

(c) Decreased Load

In carrying out the time-dependent behaviour contact tests, some samples were subject to a series of loads, the last of which was half or two thirds of the maximum load. The results showed negligible displacements occurred under the reduced loads. The attempt to reproduce this behaviour in the oedometer with the

tests on samples C.2 and C.3. was not successful. Although both samples showed negligible displacements at half the maximum stress, as the stress was increased the creep displacements also increased. The contacts were not reloaded again to see whether the increase in creep displacements would occur as in the oedometer. The contact samples were subject to the higher maintained load for some time whereas the oedometer samples were only subjected to the maximum load momentarily. Another reason for the discrepancy in behaviour may be the path-dependency of the oedometer sample. In reloading the configuration of particles, numbers of contacts and distribution of forces may alter and some contacts be subject to larger forces than previously experienced, which would produce additional crushing.

(d) Cyclic Loading

In the oedometer tests on samples C.2. and C.3. the samples were loaded to 1200 kN/m^2 and then unloaded immediately to 650 kN/m^2. The stress was then increased over four weeks back to 1200 kN/m^2 and the displacements recorded at each stage. The displacements noted on reloading were about 7-11% of those observed on the initial loading. While the magnitudes of the additional contact displacements during cyclic loading were not very consistent, there was a definite trend of decreasing displacement on each cycle and the additional displacements were much smaller than the initial displacements. In the same way the repeated impounding of the reservoir of a membrane dam produces less movement than the initial impounding.

8.2.ii Effect of Saturation

(a) Immediate Displacements

The load-displacement tests on dry and saturated rock points produced an inconclusive picture of the effect of saturation. The area of contact tests, however, showed very clearly that saturated samples require a much larger area to support a given load. For contacts of similar shape this implies that saturation increases the immediate displacements and the work of Sowers et al. (1965) supports this conclusion.

In the oedometer tests the dry sample A.1. was loaded to

1852 kN/m^2 and settled by 1.9% of its initial height, whereas saturated sample A.2. settled by 3.5% in loading up to 1715 kN/m^2. The difference in the displacements may have been due to particle breakage but a study of the breakage values, 2.2% and 2.5% for A.1. and A.2. respectively, suggests that the contact crushing was more important.

(b) Time-dependent Displacements

The time-dependent displacements of samples A.1. and A.2. show greater settlements for the saturated sample and this is again observed in the tests on samples C.4. and D.1. Similar behaviour is noted for contact creep initially, although after two-three hours the magnitudes are not substantially different.

(c) Saturation of Dry Fill

After subjecting dry rock points to cycles of load some of these were saturated and on reloading increased displacements were observed. Saturating dry points under maintained loads produced additional displacements immediately. The saturation of oedometer sample A.1. did not produce an immediate displacement but after about two minutes the creep rate increased and larger displacements were noted over the next three hours. In the tests on samples C.4. and D.1. the samples were loaded dry and allowed to creep for a week before saturating. This produced additional immediate displacements of about 50% and 30% respectively and the creep displacements in the second week were greater than those in the first.

Dams constructed with dry fill have also been saturated and have experienced large displacements. A storm yielding 383 mm of rain at the construction site of the 86 m high Cogswell Dam in California, when 80% of the dam was complete, produced settlements of 176 cm overnight and the dam continued to settle rapidly for several months (Spielman, 1960). During the construction of Venemo Dam in Norway fill placed in the winter was not sluiced until spring and Kjaernsli (1965) notes settlements for some layers of more than 1% of the overburden. In addition to these examples the initial reservoir filling of any dam has always been considered critical and large movements are usually noted.

(d) Repeated Saturation

In both the contact tests and oedometer tests on samples C.2. and C.3. repeated saturation did not appear to produce either immediate deformations or additional time-dependent displacements. Similarly the repeated impounding of reservoirs at sloping core and membrane dams has little effect on the movements once the initial filling has been completed. Central core dams are more sensitive to the reservoir level e.g. Gepatsch Dam in Austria but this may also be due to the elasticity and position of the core.

8.3 Conclusion

The above comparisons of behaviour and the preceeding discussion of the relative importance of the four mechanisms of deformation show that the contact crushing is significant in a number of different situations. The ability to predict local and overall movements of a granular mass is very useful and the evidence suggests that a prediction based on the contact displacements would give reasonable results. In view of this, a numerical computer model of a granular mass has been devised and the results from this compared with the results of the oedometer test on sample C.1. (section 7.5.ii). The details of this model and the description of contact behaviour, determined from the contact tests, are presented in Chapter 9.

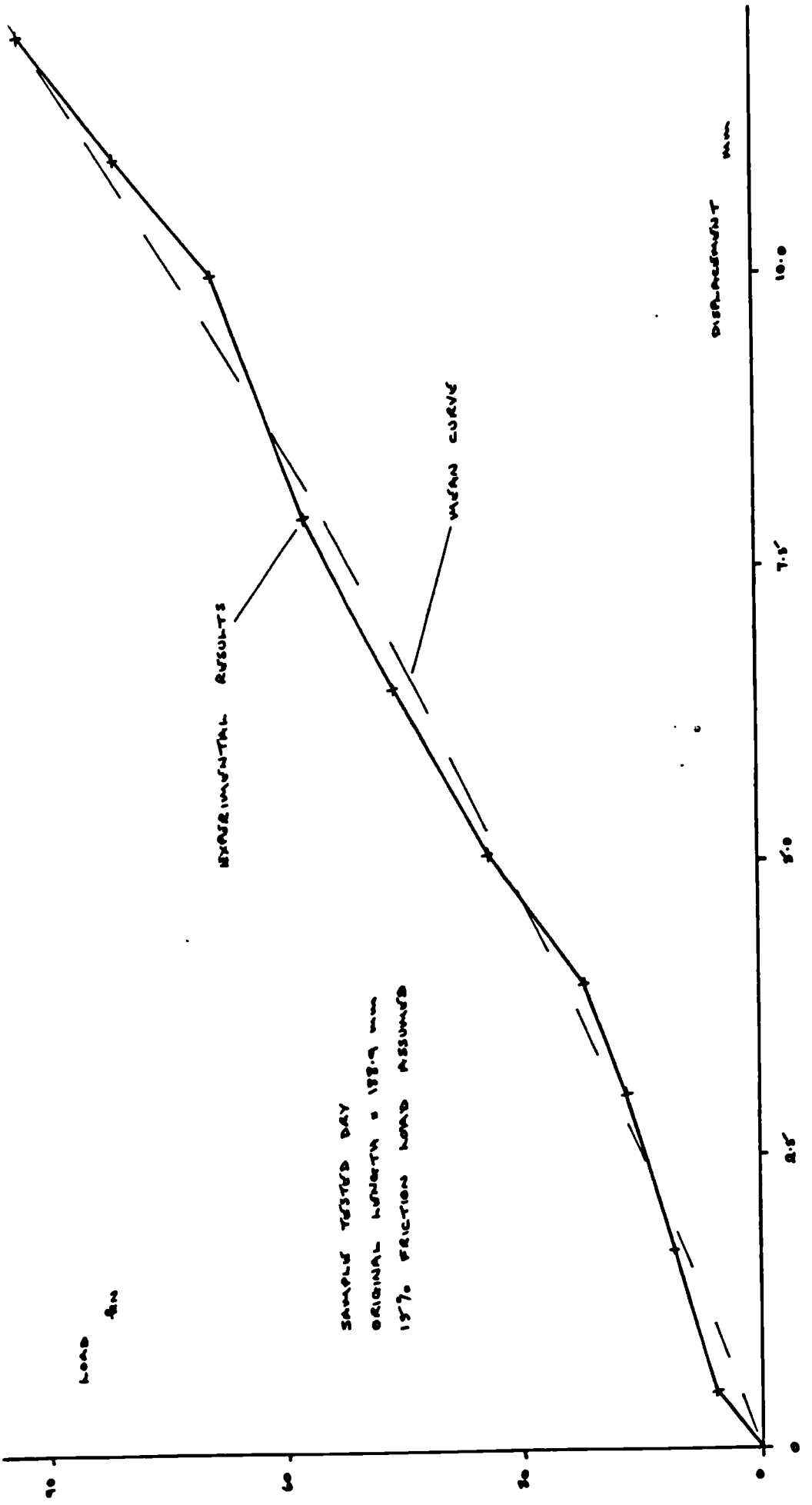

Fig. 5.1 :- LOAD - DISPLACEMENT CURVE FOR DRY UNDRAINED GRADED OTTAWA SAND C.I.

Chapter 9

The Prediction of the Behaviour of a Granular Mass of Angular Particles

The work presented in this chapter describes the development of a 2-D numerical computer model using a stiffness analysis to predict the behaviour of a granular mass. In order to assess the accuracy of the results, the situation modelled was one which could be reproduced in the laboratory, i.e. an oedometer test. Section 7.5.ii gives the details of the laboratory test used for comparison and fig. 7.10 shows the load-displacement curve obtained for this sample (C.1.). This sample had a uniform grading and was tested dry. Accordingly, the work has concentrated on the immediate displacements of a dry sample and where possible the description of contact behaviour has been based on the experimental results of dry particle contact tests.

9.1 The Granular Material Model

9.1.i The Model Structure

In developing granular models it is usual to approximate the particle shapes to circles or spheres (Ko and Scott, 1967; Serrano and Ortiz, 1973) as this aids the model building process. This simplication may be reasonable if smooth, near spherical particles are being considered but discrepancies will arise if the particles have low roundness or sphericity values. The method proposed may be applied to particles of any shape and if appropriate restrictions are used the range of sphericity values observed in the mass may be reproduced. The descriptions of contact behaviour take into account the angularity of the particles.

The model developed here is a 2-D model and therefore caution must be used in comparing the results with those of a 3-D laboratory test. However, if some agreement can be obtained, then this provides encouragement to use this 2-D model as a basis for a 3-D model. The setting up of a structural model and of the stiffness equations can be easily developed

from the 2-D model. The procedure for setting up the structural model would be exactly the same except that an extra co-ordinate and slightly different restrictions on sample boundaries would be needed.

The particles are replaced by a lattice structure with nodes at the centre of each particle, fig. 9.1. The members between nodes consist of

(a) a rigid strut from a particle centre to the contact point with an adjacent particle

(b) a deformable element to provide for local deformation in the vicinity of the contact point

(c) a rigid strut between the contact point and the centre of the adjacent particle

Lucas (1975) has used a similar structure to model configurations of ice floes.

9.1.ii Programme MODELG

Fig. 9.2 shows a flow chart of programme MODELG which was used to generate the structural models. Prior to preparing the models the number of particles, the maximum and minimum dimensions of each particle (d max, d min) and the size of the container holding the particles (in this case - 457.2 mm x 228.6 mm - the oedometer cylinder dimensions were chosen) were specified. The particle centres were generated using psuedo-random numbers and those lying within the minimum specified distance, d min, of existing centres were discarded. The lattice members were produced by connecting centres less than the maximum specified distance, d max, apart and the contacts between particles were assumed to be at the centre of each lattice member. Where two or more members were found to cross the additional members were discarded so that only one remained. Contacts with the container walls were also formed for particles at the edge of the sample, subject to the same size restrictions.

9.1.iii Models MOD1O and MOD1OR

Fig. 9.3 shows two models generated using MODELG and Table

9.1.1 gives details of these. The model, MOD1O, has been used to obtain results for comparison with the load-displacement curve of C.1. Model MOD1OR is similar to MOD1O but has more particles. This has been used to investigate the effect of denser packing.

Sample	Max particle size mm	Min. particle size mm	No. of particles	No. part. /unit vol. $x10^3/m^3$	Av. no. contacts/ particle	Total no. contacts
MOD1O	76	38	41	7.8	5.2	118
MOD1OR	76	38	47	9.5	5.4	140

Table 9.1.1:- Details of Structural Models generated using MODELG

The values shown in Table 9.1.1 for the number of particles per unit volume (nv) have been calculated from the number of particles per unit area (ns) assuming

$$ns = nv^{\frac{2}{3}}$$

This is a 3-D equation and its use in a 2-D situation provides only a rough indication of the values which would be obtained in a 3-D model. Marsal, (1963), in studying the structure of granular masses, indicates that errors of upto 18% may occur in determining the nv value with this equation. From these nv values and the average particle weight of sample C.1., initial dry density values for the models may be obtained. These values - $1.37t/m^3$ for MOD1O and $1.69t/m^3$ for MOD1OR give some indication of the range of dry densities which the models represent.

The values of the average number of contacts/particle show only a slight increase for the denser packing. Fig. 9.4 shows the frequency distribution of the contacts per particle values and it can be seen that there is not a great change in the number of particles with 4, 5 or 6 contacts. The increase in the mean is due to a few more particles with 7 or 8 contacts. It should be noted, however, that the introduction of 6 particles increases the total number of contacts by 22.

As has been noted the choice of a 2-D model to represent a 3-D cylindrical sample is difficult but it is felt that some crude basis of similarity is needed if the analysis results are to have any value. Accordingly similar sample dimensions and

maximum and minimum particle sizes have been used. Sample C.1 had a measured nv value of $7 \times 10^3/m^3$ and therefore MOD10 was used for the comparison of model and oedometer results.

9.2 Formation of the Stiffness Matrix

Using the stiffness method of analysis, the equilibrium equations relating the forces applied at all the nodes to the corresponding displacements may be expressed in terms of matrices

$$[P] = [K][u]$$

where P represents the nodel forces, u the displacements and K is the structure stiffness matrix. Usually the known applied forces will be at the nodes where the displacements are not known and vice versa. These boundary conditions may be incorporated into the stiffness equations by adjusting the appropriate stiffness matrix elements. The equations are solved to find the nodal displacements and these are used to determine the member forces.

The stiffness matrix of the whole structure can be assembled from the lattice member stiffness matrices. The member stiffness matrix has been determined by differentiating the equation of potential energy stored in the member deformable element with respect to the nodal displacements. Fig. 9.5 shows the condition of arbitrary shape and position of the deformable element from which the equation of energy stored was determined. Details of this have been presented in Appendix II. Displacement has been allowed to occur in extension, shear and rotation and three stiffness coefficients k_e, k_s and k_r have been associated with these movements.

9.3 Description of Contact Behaviour

Having set up a structural model and determined the equilibrium equations, it is necessary to provide a description of the material behaviour so that appropriate values of the stiffness coefficients can be calculated.

During the loading process each contact within a sample will be found in one of three states of loading

(a) the 'no-contact' state - where particles, previously in contact, have been moved apart, the contact will cease to exist. This is seen in the model as a member being extended beyond its original length. It should be noted that new contacts (i.e. new members) are not formed in the analysis and this state is applied only to the existing original members.

(b) the 'loading' stage - where the centres of two particles in contact are closer together than at any other previous point in the loading process.

(c) the 'un/reloading' state - where contact still exists but the particle centres are further apart than at a previous point in the loading process. Whether the contact is being unloaded or reloaded will depend on whether the particles are moving apart or closer together.

9.3.i Extension Stiffness - k_e

Fig. 9.6 shows the approximate shape of the normal load-displacement curve determined from the results of the dry contact tests presented in Chapter 4.

(a) 'No-contact' state

In the no-contact condition, since there is effectively no member between the particle centres, k_e has been set to zero.

(b) 'Loading' state

The load-displacement curve of a dry contact may be split into two types of behaviour - a smooth initial curve followed by irregular behaviour - and these are seperated by the Damage Load, fig. 9.7. Relationships are required for both types of behaviour and a method of calculating the Damage Load.

(i) Pre-Damage Load Behaviour

Although the contact behaviour under normal load is essentially inelastic it can nevertheless be described well using Hertz's theoretical equation for a spherical contact with a halfspace.

$$d = \eta' P^{\frac{2}{3}} \qquad (9.1.)$$

The Hertzian coefficient, η', is dependent upon the radius of the spherical contact whereas the experimental coefficient for angular particles has been found to be dependent upon the contact angle, α. Since granular particles may have either angular or rounded surfaces, it would be useful if a single parameter could be found which was representative of the whole range of roundness values.

Fig. 9.8 showshow an equivalent radius, Re, may be calculated for a contact with an apex angle γ. This construction produces the following relationship between Re and γ:-

$$\gamma = 2 \tan^{-1} \left(\sqrt{(Re^2 - (Re-d)^2}/d \right) \qquad (9.2.)$$

The displacement d is obtained from the Hertzian equation (9,1) i.e.

$$d = P^{\frac{2}{3}} . D^{\frac{2}{3}} . \left[\frac{1}{Re}\right]^{\frac{1}{3}} \qquad (9.3)$$

where D is dependent upon the Young's modulus and Poisson's Ratio of the material (see section 4.1.). A study of the validity of the use of this approach is presented in Appendix III and this shows that good agreement is obtained between the theoretical and experimental results if the displacement is calculated for a load equal to half the contact Damage Load, Pd.

$$d = \left[\frac{Pd}{2}\right]^{\frac{2}{3}} . D^{\frac{2}{3}} . \left[\frac{1}{Re}\right]^{\frac{1}{3}}$$

(d and Re in mm)
(Pd in kN)

Substituting this in equation (9.2)

$$\gamma = 2 \tan^{-1} \left(\left[Re^2 - \left(Re - \left[\frac{Pd}{2}\right]^{\frac{2}{3}} . D^{\frac{2}{3}} . \left[\frac{1}{Re}\right]^{\frac{1}{3}} 2\right]^{\frac{1}{2}} \Big/ \left[\left[\frac{Pd}{2}\right]^{\frac{2}{3}} . D^{\frac{2}{3}} . \left[\frac{1}{Re}\right]^{\frac{1}{3}}\right] \right)$$

and therefore

$$Re = \frac{1}{2} \left[\left[\frac{Pd}{2}\right]^{\frac{2}{3}} D^{\frac{2}{3}} \left| 1 + \tan^2 \frac{\gamma}{2} \right|\right]^{\frac{3}{4}}$$

Assuming Young's modulus = 10 kN/mm^2 and Poisson's Ratio =0.01 (determined from the classification test results - section 3.7)

then $D = 0.15\ mm^2/kN$ and therefore

$$Re = 0.23 \left[\left[\frac{Pd}{2} \right]^{\frac{2}{3}} \left[1 + \tan^2 \frac{\gamma}{2} \right] \right]^{\frac{3}{4}} \qquad (9.4)$$

The load-displacement equation used to model the initial behaviour was determined from (9.3).

$$d = 0.282\ P^{\frac{2}{3}} \left[\frac{1}{Re} \right]^{\frac{1}{3}}$$

and Re was calculated from (9.4)

(ii) Calculation of Damage Load

The graphs of Damage Load against contact angle, fig. 4.29 - 4.36, show clearly that increased angle increases the Damage Load but there is some doubt whether the angle α_{am} or α_{vm} is more representative of an irregular contact. A study of the dry contact graphs suggests that α_{vm} is more representative for this condition and the results from this graph, fig. 4.32, have been used. The graph points can be approximated by a best fit curve, fig. 9.9, with the form

$$Pd = 2.52 \times 10^{-11} \alpha^{5.02}$$

where the Damage Load, Pd, is in kN and the contact angle, α, in degrees. This formula has been used to calculate the Damage Load for each contact in the structural model.

(iii) Post-Damage Load Behaviour

This section of the contact load-displacement curve can be very complex and therefore, as a first approximation, a linear relationship has been assumed. A study of the curves produced, particularly for the smaller angle contacts, suggests that this is not an unreasonable mean curve. The gradient of this line varies with the contact angle and values taken from the sample results, figs. 4.23 - 4.26, have been plotted in fig. 9.10.

For angles greater than 86° the points lie along the line

$$\text{Gradient} = 3.61 \times 10^{-2} \alpha - 2.97 \qquad \alpha > 86^\circ$$

For angles less than this it has been assumed that at an angle of zero the gradient is also zero and the gradient may be calculated from the following relationship

$$\text{Gradient} = 1.52 \times 10^{-3}\alpha \qquad \alpha < 86^{\circ}$$

(c) 'Un/reloading' state

From the contact test results the behaviour on unloading and reloading has been assumed to be described by the same linear equation.

$$ke = 50 \text{ kN/mm}$$

As shown in fig. 9.6 this behaviour has been assumed to apply whatever the maximum normal load applied at the contact.

Fig. 9.11 shows typical curves of the contact normal load-displacement behaviour generated using the equations set out in sections (a), (b) and (c) above.

9.3.ii Shear Stiffness - k_s

As no tests were carried out on interparticle shear behaviour the value of k_s was initially assumed to be constant, except in the 'no-contact' state when it was set to zero. In later runs of the programme the relationship

$$k_s = 50d \qquad (\text{kN/mm}) \qquad (9.5)$$

was used (fig. 9.12), where d is the total normal displacement, for two reasons:-

(i) it gave slightly better agreement of the computer model and oedometer results

(ii) it had some justification from work carried out in the area of contact tests

For normal loads less than the Damage Load it has been shown that

$$\text{Area} \propto (\text{Normal Load})^{\frac{2}{3}}$$

$$A \propto P^{\frac{2}{3}}$$

and that in this region

$$P \propto d^{1.5}$$

If it is assumed that $k_s \propto A$, which is not unreasonable, then

$$k_s \propto d$$

It must be stressed that the choice of the constant of proportionality was arbitrary but this value did produce reasonable results in the model analysis. Experimental tests are needed to determine a more realistic equation for future use of the programme.

9.3.iii Rotational Stiffness - k_r

The rotational stiffness, k_r, is an expression of the possibility of rotation occurring between two particles and would be expected to be determined by the density of the sample packing. Since tests were not carried out to investigate the magnitude and variation of this parameter, it was assumed constant during particle contact and to be zero in the 'no-contact' state, fig. 9.13.

9.4 Programme IRMODF

Programme IRMODF was written to model an oedometer test using the stiffness analysis presented in Appendix II and fig. 9.14 shows its role within the particular problem being considered. A simple flowchart of the programme is given in fig. 9.15.

9.4.i Boundary Conditions

Fig. 9.16 shows the boundary conditions applying along the sides of the sample container. Along the walls the nodes cannot move in x-direction and therefore a $u_x = 0$ condition applies. Similarly the base nodes cannot move in the Y-direction and therefore $u_y = 0$. Movement along the walls and across the base is not restricted. These conditions were incorporated in the analysis by setting the appropriate rows and columns of the overall stiffness

matrix to zero, the diagonal element to 1.0 and the corresponding RHS matrix i.e. [P] element to zero.

In order to ensure that the line of the top edge nodes remains plane (as in a real oedometer test), it is necessary to specify equal applied displacements at these nodes. This is done by setting the stiffness matrix diagonal element to the root mean square value of all the diagonal elements and the appropriate RHS element to the specified displacement multiplied by the same RMS value.

9.4.ii Non-linear Behaviour

Some of the material behaviour relationships used are non-linear and an incremental, iterative approach based on the secant modulus over the interval has been used to cope with this, fig. 9.17. Initially the stiffness values were set - k_e = 10.0, k_s = 1.0 and k_r = 1.0 - and the nodal displacements generated. Using these displacements the change in length of each member was calculated. If extension had occurred then a 'no-contact' state was assumed to exist and all three stiffness coefficients were set to zero for that member. Where contact existed the shear stiffness was calculated from the member contraction using equation (9.5) and k_r remained constant. The extension stiffness was determined as the gradient from the origin of the behaviour curve to the point on the curve corresponding to the calculated compression of the member. Using these new stiffnesses a new stiffness matrix was compiled and a second set of displacements generated. This process was repeated until the solutions converged and satisfied the criterion set out in 9.4.iii.

Having achieved this first solution a second increment of displacement was applied to top edge nodes. The nodal displacements generated represented incremental movements and these had to be summed with the previous solution to obtain the total displacements. These total values were used to ascertain the state of each contact e.g. pre or post-Damage Load and appropriate stiffness values calculated for the next iteration. As shown in fig. 9.17 the extension stiffness was calculated as the gradient over the incremental displacement. This process was repeated until the convergence criterion was satisfied and then another increment of displacement applied to the top edge nodes.

9.4.iii Convergence Criterion

After generating the displacements from the stiffness equations, the forces in the members with nodes along the top edge were calculated from the member stiffness equation. The sum of these represents the effective total load increment applied to the sample. By comparing the total with the solution of the previous iteration a convergence criterion was established. If the difference in value was less than 2% of the previous solution then convergence was assumed. The possibility of using 1% was investigated but this was not warrented by the additional computation required.

9.5 The Sensitivity of the Stiffness Analysis

In producing the description of material behaviour in section 9.3 assumptions have been made about the k_s and k_r values and it is clear that the k_e value will be determined by the value of the contact angle assigned to each contact. Before using the analysis to generate results for comparison with experimental results, an investigation into the sensitivity of the analysis to changes in these unknowns was carried out.

9.5.i Contact Angle

In setting up the structural model several methods of ascribing an angle to each contact are available, e.g. random values, statistical distribution. In this research the same angle has been assigned to each contact, as it was felt that the introduction of different values would create unnecessary complications at this stage of the model development.

Fig. 9.18 shows a graph of the total normal loads generated at the top edge nodes for model MOD10 against the total applied displacements. These show that the loads increase with the contact angle for a given displacement and that the increase in load for a reasonable range of angles is fairly significant.

9.5.ii Shear Stiffness

Fig. 9.19 shows the sensitivity of the analysis to changes in the k_s value. As with the contact angle the load increases

with increasing k_s. These increases over four orders of magnitude of k_s are not very significant, particularly at the lower displacements. Lack of experimental results on the magnitude and likely variation of this value makes it difficult to gauge how important this sensitivity really is.

9.5.iii Rotational Stiffness

The variation of the positions of the load-displacement curves for three values of the rotational stiffness is shown in fig. 9.20. The variation is negligible for a wide range of values and therefore the value of k_r used in the analysis is not particularly important. This is due to the small particle rotations produced within the sample (usually less than 1^o) for this type of loading and this means that the relative particle rotations are also very small. It is interesting to note that if extremely large k_r values are used the particle rotations all approach the same absolute value.

9.6 Comparison of Computer and Oedometer Test Results

A quantitative comparison of the results obtained from the structural model MOD10 was made with the oedometer test results to enable appropriate values of contact angle and shear stiffness to be selected. As a result of this 150^o was chosen for the contact angle and the relationship $k_s = 50 \times$ (normal displacement) was used. Fig. 9.21 shows the curve shapes obtained using $k_s \propto d$ and k_s constant and it can be seen that there is little difference.

Fig. 9.22 shows the model load-displacement curve obtained using these stiffness values, together with a mean curve calculated from the oedometer results. While there is very good agreement over the first 3.5 mm of displacement, after this the curves diverge. Using what is considered to be a reasonable contact angle and a contact behaviour model obtained directly from experimental results, this agreement suggests that in this displacement range contact crushing is very important.

There appear to be two reasons for the discrepancy in the loads at large displacements:-

(a) Updating of the structural model.

No attempt has been made to update the structural model as the displacements are applied and everything is calculated relative to the original configuration. The analysis (Appendix II) involves the angle of the deformable element to the x-axis and parameters representing the relative positions of the particle centres. These values remain constant throughout the calculations, although in practice they would change as the particles move. If these were updated then the analysis would include both the compaction of the structural model and the stiffening of the contact element, producing an increase in the loads generated. The lack of this updating would be notedat larger displacements but would be of little importance at smaller displacements.

(b) Generation of new contacts

New contacts may be formed in an oedometer sample in three ways:-

(i) as particles approach each other - due to the compaction of the sample

(ii) through particle breakage - this forms new smaller particles which make new contacts with each other and the surrounding particles.

(iii) rotation of particles - when a particle rotates relative to its neighbour, the point of contact may shift slightly so that contact exists at a point where the local material has not previously been disturbed.

An increase in the number of contacts reduces the interparticle forces which means that the contacts are in the un/reloading section of the normal load-displacement curve where the extension stiffness is much higher. The material at the location of a new contact usually has not been disturbed before and therefore has not reached its Damage Load when the stiffness decreases. These effects would be expected to increase the loads at large rather than small displacements giving better agreement between the experimental and computer results.

Fig. 7.10 shows that the experimental curve is stepped whereas the computer curve gradient changes smoothly. This is perhaps

because new contacts are not formed and because the post-Damage Load behaviour has been assumed to be linear and not as complex as the experimental curves indicate.

Since good agreement of the results is obtained initially, the local behaviour of the contacts within the sample can be investigated over this range of displacements viz. 0 → 3.5 mm.

9.7 Local Behaviour at the Contacts within Sample MOD10

9.7.i Contact States

The states in which contacts may be found e.g. 'no-contact', 'un/reloading' have been defined in section 9.3 and the percentage of contacts in each of these states will reflect the behaviour of the whole sample. Fig. 9.23 shows these percentages for applied displacements ranging from 0.1 to 6.0 mm with a line representing the 3.5 mm agreement limit. The number of members in a 'no-contact' state is quite high initially (15%) but reduces quite quickly and becomes constant at 7% after about 2.0 mm displacement. This trend would be expected in a granular material although the number would not necessarily become constant.

Of more importance is the number of contacts which have reached their Damage Loads. As expected there are none initially and the first ones do not occur until 1.3 mm displacement. The curve shows the expected increasing trend but this is not smooth. The rapid increase in numbers after 4.0 mm corresponds to the divergence of the experimental and computer curves. In accordance with expected behaviour contacts in the 'un/reloading' state do not appear until other reach their Damage Load. When a contact reaches this load more crushing occurs (the stiffness is reduced) and the interparticle forces are redistributed so that some contacts are subject to lower forces than before.

9.7.ii Interparticle Forces

Fig. 9.25 shows the frequency distribution of ranges of the ratio between the calculated normal interparticle forces in each member and the Damage Load of that member at two applied displacements, i.e. 1.5 mm and 3.0 mm. Since all the contacts had equal contact angles, the Damage Loads were equal (2.12 kN)

and a line representing this load has been included on the diagram.

There is not a smooth distribution of forces at either displacement, although at 1.5 mm there is a definite peak value at about 0.64 kN. At 3.0 mm displacement the distribution is skew and although the peak occurs at the same load as for 1.5 mm, there are smaller peaks at high ratios. The results show the expected increase in the member loads with displacement and an increased number greater than the Damage Load.

9.7.iii Member Strains

Figs. 9.26 and 9.28 show the frequency of ranges of member compression and shear displacements expressed as strains with respect to the original member lengths. The mean original member length was 52.7 mm with maximum and minimum values of 76.2 mm and 38.1 mm respectively. The strains at 1.5, 3.0 and 6.0 mm have been calculated and members in a 'no-contact' state have not been included.

The compression strains show increasing mean strain with displacement as expected and both the 1.5 and 3.0 mm results have similar curve shapes and definite peaks with approximately the same frequency. The 6.0 mm results give an indication of local behaviour when good agreement does not exist between the experimental and computer results. This distribution has degenerated from a definite peak to a wide range of strains (4,000 - 20,000 μs) with a frequency of approximately 0.17. Fig. 9.25 suggests that as the displacement increases there is also a wider range of interparticle forces with the same frequency. Fig. 9.27 shows the variation of members with normal strains greater than 1% with the applied displacement and this shows the expected increasing trend althougn this is not a smooth curve.

Fig. 9.28 shows a very definite peak at 1750 μs for the shear strains at all three displacements, although the frequencies of the peak reduce slightly as the displacement increases. The shapes of the 1.5 and 3.0 mm distributions are very similar but these do suggest a slight increase in the mean values with increasing displacement. The shear strains do not seem to be as sensitive to the applied displacements as the normal strains but have a similar range of values. This is to be expected in a

confined sample when the movement of particles relative to one another is restricted.

9.7.iv Energy Stored

The frequency of the energy stored in the deformable elements at 1.5 and 3.0 mm displacement is shown in fig. 9.29. At 1.5 mm there are two peak values with approximately equal frequencies, whereas at 3.0 mm the second of these has become dominant indicating the expected increase in mean value. The double peaks noted are probably due to the choice of energy ranges being too small and the use of wider ranges would produce a single peak.

9.8 Influence of Sample Density

Tests were carried out on MOD10R to see whether the analysis would reflect the changes in behaviour expected for a denser granular mass. Fig. 9.22 shows the total load-displacement curve obtained using the same sequence of applied displacements on MOD10R. For the first 1.5 mm the MOD10 and MOD10R results are very similar but after this the curves diverge and although the curve shapes are similar, the loads generated for MOD10R are greater than those for MOD10. This is in accordance with the behaviour expected on testing a denser oedometer sample.

As before, the percentage of contacts have been plotted against the applied displacement for the various states possible, fig. 9.24. Comparing this with the graph for MOD10, fig. 23, it can be seen that there is not such a large drop initially in the numbers in a 'no-contact' state and that there are more of these members in MOD10R. The line seperating those contacts having reached their Damage Loads and those which have not could be considered to be linear and shows again the expected increasing trend. This contrasts with the sample MOD10 line which is quite irregular. The first contacts to reach their Damage Load do so at a slightly larger applied displacement than in MOD10 but a higher proportion have achieved this load at 6.0 mm. It is interesting to note that the load-displacement curves begin to diverge at about the displacement where contacts begin to reach their Damage Load.

In a denser sample the interparticle forces are smaller for a given applied load due to the greater number of contacts and this will also produce a relatively smoother change in behaviour as the load increases. This is reflected in the computer results by the steadier decrease in the number of members in the 'no-contact' state and the increase of those reaching their Damage Load. The lower interparticle forces will also mean that Damage Loads are not reached as quickly which is again reflected in the computer results. MOD10 and MOD10R are very similar and therefore would be expected to follow similar curves. It is possible that once Damage Loads begin to be reached the distributions of interparticle forces become quite different and the curves diverge. The denser sample does not reach a constant number of members in the 'no-contact' state and the slight variation is more in keeping with expected real behaviour than that seen in MOD10. As would be expected in a real granular mass the contacts appearing in the 'un/reloading' state do not occur until other contacts have reached their Damage Load.

9.9 Conclusion

The simple numerical model developed has been compared with the results of a laboratory oedometer test on a dry uniformly graded rockfill sample. Good agreement of the results has been obtained over the first 3.5 mm of applied displacement but the load-displacement curves diverge after this and reasons for this discrepancy have been suggested. A study of the local behaviour at the particle contacts has been made and the effect of denser packing investigated. In general the model behaviour has been found to respond in the same manner as a real granular mass would.

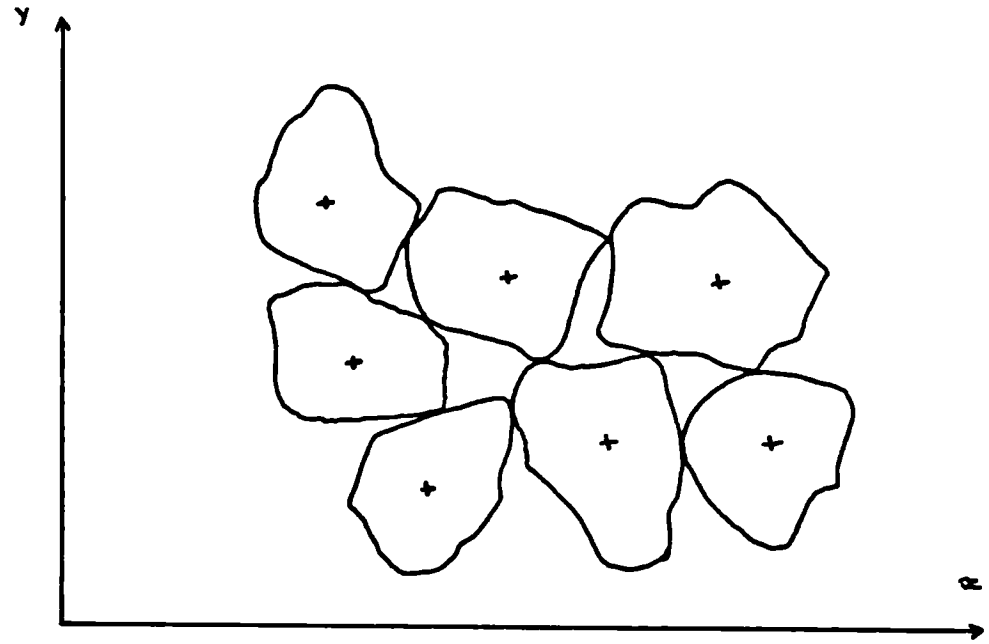

CONFIGURATION OF ROCK PARTICLES

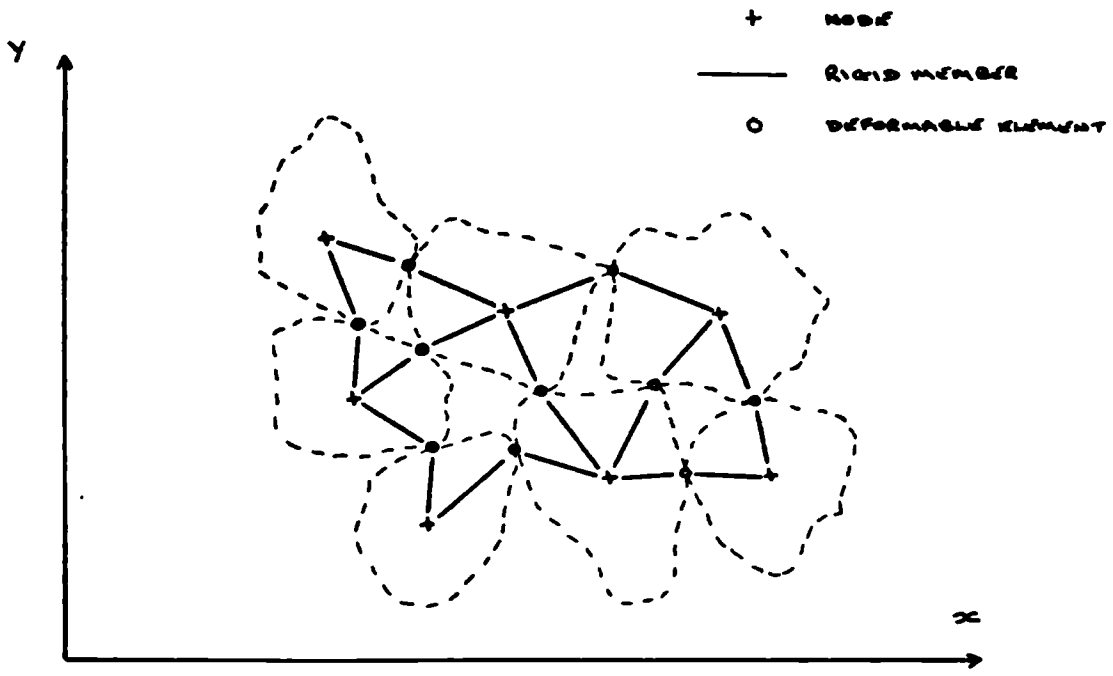

STRUCTURAL MODEL

FIG. 9.1 :- LATTICE STRUCTURE OF GRANULAR MATERIAL

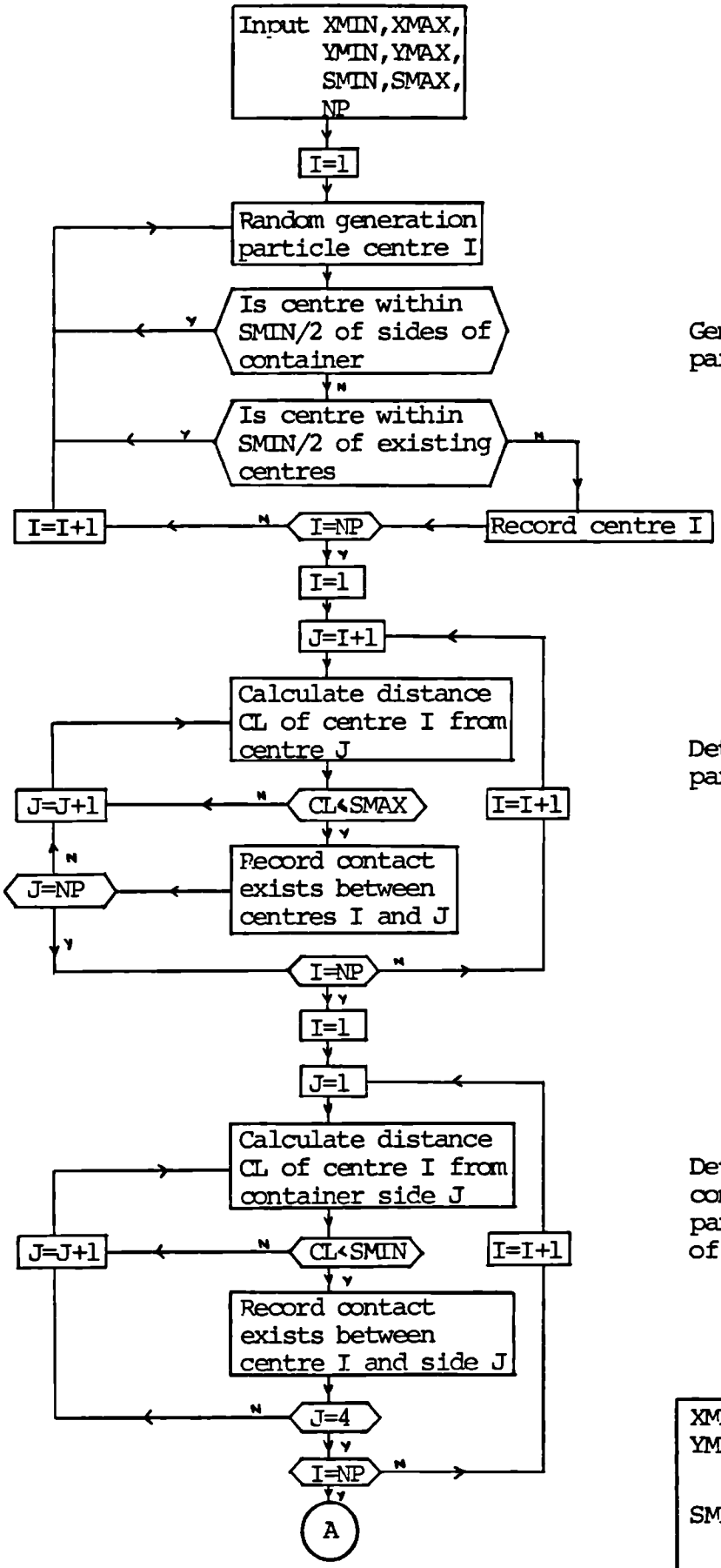

Fig.9.2 :- Flowchart MODELG

p.t.o.

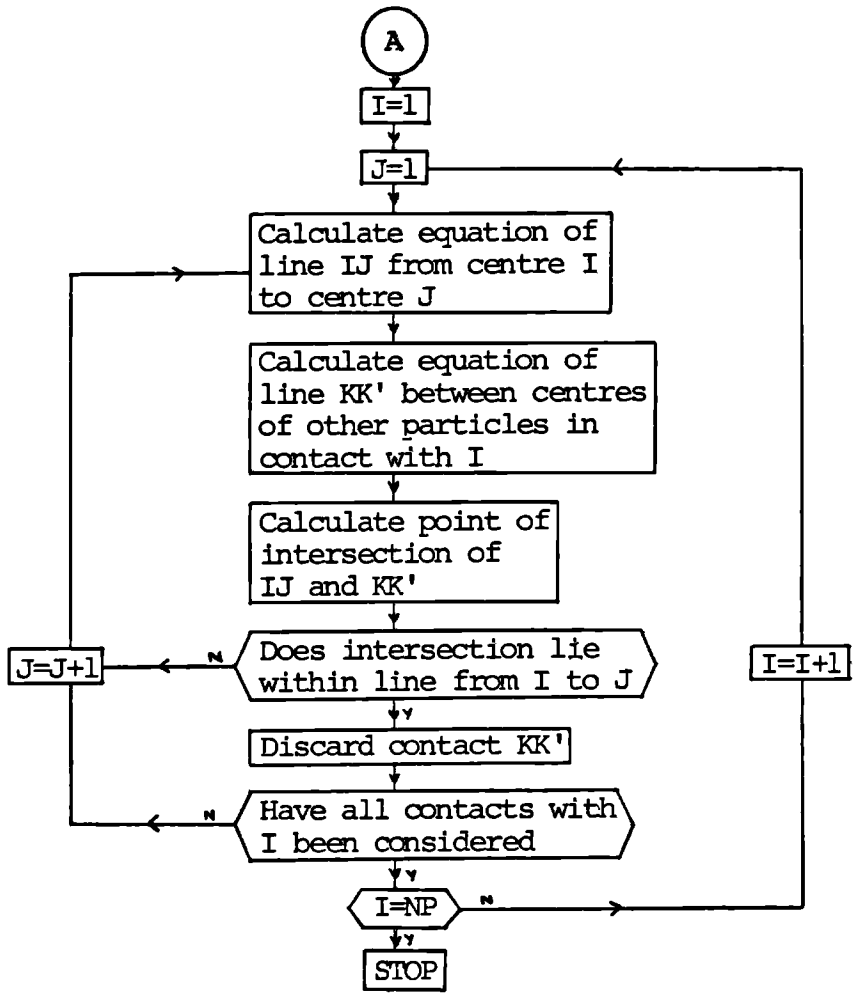

Fig.9.2 :- continued

MOD10

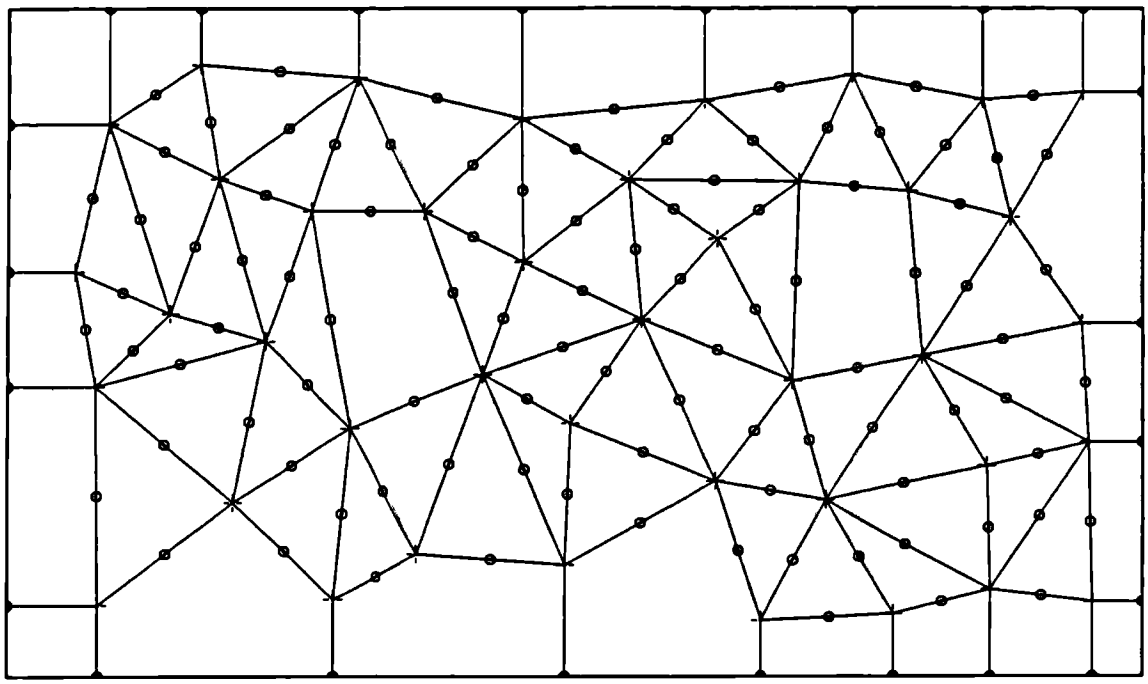

41 PARTICLES, 118 CONTACTS

MOD10R

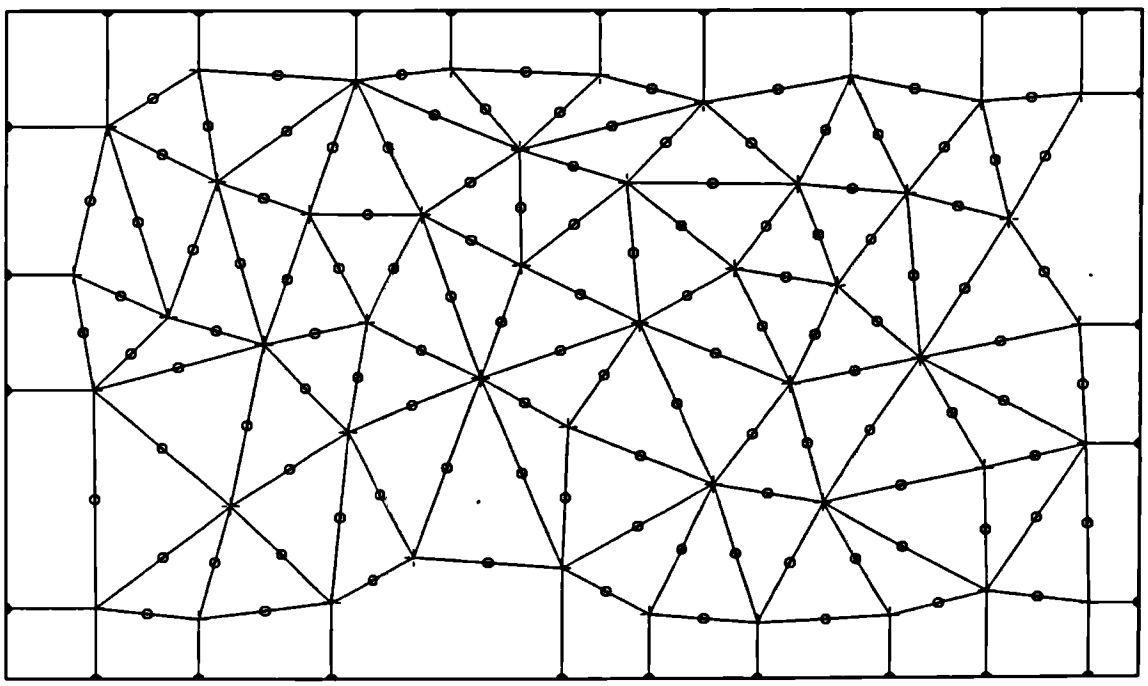

47 PARTICLES, 140 CONTACTS

FIG.9.3 : STRUCTURAL MODELS MOD10 AND MOD10R

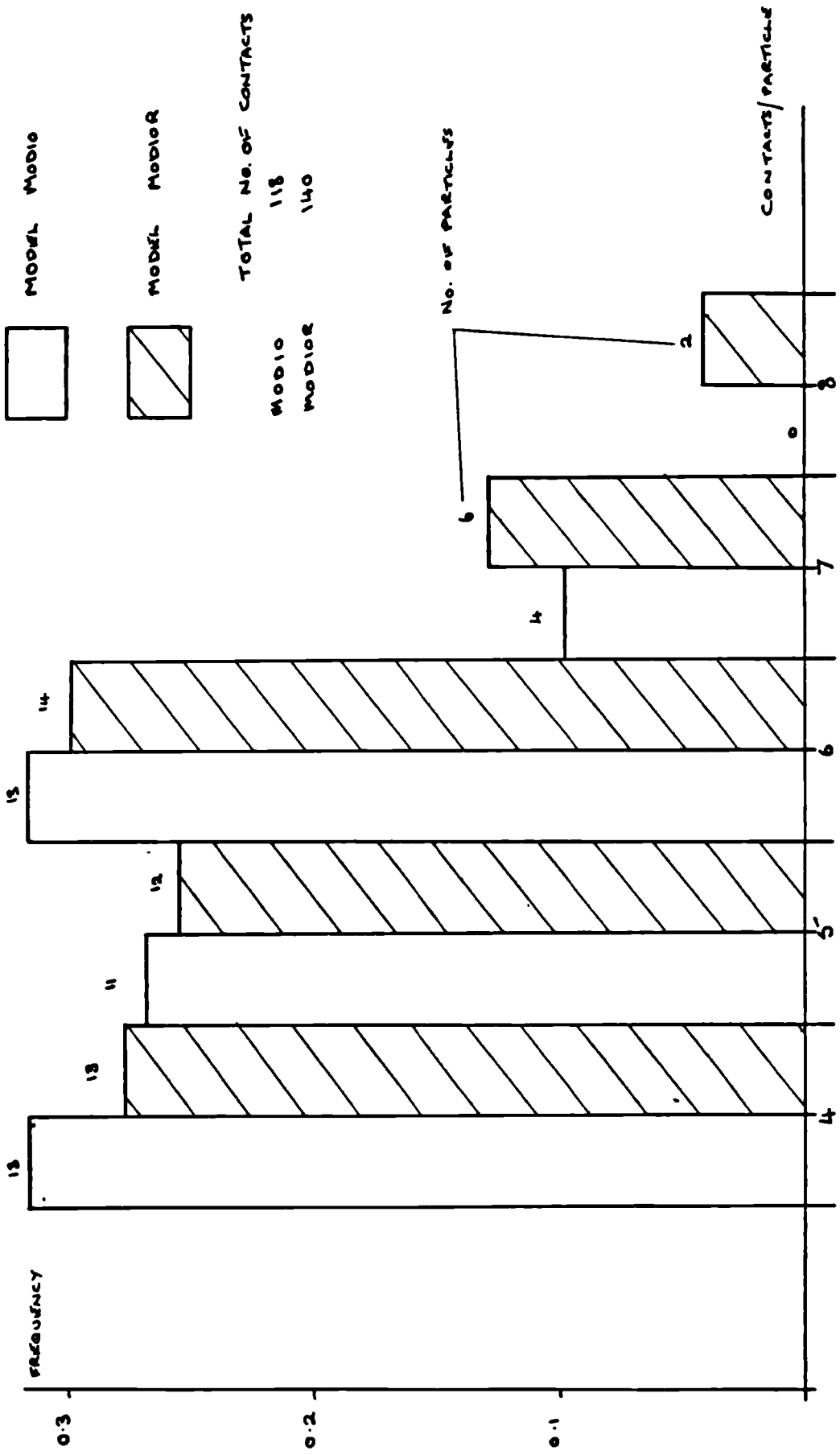

FIG. 9.4 :- FREQUENCY DISTRIBUTION OF NUMBER OF CONTACTS/PARTICLE FOR MODELS MODIO AND MODIOR

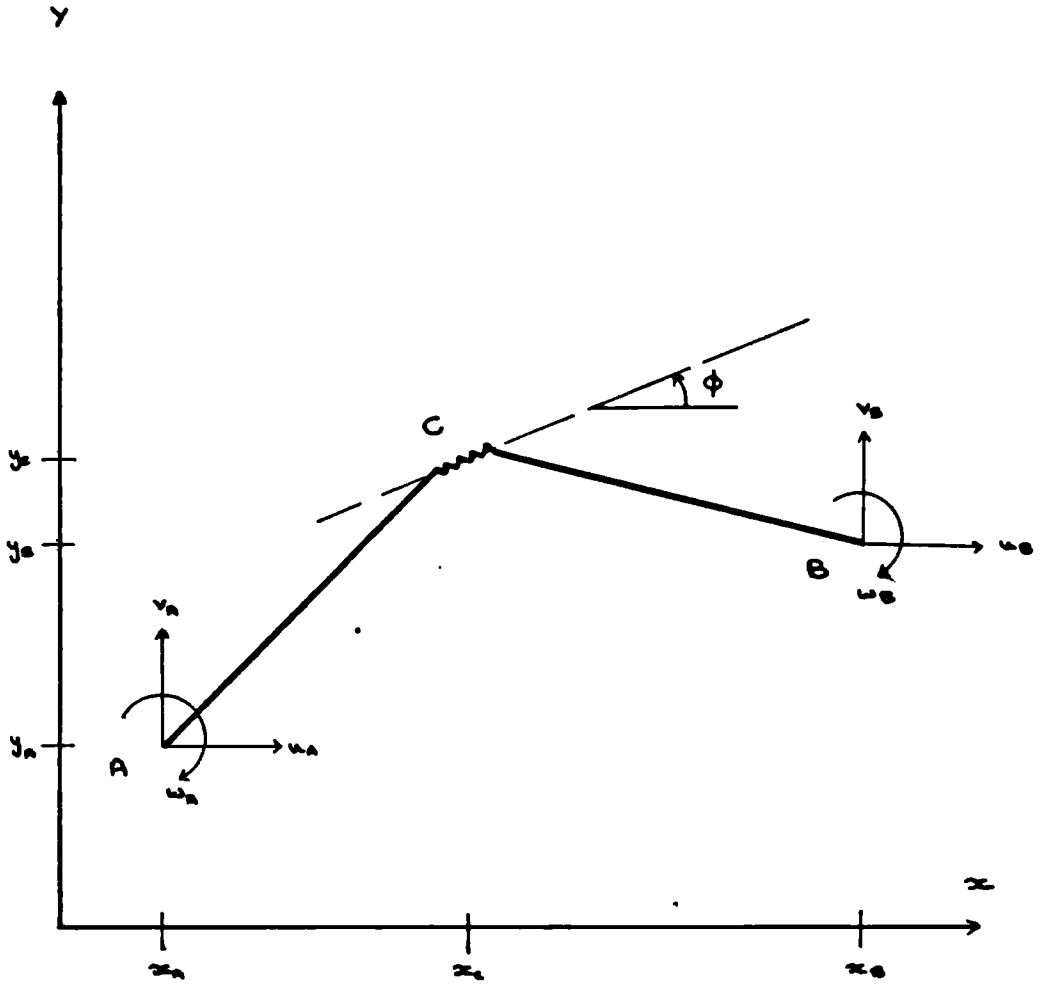

$\ell = x_c - x_A$ $\qquad L = y_c - y_A$

$\ell' = x_B - x_c$ $\qquad L' = y_B - y_c$

FIG. 9.5 :- ARBITRARY SHAPE AND POSITION OF DEFORMABLE ELEMENT OF STRUCTURAL MODEL MEMBER A-B

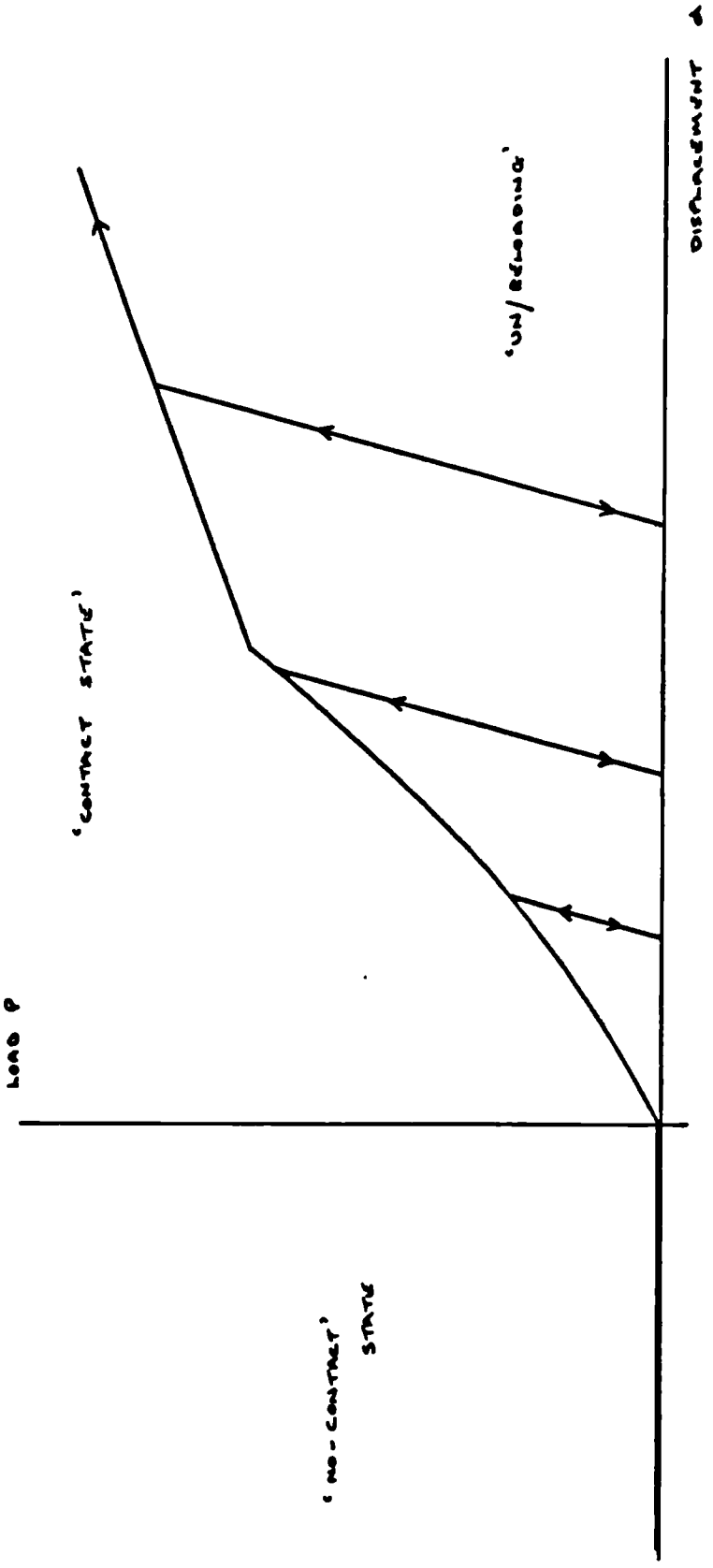

FIG. 9.6 :- CONTACT NORMAL LOAD- DISPLACEMENT CURVE

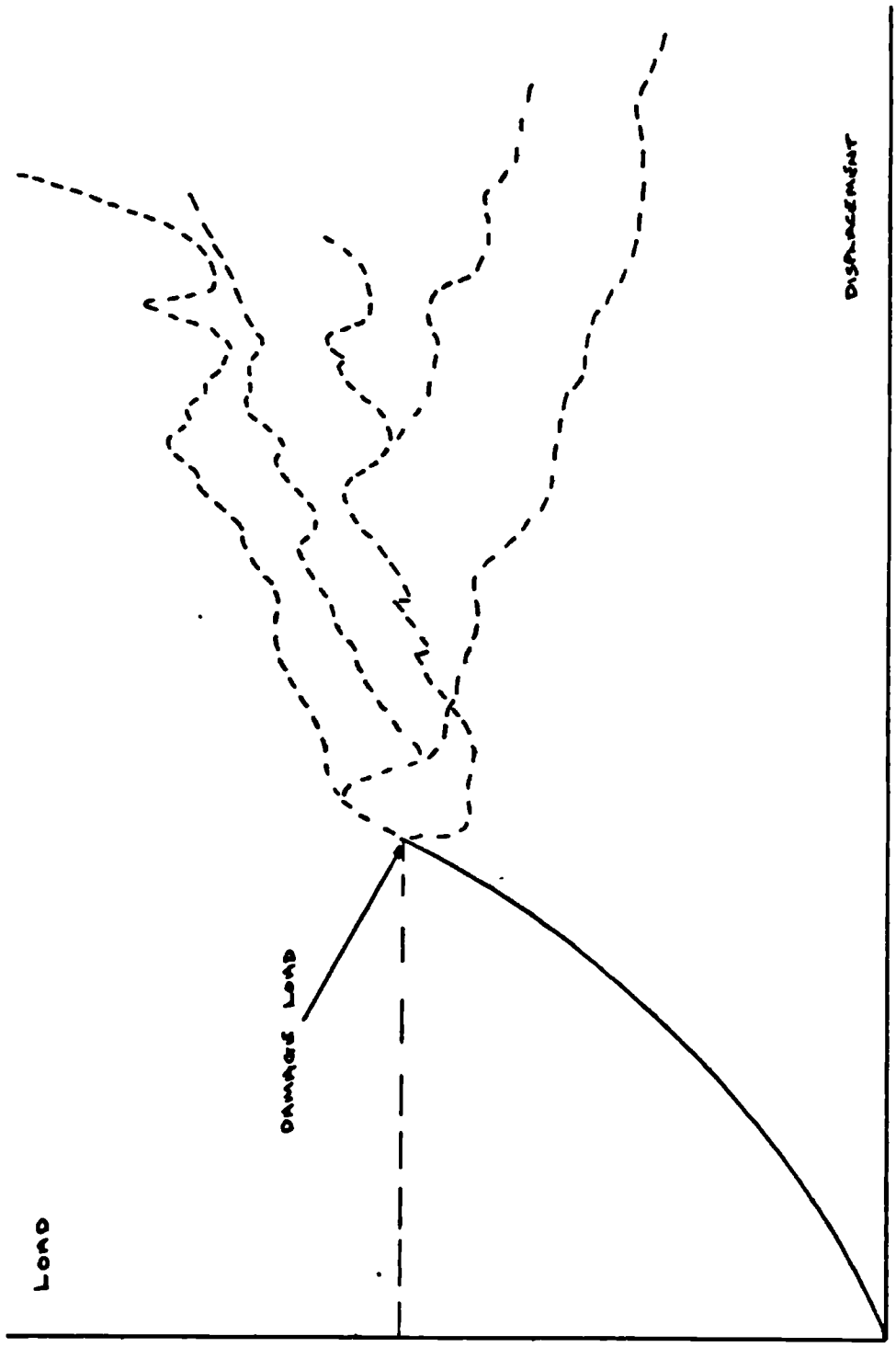

FIG. 9.7 :- TYPICAL CONTACT NORMAL LOAD - DISPLACEMENT CURVES TAKEN FROM EXPERIMENTAL RESULTS

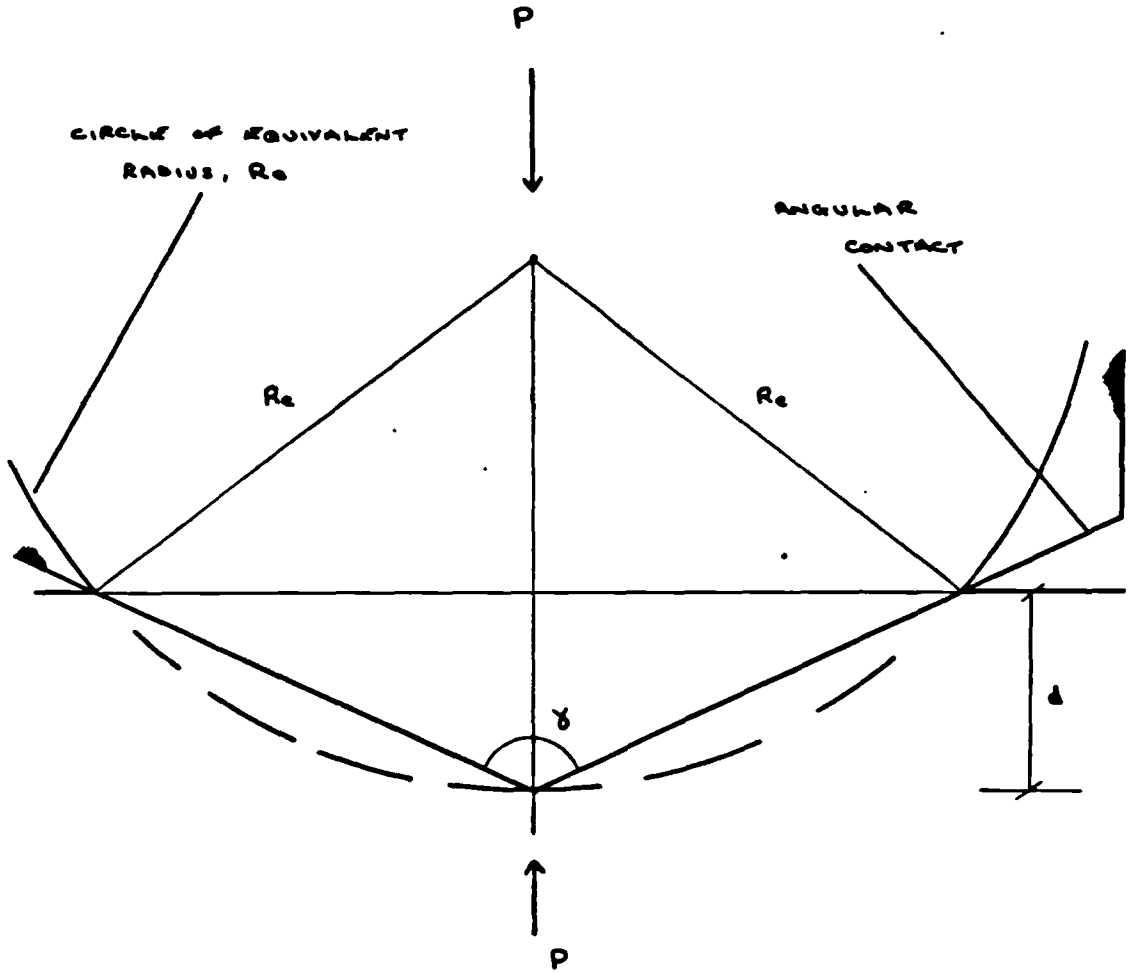

$$\gamma = 2 \tan^{-1}\left(\sqrt{R_e^2 - (R_e - d)^2}/d\right)$$

$$d = P^{2/3} D^{2/3} \left(\frac{1}{R_e}\right)^{1/3}$$

FIG. 9.8 :- THE EQUIVALENT RADIUS, R_e, OF A CONTACT WITH APEX ANGLE γ

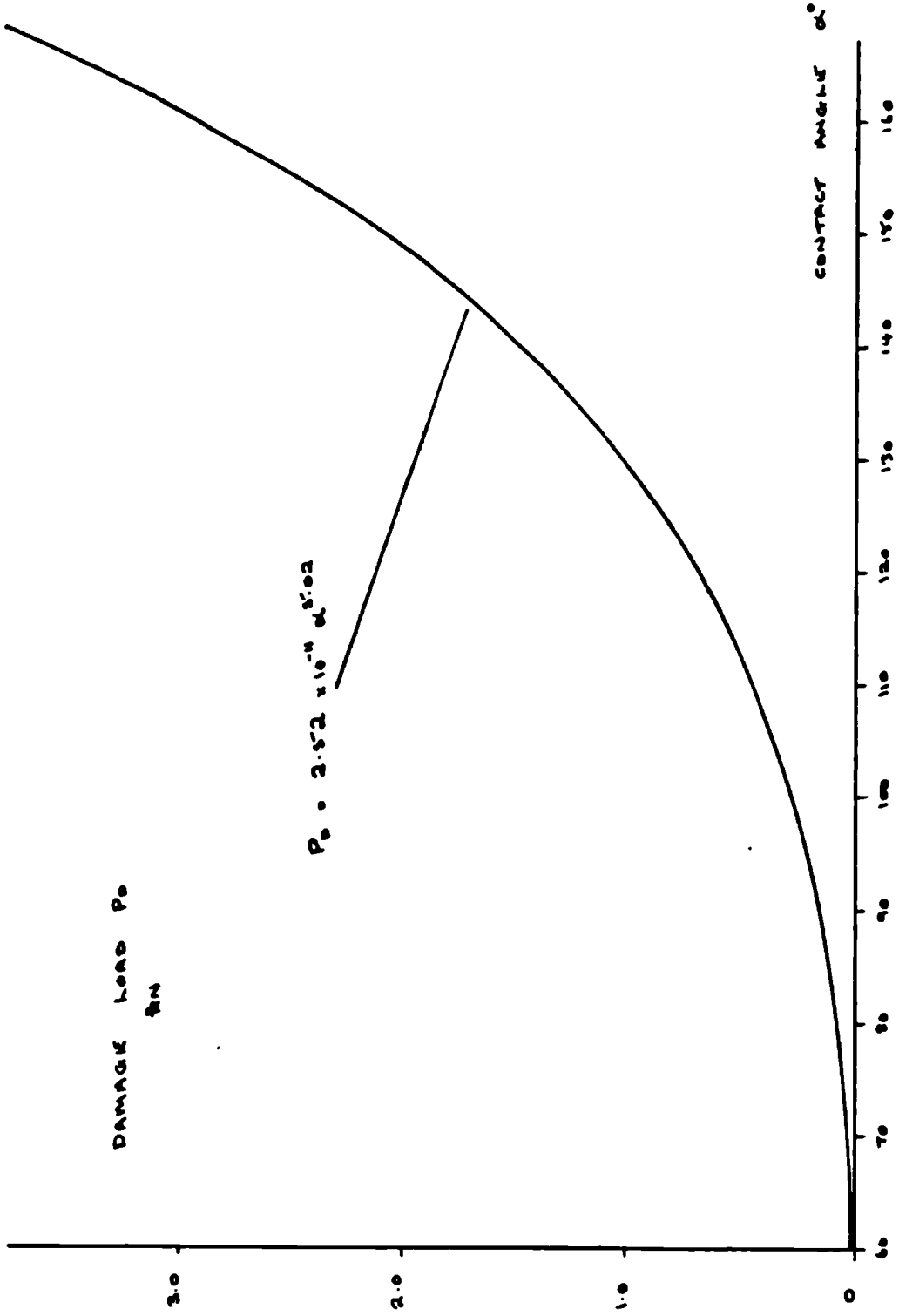

FIG. 9.9 :- VARIATION OF CONTACT DAMAGE LOAD WITH ANGLE OF CONTACT

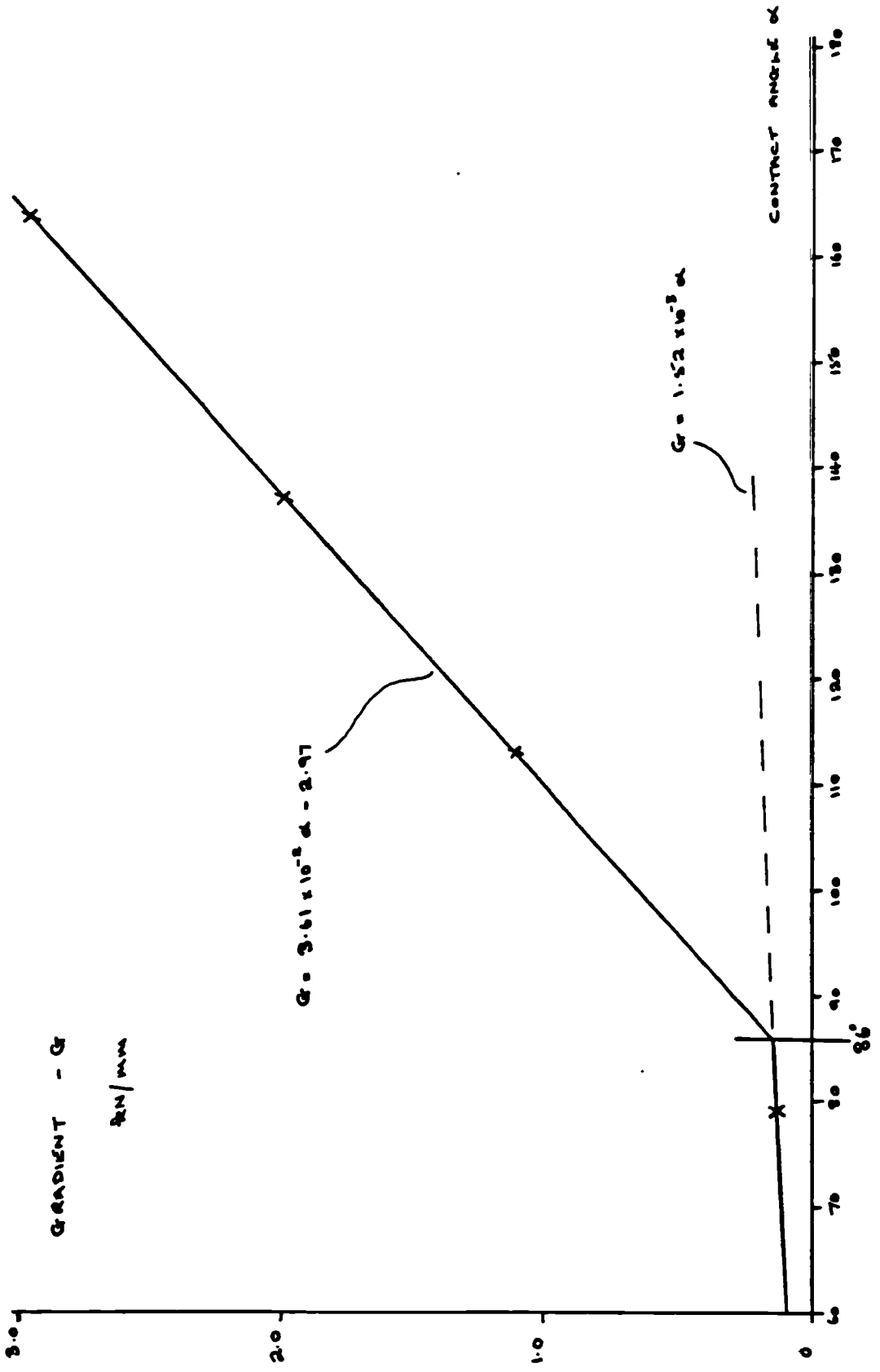

FIG. 9.10 :- VARIATION OF POST-DAMAGE LOAD GRADIENT OF LOAD-DISPLACEMENT CURVE WITH ANGLE OF CONTACT

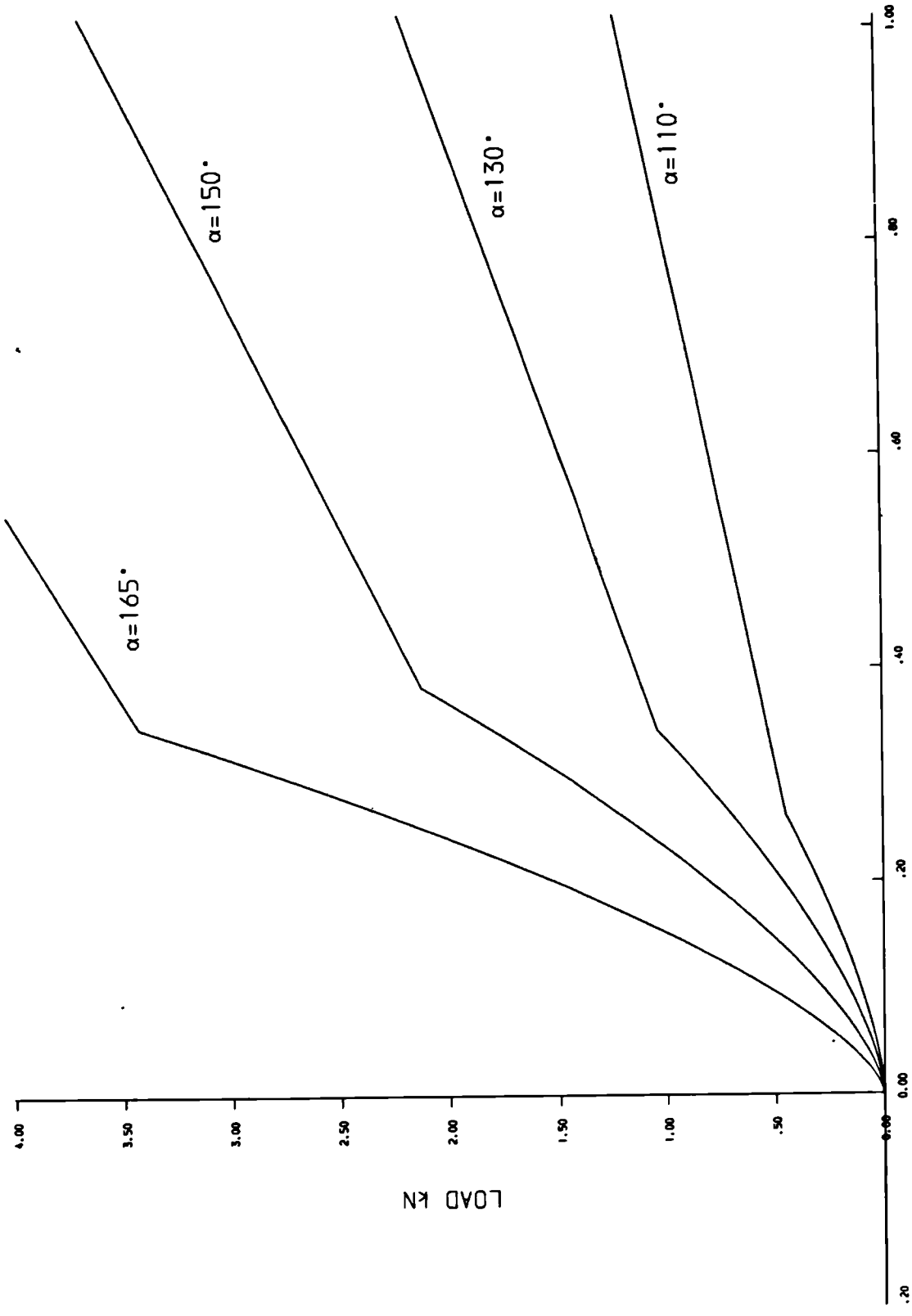

FIG.9.11 : CONTACT NORMAL LOAD-DISPLACEMENT CURVES FOR DIFFERENT CONTACT ANGLES

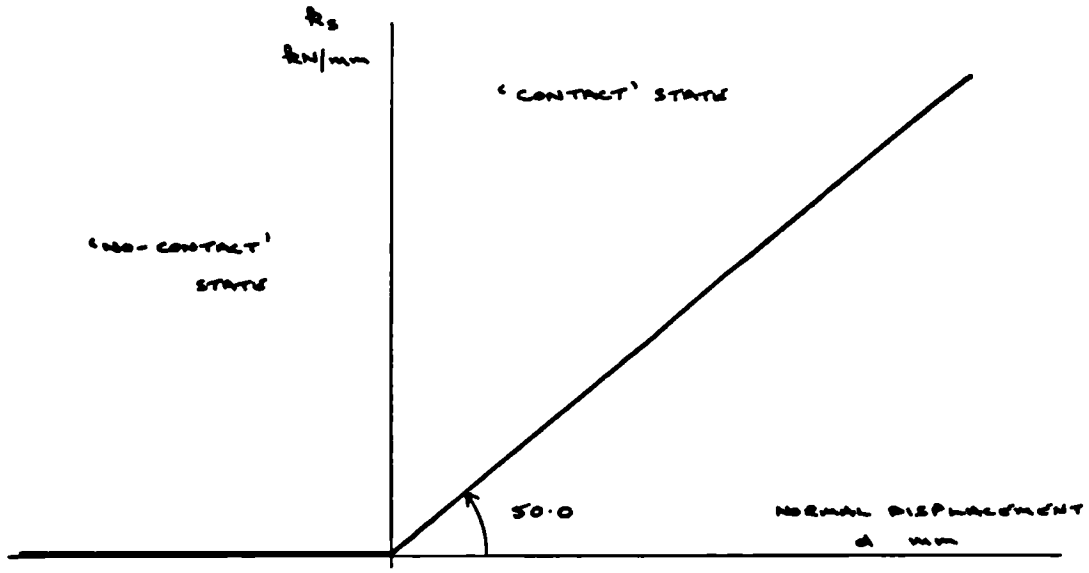

FIG. 9.12 :- PROPOSED RELATIONSHIP FOR SHEAR STIFFNESS k_s

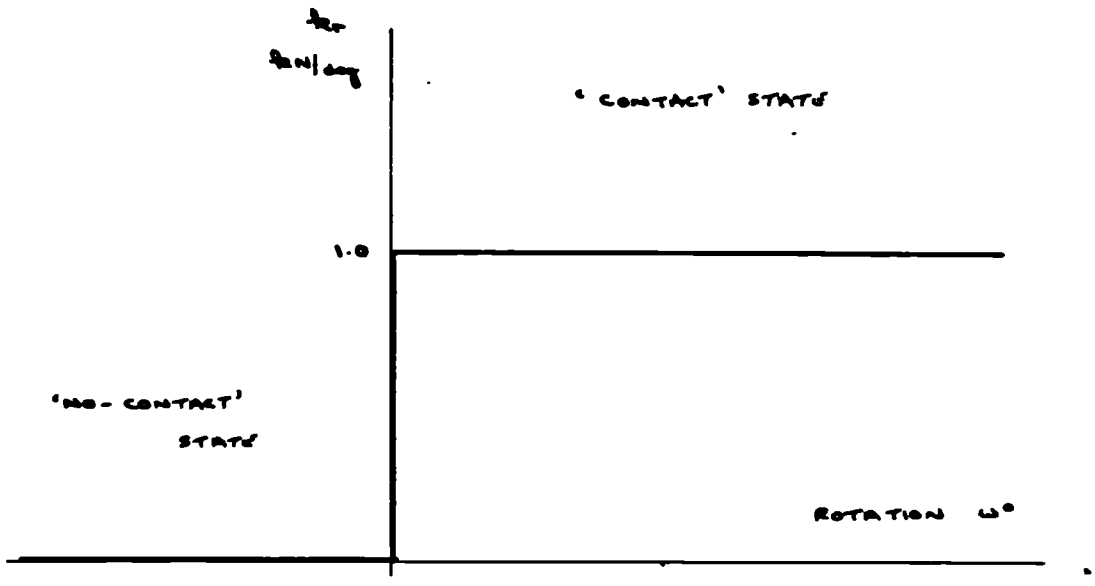

FIG. 9.13 :- PROPOSED RELATIONSHIP FOR ROTATIONAL STIFFNESS k_r

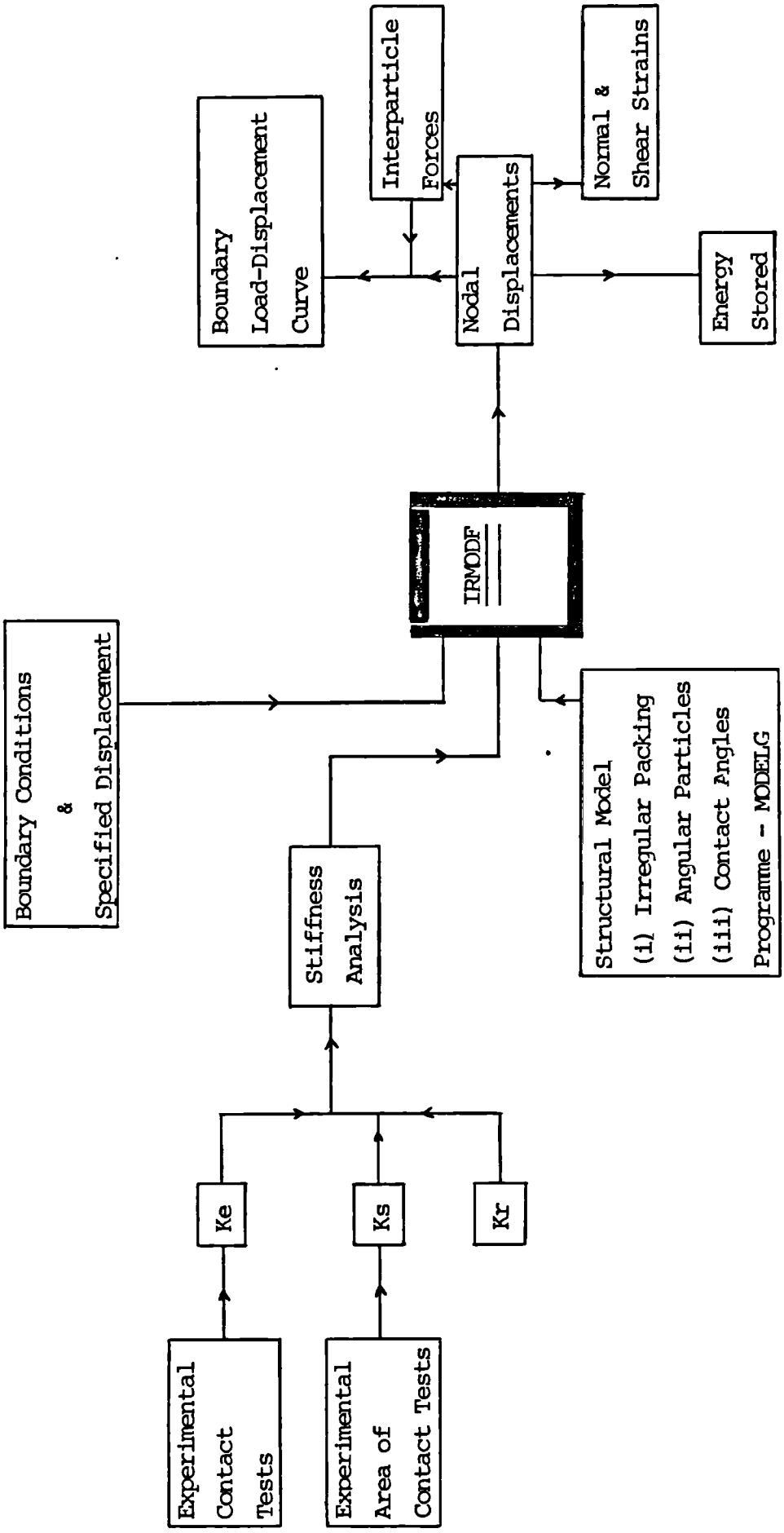

Fig.9.14 :- Role of Programme IRMODF in Modelling an Oedometer Test

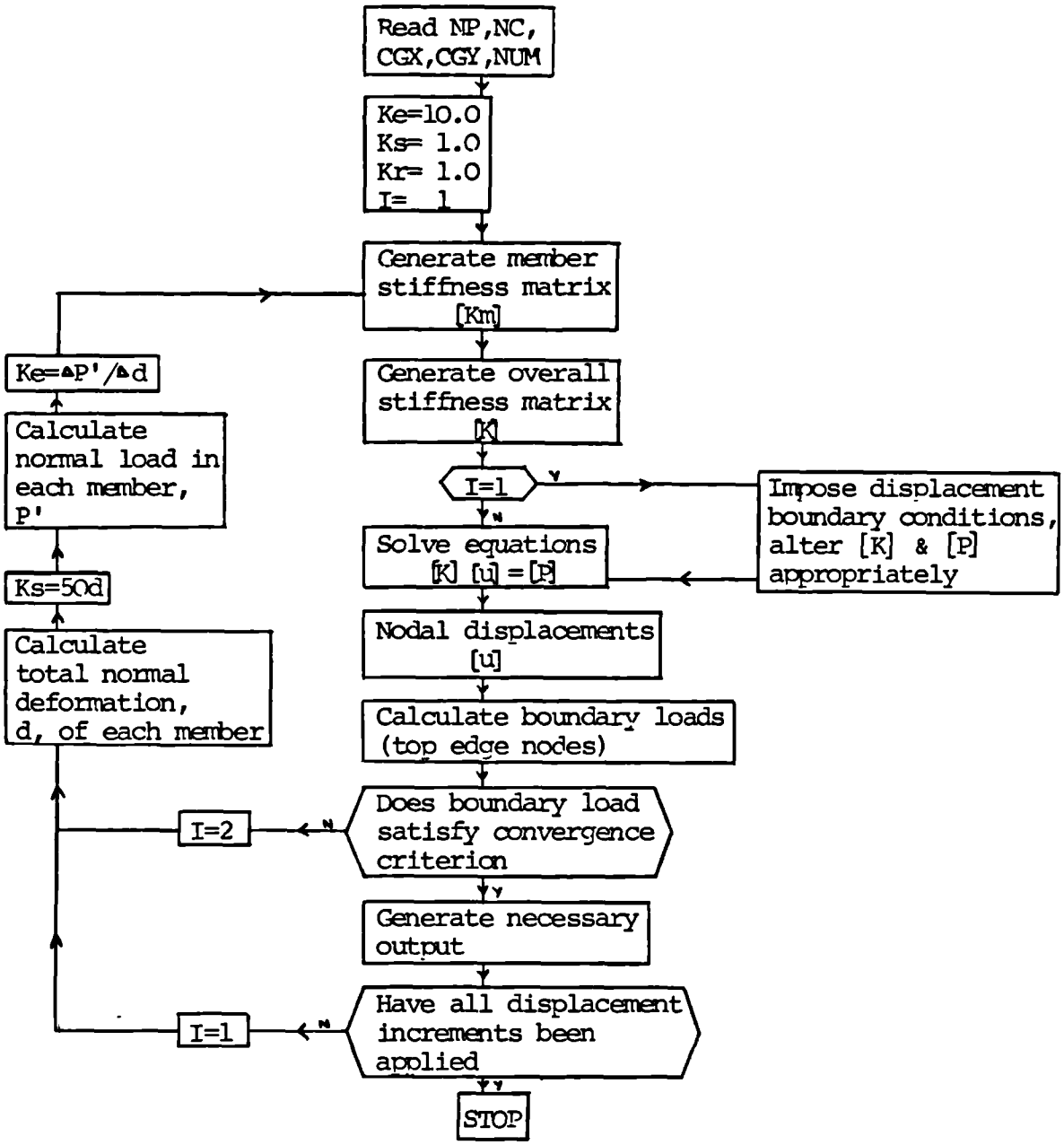

NP - no. of particles
NC - no. of contacts for each particle
NUM - numbers of particles in contact with each particle
CGX,CGY - coords of particle centres
Ke - extension stiffness
Ks - shear stiffness
Kr - rotational stiffness
[K] - overall stiffness matrix
[Km] - member stiffness matrix
[P] - nodal load matrix
[u] - nodal displacement matrix

Fig.9.15 :- Flowchart of Programme IRMODF

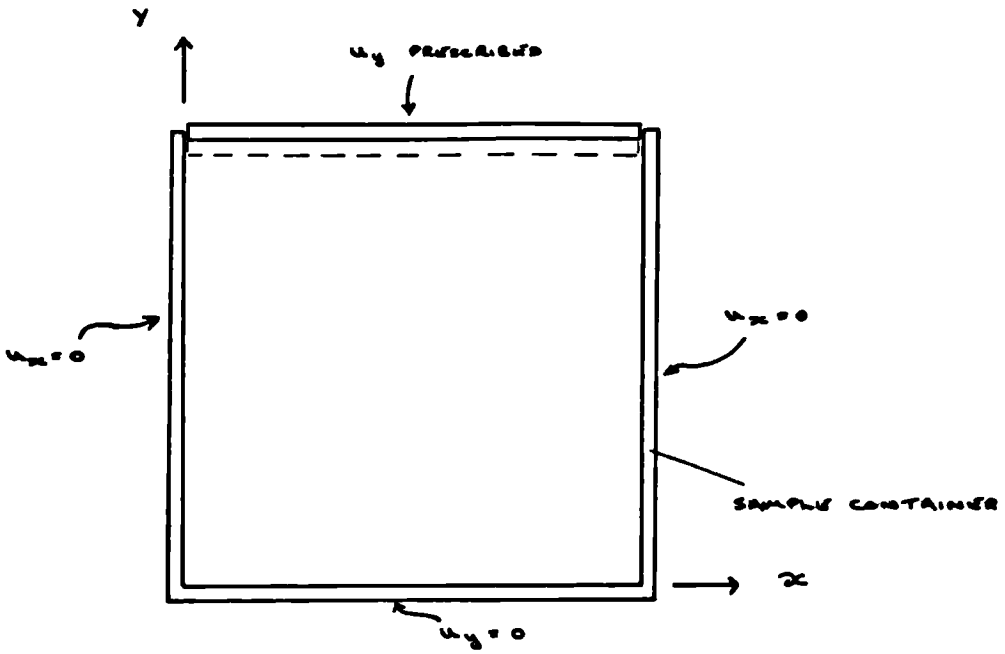

FIG. 9.16 :- BOUNDARY CONDITIONS APPLYING TO OEDOMETER SAMPLE MODEL

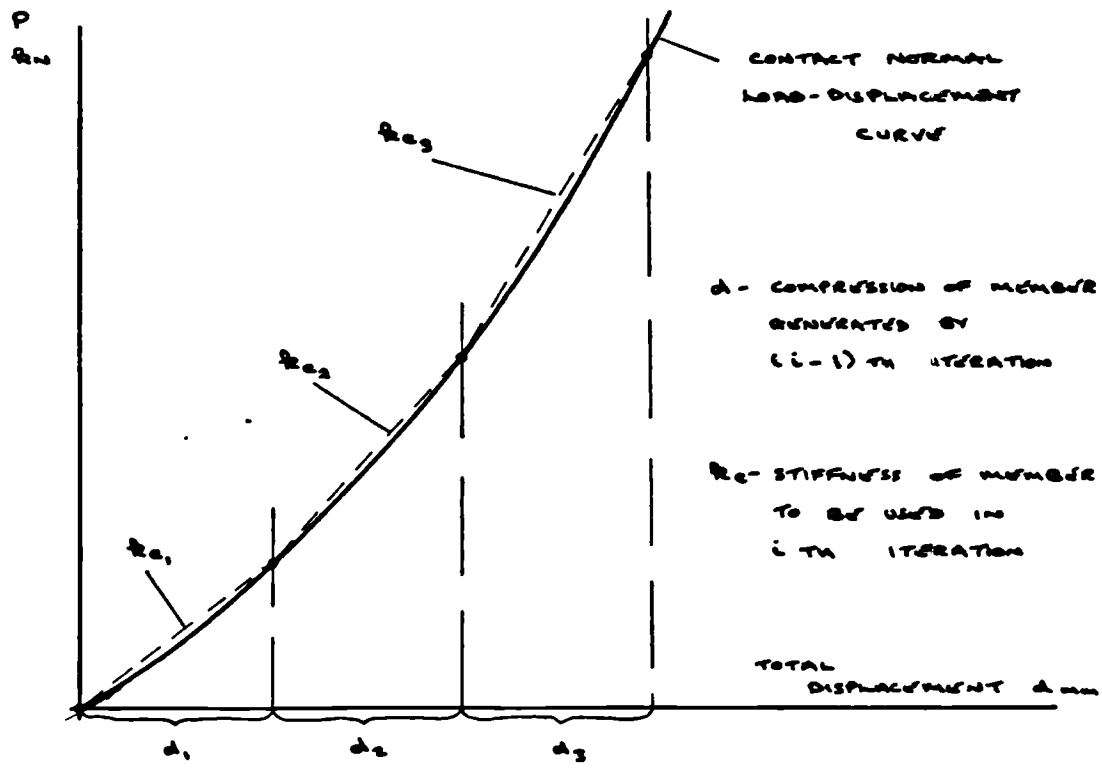

FIG. 9.17 :- CALCULATION OF EXTENSION STIFFNESS, R_e, BY INCREMENTAL SECANT APPROACH

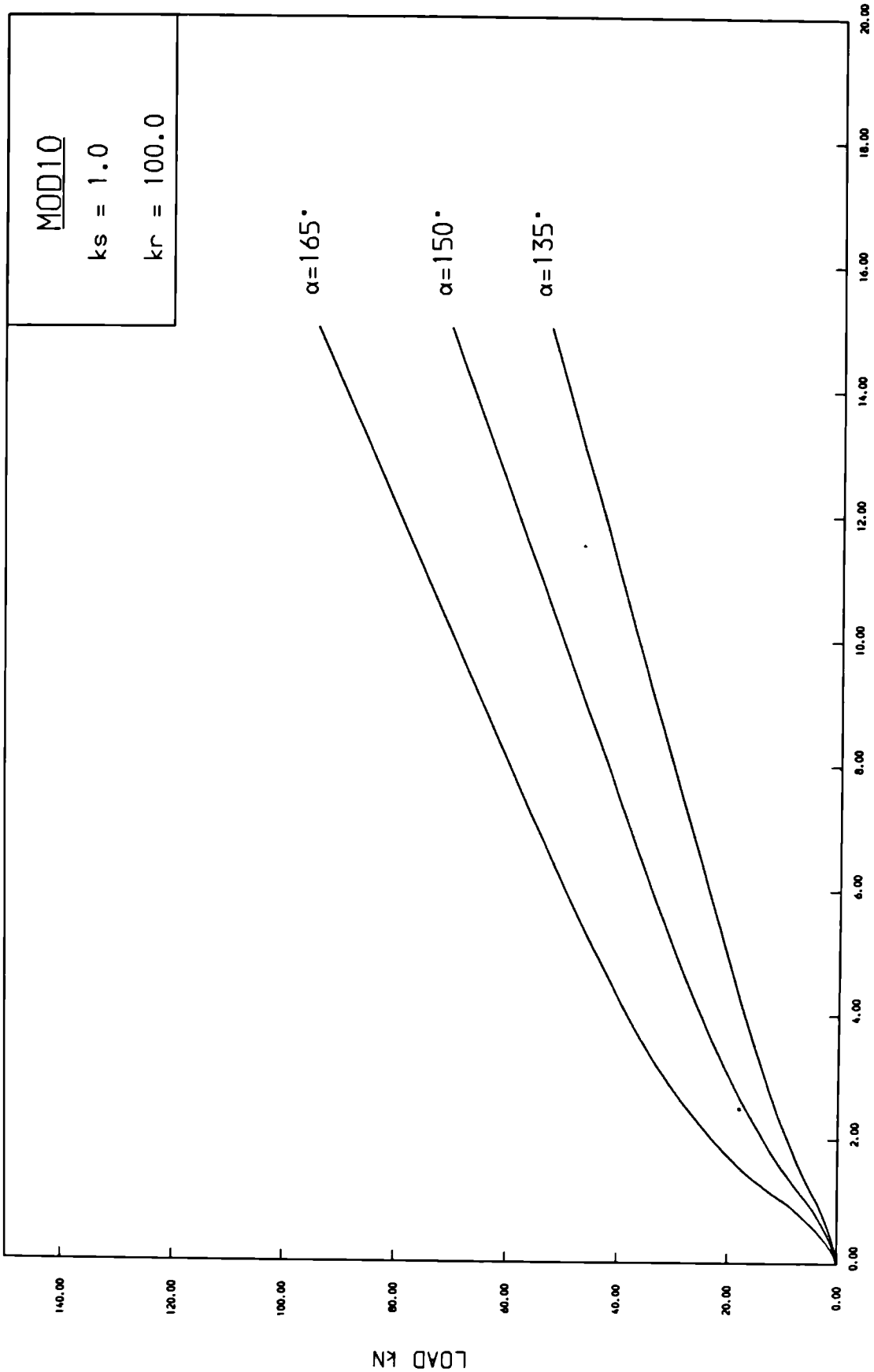

FIG.9.18 : SENSITIVITY OF STIFFNESS ANALYSIS TO CONTACT ANGLE

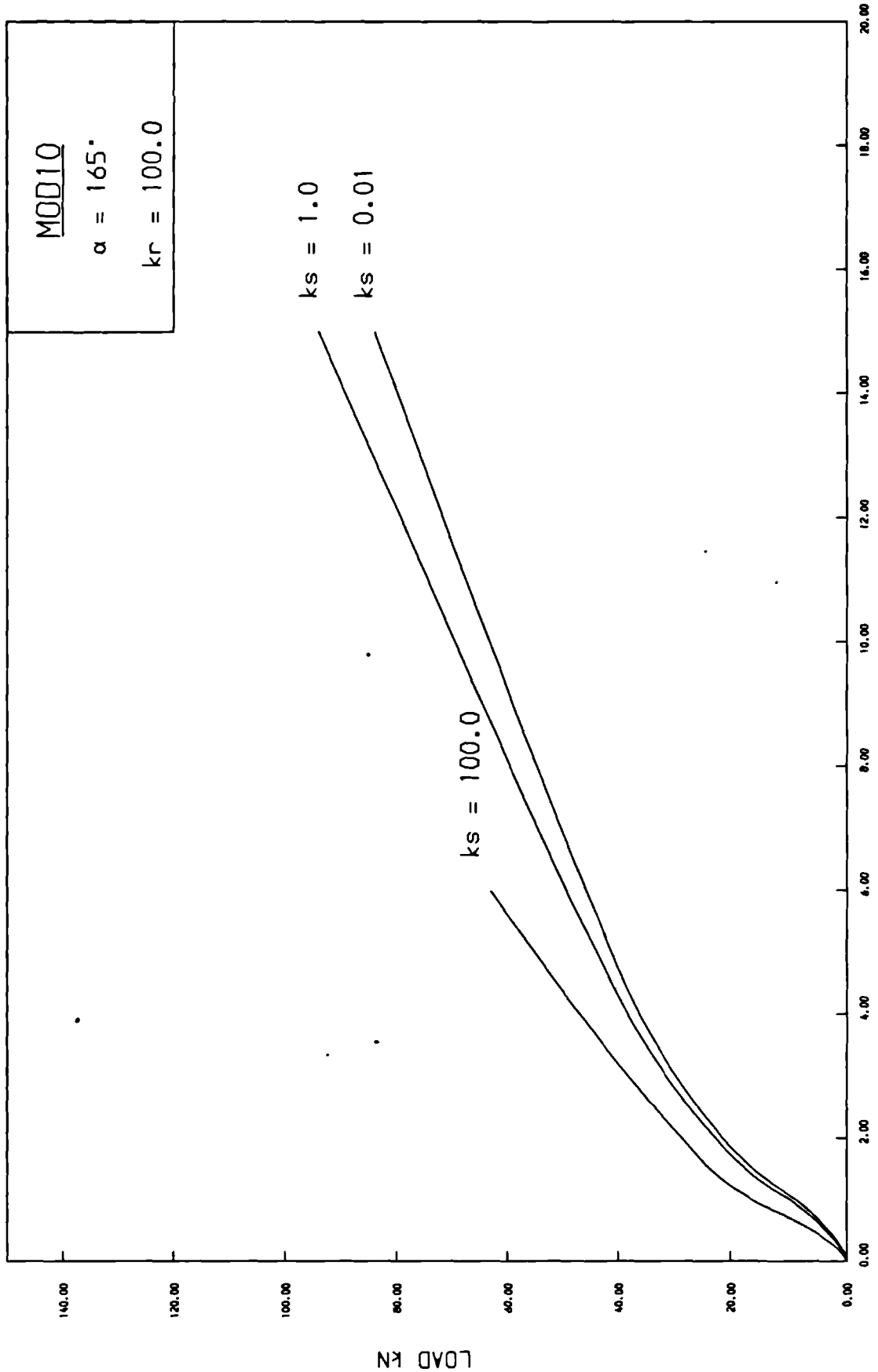

FIG.9.19 : SENSITIVITY OF STIFFNESS ANALYSIS TO SHEAR STIFFNESS, ks

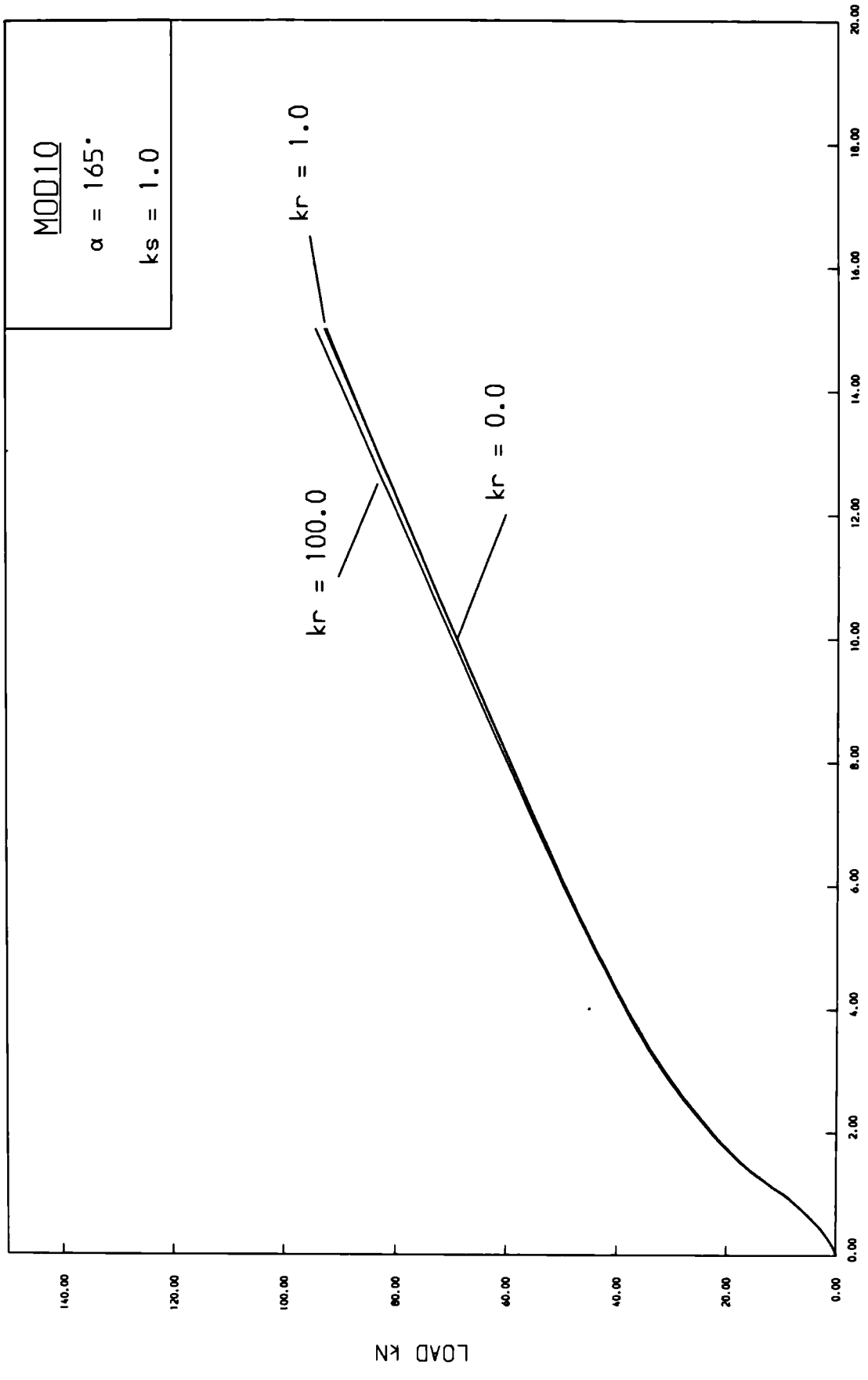

FIG.9.20 : SENSITIVITY OF STIFFNESS ANALYSIS TO ROTATIONAL STIFFNESS, kr

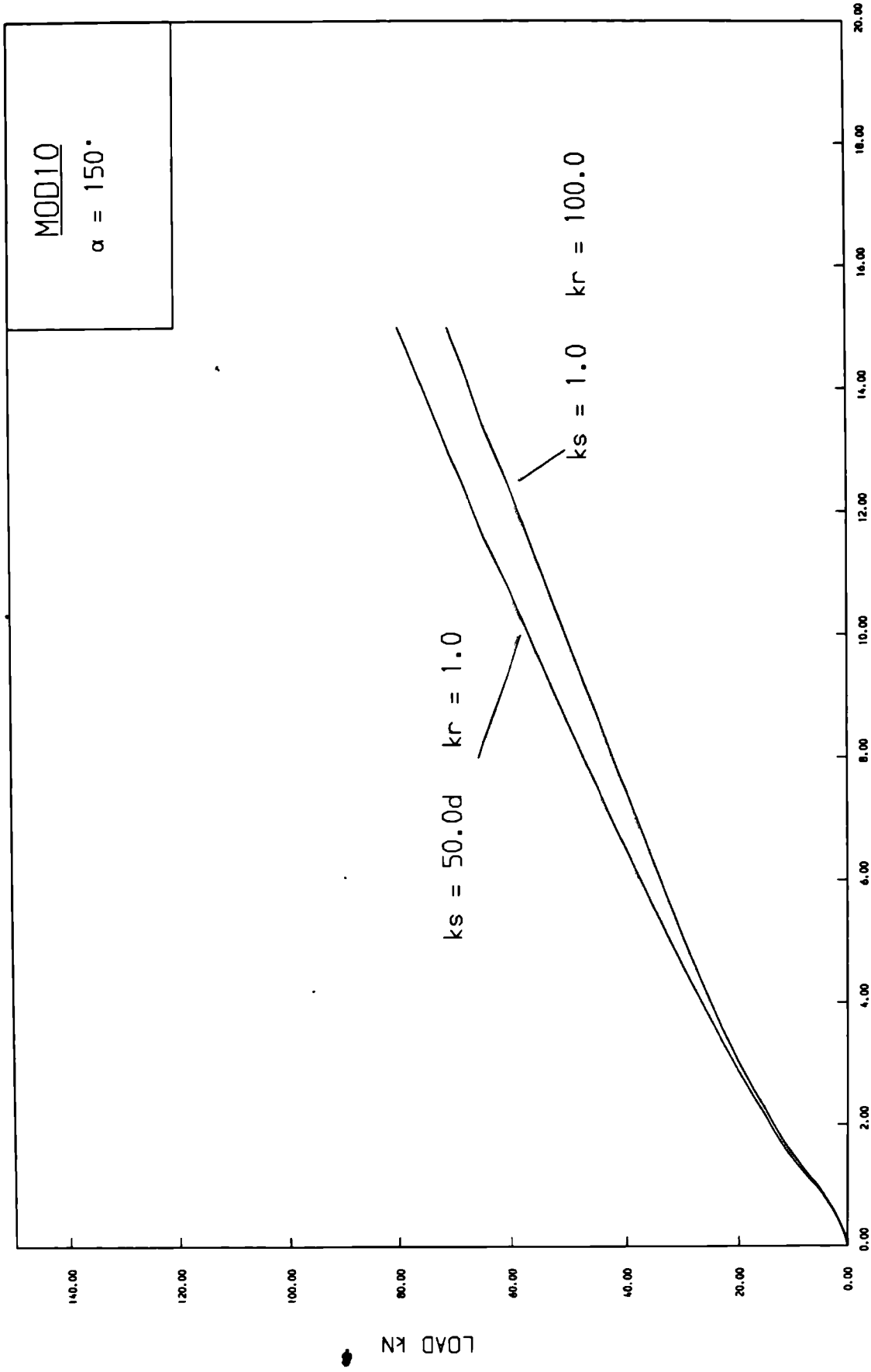

FIG.9.21 : COMPARISON OF ANALYSIS RESULTS FOR ksad AND CONSTANT ks

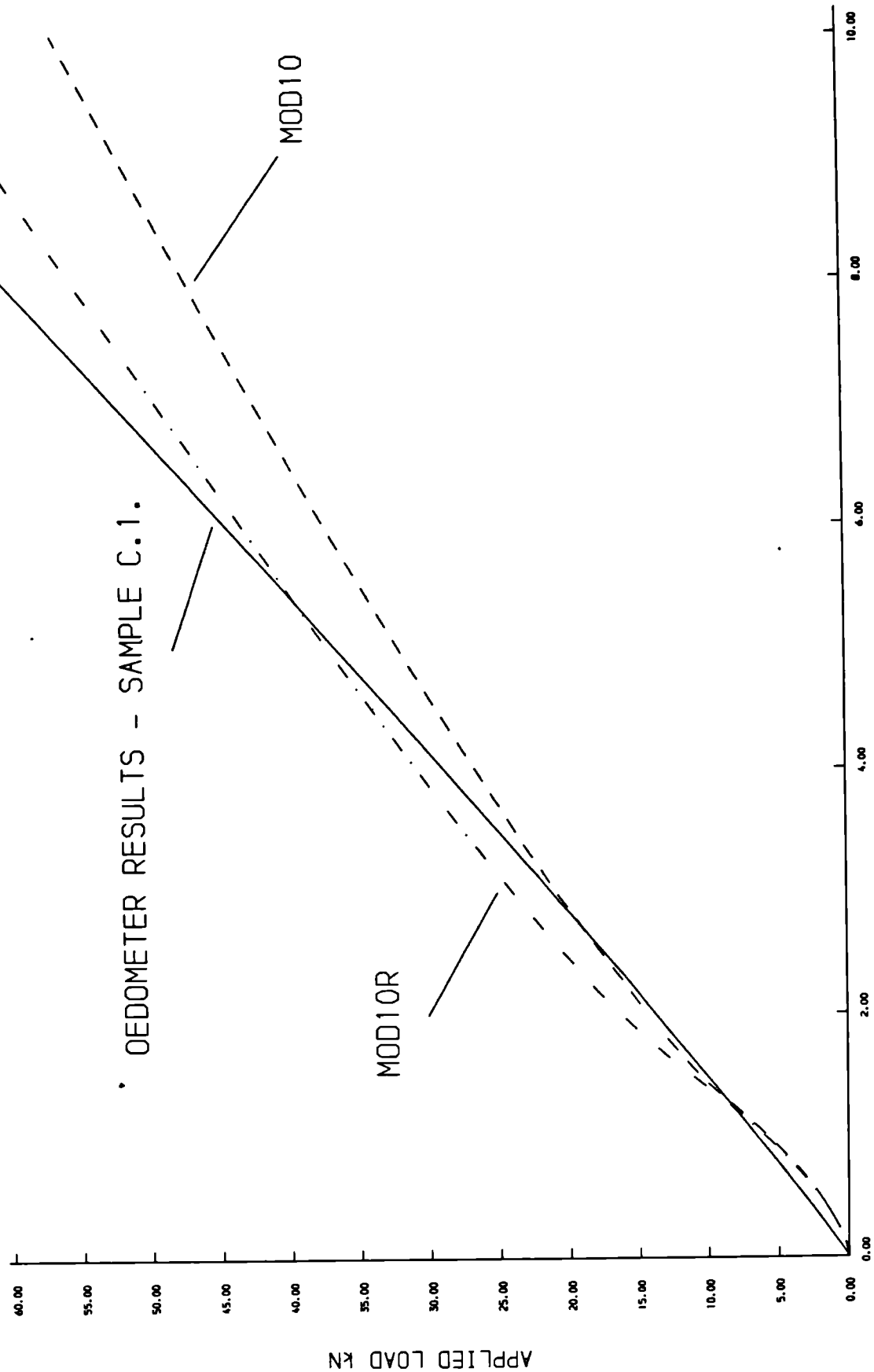

FIG.9.22 : COMPARISON OF EXPERIMENTAL AND MODEL LOAD-DISPLACEMENT CURVES

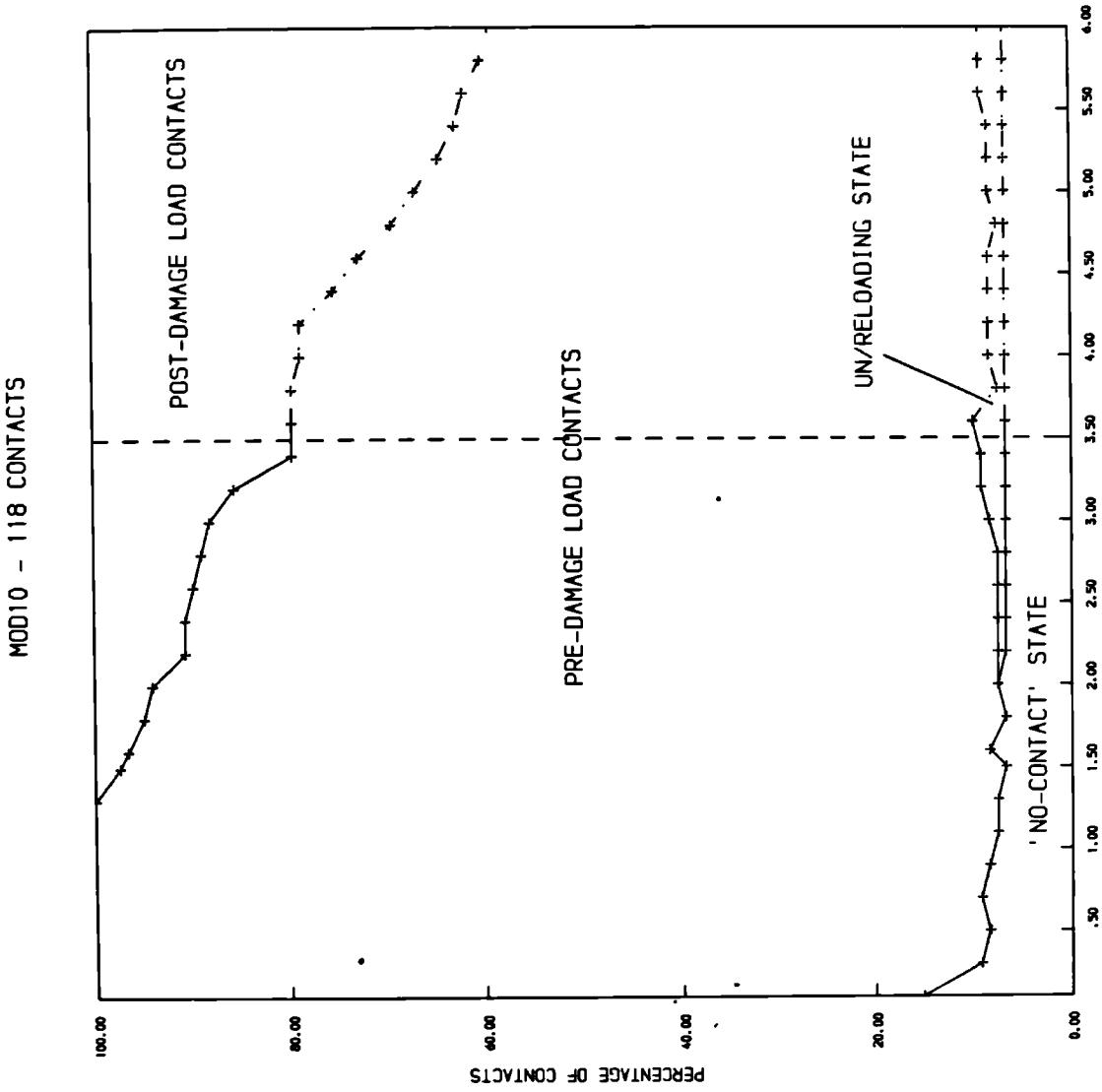

FIG.9.23 • CHANGE OF MODEL CONTACT STATES WITH APPLIED DISPLACEMENT - MOD10

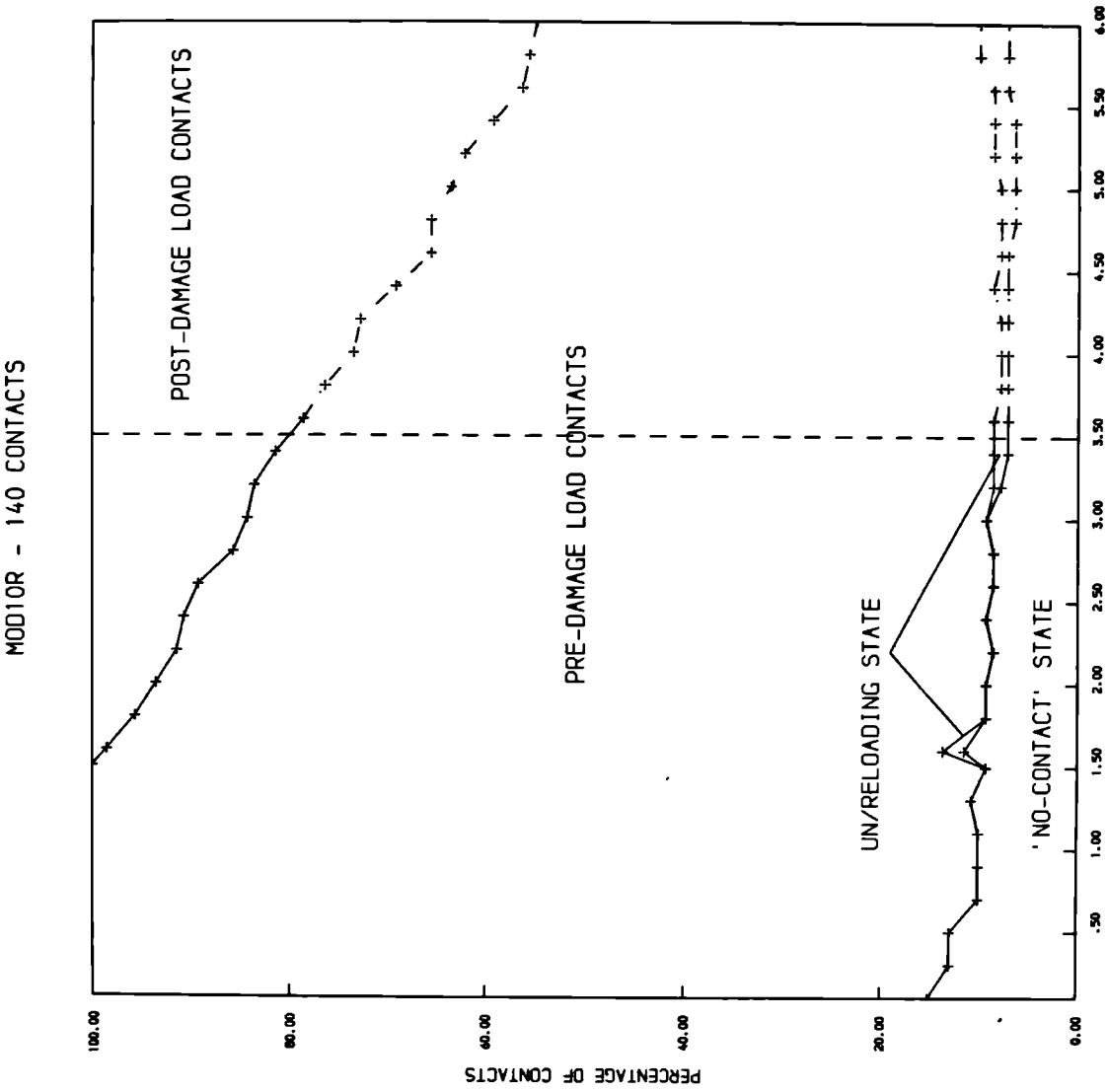

FIG.9.24 : CHANGES OF MODEL CONTACT STATES WITH APPIED DISPLACEMENT - MOD10R

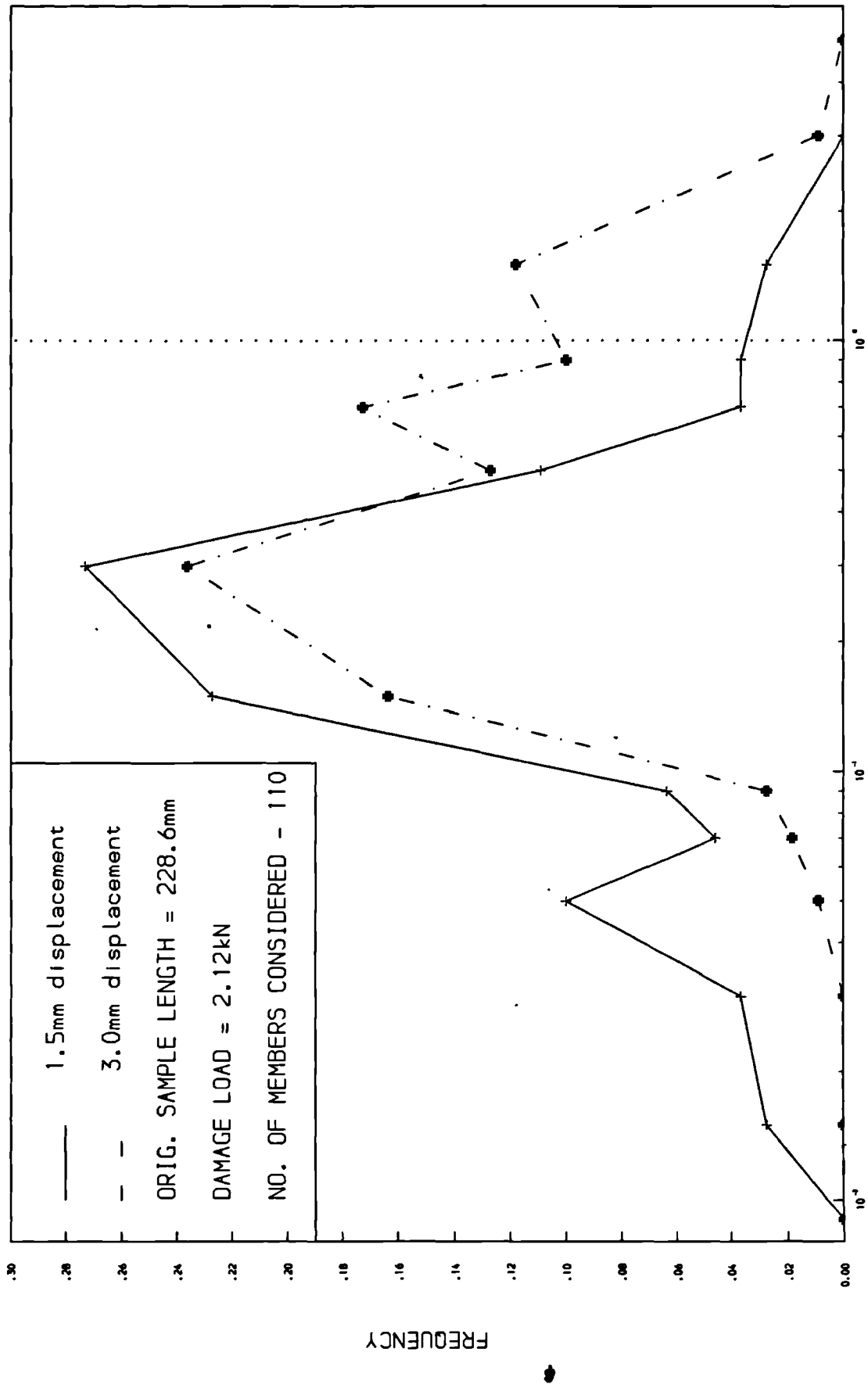

FIG.9.25 : DISTRIBUTION OF CONTACT FORCES IN MOD10 AT TWO APPLIED DISPLACEMENTS

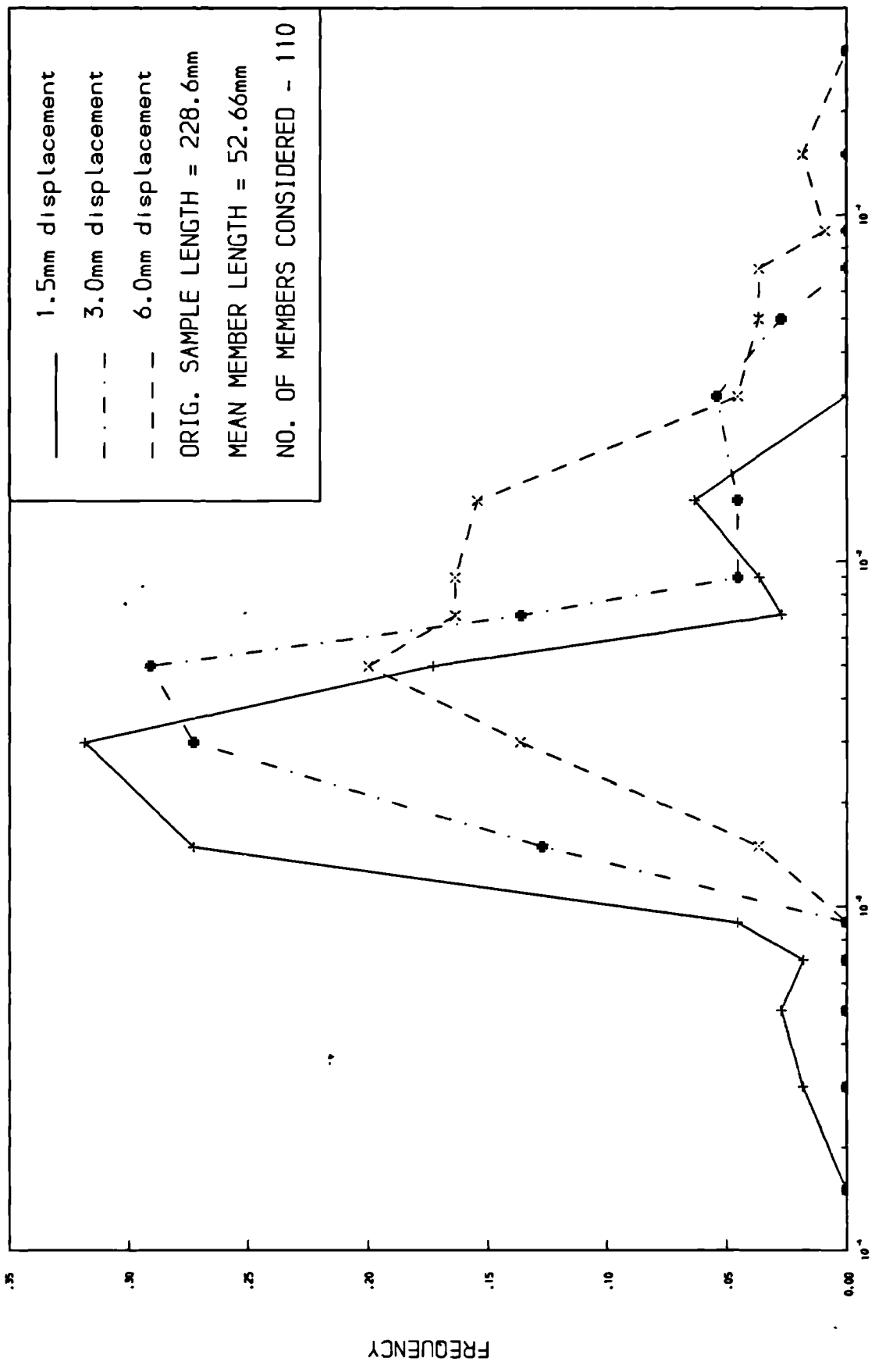

FIG.9.26 : DISTRIBUTION OF NORMAL STRAIN IN MOD10 AT THREE APPLIED DISPLACEMENTS

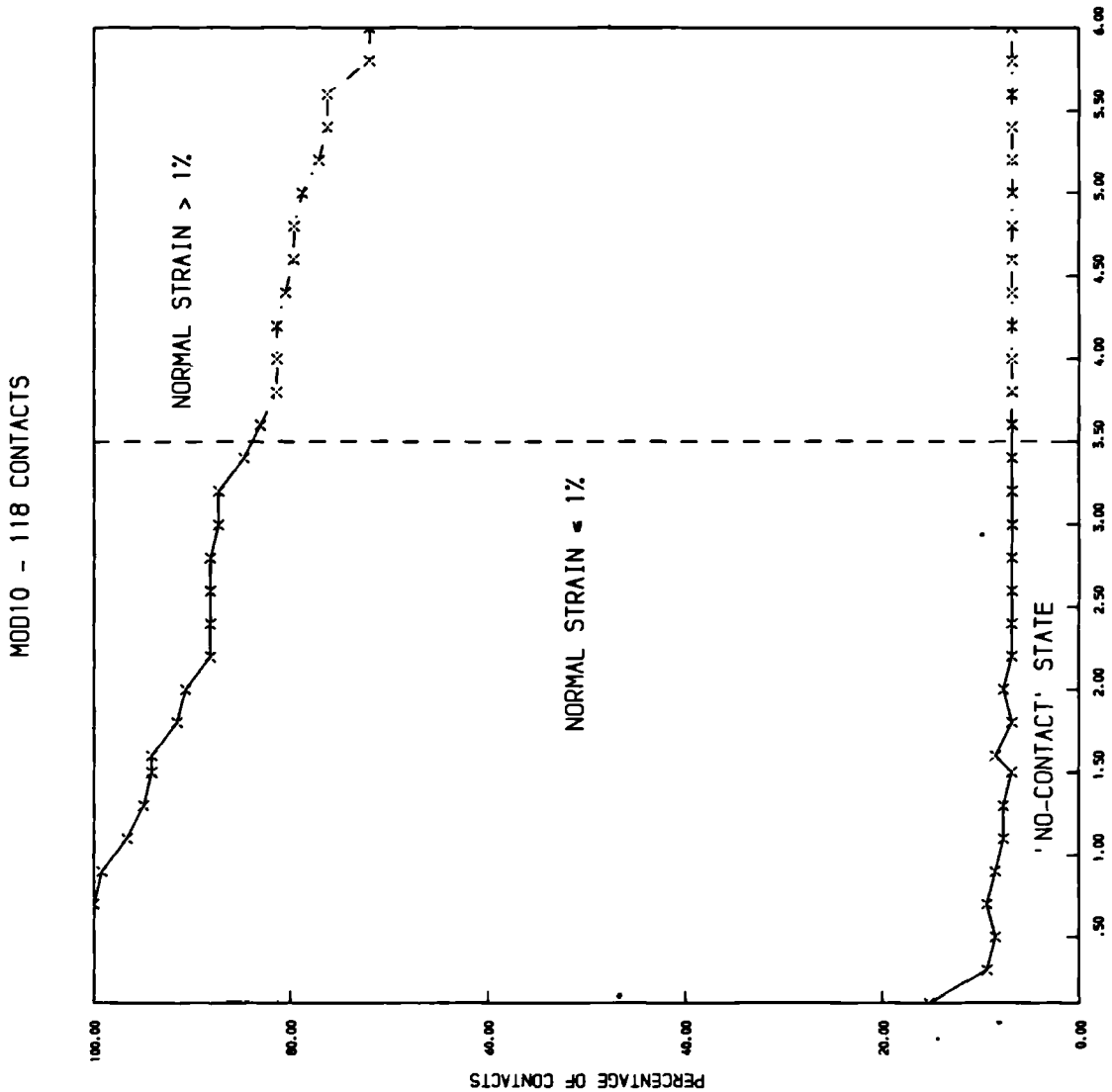

FIG.9.27 : VARIATION WITH APPLIED DISPLACEMENT OF PERCENTAGE OF MOD10 MEMBERS WITH NORMAL STRAINS > 1%

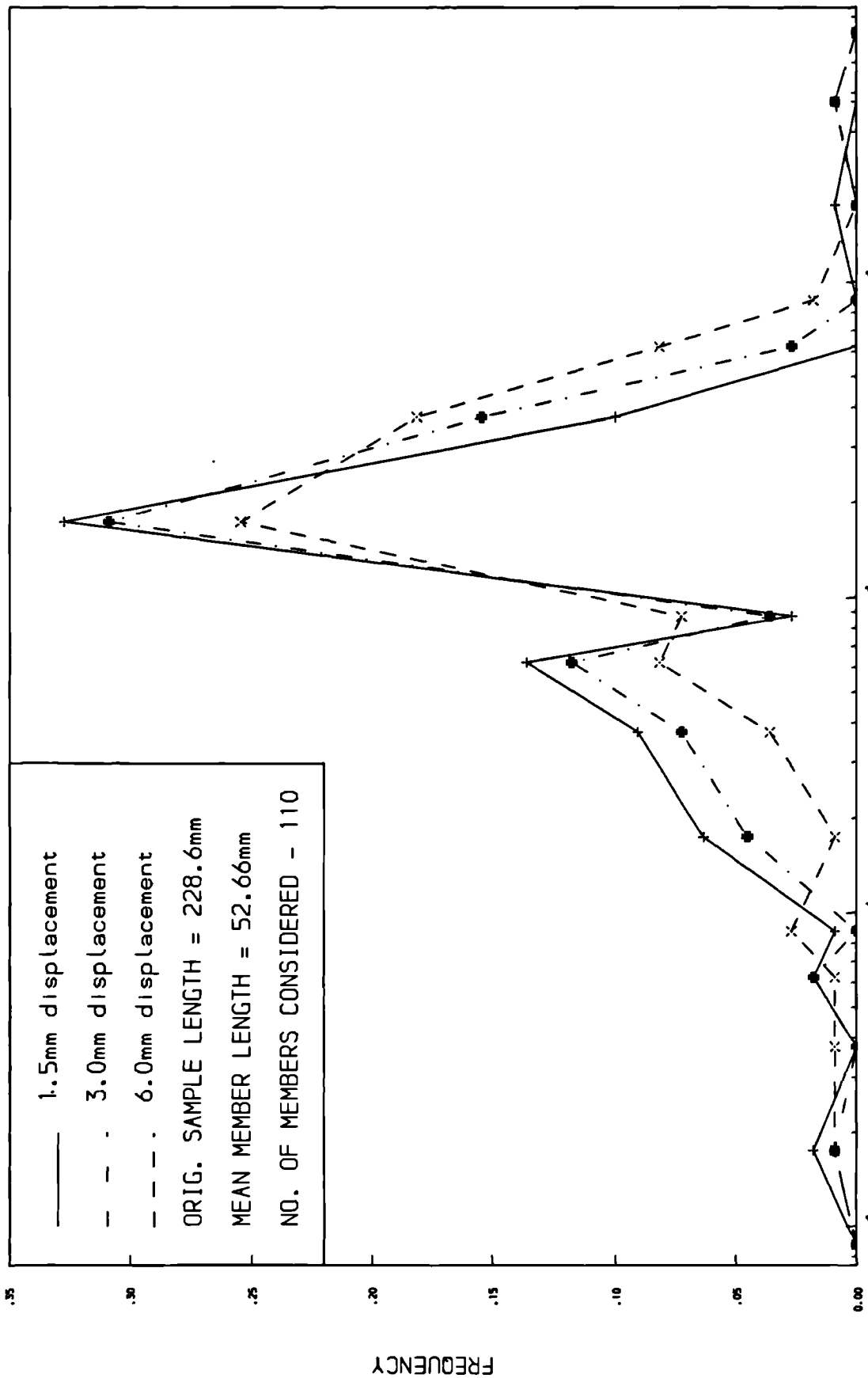

FIG.9.28 : DISTRIBUTION OF SHEAR STRAIN IN MOD10 AT THREE APPLIED DISPLACEMENTS

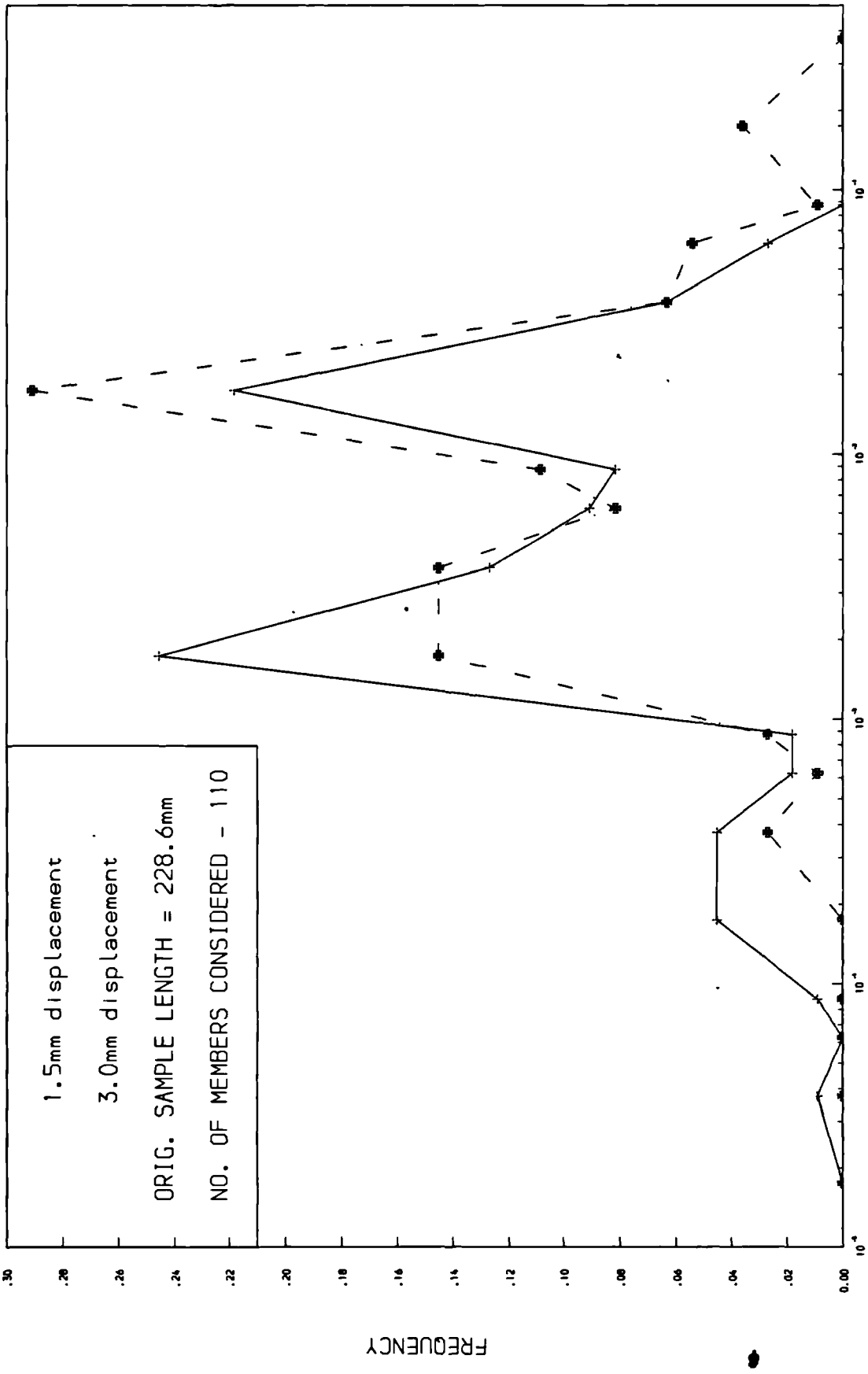

FIG.9.29 : DISTRIBUTION OF ENERGY STORED IN MOD10 MEMBERS AT TWO APPLIED DISPLACEMENTS

Chapter 10

Summary of Research and Conclusions

The work presented in this thesis has been concerned mainly with the interparticle behaviour of granular masses and of rockfill in particular. Attention has been focused on the phenomenon of contact crushing due to normal interparticle forces and the influence of this on the overall behaviour of the mass. A study of the bulk behaviour of rockfill in dams and in a series of long-term uniaxial compression tests has also been made. The results of this work led to the development of a numerical computer model of rock fill, intended for use as an aid to prediction of both overall and local behaviour.

10.1 Outline of Research

10.1.i Interparticle Behaviour

Interparticle behaviour may be considered to depend upon the amount of contact crushing and the rolling and sliding of particles relative to each other. The experimental work was concentrated on contact crushing and although the role of rolling and sliding has been discussed, this has not been investigated in any detail.

Laboratory tests have been carried out to establish a normal load-displacement relationship for rock contacts (Chapter 4). A number of shaped and irregular pointed samples were pushed either against a steel platen or the end of a cylinder of the same material. Tests were performed on both dry and saturated samples and some of the dry samples were inundated during testing. The displacements were found to depend upon the contact shape and since the particles being tested were angular, the shape has been defined in terms of a contact angle. The results have been compared with theoretical normal load-displacement relationships of elastic and plastic bodies in contact. The relationship proposed by Hertz, (1896) for elastic contacts, of the form

$$d \propto P^{\frac{2}{3}}$$

d - displacement

P - load

was found to be similar to that determined from the tests and has been discussed in some detail.

When a force is applied at a contact a region of high stress is created and the local material is crushed until the area of contact becomes large enough to support the load. Two methods of determining this area have been investigated in Chapter 5. The first involved crushing rock points against a metal platen and interposing pieces of carbon paper. The contact areas were determined by measuring the areas of the imprints. As before, shaped and irregular samples were tested and some of the irregular samples were saturated. The main disadvantages of this method were that the imprints were often torn or smudged and that the contact region was disturbed whenever the carbon paper was replaced. The second method was based on a graphical analysis which produced an upper bound approximation to the contact area. Measurements of the rock on rock contact region widths at a series of points around the samples were made from photographs and used in a computer programme to calculate the area magnitude. This method was found to be very sensitive to errors in the data and the results were not as reliable as those obtained using the first method. The results of the first method have been discussed in the light of the load-displacement behaviour and the influence of saturation, contact shape and material strength have been investigated. As before, comparisons of the results have been made with theoretical relationships and in particular with the elastic solution

$$A \propto P^{\frac{2}{3}}$$

The time-dependent behaviour of contacts has also been investigated and a rig was designed to carry out these tests (Chapter 6). The differencesin behaviour between dry and saturated samples under constant load for three - four hours were noted and particular attention paid to the effect of inundation and drying of the samples. Some samples were subjected to several different loads to determine the effect of increased and decreased load. Relaxation tests on four shaped samples (two dry and two saturated) were carried out for periods of seventy-two hours.

The material used in all these tests was a sandstone

obtained from the site of Scammonden Dam, Yorkshire. Chapter 3 describes a series of tests carried out to determine the material properties and to classify the rock. Other tests described are an investigation of the properties of the sandstone as a granular material.

10.1.ii Intra-particle Behaviour

In discussing interparticle behaviour it is necessary to assess the relative importance of the intra-particle deformations. These are observed as the bulk deformations of each particle under the interparticle forces and the breakage of particles when the stresses within the particles exceed the material strength.

In Chapter 3 details are given of the tests carried out to determine the immediate bulk deformations of cylindrical samples and values of the Young's modulus and Poisson's ratio for the material have been calculated. Tests described in Chapter 6 were carried out to investigate the time-dependent properties of the bulk material. Dry cylindrical samples were subject to either constant load or constant compressive strain and the creep strains or loss of load recorded over seventy-two hours. The recovery of the creep samples was monitored for a further seventy-two hours after unloading. The results of these tests have been compared with the results from the contact time-dependent tests as an indication of the relative importance of these two phenomena.

Particle breakage has not been considered in as much detail, although the quantities generated in each of the oedometer tests described in Chapter 7 have been calculated (using a measure of breakage proposed by Marsal, 1973) and the relative magnitudes discussed.

10.1.iii The Bulk Behaviour of Rockfill

Investigation of the bulk behaviour of rockfill has been concentrated on two areas;-

(a) rockfill dams

(b) long-term oedometer tests

The movements of rockfill dams can be measured over the whole lifetime of the structure and the observations correlated with various events occurring at the dam site. This enables a picture of the expected behaviour of a large mass of rockfill to be built up and this may be used to predict the movements of new structures. Field data of post-construction movements of sixty-eight dams has been collected in an extensive literature review and analysed (Chapter 2). From this the major influences affecting the behaviour of rockfill dams have been pinpointed and discussed. A review of methods of predicting post-construction crest movements has revealed these to be too simplistic and an alternative approach has been proposed.

Oedometer tests enabled other rockfill behaviour patterns to be studied under a degree of control which is not possible in a literature review. A large oedometer rig with a 0.45 m diameter cylinder for the samples (height:diameter ratio 1:2) was used to test three gradings of rockfill - 1 well graded and 2 uniform. Most of the tests were carried out over four weeks but one of the uniformily graded samples was subjected to a quick cycle of loading and unloading to determine a load-displacement relationship. The long term tests have been used to investigate:-

(a) the influence of saturation and the effect of cycles of wetting and drying

(b) the effect of increased and decreased load

Where possible these results have been related to dam construction practice. The friction generated along the cylinder walls has also been considered and its effect on the results discussed.

10.1.iv Numerical Computer Model of Rockfill

As a result of the studies described in the previous sections, an assessment of the relative importance of the contact crushing in the bulk behaviour of rockfill has been made (Chapter 8). This suggests that contact crushing is significant and further confirmation of this has been obtained in comparing observed contact behaviour with the behaviour of granular masses. On these grounds a 2-D numerical computer model of a granular mass has been proposed and developed in Chapter 9.

The rock particles have been modelled as a series of rigid struts radiating from the particle centres to the points of contact with other particles and small deformable elements assumed to exist at the contacts. The properties of these elements have been based on the experimental contact test results. The situation modelled was that of an oedometer test on a dry, uniformily graded sample, so that a comparison of laboratory and computer results could be made. Known displacements were applied to the top of the sample and an iterative secant stiffness analysis used to generate the boundary forces. Once the sensitivity of the model to certain unknowns had been established, direct comparisons between a real sample and the model results were made. A study of the local strains, forces and energy stored was also made. Finally the effect of increased density of the computer sample was investigated and the results compared with the expected behaviour of a real sample.

10.2 Summary of Conclusions

The main results and conclusions of this research have been listed below.

10.2.i Contact Crushing - immediate response to load (Chapter 4 and 5)

(a) The load-displacement curves for sandstone particles reveal two distinct types of behaviour - an initial smooth curve followed by complex irregular behaviour. The load at which the initial curve ceases and irregular behaviour begins has been named the Damage Load.

(b) Initial behaviour:-

The initial smooth curve can be approximated by the equation

$$d = \eta P^{\frac{2}{3}}$$

neither saturation nor the contact angle affect the $\frac{2}{3}$ index in this equation.

Saturation increases the amount of contact crushing.

Larger contact angles reduce the displacements recorded for a given applied load.

(c) Damage Load:-

The Damage Load increases with increased contact angle but is reduced by saturation if the contact angle is greater than 100^{o}.

(d) Area of Contact:-

The area of contact increases with increasing load and for loads less than the Damage Load the area-load relationship has been found to be of the form

$$A = (cP)^{\frac{2}{3}} \qquad (10.1)$$

Saturation increases the area of contact but does not affect the $\frac{2}{3}$ index in equation (10.1)
The constant c in (10.1) is inversely proportional to the material strength.
Area is not dependent upon particle shape.

(e) Other conclusions

Work-hardening usually occurs at the contact under cyclic loading.
Shaped sample behaviour is representative of the behaviour of irregular samples with similar mean contact angles.

10.2.ii Contact Crushing - time-dependent response to load (Chapter 6)

(a) Contacts continue to settle with time under constant load
Increased sustained load produces greater creep displacements and at small loads (i.e. less than 1.5 kN) linear behaviour is observed.
No creep or recovery occurs if a contact is unloaded to a lower sustained load.
A period of constant load affects the load-displacement relationship when further loading is applied: producing a sharp increase in gradient initially compared with that of the initial curve.
If the Damage Load is less than the maintained load then unpredictable behaviour may occur during constant loading.

(b) Saturation:-

Saturated samples have higher creep rates than dry samples initially but after about three hours there is little difference.

Inundation of dry samples produces large additional displacements immediately.
Draining a sample and re-saturating have a negligible effect.

(c) Creep displacements increase with decreased contact angle.

(d) Relaxation:-
Saturation increases the percentage loss of load during relaxation of a contact.
The percentage loss of load during relaxation increases with decreased contact angle.

10.2.iii The Behaviour of Rockfill Dams (Chapter 2)

(a) The crest post-construction movements of rockfill dams cannot be accurately predicted using simple height and time relationships - dam behaviour is too complex for this and varies considerably from dam to dam.

(b) Dam movements are influenced by site topography and geology

(c) Sluicing during construction increases compaction and therefore reduces post-construction settlement. No optimum volume of water is used in practice and no conclusion has been reached on this.

(d) The first reservoir filling is critical for all types of dam section but subsequent fillings appear to be significant only for central core dams - this is possibly due to differential movements allowed by deformation in the core.

(e) Single stage dumping construction produces less post-construction settlements than multi-stage construction.

10.2.iv Behaviour of Rockfill in Oedometer Tests (Chapter 7)

(a) Saturation:-
Saturated samples show greater immediate and time-dependent displacements than dry samples.

Saturation of a dry sample induces additional displacements. Repeated saturation has a negligible effect - the first wetting is important.
Similar behaviour to this is noted in contact tests.

(b) Greater compaction is obtained if the sample is saturated thoroughly beforehand rather than when in place.

(c) If the sample is first subjected to a high load, the creep displacements observed under a lower sustained load willbe reduced. Significant displacements may still be observed if the lower load is greater than 70% of the maximum previously applied load.
This behaviour was not noted in the contact tests but this may have been due to the higher maintained load being applied for some time before unloading.

(d) Rebound and recovery:-

On unloading a sample completely rebound and recovery occur - rebound was approximately 18-27% of the loading displacement for well graded samples and 4-8% for uniform samples.
Approximately 90% of the total expansions of the sample occurs within the first minute of unloading.

(e) Particle breakage increases with applied load and if the sample is saturated.

10.3 Area of Further Research

This research has concentrated on contact crushing and little attention has been paid to rolling and sliding of particles. Experimental research into the behaviour patterns of this mechanism and the factors influencing it is needed, so that its role in the deformation of granular masses can be more clearly understood.

Further development of the numerical model is needed since at larger displacements (> 3.5 mm) smaller loads than those observed in the oedometer test are predicted. This discrepancy has been attributed to

(a) not updating the model structure as displacements occur

(b) not allowing new contacts to be formed

The model has only considered the immediate displacement of a dry uniform sample but, as good initial agreement has been obtained for this, it is reasonable to assume that the model may be extended to saturated samples and time-dependent behaviour. Suitable descriptions of the contact behaviour for these conditions may be obtained from the experimental work. The contact behaviour used in the model is based on the mean experimental results although these results do show some scatter. This could be introduced into the analysis by the use of statistical models.

The numerical model has been developed to allow the local behaviour within a granular mass to be studied and also as an aid to predicting overall deformations. The model could be used to determine how appropriate proposed laboratory tests would be in reproducing field behaviour. Particle size and grading effects could be studied as well as helping in the design of a suitable rig. Clearly the amount of storage and time required to analyse a rockfill structure is prohibitive at present unless the structure is quite small. However, this type of approach could be used in analysing a section of the structure where difficulties were expected e.g. in fill around conduits. Structures are often analysed using overall behaviour models with open meshes and these highlight critical areas. Particulate analyses can be used to investigate such areas in more detail when the use of overall behaviour models is inappropriate.

10.4 Concluding Remarks

From this investigation into interparticle behaviour and the compressibility of rockfill, two conclusions stand out as being significant.

(a) Surprisingly the initial contact behaviour can be modelled using equations of the form of theoretical solutions for elastic particles, although the observed behaviour is not elastic.

(b) A 'Damage Load', at which the interparticle behaviour departs from this 'elastic' behaviour, has been shown to exist and once this has been reached the interparticle behaviour becomes very complex.

APPENDICES

APPENDIX I.

Appendix to Chapter 2 - 'The Observed Post-construction Movements of Rockfill Dams - their significance and prediction'.

1.1 Membrane Dams (dumped)

Key to figs. 2.10 and 2.13

No. D1 - Bowman (U.S.A.)
D2 - Montgomery (U.S.A.) (Note:- not considered in this research)
D3 - Lower Bear River No. 2 (U.S.A.)
D4 - Nozori (Japan)
D5 - Ishibuchi (Japan)
D6 - Salazar (Portugal)
D7 - Lower Bear River No. 1 (U.S.A.)
D8 - Malpaso (Peru)
D9 - Dix River (U.S.A.)
D10 - Salt Springs (U.S.A.)
D11 - Paradela (Portugal)

1.2 Table 1:- Membrane Dams (dumped)

NAME	COUNTRY	YEAR	HEIGHT	MAIN ROCK TYPE	FOUNDATION	CONSTRUCTION METHODS	SLUICING water/rock vol. ratio	RESERVIOR FILLING	REMARKS	REF
BONITO	NEW MEXICO	1932	28.0	-	-	-	-	-	Reinforced concrete membrane	1
BOU HANIFA	ALGERIA	1938	53.0	Hard sandstone & conglomerate	-	4.5m lifts - placed by derricks; interstices filled by hand with small stones	-	-	Reinforced concrete membrane	2,3
BOWMAN	U.S.A.	1876	29.3	-	-	Moderate to high lifts	None	-	Timber deck, dismantled in 1926	1
DIX RIVER	U.S.A.	1925	84.2	Dense, finely crystalline, light grey limestone	Limestones & shales	Dumping heights upto 35m	Poor to moderate	-	Reinforced concrete membrane Flood during constr.	1,4 5
FORDYCE	U.S.A.	1926	42.7	-	-	-	-	-	Reinforced concrete membrane	1
ISHIBUCHI	JAPAN	1953	53.0	Dacite	Decomposed & jointed liparite	u/s dumped first from 29m and 53m levels	2:1 (100 psi)	Filled Dec. 1953- April 1954 Drained Oct. 1954 Refilled Dec. "	Concrete membrane	6
LEMOLO no.1	U.S.A.	1954	36.6	Basalt	Dense basalt, tuff, basalt agglomerate layers	3 lifts	3:1	Partially filled & drained 1954; Filled May 1955	Concrete membrane Fault at site	7
LOWER BEAR RIVER no.1	U.S.A.	1952	74.7	Grey, fine-grained grano-diorite	Granite	2 lifts at 37m & 44m 1 lift used at one section of dam	3:1 (9 psi)	Seasonal variation	Concrete membrane	8
LOWER BEAR RIVER no.2	U.S.A.	1952	45.7	Grey, fine-grained grano-diorite	Granite	1 lift	?	Filled 1953 Seasonal variation	Similar design to Lower Bear River no.1	8

Table 1:- Membrane Dams (dumped) cont.

NAME	COUNTRY	YEAR	HEIGHT m	MAIN ROCK TYPE	FOUNDATION	CONSTRUCTION METHOD	SLUICING water/rock vol. ratio	RESERVOIR FILLING	REMARKS	REF
MALPASO	PERU	1936	67.4	-	Boulders, gravels, sand & clay	-	Some	-	Concrete membrane	1
NOZORI	JAPAN	1956	44.0	Andesites & propylites	-	3 lifts of 17m, 15m & 12m	4:1 (170 psi)	-	Concrete membrane	9
PARADELA	PORTUGAL	1957/8	110.0	-	Granite - weathering variable	3 lifts at levels 68m, 98m & 108m	4:1	First filling Oct. 1957-July 1958. Emptied July 1958. (seasonal variation)	Reinforced concrete slabs placed during construction	10
SALAZAR	PORTUGAL	1949	62.8	Prophry	Silicious & argillaceous shales; intensely fractured & folded	-	-	Filled 1949-50	Steel membrane	11,12 13
SALT SPRINGS	U.S.A.	1939	100.0	Sound granite	Granite; compacted gravel & boulders under d/s section	Lifts of 20-56m	Nominal for bottom half, substantial for top half	Filled 1932 (seasonal variation)	Concrete membrane	8
SHIROKOVSK	U.S.S.R.	1947	40.0	-	Ar illite & sandstone, alluvial deposits in riverbed	-	-	-	Timber membrane	14
STRAWBERRY	U.S.A.	1916	42.7	-	Gravels in riverbed	Lifts 10m	None	-	Concrete membrane	1
SWIFT	U.S.A.	1914	47.9	-	Gravels in riverbed	Moderate to high lifts	-	-	Concrete membrane	1
WISHON	U.S.A.	1958	90.2	-	Exposed glaciated granite	-	3:1 (100 psi)	Filled May 1958 in 13 days (seasonal variation)	Concrete membrane placed during construction	16

1.3 Table 2:- Membrane Dams (compacted)

NAME	COUNTRY	YEAR	HEIGHT m	MAIN ROCK TYPE	FOUNDATION	CONSTRUCTION METHOD	SLUICING water/rock vol. ratio	RESERVOIR FILLING	REMARKS	REF
BIGGE	GERMANY	1964	52.0	Shale & shaley greywacke	-	Init. 0.8m layers 3 ton tamper Later 1.2m layers 5 ton vib. roller	-	Filled 1965	Asphaltic concrete deck	17,18 19
CETHANA	TASMANIA	1971	110.0	Clean quartzite	Hard, bedded quartzite & quartzite conglomerate	Layers 0.45m, 0.9m, 1.85m; 4 passes 10 ton vib. roller	>.15	Filled Feb. - April, 1971	Face rolled 10 ton vib. roller. Reinforced concrete deck	20,21
GENKEL	GERMANY	1952	43.0	-	-	2.5 ton vib. roller & smooth steel roller	-	-	Asphaltic concrete deck	19,22
HENNE	GERMANY	1955	52.0	Crystalline limestone & sound greywacke	Volcanic ash & keratophyre tuff	Layers 0.8m; 3 ton tamper	-	-	Asphaltic concrete deck	15,17 18,19 23
KANGAROO CREEK	AUSTRALIA	1969	59.4	Zn 1:quartz gneiss Zn 2:shist, gneiss Zn 3:weak shist	L. bank : sericite shist R. bank : gneiss	Sluiced prior to compaction; 4 passes 10 ton roller	1.1	-	Reinforced concrete deck	24
NISSASTROM	SWEDEN	1950	15.0	-	-	0.45m-o.6m layers, sluiced; 10 ton roller & then 1.6 ton vib. roller	Some	-	Timber deck	25
PEDU	MALAYA	1969	63.0	Mudstones & quartzites	Conglomerates, quartzites & mudstone strata	1.8m layers; 8 passes 10.5 ton vib. roller	-	-	Asphaltic concrete deck	26
QUOICH	U.K.	1954	38.0	-	Moine shists	10 ton roller & then 3.5 ton vib. roller	Some	-	Concrete slab deck	27,28
VENEMO	NORWAY	1963	51.0	-	Granitic gneiss & zones of mica amphibolite	Init. dumped 15-20m Later 8 ton vib. roller	Some (not winter)	Filled June-Oct. 1964 (seasonal variation)	Asphaltic concrete deck Rollers: 1.5m layers 10 passes (S) 1m layers 15 passes (W)	19,29

1.4 Table 3:- Sloping Core Dams

NAME	COUNTRY	YEAR	HEIGHT m	MAIN ROCK TYPE	FOUNDATION	CONSTRUCTION METHOD	SLUICING water/rock vol. ratio	RESERVOIR FILLING	REMARKS	REF
BEAR CREEK	U.S.A.	1953	65.5	Good quality shist	Massive shist	Lift 52.5m; Top 12m constructed seperately	Some	Filled 1953	In narrow gorge; Core wet of opt.	30 31
BERSIMIS no.1	CANADA	1955	61.0	Sound granitic gneiss	Gneiss; N. abutment thick layers of till & silt	High lifts dumping from S. abutment	4:1	Started 1955 during construction. Maximum 1957, drawndown 1958	-	32
BROWNLEE	U.S.A.	1958	122.4	-	Basalts with tuff interlayers; Riverbed alluvials	Coarse rock dumped, fine rock 45cm layers - 3 passes 50 ton roller	4:1	-	Loam core. Flooding durin. constr.	15 33
CEDAR CLIFF	U.S.A.	1952	50.3	Good quality shist	-	-	-	-	-	30 31
CHILHOWEE	U.S.A.	1957	27.7	-	-	-	-	-	-	31
DESROCHES	CANADA	1955	68.6	Sound granitic gneiss	Gneiss	Dumping in high lifts 42m from North bank	4:1	Same as Bersimis no. 1	Sited next to Bersimis no.1 - similar design	32
EAST FORK	U.S.A.	1955	41.2	Good quality shist	-	-	-	Filled 1955	-	30 31
FURNAS	BRAZIL	1962	125.0	Hard, fine-grained quartzites	Quartzites with thin mica - shist interlayers	Compacted in 30-70cm layers	None	Filled shortly after construction	Decomposed shist & quartzite core	34 35 36
HOLJES	SWEDEN	1961	81.0	-	-	2-10m lifts; Sluicing in summer No sluicing in winter	2:1	Filled 1961-62 (seasonal variation)	Moraine material core	37

Table 3:- Sloping Core Dams cont.

NAME	COUNTRY	YEAR	HEIGHT m	MAIN ROCK TYPE	FOUNDATION	CONSTRUCTION METHOD	SLUICING water/rock vol. ratio	RESERVOIR FILLING	REMARKS	REF
KENNY	CANADA	1952	100.0	Massive basalt	Basalt	12m lifts from left abutment	2:1	Filled 3 years after construction	Boulder clay core	33
LOWER BJURFORS	SWEDEN	?	30.0	-	-	2m lifts	Some	Filled during 6 months after constr.	-	37
MIBORO	JAPAN	1960	131.0	Granite	Quartz porphyry with granite porphyry intrusions	~4m lifts u/s (no sluicing) ~8m lifts d/s	3:1	-	Fault zone on right abutment. Earthquake in 1961.	38
NANTAHALA	U.S.A.	1942	77.7	Hard massive arkose	Arkose	Lifts 15-40m.	4:1	Filled Feb.-July 1942 (seasonal variation)	Core - 2 % dry of opt.	30 31 39
QUEEN'S CREEK	U.S.A.	1948	23.8	Arkose	Alluvium material in riverbed	-	-	Filled 1948, emptied rapidly on several occaisions	Core of poor material	30 31
SCAMMONDEN	U.K.	1969	70.0	Sandstone	Layers of sandstone & shale	1m layers; 5 passes 11.5 ton vib. roller or 6 passes of two 5 ton rollers	Some	-	Zoned clay core	40 41
TRÄNGSLET	SWEDEN	1960	125.0	Porphry	Syenite & porphry	2-3m layers u/s, sluicing & compaction with tractors; 20m layers d/s, no sluicing	4:1	-	Core of moraine material	58
WOLF CREEK	U.S.A.	1955	50.3	Good quality shist	-	-	-	Filled shortly after construction	-	30 31

1.5 Table 4:- Central Core Dams

NAME	COUNTRY	YEAR	HEIGHT m	MAIN ROCK TYPE	FOUNDATION	CONSTRUCTION METHOD	SLUICING water/rock vol. ratio	RESERVOIR FILLING	REMARKS	REF
AKOSOMBO	GHANA	1965	112.8	Clean, strong quartzite	Riverbed sand deposits upto 38m deep	1.8m layers: 4 passes of 4 ton vib. roller or 3m layers: 4 passes of 8 ton vib. roller	Some	Filled 1969	Core 0-2% wet of opt.	42
AMBUKLAO	PHILIPPINES	1955	128.5	Diorite	Weathered andesite, tuff & lava Riverbed deposits	d/s dumped in 9-27m layers u/s compacted in 60cm layers with 50 ton roller	Some	-	Loam core	15,33
BEAS	INDIA	1974	132.5	-	Layers of sandatone & clay shales (well consolidated)	-	-	-	Clay and sand core (?)	43
CHERRY VALLEY	U.S.A.	1955	100.6	Grano-diorite	Granite	Dumped in 4.5-9m lifts	Some	Filled to ⅔ cap. May 1956; drawdown and filled July 1957 (seasonal variation)	Sandy silt core	15,44
CUPATITZIO	MEXICO	1961	72.4	Sound diorite	Right bank - diorite Left bank - conglomerate	2m layers	None (good rainfall)	Filled quickly 1961	Silt core - 7.7% wet of opt.	34,45
DHÜNN VALLEY	GERMANY	1962	35.0	Slate	Sandstone &slate, gravel in valley bed	0.6m layers: 7 ton sliding vibrator	-	-	Vertical bituminous concrete core	46
EL INFIERNILLO	MEXICO	1963	148.0	Sound diorite & silicified conglomerate	Conglomerates, alluvial deposits in riverbed	<1m layers: 4 passes of D-8 tractor	None	Filled June-Sept. 1964	Thin core; 2-6% wet of opt.	15,42
ESTREITO	BRAZIL	1968	97.0	Quart-shist, sound quartzite	Sound quartzite	0.5-0.6m layer with 2 passes of D-8 tractor	-	Filled in 10 days Nov. 1968	Thin clayey sand core	47
GEPATSCH	AUSTRIA	1964	153.0	Gneiss	Gneiss, overlain by alluvial material, talus, boulder clay	2m layers; 4 passes of 8.5 ton vib. roller	Rainfall	Filled to ⅔ cap. during construction (seasonal variation)	Talus and moraine material core	48,49 50,51

Table 4 :- Central Core Dams cont.

NAME	COUNTRY	YEAR	HEIGHT m	MAIN ROCK TYPE	FOUNDATION	CONSTRUCTION METHOD	SLUICING water/rock vol. ratio	RESVOIR FILLING	REMARKS	REF
HIGH ASWAN	EGYPT	1968	111.0	Granite, migmatites	Alluvial deposits upto 255m deep	Dumping: sluiced with sand	Some	-	Zoned dam; clay core	52,53
HYTTEJUVET	NORWAY	1965	93.0	-	-	3-5m lifts	Some	Filled May-Oct. 1966 Drawndown Feb. 1967 Filled 1967	Moraine material core- narrow at top of dam	54
KAJAKAI	AFGHANISTAN	1952	100.0	Sound limestone	Massive dolomite limestone	Dumped in 10m lifts	2:1	Filled 1952	Core- mixture of sand, silt & clay: 2-4% dry of opt.	55
LLYN BRIANNE	U.K.	1971	91.0	Slatey mudstone	Slatey, argillaceous rocks Fault in left abutment	1m layers; 4 passes of 8.6 ton roller or 13.5 ton vib. roller	Some	Filling started 2 months after completion	Moraine till core	56
MESSAURE	SWEDEN	1962	101.0	Granite	Hard, sound granite with zones of faulted, crushed rock	1.5m layers with sluicing in summer 2m layers, no sluicing in winter	Some	-	Moraine material core	57
MUDDY RUN	U.S.A.	1966	76.2	Weathered, laminated, micaceous shist	-	0.3-1m layers with vib. roller	-	-	Clayey silt core	42
MUD MOUNTAIN	U.S.A.	1941	122.0	-	Tuff, andesite, quartzite Alluvial deposits in riverbed	-	-	-	Sandy gravel & clay core	15,33
NETZHUALCO-YOTL	MEXICO	1964	137.5	Conglomerate	Conglomerate	50-100cm layers compacted by tractor	High Rainfall	Filled May-Sept. 1966	Red laterite core; 7% wet of opt.	42
NOTTELEY	U.S.A.	1942	56.1	Quartzite (20% mica shist)	-	Dumped in one stage	Some	Filled 8-9 months after completion (seasonal variation)	Wide sandy clay core	59

Table 4:- Central Core Dams cont.

NAME	COUNTRY	YEAR	HEIGHT m	MAIN ROCK TYPE	FOUNDATION	CONSTRUCTION METHOD	SLUICING water/rock vol. ratio	RESERVOIR FILLING	REMARKS	REF
PERUCA	YUGOSLAVIA (?)	1959	60.0	Limestone	'Firm rock'	Dumped in 6m lifts	4:1	Filled 1960 (seasonal variation)	Clay core at opt.	60
PRESIDENTE ALEMAN	MEXICO	1953	75.0	Limestone	Limestone	2m layers with no sluicing	High Rainfall	Seasonal filling to ⅔ cap. 1954-56 Full 1957 and kept full	Lateritic clay core; 4% wet of opt.	34,45
SOUTH HOLSTON	U.S.A.	1950	86.9	Sandstone, some shale	Sandstone	Dumped in 3 stages	Some	Filled 8-9 months after construction (seasonal variation)	Medium clay core	15,59
TOOMA	AUSTRALIA	1961	68.0	u/s dense fine-grained quartzite; d/s weathered granite	Biotite granite & granitic gneiss - generally weathered	3m layers	1.5:1	Filled 1961 Sudden drawdown 1962	Weathered biotite granite core	61
TRESNA	POLAND	1964	38.0	-	'High modulus of compressibility	-	-	-	Silty loam core; wet of opt. Culvert under dam	62,63
WATAUGA	U.S.A.	1948	96.8	Quartzite	Quartzite	Dumped in 2 stages	Some	Filled 8-9 months after construction (seasonal variation)	Clayey sand & clay core	15,59

1.6 References - Tables 1-4

1. C.V. Davis — "Handbook of Applied Hydraulics" 2nd Edit. McGraw-Hill 1952

2. K. Terzaghi — Discussion Paper No. 3065 SORD. Transactions ASCE Vol. 125 Part II 1960

3. E.E. Nonveiller — General Report - G Q 22 Vol. III 6th ICOLD 1958

4. G.W. Howson — "Design of Rockfill Dams" Transactions ASCE Vol. 104 1939

5. L.A. Schmidt — "Rockfill Dams: Dix River Dam" SORD. Transactions ASCE Vol. 125 Part II 1960

6. M. Kawase — Discussion Paper 3065 SORD. Transactions ASCE Vol. 125 Part II 1960

7. J.C. Boyle & W.R. Barrows. — "Rockfill Dams: Lemold No. 1 Dam" SORD. Transactions ASCE Vol. 125 Part II 1960

8. I.C. Steele & J.B. Cooke — "Rockfill Dams: Salt Springs and Lower Bear River Concrete Face Dams" SORD. Transactions ASCE Vol. 125 Part II 1960

9. T. Mitukoshi — Discussion Paper 3065 SORD. Transactions ASCE Vol. 125 Part II 1960

10. L.H.G. Fernandes, E. Oliveira, N. Vasconcelos Porto — "Rockfill Dams: Paradela Concrete Face Dam" SORD. Transactions ASCE Vol. 125 Part II 1960

11. A. Palma Carlos — "Valeurs Prevues et Valeurs Observees pour les Tassements des Enrochments du Barrage Salazar, Pendant et Apres sa Construction" Q.18 R 15 Vol. III 5th ICOLD 1955

12. A. Palma Carlos — Discussion Paper 3076 SORD. Transactions ASCE Vol. 125 Part II 1960

13. A.T. Morais, A. Palma Carlos — "Design & Construction of Earthfill and Rockfill Dams and their Waterproofing Blankets. Salazar & Vale Do Gaio Dams, Vale Do Sadd Irrigation Scheme of the Junta Autonoma Das Obras De Hidraulica Agricola" C.7. Vol. IV 4th ICOLD 1951

14. A.A. Nitchiporovitch — "Deformations and Stability of Rockfill Dams" Qu. 31 Vol. III 8th ICOLD 1964

15. R.A. Airapetyan — "Modern Rockfill Dams" Israel Program of Scientific Translations. Jerusalem 1973

16. J.B. Cooke — "Rockfill Dams: Wishon and Cartwright Concrete Face Dams" SORD. Transactions ASCE Vol. 125 Part II 1960

17. H.W. Koenig & K.H. Idel — "Deformation and Loading of a Rockfill Dam with Bituminous Surface Membrane" Qu. 34 9th ICOLD 1967

18. H.W. Koenig & K.H. Idel — "Report on the Behaviour of Impervious Surface of Asphalt" Qu. 42 R20 Vol. III 11th ICOLD 1973

19. C. Soydemir & B. Kjaernsli — "A Treatise on the Performance of Rockfill Dams with Unyielding Foundations in Relation to the Design of Storvass Dam" N.G.I. Report 53203 1975

20. J.K. Wilkins, W.R. Mitchell, M.D. Fitzpatrick, T.B. Liggins — "The Design of Cethana Concrete Face Rockfill Dam" Qu. 42 R3 11th ICOLD 1973

21. M.D. Fitzpatrick, T.B. Liggins, L.J. Lack, B.P. Knoop — "Instrumentation and Performance of Cethana Dam" Qu. 42 R9 11th ICOLD 1973

22. J.L. Sherard, R.J. Woodward, S.F. Gizienjki, W.A. Clevenger — Earth and Earth-Rock Dams J. Wiley and Sons N.Y. 1963

23. H.W. Koenig, K.H. Idel — "Settlement Measurements on a 52 m High Rockfill Dam with Bituminous Surface Membrane" C.2. Vol. III 8th ICOLD 1964

24. R.J. Good — "Kangaroo Creek Dam, use of a weak Schist as Rockfill for a Concrete Faced Rockfill Dam" Qu. 44 Vol. I 12th Icold 1976

25. B. Hellstrom — "Compaction of a Rockfill Dam" Vol. III 5th ICOLD 1955

26. C.L. Clarke R.G. Taylor — "Lessons Learned from Two Rockfill Dams in the Tropics" Qu. 36 Vol. I 10th ICOLD 1970

27. C.M. Roberts — "The Quoich Rockfill Dam" Qu. 22 R6 6th ICOLD 1958

28. A. Penman — "Rockfill" Building Research Station Publication April 1971

29. B. Kjaernsli, I. Torblaa — "The Venemo Asphalt Faced Rockfill Dam" N.G.I. Publication No. 69 1969

30. J.P. Growden — "Rockfill Dams: Dams with Sloping Earth Cores" SORD. Transactions ASCE Vol. 125 Part II 1960

31. J.P. Growden — "Rockfill Dams: Performance of Sloping Core Dams" SORD. Transactions ASCE Vol. 125 Part II 1960

32. F.W. Patterson, B.H. MacDonald — "Rockfill Dams: Bersimis Sloping Core Dams" SORD. Transactions ASCE Vol. 125 Part II 1960

33. F.L. Lawton M.D. Lester — "Settlement of Rockfill Dams" Qu. 31 Vol. III 8th ICOLD 1964

34. R.J. Marsal — General Report 2nd Pan-American Conf. S.M. & F.E. Vol. II 1963

35. L. Queiroz[2] — "Geotechnical Properties of Weathered Rock and Behaviour of Furnas Rockfill Dam" Qu. 28 Vol. I 8th ICOLD 1964

36. E.H. Lyra L. Queirol — "The Furnas Rockfill Dam" Qu. 31 Vol. III 8th ICOLD 1964

37. E. Reinus — "Design and Construction of Holjes Dam" Qu. 31 Vol. III 8th ICDLD 1964

38. I. Asao — "The Miboro Dam" Qu. 31 Vol. III 8th ICOLD 1964

39. J.P. Growden — "Rockfill Dams; Nantahala Sloping Core Dam" SORD. Transactions ASCE Vol. 125 . Part II 1960

40. J.A. Charles — "Correlation between Laboratory Behaviour of Rockfill and Field Performance with Particular Reference to Scammonden Dam" Ph.D. Thesis. University of London 1973

41. Private Communication — Data used with permission B.R.E. and Yorkshire Water Authority

42. S.D. Wilson — "Deformation of Earth and Rockfill Dams" Embankment-Dam Engineering Casagrande Vol. J. Wiley and Sons 1973

43. R.K. Varma, B.B. Raj — "Performance Analysis of Embankment - Case Studies" Geocon Proceedings Conference on Geotechnical Engineering India 1978

44. H.E. Lloyd, O.L. Moore, W.F. Getts — "Rockfill Dams: Cherry Valley Central Core Dam" SORD. Transactions ASCE Vol. 125 Part II 1960

45. R.J. Marsal, L. Ramiz de Arellano — "Field Measurements in Rockfill Dams" 2nd Pan-American Conf. S.M. and F.E. Vol. II 1963

46. H. Breth — "Measurements on aRockfill Dam with a Bituminous Concrete Diaphram" Qu. 29 Vol. III 8th ICOLD 1964

47. F.H. Lyra, F. Fernandes — "Estreito Rockfill Dam" Qu. 36 R44 10th ICOLD 1970

48. W. Schober — "Behaviour of theGepatsch Rockfill Dam" Qu. 34 R39 9th ICOLD 1967

49. W. Schober — Technical Session Qu. 34 9th ICOLD 1967

50. W. Schober — "Considerations and Investigations for the Design of a Rockfill Dam with a 92 m High Bituminous Mix Core" Qu. 42 R34 Vol. III 11th ICOLD 1973

51. E. Neuhaujer, W. Weissiar — "Placing the Shell Zones of the Gepatsch Rockfill Dam in Winter" Qu. 35 9th ICOLD 1967

52. I.Z. Kinawy, K. Shenovda, M. Sheta — "Selection of Construction Materials and Methods of their Placement in the High Aswan Dam" Qu. 42 R53 Vol. III 11th ICOLD 1973

53. I.Z. Kinawy, W.K. Shenovda — "Observations on Performance Settlement and Movement Measurements of High Aswan Dam" Qu. 42 R19 Vol. III 11th ICOLD 1973

54. B. Kjaernsli, I. Torblaa — "Leakage Through Horizontal Cracks in the core of Hyttejuvet Dam" N.G.I. Publ. No. 80 1968

55. G.F. Sudman — "Rockfill Dams: Kajakai Central Core Dam, Afghanistan" SORD. Transactions ASCE Vol. 125 Part II 1960

56. W.J. Carlyle — "The Design and Performance of the Core. of Brianne Dam" Qu. 42 R26 Vol. III 11th ICOLD 1973

57. L. Bernell — "Measurements in the Messaure Dam, a Rockfill Structure with wet-compacted Moraine Core" Qu. 29 Vol. II 8th ICOLD 1964

58. T. Persson — "The Trangslet Dam. Results and Interpretation of Measurements made on the Dam" Qu. 29 Vol. II 8th ICOLD 1964

59. G.K. Leonard, O.H. Raine — "Rockfill Dams: TVA Central Core Dams" SORD. Transactions ASCE Vol. 125 Part II 1960

60. E. Nonveiller — "Post Construction Deformation of Rockfill Dam Peruca" Qu. 29 R47 Vol. II 8th ICOLD 1964

61. I.L. Pinkerton, A.D. McConnell — "Behaviour of Tooma Dam" Qu. 29 Vol. II 8th ICOLD 1964

62. R. Karminski, K. Garbulenski, A. Furstenburg, W. Wolski — "Distribution of Stresses in Earth Dams Estimated by means of Small Computer ODRA 1204 - D" Criteria & Assumptions for Numerical Analysis of Dams Swansea 1975

63. W. Wolski, A. Furstenburg — "Comparison of Deformation of the Tresna Dam, Observed and Computed by means of the F.E.M." I.C.S.M. & F.E. Moscow 1977

APPENDIX II.

Appendix to Chapter 9 - The Prediction of the Behaviour of a Granular Mass of Angular Particles

Determination of overall stiffness matrix

The equilibrium equations relating the forces applied at the nodes and the corresponding nodal displacements may be expressed in terms of matrices.

$$[P] = [K][u]$$

where $[K]$ is the structure stiffness matrix. Deformation of each member of the structure is allowed to occur in extension, shear and rotation with corresponding stiffnesses k_e, k_s and k_r. The potential energy stored (U) in the deformable element of a member can be determined from the following equation

$$U = \frac{1}{2} k_e u_e^2 + \frac{1}{2} k_s u_s^2 + \frac{1}{2} k_r u_r^2$$

where u_e, u_s and u_r represent the extension, shear and rotation displacements respectively.

Fig. II.1 shows the condition of arbitrary shape and position of the deformable element and the energy stored for this case is

$$U = \frac{1}{2} k_e \left((u_A + LW_A - u_B + L' W_B) \cos \phi + (V_A - 1 W_A - V_B - 1' W_B) \sin \phi\right)^2$$

$$+ \frac{1}{2} k_s \left((u_A + LW_A - u_B + L' W_B) \sin \phi - (V_A - 1 W_A - V_B - 1' W_B) \cos \phi\right)^2$$

$$+ \frac{1}{2} k_r (W_A - W_B)^2$$

where $1 = x_c - x_A$ $\qquad 1' = x_B - x_c$

$L = y_c - y_A$ $\qquad L' = y_B - y_c$

In deriving this equation it is assumed that
(a) the size of the deformable is negligible compared with the particle size.
(b) the deformations are small.

Lucas (1975) has produced a similar equation for his work on ice floes, although there is a positive sign before the second bracket of terms in the shear displacement expression (i.e. $((-) \sin \phi + (-) \cos \phi)$)

The member stiffness matrix may be obtained from this energy expression by differentiation with respect to the nodal displacements.

$$\frac{\partial}{\partial u} [U] = [K] [u]$$

The overall stiffness matrix may be assembled from the member stiffness matrix by including the member matrix elements in the appropriate elements of the overall matrix. The member stiffness matrix for the member shown in fig. II.1 is given over.

$$
k = \begin{array}{c} \\ u_A \\ V_A \\ W_A \\ u_B \\ V_B \\ W_B \end{array}
\begin{bmatrix}
k_e \cos^2 \phi + k_s \sin^2 \phi & & \\
(k_e - k_s) \sin \phi \cos \phi & k_e \sin^2 \phi + k_s \cos^2 \phi & \\
Ak_e \cos \phi + Bk_s \sin \phi & Ak_e \sin \phi - Bk_s \cos \phi & A^2 k_e + B^2 k_s + k_r \\
-k_e \cos^2 \phi - k_s \sin^2 \phi & -(k_e - k_s) \sin \phi \cos \phi & - Ak_e \cos \phi - V k_s \sin \phi \\
-(k_e - k_s) \sin \phi \cos \phi & -k_e \sin^2 \phi - k_s \cos^2 \phi & - Ak_e \sin \phi + Bk_s \cos \phi \\
Ck_e \cos \phi + Dk_s \sin \phi & Ck_e \sin \phi - Dk_s \cos \phi & ACk_e + BDk_s - k_r
\end{bmatrix}
$$

$$
\begin{array}{c} u_A \\ V_A \\ W_A \\ u_B \\ V_B \\ W_B \end{array}
\begin{bmatrix}
 & & \\
 & \text{Symmetric} & \\
 & & \\
k_e \cos^2 \phi + k_s \sin^2 \phi & & \\
(k_e - k_s) \sin \phi \cos \phi & k_e \sin^2 \phi + k_s \cos^2 \phi & \\
-Ck_e \cos \phi - Dk_s \sin \phi & -Ck_e \sin \phi + Dk_s \cos \phi & C^2 k_e + D^2 k_s + k_r
\end{bmatrix}
$$

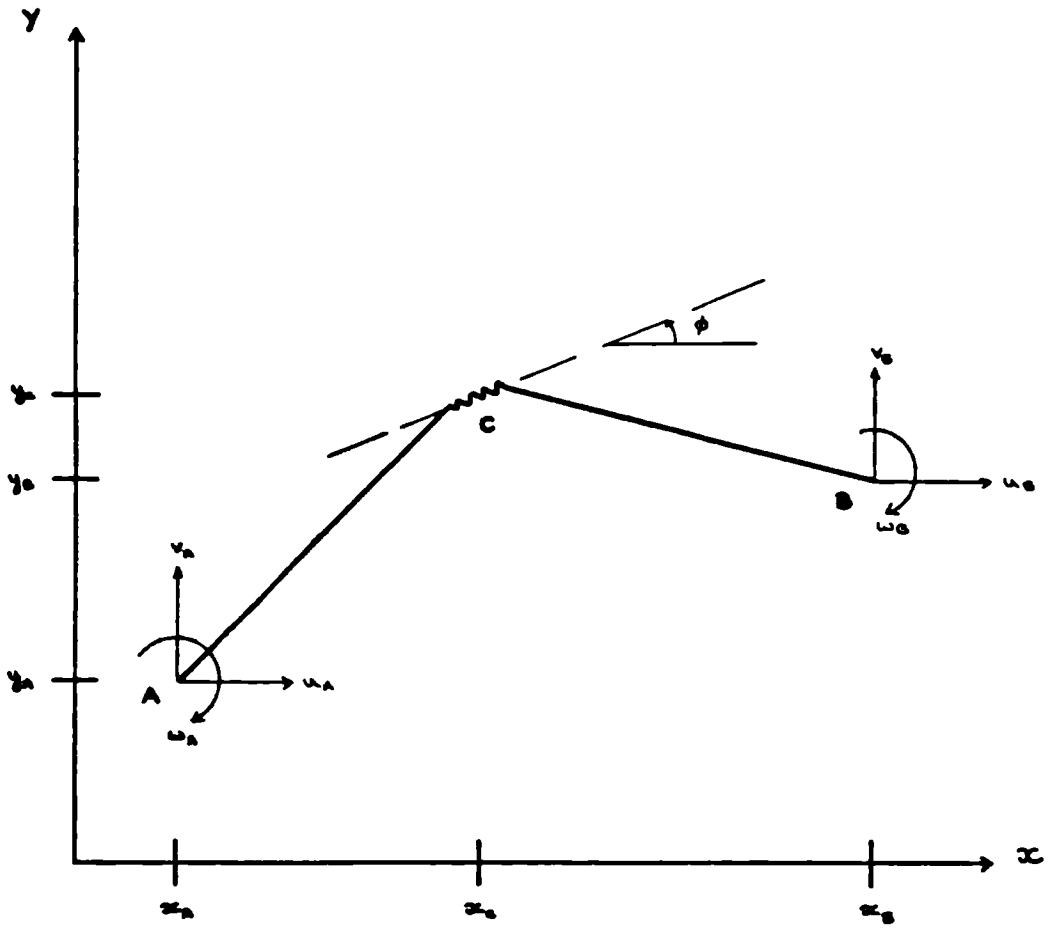

$\ell = x_c - x_A$ $\qquad L = y_c - y_A$

$\ell' = x_B - x_c$ $\qquad L' = y_B - y_c$

FIG. II.1 :- ARBITRARY SHAPE AND POSITION OF DEFORMABLE ELEMENT OF STRUCTURAL MODEL MEMBER A-B

APPENDIX III.

Appendix to Chapter 9 - The Prediction of the Behaviour of a Granular Mass of Angular Particles

Validity of use of equivalent radius R_e

In Chapter 4 the similarity between the Hertzian theoretical load-displacement equation for a spherical contact with a halfspace and the experimental relationship was noted.

Hertz:- $d = \eta' P^{\frac{2}{3}}$

Experimental:- $d = \eta P^{\frac{2}{3}}$

The experimental coefficient, η, is dependent upon the contact angle whereas η' is dependent upon the radius of the spherical contact, R, and the material parameters Young's modulus, E, and Poisson's ratio, ν.

Assuming $E = 10\ kN/mm^2$ and $\nu = 0.01$ then the Hertz equation becomes

$$d = 0.282\ P^{\frac{2}{3}}\ \left(\frac{1}{R}\right)^{\frac{1}{3}} \qquad (1)$$

If it is assumed that $\eta = \eta'$, then using the experiment values of η, values of R_e can be found from (1)

$$\eta = \eta' = \frac{0.282}{R_e^{\frac{1}{3}}}$$

$$R_e = \left|\frac{0.282}{\eta}\right|^3 \qquad (2)$$

Using the conversion equation given in section 9.3.i

$$R_e = \frac{1}{2}\left[(P)^{\frac{2}{3}}\ D^{\frac{2}{3}}\ (1 + \tan^2\ \frac{\gamma}{2})\right]^{\frac{3}{4}}$$

where P is the applied load and $D = 0.15\ mm^2/kN$

then $$\gamma = 2\ \tan^{-1}\left[\left[2\ \left(\frac{R_e^2}{P.D}\right)^{\frac{2}{3}} - 1\right]^{\frac{1}{2}}\right] \qquad (3)$$

From (3) values of γ can be found using the R_e values calculated in (2) and these may be compared with the measured contact angles of the experimental values. To do this a load P is also needed and in correlating R_e and the contact angle two specific loads were used - the Damage Load, P_o, and half this value.

Fig. III shows the graph of γ v β for the dry shaped samples using values determined from the above analysis with values of P_o and $P_o/2$ for each sample. This shows a good correlation of the angles with most of the points lying along the $\gamma = \beta$ line. Similar calculations were carried out for some of the dry irregular samples and comparisons made with the angles α_{1m}, α_{2m} and α_{5m}. This correlation was not as good with a wider spread of points.

Table 1 gives the standard deviations, S_γ, of the calculated γ values from the equal angle line where

$$S_\gamma = \left(\frac{\Sigma_o^n (\gamma - \beta)}{n} \right)^{\frac{1}{2}}$$

These indicate that calculations based on the half Damage Load give a better correlation and that the α_{5m} angle produces the best correlation of results for the irregular samples.

Angles	Samples	No. points on graph	S_γ
	Shaped Samples-P_o	5	20.47
	" " -$P_{o/2}$	5	9.63
α_{1m}	Irreg. Samples-P_o	8	44.67
	" " -$P_{o/2}$	8	31.76
α_{2m}	Irreg. Samples-P_o	8	32.00
	" " -$P_{o/2}$	8	20.03
α_{5m}	Irreg. Samples-P_o	8	23.38
	" " -$P_{o/2}$	8	21.54

Table 1:- Standard Deviations of γ values from the $\gamma = \beta$ (or α_m) line.

A similar analysis using the general Hertzian equation for an ellipsoid in contact with a halfspace (section 4.1.i) and programme contact (section 4.1.ii) indicated a slightly better correlation could be obtained using the general analysis but the increase in accuracy was not really justified by the additional computation.

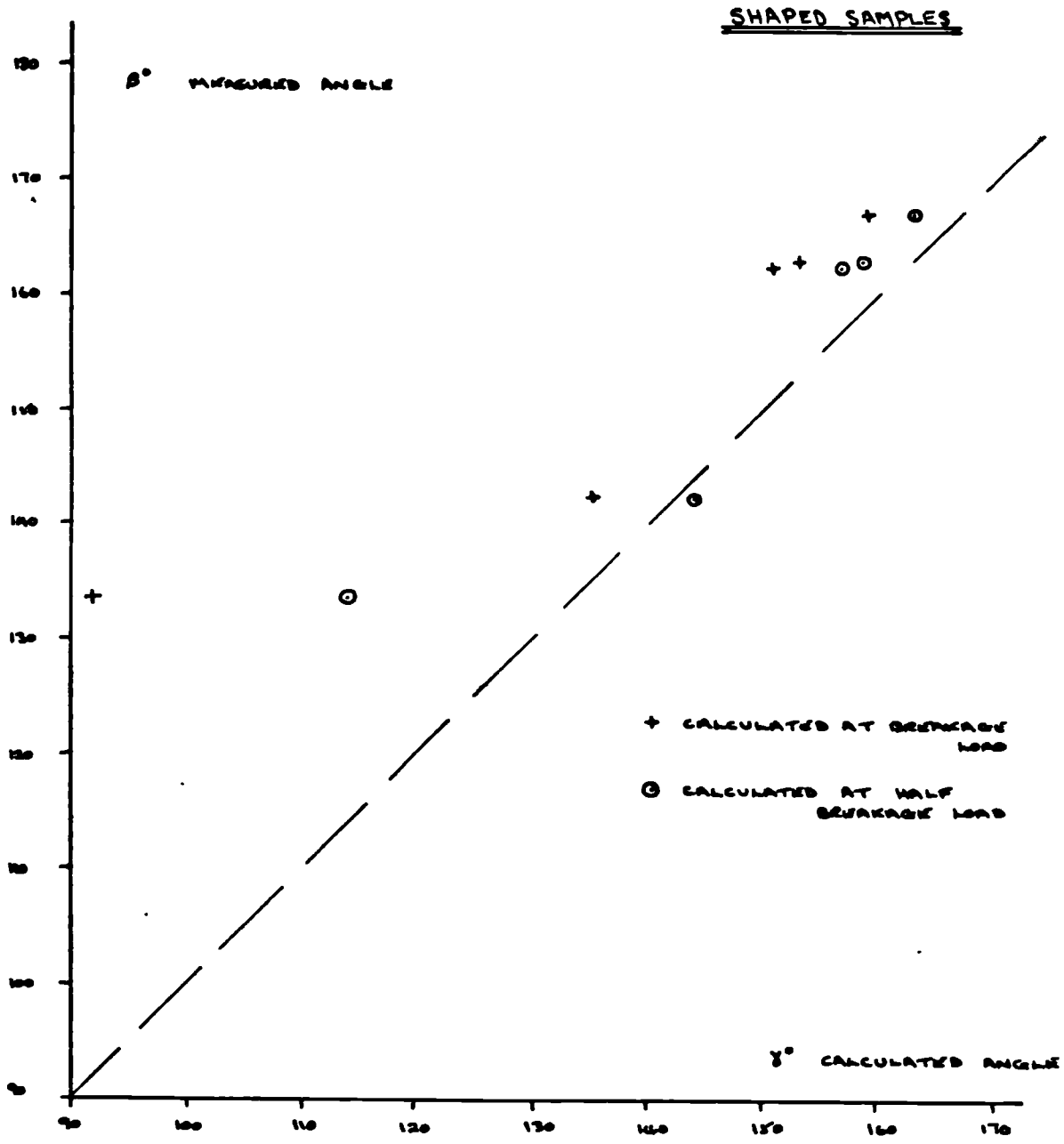

FIG. III.1 :- CORRELATION BETWEEN MEASURED AND CALCULATED APEX ANGLES

REFERENCES

A.S.C.E. "Problems in Design and Construction of Earth and Rockfill Dams"
Journal Soil Mechanics and Foundations Division
Proc. A.S.C.E. SM3 1967

BECKER E., CHAN C.K. and SEED H.B.
"Strength and Deformation Characteristics of Rockfill Materials in Plane Strain and Triaxial Compression Tests"
Report No.TE 72-3
Dept. of Civil Engineering
University of California
Berkeley U.S.A. 1972

BAUMANN P.
"Rockfill Dams: Cogswell and San Gabriel Dams"
Sord A.S.C.E. Transactions
Vol. 125 Part II 1960

BOWDEN F.P. and TABOR D.
"The Friction and Lubrication of Solids"
Clarendon Press, Oxford
Vol. I 1949
Vol. II 1964

BROS B and ORZESZYNA H.
"The Influence of Particles Angularity and Surface Roughness on Engineering Properties of Sands"
7th European Conference on Soil Mechanics and Foundation Engineering
Vol. II Brighton 1979

CATHIE D.N. and DUNGAR R.
"Evaluation of Finite Element Predictions for Constructional Behaviour of a Rockfill Dam"
Proc. Institution of Civil Engineers
No. 65 Part II 1978

CATTANEO C.

"Teoria Del Contatto Elastico in Seconda Approssimatione"
Rendiconti Di Matematica
Vol. 6 1947

CHARLES J.A.

"Correlation Between Laboratory Behaviour of Rockfill and Field Performance with Particular Reference to Scammonden Dam"
Ph. D. Thesis
London 1973

COGAN J.

"Triaxial Creep Tests of Opohonga Limestone and Ophir Shale"
International Journal of Rock Mechanics and Mining Science
Vol. 13 1976

COOPER D.H.

"Hertzian Contact - Stress Deformation Coefficients"
Journal of Applied Mechanics
Vol. 36 1969

FENG G.C.

"Contact Stress Analysis of Normally Loaded Rough Spheres" - Discussion
Journal of Applied Mechanics
Vol. 30 1963

FITZPATRICK M.D., LIGGINS T.B., LACK L.J., and KNOOP B.P.

"Instrumentation and Performance of Cethana Dam"
Qu. 42 R9
11th ICOLD 1973

FUMAGALLI E.

"Tests on Cohesionless Materials for Rockfill Dams"
Journal Soil Mechanics and Foundations Division
Proc. A.S.C.E. SM1
Vol. 95 1969

GILLAM E.

"Materials under Stress"
Newnes - Butterworths.
London 1969

GOODMAN L.E.

"Contact Stress Analysis of Normally Loaded Rough Spheres"
Journal of Applied Mechanics
Vol. 29 1962

GOODMAN L.E. and KEER L.M.

"The Contact Stress Problem for an Elastic Sphere Indenting an Elastic Cavity"
International Journal of Solids and Structures
Vol. 1 Part 4 1965

GRIGGS D.T.

"Creep of Rocks"
Journal of Geology
Vol. 47 1939

HERTZ H.

"Miscellaneous Papers"
Translated by D.E. Jones and G.A. Schott
Macmillan & Co.
London 1896

HOBBS D.W.

"A Simple Method for Assessing the Uniaxial Compressive Strength of Rock"
International Journal of Rock Mechanics and Mining Science
Vol. 1 1963

JAEGAR C.

"Rock Mechanics and Engineering"
Cambridge University Press 1972

JAEGAR J.C. and COOK N.G.W.
"Fundamentals of Rock Mechanics"
Methuen & Co. 1969

KAWASE M.
Discussion Paper 3065
Sord A.S.C.E. Transactions
Vol. 125 Part II 1960

KJAERNSLI B. and SANDE A.
"Compressibility of Some Coarse - Grained Materials"
Proc. European Conference on Soil Mechanics and Foundation Engineering
Wiesbaden 1963

KJAERNSLI B.
"Compressibility of Rockfill and Deformations of Rockfill Dams"
British Geotechnical Society
London 1965

Alternative Ref. Norwegian Geotechnical Institute Publ. F 196 1965

KO H.Y. and SCOTT R.F.
"Deformation of Sand in Hydrostatic Compression"
Journal A.S.C.E. SM3 · Soil Mechanics Division
1967

KOLBUSZEWSKI J.J.
"An Experimental Study of the Maximum and Minimum Porosities of Sands"
Proc. 2nd International Conference of Soil Mechanics and Foundation Eng.
Vol. 1 1948

KRUMBEIN W.C.
"Measurement and Geological Significance of Shape and Roundness Sedimentary Particles"
Journal of Sedimentary Petrology
Vol. II 1941

LAWTON F.L. and LESTER M.D.
"Settlement of Rockfill Dams"
Qu. 31 Vol. III
8th ICOLD 1964

LE COMPTE P.
"Creep in Rock Salt"
Journal of Geology
Vol. 73 1965

LEE E.H. and RADOK J.R.M.
"The Contact Problem for Viscoelastic Bodies"
Journal of Applied Mechanics
Vol. 27 1960

LEWIS J.G.
"Shear Strength of Rockfill"
Proc. 2nd Australia - New Zealand
Conference on Soil Mechanics
1956

LOMNITZ C.
"Creep Measurements in Igneous Rocks"
Journal of Geology
Vol. 64 1956

LUBKIN J.L.
"The Torsion of Elastic Spheres in Contact"
Journal of Applied Mechanics
Vol. 18 1951

LUCAS M.M.
"On a Mechanical Model for the Deformation of
Pack Ice"
Thesis Submitted for M.Sc.
University of Washington 1975

MARSAL R.J.
"Contact Forces in Soil and Rockfill Materials"
Proc. 2nd Pan-American Conference on
Soil Mechanics and Foundation Engineering
Brazil 1963

MARSAL R.J.
"Mechanical Properties of Rockfill"
Embankment-Dam Engineering
Casagrande Volume
J. Wiley and Sons 1973

MARSAL R.J.
"Research on Granular Materials (Rockfills and Soil-Gravel Mixtures)"
Report E-25 Instituto De Ingenieria Universidad Nacional Autonoma de Mexico 1977

MICHELSON A.A.
"The Laws of Elastico-Viscous Flow"
Journal of Geology
Vol. 25 1917

MINDLIN R.D., MASON W.P., OSMER T.F. and DERESIEWICZ H.
"Effects of an Oscillating Tangential Force on the Contact Surfaces of Elastic Spheres"
Proc. 1st U.S. National Congress of Applied Mechanics
Chicago 1951

OBERT L. and DUVAL W.I.
"Rock Mechanics and the Design of Structures in Rock"
J. Wiley and Sons 1967

PARKIN A.K.
"Application of Rate Analysis to Settlement Problems Involving Creep"
Proc. 1st Aust. - New Zealand Conference on Geomechanics
Vol. 1 1971

PARKIN A.K.
"The Compression of Rockfill"
Australian Geomechanics Journal
G. 7. 1977

PENMAN A.D.M. and MITCHELL P.B.
"Initial Behaviour of Scammonden Dam"
10th ICOLD, Montreal 1970

PENMAN A.D.M.
"Rockfill"
Current Paper 15/71
Building Research Establishment 1971

PENMAN A.D.M. and CHARLES J.A.
"Constructional Deformations in a Rockfill Dam"
Current Paper 19/72
Building Research Establishment 1972

PIGEON Y.
"The Compressibility of Rockfill"
Ph. D. Thesis
London University 1969

PRICE N.J.
"A Study of the Time-strain Behaviour of Coal-Measure Rocks"
International Journal of Rock Mechanics and Mining Science
Vol. 1. 1964

RABINOWICZ E.
"Friction and Wear of Materials"
J. Wiley and Sons 1965

REINUS E.
"Design and Construction of Holjes Dam"
Vol. III 8th ICOLD 1964

RITTENHOUSE G.
"A Visual Method of Estimating Two-Dimensional Sphericity"
Journal of Sedimentary Petrology
Vol. 13 1943

RZADKOWSKI B. and ZUREK J.
"Influence de L'Eau sur la Deformabilite des Roches Broyees et sur le Tassement des Barrages en Enrochement"
10th ICOLD Montreal 1970

SERRANO A.A. and RODRIGUEZ-ORTIZ J.M.
"A Contribution to the Mechanics of Heterogeneous Granular Media"
Proc. Symposium on the Role of Plasticity in Soil Mechanics
Cambridge 1973

SHERARD J.L., WOODWARD R.J., GIZIENSKI S.F., and CLEVENGER W.A.
"Earth and Earth-Rock Dams"
J. Wiley and Sons 1963

SHERARD J.L.
"Embankment Dam Cracking"
Embankment-Dam Engineering
Casagrande Volume
J. Wiley and Sons 1973

SOWERS G.F., WILLIAMS R.C. and WALLACE T.S.
"Compressibility of Broken Rock and the Settlement of Rockfills"
Proc. 6th International Conference on Soil Mechanics and Foundation Eng.
Montreal 1965

SOYDEMIR C. and KJAERNSLI B.
"A Treatise on the Performance of Rockfill Dams with Unyielding Foundations in Relation to the Design of Storvass Dam"
Report 53203 Norwegian Geotechnical Institute 1975

SOYDEMIR C. and KJAERNSLI B.
"Deformation of Membrane-Faced Rockfill Dams"
7th European Conference on Soil Mechanics and Foundation Engineering
Vol. 3 1979

SPIELMAN J.V.

Discussion on Cogswell and San Gabriel Dams
Transactions A.S.C.E.
Vol. 125 Part 2 1960

STEELE I.C. and COOKE J.B.

"Rockfill Dams: Salt Springs and Lower Bear River Concrete Face Dams"
Sord A.S.C.E. Transactions
Vol. 125 Part II 1960

STOREY C.

"Investigation into one of the Assumptions of the Hertz Theory of Contact"
British Journal of Applied Physics
Vol. II 1968

TAYLOR D.W.

"Fundamentals of Soil Mechanics"
J. Wiley and Sons 1948

TERZAGHI K.

"Theoretical Soil Mechanics"
J. Wiley and Sons 1943

TERZAGHI K.

Discussion Paper 3065
Sord A.S.C.E. Transactions
Vol. 125 Part II 1960

TORVIK P.J.

"Note on the Boundary Conditions for Contact Problems"
Journal of Applied Mechanics
Vol. 34 1967

WILLIAMS H. and STOTHARD J.N.

"Rock Excavation and Specification Trials for the Lancashire - Yorkshire Motorway, Yorkshire (West-Riding) Section"
Proc. Institution of Civil Engineers.
Vol. 36 1967

WILSON S.D.

"Deformation of Earth and Rockfill Dams"
Embankment-Dam Engineering
J. Wiley and Sons 1973

WILSON S.D. and MARSAL R.J.

"Current Trends in Design and Construction of Embankment Dams"
Monograph A.S.C.E. 1979

WORLD REGISTER OF DAMS

ICOLD 1964 - Updated 1968
ICOLD 1973 - Updated ICOLD 1976 and ICOLD 1979

YANG W.H.

"The Contact Problem for Viscoelastic Bodies"
Journal of Applied Mechanics
Vol. 33 1966

ZELLER J. and WULLIMANN R.

"The Shear Strength of the Shell Materials for the Goschenenalp Dam, Switzerland"
Proc. 4th International Conference on Soil Mechanics and Foundation Eng.
Vol. 2 1957